

Solid State Theory: An Introduction

U. Rössler

Solid State Theory: An Introduction

Second revised and extended edition

With 123 Figures and 6 Tables



Physica-Verlag

Prof. Dr. h.c. Ulrich Rössler
Universität Regensburg
Inst. Theoretische Physik
Universitätsstr. 31
93040 Regensburg
Germany

ISBN 978-3-540-92761-7 e-ISBN 978-3-540-92762-4
DOI 10.1007/978-3-540-92762-4
Springer Dordrecht Heidelberg London New York

Library of Congress Control Number : 2009929708

© Springer-Verlag Berlin Heidelberg 2009

This work is subject to copyright. All rights are reserved, whether the whole or part of the material is concerned, specifically the rights of translation, reprinting, reuse of illustrations, recitation, broadcasting, reproduction on microfilm or in any other way, and storage in data banks. Duplication of this publication or parts thereof is permitted only under the provisions of the German Copyright Law of September 9, 1965, in its current version, and permission for use must always be obtained from Springer. Violations are liable to prosecution under the German Copyright Law.

The use of general descriptive names, registered names, trademarks, etc. in this publication does not imply, even in the absence of a specific statement, that such names are exempt from the relevant protective laws and regulations and therefore free for general use.

Cover design: eStudio Calamar S.L.

Printed on acid-free paper

Physica-Verlag is a brand of Springer-Verlag Berlin Heidelberg
Springer is part of Springer Science+Business Media (www.springer.com)

To Erika

Preface to Second Edition

Given the fact that the first edition of this book is almost sold out, the editor has asked for a second edition. I readily accepted this opportunity, because – as many users and I myself had found out in the meantime – there were quite a lot of typing and other errors in the first edition which had to be eliminated. But more important, I saw the chance to extend the book by a new chapter on light–matter interaction, which complements the canon of the book with respect to both the physics of this interaction and the theoretical methods used for its description. Moreover, during the four years since the first edition the whole field has developed as can be seen in the list of references which now contains about 30 new titles.

Part of the contents of this book has been presented during a guest lecture at the National Mechnikov University in Odessa in the spring term of 2007. I would like to acknowledge the hospitality of the Department of Theoretical Physics and its head, Prof. V.M. Adamyan, and the contacts with the students who attended this one as their first lecture in English. Finally, I appreciate the support by and easy cooperation with the publisher.

Regensburg,
June 2009

Ulrich Rössler

Preface to First Edition

The history of my involvement in this book project starts more than 30 years ago. During the years 1969–1972, my thesis advisor, Otfried Madelung, wrote a series of three textbooks on Solid State Theory, entitled *Festkörpertheorie* I–III, which appeared in the Springer paperback series *Heidelberger Taschenbücher*. My fellow graduate students and friends Manfred Lietz, Rolf Sandrock, Joachim Treusch, and I, were the first to proof-read these books. Better still, we were given the unique opportunity to provide input based on insights gained during our studies. In 1978, when *Festkörpertheorie* I–III were partly rewritten and translated into English, Otfried Madelung again asked his former disciples, then already established in university positions, for comments and contributions based on their respective research and teaching experience in this field. The result, entitled *Introduction to Solid-State Theory*, became a widely used textbook, published in several further editions over the following years.

Like most textbooks on Solid-State Theory currently used in university physics courses all over the world, *Introduction to Solid-State Theory* has meanwhile become somewhat outdated. Solid State Physics has evolved significantly and many topics, which 30 years ago were still the subject of active research or even beyond its leading edge, have now become part of our standard knowledge. The idea of accounting for this development in a textbook has been lingering in the collective mind of the Solid State Physics community for quite a while, but it took an initiative by Springer to concretize the project. When Springer editors asked Otfried Madelung to rework on *Introduction to Solid-State Theory* accordingly, he convinced them that it would make more sense to write a completely new book, proposing me as a potential author. This is how I got involved.

Due to the formative influence of Otfried Madelung and his approach to science, my research in Solid State Theory has from the very beginning been oriented towards experimental work, often directly stimulated by concrete experimental results. This tendency was solidified during a year as postdoctoral researcher with Manuel Cardona at Brown University in Providence,

RI, USA. Quite commonly, my research projects were initiated by discussions with researchers renowned for their experimental work and have frequently been conducted in fruitful cooperations. It is to this continuous contact with the physics reality that I owe the down-to-earth approach which characterizes my research and teaching and which should also be noticeable in this book.

At the University of Regensburg, where I became professor in 1972, Solid State Physics has been a strong research field, both in experiment and theory. Over the years the topics evolved from magnetism, phase transitions, lattice dynamics, and electronic structure of bulk material to the upcoming fields of high- T_c superconductors, correlated electron systems, surface physics, quantum wells, nano-structures, and composite materials. Quite naturally, Solid State Theory has been a standard part of the physics curriculum in Regensburg. It started as a one-semester course with four weekly lectures in the fourth year of the German diploma curriculum (corresponding to the first year of the graduate education in the Anglo-American system). Soon it was supplemented by a second course on special topics, with the purpose of guiding the students into active research fields. For more than 30 years, I taught these courses on a regular basis, taking turns with my colleagues Joachim Keller, Uwe Krey, Ulrich Schröder, and Dieter Strauch. The exchange of teaching concepts and problems with these colleagues, and also our joint research projects considerably enriched my lectures. During the last decade I benefited much from the expertise of my senior coworker Michael Suhrke. Further, important input came from discussions with many colleagues from all over the world during conferences, visits, and sabbaticals in different places. My lecture notes for these courses, accumulated and continuously modified over the years, constitute the backbone of this book.

Clearly, the book follows a well-defined tradition. Target readers are those students in physics or material science who are interested in understanding the theoretical approach to Solid State Physics, while maintaining contact to the experimental facts. The contents are essentially comparable to those of other textbooks on the same subject, but emphasis is put on new aspects of the field that have resulted from more recent research. Extensive references to related literature in the form of textbooks, topical series, data collections, and selected original papers are provided to establish the connection with the sources of this subject and with active research fields. Each chapter contains a selection of problems and solutions, which are meant to help the reader gain practice with the concepts and the physics explained in the text. Since the number of pages is restricted, this book cannot claim completeness. Nevertheless, wherever possible, reference is given to those important topics that could be covered here only briefly or not at all. In short, this book is intended as an introduction to Solid State Theory, given from the perspective of more than 30 years of learning, teaching, and research in this field.

It is a pleasure to thank all those who contributed in one way or the other to this project. I have already mentioned some friends and colleagues and would like to extend my acknowledgments to the students who attended my courses

and enriched them by their constructive feedback. This applies especially to my diploma and Ph.D. students, who contributed ideas during many hours of discussion about their research projects. A highly visible contribution to this book came from Ingeburg Zirkl who prepared all the figures. A critical reading of parts of the manuscript by my friends and colleagues Joachim Keller and Dieter Strauch, and by my son Thomas has led to considerable improvements of the contents and the text. Finally, I express my gratitude to Springer, in particular to Dr. Claus Ascheron and Dr. Angela Lahee, not only for their expert help and advice but also for their patience in waiting for the final version of this book.

Regensburg,
April 2004

Ulrich Rössler

Contents

List of Symbols	XVII
1 Introduction	1
1.1 Aims and Outline	2
1.2 The Structure of Solids	4
1.3 Pair-Distribution Function and Structure Factor	9
Problems	12
2 The Solid as a Many-Particle Problem	15
2.1 The Hamiltonian of the Solid	16
2.2 Separating the Motion of Electrons and Ions	20
2.3 Thermal Expectation Values	22
2.4 Theory of Linear Response	24
2.5 Kubo's Formulas: Response Functions	28
2.6 Properties of Response Functions	32
Problems	36
3 Lattice Dynamics: Phonons	37
3.1 Harmonic Approximation	39
3.2 Normal Coordinates	42
3.3 Phonons and Occupation Number Representation	44
3.4 Acoustic Phonons	48
3.5 Optical Phonons	55
3.6 Examples: Phonon Dispersion Curves	60
3.7 The Crystal Lattice at Finite Temperature	68
Problems	73
4 The Free Electron Gas	75
4.1 Free Electrons Without Interaction	76
4.2 Free Electrons in a Magnetic Field	84
4.3 Occupation Number Representation for Electrons	93

4.4	Hartree–Fock Approximation	97
4.5	The Dielectric Function	102
4.6	Discussion of the Dielectric Function	107
4.7	Electronic Correlation	110
	Problems	115
5	Electrons in a Periodic Potential	119
5.1	Density Functional Theory	120
5.2	Bloch Electrons and Band Structure	127
5.3	Almost Free Electrons and Pseudo-Potentials	129
5.4	LCAO and Tight-Binding Approximation	139
5.5	Effective-Mass Approximation	147
5.6	Subbands in Semiconductor Quantum Structures	152
	Problems	157
6	Spin Waves: Magnons	161
6.1	Preliminaries	162
6.2	The Heisenberg Hamiltonian	166
6.3	Spin Waves in Ferromagnets	170
6.4	Spin Waves in Anti-Ferromagnets	175
6.5	Molecular Field Approximation	179
6.6	Itinerant Electron Magnetism	185
	Problems	191
7	Correlated Electrons	195
7.1	Retarded Green Function for Electrons	196
7.2	The Hubbard Model	201
7.3	Fermi Liquids	208
7.4	Luttinger Liquids	213
7.5	Heavy Fermion Systems	217
7.6	Fractional Quantum Hall States	222
	Problems	228
8	Electron–Phonon Interaction	231
8.1	Preliminaries	232
8.2	Coupling Mechanisms	235
8.3	Scattering Processes: Lifetime, Relaxation	240
8.4	The Fröhlich Polaron	247
8.5	Effective Electron–Electron Interaction	250
8.6	Cooper Pairs and the Gap	255
	Problems	263

9	Defects, Disorder, and Localization	265
9.1	Point Defects	266
9.2	Disorder	273
9.3	Approximations for Impurity Scattering	276
9.4	Electric Conductivity	280
9.5	Metal–Insulator Transition	285
	Problems	290
10	Light–Matter Interaction	291
10.1	Preliminaries	291
10.2	Single-Particle Approximation	294
10.3	Excitons	298
10.4	Polaritons	307
10.5	Light-Scattering	312
10.6	Coherent Interband Dynamics	316
10.7	Semiconductor Bloch Equations	320
	Problems	323
A	Appendices	325
A.1	Elements of Group Theory	325
A.2	Fourier Series and Fourier Transforms	329
A.3	Fermi and Bose Integrals	331
A.4	Sommerfeld Expansion	333
A.5	Calculation of the Exchange Energy	335
A.6	Operators in Fock Representation	336
	References	337
	Solutions	349
	Index	389

List of Symbols

a	Lattice constant
$a_s^\dagger(\mathbf{q}), a_s(\mathbf{q})$	Creation, annihilation operator of a phonon with quantum numbers s, \mathbf{q}
a_i^\dagger, a_i	Creation, annihilation operator of spin excitations at site i
$\mathbf{a}_i, i = 1, 2, 3$	Primitive lattice vectors
\hat{A}	Observable
\mathbf{A}	Vector potential
$\mathbf{b}_j, j = 1, 2, 3$	Primitive reciprocal lattice vectors
$b_{\mathbf{k}}^\dagger, b_{\mathbf{k}}$	Creation, annihilation operator of ferromagnetic magnons
\mathbf{B}	Magnetic induction
\hat{B}	Observable
B_0	Bulk modulus
$\mathcal{B}_S(y)$	Brillouin function
$B_{\nu\mathbf{Q}}^\dagger, B_{\nu\mathbf{Q}}$	Creation, annihilation operator of excitons
c	Velocity of light in vacuum
c_V	Specific heat at constant volume
$c_{ijkl}(c_{IJ})$	Components of the compliance tensor, elastic moduli (Voigt notation)
$c_{\mathbf{k}\sigma}^\dagger, c_{\mathbf{k}\sigma}$	Creation, annihilation operator of Bloch electrons
$C_{nn}(\mathbf{r}, \mathbf{r}')$	Density–density correlation function
$\mathbf{d}, \mathbf{d}_{cv}$	Electric dipole vector
$D, D_{1,2,3}$	Deformation potentials
$D_{\tau i, \tau' j}(\mathbf{q})$	Element of the dynamical matrix

XVIII List of Symbols

$D(\omega), D(E)$	Density of states
$\mathbf{D}, \mathbf{D}(\mathbf{q}, \omega)$	Displacement field
e	Elementary charge
e_{ijk}	Piezoelectric tensor
$\mathbf{e}^s(\mathbf{q})$	Normalized phonon eigenvector
E	Energy
	Young's modulus
$E_n(\mathbf{k}), \epsilon_{nk\sigma}$	Energy of Bloch electron
E_0	Energy of ground state
E_F	Fermi energy
$E(T)$	Thermal energy
\mathcal{E}_{el}	Energy eigenvalue of the many-body electron problem
E_ν, \mathbf{Q}	Energy of exciton
$\mathbf{E}, \mathbf{E}(\mathbf{q}, \omega)$	Electric field
f_0	Oscillator strength
$f_{\mathbf{k}}$	Fermi distribution function
F	Free energy
$g(g^*)$	Landé (effective) g factor
$g(\mathbf{r})$	Pair-distribution function
G	Rigidity modulus
$G_{\text{AB}}, G(\alpha; t, t')$	Retarded Green function
\mathbf{G}_m, \mathbf{G}	Reciprocal lattice vector
H	Hamiltonian of phonons or of electrons symmetry point of the bcc Brillouin zone, endpoint of the Δ -axis
$\mathcal{H}, \mathcal{H}_0$	Many-body Hamiltonian of the solid
$\mathcal{H}_{\text{el}}, \mathcal{H}_{\text{ion}}, \mathcal{H}_{\text{el-ion}}$	Parts of \mathcal{H} describing electrons, ions, and the electron-ion interaction
$\mathcal{H}_{\text{rad}}, \mathcal{H}_{\text{el-rad}}$	Hamiltonian of the radiation field and of the light-matter interaction
$\mathcal{H}_{\text{jell}}$	Hamiltonian of the jellium model
\mathcal{H}_{so}	Hamiltonian of spin-orbit coupling
$\mathcal{H}_{\text{spin}}$	Heisenberg's spin Hamiltonian
\mathbf{H}	Magnetic field
\mathbf{j}	Electric current density
$J, J_{\mathbf{RR}'}, J_{ij}$	Exchange integrals
k_B	Boltzmann constant
k_F	Radius of Fermi sphere

k_{FT}	Thomas–Fermi screening parameter
\mathbf{k}	Wave vector (of electron)
L	Symmetry point of the fcc Brillouin zone Lagrangian of lattice vibrations
m	Free electron mass
m^*	Effective mass of an electron
\mathbf{m}	Magnetic dipole moment
M_i, M_τ	Mass of an ion
M^E, \mathbf{M}	Electric dipole moment
M	Magnetization or magnetic dipole density
$n(\mathbf{r})$	Particle (electron) density
\hat{n}	Density operator
$n_{\mathbf{q}}$	Density fluctuation
$n_s(\mathbf{q}, T)$	Bose–Einstein distribution function
N, N_0	Number of electrons Number of unit cells in the normalization volume
$N_{\mathbf{q}}$	Number fluctuation
$N_{\pm}, N_{\uparrow\downarrow}$	Number of electrons for different spin orientation
\mathbf{p}, p_l	Momentum of an electron
\mathbf{P}	Dielectric polarization or electric dipole density
$\mathbf{P}_{n\tau}$	Momentum of an ion
$P_s(\mathbf{q})$	Conjugate momentum to $Q_s(\mathbf{q})$
\mathbf{q}	Wave vector (of phonon)
Q_i, Q_{ext}	(Point) charge
$Q_s(\mathbf{q})$	Normal coordinate of lattice vibration
r_s	Density parameter (radius of Wigner–Seitz sphere)
\mathbf{r}, r_l	Position vector of an electron
\mathbf{R}_n^0	Lattice vector, equilibrium position of an ion in a Bravais lattice
\mathbf{R}_n	Actual position of an ion in a Bravais lattice
$\mathbf{R}_{n\tau}$	Actual position of an ion in a lattice with basis
s_{ijkl}	Components of the elastic or stiffness tensor
$S(\mathbf{q})$	Static structure factor

$S(\mathbf{q}, \omega)$	Dynamic structure factor
$\mathbf{S}_{\mathbf{R}}, \mathbf{S}_i$	Vector operator for spin at \mathbf{R} or at site i
S^i, S^\pm	Components of vector spin operator
$t, t_{ij}, t_{\mathbf{R}\mathbf{R}'}$	Transfer integral
T	Absolute temperature
$T_c(T_C)$	Critical (Curie) temperature
T_N	Néel temperature
$T_{\mathbf{R}^0_{\mathbf{r}_n}}$	Translation operator
T_1, T_2	Longitudinal, transverse relaxation time
$\mathbf{u}_{n\tau}(t)$	Ion displacement from equilibrium position
U	Exchange interaction, correlation energy (Hubbard)
$\mathbf{U}(\mathbf{k}, t)$	Bloch vector
$\mathcal{U}_\alpha(\{\mathbf{R}_n\})$	Adiabatic potential
$v_{\mathbf{q}}$	Fourier transform of (Coulomb) potential
v_F	Fermi velocity
v_L, v_T	Longitudinal, transverse sound velocity
V, V_c	Crystal or normalization volume
V_{WSC}	Volume of Wigner–Seitz cell
$V_{\text{eff}}(\mathbf{r})$	Effective single particle potential
$V_{\text{xc}}(\mathbf{r})$	Exchange–correlation potential
V_{ext}	External perturbation
$\mathcal{V}_s(\mathbf{q})$	Matrix element of electron–phonon interaction
Z, Z_G	Partition function of canonical and grand-canonical ensemble
α	Thermal expansion coefficient
$\alpha_{\mathbf{k}}^\dagger, \alpha_{\mathbf{k}}; \beta_{\mathbf{k}}^\dagger, \beta_{\mathbf{k}}$	Creation, annihilation operators of anti-ferromagnetic magnons
α^F	Froehlich coupling constant
γ	Grüneisen parameter, Sommerfeld coefficient
Γ	center of the Brillouin zone, $\mathbf{k} = (0, 0, 0)$
Δ	damping parameter
	Symmetry line in the fcc (bcc) Brillouin zone connecting Γ and $X(H)$
	Gap parameter in superconductors
$\chi_{AB}(\omega)$	Response function, susceptibility
χ^E, χ^M	Dielectric, magnetic susceptibility
χ_{ij}^E, χ_{ij}^M	Tensor components of χ^E, χ^M
$\chi_{+-}^M(\mathbf{q}, \omega)$	Spin susceptibility

$\epsilon_{jl}(\epsilon_J)$	Components of the strain tensor (Voigt notation)
ϵ_0	Average ground state energy per electron
$\epsilon_c(\epsilon_{xc})$	Average correlation (exchange–correlation) energy per electron
ϵ_0	Vacuum dielectric constant
$\epsilon(0)$	Static or low-frequency dielectric constant
ϵ_∞	High-frequency dielectric constant
$\epsilon(\mathbf{q}, \omega)$	Dielectric function
ϵ_1, ϵ_2	Real, imaginary part of dielectric function
η	(Transverse) Effective charge
λ	Localization length
Λ	Symmetry line in the Brillouin zone connecting Γ and L
μ	Reduced mass chemical potential mobility
μ_B	Bohr's magneton
μ_0	Magnetic field constant
ν	Filling factor of Landau levels
ω_c	Cyclotron frequency
ω_D	Debye frequency
$\omega_s(\mathbf{q})$	Frequency of phonon with quantum numbers s, \mathbf{q}
$\omega_{L(O)}, \omega_{T(O)}$	longitudinal, transverse (optical) phonon frequency at $\mathbf{q} = 0$
ω_k	Magnon frequency
ω_p	Plasma frequency
ω_R	Rabi frequency
Ω	Grand-canonical potential
$\psi(\mathbf{r})$	Single-electron wave function
$\psi_{n\mathbf{k}}(\mathbf{r})$	Bloch function
$\Psi, \tilde{\Psi}$	Many-electron wave function (stationary, time-dependent)
$\phi_\nu(\mathbf{r} - \mathbf{R}_n^0)$	Atomic orbital centered at \mathbf{R}_n^0
$\phi_\nu(\mathbf{r})$	Exciton envelope function
Φ	Force constant Magnetic flux
Φ_0	Elementary magnetic flux quantum
$\rho, \hat{\rho}$	Statistical operator
ρ_0	Statistical operator of thermal equilibrium
ρ_M	Mass density
ρ_{AB}	Spectral function
$\rho(\mathbf{r})$	Charge density
ρ	Resistivity tensor

$\rho_{\mathbf{k}}(t)$	Time-dependent density matrix
$\rho_{cc}(\mathbf{k}, t), \rho_{vv}(\mathbf{k}, t), \rho_{cv}(\mathbf{k}, t)$	Components of the density matrix
$\sigma_{ik}(\sigma_I)$	Components of the stress tensor (Voigt notation)
σ	Conductivity tensor
Σ	Symmetry line in the Brillouin zone connecting Γ and K
$\Sigma(\alpha, E), \Sigma(\mathbf{k}, \sigma)$	Electron self-energy
Θ_D	Debye temperature
$\tau_{\mathbf{k}}$	Single-particle lifetime
τ_{tr}	Transport relaxation time
τ	Ion position relative to the lattice vector in a lattice with basis
ζ	Degree of spin polarization
$\zeta_n(z)$	Subband envelope function

Introduction

The advent of quantum mechanics in the early twentieth century has fundamentally improved our understanding of the physics of matter in general and of the solid state in particular. Consisting of a very large number of atoms, solids exhibit a rich variety of material properties, whose understanding represents a challenge to the curious scientist. These properties are at the same time a rich source for technical applications. Consequently, in the course of the last century our increasing knowledge about the relationship between the chemical composition and the structure of solids on one side and their particular properties – according to which we identify metals, semiconductors, superconductors, and magnetic materials – on the other side, has led to the invention of an enormous variety of solid state devices. Whole industries have been created based on products that make use of solid state properties. Transistors, sensors, solid state lasers, light-emitting diodes (LED), superconducting quantum interference devices (SQUID), dynamic and magnetic random access memories (DRAM and MRAM) have become essential parts of electronic appliances such as computers, mobile phones, compact disc (CD) and digital video disc (DVD) players, which have revolutionized our daily life and continue to do so. The impressive development in the technology of data storage and handling, symbolized by Moore's law, demonstrates an unprecedented technological progress, which, though driven by the market, would be unthinkable without the ingenious investigations of generations of physicists.

In the past decades, solid state research has uncovered interconnections between the structural, elastic, electronic, magnetic, and optical properties of solids and led to unpredicted fundamental discoveries like heavy fermions, the quantum Hall effects, high- T_c superconductors, the giant magnetoresistance effect, and solid state lasers. The progress in material growth and manipulation, which enables the tailoring of solid state properties by properly choosing the chemicals and the structure, together with the invention of pioneering experimental techniques, has paved the road to the world of low-dimensional systems and nanostructures with new physical and technological perspectives. Quantum dots, single electron transistors, and Carbon nanotubes are the

buzzwords in this research field, which has attracted the attention of many solid state physicists. Most recently, the electron spin has moved into the focus of interest with the perspective of applications in spintronics and quantum computation. Accompanying and enabling these developments, powerful theoretical concepts, complemented by numerical tools and computational physics, have been developed for qualitative and quantitative modeling of the solid state and its properties.

Thus, solid state physics presents itself as a dynamic and rich research field whose results and progress are well documented not only in the physics journals but also in series publications and data collections devoted to this subject [1]. Recently even an Encyclopedic Dictionary of Condensed Matter Physics appeared on the market [2]. A thorough understanding of the theoretical foundations of the field and how the properties of solids derive from the chemical composition and structure in a quantum mechanical description are an indispensable part of a university physics curriculum.

1.1 Aims and Outline

As stated in the preface, this book follows the tradition of a series of textbooks on Solid State Theory that have served generations of graduate students in physics [3–14]; but there are also a number of more recently published books in the field [15–28]. Courses on Solid State Theory, which are found in physics curricula all over the world, are based on theoretical concepts developed in quantum mechanics and statistical physics, but they also require some basic knowledge about solid state phenomena from an introductory course in Solid State Physics for which [12, 29–31] are standard references.

The aim of this book is to provide the methods required to describe a many-particle system with about 10^{23} atoms per cm^3 and its material specific properties. This can only be done in an approximate way and for special quantum mechanical states of the system. We focus here on the ground state, which defines the structure of the solid, and on low-lying excited states, which determine the response of the solid to a small external perturbation. This response characterizes material properties like dielectric or magnetic susceptibility and electrical conductivity, whose meaning is already known from more elementary courses. They establish the connection between theoretical description and the real world, explored by experiments and relevant for applications. Therefore, in the individual chapters, the relation to material properties, be it elastic, electronic, optical, or magnetic, will be emphasized in view also of recent results in the field.

The aims of the book become more transparent when one looks at the outline. In this introduction (Chap. 1), we survey the different forms of condensed matter, which can be distinguished from each other by their pair-distribution function or its Fourier transform, the structure factor. The crystalline solids,

which are the focus of this book, represent a specific form of condensed matter with a pronounced structure due to a characteristic long-range order. At the beginning of Chap. 2, the Hamiltonian of a solid composed of ions (nuclei and closed electron shells) and valence electrons will be introduced. These two kinds of constituents, with masses differing by orders of magnitude, can be treated separately as independent subsystems after applying the adiabatic or Born–Oppenheimer approximation. Before doing so, the linear response theory is introduced as the basic concept to describe the material properties of a solid. In Chap. 3, the dynamics of the ions, the heavy constituents of a solid, will be described as theory of lattice vibrations. This will first be done in a classical approach using the model of massive spheres connected by springs; but in a second step, we turn to the quantum-mechanical concept of phonons as elementary excitations of the lattice. Acoustic phonons will be discussed in the context of heat capacity, elastic properties, and sound propagation; optical phonons will be related to optical properties of solids in the far-infrared spectral range. Examples of phonon dispersion curves for quite different solids will be presented to illustrate the influence of structure and chemical composition. The next chapters (Chaps. 4–7) are devoted to electrons and their properties. The basic concept of the Fermi surface and the fundamentals of the many-particle theory, like Fock representation, Hartree–Fock approximation, dielectric screening, and electronic correlation, for free electrons in the jellium model (Chap. 4) will be introduced. The influence of the periodic lattice structure on the electron states will be treated in the single-particle approximation justified by the density–functional theory (Chap. 5). In this chapter, we also present methods for calculating the band structure, which are important to understand the material specific aspects of energy bands, and discuss the properties of two-dimensional electron systems. As a particular outcome of electron–electron interaction, the Heisenberg Hamiltonian will be the starting point in Chap. 6 to discuss spin waves as excitations out of a ground state with ferromagnetic or anti-ferromagnetic ordering. This Hamiltonian will also be used to demonstrate the molecular field approximation and the ferromagnetic phase transition. Finally, the theory of itinerant electron magnetism will be presented in this chapter. Electron–electron interaction is the focus also in Chap. 7 which is devoted to correlated electrons. For the treatment of some aspects in this field, we take advantage of using Green functions, which have to be introduced for this purpose. They will be used to deal with the Hubbard model, leading to the Mott–Hubbard metal-insulator transition. We discuss the phenomenological concept of Fermi liquids and its modification for one-dimensional electron systems. Finally, heavy fermions and the fractional quantum Hall states, both dominated by correlation, are also introduced. In Chap. 8, we go beyond the adiabatic approximation and study the electron–phonon interaction as a prototype of coupling between fermions and bosons. It is relevant in scattering processes, which are essential for the electric conductivity, for relaxation and lifetime effects of free carriers, but can also mediate an attractive electron–electron interaction that gives rise

to the formation of Cooper pairs, a basic concept of superconductivity. While the ideal crystalline order of the ions has been assumed in all these chapters, Chap. 9 will be devoted to disorder caused by impurities and other deviations from lattice periodicity, and their consequences for electron states and electric conductivity. This chapter includes an excursion to weak and strong localization and the disorder-induced metal-insulator transition. The interaction between light and matter will be the subject of Chap. 10. Besides the quantum mechanical description of the optical properties of semiconductors and insulators we present the concepts of polaritons and of semiconductor Bloch equations.

1.2 The Structure of Solids

Atoms or groups of atoms, when brought into close contact, stick together because of chemical binding. The resulting stable spatial configuration is governed by electrostatics (due to the charged ions) and quantum mechanics (for the electrons). Under given thermodynamic conditions, it represents the state of condensed matter with the lowest total energy, the *ground state*. For molecules consisting of a small number of atoms, the variety in structure and functionality results from the many possible combinations of different atoms from the periodic table. A larger number of identical atoms (or identical groups of a small number of atoms) can form a *cluster* [32–34] or *macromolecule* with identical building blocks (e.g., polymer chains). With an increasing number of atoms, this eventually results in macroscopic structures whose physical properties are determined by the chemical nature of the constituents and their configuration in space. These macroscopic structures are understood in a more restricted sense as *condensed matter*, which comprises matter in the liquid or solid phase.

Crystalline structures result from a space-filling periodic repetition of the same building blocks (an atom and its nearest and next-nearest neighbors). These configurations are characterized by a long-range order, which causes sharp Bragg¹ peaks in diffraction experiments. These Bragg peaks are used to identify *crystalline solids* (or solids in the crystalline state) by their crystal classes. Crystalline solids will be the primary subject of this book. Some elementary concepts for describing their structure shall be polished up by solving Problem 1.1.

Before discussing crystalline structures in more detail, we should mention other forms of condensed matter, namely *quasi-crystals* [35–37], *amorphous solids* [38, 39], *liquid crystals* [40], and *soft matter* [41–46]. Quasi-crystals exhibit long-range order, but they are not simple periodic structures. Instead, they result from superimposed incommensurate periodicities and are self-similar. Examples are the one-dimensional Fibonacci chain (Problem 1.2)

¹ Sir William Henry Bragg 1862–1942, Sir William Lawrence Bragg 1890–1971, shared the Nobel prize in physics 1915.

and the Penrose tilings. The latter allows a local fivefold symmetry, which is prohibited in crystalline solids. In contrast, this long-range order is missing completely in amorphous solids which are characterized by disorder in the spatial configuration (structural disorder). The X-ray diffraction patterns of quasi-crystals show sharp peaks owing to the long-range order, while those of amorphous solids are diffuse. Liquid crystals have long-range order but not in all spatial directions. The building blocks – usually large rod-like or cyclic molecules – are arranged such that a long-range order exists with respect to the orientation of these molecules in at least one direction, whereas in other directions, a liquid structure prevails. Because of their order–disorder phase transitions at room temperature which can be triggered by applied voltages, liquid crystals have seen widespread use in displays and large scale television screens. Finally, we refer to soft matter, a class of materials that comprises foams, polymer melts, biological membranes, and colloid systems. Their particular material properties result from structuring on a mesoscopic scale on which normal liquids and solids are homogeneous.

Let us return to the periodic structures. Their systematic description can be found at the beginning of most Solid State Physics books and shall be repeated here only briefly (see Problem 1.1). An infinite periodic structure can be characterized by a *point lattice*, which in three dimensions is defined by the set of lattice vectors

$$\mathbf{R}_n = n_1 \mathbf{a}_1 + n_2 \mathbf{a}_2 + n_3 \mathbf{a}_3 \quad (1.1)$$

with linearly independent vectors \mathbf{a}_i , ($i = 1, 2, 3$), the primitive lattice vectors, and integers n_i , ($i = 1, 2, 3$) combined to $\mathbf{n} = (n_1, n_2, n_3)$. Point lattices in one and two dimensions are defined analogously. While in one dimension there is only one point lattice, there are 5 in two (Problem 1.3) and 14 in three dimensions [29].

The point lattice is used to define the crystal unit cell or its particular choice, the *Wigner-Seitz² cell*, which by repetition fills the whole space. Clearly, the lattice structure is mapped onto itself under a translation by a lattice vector. Mathematically, these operations form the *translation group* of the point lattice (see Appendix). Lattice translations commute with the system Hamiltonian and allow one to characterize the quantum states of the solid by a wave vector \mathbf{k} . It corresponds to the linear momentum. However, as the crystalline solid is only invariant under the discrete lattice (and not under infinitesimal) translations, the meaning of this momentum is modified as will be explained below. Therefore, it is called *crystal momentum*.

A *crystal structure* is obtained by assigning an atom or a group of atoms to each lattice point. The former case corresponds to the *Bravais³ lattices*. For the latter case, called *lattice with basis*, the position of the atoms can be

² Eugene Paul Wigner 1902–1995, Nobel prize in physics 1963; Frederick Seitz 1911–2008.

³ Auguste Bravais 1811–1863.

described by

$$\mathbf{R}_{n\tau} = \mathbf{R}_n + \boldsymbol{\tau} \quad (1.2)$$

where $\boldsymbol{\tau}$ denotes the position of an atom of the basis relative to the lattice point.

For each point lattice, a *reciprocal lattice* is defined by the vectors

$$\mathbf{G}_m = m_1 \mathbf{b}_1 + m_2 \mathbf{b}_2 + m_3 \mathbf{b}_3 \quad (1.3)$$

with integers m_j , ($j = 1, 2, 3$), $\mathbf{m} = (m_1, m_2, m_3)$, and primitive reciprocal translations \mathbf{b}_j defined by

$$\mathbf{a}_i \cdot \mathbf{b}_j = 2\pi\delta_{ij}. \quad (1.4)$$

The Wigner–Seitz cell of the reciprocal lattice is the *Brillouin*⁴ *zone*. Thus, within the Brillouin zone, there are no two wave vectors which differ by a reciprocal lattice vector, and \mathbf{k} is unique. These \mathbf{k} vectors – or the corresponding crystal momentum – characterize the eigenstates of the crystal Hamiltonian, which at the same time are eigenstates of the translation operator (Problem 1.4). Their wavefunctions, which according to *Bloch’s theorem* are modulated plane waves, yield equal probabilities in each Wigner–Seitz cell. Therefore, they represent *extended states*.

Among the different Bravais lattices, the face-centered cubic (fcc) and the body-centered cubic (bcc) are most frequently realized in normal, noble, and transition metals. One can easily check (see Problem 1.1) that these two lattices are reciprocal to each other. Their Brillouin zones, which will be used in later chapters, are shown in Figs. 1.1 and 1.2. Owing to the point lattice, the shape of the Brillouin zone exhibits a high symmetry under operations such as rotations, reflections, and inversions, which form the *point group* (see Appendix). Different points and lines of high symmetry in the Brillouin zone, denoted by letters, e.g., $\Gamma, \Delta, \Lambda, X, W, H$, are invariant under subgroups of

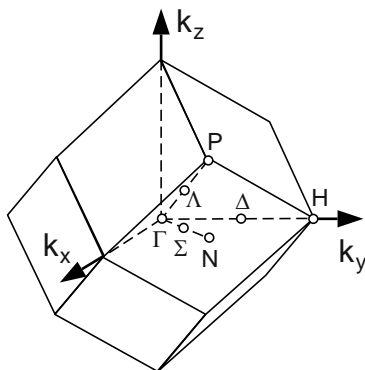


Fig. 1.1. Brillouin zone of the body-centered cubic (bcc) lattice

⁴ Léon Brillouin 1889–1969.

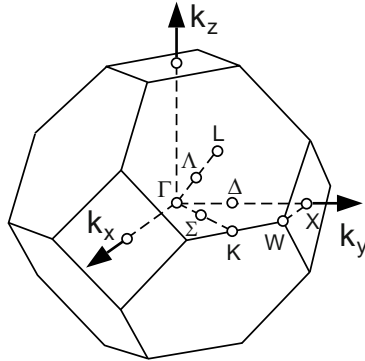


Fig. 1.2. Brillouin zone of the face-centered cubic (fcc) lattice

the point group, consisting of all operations under which \mathbf{k} is not changed, the *group of the wave vector*. For the Γ point, the center of the Brillouin zone ($\mathbf{k} = 0$), this group is identical with the point group of the crystal. The energies of quantized lattice vibrations, of electrons or spin waves will be drawn in later chapters as a function of the crystal momentum along these lines.

The fcc lattice is the point lattice of the *diamond* and *zinc blende structures*, in which the technologically most important semiconductors such as Si, Ge, and GaAs crystallize: both are lattices with a basis of two atoms (at $\boldsymbol{\tau} = \pm a(1, 1, 1)/8$, where a is the cubic lattice constant), which are identical (from the fourth group of the periodic table) for diamond, but different (e.g., from the third and the fifth group in A_3B_5 compounds) for zinc blende. Also, the *rocksalt structure*, in which most alkali halides crystallize, derives from the fcc lattice, but with the two different ions placed at $\boldsymbol{\tau} = \pm a(1, 1, 1)/4$. As demonstrated in Problem 1.5, these crystal structures lead to quite different space filling and coordination numbers, which signalize distinct types of chemical binding. More complex crystal structures with a basis of many atoms are realized, for instance, in molecular crystals and high- T_c superconductors.

The crystal structure is invariant under the operations of the *space group*, which is composed of translations and operations of the point group. Crystal eigenstates can be classified by exploiting these symmetries within the concepts of group theory [47–50]. A short introduction will be given in the Appendix A.1.

But even within the simple crystal structures, a variety of solids can be realized in mixed crystals when the positions $\mathbf{R}_{n\boldsymbol{\tau}}$ (1.2) are randomly occupied, e.g., by different kinds of atoms with the same number of valence electrons but from different rows of the periodic table. In this case, the periodicity of the point lattice still exists, but there is disorder in the occupation of the sites (*compositional disorder*). It is to be noted that already the

occupation of the lattice positions by different isotopes of the same element represents a case of compositional disorder. Compositional disorder is to be distinguished from that of amorphous material, where atoms (or groups of atoms) of the same kind are placed without long-range order to create a solid with *structural disorder*. Disorder will become important in Chap. 9 with the discussion of *localized states* whose wave functions yield a probability which decays exponentially away from its maximum.

More recently, periodic structures have become an issue in connection with *photonic crystals* [51–54]. Just as the lattice periodicity influences the electrons by Bragg reflections and causes the electronic band structure (Chap. 5), a periodic arrangement of dielectric matter or a periodicity in the refractive index gives rise to a photonic band structure. This modification of the dispersion relation of electromagnetic waves results in a wavelength dependent reflectivity which is not only observed in man-made structures, but can also be the reason for color phenomena in the natural world [55].

Any real solid has a finite size. Its *surface* is the border that separates the interior of the solid from the investigator. All experimental knowledge about a solid is based on information inter-penetrating this border and should be checked with respect to possible artifacts caused by the surface. On the other hand, the surfaces of solids – their structure, dynamics, and functionality – comprise an important part of solid state physics with a high potential for applications [56–60]. The surfaces of crystalline solids have a two-dimensional periodic structure and can be understood as a solid with reduced dimensionality. They are defined by those terminating layers of the solid whose atoms experience a surrounding that differs from that of the bulk atoms. Usually, these are the outermost two or three layers. With the changing surrounding and chemical binding, the surface atoms can take positions different from those of the bulk material given by (1.2): The lattice spacing or even the lateral periodicity can change. These changes are called relaxation and reconstruction, respectively. Some experimental techniques are more sensitive to surface effects than others and some are especially designed to study the surface of solids. Besides surface sensitive optical methods and particle scattering processes, scanning tunneling microscopy (STM), invented by Binnig and Rohrer⁵ [61], has become a diversified tool in surface physics within a short period of time. These methods allow one not only to investigate the surface of solids but also to manipulate individual atoms on the surface. The eye-catching pictures of company logos constructed by arranging individual atoms or molecules on a clean surface or of a *quantum corral* have gained some publicity [58, 62]. In the world of nanophysics [63], STM and its variants (like atomic force microscopy) play an important role.

⁵ Gerd Binnig *1947, Heinrich Rohrer *1933, shared the Nobel prize in physics 1986.

1.3 Pair-Distribution Function and Structure Factor

In order to characterize the structure of a system that consists of a very large number of constituents, it is not necessary to know the position of each individual particle. Instead, one can use a quantity which describes the probability of finding pairs of particles with given relative positions: the pair-distribution function. As we will see, this suffices to distinguish between a gas, a liquid or amorphous solid, or a crystalline solid.

Let us consider a system of N particles in a volume V (in the context of this chapter, it will be the atoms or ions of a solid, but it could also be the electrons in a plasma or the galaxies in the universe) at positions \mathbf{r}_i , with $i = 1, \dots, N$. The particle density is given by

$$n(\mathbf{r}) = \sum_{i=1}^N \delta(\mathbf{r} - \mathbf{r}_i). \quad (1.5)$$

The correlations of positions or of the density are quantified by the *density-density correlation function*

$$C_{nn}(\mathbf{r}, \mathbf{r}') = \langle n(\mathbf{r} + \mathbf{r}')n(\mathbf{r}') \rangle, \quad (1.6)$$

where $\langle \dots \rangle$ denotes the thermal average or quantum-mechanical expectation value, depending on the situation. By integration of (1.6) and normalizing we obtain the function

$$\begin{aligned} p(\mathbf{r}) &= \frac{1}{N} \left\langle \int d^3r' \sum_{ij} \delta(\mathbf{r} + \mathbf{r}' - \mathbf{r}_i) \delta(\mathbf{r}' - \mathbf{r}_j) \right\rangle \\ &= \frac{1}{N} \left\langle \sum_{ij} \delta(\mathbf{r} + \mathbf{r}_i - \mathbf{r}_j) \right\rangle \\ &= N\delta(\mathbf{r}) + \frac{1}{N} \left\langle \sum_{\substack{ij \\ i \neq j}} \delta(\mathbf{r} + \mathbf{r}_i - \mathbf{r}_j) \right\rangle, \end{aligned} \quad (1.7)$$

where the last term contains the information about the distribution of pairs $i \neq j$ with relative position $\mathbf{r}_i - \mathbf{r}_j$. Replacing the δ -function by its Fourier transform (see Appendix A.2) leads to

$$p(\mathbf{r}) = \frac{1}{V} \sum_{\mathbf{q}} e^{i\mathbf{q} \cdot \mathbf{r}} \frac{1}{N} \left\langle \sum_{i,j} e^{i\mathbf{q} \cdot (\mathbf{r}_i - \mathbf{r}_j)} \right\rangle. \quad (1.8)$$

For $\mathbf{q} = 0$, the double sum over the sites gives N^2 irrespective of the configuration. One separates this term to introduce the *static structure factor* [64]

$$S(\mathbf{q}) = \frac{1}{N} \left\langle \sum_{i,j} e^{i\mathbf{q} \cdot (\mathbf{r}_i - \mathbf{r}_j)} \right\rangle - N\delta_{\mathbf{q},0}. \quad (1.9)$$

We may also write

$$\begin{aligned} N\delta_{\mathbf{q},0} + S(\mathbf{q}) &= \frac{1}{N} \sum_i \left(1 + \left\langle \sum_{j \neq i} e^{i\mathbf{q} \cdot (\mathbf{r}_i - \mathbf{r}_j)} \right\rangle \right) \\ &= 1 + \frac{N}{V} \int_V d^3r' g(\mathbf{r}') e^{i\mathbf{q} \cdot \mathbf{r}'}, \end{aligned} \quad (1.10)$$

where $g(\mathbf{r})$ is the *pair-distribution function* [16, 64]. The last equation can be solved for $g(\mathbf{r})$ and yields

$$g(\mathbf{r}) = 1 + \frac{1}{N} \sum_{\mathbf{q}} e^{i\mathbf{q} \cdot \mathbf{r}} (S(\mathbf{q}) - 1), \quad (1.11)$$

The pair-distribution function gives the probability of finding a particle at \mathbf{r} if there is a particle at $\mathbf{r} = 0$. In general $g(\mathbf{r} = 0) = 0$ because of strong short-range repulsive forces, which prevent two particles from occupying the same position. For a crystalline solid with atoms at the fixed positions $\mathbf{R}_{n\tau}$, i.e., without thermal motion, $g(\mathbf{r})$ has sharp peaks for $\mathbf{r} = \mathbf{r}_i - \mathbf{r}_j = \mathbf{R}_{n\tau}$. This feature is a consequence of the long-range order or density–density correlation in the crystal lattice. When this order is relaxed, the peaks will become diffuse. This happens because of thermal motion and is described by the Debye–Waller factor (see Sect. 3.7), but is the case also for amorphous solids or liquids due to structural disorder. If long-range and short-range order is absent, as in a gas, $g(\mathbf{r})$ is constant for $|\mathbf{r}| > d$, where d is a characteristic parameter of the particles, e.g., the hard-core diameter.

Let us have a look also at the static structure factor written as

$$\begin{aligned} S(\mathbf{q}) &= \int d^3r p(\mathbf{r}) e^{-i\mathbf{q} \cdot \mathbf{r}} \\ &= \frac{1}{N} \left\langle \sum_{i,j} \int d^3r \delta(\mathbf{r} + \mathbf{r}_i - \mathbf{r}_j) e^{-i\mathbf{q} \cdot \mathbf{r}} \right\rangle \\ &= \frac{1}{N} \left\langle \sum_{i,j} e^{i\mathbf{q} \cdot (\mathbf{r}_i - \mathbf{r}_j)} \right\rangle = \frac{1}{N} \left\langle \sum_i e^{i\mathbf{q} \cdot \mathbf{r}_i} \sum_j e^{-i\mathbf{q} \cdot \mathbf{r}_j} \right\rangle. \end{aligned} \quad (1.12)$$

For a crystalline solid with the ions at rest, one has $\mathbf{r}_i - \mathbf{r}_j = \mathbf{R}_{n\tau}$ with $\mathbf{R}_{n\tau}$ from (1.2) giving

$$S(\mathbf{q}) = \frac{1}{N} \left\langle \sum_{\tau} e^{i\mathbf{q} \cdot \tau} \sum_{\mathbf{n}} e^{i\mathbf{q} \cdot \mathbf{R}_{\mathbf{n}}} \right\rangle. \quad (1.13)$$

Because of the periodic structure, the phases of the last sum cancel each other except for $\mathbf{q} = \mathbf{G}$, where \mathbf{G} is a vector of the reciprocal lattice, and we have $\sum_{\mathbf{n}} \exp(i\mathbf{q} \cdot \mathbf{R}_{\mathbf{n}}) = N \sum_{\mathbf{G}} \delta_{\mathbf{q},\mathbf{G}}$. Thus, the structure factor

$$S(\mathbf{q}) = \sum_{\mathbf{G}} \delta_{\mathbf{q},\mathbf{G}} \sum_{\tau} e^{i\mathbf{q} \cdot \tau} \quad (1.14)$$

is characterized by sharp peaks at the reciprocal lattice vectors \mathbf{G} . They specify sets of parallel crystal planes: Their orientation is given by the direction of \mathbf{G} and their spacing by $2\pi/|\mathbf{G}|$. The static structure factor determines the cross section for X-ray scattering, which is the standard method to identify the crystal structure of a solid (Problem 1.6).

The structure factor can also be expressed in terms of the Fourier transform (see Appendix) of the density

$$n_{\mathbf{q}} = \frac{1}{V} \int d^3r n(\mathbf{r}) e^{-i\mathbf{q}\cdot\mathbf{r}} = \frac{1}{V} \sum_j e^{-i\mathbf{q}\cdot\mathbf{r}_j}, \quad (1.15)$$

which, for $\mathbf{q} \neq 0$, describes the deviations from the average particle density $n_{\mathbf{q}=0} = n = N/V$ called *density fluctuations*. In terms of the corresponding number fluctuations $N_{\mathbf{q}} = n_{\mathbf{q}}V$, the static structure factor can be written as

$$S(\mathbf{q}) = \frac{1}{N} \langle N_{\mathbf{q}} N_{-\mathbf{q}} \rangle. \quad (1.16)$$

For describing correlations between time-dependent positions of particles, e.g., due to thermal motion of the ions, one uses the *dynamic structure factor*

$$S(\mathbf{q}, \omega) = \frac{1}{2\pi} \int e^{-i\omega t} \left\langle \sum_{i,j} e^{i\mathbf{q}\cdot\mathbf{r}_i(t)} e^{-i\mathbf{q}\cdot\mathbf{r}_j(0)} \right\rangle dt, \quad (1.17)$$

which, in terms of number fluctuations, can also be written as

$$S(\mathbf{q}, \omega) = \frac{1}{2\pi} \int e^{-i\omega t} \langle N_{\mathbf{q}}(t) N_{-\mathbf{q}}(0) \rangle dt. \quad (1.18)$$

As we shall see later, thermal motion reduces the intensity of the Bragg peaks and leads, if it gets sufficiently strong, to their complete suppression as an indication of loss of structural correlation. This is the transition to the liquid phase.

The functions, $S(\mathbf{q})$ and $g(\mathbf{r})$, containing the full information about the 3-dimensional structure, are difficult to plot due to their dependence on vectors. For practical reasons, this information is reduced to the radial distribution function $g(r)$, which determines the number of particles in a spherical shell of radius r and thickness dr : $ng(r)4\pi r^2 dr$. Plots of the radial distribution function and the corresponding structure factor are shown in Fig. 1.3 for a gas, a liquid or an amorphous solid, and a crystalline solid. For a gas with random positions of the atoms, there is equal probability in the radial distribution for $r > d$, where d is the minimum distance between pairs of particles due to repulsive forces (e.g., the diameter of hard spheres). In contrast, the crystalline solid with long-range order due to the periodic arrangement is characterized by a radial distribution that exhibits peaks corresponding to the coordination shells of nearest, next-nearest etc. neighbors. Amorphous solids

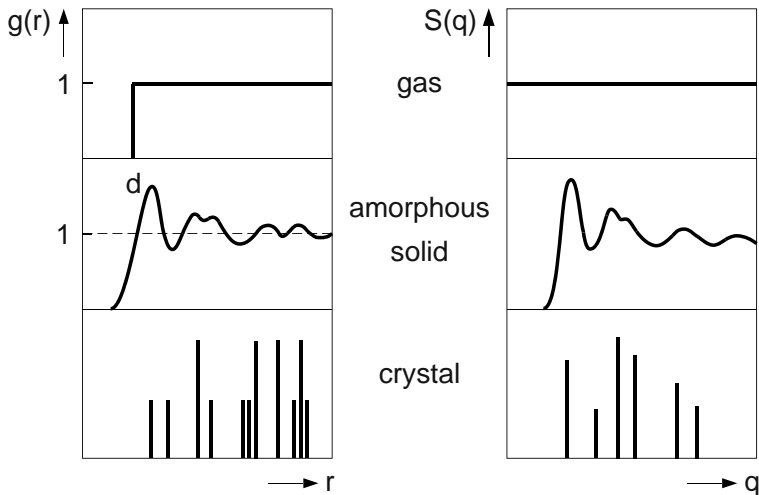


Fig. 1.3. The radial pair-distribution function (*left*) and static structure factor (*right*) of a gas, an amorphous solid, and a crystalline solid

(and liquids) still have short-range order and the nearest coordination shells are visible, while others are washed out with increasing r because of missing long-range order. The structure factor exhibits the same features as can be understood from (1.11). The more pronounced structures in these functions indicate the strength of *correlation* in the density or relative positions.

In this section, we have used the pair-distribution function and the structure factor to characterize and distinguish different forms of condensed matter with respect to correlations in their ion configuration. The concept of analyzing the pair-distribution function of a particle system is, however, quite general and will be applied in Chaps. 4 and 7 to identify and quantify correlation in electron systems.

Problems

- 1.1 The following concepts are frequently used in solid state physics: point (Bravais) lattice, lattice vector, reciprocal lattice, Wigner-Seitz cell, Brillouin zone. What is the meaning of these quantities? Give explicit descriptions (by formulas or drawings) for a two-dimensional square lattice, a simple cubic (sc), a face-centered cubic (fcc), and a body-centered cubic (bcc) lattice.
- 1.2 Consider the one-dimensional model system constructed from two building blocks of different lengths, S (for short) and L (for long), starting from the configuration LS by the following rule: replace S by L and L by LS . Construct the chain by repeated application of the rule to obtain what is

called a Fibonacci chain. Realize, that it is not periodic and that it has the same configuration when $L = S'$ is taken as the short and $LS = L'$ as the long building block! This property is called self-similarity or fractality. Although not being periodic, the structure has long-range order as can be seen by taking the Fourier transform.

- 1.3 Find the five different possible point lattices in two dimensions.
- 1.4 Explain the meaning of Bloch's theorem. On which symmetry is it based, and to which constant of motion is it related?
- 1.5 Give the coordination numbers and calculate the relative spatial filling in a simple cubic, a face centered cubic, a body centered cubic, and a diamond lattice, by considering non-overlapping spheres of maximal diameter at each lattice point for fixed lattice constant of the elementary cube.
- 1.6 The structure of solids can be investigated by diffraction experiments with photons, electrons or neutrons. The cross section for elastic scattering is determined by the scattering amplitude

$$F(\mathbf{k}, \mathbf{k}') = \int n(\mathbf{r}) e^{i(\mathbf{k}-\mathbf{k}') \cdot \mathbf{r}} d^3r, \quad (1.19)$$

where $n(\mathbf{r})$ is the mass density and $\mathbf{k}(\mathbf{k}')$ is the wave vector of the incident (scattered) wave. Make use of the periodic mass density in a crystalline solid to find the values $\mathbf{k} - \mathbf{k}'$ for which the scattering amplitude does not vanish. Give a geometrical interpretation of the result with respect to the meaning of the direction and length of reciprocal lattice vectors.

The Solid as a Many-Particle Problem

As mentioned in Sect. 1.1, we understand the solid as being composed of ions (nuclei and closed electron shells) and valence electrons. A more rigorous approach would start from nuclei and electrons, but a simple consideration of the spatial extension of electrons in different shells of the isolated atoms shows immediately that this is not necessary. The wave functions of electrons in inner shells (the core electrons) with binding energies of hundreds or thousands of eV extend over a distance much smaller than the lattice spacing in a solid, as visualized in Fig. 2.1. In fact, when the atoms are assembled into the configuration of a crystal lattice (or likewise of a molecule, cluster, liquid...) it will be the outermost, weakly bound valence electrons which first experience the presence of their nearest neighbors. They will rearrange from their states in the isolated atoms into those which establish the chemical binding. Together with the electrostatic energy of the ion configuration, this defines the stable structure. Some textbooks on Solid State Theory start with a detailed description of this structure of crystalline solids (e.g., [4, 7, 9, 11]) which is only briefly repeated here. Instead, we follow the approach of [5, 14, 21] with a presentation of the basic Hamiltonian, which defines the solid as a quantum-mechanical many-body problem.

The effectiveness of chemical binding depends on the overlap of the electronic wave functions at neighboring lattice sites and on their coordination number. Thus, metals prefer a close-packed structure, namely the body-centered cubic (bcc) and face-centered cubic (fcc) lattices, with delocalized electrons acting as glue between the positively charged ions (*metallic binding*), while in (binary) ionic crystals, electrons are transferred from the cation to the anion to complete their outer shells (*ionic* or *heteropolar binding*) and form lattices dominated by electrostatic interaction (like the rocksalt structure). Rare gases with closed shell configurations as well as larger molecules form crystalline solids due to the weak *van der Waals*¹ forces and are stable only at low temperatures. Elements of the fourth group of the periodic table

¹ Johannes Diderik van der Waals 1837–1923, Noble prize in physics 1910.

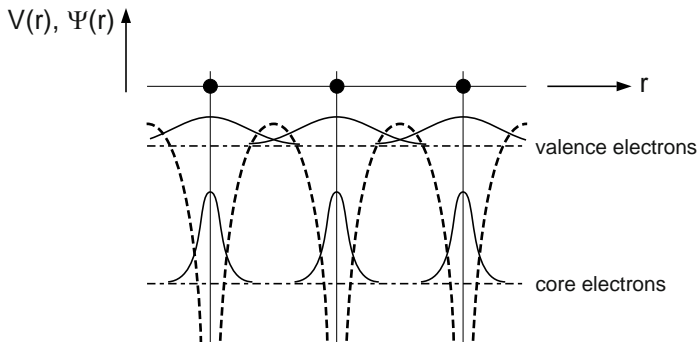


Fig. 2.1. Schematic view of a solid: periodic potential (*dashed line*) and wave functions of core and valence electrons (*solid lines*) drawn at their respective energy levels

share each of their four valence electrons with the four nearest neighbors in directed covalent bonds (*covalent* or *homopolar binding*), which results in the diamond structure. A mixture of covalent and ionic binding, whereby the contribution of the latter increases with the polarity of the material, is typical for the zinc blende structure realized in A_3B_5 , A_2B_6 , and A_1B_7 compounds. A dominant covalent binding is typical for semiconductors.

In most cases, the distinction between valence and closed shell electrons is justified by the large energy separation, which can be detected by photoelectron spectroscopy (PES [65, 66]). With reference to the heavier elements (including transition-metals and rare-earths) and their compounds, for which d states are in the same energy range as the s like valence electrons, one should keep in mind, however, that even complete d shells can participate in the chemical binding and influence the electronic structure. In Chap. 5, we shall come back to this case but will rely here on a clear separation between closed-shell ions and valence electrons.

2.1 The Hamiltonian of the Solid

These introductory considerations about the composition of a solid out of valence electrons and ions justify writing the Hamiltonian as

$$\mathcal{H}_0 = \mathcal{H}_{\text{ion}} + \mathcal{H}_{\text{el}} + \mathcal{H}_{\text{el-ion}}. \quad (2.1)$$

The first term depends only on the coordinates of the ions and reads

$$\mathcal{H}_{\text{ion}} = \sum_{i=1}^{N_I} \frac{\mathbf{P}_i^2}{2M_i} + \frac{1}{2} \sum_{\substack{i,j=1 \\ i \neq j}}^{N_I} V(\mathbf{R}_i - \mathbf{R}_j) \quad (2.2)$$

where \mathbf{P}_i , \mathbf{R}_i , and M_i denote the momentum, position, and mass of the i th ion, respectively, and N_I is the number of ions in the crystal volume V_C .

$V(\mathbf{R}_i - \mathbf{R}_j)$ can be a quite general ion-ion interaction potential, but for point-like ions with charge $Q_i = \text{sign}(Q_i)Z_i e$ and positive integer Z_i , it will be the Coulomb interaction

$$V(\mathbf{R}_i - \mathbf{R}_j) = \frac{Q_i Q_j}{4\pi\epsilon_0 |\mathbf{R}_i - \mathbf{R}_j|}. \quad (2.3)$$

Here, ϵ_0 is the vacuum dielectric constant. The assumption of point-like ions is justified for closed shells with tightly bound electrons. This situation is visualized in Fig. 2.1.

The electron part of \mathcal{H}_0 is given by

$$\mathcal{H}_{\text{el}} = \sum_{l=1}^{N_e} \frac{\mathbf{p}_l^2}{2m} + \frac{1}{2} \sum_{\substack{k,l=1 \\ k \neq l}}^{N_e} \frac{e^2}{4\pi\epsilon_0 |\mathbf{r}_l - \mathbf{r}_k|} \quad (2.4)$$

where \mathbf{p}_l and \mathbf{r}_l are the momentum and position of the l th electron, m is the free electron mass, and N_e is the number of electrons in the crystal volume. The charge neutrality of the solid requires that

$$\sum_{i=1}^{N_I} Q_i - eN_e = 0. \quad (2.5)$$

The interaction between electrons and ions is described by

$$\mathcal{H}_{\text{el-ion}} = \sum_{l=1}^{N_e} \sum_{i=1}^{N_I} v(\mathbf{r}_l - \mathbf{R}_i) \simeq \sum_{l=1}^{N_e} \sum_{i=1}^{N_I} \frac{Q_i e}{4\pi\epsilon_0 |\mathbf{r}_l - \mathbf{R}_i|} \quad (2.6)$$

where the last expression is the approximation for point-like ions.

It is conceivable that the physical properties of the system described by \mathcal{H}_0 do not depend on $N_{I,e}$ as long as these numbers are sufficiently large. These properties will be considered in the thermodynamic limit $N_{I,e} \rightarrow \infty$, with the corresponding densities $N_{I,e}/V_c$ kept constant. This situation, valid for macroscopic solids, is to be distinguished from that of *mesoscopic systems* for which *clusters* are a representative example. The number of their surface ions is comparable with that of the bulk ions with the consequence that their properties depend on the shape defined by the surface. The physics of clusters has become a research field in its own right [32–34]. Nevertheless, it is interesting to note that the properties of macroscopic solids can be thought of as evolving with increasing size from those of clusters as the ratio of the number of surface ions divided by the number of bulk ions goes to zero.

So far the spin of electrons or ions did not appear because neither the kinetic energy nor the Coulomb interaction depends on spin. The expression for the kinetic energy is that of the non-relativistic formulation. In principle, one could have started, e.g., for the electrons, from the relativistic Dirac operator (which is in fact used in band structure theory and becomes relevant for

solids composed of atoms with large Z_i , see Chap. 5). However, in most cases, it is sufficient to consider just the spin-orbit coupling in the electron part of the Hamiltonian

$$\mathcal{H}_{\text{so}} = \frac{\hbar}{4m^2c^2} \sum_l (\nabla_l V_{\text{eff}}(\mathbf{r}_l) \times \mathbf{p}_l) \cdot \boldsymbol{\sigma}_l \quad (2.7)$$

where $V_{\text{eff}}(\mathbf{r}_l)$ is the effective single-particle potential, which will be introduced in Chap. 5, and $\boldsymbol{\sigma}_l$ is the vector of the Pauli spin matrices of the l th electron. A similar term can be added to the ion part of the Hamiltonian, in order to account for the nuclear spins, if their influence is addressed. But even without spin-orbit coupling, the spin becomes important in the presence of a magnetic field, when the Zeeman term causes removal of spin degeneracy, and, because of the fermion character of the electrons, by considering the Pauli principle, when dealing with the many-particle aspect of the problem (see Chap. 4). Moreover, spin alignment and spin excitation are essential for magnetic properties (see Chap. 6).

As mentioned already in Sect. 1.2, we consider a solid primarily for the case of the crystalline periodic order of the ions. Only in Chap. 9, we shall remove this restriction by allowing structural disorder and its effect on the electronic eigenstates and transport. The perfect crystalline configuration – which, in order to simplify the notation, is assumed here to be a Bravais lattice – is characterized by ion positions \mathbf{R}_i forming a point lattice (see Sect. 1.2)

$$\mathbf{R}_n^0 = n_1 \mathbf{a}_1 + n_2 \mathbf{a}_2 + n_3 \mathbf{a}_3 \quad (2.8)$$

where the upper index 0 indicates that these vectors now mark the equilibrium positions, while the actual position of an ion is given by

$$\mathbf{R}_n = \mathbf{R}_n^0 + \mathbf{u}_n \quad (2.9)$$

with a displacement \mathbf{u}_n accounting for the motion of the ion about its equilibrium position. These displacements will be assumed to be small in comparison with the lattice constant to motivate a separation of the ion-ion potential according to

$$\begin{aligned} V(\mathbf{R}_n - \mathbf{R}_m) &= V(\mathbf{R}_n^0 - \mathbf{R}_m^0 + \mathbf{u}_n - \mathbf{u}_m) \\ &= V(\mathbf{R}_n^0 - \mathbf{R}_m^0) + \delta V(\mathbf{R}_n - \mathbf{R}_m), \end{aligned} \quad (2.10)$$

where $V(\mathbf{R}_n^0 - \mathbf{R}_m^0)$ is determined by the equilibrium configuration and δV can be explicitly expressed as a Taylor series in the displacements. In the same way we may proceed with the electron-ion potential

$$v(\mathbf{r}_l - \mathbf{R}_n) = v(\mathbf{r}_l - \mathbf{R}_n^0) + \delta v(\mathbf{r}_l - \mathbf{R}_n). \quad (2.11)$$

The Hamiltonian of the solid may now be written as

$$\begin{aligned}
 \mathcal{H}_0 = & \sum_{\mathbf{n}} \frac{\mathbf{P}_{\mathbf{n}}^2}{2M_{\mathbf{n}}} + \frac{1}{2} \sum_{\substack{\mathbf{n}, \mathbf{m} \\ \mathbf{n} \neq \mathbf{m}}} \delta V(\mathbf{R}_{\mathbf{n}} - \mathbf{R}_{\mathbf{m}}) \\
 & + \sum_{l=1}^{N_e} \frac{p_l^2}{2m} + \frac{1}{2} \sum_{\substack{k, l=1 \\ k \neq l}}^{N_e} \frac{e^2}{4\pi\epsilon_0 |\mathbf{r}_l - \mathbf{r}_k|} + \sum_{\mathbf{n}, l} v(\mathbf{r}_l - \mathbf{R}_{\mathbf{n}}^0) \\
 & + \frac{1}{2} \sum_{\substack{\mathbf{n}, \mathbf{m} \\ \mathbf{n} \neq \mathbf{m}}} V(\mathbf{R}_{\mathbf{n}}^0 - \mathbf{R}_{\mathbf{m}}^0) + \sum_{\mathbf{n}, l} \delta v(\mathbf{r}_l - \mathbf{R}_{\mathbf{n}}). \quad (2.12)
 \end{aligned}$$

The first line of (2.12), depending only on the positions and momenta of the heavy constituents of the solid, will be the subject of Chap. 3, the lattice dynamics. In the quantum mechanical version, it is characterized by phonons, the quanta of lattice vibrations, which determine the elastic properties, the specific heat, and the optical properties in the far-infrared spectral range.

The second line, describing the electrons in a static periodic lattice potential and their mutual interaction, will be the starting point of Chaps. 4–7. In Chap. 4, we will present the properties of the homogeneous electron gas (for which the periodic potential will be smeared out into a homogeneous positive charge background defining the jellium model) and learn how to treat the electron–electron interaction. In Chap. 5, the single-particle concepts of band structure, which allow one to distinguish metals from insulators will be introduced. Also, spin dynamics and magnetic properties (Chap. 6) and correlated electron systems (Chap. 7) will be treated, essentially by starting from the second line of (2.12).

The third line of (2.12) contains two contributions. The first one is the electrostatic interaction energy of the ions in their equilibrium configuration, representing a constant energy which becomes important in total energy calculations. For a binary cubic lattice, with a basis consisting of two point-like ions with opposite charge $\pm Ze$ (e.g., the zinc blende and rocksalt structure), this term can be expressed using

$$\frac{1}{2} \sum_{j \neq i} \text{sign}(Q_i) \text{sign}(Q_j) \frac{(Ze)^2}{4\pi\epsilon_0 |\mathbf{R}_i - \mathbf{R}_j|} = \frac{1}{2} \frac{(Ze)^2}{4\pi\epsilon_0 R} \alpha_M, \quad (2.13)$$

where $|\mathbf{R}_i - \mathbf{R}_j| = Rp_{ij}$, with the nearest neighbor distance R , and

$$\alpha_M = \sum_{j \neq i} \text{sign}(Q_i) \text{sign}(Q_j) \frac{1}{p_{ij}} \quad (2.14)$$

is the Madelung² constant. It is independent of the reference lattice point i [29]. The second contribution depends on the actual positions of the ions

² Erwin Madelung 1881–1972.

and electrons and couples the dynamics of both subsystems, thus giving rise to electron–phonon interaction (Chap. 8). It is important for electron transport properties, relaxation phenomena, and superconductivity.

The structuring of \mathcal{H}_0 as given in (2.12) is by purpose quite suggestive: Without the third line, the electron and ion subsystems are separated and can be considered as independent. We will discuss in the next section the conditions under which such an approximation is justified.

2.2 Separating the Motion of Electrons and Ions

In order to describe a solid and its properties, we have to solve the quantum mechanical problem:

$$\mathcal{H}_0 \tilde{\Psi} = i\hbar \dot{\tilde{\Psi}} \quad \text{with} \quad \tilde{\Psi} = \tilde{\Psi}(\{\mathbf{r}_l\}, \{\mathbf{R}_n(t)\}). \quad (2.15)$$

Here, $\{\mathbf{r}_l\}, \{\mathbf{R}_n(t)\}$ denote the configurations of the electrons and ions of the system, of which the latter is considered time-dependent because of the thermal motion of the ions.

Employing thermodynamic concepts, electrons and ions can be considered as two systems which are in contact as mediated by the last term of (2.12). Let us assume that the thermal equilibrium of the whole system, i.e., electrons and ions have the same temperature and the same average thermal energy per degree of freedom. This can be quantified by the mean values of the kinetic energy and we may write

$$\left\langle \frac{p_l^2}{2m} \right\rangle = \left\langle \frac{P_n^2}{2M} \right\rangle. \quad (2.16)$$

Because of the mass ratio $m/M \simeq 10^{-4}$, this equation indicates that the electrons move much faster than the ions. Thus, the electrons will experience any actual configuration of the ions (caused by thermal fluctuation) as a stationary potential to which they adjust instantaneously by adopting the state of lowest energy. This fact can be used to formulate the conditions for separating the motions of ions and electrons.

Consider the stationary Schrödinger³ equation of the electrons moving in the electrostatic potential, defined by the actual configuration of the ions,

$$(\mathcal{H}_{\text{el}} + \mathcal{H}_{\text{el-ion}}) \Psi_\alpha = \mathcal{E}_{\text{el},\alpha} \Psi_\alpha \quad (2.17)$$

as being solved. The eigensolutions $\Psi_\alpha(\{\mathbf{r}_l\}, \{\mathbf{R}_n\})$ and energy eigenvalues $\mathcal{E}_{\text{el},\alpha}(\{\mathbf{R}_n\})$ are characterized by a complete set of quantum numbers α and depend parametrically on the ion configuration $\{\mathbf{R}_n\}$. For a given configuration, the Ψ_α form a complete set and can be used to expand the solution of the time-dependent problem (2.15) in the form

³ Erwin Schrödinger 1887–1961, shared in 1933 the Nobel prize in physics with P.A.M. Dirac.

$$\tilde{\Psi}(\{\mathbf{r}_l\}, \{\mathbf{R}_n(t)\}) = \sum_{\alpha} \Phi_{\alpha}(\{\mathbf{R}_n\}, t) \Psi_{\alpha}(\{\mathbf{r}_l\}, \{\mathbf{R}_n\}) \quad (2.18)$$

with the expansion coefficients Φ_{α} depending on the ion configuration and on t . Then the full problem (2.15) reads

$$\mathcal{H}_0 \tilde{\Psi} = \sum_{\alpha} \left[\underbrace{(\mathcal{H}_{\text{el}} + \mathcal{H}_{\text{el-ion}})}_{=\mathcal{E}_{\text{el},\alpha} \Psi_{\alpha}} \Psi_{\alpha} \Phi_{\alpha} + \mathcal{H}_{\text{ion}} \Psi_{\alpha} \Phi_{\alpha} \right] = i\hbar \sum_{\alpha} \Psi_{\alpha} \dot{\Phi}_{\alpha}. \quad (2.19)$$

Using the completeness of the Ψ_{α} , we eliminate the electron coordinates by multiplying from left with Ψ_{β}^* and integrating over all \mathbf{r}_l to obtain

$$\mathcal{E}_{\text{el},\beta} \Phi_{\beta} + \sum_{\alpha} \int \dots \int \Psi_{\beta}^* \mathcal{H}_{\text{ion}} \Psi_{\alpha} d^3\{\mathbf{r}_l\} \Phi_{\alpha} = i\hbar \dot{\Phi}_{\beta}. \quad (2.20)$$

The operator \mathcal{H}_{ion} contains the momentum operators \mathbf{P}_n which act on the ion coordinates of both Ψ_{α} and Φ_{α} . Thus the integration over electron coordinates in the second term of (2.20) can be performed by writing (as operator equation applied to Φ_{α})

$$\int \dots \int \Psi_{\beta}^* \mathcal{H}_{\text{ion}} \Psi_{\alpha} d^3\{\mathbf{r}_l\} = \sum_{\mathbf{n}} \frac{1}{2M} (2(\mathbf{P}_{\mathbf{n}})_{\beta\alpha} \cdot \mathbf{P}_{\mathbf{n}} + (\mathbf{P}_{\mathbf{n}}^2)_{\beta\alpha}), \quad (2.21)$$

where the matrix elements (for $\kappa = 1, 2$)

$$(\mathbf{P}_{\mathbf{n}}^{\kappa})_{\beta\alpha} = \int \dots \int \Psi_{\beta}^*(\{\mathbf{r}_l\}, \{\mathbf{R}_n\}) \mathbf{P}_{\mathbf{n}}^{\kappa} \Psi_{\alpha}(\{\mathbf{r}_l\}, \{\mathbf{R}_n\}) d^3\{\mathbf{r}_l\} \quad (2.22)$$

couple between different electron states $\Psi_{\alpha}, \Psi_{\beta}$. When writing the momentum in atomic units (Bohr radius $a_{\text{B}} = 4\pi\epsilon_0\hbar^2/me^2$ and Rydberg energy $1 \text{ Ry} = me^4/(4\pi\epsilon_0)^2 2\hbar^2$), $\mathbf{P}_{\mathbf{n}} = \mathbf{P}'_{\mathbf{n}}\hbar/a_{\text{B}}$, this coupling, expressed in terms of

$$\frac{P^2}{2M} = \frac{m}{M} P'^2 \text{ Ry},$$

is seen to carry a factor $m/M \ll 1$, thus representing a small term. If this coupling is neglected, one arrives at the *Born–Oppenheimer*⁴ *approximation*. It is sometimes also called *adiabatic approximation* because the electrons follow the (slow) motion of the ions adiabatically, i.e., without changing their eigenstate. Within this approximation, the motion of the electrons is separated from that of the ions, and we may write for these two systems, the equations

$$(\mathcal{H}_{\text{ion}} + \mathcal{E}_{\text{el},\alpha}) \Phi_{\alpha} = i\hbar \dot{\Phi}_{\alpha} \quad (2.23)$$

with

$$\mathcal{H}_{\text{ion}} + \mathcal{E}_{\text{el},\alpha} = \sum_{\mathbf{n}} \frac{P_{\mathbf{n}}^2}{2M} + \mathcal{E}_{\text{el},\alpha}(\{\mathbf{R}_n\}) + \frac{1}{2} \sum_{\substack{\mathbf{n}, \mathbf{m} \\ \mathbf{n} \neq \mathbf{m}}} V(\mathbf{R}_n - \mathbf{R}_m) \quad (2.24)$$

⁴ Max Born 1882–1970, Nobel prize in physics 1954; J. Robert Oppenheimer 1904–1967.

and (see (2.17))

$$(\mathcal{H}_{\text{el}} + \mathcal{H}_{\text{el-ion}}) \Psi_{\alpha} = \mathcal{E}_{\text{el},\alpha} \Psi_{\alpha}. \quad (2.25)$$

Equation (2.23) is the time-dependent Schrödinger equation for the ions which move in the *adiabatic potential*

$$\mathcal{U}_{\alpha}(\{\mathbf{R}_n\}) = \mathcal{E}_{\text{el},\alpha}(\{\mathbf{R}_n\}) + \frac{1}{2} \sum_{\substack{n,m \\ n \neq m}} V(\mathbf{R}_n - \mathbf{R}_m) \quad (2.26)$$

defined by the ion configuration and the energy of the eigenstate α of the electron system. This problem will be studied in more detail in Chap. 3. Equation (2.25) is the stationary eigenvalue problem of the electron system for a given ion configuration. We will discuss its solution in Chaps. 4–7 with the simplification of always replacing $\{\mathbf{R}_n\}$ by the equilibrium configuration $\{\mathbf{R}_n^0\}$. It should be mentioned that the Born–Oppenheimer approximation does not apply only to solids but also to molecules.

2.3 Thermal Expectation Values

One of the important aims of a theory is to explain experimental results and possibly arrive at a quantitative description of measurements. Experiments yield information about physical observables, which in quantum formulation are Hermitian operators $\hat{A} = \hat{A}^{\dagger}$. Thus, our theory has to aim at the description of the expectation values $\langle \hat{A} \rangle$ of such operators. For solids, which are macroscopic thermodynamic systems, they have to be understood as thermal expectation values. Therefore, a brief repetition of the related concepts of statistical mechanics is required.

Simple quantum mechanical systems (e.g., an atom, an oscillator) can be prepared in a state $|i\rangle$ and the expectation (or mean) value is given by

$$\langle \hat{A} \rangle = \langle i | \hat{A} | i \rangle. \quad (2.27)$$

The state $|i\rangle$ can be an eigenstate or a mixture of eigenstates and thus, in repeated measurements, the measured values will be sharp (an eigenvalue of \hat{A}) or fluctuate around the mean value, respectively. A solid, consisting of many particles, is not a simple system and cannot be prepared in a well defined quantum state. Instead, being a thermodynamic system, the solid can be prepared in a state characterized by a set of thermodynamic variables like temperature T , particle number N , volume V . These thermodynamic quantities specify the state of the solid as a statistical ensemble of quantum mechanical micro-states $\{|i\rangle, i = 1, \dots, I; T, N, \dots \text{ fixed}\}$, and the experimental values for the observable \hat{A} are described by the thermal expectation value (or ensemble mean value)

$$\langle \hat{A} \rangle = \frac{1}{I} \sum_{i=1}^I \langle i | \hat{A} | i \rangle. \quad (2.28)$$

Making use of a complete orthonormal set of states $|n\rangle$ and of the property that factors under the trace operation $\text{Tr}(\dots) = \sum_n \langle n | \dots | n \rangle$ can be interchanged, we may formulate the expectation or *thermal mean value* as

$$\langle \hat{A} \rangle = \sum_n \langle n | \left(\frac{1}{I} \sum_{i=1}^I |i\rangle \langle i| \right) \hat{A} | n \rangle \quad (2.29)$$

or in short

$$\langle \hat{A} \rangle = \text{Tr} \left(\hat{\rho} \hat{A} \right), \quad (2.30)$$

where

$$\hat{\rho} = \frac{1}{I} \sum_{i=1}^I |i\rangle \langle i| \quad (2.31)$$

is the statistical operator.

Let us repeat the important properties of the statistical operator:

1. It is Hermitian: $\hat{\rho} = \hat{\rho}^\dagger$
2. It is positive semi-definite: $\langle \psi | \hat{\rho} | \psi \rangle = \frac{1}{I} \sum_i |\langle \psi | i \rangle|^2 \geq 0$, for arbitrary $|\psi\rangle$
3. It is normalized: $\text{Tr} \hat{\rho} = \frac{1}{I} \sum_{n,i} \langle n | i \rangle \langle i | n \rangle = \frac{1}{I} \sum_i \langle i | (\sum_n |n\rangle \langle n|) | i \rangle = 1$ in any representation.

These properties qualify $\hat{\rho}$ as the operator of probability distributions. It satisfies the eigenvalue equation

$$\hat{\rho} |n\rangle = p_n |n\rangle \quad (2.32)$$

with the eigenvalue

$$p_n = \langle n | \hat{\rho} | n \rangle = \frac{1}{I} \sum_i |\langle i | n \rangle|^2, \quad (2.33)$$

which quantifies the probability of finding the state $|n\rangle$ in the ensemble of micro-states $\{|i\rangle \dots\}$.

In thermal equilibrium, one has

$$\hat{\dot{\rho}} = \frac{1}{i\hbar} [\hat{H}, \hat{\rho}] = 0, \quad (2.34)$$

where \hat{H} is the Hamiltonian of the system in which the states $|i\rangle$ are realized (in our case that of the solid). In the representation of eigenstates of \hat{H} , the statistical operator, which commutes with \hat{H} , is diagonal (Problem 2.1).

The following statistical ensembles are of importance in solid state physics and will be used throughout the book:

1. The canonical ensemble with fixed temperature T and particle number N ($\beta = 1/k_B T$ where k_B is the Boltzmann⁵ constant):

$$\hat{\rho} = \frac{1}{Z} e^{-\beta \hat{H}} \quad (2.35)$$

with the canonical partition function $Z = \text{Tr}(e^{-\beta \hat{H}})$. In the energy representation $\hat{\rho}$ becomes $p_n = Z^{-1} \exp(-\beta E_n)$.

2. The grand-canonical ensemble with fixed temperature T and variable particle number N :

$$\hat{\rho}_G = \frac{1}{Z_G} e^{-\beta(\hat{H} - \mu \hat{N})} \quad (2.36)$$

with the grand-canonical partition function $Z_G = \text{Tr}\{e^{-\beta(\hat{H} - \mu \hat{N})}\}$, where \hat{N} is the particle number operator and μ the chemical potential. In the energy representation, $\hat{\rho}_G$ becomes $p_n = Z_G^{-1} \exp(-\beta(E_n - \mu N_n))$, where N_n is the particle number in the state $|n\rangle$.

In the next section, the thermal expectation values of observables will be evaluated, especially for thermal equilibrium formulated in terms of eigenstates of the Hamiltonian \mathcal{H}_0 (see (2.12)). A particular situation is obtained for very low temperatures, at which the thermal expectation value becomes the ground state expectation value (Problem 2.2). When considering the number operator as observable for a system in thermal equilibrium, one obtains the well-known distribution functions of the Fermi–Dirac⁶ or Bose–Einstein⁷ statistics (depending on the system), and of their high-temperature limit, the Maxwell distribution (Problem 2.3).

2.4 Theory of Linear Response

Any experiment constitutes a perturbation of the system under investigation: By scattering light or particles, we obtain information on the structure of the solid or of its characteristic excitations; by applying an electric or magnetic field, we study the transport or magnetic properties; by probing with light, we detect the optical properties. If we do this to characterize the material, these perturbations have to be weak and must not change the system properties. This defines the regime of *linear response*.

The system (in our case the solid) plus the external perturbation applied to investigate its properties, is described by the Hamiltonian

$$\mathcal{H} = \mathcal{H}_0 + V_{\text{ext}}. \quad (2.37)$$

⁵ Ludwig Boltzmann 1844–1906.

⁶ Enrico Fermi 1901–1954, Nobel prize in physics 1938; Paul Adrien Maurice Dirac 1902–1984, Nobel prize in physics 1933.

⁷ Satyendra Nath Bose 1894–1974; Albert Einstein 1879–1955, Nobel prize in physics 1922.

Table 2.1. Examples of observables used in the response formalism

\hat{A}, \hat{B}	V_{ext}	F	Response function
Electric current density	$-\mathbf{j} \cdot \mathbf{A}$	Electric field	Electric conductivity
Dielectric polarization	$-\mathbf{P} \cdot \mathbf{E}$	Electric field	Dielectric function
Magnetic polarization	$-\mathbf{m} \cdot \mathbf{H}$	Magnetic field	Magnetic susceptibility
Heat current density	$-\mathbf{v} \cdot \nabla T$	Temp. gradient	Heat conductivity

\mathcal{H}_0 is the Hamiltonian (2.12) of the unperturbed solid and the perturbation, (assumed for simplicity as being independent of space variables) can be written as.

$$V_{\text{ext}}(t) = -\hat{B}F(t). \quad (2.38)$$

Here, \hat{B} is an observable and $F(t)$, a (in general, time-dependent) scalar function. We may distinguish between dynamic (time-dependent) and static (time-independent) perturbations. Consider the measurement of an observable \hat{A} . The measured values can be described by

$$\langle \hat{A} \rangle_t = \text{Tr} \left(\hat{\rho} \hat{A} \right) = \int dt' R(t, t') F(t'). \quad (2.39)$$

They are ruled by a linear response function $R(t, t')$, which is expected to depend on \hat{A} and \hat{B} . It will turn out to be a correlation function of these observables as shown later in this section. But before doing this, let us look at the examples of experimental situations listed in Table 2.1 together with their translation into the response formalism.

To determine the electric conductivity as a material property of a solid one has to design a measurement of the electric current density \mathbf{j} by exposing the sample to an electric field, which can be formulated as the time-derivative of the vector potential \mathbf{A} . The perturbation results from the minimal coupling according to which the particle momenta in \mathcal{H}_0 are replaced by $\mathbf{p} + e\mathbf{A}$ which, to lowest order in \mathbf{A} , leads to $V_{\text{ext}}(t) = -\mathbf{j} \cdot \mathbf{A}(t)$ with the electric current density $\mathbf{j} = -e \sum_l \mathbf{p}_l/m$. Thus the electric conductivity is a current–current (or velocity–velocity) correlation function. Due to the vector character of \mathbf{j} and \mathbf{A} , the response function is a second rank tensor. Likewise, the dielectric function, characterizing the optical and dielectric properties, follows from measuring the dielectric polarization by probing with an electric field as perturbation. The dielectric function will turn out to be a correlation function between polarizations (or electric dipole moments). A similar situation leads to the magnetic susceptibility. A heat current is caused by a temperature gradient; its measurement provides the heat conductivity.

In generalizing (2.39) to also include dependence on space variables, we may write

$$\langle \hat{A}(\mathbf{r}) \rangle_t = \int dt' \int d^3 r' R(\mathbf{r}, t; \mathbf{r}', t') F(\mathbf{r}', t'). \quad (2.40)$$

For homogeneous systems, the response function depends only on $\mathbf{r} - \mathbf{r}'$ and, therefore, a spatially harmonic external perturbation of the form $F(\mathbf{r}', t') = F_{\mathbf{q}}(t') \exp(i\mathbf{q} \cdot \mathbf{r}')$ leads to the same spatial dependence of the observable, which in brief means

$$\langle \hat{A}_{\mathbf{q}} \rangle_t = \int dt' R(\mathbf{q}; t, t') F_{\mathbf{q}}(t') \quad (2.41)$$

with $R(\mathbf{q}; t, t')$ being the Fourier transform of $R(\mathbf{r} - \mathbf{r}'; t, t')$.

Let us return to the task of finding an expression for the thermal expectation value of \hat{A} , which is linear in the perturbing field $F(t)$ for the system described by the Hamiltonian \mathcal{H} of (2.37). In view of (2.39), the dependence on the field enters through the statistical operator, which contains the system Hamiltonian including the external perturbation. Without this perturbation, the system is in equilibrium, and the statistical operator satisfies the equation of motion (in the following the $\hat{\cdot}$ -sign, indicating operators, is dropped)

$$[\mathcal{H}_0, \rho_0] = i\hbar \dot{\rho}_0 = 0. \quad (2.42)$$

If the perturbation is switched on, the system is driven out of the thermal equilibrium described by ρ_0 , and the statistical operator will become time-dependent:

$$\rho_0 \rightarrow \rho(t) = \rho_0 + \Delta\rho(t). \quad (2.43)$$

In order to find the deviation $\Delta\rho(t)$ from equilibrium, caused by the perturbation, we have to solve the equation of motion for $\rho(t)$:

$$[\mathcal{H}, \rho(t)] = i\hbar \dot{\rho}(t). \quad (2.44)$$

Looking for the first order perturbation correction to the equilibrium distribution, we rewrite this equation as

$$\begin{aligned} [\mathcal{H}_0 + V_{\text{ext}}, \rho_0 + \Delta\rho(t)] &= [\mathcal{H}_0, \rho_0] + [\mathcal{H}_0, \Delta\rho(t)] \\ &+ [V_{\text{ext}}, \rho_0] + [V_{\text{ext}}, \Delta\rho(t)] = i\hbar \dot{\rho}(t) \end{aligned} \quad (2.45)$$

and keep only those terms, which are of first order in the perturbation (i.e., we neglect $[V_{\text{ext}}, \Delta\rho]$) to write

$$[V_{\text{ext}}, \rho_0] \simeq i\hbar \left\{ \frac{\partial}{\partial t} \rho(t) - \frac{1}{i\hbar} [\mathcal{H}_0, \Delta\rho(t)] \right\}. \quad (2.46)$$

By multiplying from left and right with the proper exponentials we change from the Schrödinger into the interaction picture (indicated by an overbar), which for the deviation from the equilibrium distribution reads

$$\Delta\bar{\rho}(t) = e^{\frac{i}{\hbar}\mathcal{H}_0 t} \Delta\rho(t) e^{-\frac{i}{\hbar}\mathcal{H}_0 t}. \quad (2.47)$$

Note, that the time dependence of $\Delta\rho(t)$ on the *rhs* (in the Schrödinger picture) is that of the external field, while that on the *lhs* also includes the time

evolution due to \mathcal{H}_0 . In the interaction picture, the equation of motion for the first order correction $\Delta\bar{\rho}$ to the equilibrium distribution reads

$$i\hbar \frac{\partial}{\partial t} \Delta\bar{\rho}(t) = e^{\frac{i}{\hbar}\mathcal{H}_0 t} [V_{\text{ext}}(t), \rho_0] e^{-\frac{i}{\hbar}\mathcal{H}_0 t}. \quad (2.48)$$

It is an inhomogeneous linear differential equation indicating a linear relation between $\Delta\bar{\rho}(t)$ and the external perturbation V_{ext} . By direct integration one finds

$$\Delta\bar{\rho}(t) = \frac{1}{i\hbar} \int_{-\infty}^t e^{\frac{i}{\hbar}\mathcal{H}_0 t'} [V_{\text{ext}}(t'), \rho_0] e^{-\frac{i}{\hbar}\mathcal{H}_0 t'} dt', \quad (2.49)$$

and in the Schrödinger picture

$$\Delta\rho(t) = \frac{1}{i\hbar} \int_{-\infty}^t e^{-\frac{i}{\hbar}\mathcal{H}_0(t-t')} [V_{\text{ext}}(t'), \rho_0] e^{\frac{i}{\hbar}\mathcal{H}_0(t-t')} dt', \quad (2.50)$$

which is explicitly a linear expression in the external perturbation.

Let us now calculate the thermal expectation value of the observable A (the index t indicates the possible time dependence)

$$\langle A \rangle_t = \text{Tr}((\rho_0 + \Delta\rho(t))A) = \text{Tr}(\rho_0 A) + \text{Tr}(\Delta\rho(t)A). \quad (2.51)$$

The first term is the thermal expectation value of A of the unperturbed system (i.e., in equilibrium), which may be written A_0 . The second term, depending on the perturbation (2.38), can be transformed in several steps by exploiting the meaning of the trace operation:

$$\begin{aligned} \langle A \rangle_t &= A_0 + \frac{i}{\hbar} \int_{-\infty}^t \text{Tr} \left(e^{-\frac{i}{\hbar}\mathcal{H}_0(t-t')} [BF(t'), \rho_0] e^{\frac{i}{\hbar}\mathcal{H}_0(t-t')} A \right) dt' \\ &= A_0 + \frac{i}{\hbar} \int_{-\infty}^t \text{Tr} (A(t-t') \{BF(t')\rho_0 - \rho_0 BF(t')\}) dt' \\ &= A_0 + \frac{i}{\hbar} \int_{-\infty}^t \text{Tr} (\rho_0 \{A(t-t')B - BA(t-t')\}) F(t') dt'. \end{aligned} \quad (2.52)$$

In the first step, we applied a cyclic permutation of operators under the trace operation, in the second step we introduced the interaction picture for the observable A written as $A(t-t')$, and in the last step, we extracted the scalar factor $F(t')$ (note, that it is not an operator) and performed a cyclic permutation in the second term. We may now write $B = B(0)$ because, for vanishing time argument, the Schrödinger picture coincides with the interaction picture. Moreover, the upper limit of the integral can be shifted to infinity when the integrand is multiplied by the unit step function $\theta(t-t')$. Thus we find

$$\langle A \rangle_t = A_0 + \frac{i}{\hbar} \int_{-\infty}^{\infty} \theta(t-t') \langle [A(t-t'), B(0)] \rangle_0 F(t') dt' \quad (2.53)$$

which has the form of (2.39). The expectation value $\langle \dots \rangle_0$ under the integral is to be taken with the statistical operator ρ_0 in the equilibrium. The usual writing is by taking the Fourier transform

$$\begin{aligned} \Delta A(\omega) &= \int_{-\infty}^{+\infty} e^{i\omega t} (\langle A \rangle_t - A_0) dt \\ &= \frac{i}{\hbar} \int \int_{-\infty}^{+\infty} dt dt' e^{i\omega(t-t')} \theta(t-t') \langle [A(t-t'), B(0)] \rangle_0 e^{i\omega t'} F(t'). \end{aligned}$$

Finally, by changing the two time integrations with the substitution $t-t' = \tau$ we have

$$\Delta A(\omega) = \frac{i}{\hbar} \int_{-\infty}^{+\infty} d\tau e^{i\omega\tau} \theta(\tau) \langle [A(\tau), B(0)] \rangle_0 \int_{-\infty}^{+\infty} dt' e^{i\omega t'} F(t') \quad (2.54)$$

and

$$\Delta A(\omega) = \chi_{AB}(\omega) F(\omega). \quad (2.55)$$

This is the linear response of the system when measuring the observable \hat{A} (now using the $\hat{\cdot}$ -sign again) by applying a (time-dependent) perturbation $-\hat{B}F(\omega)$. It is expressed as the Fourier transform of the difference between the thermal expectation value of \hat{A} and its equilibrium value and written as a product of the perturbing field and a response function or susceptibility

$$\chi_{AB}(\omega) = \frac{i}{\hbar} \int_{-\infty}^{+\infty} d\tau e^{i\omega\tau} \theta(\tau) \langle [\hat{A}(\tau), \hat{B}(0)] \rangle_0. \quad (2.56)$$

The response function is completely defined by the unperturbed system (in our case the solid in thermal equilibrium) and describes a material property of the solid. It is a correlation function between the measured observable \hat{A} and the observable \hat{B} appearing in the perturbation. As will be seen later, the observables \hat{A} and \hat{B} are Hermitian adjoints of each other. The time dependent integrand with the step function warrants the causality between perturbation and response. This characteristic structure will be identified later (Sect. 7.1) as that of a retarded Green function. Having anticipated a periodic time dependence of the perturbation with the frequency ω , we obtain the response depending on ω (dynamical response). The special case of $\omega = 0$ refers to the static response.

2.5 Kubo's Formulas: Response Functions

The general concept of linear response has been developed in an earlier paper by Ryogo Kubo[67] and can be found in some text books (e.g., [9, 13, 18]). In this section, we restrict ourselves to the response functions of importance in solid state physics, some of which have already been mentioned in Table 2.1.

1. Dielectric Susceptibility: When exposing a piece of matter to an electric field, the matter will be polarized, i.e., it responds by shifting positive and

negative charges against each other or by aligning existing electric dipoles which, without the field, are randomly oriented. The polarization or electric dipole density $\mathbf{P} = \mathbf{M}^E/V$ (here V is the volume) is given by the relation

$$\mathbf{P} = \chi^E \cdot \mathbf{E}, \quad (2.57)$$

which has the form of (2.55). The dielectric susceptibility χ^E is a symmetric second rank tensor. Its principal values depend on the crystal structure of the solid as will be seen later. This tensor property allows the two vectors \mathbf{P} and \mathbf{E} to have different directions and to describe birefringence. This is the case in solids with axial anisotropy, while in cubic crystals the principal values of χ^E are equal to each other.

In order to formulate the dielectric susceptibility as a correlation function as in (2.56), we have to identify the two observables \hat{A} and \hat{B} . The perturbation is the potential energy of the electric dipole moment \mathbf{M}^E in the applied electric field $\mathbf{E}(t)$

$$V_{\text{ext}}(t) = -\mathbf{M}^E \cdot \mathbf{E}(t) = -\sum_j M_j^E E_j(t). \quad (2.58)$$

We find the observable \hat{B} to be one of the components of the electric dipole moment and the scalar field $F(t)$ to be the corresponding component of the applied electric field. The observable to be measured for investigating the dielectric susceptibility (or one of its tensor components) is a component of the electric dipole density, say P_i , and we may write (2.53) in the form

$$\langle P_i \rangle_t - P_{i0} = \sum_j \frac{i}{\hbar V} \int_{-\infty}^{+\infty} \theta(t-t') \langle [M_i^E(t-t'), M_j^E(0)] \rangle_0 E_j(t') dt' \quad (2.59)$$

and obtain after Fourier transformation, the response function

$$\chi_{ij}^E(\omega) = \frac{i}{\hbar V} \int_{-\infty}^{+\infty} e^{i\omega\tau} \theta(\tau) \langle [M_i^E(\tau), M_j^E(0)] \rangle_0 d\tau. \quad (2.60)$$

This is the Kubo formula for the *dielectric susceptibility*, which is a correlation function of components of the electric dipole moment. The contribution of the crystal lattice to the dielectric susceptibility will be described in more detail in Sect. 3.5. We mention in passing that systems with $P_{i0} \neq 0$ are called ferroelectric; their configuration of electrons and ions allows for a spontaneous dielectric polarization.

2. Magnetic Susceptibility: Magnetic properties of matter can be characterized by the response of the system to an applied magnetic field \mathbf{B} . The measured quantity will be the magnetization $\mathbf{M} = \mathbf{m}/V$, which in complete analogy to the dielectric case is the magnetic dipole density. Making use of this analogy, we may write the perturbation $V_{\text{ext}}(t) = -\mathbf{m} \cdot \mathbf{B}(t)$ and identify the observable \hat{A} with a component of the magnetization and the observable \hat{B} with a

component of the magnetic dipole moment to write the Kubo formula for the *magnetic susceptibility*

$$\chi_{ij}^M(\omega) = \frac{i}{\hbar V} \int_{-\infty}^{+\infty} e^{i\omega\tau} \theta(\tau) \langle [m_i(\tau), m_j(0)] \rangle_0 d\tau. \quad (2.61)$$

It is a correlation function between the components of the magnetic dipole moment.

In Chap. 6, we shall express the magnetic dipole moment in terms of the electron spin operators \mathbf{S}_l as

$$\mathbf{m} = g\mu_B \sum_l \mathbf{S}_l, \quad (2.62)$$

with the Landé⁸ g factor and the Bohr⁹ magneton μ_B . For this case, the magnetic susceptibility

$$\chi_{ij}^M(\omega) = \frac{i}{\hbar V} g^2 \mu_B^2 \sum_{ll'} \int_{-\infty}^{+\infty} e^{i\omega\tau} \theta(\tau) \langle [S_{l,i}(\tau), S_{l',j}(0)] \rangle_0 d\tau. \quad (2.63)$$

turns out to be a correlation function between the components of the electron spin operator or in short, a spin–spin correlation function.

3. Dielectric Function: The dielectric function (or frequency dependent dielectric constant) is known from electrodynamics; it connects the displacement field with the electric field according to

$$\mathbf{D}(\mathbf{q}, \omega) = \varepsilon_0 \varepsilon(\mathbf{q}, \omega) \mathbf{E}(\mathbf{q}, \omega). \quad (2.64)$$

The space and time dependence of the quantities are specified by the wave vector \mathbf{q} and the frequency ω , respectively. Depending on the experimental situation, one distinguishes between the response to a longitudinal or transverse perturbation. Let us consider here, the case of probing the dielectric system with an external test charge, which exerts a longitudinal electric field. This scenario is typical for a scattering experiment. It is intuitively clear that the charges of the dielectric will rearrange in the presence of the test charge, and this rearrangement is quantified by an induced charge density en_{ind} . The fields are determined by their respective charges via Poisson's equation. For the displacement field, these are the external charges $en_{\text{ext}}(\mathbf{q}, \omega)$ (the Fourier transform of the external charge density $en_{\text{ext}}(\mathbf{r}, t)$)

$$i\mathbf{q} \cdot \mathbf{D}(\mathbf{q}, \omega) = en_{\text{ext}}(\mathbf{q}, \omega) \quad (2.65)$$

and for the electric field, in addition the induced charges (due to polarization in the presence of the external charge) $en_{\text{ind}}(\mathbf{q}, \omega)$

⁸ Alfred Landé 1888–1975.

⁹ Niels Bohr 1885–1962, Nobel prize in physics 1922.

$$\mathbf{i}\mathbf{q} \cdot \mathbf{E}(\mathbf{q}, \omega) = \frac{e}{\varepsilon_0} (n_{\text{ext}}(\mathbf{q}, \omega) + n_{\text{ind}}(\mathbf{q}, \omega)). \quad (2.66)$$

It is straightforward to eliminate the fields from (2.64) to (2.66) and to write

$$n_{\text{tot}}(\mathbf{q}, \omega) = n_{\text{ind}}(\mathbf{q}, \omega) + n_{\text{ext}}(\mathbf{q}, \omega) = \frac{n_{\text{ext}}(\mathbf{q}, \omega)}{\varepsilon(\mathbf{q}, \omega)}. \quad (2.67)$$

The last relation is the standard expression for the *dielectric screening* of a test charge in dielectric matter. In general, for time-dependent processes, it depends on ω , and describes dynamical screening.

We may read this relation also from the viewpoint of linear response: The system responds to the external or test charge by building up the total charge density $en_{\text{tot}}(\mathbf{q}, \omega)$ with the inverse dielectric function as the response function. In order to cast it into the form of (2.56), we identify the observable \hat{A} as the charge density operator

$$e\hat{n}(\mathbf{r}) = e \sum_{\mathbf{q}} \hat{n}_{\mathbf{q}} e^{i\mathbf{q} \cdot \mathbf{r}} \quad (2.68)$$

or its Fourier transform, the operator of density fluctuations $\hat{n}_{\mathbf{q}}$. The time dependent induced density fluctuations are given by

$$n_{\text{ind}}(\mathbf{q}, t) = \langle \hat{n}_{\mathbf{q}} \rangle_t - n_0. \quad (2.69)$$

The perturbation is caused by the charge density of the external (or test) charge

$$en_{\text{ext}}(\mathbf{r}, t) = e \sum_{\mathbf{q}'} n_{\text{ext}}(\mathbf{q}', t) e^{i\mathbf{q}' \cdot \mathbf{r}} \quad (2.70)$$

with the interaction energy

$$\begin{aligned} V_{\text{ext}}(t) &= \frac{-e^2}{4\pi\varepsilon_0} \int \int d^3\mathbf{r} d^3\mathbf{r}' \frac{\hat{n}(\mathbf{r}) n_{\text{ext}}(\mathbf{r}', t)}{|\mathbf{r} - \mathbf{r}'|} \\ &= \frac{-e^2}{4\pi\varepsilon_0} \sum_{\mathbf{q}\mathbf{q}'} \hat{n}_{\mathbf{q}} n_{\text{ext}}(\mathbf{q}', t) \int \int d^3\mathbf{r} d^3\mathbf{r}' \frac{e^{i(\mathbf{q} \cdot \mathbf{r} + \mathbf{q}' \cdot \mathbf{r}')}}{|\mathbf{r} - \mathbf{r}'|}. \end{aligned} \quad (2.71)$$

The double integral can be expressed in terms of the Fourier transform, and one obtains

$$V_{\text{ext}}(t) = - \sum_{\mathbf{q}} v_{\mathbf{q}} \hat{N}_{-\mathbf{q}} N_{\text{ext}}(\mathbf{q}, t), \quad (2.72)$$

where $v_{\mathbf{q}} = e^2/V\varepsilon_0q^2$ is the Fourier transform of the Coulomb potential (see Appendix), $\hat{N}_{-\mathbf{q}} = V\hat{n}_{-\mathbf{q}}$ and $N_{\text{ext}}(\mathbf{q}, t) = Vn_{\text{ext}}(\mathbf{q}, t)$. By identifying $\hat{N}_{-\mathbf{q}}$ as the observable \hat{B} and $n_{\text{ext}}(\mathbf{q}, t)$ as the scalar time dependent field $F(t)$ of the general response formalism, we may now write

$$n_{\text{ind}}(\mathbf{q}, \omega) = v_{\mathbf{q}} \frac{i}{\hbar} \int_{-\infty}^{+\infty} e^{i\omega\tau} \theta(\tau) \langle [\hat{N}_{\mathbf{q}}(\tau), \hat{N}_{-\mathbf{q}}(0)] \rangle_0 n_{\text{ext}}(\mathbf{q}, \omega) d\tau. \quad (2.73)$$

In comparison with (2.67), we find as the Kubo formula for the *inverse dielectric function*

$$\frac{1}{\varepsilon(\mathbf{q}, \omega)} = 1 + v_{\mathbf{q}} \frac{i}{\hbar} \int_{-\infty}^{+\infty} e^{i\omega\tau} \theta(\tau) \langle [\hat{N}_{\mathbf{q}}(\tau), \hat{N}_{-\mathbf{q}}(0)] \rangle_0 d\tau. \quad (2.74)$$

It is a correlation function of the number (or density) fluctuations and will be discussed in more detail in Chap. 4 as *energy-loss function*.

As further examples, one may consider the tensor components of the electric conductivity $\sigma_{\mu\nu}(\omega)$ (Problem 2.4) or the thermal conductivity mentioned in Table 2.1. The response concept can be generalized beyond the linear regime by considering higher order terms in the external perturbation (Problem 2.5). The corresponding response functions describe the nonlinear properties of the material, which become important, for instance, in the response of a solid to intense laser light (nonlinear optics) or strong electric fields (nonlinear transport) [68].

2.6 Properties of Response Functions

Because response functions will be used throughout the book, some of their properties have to be compiled at the beginning [64, 69, 70]. Response functions $\chi_{AB}(\omega)$ of the general form (2.56) are complex valued functions for real frequencies. If they are considered in the complex frequency plane with $z = \omega + i\delta$, they represent analytic functions in the upper half-plane. The analyticity is a consequence of the causal connection between the perturbation and its effect on the system as expressed by the unit step function under the integral. Due to this property, Cauchy's theorem holds, which reads

$$\chi_{AB}(z) = \frac{1}{2\pi i} \oint \frac{\chi_{AB}(z')}{z' - z} dz', \quad (2.75)$$

where the contour integral is along the real axis and closes along the great semicircle in the upper half-plane. Assuming that $\chi_{AB}(z')$ vanishes sufficiently rapidly at infinity, the semicircle does not contribute to the integral, and we have

$$\chi_{AB}(z) = \frac{1}{2\pi i} \int_{-\infty}^{+\infty} \frac{\chi_{AB}(\omega')}{\omega' - z} d\omega'. \quad (2.76)$$

This relation can be evaluated for real z with

$$\lim_{\Gamma \rightarrow 0} \frac{1}{\omega' - \omega - i\Gamma} = \mathcal{P} \left(\frac{1}{\omega' - \omega} \right) + i\pi\delta(\omega' - \omega), \quad (2.77)$$

where \mathcal{P} denotes the principal part. Using (2.77) in (2.76) and rearranging terms gives

$$\chi_{AB}(\omega) = \frac{1}{i\pi} \mathcal{P} \int_{-\infty}^{+\infty} \frac{\chi_{AB}(\omega')}{\omega' - \omega} d\omega'. \quad (2.78)$$

By separating this relation into real and imaginary part,

$$\chi_{AB}(\omega) = \text{Re}\chi_{AB}(\omega) + i\text{Im}\chi_{AB}(\omega), \quad (2.79)$$

one finds the *dispersion* or *Kramers–Kronig*¹⁰ relations

$$\text{Re}\chi_{AB}(\omega) = \frac{1}{\pi} \mathcal{P} \int_{-\infty}^{+\infty} \frac{\text{Im}\chi_{AB}(\omega')}{\omega' - \omega} d\omega' \quad (2.80)$$

$$\text{Im}\chi_{AB}(\omega) = -\frac{1}{\pi} \mathcal{P} \int_{-\infty}^{+\infty} \frac{\text{Re}\chi_{AB}(\omega')}{\omega' - \omega} d\omega' \quad (2.81)$$

which are a consequence of causality. The real and imaginary parts of the susceptibility are also called the dissipative and absorptive parts, respectively.

The meaning of these relations can be illustrated by considering the imaginary part of a susceptibility of the form $\text{Im}\chi(\omega') \sim (\delta(\omega_0 - \omega') - \delta(\omega_0 + \omega'))$ (as will be shown in Chap. 3, this describes the absorption (and emission) of a harmonic oscillator with eigenfrequency ω_0). For this case, the real part of $\chi(\omega)$ takes the form $1/(\omega_0^2 - \omega^2)$, characteristic for the anomalous dispersion of an oscillator (Problem 2.6).

According to the structure of (2.56), the susceptibility is the Fourier transform of an object of the more general form

$$G_{AB}(\tau) = -\frac{i}{\hbar} \theta(\tau) \langle [\hat{A}(\tau), \hat{B}(0)]_{\pm} \rangle \quad (2.82)$$

which is a *retarded Green*¹¹ *function*. Depending on whether \hat{A} , \hat{B} are fermion or boson operators, one has to take the anti-commutator $[\hat{A}, \hat{B}]_+ = \hat{A}\hat{B} + \hat{B}\hat{A}$ or the commutator $[\hat{A}, \hat{B}]_- = \hat{A}\hat{B} - \hat{B}\hat{A}$, respectively. Note, that a response function χ_{AB} is always written in terms of the commutator. The thermal expectation value is evaluated for the system Hamiltonian (in case of a response function it is the one without external perturbation).

The retarded Green function $G_{AB}(\tau)$ can be decomposed into the correlation functions $C_{AB}^>(\tau) = \langle \hat{A}(\tau)\hat{B}(0) \rangle$ and $C_{AB}^<(\tau) = \langle \hat{B}(0)\hat{A}(\tau) \rangle$

$$G_{AB}(\tau) = -\frac{i}{\hbar} \theta(\tau) (C_{AB}^>(\tau) \pm C_{AB}^<(\tau)). \quad (2.83)$$

Its Laplace transform, to which the Fourier transform reduces because of the step function in $G_{AB}(\tau)$,

¹⁰ Hendrik Anton Kramers 1894–1952; Ralph de Laer Kronig 1904–1995.

¹¹ George Green 1793–1841.

$$\begin{aligned}
G_{AB}(z) &= \int_0^{\infty} e^{iz\tau} G_{AB}(\tau) d\tau \\
&= -\frac{i}{\hbar} \int_0^{\infty} d\tau e^{iz\tau} \int_{-\infty}^{+\infty} \frac{d\omega}{2\pi} e^{-i\omega\tau} (C_{AB}^>(\omega) \pm C_{AB}^<(\omega)) \quad (2.84)
\end{aligned}$$

can be expressed in terms of the Fourier transforms $C_{AB}^>(\omega)$ and $C_{AB}^<(\omega)$ of the correlation functions. After performing the time integration, one finds the *spectral representation* of the Green function

$$G_{AB}(z) = \frac{1}{\pi} \int_{-\infty}^{+\infty} \frac{\rho_{AB}(\omega')}{\omega' - z} d\omega' \quad (2.85)$$

with the *spectral function*

$$\rho_{AB}(\omega) = -\frac{1}{2\hbar} (C_{AB}^>(\omega) \pm C_{AB}^<(\omega)). \quad (2.86)$$

The upper(lower) sign refers to expressions formed with fermion(boson) operators. The spectral representation (2.85) can be used to express $\rho_{AB}(\omega)$ in terms of the Green function

$$\rho_{AB}(\omega) = \frac{1}{2i} \lim_{\Gamma \rightarrow 0} (G_{AB}(\omega + i\Gamma) - G_{AB}(\omega - i\Gamma)) \quad (2.87)$$

which, under the conditions given below, is real valued.

Some properties of the spectral function $\rho_{AB}(\omega)$ can be obtained by writing the time-dependent correlation functions in the energy or spectral representation (using eigenstates $|n\rangle$, $|m\rangle$ of the system Hamiltonian H)

$$\begin{aligned}
C_{AB}^>(\tau) &= \langle e^{\frac{i}{\hbar}H\tau} \hat{A} e^{-\frac{i}{\hbar}H\tau} \hat{B} \rangle \\
&= \sum_{nm} p_n A_{nm} B_{mn} e^{\frac{i}{\hbar}(E_n - E_m)\tau}. \quad (2.88)
\end{aligned}$$

Here p_n is the statistical factor, E_n , E_m are the eigenvalues of H and A_{nm} , B_{mn} the matrix elements of \hat{A} and \hat{B} . The Fourier transform of $C_{AB}^>(\tau)$ is given by

$$C_{AB}^>(\omega) = \sum_{nm} p_n A_{nm} B_{mn} 2\pi \delta(\hbar\omega + E_n - E_m). \quad (2.89)$$

Similarly we find

$$C_{AB}^<(\omega) = \sum_{nm} p_m B_{mn} A_{nm} 2\pi \delta(\hbar\omega + E_n - E_m). \quad (2.90)$$

The following relations hold for the correlation functions:

$$C_{AB}^>(\omega) = C_{BA}^<(-\omega) \quad (2.91)$$

$$C_{AB}^<(\omega) = e^{-\beta\hbar\omega} C_{AB}^>(\omega). \quad (2.92)$$

The first of these relations is obtained by interchanging n and m under the sum in (2.89) and (2.90). The second is found by using the ratio $p_m/p_n = \exp(-\beta\hbar\omega)$ of the statistical factors. (This relation holds not only for the canonical ensemble, but also for the grand-canonical ensemble if the operators \hat{A} and \hat{B} do not change the particle numbers.) Because of (2.91), the spectral function has the property

$$\rho_{AB}(-\omega) = \pm \rho_{BA}(\omega), \quad (2.93)$$

which in connection with (2.85), implies $G_{AB}(-z) = \mp G_{BA}(z)$, where again, the upper(lower) sign refers to the quantity defined for fermion(boson) operators. For $\hat{B} = \hat{A}^\dagger$, and using (2.89), (2.90), and (2.92) we may write $\rho_{BA}(\omega)$ in the form

$$\rho_{AA^\dagger} = -\frac{\pi}{\hbar} (1 \pm e^{-\beta\hbar\omega}) \sum_{m,n} p_n A_{nm} A_{mn} \delta(\hbar\omega + E_n - E_m), \quad (2.94)$$

to see with $A_{mn} = A_{nm}^*$ that it is real, and with (2.87) that $\rho_{AA^\dagger}(\omega) = \text{Im}\{G_{AA^\dagger}(\omega)\}$. In the special case of Hermitian operators, $\hat{B} = \hat{A}$, one has $\text{Im}\{G_{AA}(-\omega)\} = -\text{Im}\{G_{AA}(\omega)\}$. Using (2.92), the correlation function $C_{AB}^>(\omega)$ can be expressed also as

$$C_{AB}^>(\omega) = -2\hbar \frac{\rho_{AB}(\omega)}{1 \pm e^{-\beta\hbar\omega}} \quad (2.95)$$

and its Fourier transform is

$$\langle A(\tau)B(0) \rangle = -\frac{\hbar}{\pi} \int_{-\infty}^{+\infty} e^{-i\omega\tau} \frac{\rho_{AB}(\omega)}{1 \pm e^{-\beta\hbar\omega}} d\omega. \quad (2.96)$$

Let us finally specialize to the case of G_{AB} being a response function with $\hat{B} = \hat{A}^\dagger$ and consider the case $\tau = 0$. Then with $\rho_{AA^\dagger}(\omega) = -\text{Im} \chi_{\hat{A}\hat{A}^\dagger}(\omega)$ the last relation takes the form

$$\langle \hat{A}\hat{A}^\dagger \rangle = \frac{\hbar}{\pi} \int_{-\infty}^{+\infty} \frac{\text{Im}\chi_{\hat{A}\hat{A}^\dagger}(\omega)}{1 - e^{-\beta\hbar\omega}} d\omega, \quad (2.97)$$

which connects the imaginary (or dissipative) part of the response function with a quantity that describes the fluctuations in the observable \hat{A} and is therefore known as the *dissipation-fluctuation theorem*.

Due to the hermiticity of the operators \hat{A} and \hat{B} and the appearance of their commutator in the response function, its imaginary part fulfills the relations

$$\text{Im} \chi_{AB}(-\tau) = -\text{Im} \chi_{BA}(\tau) \quad (2.98)$$

$$\text{Im} \chi_{AB}(-\omega) = -\text{Im} \chi_{BA}(\omega) \quad (2.99)$$

and with

$$\chi_{AB}^*(\omega) = \chi_{AB}(-\omega), \quad (2.100)$$

the response $\Delta A(\omega)$ in (2.55) is real as required for an observable.

Problems

- 2.1 Formulate the matrix representation of the statistical operator with the eigenstates of the system Hamiltonian and show that it is diagonal.
- 2.2 Show that the thermal expectation value of an observable reduces for $T = 0$ K to the expectation value of this observable in the ground state of the system.
- 2.3 Calculate the thermal expectation value of the particle number operator for a system of (free) fermions in thermal equilibrium to find the Fermi–Dirac distribution. Do the same for a system of bosons to obtain the Bose–Einstein distribution. Consider the high temperature limit.
- 2.4 In order to derive the Kubo formula for the electric conductivity $\sigma_{\mu\nu}(\omega)$, identify the observables \hat{A} and \hat{B} in (2.56). Keep in mind which quantity is measured in transport experiments, and how the coupling between electrons and the electromagnetic field is described.
- 2.5 Develop the concept of nonlinear response by considering (as in perturbation theory) corrections to the equilibrium distribution $\Delta\rho = \Delta\rho_1 + \Delta\rho_2 + \dots$ of increasing order in the external perturbation. Find the structure of the lowest order nonlinear response function for the observable \hat{A} due to the perturbation V_{ext} (2.38).
- 2.6 Let the imaginary part of a response function be of the form $\text{Im}\chi_{AB}(\omega) = \chi_0(\delta(\omega_0 - \omega) - \delta(\omega_0 + \omega))$. Calculate the real part of the response function using (2.80).

Lattice Dynamics: Phonons

The motion of the heavy constituents of the solid and the solid state properties, which are essentially determined by this motion, are the subject of this chapter. Lattice dynamics is a standard topic in textbooks on Solid State Physics, but there is also a variety of monographs on this subject, e.g., [71–83], of which the one by Born and Huang [71], entitled “Dynamical Theory of Crystal Lattices” is the pioneering textbook in this field. The progress in Lattice Dynamics, especially the strong mutual influence between experimental and theoretical investigations, is well documented in the three volumes “Phonons: Theory and Experiment,” edited by Brüesch [77–79].

In simplest terms, the dynamics of a lattice can be described by employing a classical model with massive spheres (representing the atoms or ions) connected by springs (representing the chemical bonds) in a periodic array (see Fig. 3.1).

For a more rigorous description, the starting point is the adiabatic approximation of Sect. 2.2, according to which the motion of the ions is governed by the time-dependent Schrödinger equation (see 2.23)

$$(\mathcal{H}_{\text{ion}} + \mathcal{E}_{\text{el},\alpha})\Phi_{\alpha} = i\hbar\dot{\Phi}_{\alpha}, \quad (3.1)$$

where (see 2.24)

$$\mathcal{H}_{\text{ion}} + \mathcal{E}_{\text{el},\alpha} = \sum_{\mathbf{n}} \frac{\mathbf{P}_{\mathbf{n}}^2}{2M} + \mathcal{E}_{\text{el},\alpha}(\{\mathbf{R}_{\mathbf{n}}\}) + \frac{1}{2} \sum_{\substack{\mathbf{n}, \mathbf{m} \\ \mathbf{n} \neq \mathbf{m}}} V(\mathbf{R}_{\mathbf{n}} - \mathbf{R}_{\mathbf{m}}). \quad (3.2)$$

The last two terms on the *rhs* represent the adiabatic potential energy $\mathcal{U}_{\alpha}(\{\mathbf{R}_{\mathbf{n}}\})$ of the ion configuration $\{\mathbf{R}_{\mathbf{n}}\}$, with the electron system being in the state described by the wave function $\Psi_{\alpha}(\{\mathbf{r}_l\}, \{\mathbf{R}_{\mathbf{n}}\})$ as introduced in Sect. 2.2. Thus, the motion of the ions, described by the wave function $\Phi_{\alpha}(\{\mathbf{R}_{\mathbf{n}}\})$, is not only determined by the potential energy of the ion configuration but also by the energy of the electrons $\mathcal{E}_{\text{el},\alpha}(\{\mathbf{R}_{\mathbf{n}}\})$ in this configuration. Instead of considering the dependence of this motion on α , let us assume,

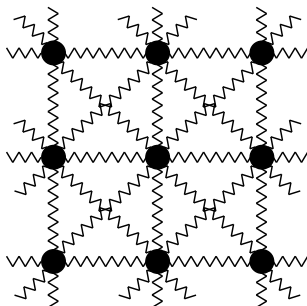


Fig. 3.1. Classical model for lattice dynamics: spheres and springs

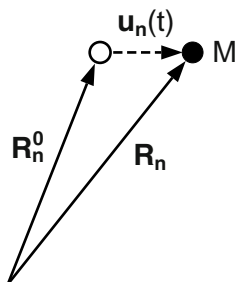


Fig. 3.2. Equilibrium position and displacement of an ion

for simplicity, the electron system to be in its ground state (see Chaps. 4 and 5) and drop the index α . Hence, in this chapter, we are dealing with the Hamiltonian

$$H = \mathcal{H}_{\text{ion}} + \mathcal{E}_{\text{el}} = \sum_{n\tau} \frac{\mathbf{P}_{n\tau}^2}{2M_\tau} + \mathcal{U}(\{\mathbf{R}_{n\tau}\}) \quad (3.3)$$

to describe the dynamics of the crystal lattice, which, in general, can be a lattice with basis as indicated by the vector index τ .

In a crystalline solid, the ion configuration is characterized by the actual positions of the atoms

$$\mathbf{R}_{n\tau}(t) = \mathbf{R}_{n\tau}^0 + \mathbf{u}_{n\tau}(t), \quad (3.4)$$

with equilibrium positions $\mathbf{R}_{n\tau}^0$ at the points of a lattice with basis (see Sect. 1.2) and time-dependent displacements $\mathbf{u}_{n\tau}(t)$ around these positions (see Fig. 3.2). The vector indices $\mathbf{n} = (n_1, n_2, n_3)$ for the lattice cell and τ for the atoms of the basis have been introduced in Sect. 1.2. The aim of lattice dynamics is to set up and solve equations of motion for the displacement vectors $\mathbf{u}_{n\tau}(t)$.

3.1 Harmonic Approximation

It is reasonable and required for the Born–Oppenheimer approximation to start with displacements $|\mathbf{u}_{n\tau}(t)|$ which are small compared to the lattice spacings $|\mathbf{a}_j|$, i.e., the springs are only slightly distorted and the ions remain close to their equilibrium positions. (The other extreme, when $|\mathbf{u}_{n\tau}(t)|$ becomes comparable with $|\mathbf{a}_j|$, would lead to a destruction of the lattice, e.g., in the case of melting, which is not the subject here.) Under this condition the adiabatic potential can be expanded in a power series with respect to the components of $\mathbf{u}_{n\tau}(t)$ around the equilibrium positions. Let us adopt here a frequently used notation [84]

$$u_{n\tau i} =: u \begin{pmatrix} \mathbf{n} \\ \boldsymbol{\tau} \\ i \end{pmatrix} \begin{array}{l} \leftarrow \text{lattice cell} \\ \leftarrow \text{atom of basis} \\ \leftarrow \text{vector component} \end{array} \quad (3.5)$$

to write the expansion

$$\begin{aligned} \mathcal{U}(\{\mathbf{R}_{n\tau}\}) &= \mathcal{U}(\{\mathbf{R}_{n\tau}^0\}) + \sum_{n\tau i} \Phi \begin{pmatrix} \mathbf{n} \\ \boldsymbol{\tau} \\ i \end{pmatrix} u \begin{pmatrix} \mathbf{n} \\ \boldsymbol{\tau} \\ i \end{pmatrix} \\ &+ \frac{1}{2} \sum_{\substack{n\tau i \\ m\tau' j}} \Phi \begin{pmatrix} \mathbf{n} & \mathbf{m} \\ \boldsymbol{\tau} & \boldsymbol{\tau}' \\ i & j \end{pmatrix} u \begin{pmatrix} \mathbf{n} \\ \boldsymbol{\tau} \\ i \end{pmatrix} u \begin{pmatrix} \mathbf{m} \\ \boldsymbol{\tau}' \\ j \end{pmatrix} + \mathcal{O}(u^3), \end{aligned} \quad (3.6)$$

with

$$\Phi \begin{pmatrix} \mathbf{n} \\ \boldsymbol{\tau} \\ i \end{pmatrix} = \left. \frac{\partial \mathcal{U}}{\partial u_{n\tau i}} \right|_{\{\mathbf{R}_{n\tau}^0\}} \quad \text{and} \quad \Phi \begin{pmatrix} \mathbf{n} & \mathbf{m} \\ \boldsymbol{\tau} & \boldsymbol{\tau}' \\ i & j \end{pmatrix} = \left. \frac{\partial^2 \mathcal{U}}{\partial u_{n\tau i} \partial u_{m\tau' j}} \right|_{\{\mathbf{R}_{n\tau}^0\}}. \quad (3.7)$$

For the equilibrium configuration, the potential energy $\mathcal{U}(\{\mathbf{R}_{n\tau}\})$ is at its minimum and all first derivatives vanish; those of second order become the leading terms and are the only ones if higher order terms are neglected because of their smallness. This defines the *harmonic approximation* with the Hamiltonian

$$H = \sum_{n\tau} \frac{\mathbf{P}_{n\tau}^2}{2M_{n\tau}} + \frac{1}{2} \sum_{\substack{n\tau i \\ m\tau' j}} \Phi \begin{pmatrix} \mathbf{n} & \mathbf{m} \\ \boldsymbol{\tau} & \boldsymbol{\tau}' \\ i & j \end{pmatrix} u \begin{pmatrix} \mathbf{n} \\ \boldsymbol{\tau} \\ i \end{pmatrix} u \begin{pmatrix} \mathbf{m} \\ \boldsymbol{\tau}' \\ j \end{pmatrix} \quad (3.8)$$

formulated in terms of the displacements $\mathbf{u}_{n\tau}$ and their conjugate momenta $\mathbf{P}_{n\tau}$. It corresponds to that of a set of coupled harmonic oscillators for which the canonical equations of motion

$$\dot{P}_{n\tau i} = - \frac{\partial H}{\partial u_{n\tau i}}, \quad \dot{u}_{n\tau i} = \frac{\partial H}{\partial P_{n\tau i}} = \frac{P_{n\tau i}}{M_{n\tau}} \quad (3.9)$$

or Newton's equations of motion

$$M_{\tau} \ddot{u} \begin{pmatrix} \mathbf{n} \\ \tau \\ i \end{pmatrix} = - \sum_{\mathbf{m}\tau'j} \Phi \begin{pmatrix} \mathbf{n} & \mathbf{m} \\ \tau & \tau' \\ i & j \end{pmatrix} u \begin{pmatrix} \mathbf{m} \\ \tau' \\ j \end{pmatrix} \quad (3.10)$$

are easily obtained. These equations generalize the simple pendulum model, a mass attached to a spring, to a network like that of Fig. 3.1: The *rhs* of (3.10) represents the force exerted onto the mass M_{τ} at $\mathbf{R}_{\mathbf{n}\tau}$ in direction i if the masses at $\mathbf{R}_{\mathbf{m}\tau'}$ are moved in directions j . The Φ are the *force constants* symbolized in Fig. 3.1 by the springs, but their microscopic meaning derives from the adiabatic potential by means of (3.7). Simple examples are the subject of Problem 3.1 (the linear chain with two different atoms in the unit cell) and Problem 3.2 (the two-dimensional square lattice).

Supplement: Reducing the number of force constants

The number of force constants, which is the squared number of degrees of freedom, can drastically be reduced in the following way (see also Problem 3.2):

1. According to Newton's third axiom (action = reaction), we can write

$$\Phi \begin{pmatrix} \mathbf{n} & \mathbf{m} \\ \tau & \tau' \\ i & j \end{pmatrix} = \Phi \begin{pmatrix} \mathbf{m} & \mathbf{n} \\ \tau' & \tau \\ j & i \end{pmatrix}. \quad (3.11)$$

2. If the displacements $\mathbf{u}_{\mathbf{m}\tau'}$ are the same for all $\mathbf{m}\tau'$, the solid experiences a translation by \mathbf{u} , which (in the absence of external forces) does not change the potential energy. Formally, this means

$$\sum_{\mathbf{m}\tau'j} \Phi \begin{pmatrix} \mathbf{n} & \mathbf{m} \\ \tau & \tau' \\ i & j \end{pmatrix} u_j = 0 \quad \text{for arbitrary } u_j, j = 1, 2, 3 \quad (3.12)$$

or

$$\sum_{\mathbf{m}\tau'} \Phi \begin{pmatrix} \mathbf{n} & \mathbf{m} \\ \tau & \tau' \\ i & j \end{pmatrix} = 0 \quad \text{for } i, j = 1, 2, 3. \quad (3.13)$$

3. Due to the invariance of the lattice under discrete translations or by replacing $\mathbf{R}_n^0 \rightarrow \mathbf{R}_n^0 + \mathbf{R}_{n'}^0$, we have

$$\Phi \begin{pmatrix} \mathbf{n} & \mathbf{m} \\ \tau & \tau' \\ i & j \end{pmatrix} = \Phi \begin{pmatrix} \mathbf{n} + \mathbf{n}' & \mathbf{m} + \mathbf{n}' \\ \tau & \tau' \\ i & j \end{pmatrix} = \Phi \begin{pmatrix} \mathbf{n} - \mathbf{m} & \mathbf{0} \\ \tau & \tau' \\ i & j \end{pmatrix}, \quad (3.14)$$

where the last equation follows for the choice $\mathbf{n}' = -\mathbf{m}$.

4. Making use of the symmetry of the lattice under operations of the *point group* (rotations, mirror reflections, inversion), the number of independent force constants is further reduced depending on the actual lattice structure.
5. Finally, the forces reduce with increasing distance between the masses and usually only those between nearest and next nearest neighbors need to be considered (see Problems 3.1 and 3.2).

The equations of motion (3.10), being a homogeneous set of coupled linear differential equations, can be solved by the standard procedure assuming

$$u_{\mathbf{n}\tau i}(t) = \frac{1}{\sqrt{M_\tau}} \bar{u} \begin{pmatrix} \mathbf{n} \\ \tau \\ i \end{pmatrix} e^{-i\omega t}, \quad (3.15)$$

where, by convention, a factor with the square-root of the mass is extracted. It yields a homogeneous system of coupled linear equations for the displacements

$$\omega^2 \bar{u} \begin{pmatrix} \mathbf{n} \\ \tau \\ i \end{pmatrix} = \sum_{\mathbf{m}\tau'j} \frac{1}{\sqrt{M_\tau M_{\tau'}}} \Phi \begin{pmatrix} \mathbf{n} & \mathbf{m} \\ \tau & \tau' \\ i & j \end{pmatrix} \bar{u} \begin{pmatrix} \mathbf{m} \\ \tau' \\ j \end{pmatrix}. \quad (3.16)$$

We make use of the *Bloch theorem* (see Problem 1.4), according to which the displacements on different lattice sites differ only by phase factors

$$\bar{u} \begin{pmatrix} \mathbf{n} + \mathbf{m} \\ \tau \\ i \end{pmatrix} = \bar{u} \begin{pmatrix} \mathbf{n} \\ \tau \\ i \end{pmatrix} e^{i\mathbf{q} \cdot \mathbf{R}_m^0} = \bar{u} \begin{pmatrix} \mathbf{0} \\ \tau \\ i \end{pmatrix} e^{i\mathbf{q} \cdot (\mathbf{R}_m^0 + \mathbf{R}_n^0)}, \quad (3.17)$$

and apply the periodic boundary conditions (Problem 3.3), which restrict the components of the wave vector to the discrete values

$$q_i = \frac{2\pi}{N_i a_i} \nu_i, \quad \nu_i = 0, \dots, N_i - 1, \quad i = 1, 2, 3. \quad (3.18)$$

Here $N = N_1 N_2 N_3 \gg 1$ is the number of unit cells in the periodicity (or crystal) volume V . Thus, (3.10) can be written in the compact form

$$\omega^2 \bar{u}_{\tau i}(\mathbf{q}) = \sum_{\tau'j} D_{\tau i, \tau' j}(\mathbf{q}) \bar{u}_{\tau' j}(\mathbf{q}), \quad (3.19)$$

with the *dynamical matrix*

$$D_{\tau i, \tau' j}(\mathbf{q}) = \sum_{\mathbf{m}} \frac{1}{\sqrt{M_\tau M_{\tau'}}} \Phi \begin{pmatrix} \mathbf{n} - \mathbf{m} & \mathbf{0} \\ \tau & \tau' \\ i & j \end{pmatrix} e^{i\mathbf{q} \cdot (\mathbf{R}_m^0 - \mathbf{R}_n^0)}. \quad (3.20)$$

It does not depend on the index \mathbf{n} and on the sign of \mathbf{q} (as can be seen by rearranging the sum over \mathbf{m}), thus $D_{\tau i, \tau' j}(\mathbf{q}) = D_{\tau i, \tau' j}(-\mathbf{q})$. The number of solutions of (3.19) is the same as the number $3rN$ of degrees of freedom of the system, where r is the number of atoms in the basis and N the number of lattice cells (equal to the number of different \mathbf{q} in the first Brillouin zone). For each \mathbf{q} , the secular problem

$$\|D_{\tau i, \tau' j}(\mathbf{q}) - \omega^2 \delta_{\tau\tau'} \delta_{ij}\| = 0 \quad (3.21)$$

yields $3r$ eigenfrequencies $\omega_s(\mathbf{q}) = \omega_s(-\mathbf{q})$, $s = 1, \dots, 3r$, with corresponding normalized eigenvectors $\mathbf{e}_\tau^s(\mathbf{q})$. It is important to note that the solutions of (3.19) describe *collective modes* or *excitations*, for which all ions of the lattice move with the same time dependence but phase shifted with respect to each other according to Bloch's theorem. For the collective mode $s\mathbf{q}$, the motion of the individual ion (or mass) at $\mathbf{R}_{n\tau}$ is described by the displacement

$$\mathbf{u}_{n\tau}^s(\mathbf{q}, t) \sim \frac{1}{\sqrt{M_\tau}} \mathbf{e}_\tau^s(\mathbf{q}) e^{i(\mathbf{q} \cdot \mathbf{R}_n^0 - \omega_s(\mathbf{q})t)}. \quad (3.22)$$

As usual, the eigenmodes form a complete set of solutions that can be used as the basis for representing an arbitrary motion of the lattice or of the individual ion.

Essential aspects of lattice dynamics in the harmonic approximation, such as the dependence of the frequencies on the force constants and masses, the distinction between acoustic and optical branches (see Sects. 3.4 and 3.5), and the anisotropy of the dispersion curves, can be studied already in simplified models as those of Problems 3.1 and 3.2. Moreover, even the reduced dimension assumed in these problems is not hypothetical but corresponds to physical reality: Take the atoms at the surfaces of solids, they move differently from those in the bulk and give rise to investigate surface phonons [85–87]. They represent a (quasi) two-dimensional dynamical system with phonon amplitudes that decay over a few lattice constants away from the surface.

3.2 Normal Coordinates

Having found the eigensolutions of the Hamiltonian (3.8) in the previous section, we now aim at formulating this Hamiltonian in terms of these eigensolutions or *normal coordinates*. We expect that in this representation the Hamiltonian will be that of a set of uncoupled harmonic oscillators, each corresponding to a collective mode.

The displacement of an ion (or atom) can be expressed in terms of the complete set of eigensolutions (3.22)

$$u_{n\tau i}(t) = \frac{1}{\sqrt{NM_\tau}} \sum_{s\mathbf{q}} f_s(\mathbf{q}) e^{-i\omega_s(\mathbf{q})t} e_{\tau i}^s(\mathbf{q}) e^{i\mathbf{q} \cdot \mathbf{R}_n^0}, \quad (3.23)$$

with expansion coefficients $f_s(\mathbf{q})$. The normal coordinate for the collective lattice mode $s\mathbf{q}$ is defined by

$$Q_s(\mathbf{q}, t) = f_s(\mathbf{q}) e^{-i\omega_s(\mathbf{q})t}. \quad (3.24)$$

The following scheme demonstrates the intended transformation from a system with coupled localized motions of the individual masses (or ions) around their equilibrium position to the uncoupled delocalized collective motions with all ions moving in phase:

coupled motion	\Rightarrow	uncoupled collective motion
localized		delocalized
$u_{\mathbf{n}\tau i}(t)$	\rightarrow	$Q_s(\mathbf{q}, t)$
$D_{\tau i, \tau' j}(\mathbf{q})$	\rightarrow	diagonal form with $\omega_s^2(\mathbf{q})$
$H(\mathbf{u}_{\mathbf{n}\tau}, \mathbf{P}_{\mathbf{n}\tau})$	\rightarrow	$H(Q_s(\mathbf{q}), P_s(\mathbf{q}))$.

Starting from the original Hamiltonian $H(\mathbf{u}_{\mathbf{n}\tau}, \mathbf{P}_{\mathbf{n}\tau})$ (3.8) and making use of (3.23) and

$$P_{\mathbf{n}\tau i} = M_\tau \dot{u}_{\mathbf{n}\tau i} = \sqrt{\frac{M_\tau}{N}} \sum_{s\mathbf{q}} \dot{Q}_s(\mathbf{q}, t) e_{\tau i}^s(\mathbf{q}) e^{i\mathbf{q} \cdot \mathbf{R}_n^0}, \quad (3.25)$$

we find the Lagrangian corresponding to $H(Q_s(\mathbf{q}), P_s(\mathbf{q}))$, which can be written as

$$L = \frac{1}{2N} \left(\sum_{\mathbf{n}\tau i} \sum_{s'\mathbf{q}'} \dot{Q}_s(\mathbf{q}) \dot{Q}_{s'}(\mathbf{q}') e^{i(\mathbf{q}+\mathbf{q}') \cdot \mathbf{R}_n^0} e_{\tau i}^s(\mathbf{q}) e_{\tau i}^{s'}(\mathbf{q}') \right. \\ \left. - \sum_{\substack{\mathbf{n}\tau i \\ \tau' j}} \sum_{s'\mathbf{q}'} D_{\tau i, \tau' j}(\mathbf{q}') Q_s(\mathbf{q}) Q_{s'}(\mathbf{q}') e_{\tau i}^s(\mathbf{q}) e_{\tau' j}^{s'}(\mathbf{q}') e^{i(\mathbf{q}+\mathbf{q}') \cdot \mathbf{R}_n^0} \right), \quad (3.26)$$

where, in the second term, the force constants are expressed by the dynamical matrix (3.20). The sum over the lattice points \mathbf{n} can be performed with

$$\frac{1}{N} \sum_{\mathbf{n}} e^{i(\mathbf{q}+\mathbf{q}') \cdot \mathbf{R}_n^0} = \sum_{\mathbf{G}} \delta_{\mathbf{q}', -\mathbf{q}+\mathbf{G}}, \quad (3.27)$$

where \mathbf{G} is a vector of the reciprocal lattice. On the *rhs*, only the term with $\mathbf{G} = 0$ contributes, because \mathbf{q} and \mathbf{q}' are vectors in the first Brillouin zone. The displacements $\mathbf{u}_{\mathbf{n}\tau}$ are real and, therefore,

$$e_{\tau i}^s(-\mathbf{q}) Q_s(-\mathbf{q}, t) = e_{\tau i}^{s*}(\mathbf{q}) Q_s^*(\mathbf{q}, t). \quad (3.28)$$

As this relation holds for arbitrary Q_s and all $e_{\tau i}^s$, we have

$$e_{\tau i}^s(-\mathbf{q}) = e_{\tau i}^{s*}(\mathbf{q}) \quad \text{and} \quad Q_s(-\mathbf{q}, t) = Q_s^*(\mathbf{q}, t), \quad (3.29)$$

and can write the Lagrangian as

$$L = \frac{1}{2} \sum_{\tau i} \sum_{s s'} \left\{ \dot{Q}_s(\mathbf{q}) \dot{Q}_{s'}^*(\mathbf{q}) e_{\tau i}^s(\mathbf{q}) e_{\tau i}^{s'*}(\mathbf{q}) \right. \\ \left. - Q_s(\mathbf{q}) Q_{s'}^*(\mathbf{q}) e_{\tau i}^s \sum_{\tau' j} D_{\tau i, \tau' j}(-\mathbf{q}) e_{\tau' j}^{s'*}(\mathbf{q}) \right\}. \quad (3.30)$$

The sum in the last term on the *rhs* of (3.30) simplifies, because $e_{\tau' j}^{s'*}(\mathbf{q}) = e_{\tau' j}^{s'}(-\mathbf{q})$ is an eigenvector of the dynamical matrix (see (3.19)). The

Hamiltonian (3.8) corresponding to L , formulated in terms of the normal coordinates $Q_s(\mathbf{q}, t)$ and their conjugate momenta

$$P_s(\mathbf{q}, t) = \frac{\partial L}{\partial \dot{Q}_s(\mathbf{q}, t)} = \dot{Q}_s^*(\mathbf{q}, t) \quad (3.31)$$

takes the form

$$H(Q_s(\mathbf{q}), P_s(\mathbf{q})) = \frac{1}{2} \sum_{s\mathbf{q}} \{P_s^*(\mathbf{q})P_s(\mathbf{q}) + \omega_s^2(\mathbf{q})Q_s^*(\mathbf{q})Q_s(\mathbf{q})\}. \quad (3.32)$$

As expected, it describes $3rN$ uncoupled harmonic oscillators, each of which corresponds to a *collective mode* or *elementary excitation* of the lattice (characterized by s and \mathbf{q}). For the individual mode, the equation of motion follows from (3.32)

$$\dot{P}_s^*(\mathbf{q}, t) = -\frac{\partial H}{\partial Q_s^*(\mathbf{q}, t)} \quad \text{or} \quad \ddot{Q}_s(\mathbf{q}, t) = -\omega_s^2(\mathbf{q})Q_s(\mathbf{q}, t), \quad (3.33)$$

and is easily identified as that of a harmonic oscillator.

Note, that the decoupling of the ion motions is possible only in the harmonic approximation. If in the expansion of the adiabatic potential (3.6) higher order terms in the displacements are taken into account, one arrives at nonlinear lattice dynamics, which has to be invoked to describe thermal lattice expansion or the temperature dependence of the frequencies $\omega_s(\mathbf{q})$ [84]. We come back to these properties in Sect. 3.7.

3.3 Phonons and Occupation Number Representation

The lattice dynamics, so far formulated in terms of classical mechanics, can be cast into the language of quantum mechanics by using $Q_s^*(\mathbf{q}) = Q_s(-\mathbf{q})$, $P_s^*(\mathbf{q}) = P_s(-\mathbf{q})$, and converting the conjugate variables $Q_s(\mathbf{q})$ and $P_s(\mathbf{q})$ of the system into operators $\hat{Q}_s(\mathbf{q})$ and $\hat{P}_s(\mathbf{q})$, for which we postulate the commutation relations

$$[\hat{Q}_s(\mathbf{q}), \hat{P}_{s'}(\mathbf{q}')] = i\hbar\delta_{ss'}\delta_{\mathbf{q}\mathbf{q}'} \quad (3.34)$$

$$[\hat{Q}_s(\mathbf{q}), \hat{Q}_{s'}(\mathbf{q}')] = [\hat{P}_s(\mathbf{q}), \hat{P}_{s'}(\mathbf{q}')] = 0. \quad (3.35)$$

Instead of using $\hat{Q}_s(\mathbf{q})$, and $\hat{P}_s(\mathbf{q})$ it is more convenient to introduce for each mode s, \mathbf{q} creation and annihilation operators known from the harmonic oscillator of elementary quantum mechanics

$$a_s^\dagger(\mathbf{q}) = (2\hbar\omega_s(\mathbf{q}))^{-1/2}(\omega_s(\mathbf{q})\hat{Q}_s(-\mathbf{q}) - i\hat{P}_s(\mathbf{q})) \quad (3.36)$$

$$a_s(\mathbf{q}) = (2\hbar\omega_s(\mathbf{q}))^{-1/2}(\omega_s(\mathbf{q})\hat{Q}_s(\mathbf{q}) + i\hat{P}_s(-\mathbf{q})). \quad (3.37)$$

They obey the commutation relations (Problem 3.4)

$$[a_s(\mathbf{q}), a_{s'}^\dagger(\mathbf{q}')] = \delta_{ss'}\delta_{\mathbf{q}\mathbf{q}'}, [a_s(\mathbf{q}), a_{s'}(\mathbf{q}')] = [a_s^\dagger(\mathbf{q}), a_{s'}^\dagger(\mathbf{q}')] = 0. \quad (3.38)$$

With the inverted relations of (3.36) and (3.37),

$$Q_s(\mathbf{q}) = \left(\frac{\hbar}{2\omega_s(\mathbf{q})} \right)^{1/2} (a_s^\dagger(-\mathbf{q}) + a_s(\mathbf{q})) \quad (3.39)$$

$$P_s(\mathbf{q}) = i \left(\frac{\hbar\omega_s(\mathbf{q})}{2} \right)^{1/2} (a_s^\dagger(\mathbf{q}) - a_s(-\mathbf{q})), \quad (3.40)$$

and with $\omega_s(\mathbf{q}) = \omega_s(-\mathbf{q})$, the Hamiltonian of uncoupled harmonic oscillators (3.32) can be written as

$$\hat{H} = \sum_{s\mathbf{q}} \hbar\omega_s(\mathbf{q}) \left(a_s^\dagger(\mathbf{q})a_s(\mathbf{q}) + \frac{1}{2} \right). \quad (3.41)$$

Here, $\hbar\omega_s(\mathbf{q})$ is the energy quantum of the collective lattice mode. This excitation out of the ground state is called *phonon* and $\hbar\omega_s(\mathbf{q})$ is the phonon energy.

Let us contemplate briefly on how we arrived at this Hamiltonian: We started from a classical formulation of the field of lattice displacements in terms of the normal coordinates, imposed the quantization conditions (3.34, 3.35), introduced the creation and annihilation operators (3.36) and (3.37), and achieved a representation in terms of phonons as the quanta of the moving lattice. This procedure is an example of the general concept of *field quantization* [10].

As a reminder of quantum mechanics, we briefly present the properties of annihilation and creation operators for a harmonic oscillator: If $|\Psi\rangle$ is an eigenstate of \hat{H} (3.41) with energy E , then $a_s^\dagger(\mathbf{q})|\Psi\rangle$ (or $a_s(\mathbf{q})|\Psi\rangle$) is also an eigenstate but with energy $E + \hbar\omega_s(\mathbf{q})$ (or $E - \hbar\omega_s(\mathbf{q})$), i.e., with the energy increased (decreased) by one quantum. In other words, applying $a_s^\dagger(\mathbf{q})$ (or $a_s(\mathbf{q})$) to an eigenstate of \hat{H} creates a new eigenstate with one phonon added (removed). As the spectrum of the harmonic oscillator is positive definite, there must be a state $|\Psi_0\rangle$ with the lowest non-negative energy, such that $a_s(\mathbf{q})|\Psi_0\rangle = 0$, indicating that there is no phonon in this state. $|\Psi_0\rangle = |\{0\}\rangle$ is, therefore, called the ground state of the lattice or *phonon vacuum*. Its energy

$$E_0 = \frac{1}{2} \sum_{s\mathbf{q}} \hbar\omega_s(\mathbf{q}) \quad (3.42)$$

is that of the zero point motion of the ions about their equilibrium positions, due to the uncertainty principle. The notation $\{0\}$ is a short writing for entries 0 for all quantum numbers s, \mathbf{q} : $|\{0\}\rangle = |0 \dots 0, \text{all } s, \mathbf{q}\rangle$. Excited states can be generated from the phonon vacuum by applying creation operators that turn the zeros into numbers $n_s(\mathbf{q})$ according to the number of $a_s^\dagger(\mathbf{q})$ applied

to $|\{0\}\rangle$. Because of the commutation relations (3.38) (typical for boson operators), the result is independent of the order of the applied operators. Thus, the eigenstates of \hat{H} have the form $|\{n_s(\mathbf{q})\}\rangle$, all s, \mathbf{q} indicating the number of phonons present in the state: this is the *occupation number representation*. In general, we can write these states as

$$|\{n_s(\mathbf{q})\}\rangle = \prod_{s\mathbf{q}} \frac{1}{\sqrt{n_s(\mathbf{q})!}} (a_s^\dagger(\mathbf{q}))^{n_s(\mathbf{q})} |\{0\}\rangle, \quad (3.43)$$

with a factor introduced for normalization. Their energy eigenvalues are

$$E(\{n_s(\mathbf{q})\}) = E_0 + \sum_{s\mathbf{q}} n_s(\mathbf{q}) \hbar \omega_s(\mathbf{q}). \quad (3.44)$$

By comparing with the Hamiltonian (3.41), $n_s(\mathbf{q})$ is identified as the eigenvalue of the *occupation number operator* $\hat{n}_s(\mathbf{q}) = a_s^\dagger(\mathbf{q})a_s(\mathbf{q})$.

In general, a solid cannot be prepared in a certain eigenstate of the Hamiltonian (3.41), but it can be prepared in a thermodynamic state defined by the temperature. The energy of this state will be given by the thermal expectation value

$$\langle \hat{H} \rangle = \sum_{s\mathbf{q}} \hbar \omega_s(\mathbf{q}) \left(\langle \hat{n}_s(\mathbf{q}) \rangle + \frac{1}{2} \right), \quad (3.45)$$

which, up to the energy of the zero point motion, is the thermal expectation value of the occupation number operator $\hat{n}_\alpha = a_\alpha^\dagger a_\alpha$, $\alpha = s, \mathbf{q}$. As outlined in Sect. 2.3, it is given by

$$\langle \hat{n}_\alpha \rangle = \frac{1}{Z_G} \text{Tr} \left(\hat{n}_\alpha e^{-\beta(\hat{H} - \mu \hat{N})} \right), \quad (3.46)$$

with $\beta = 1/k_B T$, $\hat{N} = \sum_\alpha \hat{n}_\alpha$, the grand-canonical partition function Z_G , and the chemical potential μ , which for massless particles (as for phonons) is zero. We may write $\hat{H} = E_0 + \sum_{\alpha'} \hat{n}_{\alpha'} \hbar \omega_{\alpha'}$ and obtain in occupation number representation

$$\langle \hat{n}_\alpha \rangle = \frac{e^{-\beta E_0}}{Z_G} \sum_{N=0}^{\infty} \sum_{\{n_{\alpha'}\}_N} n_\alpha e^{-\beta \sum_{\alpha'} n_{\alpha'} \hbar \omega_{\alpha'}}. \quad (3.47)$$

Here $\{n_{\alpha'}\}_N$ stands for sets of occupation numbers $n_{\alpha'}$ with $\sum_{\alpha'} n_{\alpha'} = N$. Instead of summing over N and sets of occupation numbers with total occupancy N , we can sum over all sets of occupation numbers without restriction. Moreover, the sum over the occupation number n_α for the mode α may be separated as a factor to yield

$$\langle \hat{n}_\alpha \rangle = \frac{e^{-\beta E_0}}{Z_G} \sum_{n_\alpha=0}^{\infty} n_\alpha e^{-\beta \sum_\alpha n_\alpha \hbar \omega_\alpha} \sum_{\substack{\{n_{\alpha'}\} \\ \alpha' \neq \alpha}} e^{-\beta \sum_{\alpha' \neq \alpha} n_{\alpha'} \hbar \omega_{\alpha'}}. \quad (3.48)$$

Given the grand-canonical partition function

$$Z_G = e^{-\beta E_0} \sum_{\{n_{\alpha'}\}} e^{-\beta \sum_{\alpha'} n_{\alpha'} \hbar \omega_{\alpha'}}, \quad (3.49)$$

this reduces to

$$\langle \hat{n}_\alpha \rangle = \frac{\sum_n n e^{-\beta n \hbar \omega_\alpha}}{\sum_n e^{-\beta n \hbar \omega_\alpha}} = \frac{\sum_n n x^n}{\sum_n x^n}, \quad (3.50)$$

where $x = e^{-\beta \hbar \omega_\alpha}$, which can be evaluated with

$$\langle \hat{n}_\alpha \rangle = \frac{x(1 + 2x + 3x^2 + \dots)}{1 + x + x^2 + \dots} = \frac{x(1-x)}{(1-x)^2} = \frac{x}{1-x}. \quad (3.51)$$

The final result for the thermal expectation value $\langle \hat{n}_s(\mathbf{q}) \rangle$ of the number of phonons with s, \mathbf{q} written as

$$n_s(\mathbf{q}, T) = \frac{1}{e^{\beta \hbar \omega_s(\mathbf{q})} - 1} \quad (3.52)$$

is the *Bose–Einstein distribution* function. Here, the dependence of the phonon occupancy on the temperature (remember: $\beta = 1/k_B T$) is explicitly considered in the notation. More complex thermal expectation values of phonon operators like those of Problem 3.5 can be calculated and will be needed later.

A quantity frequently used to characterize a phonon spectrum and to interpret experimental data is the *density of states* (or phonon density of states, to distinguish from the electron density of states that will be introduced in Chaps. 4 and 5), defined by

$$D(\omega) = \sum_{s\mathbf{q}} \delta(\omega - \omega_s(\mathbf{q})). \quad (3.53)$$

It counts the number of phonon modes (or states) at a frequency ω by summing over all branches in the first Brillouin zone. Instead of summing over the discrete \mathbf{q} values (see (3.18)), we may assign to each of them the volume $(2\pi)^3/V$ in \mathbf{q} space (see Problem 3.3), to write $D(\omega)$ as an integral over the Brillouin zone (here V is the crystal volume)

$$D(\omega) = \frac{V}{(2\pi)^3} \sum_s \int_{BZ} \delta(\omega - \omega_s(\mathbf{q})) d^3\mathbf{q}. \quad (3.54)$$

The three-dimensional integration over the δ function reduces to a two-dimensional integral over surfaces $S_{\mathbf{q}}$ in \mathbf{q} space, for which $\omega = \omega_s(\mathbf{q})$ and we may write

$$D(\omega) = \frac{V}{(2\pi)^3} \sum_s \int_{S_{\mathbf{q}}} \frac{dS_{\mathbf{q}}}{|\nabla_{\mathbf{q}} \omega_s(\mathbf{q})|}. \quad (3.55)$$

The integrand increases with the flatness of the dispersion curve and we expect singular behavior if $|\nabla_{\mathbf{q}}\omega_s(\mathbf{q})| = 0$, which defines a *van Hove singularity* [88] and the corresponding \mathbf{q} as *critical point* (for a classification of the critical points see [21, 89]). An example of $D(\omega)$ is shown in Fig. 3.13 for GaAs. It is clearly seen that the critical points cause pronounced structures in the density of states. Especially the rather flat dispersion curves of the optical phonons result in characteristic peaks.

3.4 Acoustic Phonons

Common to the phonon dispersions of all solids is the group of lowest branches with frequencies starting from the center of the Brillouin zone, with linear dependence on the wave vector (see the solutions of Problems 3.1 and 3.2). This particular property being connected with sound propagation, as will be discussed later in this section, has led to the term *acoustic phonons*. The other important aspect of these phonons with the smallest quanta of energy is that they dominate the low-temperature *specific heat* of the crystal lattice. If the solid is heated, starting from the ground state at $T = 0$ K, the macroscopic change of the temperature is connected microscopically with the creation, first of all, of acoustic phonons. This addition of energy in a quantized form is responsible for a peculiar behavior of the specific heat at low temperatures to which we turn our attention at the beginning of this section.

The specific heat is the change of the thermal energy $E(T)$ with the temperature T . The thermal energy of the crystal lattice, connected with the thermal motion of the ions (or atoms), can be calculated as the thermal expectation value of the Hamiltonian \hat{H} (3.41)

$$E(T) = E_0 + \sum_{s\mathbf{q}} n_s(\mathbf{q}, T) \hbar\omega_s(\mathbf{q}). \quad (3.56)$$

Let us first consider the classical limit of this general expression, which is valid for sufficiently large temperatures $\hbar\omega_s(\mathbf{q}) \ll k_B T$, i.e., for a phonon energy much smaller than the average thermal energy per degree-of-freedom. In this case, the phonon occupation simplifies according to

$$n_s(\mathbf{q}, T) = \left(e^{\beta\hbar\omega_s(\mathbf{q})} - 1 \right)^{-1} \simeq \frac{k_B T}{\hbar\omega_s(\mathbf{q})}. \quad (3.57)$$

As we can also neglect the ground state energy E_0 (as compared to $k_B T$), the thermal energy of the lattice is given by

$$E(T) \simeq \sum_{s\mathbf{q}} k_B T = 3r N k_B T. \quad (3.58)$$

Taking the derivative with respect to T (at constant volume)

$$c_V = \left. \frac{dE(T)}{dT} \right|_{V=\text{const}} = 3rNk_B, \quad (3.59)$$

we find the classical result of the *Dulong–Petit law*, according to which at high temperatures each degree of freedom contributes k_B to the specific heat.

When approaching the low temperature regime, the phonon energy $\hbar\omega_s(\mathbf{q})$ is not much smaller than $k_B T$, and its discreteness has to be taken into account in evaluating the thermal energy. This can be done within what is known as the *Debye¹ model*. It is based on the assumption that at low temperatures only acoustic phonons are excited and that their dispersion is isotropic and follows $\omega_s(\mathbf{q}) = vq$ with the same *sound velocity* v for all three acoustic branches. Under these assumptions the sum over \mathbf{q} in (3.56) can be evaluated as an integral

$$E(T) = E_0 + \frac{V}{(2\pi)^3} \sum_s \int \frac{\hbar\omega_s(q)}{e^{\beta\hbar\omega_s(q)} - 1} d^3\mathbf{q}. \quad (3.60)$$

The limitation of the sum over \mathbf{q} to values within the first Brillouin zone has to be considered in the integral over q by a cut-off radius q_D , thus the Brillouin zone is replaced by a sphere of the same size, containing N states

$$N = \frac{V}{(2\pi)^3} 4\pi \int_0^{q_D} q^2 dq, \quad (3.61)$$

which yields $q_D = (6\pi^2 N/V)^{1/3}$. This cut-off in q space can be converted into a cut-off frequency, the *Debye frequency*

$$\omega_D = v \left(6\pi^2 \frac{N}{V} \right)^{1/3}. \quad (3.62)$$

The energy quantum $\hbar\omega_D$ is frequently expressed as a temperature $\Theta_D = \hbar\omega_D/k_B$, the *Debye temperature*. A collection of Debye temperatures is given in Table 3.1. Note that ω_D and Θ_D are proportional to the sound velocity v . For C(diamond), it is with 10,000–20,000 m s^{-1} (depending on the acoustic branch and the direction of propagation), the highest known for solids, while for Ne, which can be solidified only at low temperatures, it is significantly smaller. Within the solids consisting of group-IV elements (C, Si, Ge, all in the diamond structure) the Debye temperature decreases with increasing mass

Table 3.1. Debye temperatures in K of some solids

	C	Si	Ge	Al	Cu	Ne
Θ_D	1,860	625	360	394	315	63

¹ Peter Joseph Debye 1884–1966, Nobel prize in chemistry 1936

of the ions. The fcc metals Al and Cu, in spite of their different ion masses, have quite similar Debye temperatures.

Substituting $q = \omega/v$, the thermal energy of the lattice (3.60) can be written as

$$E(T) = E_0 + \frac{3V}{2\pi^2 v^3} \int_0^{\omega_D} \frac{\hbar\omega^3}{e^{\beta\hbar\omega} - 1} d\omega, \quad (3.63)$$

where we may identify $D(\omega) = V\omega^2/2\pi^2 v^3$ with the density of states for each branch of the Debye model. It is a smooth function and does not exhibit critical points, because of the assumed linear dispersion and the neglect of Bragg reflection at Brillouin zone boundaries. By introducing the dimensionless variable $x = \beta\hbar\omega$ ($x_D = \beta\hbar\omega_D$), one has

$$E(T) = E_0 + 3Nk_B T \frac{3}{x_D^3} \int_0^{x_D} \frac{x^3}{e^x - 1} dx. \quad (3.64)$$

The integral belongs to a class of similar expressions with different powers of x (see Appendix A.3). For $T \rightarrow 0$ (and $x_D \rightarrow \infty$) it approaches $\pi^4/15$, giving for the thermal energy

$$E(T) \rightarrow E_0 + 3Nk_B T \frac{\pi^4}{5} \left(\frac{T}{\Theta_D} \right)^3. \quad (3.65)$$

Thus, in the low-temperature limit the specific heat exhibits a characteristic T^3 dependence

$$c_V(T) = \left. \frac{dE(T)}{dT} \right|_{V=\text{const}} = 3Nk_B \frac{4\pi^4}{5} \left(\frac{T}{\Theta_D} \right)^3 \quad (3.66)$$

which is known as the *Debye law*.

The observed vanishing of the lattice specific heat at low temperatures had puzzled physicists for quite some time. In 1905, Einstein came up with a first explanation based on the assumption of dispersionless oscillators, as in the derivation of the law for black-body radiation by Max Planck² in 1900, but did not yield the experimental T^3 -law. Therefore, the correct derivation of this law within the Debye model in 1912 was the breakthrough in demonstrating the quantum nature of lattice vibrations. In Chap. 4, the specific heat of free electrons in metals will be discussed, which adds a contribution depending linearly on T at low temperature.

Another effect of the thermal motion of the lattice can be detected in scattering experiments as a reduction of the scattering amplitude. It is described by the *Debye-Waller factor* (see Sect. 3.7), which is calculated in Problem 3.6.

Let us now turn to the elastic properties of solids by studying acoustic phonons in the long-wavelength limit $q \rightarrow 0$, for which all atoms in a unit cell

² Max Karl Ernst Ludwig Planck 1858–1947, Noble prize in physics 1918

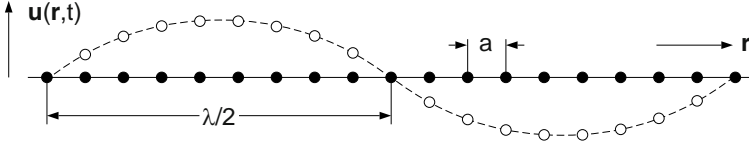


Fig. 3.3. Transverse ion displacements of an acoustic mode in the long-wavelength limit

move with the same phase. In this case, the equation of motion (3.10) can be written in the form

$$M\ddot{u}\left(\begin{matrix} \mathbf{n} \\ i \end{matrix}\right) = -\sum_{\mathbf{m}j} \Phi\left(\begin{matrix} \mathbf{n} & \mathbf{m} \\ i & j \end{matrix}\right) u\left(\begin{matrix} \mathbf{m} \\ j \end{matrix}\right), \quad (3.67)$$

where $M = \sum_{\tau} M_{\tau}$. If the lattice moves in an acoustic mode, the displacements at nearby lattice points differ only little from each other, thus, making up a wave like distortion with a wavelength λ much larger than the lattice constant a . The situation is depicted in Fig. 3.3 for a transverse mode of the linear chain.

The limit $q \rightarrow 0$, called the continuum limit, allows us to consider instead of the displacements of the discrete ions, a continuous displacement field $\mathbf{u}(\mathbf{r}, t)$ with the aim to derive the equation of motion. In view of this continuous displacement field, let us write

$$u\left(\begin{matrix} \mathbf{n} \\ i \end{matrix}\right) = u_i(\mathbf{R}_{\mathbf{n}}^0, t) \quad (3.68)$$

and expand the displacement $u_j(\mathbf{R}_{\mathbf{m}}^0, t)$ at a nearby lattice point $\mathbf{R}_{\mathbf{m}}^0$ around $\mathbf{R}_{\mathbf{n}}^0$

$$\begin{aligned} u_j(\mathbf{R}_{\mathbf{m}}^0, t) &= u_j(\mathbf{R}_{\mathbf{n}}^0, t) + \sum_k \left. \frac{\partial u_j}{\partial r_k} \right|_{\mathbf{R}_{\mathbf{n}}^0} \mathbf{R}_{\mathbf{m}k}^0 \\ &+ \frac{1}{2} \sum_{kl} \left. \frac{\partial^2 u_j}{\partial r_k \partial r_l} \right|_{\mathbf{R}_{\mathbf{n}}^0} \mathbf{R}_{\mathbf{m}k}^0 \mathbf{R}_{\mathbf{m}l}^0 + \dots \end{aligned} \quad (3.69)$$

with derivatives of the continuous function $u_j(\mathbf{r}, t)$, with respect to the components of \mathbf{r} . When being used in the equation of motion (3.67), the first and second term of this expansion do not contribute because of the properties of the force constants discussed in Sect. 3.1, and we find

$$M\ddot{u}\left(\begin{matrix} \mathbf{n} \\ i \end{matrix}\right) = -\frac{1}{2} \sum_{jkl} \sum_{\mathbf{m}} \Phi\left(\begin{matrix} \mathbf{n} & \mathbf{m} \\ i & j \end{matrix}\right) \mathbf{R}_{\mathbf{m}k}^0 \mathbf{R}_{\mathbf{m}l}^0 \left. \frac{\partial^2 u_j}{\partial r_k \partial r_l} \right|_{\mathbf{R}_{\mathbf{n}}^0} + \dots \quad (3.70)$$

still expressed in terms of the discrete lattice points. The continuum limit is now completed by replacing the discrete masses M with the mass density

per unit (or Wigner–Seitz) cell, $\rho_M = M/V_{\text{cell}}$ and the displacements at the discrete lattice points by the continuous displacement field $u_i(\mathbf{r}, t)$:

$$\rho_M \ddot{u}_i = \sum_{jkl} c_{ijkl} \frac{\partial^2 u_j}{\partial r_k \partial r_l}. \quad (3.71)$$

Here, the coefficients

$$c_{ijkl} = -\frac{1}{2V_{\text{cell}}} \sum_{\mathbf{m}} \Phi \begin{pmatrix} \mathbf{n} & \mathbf{m} \\ i & j \end{pmatrix} \mathbf{R}_{\mathbf{m}k}^0 \mathbf{R}_{\mathbf{m}l}^0 \quad (3.72)$$

are the *elastic* or *stiffness constants*.

Equation (3.71), which is the wave equation for the elastic continuum, can be simplified by making the reasonable assumption that the force constants derived from the adiabatic potential $\mathcal{U}(\{\mathbf{R}_n\})$ are due to central forces between the ions, thus,

$$\Phi \begin{pmatrix} \mathbf{n} & \mathbf{m} \\ i & j \end{pmatrix} = g(|\mathbf{R}_m - \mathbf{R}_n|) \mathbf{R}_{\mathbf{m}i}^0 \mathbf{R}_{\mathbf{m}j}^0 \quad (3.73)$$

and

$$c_{ijkl} = -\frac{1}{V_{\text{cell}}} \sum_{\mathbf{m}} g(|\mathbf{R}_m - \mathbf{R}_n|) \mathbf{R}_{\mathbf{m}i}^0 \mathbf{R}_{\mathbf{m}j}^0 \mathbf{R}_{\mathbf{m}k}^0 \mathbf{R}_{\mathbf{m}l}^0. \quad (3.74)$$

In this form, i.e., due to the assumed central forces, the components of the elasticity tensor are invariant under exchange of any two of the indices, and the *rhs* of (3.71) can be rewritten as

$$\sum_{jkl} c_{ijkl} \frac{\partial^2 u_j}{\partial r_k \partial r_l} = \sum_j \sum_{kl} c_{ikjl} \frac{\partial \epsilon_{jl}}{\partial r_k}, \quad (3.75)$$

where we have introduced the components of the *strain tensor*

$$\epsilon_{jl} = \frac{1}{2} \left(\frac{\partial u_j}{\partial r_l} + \frac{\partial u_l}{\partial r_j} \right). \quad (3.76)$$

The long-wave length limit or continuum approximation, considered here, implies that the strain tensor field is locally homogeneous on a length-scale, limited by the wave length λ of the acoustic phonon mode. This homogeneous strain is related to a homogeneous stress, σ_{ik} , by *Hooke's³ law*

$$\sigma_{ik} = \sum_{jl} c_{ikjl} \epsilon_{jl}, \quad (3.77)$$

which belongs to the family of linear-response relations (see Chap. 1), with the fourth rank tensor of elastic constants as the response function. As the

³ Robert Hooke 1635–1703

stress and strain tensors are symmetric, one has $c_{ikjl} = c_{kijl} = c_{iklj} = c_{kilj}$ and the number of independent elastic constants c_{ikjl} is reduced to 21. If the strain is understood as the response of the elastic continuum to an applied stress, the inverted relation to (3.77) reads

$$\epsilon_{ij} = \sum_{kl} s_{ijkl} \sigma_{kl}, \tag{3.78}$$

with the *elastic moduli* or *compliance constants* s_{ijkl} . With Hooke’s law, the wave equation for the elastic continuum takes the final form

$$\rho_M \ddot{u}_i = \sum_k \frac{\partial}{\partial r_k} \sigma_{ik}. \tag{3.79}$$

By definition, the strain and stress tensors are symmetric, e.g.,

$$\epsilon = \begin{pmatrix} \epsilon_{11} & \epsilon_{12} & \epsilon_{13} \\ \epsilon_{12} & \epsilon_{22} & \epsilon_{23} \\ \epsilon_{13} & \epsilon_{23} & \epsilon_{33} \end{pmatrix}, \tag{3.80}$$

thus having in general six independent components, which frequently are cast into a vector or *Voigt⁴ notation* according to the scheme

<i>ik</i>	11	22	33	23	13	12	matrix notation
<i>I</i>	1	2	3	4	5	6	Voigt notation

in which Hooke’s law (3.77) takes the form

$$\sigma_I = \sum_{J=1}^6 c_{IJ} \epsilon_J. \tag{3.81}$$

The number of independent elastic constants is further decreased by crystal symmetry (as was the case for the force constants) and can be looked up in the literature [90, 91]. For cubic crystal structures, there are only three independent elastic constants, which in Voigt notation are $c_{11} = c_{22} = c_{33}$, $c_{23} = c_{13} = c_{12}$, and $c_{44} = c_{55} = c_{66}$ (Problem 3.7). For this case, the wave equation (10.6) can be turned into eigenvalue equations for the components of the normalized eigenvector \mathbf{e} , using

$$\mathbf{u}(\mathbf{r}, t) \sim \mathbf{e} e^{i(\mathbf{q} \cdot \mathbf{r} - \omega t)}. \tag{3.82}$$

For the first component, it reads

$$\omega^2 \rho_M e_1 = (c_{11} q_1^2 + c_{44} (q_2^2 + q_3^2)) e_1 + (c_{12} + c_{44}) q_1 (q_2 e_2 + q_3 e_3) \tag{3.83}$$

and similar equations for the other components are obtained by cyclic permutation of the indices. The eigenfrequencies depend on the direction of

⁴ Woldemar Voigt 1850–1919

propagation and the surfaces of constant frequency are not spherical but warped. As a consequence, the group velocity is anisotropic and phonon wave packets propagate preferentially in the direction of zero curvature, giving rise to caustics. This *phonon focusing* is connected with the energy flux and can be measured by propagating heat pulses [74, 92, 93].

A further simplification is possible by assuming, instead of cubic symmetry, an isotropic solid (conceivable in the continuum limit), for which $c_{11} = c_{12} + 2c_{44}$ and

$$\omega^2 \rho_M \mathbf{e} = (c_{12} + c_{44}) \mathbf{q}(\mathbf{q} \cdot \mathbf{e}) + c_{44} q^2 \mathbf{e}. \quad (3.84)$$

The solutions of this equation can clearly be distinguished as longitudinal waves, with $\mathbf{e} \parallel \mathbf{q}$ and $\rho_M \omega_L^2 = (c_{12} + 2c_{44})q^2$, and transverse waves, with $\mathbf{e} \perp \mathbf{q}$ and $\rho_M \omega_T^2 = c_{44}q^2$. The corresponding sound velocities $v = \omega/q$ are

$$\begin{aligned} \text{longitudinal sound velocity : } v_L &= \sqrt{\frac{c_{12} + 2c_{44}}{\rho_M}} \\ \text{transverse sound velocity : } v_T &= \sqrt{\frac{c_{44}}{\rho_M}} < v_L. \end{aligned} \quad (3.85)$$

Measuring the sound velocities in solids provides information about the elastic properties and allows one to determine the elastic constants (see Problem 3.7). In general, the velocities for longitudinal sound propagation (and the corresponding frequencies) are larger than those for transverse sound propagation in the same direction. Within the simple mechanical model this can be understood by the stronger distortions of the springs, if the masses are displaced parallel (and not perpendicular) to the propagation direction. This fact can also be expressed in terms of the compliance constants (or elastic moduli) s_{IJ} . The isotropic solid is characterized by only two independent moduli, s_{11} and s_{12} , which are used to define [94]

$$\text{Young's modulus } E = 1/s_{11} \quad (3.86)$$

$$\text{rigidity modulus } G = 1/(2(s_{11} - s_{12})) \quad (3.87)$$

$$\text{bulk modulus } B_0 = 1/(3(s_{11} + 2s_{12})) \quad (3.88)$$

$$\text{Poisson's ratio } \nu = -s_{12}/s_{11} \quad (3.89)$$

corresponding to longitudinal (E) and transverse (G) distortions and volume changes (B_0). The rigidity modulus also is called shear modulus. The bulk modulus is the inverse of the volume *compressibility*. The elastic properties of isotropic homogeneous systems can be characterized by two parameters, the Lamé constants, which can be expressed by Poisson's ratio and Young's modulus according to

$$\lambda = \frac{\nu E}{(1 + \nu)(1 - 2\nu)} \quad (3.90)$$

$$\mu = \frac{E}{2(1 + \nu)}. \quad (3.91)$$

3.5 Optical Phonons

Phonon dispersions of solids with a crystal structure, containing more than one atom in the unit cell exhibit, besides the acoustic phonons, additional branches starting with finite frequencies at $\mathbf{q} = 0$ in the center of the Brillouin zone. An example has been dealt with in Problem 3.1. We know from its solution, that in this phonon mode the atoms of the unit cell move π out of phase with each other as demonstrated in Fig. 3.4. Some of these phonons are dipole active, i.e., they can be excited optically by infra-red light, thus, determining the response of the solid to the external electric field of an electromagnetic wave in this spectral range. They are, therefore, called *optical phonons*. Their properties will be the subject of this section.

Let us consider the situation for a crystal unit cell with two ions carrying charges η_τ , where $\tau = \pm$ is the index for the basis, as depicted in Fig. 3.4. The electric dipole moment of the solid (here denoted as \mathbf{M}) can be expressed as

$$\mathbf{M} = \sum_{\mathbf{n}, \tau} \eta_\tau (\mathbf{R}_{\mathbf{n}\tau}^0 + \mathbf{u}_{\mathbf{n}\tau}). \quad (3.92)$$

For the static lattice in equilibrium, $\mathbf{M}^0 = \sum_{\mathbf{n}, \tau} \eta_\tau \mathbf{R}_{\mathbf{n}\tau}^0$ defines the spontaneous electric dipole moment. Solids with $\mathbf{M}^0 \neq 0$ are called ferroelectric. We consider here the case $\mathbf{M}^0 = 0$, which results for the considered binary solid with two ions with opposite charge in the unit cell. An electric field drives the two charged ions into opposite directions, thus, inducing a dipole moment. In a time-dependent electric field $\mathbf{E}(t)$, this system can be resonantly excited at the frequency of the optical phonon. In the language of the response formalism, the system Hamiltonian (3.41) has to be extended by the time-dependent perturbation (see (2.58))

$$V_{\text{ext}}(t) = -\mathbf{M} \cdot \mathbf{E}(t). \quad (3.93)$$

It causes a (dielectric) polarization with components

$$P_i = \frac{M_i}{V} = \sum_j \chi_{ij} E_j, \quad i, j = 1, 2, 3 \quad (3.94)$$

with the *dielectric susceptibility* χ as a response function, which is a symmetric second rank tensor. The vector components P_i and M_j can be identified with

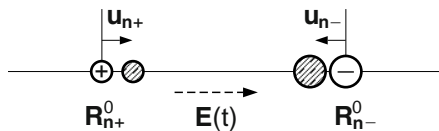


Fig. 3.4. Characteristic ion displacements in a unit cell for an optical phonon

the observables \hat{A} and \hat{B} , respectively, of the response formalism outlined in Chap. 2. After Fourier transformation, we write

$$\langle P_i \rangle_\omega = \sum_j \frac{i}{\hbar V} \int_{-\infty}^{+\infty} e^{i\omega t} \theta(t) \langle [\hat{M}_i(t), \hat{M}_j(0)] \rangle_0 dt E_j(\omega) \quad (3.95)$$

$$= \sum_j \chi_{ij}(\omega) E_j(\omega), \quad (3.96)$$

with the dipole operator given by

$$\hat{M}(t) = \sum_{n\tau} \eta_\tau \hat{u}_{n\tau}(t) = \sum_{s\mathbf{q}} \sum_{n\tau} \frac{\eta_\tau}{\sqrt{NM_\tau}} e_\tau^s(\mathbf{q}) e^{i\mathbf{q} \cdot \mathbf{R}_n^0} Q_s(\mathbf{q}, t). \quad (3.97)$$

The normal coordinate $Q_s(\mathbf{q}, t)$ can be expressed in terms of phonon operators to write

$$\hat{M}_i(t) = \sum_{s\mathbf{q}} M_i^s(\mathbf{q}) (a_s^\dagger(-\mathbf{q}, t) + a_s(\mathbf{q}, t)), \quad (3.98)$$

with the component

$$M_i^s(\mathbf{q}) = \sum_{n\tau} \eta_\tau \left(\frac{\hbar}{2NM_\tau \omega_s(\mathbf{q})} \right)^{1/2} e_{\tau i}^s(\mathbf{q}) e^{i\mathbf{q} \cdot \mathbf{R}_n^0} \quad (3.99)$$

of the dipole moment connected with a phonon in the mode s, \mathbf{q} . The dipole correlation function $\langle [\hat{M}_i(t), \hat{M}_j(0)] \rangle_0$ can be evaluated using Problem 3.5, together with $n_s(\mathbf{q}, T) = n_s(-\mathbf{q}, T)$ to write

$$\langle [a_s^\dagger(-\mathbf{q}, t), a_{s'}(\mathbf{q}', 0)] \rangle_0 = -\delta_{ss'} \delta_{-\mathbf{q}\mathbf{q}'} e^{i\omega_s(-\mathbf{q})t} \quad (3.100)$$

and yields, with $\omega_s(\mathbf{q}) = \omega_s(-\mathbf{q})$,

$$\langle [\hat{M}_i(t), \hat{M}_j(0)] \rangle_0 = \sum_{s\mathbf{q}} M_i^s(\mathbf{q}) M_j^s(-\mathbf{q}) \left\{ -e^{i\omega_s(\mathbf{q})t} + e^{-i\omega_s(\mathbf{q})t} \right\}. \quad (3.101)$$

Let us now consider the limit of long wavelengths $\lambda \gg a$ (where $|\mathbf{q}| = 2\pi/\lambda$ and a is the lattice constant), which holds for far-infrared light, to simplify $M_i(\mathbf{q})$ with the dipole approximation

$$e^{i\mathbf{q} \cdot \mathbf{R}_n^0} = 1 + i\mathbf{q} \cdot \mathbf{R}_n^0 + \dots \simeq 1 \quad (3.102)$$

and distinguish between longitudinal ($s = \text{L}$) and transverse phonons ($s = \text{T}$) with the properties

$$\mathbf{M}^{\text{L}} \parallel \mathbf{e}_\tau^{\text{L}}(\mathbf{q}) \parallel \mathbf{q} \quad \text{and} \quad \mathbf{M}^{\text{T}} \parallel \mathbf{e}_\tau^{\text{T}}(\mathbf{q}) \perp \mathbf{q}, \quad \text{respectively.} \quad (3.103)$$

In the first case and for an electromagnetic wave propagating in the direction of \mathbf{q} , one has $\mathbf{M}^{\text{L}} \cdot \mathbf{E} = 0$, i.e., the transverse light cannot excite a longitudinal

phonon mode. In the second case, there is a contribution to $\langle \mathbf{P} \rangle_\omega$ and thus, to the susceptibility. In the long-wavelength limit, with

$$M_i^T(\mathbf{q} \rightarrow 0) = \left(\frac{\hbar}{2\omega_T(0)} \right)^{1/2} \sum_\tau \eta_\tau \sqrt{\frac{N}{M_\tau}} e_{\tau i}^T(0) =: M_i^T, \quad (3.104)$$

one finds for the dielectric susceptibility

$$\chi_{ij}(\omega) = \lim_{\Gamma \rightarrow 0} \frac{iM_i^T M_j^{T*}}{\hbar V} \int_0^\infty \left\{ e^{i(\omega_T(0) + \omega + i\Gamma)t} - e^{-i(\omega_T(0) - \omega - i\Gamma)t} \right\} dt. \quad (3.105)$$

Here, the exponential with the parameter Γ has been introduced for the adiabatic switching on of the perturbation V_{ext} of (3.93), and the lower integration limit is a consequence of the step function in (3.95). After integration, one has

$$\chi_{ij}(\omega) = \lim_{\Gamma \rightarrow 0} \frac{M_i^T M_j^{T*}}{\hbar V} \left\{ \frac{1}{\omega_T(0) + \omega + i\Gamma} + \frac{1}{\omega_T(0) - \omega - i\Gamma} \right\}. \quad (3.106)$$

The susceptibility exhibits a characteristic pole structure in the complex ω -plane, with poles at $\omega = \pm\omega_T(0) - i\Gamma$ (see Fig. 3.5a) and frequencies $\omega_T(0) = \omega_T$ in the infra-red spectral range.

For solids with a cubic lattice, $\chi_{ij}(\omega)$ simplifies to a scalar $\chi_{ij}(\omega) = \chi(\omega)\delta_{ij}$, which determines the complex frequency-dependent dielectric function

$$\varepsilon(\omega) = \varepsilon_\infty + \frac{1}{\varepsilon_0} \chi(\omega) = \varepsilon_1(\omega) + i\varepsilon_2(\omega), \quad (3.107)$$

where ε_0 is the vacuum dielectric constant, while ε_∞ accounts for the dielectric background, which is caused by contributions of oscillators in the electronic

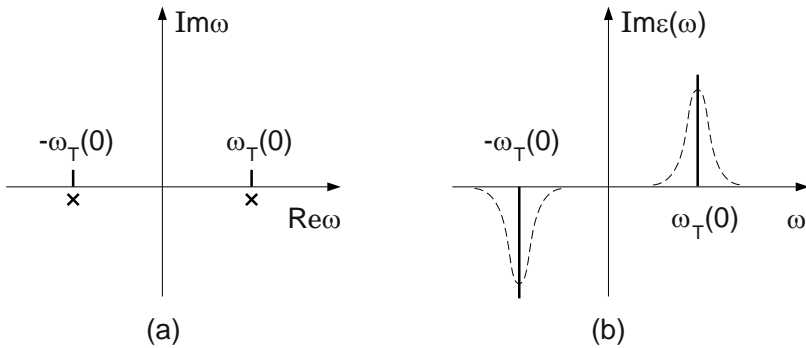


Fig. 3.5. (a) Complex ω plane with poles of the dielectric function; (b) Real part of the dielectric function without (*solid*) and with (*dashed*) damping vs. frequency

system of the solid (see Chaps. 4 and 5), with resonances at much higher frequencies than those of the optical phonons. Therefore, it is called *high-frequency dielectric constant*. The imaginary part of the dielectric function is related to the *absorption coefficient* (see Chap. 10) and takes the form

$$\begin{aligned}\varepsilon_2(\omega) &= \text{Im} \frac{\chi(\omega)}{\varepsilon_0} \\ &= \lim_{\Gamma \rightarrow 0} \frac{|M^\Gamma|^2}{\hbar V \varepsilon_0} \left\{ \frac{\Gamma}{(\omega_T - \omega)^2 + \Gamma^2} - \frac{\Gamma}{(\omega_T + \omega)^2 + \Gamma^2} \right\}. \quad (3.108)\end{aligned}$$

Each term in the last bracket is a Lorentzian, which for $\Gamma \rightarrow 0$ becomes a δ function peaked at $\omega = -\omega_T$ and $\omega = \omega_T$ (see Fig. 3.5b), corresponding to emission and absorption respectively of an optical phonon at $\mathbf{q} = 0$. Note, that this final result with the δ functions would also result by applying (2.77) directly to (3.106) for $i = j$. Combining both terms, the real and imaginary part of the dielectric function can be written as

$$\varepsilon_1(\omega) = \varepsilon_\infty + \lim_{\Gamma \rightarrow 0} \frac{|M^\Gamma|^2}{\hbar V \varepsilon_0} \frac{2\omega_T(\omega_T^2 - \omega^2)}{(\omega_T^2 - \omega^2)^2 + \omega^2\Gamma^2}, \quad (3.109)$$

$$\varepsilon_2(\omega) = \lim_{\Gamma \rightarrow 0} \frac{|M^\Gamma|^2}{\hbar V \varepsilon_0} \frac{2\omega_T\omega\Gamma}{(\omega_T^2 - \omega^2)^2 + \omega^2\Gamma^2}. \quad (3.110)$$

We note in passing that $\varepsilon_1(\omega)$ and $\varepsilon_2(\omega)$ are connected with each other by the Kramers–Kronig relations (see Sect. 2.6).

The parameter Γ is introduced as a mathematical trick to regularize the integral in (3.105). But in a more general view, it can be understood as also being caused by interactions not explicitly included in the present model. By taking into account electron–phonon interaction (see Chap. 7) or anharmonic effects due to higher order terms in the expansion (3.6) it would be finite, thus, indicating a finite phonon lifetime or a damping of the phonon oscillator. In fact, an optical phonon can decay into two acoustic phonons. Microscopically, such processes mean dissipation of energy from the optical phonon to other degrees of freedom.

We go into a more detailed discussion of the optical properties by looking at $\varepsilon_1(\omega)$ and the reflection coefficient $R(\omega)$, which are plotted in Fig. 3.6. For $\omega = 0$ (and $\Gamma = 0$), the real part of the dielectric function can be written as $\varepsilon(0) = \varepsilon_\infty + S/\omega_T^2$, known as the *static dielectric constant*, while for frequencies $\omega \gg \omega_T$ (or $\omega \rightarrow \infty$ in (3.109)) it approaches the high frequency value ε_∞ . In-between, it passes through the resonance at ω_T and is negative up to a frequency identified with that of the longitudinal phonon ω_L at which $\varepsilon_1(\omega_L) = 0$. Without damping, this relation yields

$$\omega_L^2 = \omega_T^2 + \frac{S}{\varepsilon_\infty} > \omega_T^2. \quad (3.111)$$

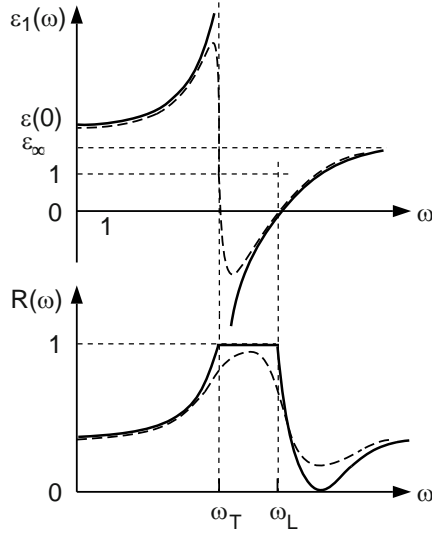


Fig. 3.6. Real part of the dielectric function (*upper part*) and reflection coefficient (*lower part*) without (*solid*) and with (*dashed*) damping vs. frequency

By including Γ , one obtains the dashed curve for $\varepsilon_1(\omega)$ in Fig. 3.6, which is characteristic for a damped oscillator with frequency ω_T .

The reflection coefficient is defined by the complex index of refraction $N = n_1 + in_2$ (all quantities depending on ω):

$$R(\omega) = \left| \frac{1 - N(\omega)}{1 + N(\omega)} \right| = \left(\frac{(1 - n_1(\omega))^2 + n_2^2(\omega)}{(1 + n_1(\omega))^2 + n_2^2(\omega)} \right)^{1/2}. \quad (3.112)$$

Without damping, using $\varepsilon_1 = n_1^2 - n_2^2$, and $\varepsilon_2 = 2n_1n_2$, we find in the interval $\omega_T < \omega < \omega_L$ that ε_1 is negative while ε_2 vanishes, which leads to $n_1 = 0$ and $n_2 \neq 0$ and consequently to $R(\omega) = 1$. In other words, the solid cannot propagate light in this frequency range, i.e., all light is perfectly reflected from the surface. It is called *Reststrahlen band* because the reflected light is dominated by these frequencies. Taking into account damping gives the more realistic (dashed) curve shown in Fig. 3.6. It is in accordance with experimental spectra, which can be picked up from textbooks like [89] or from data collections like [94].

From (3.111), we have $S = \varepsilon_\infty(\omega_L^2 - \omega_T^2)$ and can express the (real part of the) dielectric function (see (3.109) for $\Gamma = 0$) as

$$\varepsilon(\omega) = \varepsilon_\infty \frac{\omega_L^2 - \omega^2}{\omega_T^2 - \omega^2} \quad (3.113)$$

in terms of the characteristic optical phonon frequencies and the material constant ε_∞ . For $\omega = 0$, this expression reduces to

$$\frac{\varepsilon(0)}{\varepsilon_\infty} = \frac{\omega_L^2}{\omega_T^2} \quad (3.114)$$

known as the *Lyddane–Sachs–Teller*⁵ relation. Making use of this relation, we also may write $S = \omega_T^2(\varepsilon(0) - \varepsilon_\infty)$ in terms of the macroscopic quantities ω_T , $\varepsilon(0)$, and ε_∞ . On the other hand, $S = 2\omega_T|M^T|^2/\hbar V\varepsilon_0$ is determined by the microscopic parameters of the system (see (3.104)), the charge $\eta_\pm = \pm\eta$ and the masses M_\pm of the ions. In the long-wavelength limit of the optical mode the latter move against each other with eigenvectors $e_\pm^T = \pm\sqrt{(M_\mp/M)}$, where $M = M_+ + M_-$. This allows us to express

$$\eta = \left(\frac{\mu V \varepsilon_0}{N} (\varepsilon(0) - \varepsilon_\infty) \right)^{1/2} \omega_T \quad (3.115)$$

in terms of the macroscopic material parameters (here the reduced mass $\mu = (1/M_+ + 1/M_-)^{-1}$ appears because of the relative motion of the two ions in the unit cell, see Problem 3.1). As this expression for η contains also the transverse phonon frequency ω_T , it is called the *transverse charge* [89]. It is related to the strength of the phonon oscillator and can be determined from the measured spectrum by a line-shape fit.

In crystalline solids with more complex unit cells than the one with two oppositely charged ions assumed here, there are several triples of optical phonon branches with different longitudinal-transverse splittings, giving rise to different transverse effective charges [95].

3.6 Examples: Phonon Dispersion Curves

Phonon dispersion curves, showing the phonon frequencies $\omega_s(\mathbf{q})$ for different branches s , are usually plotted versus \mathbf{q} along different high symmetry directions in the Brillouin zone. For the examples to be discussed in this section, which all have fcc or bcc point lattices, we refer to the Brillouin zones depicted in Figs. 1.1 and 1.2. Phonon dispersion curves are obtained either experimentally from inelastic scattering preferentially with neutrons (for a more recent introduction and examples see [96, 97]) and also with photons and atoms, or from model calculations of different sophistication. Both kinds of investigation have influenced and stimulated each other and are well documented [77–79], thus, at present the phonon dispersion curves of solids are well known. For collections of phonon dispersion curves, together with a compilation of the original references, we refer to [76, 81, 94]. A selection will be presented and discussed in this section to provide the knowledge how to read phonon dispersion curves and understand their principal material specific features.

⁵ Russell Hancock Lyddane 1913–2001, Robert Green Sachs 1916–1990, Edward Teller 1908–2003

In all the examples presented below, experimental data are shown together with calculated dispersion curves. In order to judge the quality of the theoretical data, it is necessary to briefly characterize the different models used. Historically (and this has been in the first place a matter of available computer power), a variety of phenomenological models has been developed. Depending on their complexity, these models are characterized by a number of parameters, which have to be determined by fits to the experimental data. We have already learned about the simplest of these phenomenological models with massive spheres (representing rigid ions) and springs (representing the interionic forces due to chemical binding) in Sects. 3.1 and 3.2 (including Problems 3.1 and 3.2). For given masses of the ions, this *rigid-ion model* contains the force constants as adjustable parameters (their number depending on the symmetry of the lattice and the considered number of neighbors coupled by springs, see Problem 3.2). As demonstrated by comparing measured with fitted dispersion curves for Al in Fig. 3.7 and for Fe in Fig. 3.8, this model works well for metals.

However, this rigid-ion model does not account for a polarization connected with a motion of the ions in ionic crystals. For these systems, so-called *shell models* of different complexity have been developed. By decomposing the ion into the nucleus with the closed shells of core electrons and the shell of valence electrons, responsible for the chemical binding, it becomes possible to introduce additional parameters or force constants representing springs between each two movable parts of the model. Especially, a spring between the closed-shell ion and the shell of valence electrons can be used to account for the polarization of the atom. With this increased number of parameters, shell models are quite flexible and have been successfully applied to ionic crystals with heteropolar binding like KI (Fig. 3.9). KI crystallizes in the rocksalt structure with two ions in the Wigner–Seitz cell and, therefore, its phonon dispersion curves have acoustic (TA, LA) and optical branches (TO, LO).

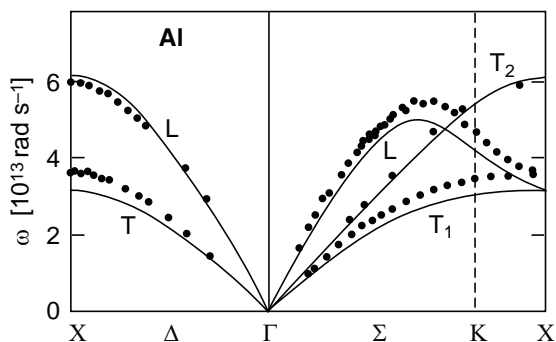


Fig. 3.7. Phonon dispersion curves for Al (fcc structure). Symbols are experimental data from inelastic neutron scattering, dispersion curves calculated with the rigid ion model using three force constants fitted to elastic constants (after [77])

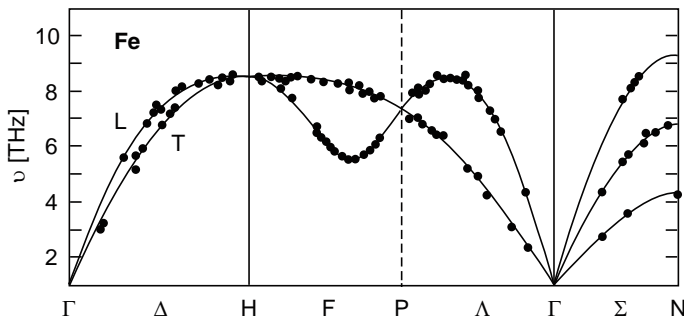


Fig. 3.8. Phonon dispersion curves for α -Fe (bcc structure). Symbols are experimental data from inelastic neutron scattering, dispersion curves calculated with the rigid ion model using force constants for up to five nearest neighbors (after [81])

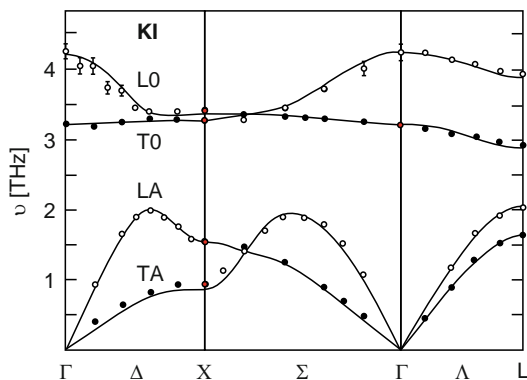


Fig. 3.9. Phonon dispersion curves for KI (rocksalt structure). Symbols (*open* for L, *full* for T modes) are experimental data from inelastic neutron scattering, dispersion curves calculated with an 11-parameter shell model (after [76])

In solids with dominating covalent binding, like those made of the group-IV elements, which crystallize in the diamond structure (two interpenetrating fcc lattices with four nearest neighbors to each atom), the valence electron density exhibits a strong maximum halfway between each pair of nearest neighbors (see Chap. 5). This bond charge is characteristic for covalent binding. It turns out to be important not only for the stability of the diamond structure but also for the lattice dynamics. Because the rigid-ion models as well as the shell models fall short of describing the bond charge and its motion, a *bond charge model* has been invented, which introduces springs between neighboring bond charges. This model has been used to calculate the phonon dispersion curves of Si in Fig. 3.10.

Of particular nature are solid rare gases, which, due to the weak van der Waals forces, exist only at low temperatures. Their characteristic phonon frequencies are much smaller than those of other solids, therefore, already very

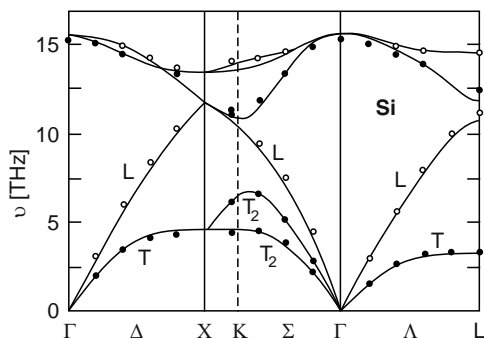


Fig. 3.10. Phonon dispersion curves for Si (diamond structure). Symbols (*open* for L, *full* for T modes) are experimental data from inelastic neutron scattering, dispersion curves calculated with the bond-charge model (after [76])

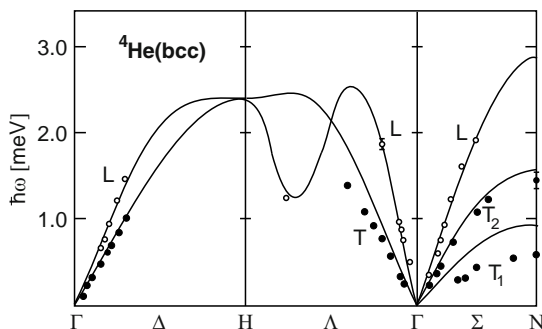


Fig. 3.11. Phonon dispersion curves for solid ^4He in the bcc structure. Symbols (*open* for L and *full* for T modes) are experimental data from inelastic neutron scattering, dispersion curves calculated with the self-consistent harmonic approximation (after [76])

little thermal energy creates lattice displacements that require the consideration of anharmonic corrections. This is done in the *self-consistent harmonic approximation* (SCHA) used in Figs. 3.11 and 3.12 (see also Problem 3.8).

These different models, although successful in many cases, turned out to be in conflict with experimental data of increasing accuracy. Discrepancies were found in particular for phonon eigenvectors, which have been measured besides the frequencies [98]. At the same time, theoretical concepts and computer power became available for microscopic lattice dynamics based on ab-initio methods [99, 100]. These methods aim at the self-consistent solution of the time-dependent Schrödinger equation for the motion of the ions in the adiabatic potential (3.1)

$$\left(\sum_n \frac{P_n^2}{2M} + \mathcal{U}(\{\mathbf{R}_n\}) \right) \Phi = i\hbar \dot{\Phi} \quad (3.116)$$

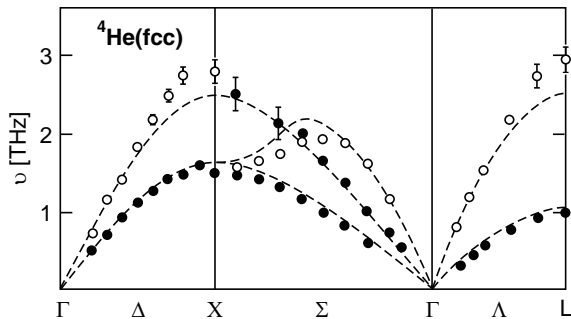


Fig. 3.12. Phonon dispersion curves for solid ${}^4\text{He}$ under hydrostatic pressure in the fcc structure. For symbols (experiment) and lines (model calculations) see caption of Fig. 3.11 (after [76])

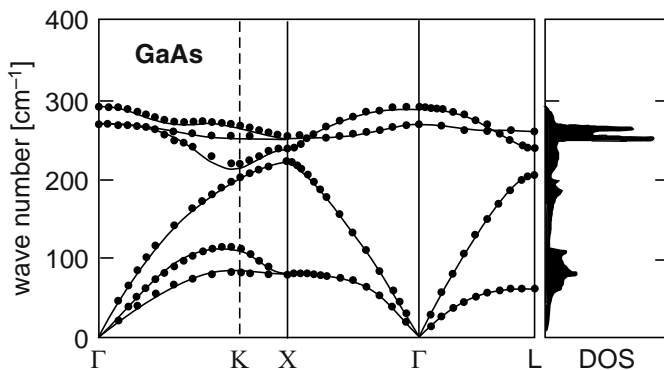


Fig. 3.13. Phonon dispersion curves and density of states (DOS) for GaAs (zinc blende structure). Symbols are experimental data from inelastic neutron scattering, dispersion curves are ab-initio results from DFPT (after [101])

and of the time-independent Schrödinger equation for the electrons in the equilibrium configuration of the ions

$$\left(\sum_l \frac{p_l^2}{2m} + \frac{1}{8\pi\epsilon_0} \sum_{\substack{k,l \\ k \neq l}} \frac{e^2}{|\mathbf{r}_k - \mathbf{r}_l|} + \sum_{n,l} v(\mathbf{r}_l - \mathbf{R}_n) \right) \Psi_0 = \mathcal{E}_{el} \Psi_0. \quad (3.117)$$

This becomes possible within the density–functional theory (DFT), which will be introduced in Chap. 5, as an extension to the density–functional perturbation theory (DFPT) [98–100]. As an example of such calculations we show phonon dispersion curves of GaAs in Fig. 3.13, together with the phonon density of states.

When looking at the phonon dispersion curves, one finds different units for the phonon frequencies ν , wave numbers $\bar{\nu}$, or energies $\hbar\omega$, following from the relations $E = \hbar\omega = h\nu = hc\bar{\nu}$. The scales are typically THz or 10^{12} s^{-1}

for ν , 100 cm^{-1} for $\bar{\nu}$, and a few meV for $\hbar\omega$. In order to convert these units for comparison of the different dispersion curves, the following scheme can be used (e.g., $1\text{ THz} = 10^{12}\text{ s}^{-1} \equiv 4.136\text{ meV}$):

	THz	100 cm^{-1}	10 meV
THz	1	0.3336	0.4136
100 cm^{-1}	2.9979	1	1.2398
10 meV	2.4181	0.8066	1

Let us first discuss the phonon dispersion curves of solids with Bravais lattices (with only one atom per unit cell) shown for Al (Fig. 3.7), Fe (Fig. 3.8) and solid ^4He (Figs. 3.11 and 3.12).

The dispersion is depicted for the directions $[100]$, $[111]$, and $[110]$ in the Brillouin zone which correspond, respectively, to the lines Δ , Λ , and Σ (see Figs. 1.1 and 1.2). In each case, one has only acoustic branches, one longitudinal (L) and two transverse ones (T or T_1 , T_2). The transverse branches are degenerate for the $[100]$ and $[111]$ directions, whose group of the wave vector contains fourfold and threefold rotations, respectively, but split into two separate branches for the $[110]$ direction (which is invariant only under twofold rotation). By comparison of bcc ^4He and Fe on one side and those of fcc ^4He and Al we recognize a remarkable correlation between lattice structure and topology of the phonon dispersion curves. This is most striking for the dispersion along the Λ line (or $[111]$ direction), for which the longitudinal branch from Γ to H of bcc ^4He and Fe exhibits a pronounced dip, while it increases monotonously from Γ to L for the fcc solids. For a given crystal structure, the difference in the material and its specific chemical binding determines the force constants and therefore, the phonon frequencies. Thus, the phonon spectrum of the metals Al and Fe spreads over a much larger interval than those of both modifications of solid ^4He . But already the comparison of bcc ^4He and fcc ^4He (obtained by applying hydrostatic pressure) shows an increase of the phonon frequencies as the strength of the chemical binding (here van der Waals forces) is increased by compression.

The next group of examples consists of solids, all based on the fcc point lattice but with different basis: diamond structure for Si (Fig. 3.10), zinc blende structure for GaAs (Fig. 3.13), and rocksalt structure for KI (Fig. 3.9). With two atoms per unit cell, these solids have phonon dispersion curves exhibiting three optical branches with similarities as well as pronounced differences inside the acoustic branches. For the acoustic branches, with dispersion curves similar to those of Al and fcc He^4 , we mention only the differences in the slopes. They are largest for Si, which, similar to C(diamond), is a rather rigid material due to the covalent bonds, and its Debye temperature is about 50% larger than that of Al. Note the degeneracy of the transverse phonons in KI along the Σ axis. It is a consequence of the higher symmetry of the rocksalt lattice compared to that of the zinc blende lattice. The optical branches of Si differ

from those of GaAs and KI by convergence toward a degeneracy with the acoustic branches, e.g., at the X point, while these two groups of branches do not interpenetrate for GaAs and are even well separated by a gap for KI. This behavior can be understood from the solution for Problem 3.1, the linear chain with two atoms in the unit cell: If the two atoms in the unit cell have different masses, the dispersion curves show a gap at the boundary of the Brillouin zone (as for GaAs and KI); this gap closes, if the masses are equal (as for Si). Even the difference between these gaps of GaAs and KI can be explained within this model, it increases with increasing mass difference. The other striking difference is the splitting of the optical phonon branches at the Γ point for GaAs and KI – the longitudinal–transverse (or LT) splitting – while these branches are threefold degenerate in Si. The splitting is a consequence of the macroscopic polarization inherent with a longitudinal optical mode in a binary compound solid (such as GaAs and KI) that gives rise to a stronger restoring force than for the transverse mode, i.e., $\omega_L > \omega_T$, as discussed in Sect. 3.5, and is connected with the Reststrahlen band. The rather flat optical phonon branches lead to a pronounced peak in the density of states (DOS), shown for GaAs in Fig. 3.13. Nevertheless, the phonon dispersion curves for Si and GaAs resemble each other much more than those of GaAs and KI. This is due to the similarity of the diamond and zinc blende structure and the small mass difference between Ga and As. On the other hand, the characteristic frequencies are higher in Si than in GaAs, which can be ascribed to a weakening of the covalent binding in GaAs (which becomes partially ionic) and to the larger masses of Ga and As as compared to the mass of Si.

With these aspects of selected phonon curves in mind, it is not difficult to make an excursion to other materials maintaining the same crystal structure but replacing the atoms. As an example, we may consider AlAs and GaP, both in the zinc blende structure. Compared to GaAs, we expect a more pronounced separation of acoustic and optical branches in the phonon spectrum of both materials, because the mass difference of the two atoms in the unit cell, taken from different rows of the periodic table, has increased. Moreover, due to the lighter masses of Al and P, compared to those of Ga and As, respectively, the characteristic phonon frequencies are higher than those of GaAs. These features are found in the phonon dispersion curves of AlAs and GaP (see [94]).

The lattice dynamics presented in this chapter is designed for the extended solid without regarding its surface. Surface atoms experience a different structural surrounding and forces, which differ from those acting on the bulk atoms. Consequently, they have their own dynamics, which, in a simplified two-dimensional model, has been treated already in Problem 3.2. For a more detailed description we refer to [85–87]. A simple example is the phonons of a Cu(100) surface as shown in Fig. 3.14. Calculations of surface phonons are usually performed for slab configurations where the outermost atomic layers experience the modified environment of the surface, while the central layers reproduce the bulk situation. The results are plotted for wave vectors in the first BZ of the 2D periodic surface structure. The shaded area in Fig. 3.14

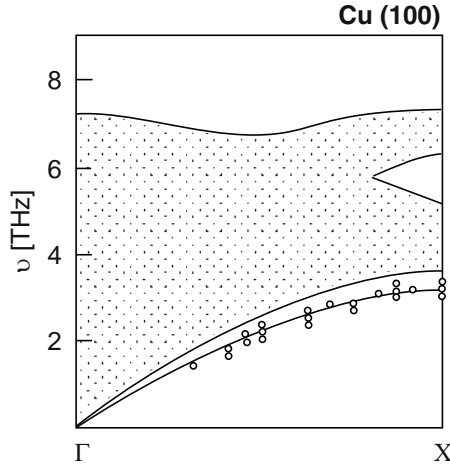


Fig. 3.14. Projected bulk phonons and surface phonons for a Cu(100) surface. Experimental data (*circles*) are from HREELS (after [102])

results from the bulk modes that have the same component of the wave vector in the surface along $\Gamma - X$, while the solid lines represent the collective modes of the surface layers, whose frequency is below the continuum of the projected bulk phonon frequencies. The surface phonons have been measured by high resolution electron energy loss spectroscopy (HREELS).

A more complex spectrum results for the clean GaAs(110) surface shown in Fig. 3.15. This surface represents a rectangular 2D lattice, whose BZ is depicted in the inset. Results from DFPT calculations [103] show again the projected bulk phonon spectrum (shaded area), but in addition solid lines from surface phonons, which partially overlap with the bulk continuum. Experimental data are from inelastic scattering with He atoms and from HREELS. Adsorbate layers modify the surface phonon spectrum.

Modern epitaxial material growth has created new solids with artificial periodicity by periodically changing the kind of atoms supplied during the growth process [104, 105]. These new materials are called superlattices. Their period is larger than that of the underlying crystal structure and thus, the Brillouin zone and the phonon branches for the growth direction are backfolded. If the masses of the atoms in the different layers differ strongly from each other, the optical phonons of one layer may fall into a frequency range outside of the optical phonon branch of the other layer. This means that these optical modes cannot propagate along the growth direction but only along their respective layers. They are called *confined phonon modes* (see Sect. 9.3 in [89]).

As already mentioned in Sect. 1.2, solids are, in general, compositionally disordered due to the natural abundance of isotopes for each element. As a consequence, not all oscillators in the model of Fig. 3.1 have the same resonance frequency. This becomes relevant especially for the optical phonons

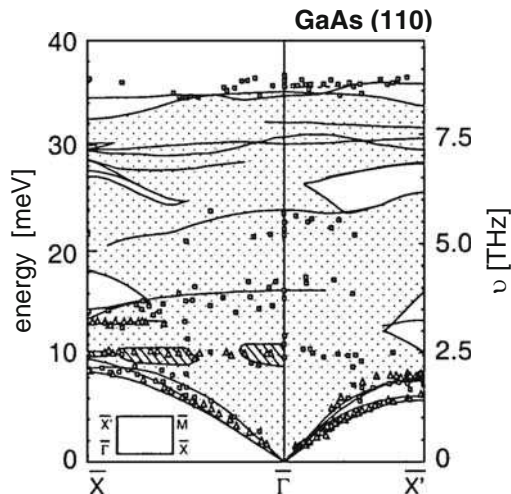


Fig. 3.15. Projected bulk phonons and surface phonons for a clean GaAs(110) surface. Experimental data are from inelastic He scattering (*triangles*) and HREELS (*squares*) (after [103])

and results in an inhomogeneously broadened infrared absorption line. This broadening can be (and has been) overcome by growing isotopically clean crystals [106]. The mass difference of isotopes also has been exploited in growing isotope superlattices, e.g., of ^{70}Ge and ^{74}Ge and to investigate their phonon spectra by inelastic light scattering [107].

3.7 The Crystal Lattice at Finite Temperature

The experimental phonon energies presented in the last section were all obtained from inelastic scattering. Besides the most frequently employed and versatile neutron scattering, inelastic scattering with photons and atoms is also in use [96, 97]. A quantitative analysis has to ask for the scattering intensity including its dependence on the temperature. The key quantity is the differential cross section. It describes the probability that an incoming particle (neutron, photon, light atom) with momentum $\hbar\mathbf{k}$ is scattered by a solid (or its surface) into an outgoing particle with momentum $\hbar\mathbf{k}'$. In the scattering process, the energy $\hbar\omega$ (the difference of the kinetic energies of the particle before and after the encounter with the solid) and the momentum $\hbar\mathbf{q} = \hbar(\mathbf{k} - \mathbf{k}')$ are exchanged with the solid. Under the assumption of weak scattering efficiency, which justifies the Born approximation, an excitation with just this energy and momentum is created (or destroyed) in the solid. For this situation, the scattering cross section can be written as [4, 83, 96, 97]

$$\frac{d^2\sigma}{d\omega d\Omega} = A_{\mathbf{q}} S(\mathbf{q}, \omega), \quad (3.118)$$

where Ω refers to the direction of the scattered particle relative to the direction of the incoming particle, $A_{\mathbf{q}}$ accounts for the details of the interaction mechanism giving rise to the scattering, and $S(\mathbf{q}, \omega)$ is the dynamic structure factor (see Sect. 1.3). It is the Fourier transform of the density–density correlation function

$$S(\mathbf{q}, \omega) = \frac{1}{2\pi} \int d^3\mathbf{r} \int d^3\mathbf{r}' e^{i\mathbf{q}\cdot(\mathbf{r}-\mathbf{r}')} \int e^{-i\omega t} \langle n(\mathbf{r}, t) n(\mathbf{r}', 0) \rangle dt. \quad (3.119)$$

Its static counterpart has been introduced already in Sect. 1.3. The time dependence of the density

$$n(\mathbf{r}, t) = \sum_{\mathbf{n}} \delta(\mathbf{r} - \mathbf{R}_{\mathbf{n}}(t)), \quad \mathbf{R}_{\mathbf{n}}(t) = \mathbf{R}_{\mathbf{n}}^0 + \mathbf{u}_{\mathbf{n}}(t) \quad (3.120)$$

has its origin in the time-dependent positions of the ions, which can be expressed by the departures from their equilibrium positions $\mathbf{R}_{\mathbf{n}}^0$ (here we assume a Bravais lattice). Thus, the dynamical structure factor can be written as

$$S(\mathbf{q}, \omega) = \frac{1}{2\pi} \int dt e^{-i\omega t} \sum_{\mathbf{nn}'} \left\langle e^{-i\mathbf{q}\cdot(\mathbf{R}_{\mathbf{n}}^0 + \mathbf{u}_{\mathbf{n}}(t))} e^{i\mathbf{q}\cdot(\mathbf{R}_{\mathbf{n}'}^0 + \mathbf{u}_{\mathbf{n}'}(0))} \right\rangle. \quad (3.121)$$

When evaluating the thermal expectation value under the integral, the displacements $\mathbf{u}_{\mathbf{n}}$ have to be understood as quantum-mechanical operators (in actual calculations they will be expressed by phonon operators), while the equilibrium positions are parameters. Therefore, we can write

$$\begin{aligned} \langle \dots \rangle &= e^{-i\mathbf{q}\cdot(\mathbf{R}_{\mathbf{n}}^0 - \mathbf{R}_{\mathbf{n}'}^0)} \langle e^{-i\mathbf{q}\cdot\mathbf{u}_{\mathbf{n}}(t)} e^{i\mathbf{q}\cdot\mathbf{u}_{\mathbf{n}'}(0)} \rangle \\ &= e^{-i\mathbf{q}\cdot(\mathbf{R}_{\mathbf{n}}^0 - \mathbf{R}_{\mathbf{n}'}^0)} \langle e^{-i\mathbf{q}\cdot(\mathbf{u}_{\mathbf{n}}(t) - \mathbf{u}_{\mathbf{n}'}(0))} e^{[\mathbf{q}\cdot\mathbf{u}_{\mathbf{n}}(t), \mathbf{q}\cdot\mathbf{u}_{\mathbf{n}'}(0)]/2} \rangle, \end{aligned} \quad (3.122)$$

where the last expression was obtained by using the operator relation

$$e^{\hat{A}} e^{\hat{B}} = e^{\hat{A} + \hat{B}} e^{[\hat{A}, \hat{B}]/2}. \quad (3.123)$$

If the lattice sum of the prefactor with the difference $\mathbf{R}_{\mathbf{n}}^0 - \mathbf{R}_{\mathbf{n}'}^0$ could be performed irrespective of the second factor, it would give a $\delta_{\mathbf{q}, \mathbf{G}}$, indicating the Bragg peaks, which correspond to the set of parallel lattice planes defined by the reciprocal lattice vector \mathbf{G} (see Problem 1.6). In fact, the second factor simplifies for elastic scattering, which corresponds to the limit $t \rightarrow \infty$, where all correlations are lost. Thus, the commutator in the exponential vanishes and we may write

$$\lim_{t \rightarrow \infty} \langle e^{-i\mathbf{q}\cdot\mathbf{u}_{\mathbf{n}}(0)} e^{i\mathbf{q}\cdot\mathbf{u}_{\mathbf{n}'}(t)} \rangle = \left| \langle e^{-i\mathbf{q}\cdot\mathbf{u}_{\mathbf{n}}} \rangle \right|^2 = e^{-2W}. \quad (3.124)$$

This is the *Debye–Waller factor*, with $W = \langle (\mathbf{q}\cdot\mathbf{u})^2 \rangle / 2$. It is independent of the lattice site (because of the translational symmetry) and describes the reduction of the intensity of the Bragg peaks due to the thermal motion of the ions.

For a more detailed evaluation of $\langle \dots \rangle$ (3.122), we first restrict to the longitudinal modes by writing $\mathbf{q} \cdot \mathbf{u}_n = u_n$ and express the displacement by phonon operators (see (3.23) together with (3.39))

$$u_n(t) = \sum_{\mathbf{q}} \frac{1}{\sqrt{2NM\omega(\mathbf{q})}} \left(a(\mathbf{q}) e^{i(\mathbf{q} \cdot \mathbf{R}_n^0 - \omega(\mathbf{q}t)} + a^\dagger(-\mathbf{q}) e^{-i(\mathbf{q} \cdot \mathbf{R}_n^0 - \omega(\mathbf{q}t)} \right). \quad (3.125)$$

We find that the commutator

$$\begin{aligned} [u_{n'}(t), u_n(0)] &= \frac{1}{2NM} \sum_{\mathbf{q}} \frac{1}{\omega(\mathbf{q})} \left([a_{\mathbf{q}}, a_{\mathbf{q}}^\dagger] e^{i\alpha_{n'n}(t)} + [a_{\mathbf{q}}^\dagger, a_{\mathbf{q}}] e^{-i\alpha_{n'n}(t)} \right) \\ &= \frac{i}{NM} \sum_{\mathbf{q}} \frac{1}{\omega(\mathbf{q})} \sin(\alpha_{n'n}(t)), \end{aligned} \quad (3.126)$$

with $\alpha_{n'n}(t) = \omega(\mathbf{q})t + \mathbf{q} \cdot (\mathbf{R}_{n'}^0 - \mathbf{R}_n^0)$, is a scalar and the exponential with this argument becomes a factor in front of the thermal expectation value of the first exponential. For a harmonic oscillator, it can be shown [4] that

$$\langle e^{iq(u_{n'}(t) - u_n(0))} \rangle = \exp \left(-\frac{q^2}{2} \langle (u_{n'}(t) - u_n(0))^2 \rangle \right). \quad (3.127)$$

We evaluate the argument of the exponential with the substitution (3.125) and obtain

$$(u_{n'}(t) - u_n(0))^2 = \frac{1}{NM} \sum_{\mathbf{q}} \frac{1}{\omega(\mathbf{q})} (1 - \cos \alpha_{n'n}(t)) (2a_{\mathbf{q}}^\dagger a_{\mathbf{q}} + 1) \quad (3.128)$$

up to terms containing two creation or two annihilation operators (which would vanish when taking the thermal expectation value). Thus, the thermal expectation value in (3.122) can be expressed as

$$\begin{aligned} \langle \dots \rangle &= \exp \left\{ -\frac{q^2}{2NM} \sum_{\mathbf{q}'} \frac{1}{\omega(\mathbf{q}')} (2n(\mathbf{q}', T) + 1) \right\} \exp \left\{ \frac{q^2}{2NM} \sum_{\mathbf{q}'} \frac{1}{\omega(\mathbf{q}')} \right. \\ &\quad \left. \times ((2n(\mathbf{q}', T) + 1) \cos \alpha_{n'n}(t) + i \sin \alpha_{n'n}(t)) \right\} \end{aligned}$$

where $n(\mathbf{q}, T)$ is the phonon occupation function. The first exponential, which is time-independent, can be identified as the Debye–Waller factor (see Problem 3.6), while the second exponential can be expanded with the leading terms

$$\begin{aligned} &\simeq 1 + \frac{q^2}{2NM} \sum_{\mathbf{q}'} \frac{1}{\omega(\mathbf{q}')} ((2n(\mathbf{q}', T) + 1) \cos \alpha_{n'n}(t) + i \sin \alpha_{n'n}(t)) \\ &= 1 + \frac{q^2}{2NM} \sum_{\mathbf{q}'} \frac{1}{\omega(\mathbf{q}')} \{ (n(\mathbf{q}', T) + 1) e^{i\alpha_{n'n}(t)} + n(\mathbf{q}', T) e^{-i\alpha_{n'n}(t)} \} \end{aligned}$$

and we obtain, after time-integration and performing the lattice sums for the structure factor,

$$\begin{aligned}
 S(\mathbf{q}, \omega) &= \delta(\omega) e^{-2W} \sum_{\mathbf{G}} \delta_{\mathbf{q}, \mathbf{G}} \\
 &+ \sum_{\mathbf{q}'} \frac{q^2}{2NM\omega(\mathbf{q}')} \{ (n(\mathbf{q}', T) + 1) \delta(\omega - \omega(\mathbf{q}')) \delta_{\mathbf{q}, \mathbf{q}'+\mathbf{G}} \\
 &+ n(\mathbf{q}', T) \delta(\omega + \omega(\mathbf{q}')) \delta_{\mathbf{q}, \mathbf{q}'-\mathbf{G}} \}. \tag{3.129}
 \end{aligned}$$

The first term is the elastic peak that corresponds to the static structure of the lattice. It is modified by the thermal motion as quantified by the Debye–Waller factor. The second and third term, are the lowest order inelastic contributions describing absorption and emission, respectively, of a single phonon, with their particular energy and momentum conservation. Note that phonon emission is possible only if phonons are thermally excited, i.e., if $n(\mathbf{q}, T) \neq 0$. More-phonon processes would follow from the higher order terms in the expansion of the exponential.

One of the most prominent effects that heat causes in matter is thermal expansion. It is quantified by the linear *thermal expansion coefficient* at constant pressure P

$$\alpha = \frac{1}{l} \left(\frac{\partial l}{\partial T} \right)_P. \tag{3.130}$$

Here, l is the linear extension of a piece of matter. With the substitution $\Delta V/V = 3\Delta l/l$, this can also be written as

$$\alpha = \frac{1}{3V} \left(\frac{\partial V}{\partial T} \right)_P = \frac{1}{3V} \left(-\frac{(\partial P/\partial T)_V}{(\partial P/\partial V)_T} \right) = \frac{1}{3B} \left(\frac{\partial P}{\partial T} \right)_V, \tag{3.131}$$

with the *bulk modulus*

$$B_0 = -V (\partial P/\partial V)_T. \tag{3.132}$$

The thermal expansion can be expressed in terms of phonons by considering the latter as a gas and using the statistical expression for the free energy $F = U - TS$, from which the pressure is obtained by

$$P = - \left(\frac{\partial F}{\partial V} \right)_T = - \frac{\partial}{\partial V} (U - TS). \tag{3.133}$$

Using $S(T)$, obtained by integrating the differential equation

$$\left(\frac{\partial U}{\partial T} \right)_V = T \left(\frac{\partial S}{\partial T} \right)_V, \tag{3.134}$$

one can write (3.133) in the form

$$P(T, V) = -\frac{\partial}{\partial V} \left(U(T, V) - T \int_0^T \frac{1}{T'} \frac{\partial U(T', V)}{\partial T'} dT' \right). \quad (3.135)$$

The inner energy U of the phonon gas is given by

$$U = \text{Tr}(\rho_0 H) = \sum_{s, \mathbf{q}} \hbar \omega_s(\mathbf{q}) \left(n_s(\mathbf{q}, T) + \frac{1}{2} \right), \quad (3.136)$$

with the Hamiltonian H from (3.41), and we find

$$P(T, V) = -\frac{\partial}{\partial V} \sum_{s, \mathbf{q}} \frac{1}{2} \hbar \omega_s(\mathbf{q}) + \sum_{s, \mathbf{q}} n_s(\mathbf{q}, T) \left(-\frac{\partial}{\partial V} \hbar \omega_s(\mathbf{q}) \right). \quad (3.137)$$

Taking the derivative with respect to the temperature we arrive at

$$\alpha = \frac{1}{3B_0} \sum_{s, \mathbf{q}} \left(-\frac{\partial}{\partial V} \hbar \omega_s(\mathbf{q}) \right) \frac{\partial}{\partial T} n_s(\mathbf{q}, T). \quad (3.138)$$

This expression allows one to recognize two mechanisms responsible for the thermal expansion in terms of the phonons: One is the change of the thermal occupation with the temperature, the other is the change of the phonon energy with the volume. The latter is specified by the mode Grüneisen parameter

$$\gamma_{s\mathbf{q}} = -\frac{V}{\omega_s(\mathbf{q})} \frac{\partial \omega_s(\mathbf{q})}{\partial V} = -\frac{\partial(\ln \omega_s(\mathbf{q}))}{\partial \ln V}. \quad (3.139)$$

In order to characterize the temperature dependence of the whole spectrum with a single parameter, the *Grüneisen parameter*

$$\gamma(T) = \frac{1}{c_V} \sum_{s, \mathbf{q}} \gamma_{s\mathbf{q}} \frac{\hbar \omega_s(\mathbf{q})}{V} \frac{\partial}{\partial T} n_s(\mathbf{q}, T) \quad (3.140)$$

is introduced. It is the average of the mode Grüneisen parameter weighted with the contribution of each mode to the lattice specific heat

$$c_V = \sum_{s, \mathbf{q}} \frac{\hbar \omega_s(\mathbf{q})}{V} \frac{\partial}{\partial T} n_s(\mathbf{q}, T). \quad (3.141)$$

The quantities α , B_0 , γ , and c_V are connected with each other by the *Grüneisen relation*

$$3B_0(T)\alpha(T) = \gamma(T)c_V(T). \quad (3.142)$$

For reasons of technical applications material research has been conducted very early on solids that do not show thermal expansion, at least in some relevant temperature range. The prominent first outcome has been the alloy

$\text{Fe}_{0.65}\text{Ni}_{0.35}$ (called INVAR) found by Guillaume.⁶ A more recently investigated material to show this property is YbGaGe [108]. Although this effect is not yet understood microscopically, there are indications that it is related to the electronic properties of these materials.

Problems

- 3.1 Consider a linear chain with two different masses (M_1, M_2) per unit cell (lattice constant a) connected by springs (spring constant f) as shown in Fig. 3.16.
 Give the possible different force constants of the model and verify the symmetry properties of the matrix of force constants presented in Sect. 3.1! Formulate the dynamical matrix and solve the eigenvalue problem! Discuss the dispersion $\omega_s(\mathbf{q})$ close to the center and the boundary of the Brillouin zone and visualize the corresponding motion of the masses! What happens for $M_1 = M_2 = M$?
- 3.2 In a two-dimensional square lattice, let elastic forces (described by harmonic force constants Φ_1, Φ_2) act between the nearest and next nearest neighbors (see Fig. 3.17).
 Calculate the frequencies of the lattice vibrations $\omega(\mathbf{q})$ for wave vectors \mathbf{q} along the symmetry lines $\Gamma - X, \Gamma - M$, and $X - M$ in the Brillouin zone! Discuss the eigenvectors (normal coordinates) and visualize the vibrations!
- 3.3 Explain the concept of periodic (or Born-von Kármán) boundary conditions! What are they good for? Show explicitly the relation between the

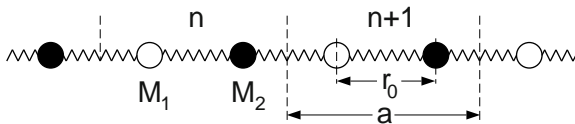


Fig. 3.16. Linear chain model with two different masses per unit cell

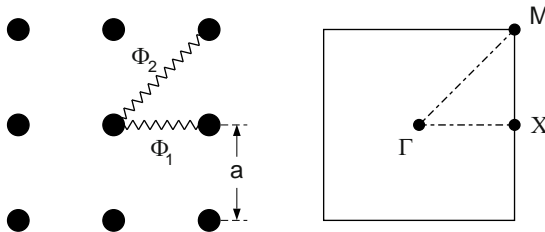


Fig. 3.17. Model for a quadratic lattice (left) and corresponding Brillouin zone with symmetry points (right)

⁶ Charles-Edouard Guillaume 1861–1938, Noble prize in physics 1920

crystal volume and the possible values of the wave vector \mathbf{q} and give their number! How can a sum over all \mathbf{q} be converted into an integral?

- 3.4 Verify the commutation relations (3.38) for the phonon creation and annihilation operators $a_s^\dagger(\mathbf{q})$ and $a_{s'}(\mathbf{q}')$ by making use of those introduced for the normal coordinates and their conjugate momenta.
- 3.5 Show the validity of the following thermal expectation values:

$$\begin{aligned}\langle a_s(\mathbf{q}, t) a_{s'}^\dagger(\mathbf{q}', 0) \rangle &= \delta_{ss'} \delta_{\mathbf{q}\mathbf{q}'} (n_s(\mathbf{q}, T) + 1) e^{-i\omega_s(\mathbf{q})t} \\ \langle a_s^\dagger(\mathbf{q}, t) a_{s'}(\mathbf{q}', 0) \rangle &= \delta_{ss'} \delta_{\mathbf{q}\mathbf{q}'} n_s(\mathbf{q}, T) e^{+i\omega_s(\mathbf{q})t} \\ \langle a_s(\mathbf{q}, t) a_{s'}(\mathbf{q}', 0) \rangle &= 0!\end{aligned}$$

- 3.6 The thermal motion of the lattice reduces the scattering amplitude (see Problem 1.6) of the rigid lattice by the Debye–Waller factor $\exp(-2W)$ with $W = \langle (\mathbf{q} \cdot \mathbf{u}(0))^2 \rangle / 2$. Here, $\mathbf{u}(0)$ is the ion displacement in the unit cell which is taken as the origin. Show, that $\langle (\mathbf{q} \cdot \mathbf{u}(t))^2 \rangle$ does not depend on t ! Calculate W by making use of the thermal expectation values given in Problem 3.5! Discuss the temperature dependence of W in the high and low temperature limits! Use the Debye model for the latter case!
- 3.7 (a) Show that due to spatial symmetry the number of independent elastic constants for a cubic crystal is reduced to 3 (make use of the transformation properties of a tensor!) (b) Solve for this case the equation of motion (3.71) for the elastic continuum with $u_i(\mathbf{r}, t) = u_i \exp i(\mathbf{q} \cdot \mathbf{r} - \omega t)$ for \mathbf{q} along $\Gamma - X$ and $\Gamma - K$! How do the sound velocities depend on the elastic constants? Take (measured or calculated) phonon dispersion curves (e.g., those of GaAs, Fig. 3.13) and determine the nonvanishing elastic constants via the sound velocities! To compare with values from the literature see [94]!
- 3.8 Calculate the correction to the frequency of an oscillator in its ground state due to a cubic anharmonicity. It arises by expanding the adiabatic potential beyond the harmonic terms. This corresponds to an oscillator problem with the Hamiltonian

$$H = \hbar\omega_0 a^\dagger a + \Delta(a^\dagger + a)^3.$$

Treat the anharmonicity by bringing the third order terms in the phonon operators first into normal order and reduce them by replacing the number operator whenever possible by the thermal expectation value $n(T)$. The self-consistent harmonic phonon approximation consists in considering the anharmonic correction in Brillouin–Wigner perturbation theory. Find the lowest eigenvalue and discuss its dependence on T to understand the meaning of a soft mode.

The Free Electron Gas

The structure of a solid, its composition of atoms, as well as the electronic, optical, and lattice properties are essentially determined by the electrons. However, not all electrons of the atoms constituting the solid are involved in the same way. At the beginning of Chap. 2 we have distinguished between the core electrons and the valence electrons. The former are tightly bound to the nuclei and extend over a distance (much) smaller than the lattice constant, while the wave functions of the latter overlap with those of the neighboring atoms, thus giving rise to the chemical binding. Therefore, we describe the solid as being composed of ions (nuclei plus closed shell electrons) in equilibrium positions at \mathbf{R}_n^0 and valence electrons, which are responsible for the stability of the solid and its electronic properties. They are ruled by the Hamiltonian (see discussion of (2.12))

$$\mathcal{H} = \sum_{l=1}^N \frac{\mathbf{p}_l^2}{2m} + \frac{1}{2} \sum_{\substack{k,l=1 \\ k \neq l}}^N \frac{e^2}{4\pi\epsilon_0 |\mathbf{r}_k - \mathbf{r}_l|} + \sum_{n,l} v(\mathbf{r}_l - \mathbf{R}_n^0) + \frac{1}{2} \sum_{mn} V(\mathbf{R}_n^0 - \mathbf{R}_m^0), \quad (4.1)$$

where N denotes the number of electrons. The first and second term describe the kinetic energy of the electrons and the electron–electron interaction, respectively. The third term, the interaction between valence electrons and ions, and the fourth term, the ion–ion interaction, depend on the equilibrium positions \mathbf{R}_n^0 of the ions (for simplicity a Bravais lattice is assumed) and are responsible for the structural aspects. The structure of the solid is defined by the configuration $\{\mathbf{R}_n^0, \text{all } \mathbf{n}\}$ with the lowest eigenvalue of \mathcal{H} . This operator comprises all terms of the Hamiltonian of the solid (2.12), if the ions are fixed at their equilibrium positions. It has to be augmented by spin-dependent terms if related effects (e.g., spin-orbit coupling, Zeeman effect) shall be considered (see Sects. 4.2, 4.3, and Chap. 5).

Instead of this complex problem, for which only approximate solutions can be found with numerical methods, we want to consider in this chapter the much simpler problem of the homogeneous electron gas. It is characterized by neglecting the structural aspects and by replacing the configuration of point-like positive ions by a homogeneous positive background charge to ensure charge neutrality of the system (Problem 4.1). This so-called *jellium model* (remember the difference between jelly and confiture) represents a many-body system of free charged fermions, which – replacing the Coulomb interaction by a more general two-particle interaction – applies also to physical systems beyond solid state physics. Thus, the treatment of the homogeneous electron gas, the calculation of its ground state energy per particle (which in different approximations can be done even analytically) becomes an introduction to the concepts of many-body theory, which have their bearings also in nuclear or astrophysics.

4.1 Free Electrons Without Interaction

In order to have a simple first look at the homogeneous electron gas, we want to neglect for the moment the interaction between the electrons (the second term in (4.1)) and the interaction with the positive background charge (corresponding to the third term in (4.1)) together with the fourth term, the electrostatic interaction energy of the ion configuration. This simplification is reasonable because in the jellium model these terms compensate exactly if one also considers the electrons as being smeared out just as the positive ions (see Problem 4.1). Thus instead of the Hamiltonian \mathcal{H} of (4.1) we consider

$$H_N = \sum_{l=1}^N H_l, \quad \text{where} \quad H_l = \frac{\mathbf{p}_l^2}{2m}, \quad (4.2)$$

with the Schrodinger equation

$$H_N \Psi(\{\mathbf{r}_l\}) = E \Psi(\{\mathbf{r}_l\}), \quad (4.3)$$

where Ψ depends on the configuration $\{\mathbf{r}_l\} = \{\mathbf{r}_1, \dots, \mathbf{r}_N\}$ of the N electrons. With H_N being a sum of single-particle operators, this N -particle problem can be separated by assuming $\Psi(\{\mathbf{r}_l\})$ to be a product of single-particle wave functions

$$\Psi(\{\mathbf{r}_l\}) = \prod_{l=1}^N \Psi_l(\mathbf{r}_l). \quad (4.4)$$

We employ Ritz' variational principle

$$\delta \left\{ \langle \Psi | H_N | \Psi \rangle - \sum_l \epsilon_l (\langle \psi_l | \psi_l \rangle - 1) \right\} = 0 \quad (4.5)$$

to minimize the expectation value of H_N under the constraint of normalized single-particle wave functions $\psi_l(\mathbf{r}_l)$. The constraint is weighted with the Lagrangian parameter ϵ_l . Using (4.2) and (4.4) we formulate (4.5) as variational derivative with respect to ψ_l^*

$$\frac{\delta}{\delta \psi_l^*} \left\{ \sum_l (\langle \psi_l | H_l - \epsilon_l | \psi_l \rangle + \epsilon_l) \right\} = 0 \quad (4.6)$$

to obtain the single-particle problem

$$H_l \psi_l(\mathbf{r}_l) = \epsilon_l \psi_l(\mathbf{r}_l), \quad (4.7)$$

which is the same for all electrons. Note, that the Lagrangian parameter ϵ_l takes the role of the single-particle energy. The total energy of the N -electron system can be represented as the sum of the energies ϵ_l

$$E = \sum_{l=1}^N \epsilon_l \quad (4.8)$$

of the occupied single-particle states.

The single-particle problem (4.7) with H_l from (4.2) is that of a free particle and has the solution

$$\psi_{\mathbf{k}}(\mathbf{r}) = \frac{1}{\sqrt{V}} e^{i\mathbf{k} \cdot \mathbf{r}} \quad (4.9)$$

with the eigenvalues

$$\epsilon(\mathbf{k}) = \frac{\hbar^2 k^2}{2m}. \quad (4.10)$$

The single-particle wave function is normalized to the fictitious (or crystal) volume V , which encloses the considered N electrons (*particle in the box*). Let V be a cuboid with side lengths L_i , $i = 1, 2, 3$ and assume *periodic boundary conditions* (see problem 3.3), according to which $\psi_{\mathbf{k}}(\mathbf{r})$ is periodic with the L_i . These conditions restrict the components of \mathbf{k} to the discrete values (see (3.18))

$$k_i = \frac{2\pi}{L_i} n_i, \quad n_i \text{ integer}, \quad i = 1, 2, 3 \quad (4.11)$$

as shown in Fig. 4.1. The periodic boundary conditions are a trick to obtain discrete states, which can be counted. It should be clear, however, that the relevant physical quantity, on which all observables of the system depend, is the single-particle density $n = N/V$ (and not the particle number N). It is kept constant for $V \rightarrow \infty$.

The wave vector \mathbf{k} (or else the triple n_1, n_2, n_3 of (4.11)) characterizes the single-particle state except for the spin degree of freedom. Each of the (quasi-discrete) \mathbf{k} takes a volume $(2\pi)^3/V$. The state with lowest energy at $T = 0$ K

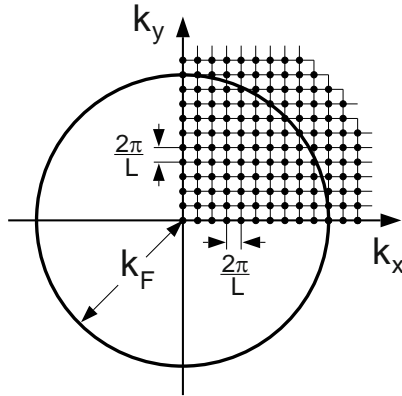


Fig. 4.1. (k_x, k_y) plane with discrete \mathbf{k} values due to the periodic boundary conditions. In the ground state at $T = 0$ K all points up to the radius k_F , defining the Fermi sphere, are occupied

for N electrons in the volume V , the *ground state*, is obtained by occupying the single-particle states with lowest possible energy with the constraint of Pauli's principle¹ which allows two electrons with opposite spin at each \mathbf{k} . This is known as the *ideal Fermi gas* or *Sommerfeld*² *model* [109]. To evaluate the ground state energy we first make use of the energy dispersion (4.10), which is isotropic in \mathbf{k} , to find the number of states in a spherical shell with radius k and thickness dk :

$$D(k)dk = \frac{2V}{(2\pi)^3} 4\pi k^2 dk . \quad (4.12)$$

The factor 2 is due to the spin degeneracy. The ground state is defined by filling concentric spherical shells around $\mathbf{k} = 0$ with increasing radius k until the stock of N electrons is exhausted:

$$N = \int_0^{k_F} D(k)dk = \frac{V}{\pi^2} \int_0^{k_F} k^2 dk = \frac{V}{3\pi^2} k_F^3 . \quad (4.13)$$

Here k_F denotes the radius of the sphere in \mathbf{k} space, the *Fermi sphere*, within which at $T = 0$ K all states are occupied (Fig. 4.1). This radius is determined by the density $n = N/V$ of the homogeneous electron gas:

$$k_F = (3\pi^2 n)^{1/3}, \quad \text{radius of the Fermi sphere} . \quad (4.14)$$

¹ Wolfgang Pauli 1900–1958, Nobel prize in physics 1945

² Arnold Sommerfeld 1868–1951

Particles with k_F have the energy

$$E_F = \frac{\hbar^2 k_F^2}{2m}, \quad \text{Fermi energy} \quad (4.15)$$

which separates the occupied states from the empty ones. The ground state energy of the system containing N electrons follows to be

$$E_0 = \int_0^{k_F} \frac{\hbar^2 k^2}{2m} D(k) dk = \frac{3}{5} N E_F \quad (4.16)$$

which, when divided by N , gives the average energy per particle in the ground state

$$\epsilon_0 = \frac{E_0}{N} = \frac{3}{5} E_F. \quad (4.17)$$

With (4.15) and (4.14), one obtains the relation between ϵ_0 and the particle density n

$$\epsilon_0 = \frac{3}{5} \frac{\hbar^2}{2m} (3\pi^2 n)^{2/3}. \quad (4.18)$$

Frequently, a dimensionless *density parameter* r_s is used. In the proper unit of length (Bohr's radius $a_B = 4\pi\epsilon_0\hbar^2/me^2$) it defines for a given density the radius of the *Wigner-Seitz sphere* whose volume can be allocated to each particle, $V/N = 1/n = 4\pi(r_s a_B)^3/3$. One finds easily

$$k_F = \left(\frac{9\pi}{4}\right)^{1/3} \frac{1}{r_s a_B} \quad (4.19)$$

and (in the unit $1 \text{ Ry} = me^4/2(4\pi\epsilon_0\hbar)^2$ of energy)

$$\epsilon_0 = \frac{3}{5} \left(\frac{9\pi}{4}\right)^{2/3} \frac{1}{r_s^2} \text{Ry} = \frac{2.2099}{r_s^2} \text{Ry}. \quad (4.20)$$

Corresponding to this relation, the mean energy per particle increases with increasing density to the extent by which states with larger \mathbf{k} are occupied under the constraint of Pauli's principle. Characteristic quantities related to k_F or E_F are the *Fermi velocity* $v_F = \hbar k_F/m$, the Fermi wave length $\lambda_F = 2\pi/k_F$, and the *Fermi temperature* $T_F = E_F/k_B$, where k_B is the Boltzmann constant.

Supplement: Parameters of fermion systems

The concepts developed so far allow one to distinguish fermion systems by their different particle densities n (or r_s) and the derived quantities. They are given for a selection of solid state fermion systems in Table 4.1. Potassium (K) has one valence electron and crystallizes in the body centered cubic lattice with two atoms and thus two electrons in the elementary cube. Copper (Cu), also with one valence electron

Table 4.1. Parameters (n in cm^{-3} , k_F in \AA^{-1} , v_F in 10^8 cm s^{-1} , E_F in eV, T_F in 10^4 K) for different fermion systems realized in solids

System	n	r_s	k_F	v_F	E_F	T_F
K	$1.43 \cdot 10^{22}$	4.83	0.75	0.87	2.14	2.48
Cu	$8.53 \cdot 10^{22}$	2.66	1.36	1.57	7.05	8.18
n-GaAs	10^{17}	1.29	0.014	0.25	$0.75 \cdot 10^{-3}$	0.0009
n-GaAs	10^{20}	0.129	0.143	2.5	0.078	0.09

per atom, forms a face centered cubic lattice with four atoms and consequently four electrons in the elementary cube. Given the lattice constants $a_K = 5.31 \text{ \AA}$ and $a_{\text{Cu}} = 3.61 \text{ \AA}$ one easily obtains the electron density n and the other system parameters depending on n . The values given in Table 4.1 for K and Cu are characteristic for normal and noble metals, respectively. For comparison we also quote numbers for n-GaAs with two different doping concentrations.

In evaluating the electron density of the metals, we have only considered the valence electrons outside of closed shells. Similarly, in doped semiconductors we count only the extra electrons provided by electron donating impurity atoms (e.g., Si substituting Ga in GaAs) to determine n . The properties of these extra electrons deviate, however, from those of free electrons in vacuum. Their energy–momentum relation is modified by the periodic crystal potential and becomes a band structure (see Chap. 5), in which these extra electrons occupy states at the bottom of the conduction band with a dispersion similar to free particles but with an effective mass m^* different from the free electron mass m ; their charge is screened with the (relative) dielectric constant ϵ . Correspondingly, the system Hamiltonian would contain these modified electron parameters in the kinetic energy and in the electron–electron interaction. Therefore, the atomic units are redefined as effective units $a_B^* = (\epsilon m / m^*) a_B$ and $1 \text{ Ry}^* = (m^* / m \epsilon^2) \text{ Ry}$. In these units, one obtains for the two doping concentrations in n-GaAs with $m^*/m = 0.066$ and $\epsilon = 12.9$ the corresponding parameter values given in Table 4.1. In spite of their much lower particle density the doped semiconductors appear as interacting fermion systems with much higher density (smaller r_s) than the metals. This is due to the much larger effective Bohr radius, which is the length scale for the interaction.

Fermion systems with quite different densities are realized in neutron stars and systems of atoms confined in electromagnetic traps. Neutron stars have a radius of about 10 km and evolve from the gravitational collapse of small stars with about the mass of the sun. They can be described as an ideal Fermi gas with the extremely high density of 10^{38} cm^{-3} ! The other extreme of very low densities is obtained by cooling ensembles of fermionic atoms confined in electromagnetic traps to extremely low temperatures ($T_F < 1 \mu \text{ K}$), at which they represent degenerate Fermi systems (see Physics Today, October 2003, p. 18).

Knowing the single-particle energy-momentum relation $\epsilon(\mathbf{k})$ of (4.10), one can derive the spectral distribution of the electrons using (4.12):

$$D(E)dE = D(k) \frac{dk}{dE} dE = \frac{mV}{\pi^2 \hbar^2} \sqrt{\frac{2m}{\hbar^2}} \sqrt{E} dE. \quad (4.21)$$

The number of states with energy E , the electron *density of states*, given by

$$D(E) = \frac{V}{2\pi^2} \left(\frac{2m}{\hbar^2} \right)^{3/2} \sqrt{E} \tag{4.22}$$

is the well-known square root relation shown in Fig. 4.2. Alternatively, one can calculate the density of states also from $D(E) = 2 \sum_{\mathbf{k}} \delta(E - \epsilon(\mathbf{k}))$ (see for comparison the phonon density of states (3.53)), by collecting in \mathbf{k} space all single-particle energies with $\epsilon(\mathbf{k}) = E$. The factor 2 takes into account the spin degeneracy.

At $T = 0$ K, all states with energy smaller than E_F are occupied and the ground state energy E_0 for N particles is obtained by integrating $ED(E)$ up to the Fermi energy E_F . More generally, to include finite temperatures the ground state energy follows from

$$E_0(T) = \int_0^\infty ED(E)f(E, \mu, T)dE \tag{4.23}$$

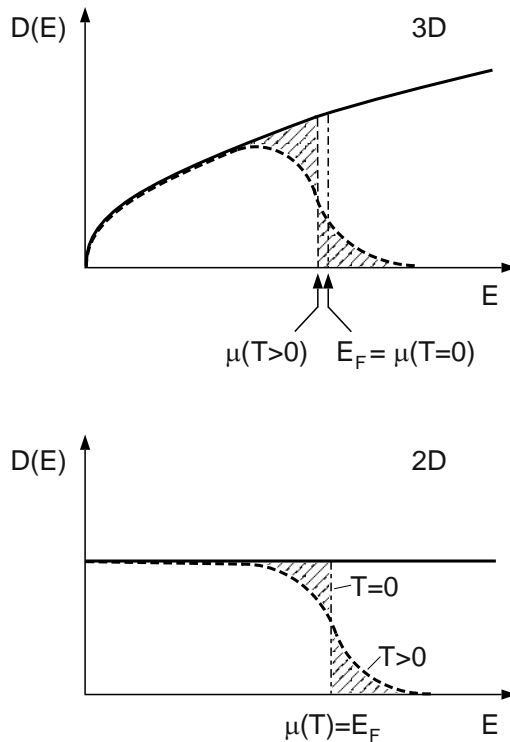


Fig. 4.2. Density of states of free electrons in three (*upper part*) and two (*lower part*) dimensions. At $T = 0$ K all states with $E \leq E_F$ are occupied. For finite temperatures the occupation around the Fermi energy is smeared out and is determined by the chemical potential $\mu(T)$

with the *Fermi–Dirac distribution function*

$$f(E, \mu, T) = \frac{1}{e^{(E-\mu)/k_B T} + 1}. \quad (4.24)$$

Here the chemical potential μ is fixed (similar to k_F in (4.13)) by the particle density $n = N/V$:

$$\frac{N}{V} = \int_0^\infty D(E) f(E, \mu, T) dE. \quad (4.25)$$

Due to the interplay between density of states and distribution function the chemical potential depends in general on T (Problem 4.2). However, for a two-dimensional electron system with constant density of states (as depicted in the lower part of Fig. 4.2) this is not the case (provided the Fermi energy is sufficiently high up in the band). At $T = 0$ K, $f(E, \mu, T)$ degenerates to a step function with a step at E_F and one identifies $\mu(T \rightarrow 0) \rightarrow E_F$ (see Fig. 4.2). But for finite T in general, quantities such as the ground state energy or the particle density, which require to integrate some power function in E with the Fermi–Dirac distribution function, can be expressed in terms of Fermi integrals (see Appendix).

Taking the T dependent chemical potential from Problem 4.2 (which applies for $T \rightarrow 0$), the thermal energy density of free electrons at fixed volume is found (*Sommerfeld expansion*, see Appendix)

$$\epsilon(T) = \epsilon_0 + \frac{\pi^2}{6} (k_B T)^2 D(E_F) + \dots \quad (4.26)$$

with ϵ_0 from (4.20). Its derivative with respect to T is the electron contribution to the specific heat (at constant V)

$$c_V(T) = \left(\frac{\partial \epsilon(T)}{\partial T} \right)_V = \frac{\pi^2}{3} k_B^2 T D(E_F) = \frac{\pi^2}{2} \frac{k_B T}{E_F} n k_B. \quad (4.27)$$

This linear dependence on T is characteristic for metals and can be detected experimentally at low temperatures. Taking into account the simultaneously present lattice contribution also (see Chap. 3), we write $c_V(T) = \gamma T + A T^3$, and find in a plot of $c_V(T)/T$ versus T^2 the *Sommerfeld coefficient* γ (see Fig. 4.3).

Sommerfeld parameters obtained from experimental data of the specific heat (γ_{exp}) can be compared with those from the Sommerfeld model (γ_S) calculated with the respective particle density (see Table 4.2). The comparison can be quantified by realizing that according to (4.27) the specific heat is proportional to the density of states at the Fermi energy and thus to the particle mass. Thus the ratio of the Sommerfeld parameters corresponds to the ratio of the fermion mass obtained from the measured specific heat (m_{c_V}) to the free electron mass m . In Table 4.2 we find good agreement between the

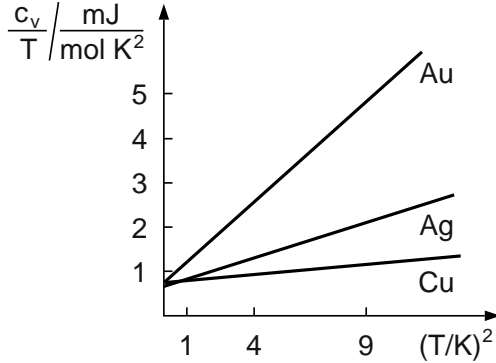


Fig. 4.3. Measured values of c_V/T for Au, Ag, Cu vs. temperature. The extrapolated value for $T = 0$ K gives the Sommerfeld coefficient γ_{exp}

Table 4.2. Sommerfeld coefficients from the free electron model (γ_S) and from experiment (γ_{exp}) (in mJ Mol K^{-2}) and the corresponding mass ratio [29]

System	γ_S	γ_{exp}	m_{c_V}/m
Na	1.38	1.094	1.26
K	2.08	1.668	1.25
Al	1.35	0.912	1.48
Cu	0.695	0.505	1.38
Ag	0.646	0.645	1.00
Au	0.729	0.642	1.14
Fe	4.98	0.498	10.0
Ni	7.02	0.459	15.3

Sommerfeld model and the experimental data, i.e., $m_{c_V}/m \simeq 1$, for the alkali and noble metals, whose valence shells contain s and p electrons. However, even dramatic deviations, $m_{c_V}/m \gg 1$, are observed for transition metals and rare earth compounds. As an example, the mass ratio of about 15 for Ni is given in Table 4.2. It can be ascribed to the influence of the periodic potential (Chap. 5) and understood as a single-particle or band structure effect. However, mass ratios of the order of 10^3 found for the rare earth compounds are in addition due to electron–electron interaction or electronic correlation (see Sect. 7.5). The latter materials are called *heavy fermion systems* [110].

In this section, we have assumed a three-dimensional electron system in deriving e.g., the density of states in (4.12) and (4.22) and the parameters of the Fermi sphere. But electron systems of lower dimension ($d = 2, 1$, and 0) can also be realized at semiconductor hetero-interfaces, by using modern device technologies to produce quantum wires or dots, or in molecular systems like carbon nanotubes [21, 111–114]. These low-dimensional electron systems exhibit characteristic phenomena which can be understood in parts from the

dimension-specific density of states (see e.g., Fig. 4.2 for the two-dimensional case and Problem 4.3).

4.2 Free Electrons in a Magnetic Field

The orbital motion of electrons and their energy spectrum change in a homogeneous magnetic field. At the same time, the magnetic field acts on the electron spin. Both effects result in some of the magnetic properties of the electron system. For their description the single-particle Hamiltonian H_I in (4.2) is to be replaced by

$$H = \frac{1}{2m}(\mathbf{p} + e\mathbf{A})^2 + \frac{e\hbar}{2m}\boldsymbol{\sigma} \cdot \mathbf{B}. \quad (4.28)$$

Here we denote the magnetic induction $\mathbf{B} = \mu_0\mathbf{H}$, connected with the external homogeneous field by the vacuum permeability μ_0 , as magnetic field. If its direction is along z , $\mathbf{B} = (0, 0, B)$, it can be described in the *Landau gauge*³ by the vector potential $\mathbf{A} = (0, Bx, 0)$. In a classical description, the first term in (4.28) leads to the circular motion as a consequence of the Lorentz force. It represents a harmonic oscillator with the *cyclotron frequency* $\omega_c = eB/m$, which in the quantum mechanical treatment gives the characteristic oscillator spectrum. The second term, containing the vector $\boldsymbol{\sigma}$ of the Pauli spin matrices, is the Zeeman⁴ term responsible for the removal of the spin degeneracy by the magnetic field.

Let us calculate first the eigenvalues of H by considering the commutation relations for the components of the vector operator $\boldsymbol{\pi} = \mathbf{p} + e\mathbf{A}$:

$$[\pi_x, \pi_y] = e(p_x A_y - A_y p_x) = -i\hbar eB, \quad [\pi_z, \pi_x] = [\pi_y, \pi_z] = 0. \quad (4.29)$$

They can be written in the compact form of a vector relation

$$\boldsymbol{\pi} \times \boldsymbol{\pi} = -ie\hbar\mathbf{B}. \quad (4.30)$$

Because of the translational invariance of H in the z -direction (parallel to the magnetic field) we have $[p_z, H] = 0$, and the linear momentum $p_z = \hbar k_z$ is a constant of motion. The Hamiltonian

$$H = \frac{1}{2m}(\pi_x^2 + \pi_y^2) + \frac{\hbar^2 k_z^2}{2m} + \mu_B \sigma_z B \quad (4.31)$$

(with the Bohr magneton $\mu_B = e\hbar/2m$) can now be rewritten by making use of oscillator operators a, a^\dagger according to

³ Lev Davidovich Landau 1908–1968, Nobel prize in physics 1962

⁴ Pieter Zeeman 1865–1943, Nobel prize in physics 1902

$$\pi_x = \frac{\hbar}{\sqrt{2}l}(a^\dagger + a), \quad \pi_y = -\frac{i\hbar}{\sqrt{2}l}(a^\dagger - a), \quad (4.32)$$

where a and a^\dagger fulfill the commutation relation

$$[a, a^\dagger] = aa^\dagger - a^\dagger a = 1 \quad (4.33)$$

and $l = \sqrt{(\hbar/eB)}$ is the *magnetic length*. Thus H takes the form

$$H = \hbar\omega_c(a^\dagger a + \frac{1}{2}) + \frac{\hbar^2 k_z^2}{2m} + \mu_B \sigma_z B. \quad (4.34)$$

Its eigenvalues are given by:

$$\epsilon(n, k_z, \pm) = \hbar\omega_c \left(n + \frac{1}{2} \right) + \frac{\hbar^2 k_z^2}{2m} \pm \frac{g}{2} \mu_B B. \quad (4.35)$$

In comparison with the magnetic field-free case (4.10), these single-particle energies differ by replacing $\hbar^2(k_x^2 + k_y^2)/2m \rightarrow \hbar\omega_c(n + 1/2)$ and adding the Zeeman term. The first term describes the equidistant energy levels of the cyclotron oscillator (*Landau levels*), the second the free motion parallel to the magnetic field, and the third the Zeeman spin-splitting with the *g factor*, which for the free electron is (very close to) two. The spectrum is visualized in Fig. 4.4.

Experimentally, this spectrum can be detected by absorption of electromagnetic waves propagating parallel to the magnetic field, i.e., with an electric field vector in the (x, y) plane. From the resonant absorption at $\omega = \omega_c$ (*cyclotron resonance*) with

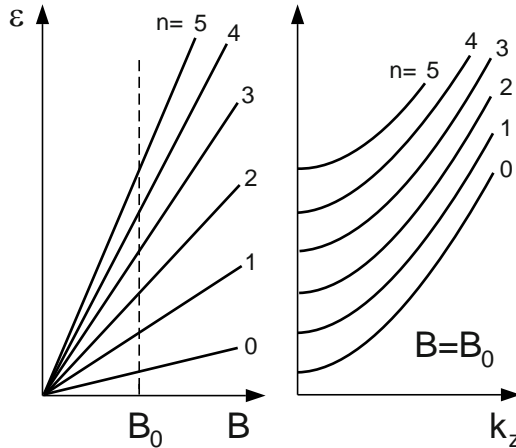


Fig. 4.4. Dependence of the single-particle energies $\epsilon(n, k_z)$ on the magnetic field at $k_z = 0$ (*left*) and on k_z at the magnetic field B_0 (*right*). The Zeeman splitting is not shown

$$\hbar\omega_c = \epsilon(n+1, k_z, \pm) - \epsilon(n, k_z, \pm) = \frac{\hbar e B}{2m} \quad (4.36)$$

and the *electron-spin resonance* (also known as *spin-flip* or *paramagnetic resonance*) at $\omega = \omega_{\text{esr}}$ with

$$\hbar\omega_{\text{esr}} = \epsilon(n, k_z, +) - \epsilon(n, k_z, -) = g\mu_B B \quad (4.37)$$

the system parameters m and g can be determined. This possibility is important because for electron systems in solids these parameter values differ from those of free electrons in vacuum due to the influence of the periodic potential and become material specific (see Sect. 4.1 and Chap. 5). Thus, cyclotron and electron spin resonance allow to determine the material specific effective mass m^* and g factor g^* of free charge carriers in a solid.

The drastic change of the free electron energy spectrum by the magnetic field results in a change of the density of states and of the electronic wave functions. While in the magnetic field-free case the eigenfunctions are plane waves with the wave vector \mathbf{k} determined by the periodic boundary conditions, now we have oscillator functions with the quantum number n in the plane perpendicular to the magnetic field. A closer inspection shows that the Landau levels are highly degenerate with a degeneracy depending on the magnetic field. It can be obtained by starting from the Hamiltonian H (4.28) with the Landau gauge in the form

$$H = \frac{1}{2m} (p_x^2 + (p_y + eBx)^2 + p_z^2) + \mu_B \sigma_z B, \quad (4.38)$$

satisfying the commutation relations $[H, p_y] = [H, p_z] = 0$. Thus, besides k_z , k_y is also a good quantum number. Making use of this fact we write

$$H = \frac{p_x^2}{2m} + \frac{1}{2}m\omega_c^2(x - x_0)^2 + \frac{\hbar^2 k_z^2}{2m} + \mu_B \sigma_z B. \quad (4.39)$$

Here $x_0 = \hbar k_y / m\omega_c = l^2 k_y$ is the so-called *center coordinate* of the classical cyclotron orbit. It becomes quantized by applying periodic boundary conditions in y (as in Sect. 4.1) with $k_y = 2\pi n_y / L_y$. Assuming in x direction a width L_x of the solid, the natural condition $0 < x_0 < L_x$ for the center coordinate leads to

$$0 < n_y < \frac{L_x L_y}{2\pi l^2} = \frac{L_x L_y}{2\pi \hbar} eB. \quad (4.40)$$

This defines the degree of degeneracy, which is the maximum number of states (counted by n_y) in a Landau level at fixed k_z for a given spin in a system with area $L_x L_y$ perpendicular to the magnetic field \mathbf{B} . As $BL_x L_y$ is the flux Φ of the magnetic induction threading the system area, the degeneracy can also be written as

$$\frac{L_x L_y}{2\pi \hbar} eB = \frac{\Phi}{\Phi_0} \quad (4.41)$$

where $\Phi_0 = h/e$ is the *elementary flux quantum*.

For a two-dimensional system with N electrons in the plane perpendicular to the magnetic field, the ratio $\nu = N\Phi_0/\Phi$ gives the number of filled Landau levels (note that in this case there is no dispersion with k_z) and is called *filling factor*. Its inverse gives the number of elementary flux quanta per electron. As we shall see in Sects. 5.7 and 7.6, the integer (fractional) filling factor marks the characteristic features in the magneto-transport data connected with the integer (fractional) quantum Hall effect.

For three-dimensional systems one has to consider also the dispersion parallel to the magnetic field. By applying periodic boundary conditions to make k_z countable, the number of states at k_z is $2L_z\Phi/2\pi V\Phi_0 = eB/2\pi^2\hbar$ and leads to the energy dependent density of states

$$D(E, B) = \frac{eBV}{2\pi^2\hbar} \frac{dk_z}{dE}. \quad (4.42)$$

Solving (4.35) for k_z as a function of the single-particle energy (here denoted by E) this can be expressed as

$$D(E, B) = \sum_{n, \sigma = \pm 1} \frac{eBV}{2\pi^2\hbar} \left(\frac{2m}{\hbar^2}\right)^{1/2} \frac{1}{2} \left\{ E - \hbar\omega_c \left(n + \frac{1}{2} + \frac{\sigma}{2}\right) \right\}^{-\frac{1}{2}} \quad (4.43)$$

or, using the cyclotron frequency ω_c , as

$$D(E, B) = \frac{V\sqrt{\hbar\omega_c}}{8\pi^2} \left(\frac{2m}{\hbar^2}\right)^{3/2} \sum_{n, \sigma = \pm} \left\{ \frac{E}{\hbar\omega_c} - \left(n + \frac{1}{2} + \frac{\sigma}{2}\right) \right\}^{-\frac{1}{2}}. \quad (4.44)$$

The sum includes only contributions with positive radicands. For 3D electrons, the density of states $D(E, B)$ (4.44) is a superposition of inverse square root functions resulting from the free particle motion parallel to the magnetic field (see the solution of Problem 4.3 for the one-dimensional case). The singularities of the inverse square-root functions mark the discrete energies of the Landau levels. They move with changing B and also their strength (related to the degeneracy) changes with B . This density of states differs strongly from the case for $B = 0$ (see Fig. 4.2) and gives rise to the characteristic properties of the free electron system in a magnetic field. They will be discussed in the following paragraph.

The Fermi energy (at $T = 0$ K) is given in analogy to (4.13) by the relation

$$\begin{aligned} N &= \int_0^{E_F(B)} D(E, B) dE \\ &= \frac{1}{4\pi^2} \left(\frac{2m}{\hbar^2}\hbar\omega_c\right)^{3/2} \sum_{n, \sigma} \left\{ \frac{E_F(B)}{\hbar\omega_c} - \left(n + \frac{1}{2} + \frac{\sigma}{2}\right) \right\}^{1/2}, \quad (4.45) \end{aligned}$$

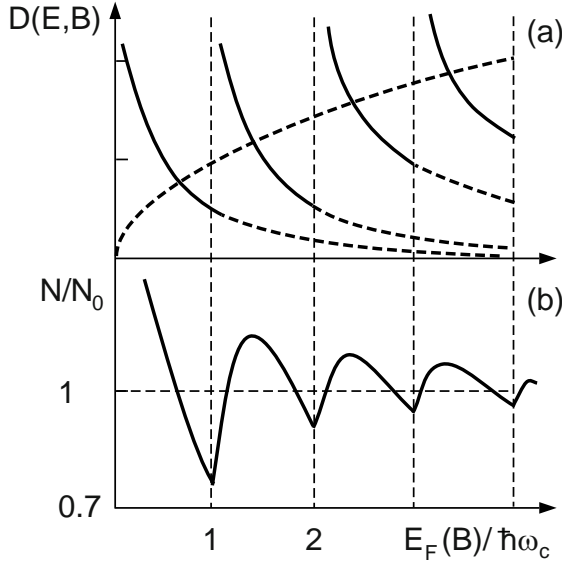


Fig. 4.5. (a) Density of states of free electrons with (*solid line*) and without (*dashed line*) magnetic field; (b) Ratio of electron numbers for occupying all states with and without magnetic field up to $E_F(B)$

which, however, cannot be solved for $E_F(B)$. Therefore, we first compare with the case without magnetic field

$$N_0 = \int_0^{E_F} D(E)dE = \frac{1}{3\pi^2} \left(\frac{2m}{\hbar^2} E_F \right)^{3/2} \quad (4.46)$$

by writing

$$\frac{N}{N_0} = \frac{3}{4} \left(\frac{\hbar\omega_c}{E_F} \right)^{3/2} \sum_{n,\sigma} \left\{ \frac{E_F(B)}{\hbar\omega_c} - \left(n + \frac{1}{2} + \frac{\sigma}{2} \right) \right\}^{1/2}. \quad (4.47)$$

Let us now fill the densities of states $D(E, B)$ and $D(E)$ up to the same energy $E_F(B)$ and look for the ratio N/N_0 (see Fig. 4.5) : For $0 < E_F(B)/\hbar\omega_c < 1$ we start with $N/N_0 > 1$ but N/N_0 decreases monotonously with increasing $E_F(B)$, finally falling below 1 (Fig. 4.5b). In the interval $1 < E_F(B)/\hbar\omega_c < 2$ the ratio N/N_0 first increases strongly, reaches a maximum value > 1 and then for $E_F(B) \rightarrow 2\hbar\omega_c$ falls again below the value 1. This behavior is repeated with increasing values of $E_F(B)$ and we find an oscillating function with a characteristic period in the dependence on $1/B$ given by

$$\Delta_{1/B} = e\hbar/mE_F(B). \quad (4.48)$$

This oscillation is a consequence of the quantization into Landau levels. The Fermi energy $E_F(B)$ for the given number of electrons $N = N_0$ is found by the

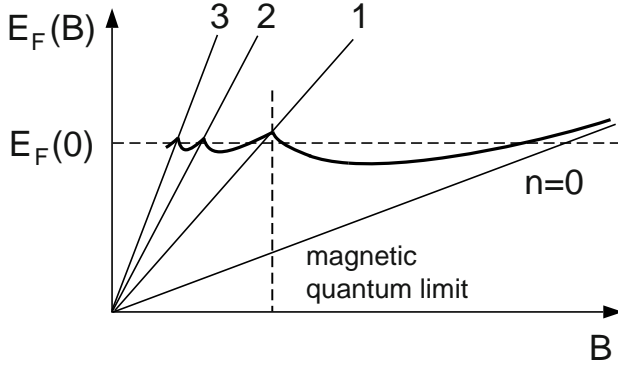


Fig. 4.6. Energies of Landau levels and Fermi energy versus magnetic field (spin-splitting is not shown)

lowering (raising) of $E_F(B)$ relative to $E_F(0)$ in intervals in which, according to Fig. 4.5b, $N/N_0 > 1$ ($N/N_0 < 1$). The result is shown in Fig. 4.6 with $E_F(B)$ oscillating around $E_F(0)$ with the period $\Delta_{1/B}$. This behavior of the Fermi energy, resulting from the Landau quantization, leads to a characteristic oscillating dependence of solid state properties on the magnetic field, the *quantum oscillations*. By measuring this period the magnetic field dependent Fermi energy $E_F(B)$ and thus the particle density can be determined. With increasing magnetic field the oscillations become weaker (and smoothen out at finite temperature). Therefore, they can be detected only at sufficiently high magnetic fields and low temperatures given by $\hbar\omega_c > k_B T$. For $\hbar\omega_c > E_F(B)$, when only states in the lowest Landau level are occupied, we reach the so-called *magnetic quantum limit* (Problem 4.4).

Let us draw attention to the magnetization as the basic material property in this context. Starting point for describing the magnetization is the Gibbs free energy $F = \mu N + \Omega$, with the chemical potential μ , the particle number N , and the grand-canonical potential ($\beta = 1/k_B T$)

$$\Omega = -\frac{1}{\beta} \ln Z_G = -\frac{1}{\beta} \sum_{\alpha} \ln(1 + e^{-\beta(\epsilon_{\alpha} - \mu)}). \quad (4.49)$$

The sum is over the single-particle states with $\epsilon_{\alpha} = \epsilon(n, k_z, \sigma)$ (see (4.35)). For its evaluation, we refer to the literature [115, 116]. The magnetization, which for the isotropic system of free electrons has only one nonvanishing component parallel to the external magnetic field, is obtained from the free energy F according to

$$M_z = -\frac{1}{V} \left(\frac{dF}{dB} \right)_{T, \mu} \quad (4.50)$$

and reads (with $x = E_F/\mu_B B$ and $y = \pi k_B T/\mu_B B$)

$$M_z = \frac{3}{2} \frac{N}{V} \frac{\mu_B^2}{E_F} B \left[1 - \frac{1}{3} + y(x)^{1/2} \sum_{n=1}^{\infty} \frac{(-1)^n}{\sqrt{n}} \cos(n\pi) \frac{\sin(\pi/4 - n\pi x)}{\sinh(n\pi y)} \right]. \quad (4.51)$$

Here we have replaced the chemical potential $\mu(B, T)$ by its value at $T = 0$ K, briefly written as E_F .

In the context of linear response, the magnetization, expressed in the form $M_z = \chi^M B/\mu_0$, is determined by a response function, the *magnetic susceptibility* χ^M which (up to the vacuum permittivity μ_0) is the derivative

$$\chi^M = \mu_0 \left(\frac{\partial M_z}{\partial B} \right)_T \quad (4.52)$$

of M_z from (4.51). χ^M is an experimentally accessible function of B and T . The individual terms in (4.51) have the following physical meaning:

- *Pauli spin paramagnetism*: The first term, showing an increase with increasing magnetic field, is a paramagnetic contribution. It can be traced back to the spin-splitting due to the Zeeman term. Suppressing the Landau quantization, we obtain the picture of Fig. 4.7: The energy levels and therefore the density of states $D_{\uparrow\downarrow}(E)$ of electrons with different spin are shifted against each other by the Zeeman energy $\mu_B B$. Filling the states with $D_{\uparrow\downarrow}(E)$ up to E_F , there are more electrons with spin down than with spin up. Assuming $E_F \gg \mu_B B$ one finds the resulting magnetization (Problem 4.5)

$$M_z^{\text{para}} = \frac{3}{2} \frac{N}{V} \frac{\mu_B^2}{E_F} B. \quad (4.53)$$

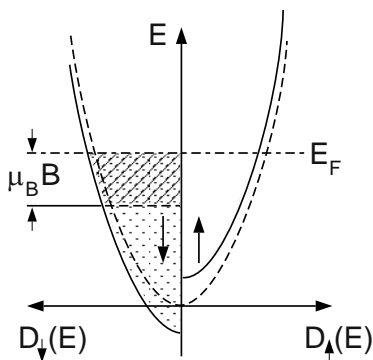


Fig. 4.7. Density of states for spin-up and spin-down electrons (Landau quantization is suppressed). The dashed lines show the situation for $B = 0$

As can be seen from Fig. 4.7, M_z^{para} depends on the density of states (or the electron mass) and on the g factor at the Fermi energy. In solids, we expect material specific deviations of the experimental values for the Pauli susceptibility

$$\chi_{\text{spin}} = \frac{dM_z^{\text{para}}}{dB} = \frac{2}{3}D(E_F)\mu_B^2, \quad (4.54)$$

from the free electron value indicating the already mentioned modifications of these parameters due to the periodic potential and the electron–electron interaction. In fact such deviations are particularly strong, e.g., for heavy fermion systems, as was the case for the specific heat.

- *Landau–Peierls*⁵ *diamagnetism*: The second term is negative, acting against the external magnetic field according to the Lenz rule applied to the cyclotron motion of the electrons. The magnetic moment connected with this motion has a direction opposite to the external magnetic field and results in a diamagnetic contribution. For free electrons in a periodic potential, which can be described as particles with an effective mass m^* , the diamagnetic contribution is to be multiplied by a factor $(m^*/m)^2$:

$$M_z^{\text{dia}} = -\frac{1}{2} \frac{N}{V} \frac{\mu_B^2 B}{E_F} \left(\frac{m^*}{m}\right)^2 \quad (4.55)$$

For mass ratios $m^*/m \simeq 1$ (see Table 4.2), we expect comparable values of the para- and dia-magnetic contributions. But there are also systems with $m^*/m \gg 1$ due to orbital contributions of d and f electrons, for which the diamagnetic term dominates.

- *de Haas–van Alphen*⁶ *effect*: The third term describes the already mentioned oscillating contribution, periodic in $1/B$ with a period determined by the Fermi energy, which is characteristic for Landau quantization. In fact, this behavior of the magnetic susceptibility is found in metals and known as *de Haas–van Alphen effect*. It can be used to determine the Fermi energy or, more precisely, the parameters of the *Fermi surface*, which for solids can deviate from the spherical form (see Sect. 5.7). The sum in the oscillating contribution converges rapidly due to the denominator and usually it suffices to consider only the first term with $n = 1$:

$$\chi_{\text{osc}}(B) \simeq -\mu_0 \frac{3}{2} \frac{N}{V} \frac{\pi^2 k_B T}{B^2} \left(\frac{m^*}{m} x\right)^{1/2} \cos\left(\pi \frac{m^*}{m}\right) \frac{\cos\left(\frac{\pi}{4} - \frac{m^* \pi x}{m}\right)}{\sinh\left(\frac{m^* \pi y}{m}\right)}. \quad (4.56)$$

Here we have considered again possible deviations of the effective mass from the free electron mass. An example of de Haas–van Alphen oscillations measured for Cu is shown in Fig. 4.8.

⁵ Sir Rudolf Ernst Peierls 1907–1995

⁶ Wander Johannes de Haas 1878–1960, P.M. van Alphen 1906–1967

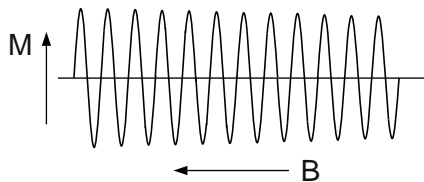


Fig. 4.8. Oscillating part of the magnetization (de Haas–van Alphen oscillations) for Cu (after [117])

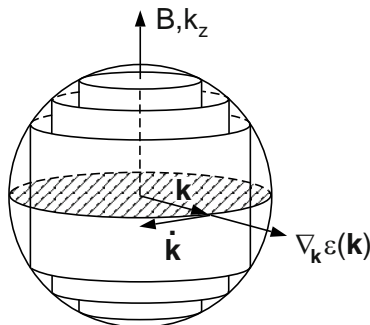


Fig. 4.9. Fermi sphere and extremal cross section perpendicular to the magnetic field to illustrate the cyclotron motion in \mathbf{k} space

It should be noted that the Landau quantization also shows up in other magnetic field dependent electronic properties of solids. One important example represent the *Shubnikov⁷–de Haas oscillations* in the magneto conductivity, which for two-dimensional electron systems at high magnetic fields and low temperature evolve into the *quantum Hall effect* (see Sect. 5.6).

All these quantum oscillations can be understood in a semi-classical description. It starts from the classical equation of motion of an electron under the Lorentz force

$$\dot{\mathbf{p}} = e(\mathbf{v} \times \mathbf{B}), \quad (4.57)$$

leading to the cyclotron motion. In semi-classical terms, we use $\mathbf{p} = \hbar\mathbf{k}$ and the group velocity $\mathbf{v} = \nabla_{\mathbf{k}}\epsilon(\mathbf{k})/\hbar$ to obtain the corresponding equation of motion in \mathbf{k} space

$$\frac{d\mathbf{k}}{dt} = \frac{e}{\hbar^2} (\nabla_{\mathbf{k}}\epsilon(\mathbf{k}) \times \mathbf{B}). \quad (4.58)$$

While in real space the electrons perform the classical cyclotron motion, their momentum (or wave vector) moves along the contour defined by cutting the Fermi sphere with a plane perpendicular to the magnetic field (see Fig. 4.9),

⁷ Lev Vasiljevich Shubnikov 1901–1937

which is the circle with radius k_F . The period of this motion is obtained after separation of variables as

$$\Theta = \frac{\hbar^2}{e} \frac{1}{B} \oint_{\epsilon(\mathbf{k})=E_F} \frac{d\mathbf{k}}{|\nabla_{\mathbf{k}}\epsilon(\mathbf{k})_{\perp}|}, \quad (4.59)$$

where the denominator is the modulus of the gradient of $\epsilon(\mathbf{k})$ in the direction perpendicular to \mathbf{B} . The contour integral equals the area of the extremal cross section of the Fermi sphere. As will be shown in Chap. 5, the relation between the period of these quantum oscillations (in $1/B$) and extremal cross sections perpendicular to the magnetic field applies to Fermi surfaces of nonspherical shape as well and is used for their exploration.

4.3 Occupation Number Representation for Electrons

In Sect. 4.1, we have introduced the many-particle wave function of the N electron system in the form of (4.4) as a product of single particle wave functions and considered the Pauli principle in the construction of the Fermi sphere only by avoiding double occupancies. However, the important property of a many-fermion wave function, which has to be antisymmetric with respect to interchanging two particles, is not fulfilled by this form. Therefore, we replace it now by an antisymmetrised product. For $N = 2$ the two-particle wave function is

$$\Psi(x_1, x_2) = \frac{1}{\sqrt{2}} (\psi_{\alpha_1}(x_1)\psi_{\alpha_2}(x_2) - \psi_{\alpha_1}(x_2)\psi_{\alpha_2}(x_1)) \quad (4.60)$$

with $\psi_{\alpha_i}(x_j)$ being ortho-normalized single-particle wave functions for states characterized by a complete set of quantum numbers α_i (for free electrons $\alpha_i = \mathbf{k}_i\sigma_i$) and x_j denotes space and spin variables. The corresponding generalization for N electrons is the *Slater*⁸ *determinant* (with i short for α_i)

$$\Psi_{\text{Slater}}(\{x_j, j = 1 \dots N\}) = \frac{1}{\sqrt{N!}} \begin{vmatrix} \psi_1(x_1) & \psi_1(x_2) & \dots & \psi_1(x_N) \\ \psi_2(x_1) & \psi_2(x_2) & \dots & \psi_2(x_N) \\ \dots & \dots & \dots & \dots \\ \psi_N(x_1) & \psi_N(x_2) & \dots & \psi_N(x_N) \end{vmatrix}. \quad (4.61)$$

By construction, it is antisymmetric under the exchange of two rows or columns and thus equals zero if two rows, i.e., the corresponding α , are identical. Thus double occupancy is avoided. Calculations with the Slater determinant are very clumsy and a more elegant formulation, the *occupation number* or *Fock*⁹ *representation*, is used instead.

⁸ John Clarke Slater 1900–1976

⁹ Vladimir Fock 1898–1974

The N -electron state can be represented in the form similar to the one used for phonons in Sect. 3.3

$$|\Psi\rangle = |\{n_\alpha, \text{all } \alpha\}\rangle, \quad (4.62)$$

but here the occupancy n_α of the single-particle state with quantum numbers α is restricted to 0 or 1 to account for the Pauli principle. The total number of electrons in the state $|\Psi\rangle$ is given by $N = \sum_\alpha n_\alpha$. N -particle states can be obtained in a systematic way from the *fermion vacuum*

$$|0\rangle = |\{n_\alpha = 0, \text{all } \alpha\}\rangle \quad (4.63)$$

by successively applying N fermion creation operators

$$|\Psi\rangle = c_{\alpha_1}^\dagger c_{\alpha_2}^\dagger \dots c_{\alpha_N}^\dagger |0\rangle. \quad (4.64)$$

In contrast to the case of the creation operators for phonons introduced in Sect. 3.3, now the order in which the operators are applied becomes important. The anti-symmetry of the N particle state is guaranteed by the anti-commutation relations for fermion creation and annihilation operators

$$\{c_\alpha^\dagger, c_{\alpha'}\} = c_\alpha^\dagger c_{\alpha'} + c_{\alpha'} c_\alpha^\dagger = \delta_{\alpha\alpha'} \quad (4.65)$$

$$\{c_\alpha, c_{\alpha'}\} = \{c_\alpha^\dagger, c_{\alpha'}^\dagger\} = 0. \quad (4.66)$$

Let us first look at the 2-electron state which can be generated by applying two creation operators to the fermion vacuum: according to the commutation relation we have

$$|\Psi\rangle = c_{\alpha_1}^\dagger c_{\alpha_2}^\dagger |0\rangle \quad \text{but} \quad c_{\alpha_2}^\dagger c_{\alpha_1}^\dagger |0\rangle = -|\Psi\rangle. \quad (4.67)$$

The adopted order of the applied fermion operators (with $\alpha_1 \neq \alpha_2$) determines the result obtained when applying c_{α_1} or c_{α_2} . One finds

$$c_{\alpha_1} |\Psi\rangle = c_{\alpha_1} c_{\alpha_1}^\dagger c_{\alpha_2}^\dagger |0\rangle = (1 - c_{\alpha_1}^\dagger c_{\alpha_1}) c_{\alpha_2}^\dagger |0\rangle = c_{\alpha_2}^\dagger |0\rangle, \quad (4.68)$$

but $c_{\alpha_2} |\Psi\rangle = -c_{\alpha_1}^\dagger |0\rangle$, because in the first step c_{α_2} has to be interchanged with $c_{\alpha_1}^\dagger$ which results in a sign change. This example for $N = 2$ demonstrates the influence of the order in which the fermion operators are applied to the vacuum state to create $|\Psi\rangle$. In general, for an N -electron state $|\Psi\rangle = c_{\alpha_1}^\dagger \dots c_{\alpha_N}^\dagger |0\rangle = |\{n_\alpha, \text{all } \alpha; N = \sum_\alpha n_\alpha\}\rangle$ we have

$$c_{\alpha_i} |\Psi\rangle = (-1)^{\nu_i} n_{\alpha_i} |\dots, n_{\alpha_i} - 1, \dots\rangle, \quad \nu_i = \sum_{k=1}^{i-1} n_{\alpha_k} \quad (4.69)$$

$$c_{\alpha_i}^\dagger |\Psi\rangle = (-1)^{\nu_i} (1 - n_{\alpha_i}) |\dots, n_{\alpha_i} + 1, \dots\rangle, \quad (4.70)$$

where the dots indicate unchanged entries. Note that the sum of the occupation numbers in the first equation is $N - 1$, because one fermion of $|\Psi\rangle$ is

annihilated, while for the second equation it is $N + 1$ due to the addition of one particle to $|\Psi\rangle$.

The meaning of *occupation number representation* can be also illustrated by applying $c_{\alpha_i}^\dagger c_{\alpha_i}$ to the N -particle state $|\Psi\rangle$. We find

$$c_{\alpha_i}^\dagger c_{\alpha_i} |\Psi\rangle = (-1)^{\nu_i} n_{\alpha_i} c_{\alpha_i}^\dagger |\dots n_{\alpha_i} - 1 \dots\rangle \quad (4.71)$$

$$= (-1)^{2\nu_i} n_{\alpha_i} (1 - (n_{\alpha_i} - 1)) |\dots n_{\alpha_i} \dots\rangle \quad (4.72)$$

$$= \begin{cases} |\Psi\rangle & n_{\alpha_i} = 1 \\ 0 & n_{\alpha_i} = 0 \end{cases} \quad (4.73)$$

or in short

$$c_{\alpha_i}^\dagger c_{\alpha_i} |\Psi\rangle = n_{\alpha_i} |\Psi\rangle. \quad (4.74)$$

Thus the eigenvalue of $c_{\alpha_i}^\dagger c_{\alpha_i}$ is the occupation number n_{α_i} of the single-particle state with quantum numbers α_i in $|\Psi\rangle$ and

$$\hat{N} = \sum_{\alpha} c_{\alpha}^\dagger c_{\alpha} = \sum_{\alpha} \hat{n}_{\alpha} \quad (4.75)$$

is the number operator with the eigenvalue equation $\hat{N}|\Psi\rangle = N|\Psi\rangle$.

The occupation number or Fock representation allows one to formulate the system Hamiltonian in terms of creation and annihilation operators. We give here only the rules for how the one- (\hat{A}_1) and two-particle (\hat{A}_2) terms of the Hamiltonian (or any other operator) have to be rewritten and refer for details to the Appendix (A.6):

$$\hat{A}_1 \rightarrow \sum_{ij} \langle \psi_{\alpha_i} | \hat{A}_1 | \psi_{\alpha_j} \rangle c_{\alpha_i}^\dagger c_{\alpha_j} \quad (4.76)$$

$$\hat{A}_2 \rightarrow \sum_{ijkl} \langle \psi_{\alpha_i}^{(1)} \psi_{\alpha_j}^{(2)} | \hat{A}_2 | \psi_{\alpha_l}^{(1)} \psi_{\alpha_k}^{(2)} \rangle c_{\alpha_i}^\dagger c_{\alpha_j}^\dagger c_{\alpha_k} c_{\alpha_l}. \quad (4.77)$$

These expressions have an obvious meaning: The one-particle operator (depending on the coordinates of only one particle) replaces a particle with quantum numbers α_j by a particle with α_i , the two-particle or interaction operator removes first a particle in the state α_l and then another one in the state α_k and adds particles in the states α_j and α_i . The weight of the operators are matrix elements of the original operators taken with the single-particle wave functions ψ_{α} of an orthonormal set. The upper index (1) and (2) in the matrix element of the two-particle operator indicates the pairs of wave functions which have the same coordinates when integrating in position representation.

This concept is now applied to the system of free electrons for which

$$\{c_{\mathbf{k}\sigma}^\dagger, c_{\mathbf{k}'\sigma'}\} = \delta_{\mathbf{k}\mathbf{k}'} \delta_{\sigma\sigma'} \quad (4.78)$$

and

$$\hat{N} = \sum_{\mathbf{k}\sigma} \hat{n}_{\mathbf{k}\sigma}, \quad \hat{n}_{\mathbf{k}\sigma} = c_{\mathbf{k}\sigma}^\dagger c_{\mathbf{k}\sigma}, \quad \psi_{\mathbf{k}\sigma}(x) = \frac{1}{\sqrt{V}} e^{i\mathbf{k}\cdot\mathbf{r}} \chi_\sigma(s), \quad (4.79)$$

where $\chi_\sigma(s)$ is a Pauli spinor and s denotes the spin variable. The Hamiltonian for the jellium model of free electrons (with the jellium term H_+ from Problem 4.1)

$$\mathcal{H}_{\text{jell}} = \sum_l \frac{\mathbf{p}_l^2}{2m} + \frac{1}{8\pi\epsilon_0} \sum_{\substack{k,l \\ k \neq l}} \frac{e^2}{|\mathbf{r}_k - \mathbf{r}_l|} + H_+, \quad (4.80)$$

can be rewritten (by making use of (4.76) and (4.77)) with

$$\sum_l \frac{\mathbf{p}_l^2}{2m} \rightarrow \sum_{\mathbf{k}\sigma} \frac{\hbar^2 k^2}{2m} c_{\mathbf{k}\sigma}^\dagger c_{\mathbf{k}\sigma} \quad (4.81)$$

and

$$\sum_{\substack{k,l \\ k \neq l}} \frac{e^2}{4\pi\epsilon_0 |\mathbf{r}_k - \mathbf{r}_l|} \rightarrow \langle \psi_{\mathbf{k}_1\sigma_1} \psi_{\mathbf{k}_2\sigma_2} | \frac{e^2}{4\pi\epsilon_0 |\mathbf{r}_1 - \mathbf{r}_2|} | \psi_{\mathbf{k}'_1\sigma'_1} \psi_{\mathbf{k}'_2\sigma'_2} \rangle \quad (4.82)$$

$$= \delta_{\sigma_1\sigma'_1} \delta_{\sigma_2\sigma'_2} \sum_{\mathbf{k}} v_{\mathbf{k}} \delta_{\mathbf{k}_1, \mathbf{k}'_1 + \mathbf{k}} \delta_{\mathbf{k}_2, \mathbf{k}'_2 - \mathbf{k}} \quad (4.83)$$

where $v_{\mathbf{k}} = e^2/\epsilon_0 V k^2$ is the Fourier transform of the Coulomb potential (see Appendix). With the replacements $\sigma_1 = \sigma'_1 = \sigma$, $\sigma_2 = \sigma'_2 = \sigma'$ and $\mathbf{k}'_1 \rightarrow \mathbf{p}$, $\mathbf{k}'_2 \rightarrow \mathbf{q}$ we find

$$\mathcal{H}_{\text{jell}} = \sum_{\mathbf{k}\sigma} \frac{\hbar^2 k^2}{2m} c_{\mathbf{k}\sigma}^\dagger c_{\mathbf{k}\sigma} + \frac{1}{2} \sum_{\substack{\mathbf{p}, \mathbf{q}, \mathbf{k} \\ \sigma, \sigma'}} v_{\mathbf{k}} c_{\mathbf{p}+\mathbf{k}\sigma}^\dagger c_{\mathbf{q}-\mathbf{k}\sigma'}^\dagger c_{\mathbf{q}\sigma'} c_{\mathbf{p}\sigma} + H_+. \quad (4.84)$$

The interaction term becomes divergent for $\mathbf{k} \rightarrow 0$. However, this divergence is exactly compensated by the jellium term for which we obtained as solution of Problem 4.1 $H_+ = -\frac{1}{2} v_0 N^2$ while $\frac{1}{2} \sum_{\mathbf{p}, \mathbf{q}, \sigma, \sigma'} v_0 c_{\mathbf{p}\sigma}^\dagger c_{\mathbf{q}\sigma'}^\dagger c_{\mathbf{q}\sigma'} c_{\mathbf{p}\sigma} = \frac{1}{2} v_0 \sum_{\mathbf{p}\sigma} \hat{n}_{\mathbf{p}\sigma} \sum_{\mathbf{q}\sigma'} \hat{n}_{\mathbf{q}\sigma'} = \frac{1}{2} v_0 N^2$. Thus we arrive at the Hamiltonian for free electrons in the jellium model

$$\mathcal{H}_{\text{jell}} = \sum_{\mathbf{k}\sigma} \frac{\hbar^2 k^2}{2m} c_{\mathbf{k}\sigma}^\dagger c_{\mathbf{k}\sigma} + \frac{1}{2} \sum_{\substack{\mathbf{p}, \mathbf{q}, \mathbf{k} \neq 0 \\ \sigma, \sigma'}} v_{\mathbf{k}} c_{\mathbf{p}+\mathbf{k}\sigma}^\dagger c_{\mathbf{q}-\mathbf{k}\sigma'}^\dagger c_{\mathbf{q}\sigma'} c_{\mathbf{p}\sigma}. \quad (4.85)$$

Its first term accounts for the single-particle energy of free noninteracting electrons, while the second term describes the electron–electron interaction. The interaction term is visualized in Fig. 4.10 as a Feynman diagram with the solid lines representing incoming and outgoing electrons with their respective

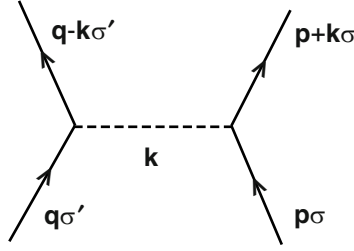


Fig. 4.10. Feynman diagram of the electron–electron interaction. The *solid lines* represent propagating electrons, the *dashed line* the Coulomb potential

wave vector and spin and the dashed line symbolizes the Coulomb interaction. This Hamiltonian does not only apply to electron systems in vacuum, but also to those realized in matter (see Table 4.1), however, by replacing the free electron mass by an effective mass and screening the Coulomb interaction with the dielectric constant of the matter. Moreover it applies also to electron systems in energy bands, however, with a matrix element between full Bloch states (see Chaps. 5 to 7). In the following sections we develop the concepts for approximate solutions of the ground state problem for the jellium model.

4.4 Hartree–Fock Approximation

In Sect. 4.1, we have characterized the ground state of the noninteracting electron system (at $T = 0$ K) as the filled Fermi sphere. The corresponding N -particle wave function, that takes into account the Pauli principle, is a Slater determinant composed of the wave functions of occupied single-particle states, i.e., plane waves with $|\mathbf{k}| \leq k_F$ but it can also be obtained by applying creation operators to the fermion vacuum to fill the Fermi sphere. Let us denote this ground state by $|\Psi_0\rangle$. We may now calculate the expectation value of $\mathcal{H}_{\text{jell}}$ from (4.85) with $|\Psi_0\rangle$ giving the ground state energy in *Hartree*¹⁰–*Fock* (HF) *approximation*

$$\begin{aligned}
 E_0^{\text{HF}} = \langle \Psi_0 | \mathcal{H}_{\text{jell}} | \Psi_0 \rangle &= \sum_{\mathbf{k}\sigma} \langle \Psi_0 | \frac{\hbar^2 k^2}{2m} c_{\mathbf{k}\sigma}^\dagger c_{\mathbf{k}\sigma} | \Psi_0 \rangle \\
 &+ \frac{1}{2} \sum_{\substack{\mathbf{k} \neq 0 \\ \mathbf{q}, \mathbf{p}, \sigma, \sigma'}} \langle \Psi_0 | v_{\mathbf{k}} c_{\mathbf{p}+\mathbf{k}\sigma}^\dagger c_{\mathbf{q}-\mathbf{k}\sigma'}^\dagger c_{\mathbf{q}\sigma'} c_{\mathbf{p}\sigma} | \Psi_0 \rangle. \quad (4.86)
 \end{aligned}$$

The first term reproduces the ground state energy $\frac{3}{5} N E_F$ of the noninteracting electron gas obtained in the Sommerfeld model (Sect. 4.1). The second term is the first order correction due to the Coulomb interaction, which is treated

¹⁰ Douglas Rayner Hartree 1897–1958

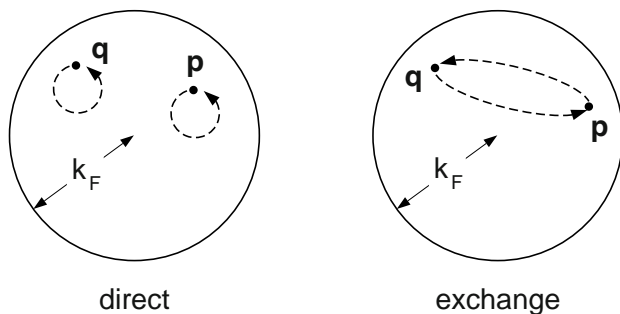


Fig. 4.11. Illustration of the direct and exchange terms in the Fermi sphere

here as a perturbation. Before we discuss the quality of this approximation, this correction has to be calculated. Two contributions, depicted in Fig. 4.11 can be distinguished:

1. Proceeding from right to left the two annihilation operators remove the electrons with $p\sigma$ and $q\sigma'$ from the filled Fermi sphere ($|\Psi_0\rangle$) and the two creation operators add electrons at $p+k\sigma$ and $q-k\sigma'$, respectively. In order to obtain the filled Fermi sphere (or $\langle\Psi_0|$) k has to be zero. However, this term is excluded from the sum over k in the interaction term as a result of the jellium model and hence does not modify the ground state energy of the Sommerfeld model. It should be mentioned, however, that this so-called *direct term* describes the electrostatic interaction energy for a system with charge density n (see Problem 4.1), which becomes important for inhomogenous electron systems (see Chaps. 5 and 6) and defines the *Hartree approximation*.

2. As before, the two annihilation operators remove two electrons from the Fermi sphere, while the two creation operators put them back but now with interchanged wave vectors. This exchange within the Fermi sphere is possible only for electrons having the same spin ($\sigma = \sigma'$) and whose wave vectors differ by $k = q - p$ (see Fig. 4.11). This *exchange term* results from the Pauli principle and does not have a classical analogue (in contrast with the direct term). The *Hartree-Fock approximation* is also understood to have considered the exchange contribution.

The exchange term is evaluated under the constraints of the exchange process ($k = q - p$, $\sigma = \sigma'$) giving

$$E_0^{\text{HF}} = E_0^{\text{H}} + \sum_{\substack{\sigma, q, p \\ q \neq p}} \frac{e^2}{2\varepsilon_0 V |\mathbf{q} - \mathbf{p}|^2} \langle \Psi_0 | c_{q\sigma}^\dagger c_{p\sigma}^\dagger c_{q\sigma} c_{p\sigma} | \Psi_0 \rangle \quad (4.87)$$

with E_0^{H} being the ground state energy in the Hartree approximation. Because of $p \neq q$ the operators, $c_{p\sigma}^\dagger$ and $c_{q\sigma}$ can be interchanged with a sign change and the four-operator expression becomes a product of number operators or their respective eigenvalues, the occupation factors $n_{q\sigma}$, $n_{p\sigma}$. Thus one finds

$$E_0^{\text{HF}} = E_0^{\text{H}} - \sum_{\substack{\sigma, q, p \\ q \neq p}} \frac{e^2}{2\varepsilon_0 V |\mathbf{q} - \mathbf{p}|^2} n_{q\sigma} n_{p\sigma}. \quad (4.88)$$

Taking E_0^{H} from (4.16) and after summing over σ and considering the occupation factors, gives

$$E_0^{\text{HF}} = \frac{3}{5} N E_{\text{F}} - \sum_{\substack{q, p, q \neq p \\ |\mathbf{q}|, |\mathbf{p}| \leq k_{\text{F}}}} \frac{e^2}{\varepsilon_0 V |\mathbf{q} - \mathbf{p}|^2}. \quad (4.89)$$

The evaluation of the sums is explicitly carried out in the Appendix (A.5). It gives

$$E_{\text{exch}} = -\frac{3}{16\pi^2 \varepsilon_0} N e^2 k_{\text{F}}. \quad (4.90)$$

and leads to the important result of this calculation, the ground state energy of the electron gas in HF approximation

$$E_0^{\text{HF}} = \frac{3}{5} N \frac{\hbar^2 k_{\text{F}}^2}{2m} - \frac{3}{16\pi^2 \varepsilon_0} N e^2 k_{\text{F}}. \quad (4.91)$$

Due to the negative contribution of the exchange interaction it is lower than the result of the Sommerfeld model. In the formulation with the dimensionless density parameter r_{s} defined in Sect. 4.1 it reads

$$E_0^{\text{HF}} = N \left\{ \frac{3}{5} \left(\frac{9\pi}{4} \right)^{2/3} \frac{1}{r_{\text{s}}^2} - \frac{3}{4\pi} \left(\frac{9\pi}{4} \right)^{1/3} \frac{2}{r_{\text{s}}} \right\} \text{Ry}. \quad (4.92)$$

As mean value energy per electron the result is written in the form

$$\epsilon_0^{\text{HF}} = \frac{1}{N} E_0^{\text{HF}} = \left\{ \frac{2.2099}{r_{\text{s}}^2} - \frac{0.916}{r_{\text{s}}} \right\} \text{Ry}. \quad (4.93)$$

It is expressed in terms of inverse powers of the density parameter r_{s} , which for the same electron density n can have quite different values depending on the material (see Table 4.1) in which it is realized (Problem 4.6).

In order to go beyond the HF approximation (which is a first order perturbation calculation) one may consider the second order correction because of the Coulomb interaction. This is formulated in Problem 4.7. As it will turn out, this term is logarithmically divergent. Thus higher order perturbation calculation seems not to be the proper way to treat Coulomb interaction and special many-body techniques are required to improve the result. But we can take from (4.93) the message that the HF approximation works well in the high density limit ($r_{\text{s}} \ll 1$).

At this point, two considerations about the HF approximation can be made. The first one aims at an approximate formulation of $\mathcal{H}_{\text{jell}}$ (4.85) as an effective single-particle operator

$$\mathcal{H}_{\text{jell}} \simeq \sum_{\mathbf{k}\sigma} \epsilon_{\mathbf{k}\sigma}^{\text{HF}} c_{\mathbf{k}\sigma}^\dagger c_{\mathbf{k}\sigma} \quad (4.94)$$

with single-particle energies $\epsilon_{\mathbf{k}\sigma}^{\text{HF}}$, which besides the kinetic energy of free particles contain a contribution from the Coulomb interaction according to the HF approximation. A systematic way to calculate $\epsilon_{\mathbf{k}\sigma}^{\text{HF}}$ is the formulation of the equation of motion for the time-dependent fermion operator

$$\frac{d}{dt} c_{\mathbf{k}\sigma}^\dagger = \frac{1}{i\hbar} \left[\mathcal{H}_{\text{jell}}, c_{\mathbf{k}\sigma}^\dagger \right]. \quad (4.95)$$

The commutator of $c_{\mathbf{k}\sigma}$ with the interaction term generates terms consisting of three fermion operators. Here the HF approximation means to replace these terms by the product of an expectation value of the number operator and the remaining fermion operator. This classifies the HF approximation as a *mean field approximation*, see Sect. 6.5. The result takes the form

$$\frac{d}{dt} c_{\mathbf{k}\sigma}^\dagger = \frac{1}{i\hbar} \epsilon_{\mathbf{k}\sigma}^{\text{HF}} c_{\mathbf{k}\sigma}^\dagger \quad (4.96)$$

with the single-particle energy

$$\epsilon_{\mathbf{k}\sigma}^{\text{HF}} = \frac{\hbar^2 k^2}{2m} - \frac{e^2}{\varepsilon_0 V} \sum_{\substack{q \neq k \\ |q| \leq k_F}} \frac{1}{|\mathbf{q} - \mathbf{k}|^2}. \quad (4.97)$$

The evaluation of the sum over \mathbf{q} in the Fermi sphere can be performed as an integral in polar coordinates with ϑ being the angle between \mathbf{q} and \mathbf{k}

$$\begin{aligned} \sum_{\substack{q \neq k \\ |q| \leq k_F}} \frac{1}{|\mathbf{q} - \mathbf{k}|^2} &= \frac{V}{(2\pi)^3} 2\pi \int_0^{k_F} dq q^2 \int_{-1}^{+1} \frac{d \cos \vartheta}{q^2 + k^2 - 2kq \cos \vartheta} \\ &= \frac{V}{(2\pi)^2} \int_0^{k_F} dq \frac{q}{2k} \ln \frac{(q-k)^2}{(q+k)^2}. \end{aligned} \quad (4.98)$$

The last integral can be found in an integral table. Finally, we obtain for the single-particle energy in HF approximation

$$\epsilon_{\mathbf{k}\sigma}^{\text{HF}} = \frac{\hbar^2 k^2}{2m} - \frac{e^2 k_F}{4\pi^2 \varepsilon_0} \left(1 + \frac{k_F^2 - k^2}{2k k_F} \ln \left| \frac{k_F + k}{k_F - k} \right| \right). \quad (4.99)$$

A plot of $\epsilon_{\mathbf{k}\sigma}^{\text{HF}}$ is shown in Fig. 4.12 for a particular choice of the electron density n in reduced units together with the free electron dispersion.

As for the ground state energy, we find for the single-particle energies in the HF approximation a lowering with respect to the free particle energy. Taking the sum over these single particle energies in the Fermi sphere leads back to the result of (4.93). Replacing the Hamiltonian of the jellium model (4.85) as indicated in (4.94) corresponds to describing the interacting free electrons as

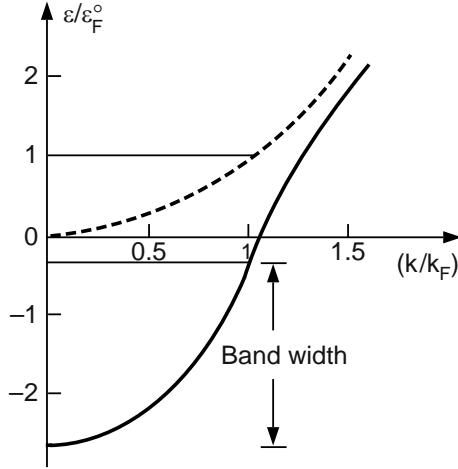


Fig. 4.12. Single-particle HF energy (*solid line*) for $r_s = 4$ in comparison with free particle energy (*dashed line*), after [12]

noninteracting *quasi-particles*, whose single-particle energies incorporate part of the Coulomb interaction. This quasi-particle concept is frequently used in many-body theory.

The second consideration concerns the charge density connected with the exchange interaction. For this purpose, we may rewrite the exchange correction with the Fourier transform of the Coulomb interaction as

$$\begin{aligned}
 - \sum_{\substack{q \neq k \\ |q| \leq k_F}} \frac{e^2}{\varepsilon_0 V} \frac{1}{|\mathbf{q} - \mathbf{k}|^2} &= - \frac{e^2}{4\pi\varepsilon_0} \sum_{\substack{q \neq k \\ |q| \leq k_F}} \frac{1}{V} \int \frac{e^{i(\mathbf{q}-\mathbf{k})\cdot\mathbf{r}}}{r} d^3\mathbf{r} \\
 &= - \int \frac{e\rho_{\mathbf{k}}^{\text{HF}}(\mathbf{r})}{4\pi\varepsilon_0 r} d^3\mathbf{r}.
 \end{aligned} \tag{4.100}$$

The last expression corresponds to the potential energy of an electron at $\mathbf{r} = 0$ in a charge density $\rho_{\mathbf{k}}^{\text{HF}}(\mathbf{r})$ (the HF or exchange charge density) resulting from all electrons in the Fermi sphere having the same spin:

$$\rho_{\mathbf{k}}^{\text{HF}}(\mathbf{r}) = \frac{e}{V} \sum_{\substack{q \neq k \\ |q| \leq k_F}} e^{i(\mathbf{q}-\mathbf{k})\cdot\mathbf{r}} = \frac{e}{V} e^{-i\mathbf{k}\cdot\mathbf{r}} \sum_{\substack{q \neq k \\ |q| \leq k_F}} e^{i\mathbf{q}\cdot\mathbf{r}}. \tag{4.101}$$

By performing the sum over \mathbf{q} as integral over the Fermi sphere in polar coordinates one obtains

$$\rho_{\mathbf{k}}^{\text{HF}}(\mathbf{r}) = \frac{2e}{(2\pi)^2} \frac{e^{-i\mathbf{k}\cdot\mathbf{r}}}{r^3} (\sin(k_F r) - k_F r \cos(k_F r)). \tag{4.102}$$

The mean value of $\rho_{\mathbf{k}}^{\text{HF}}(\mathbf{r})$ over the Fermi sphere gives the averaged HF charge density

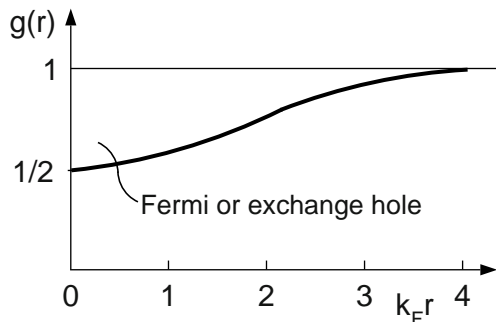


Fig. 4.13. Pair-distribution function $g(r) = 1 - \rho^{\text{HF}}(r)/en$ showing the depression in the vicinity of $r = 0$ known as Fermi or exchange hole

$$\begin{aligned} \rho^{\text{HF}}(r) &= \frac{2}{N} \sum_{|\mathbf{k}| \leq k_F} \rho_{\mathbf{k}}^{\text{HF}}(r) \\ &= \frac{9N}{2V} \frac{e}{(k_F r)^6} (\sin(k_F r) - k_F r \cos(k_F r))^2. \end{aligned} \quad (4.103)$$

The limits

$$\rho^{\text{HF}}(r \rightarrow \infty) = 0 \quad \text{and} \quad \rho^{\text{HF}}(r \rightarrow 0) = \frac{1}{2}en \quad (4.104)$$

indicate the modification of the constant charge density $-en$ of the noninteracting electron gas due to the exchange correction. In the vicinity of an electron with given spin, the charge density is reduced by 50% corresponding to the interaction with all electrons having the same spin. With increasing r , the density approaches the value of the noninteracting electron system. This result can be expressed in terms of the pair-distribution function (see Sect. 1.3)

$$g(r) = 1 - \rho^{\text{HF}}(r)/en \quad (4.105)$$

for free electrons in the HF approximation, which is depicted in Fig. 4.13. It shows a depression around $r = 0$ which is the *Fermi* or *exchange hole* and visualizes the correlation due to the exchange interaction or the Pauli principle.

4.5 The Dielectric Function

The *dielectric function* is the response of the system (here the homogeneous electron system) to a perturbation by an electromagnetic field. It is convenient to consider this perturbation as having the characteristic space and

time dependence given by $\exp(i(\mathbf{q} \cdot \mathbf{r} - \omega t))$ typical for a Fourier component with \mathbf{q} and ω . One can distinguish this perturbation caused by a moving charge (as in a particle scattering process) from that of an electromagnetic wave. The latter case, leading to the *transverse dielectric function* has been the subject of Sect. 3.5. Here we consider the former case: The moving charge is connected with a longitudinal field (directed parallel to the momentum of the moving particle) and the response is the *longitudinal dielectric function* $\varepsilon(\mathbf{q}, \omega)$. For $\omega = 0$ this case includes also the response of the electron system to a static charge placed into the electron system: The electrons will arrange around this static charge due to Coulomb attraction (if the static charge is positive) or repulsion (if it is negative), thus increasing or reducing the otherwise homogeneous density. This effect is known as static *screening*.

In Sect. 2.5, the inverse dielectric function has been introduced already in an exact formulation for an arbitrary system as density–density correlation function between density and number fluctuations. Here we want to derive the inverse dielectric function for the homogeneous electron gas. Starting point is the electron system described by $\mathcal{H}_{\text{jell}}$ and the external perturbation by V_{ext}

$$\mathcal{H} = \mathcal{H}_{\text{jell}} + V_{\text{ext}}. \quad (4.106)$$

Having in mind the results of Sect. 2.5, it is advantageous to use the formulation of $\mathcal{H}_{\text{jell}}$ in terms of number fluctuations $\hat{N}_{\mathbf{k}} = \sum_{\mathbf{p}\sigma} c_{\mathbf{p}+\mathbf{k}\sigma}^\dagger c_{\mathbf{p}\sigma}$ (see Problem 4.8)

$$\mathcal{H}_{\text{jell}} = \sum_{\mathbf{k}\sigma} \frac{\hbar^2 k^2}{2m} c_{\mathbf{k}\sigma}^\dagger c_{\mathbf{k}\sigma} + \frac{1}{2} \sum_{\mathbf{k} \neq 0} v_{\mathbf{k}} \left(\hat{N}_{\mathbf{k}}^\dagger \hat{N}_{\mathbf{k}} - N \right) \quad (4.107)$$

and write the perturbation as

$$V_{\text{ext}} = -v_{\mathbf{q}} N_{\text{ext}} e^{i\mathbf{q} \cdot \mathbf{r} - i\omega t} = -v_{\mathbf{q}} \hat{N}_{-\mathbf{q}} N_{\text{ext}} e^{-i\omega t} \quad (4.108)$$

where we have replaced $\exp(i\mathbf{q} \cdot \mathbf{r})$ by $\hat{N}_{-\mathbf{q}}$.

The response of the homogeneous electron system to a perturbation by an external charge will be a deviation from the homogeneous density in terms of number (or density) fluctuations. For V_{ext} as given in (4.108) the induced number fluctuations are described by

$$N(\mathbf{r}, t) = \langle \hat{N}_{\mathbf{q}} \rangle e^{i\mathbf{q} \cdot \mathbf{r} - i\omega t}. \quad (4.109)$$

In the context of Poisson's equation, the external test charge eN_{ext} and the induced charge (density) fluctuation $eN(\mathbf{r}, t)$ play the role of free and polarization charges, respectively, or in other words: eN_{ext}/V is the source of the dielectric displacement field \mathbf{D} while both eN_{ext} and $eN(\mathbf{r}, t)$ determine the electric field \mathbf{E} , both fields being connected by the dielectric function: $\mathbf{D}(\mathbf{q}, \omega) = \varepsilon_0 \varepsilon(\mathbf{q}, \omega) \mathbf{E}(\mathbf{q}, \omega)$. Thus, as in Sect. 2.5 we may write

$$\mathbf{iq} \cdot \mathbf{E}(\mathbf{q}, \omega) = \frac{e}{V\varepsilon_0} \left(N_{\text{ext}} + \langle \hat{N}_{\mathbf{q}} \rangle \right) \quad (4.110)$$

$$\mathbf{iq} \cdot \mathbf{D}(\mathbf{q}, \omega) = \frac{e}{V} N_{\text{ext}} \quad (4.111)$$

and obtain from these equations the relation

$$\frac{1}{\varepsilon(\mathbf{q}, \omega)} = 1 + \frac{\langle \hat{N}_{\mathbf{q}} \rangle}{N_{\text{ext}}}. \quad (4.112)$$

From (4.108) and (4.109) we identify $\hat{N}_{-\mathbf{q}}$ and $\hat{N}_{\mathbf{q}}$ as the operators \hat{B} and \hat{A} , respectively, of the response formalism, to write the exact expression for the inverse longitudinal dielectric constant as (see (2.80))

$$\frac{1}{\varepsilon(\mathbf{q}, \omega)} = 1 + \lim_{\Gamma \rightarrow 0} v_{\mathbf{q}} \frac{i}{\hbar} \int_0^{\infty} d\tau e^{i\omega\tau - \Gamma\tau} \langle [\hat{N}_{\mathbf{q}}(\tau), \hat{N}_{-\mathbf{q}}(0)] \rangle_0 \quad (4.113)$$

where the damping factor regularizes the integral.

The thermal expectation value under the integral is to be evaluated with the eigenstates of the Hamiltonian $\mathcal{H}_{\text{jell}}$ of the unperturbed system. As these are not known, this can be done only approximately. For $T = 0$ K the thermal expectation value reduces to the expectation value of the ground state $|\Psi_0\rangle$ (see Problem 2.2) and we may write

$$\begin{aligned} \langle \Psi_0 | [\hat{N}_{\mathbf{q}}(\tau), \hat{N}_{-\mathbf{q}}(0)] | \Psi_0 \rangle &= \sum_m \left\{ \langle \Psi_0 | \hat{N}_{\mathbf{q}}(\tau) | \Psi_m \rangle \langle \Psi_m | \hat{N}_{-\mathbf{q}}(0) | \Psi_0 \rangle \right. \\ &\quad \left. - \langle \Psi_0 | \hat{N}_{-\mathbf{q}}(0) | \Psi_m \rangle \langle \Psi_m | \hat{N}_{\mathbf{q}}(\tau) | \Psi_0 \rangle \right\}. \end{aligned} \quad (4.114)$$

The matrix elements can be evaluated by making use of

$$\hat{N}_{\mathbf{q}}(\tau) = e^{\frac{i}{\hbar} \mathcal{H}_{\text{jell}} \tau} \hat{N}_{\mathbf{q}} e^{-\frac{i}{\hbar} \mathcal{H}_{\text{jell}} \tau} \quad \text{and} \quad \hat{N}_{-\mathbf{q}} = \hat{N}_{\mathbf{q}}^\dagger \quad (4.115)$$

to yield $\hbar\omega_{m0} = E_m - E_0$

$$\langle \Psi_0 | [\hat{N}_{\mathbf{q}}(\tau), \hat{N}_{-\mathbf{q}}(0)] | \Psi_0 \rangle = \sum_m |\langle \Psi_0 | \hat{N}_{\mathbf{q}} | \Psi_m \rangle|^2 \{ e^{-i\omega_{m0}\tau} - e^{i\omega_{m0}\tau} \}. \quad (4.116)$$

Thus we obtain the exact expression for the longitudinal dielectric function at $T = 0$ K

$$\begin{aligned} \frac{1}{\varepsilon(\mathbf{q}, \omega)} &= 1 + \lim_{\Gamma \rightarrow 0} \frac{v_{\mathbf{q}}}{\hbar} \sum_m |\langle \Psi_0 | \hat{N}_{\mathbf{q}} | \Psi_m \rangle|^2 \left\{ \frac{1}{\omega_{m0} + \omega + i\Gamma} \right. \\ &\quad \left. + \frac{1}{\omega_{m0} - \omega - i\Gamma} \right\}. \end{aligned} \quad (4.117)$$

Formally, this result is the same as for $\chi(\omega)$ derived in Sect. 3.5 for a transverse perturbation, where however the matrix elements are those of the dipole operator while here they are those of the operator of number fluctuations.

The inverse dielectric function has poles at $\omega = \pm\omega_{m0} - i\Gamma$ in the lower complex ω -plane (see Fig. 3.5), thus measurements of $1/\varepsilon(\mathbf{q}, \omega)$ provide information about the exact excitation energies $\hbar\omega_{m0} = E_m - E_0$. Such experiments are performed as inelastic scattering of charged particles (electrons), in which energy and momentum is transferred to the electron system. This experimental technique is known as *energy-loss spectroscopy*.

Let us evaluate the inverse dielectric function at $T = 0$ K in HF approximation. This is done by calculating the matrix elements of the number fluctuations between the HF ground state (which is the filled Fermi sphere) and excited states, which are obtained by removing an electron from the Fermi sphere and placing it into a state outside (see Fig. 4.14). In other words, the excited states are the Fermi sphere plus an electron-hole excitation. The matrix elements can be evaluated and yield $\hat{N}_{\mathbf{q}} = \sum_{\mathbf{k}\sigma} c_{\mathbf{k}+\mathbf{q}\sigma}^\dagger c_{\mathbf{k}\sigma}$

$$\langle \Psi_{\mathbf{k}\mathbf{q}\sigma} | \hat{N}_{\mathbf{q}'} | \Psi_0 \rangle = \begin{cases} \delta_{\mathbf{q}\mathbf{q}'} & |\mathbf{k}| \leq k_F, |\mathbf{k} + \mathbf{q}| > k_F \\ 0 & \text{otherwise} \end{cases} \quad (4.118)$$

and one finds (with $\hbar\Gamma = \delta$)

$$\frac{1}{\varepsilon^{\text{HF}}(\mathbf{q}, \omega)} = 1 + \lim_{\delta \rightarrow 0} v_{\mathbf{q}} \sum_{\substack{|\mathbf{k}| \leq k_F, \sigma \\ |\mathbf{k} + \mathbf{q}| > k_F}} \left\{ \frac{1}{\hbar\omega + \epsilon_{\mathbf{k}+\mathbf{q}} - \epsilon_{\mathbf{k}} + i\delta} - \frac{1}{\hbar\omega - \epsilon_{\mathbf{k}+\mathbf{q}} + \epsilon_{\mathbf{k}} + i\delta} \right\}. \quad (4.119)$$

Here the energies $\epsilon_{\mathbf{k}}$ ought to be the HF single particle energies, but can be replaced by $\hbar^2 k^2 / 2m$ which is a good approximation for $r_s \ll 1$. The restricted sum can be considered by using the Fermi distribution function $f_{\mathbf{k}}$ and if in addition we replace in the first term $\mathbf{k} + \mathbf{q} \rightarrow -\mathbf{k}$ the *rhs* of (4.119) reads

$$= 1 + \lim_{\delta \rightarrow 0} v_{\mathbf{q}} \sum_{\mathbf{k}, \sigma} \left\{ \frac{f_{-\mathbf{k}-\mathbf{q}}(1 - f_{-\mathbf{k}})}{\hbar\omega + \epsilon_{-\mathbf{k}} - \epsilon_{-\mathbf{k}-\mathbf{q}} + i\delta} - \frac{f_{\mathbf{k}}(1 - f_{\mathbf{k}+\mathbf{q}})}{\hbar\omega - \epsilon_{\mathbf{k}+\mathbf{q}} + \epsilon_{\mathbf{k}} + i\delta} \right\}. \quad (4.120)$$

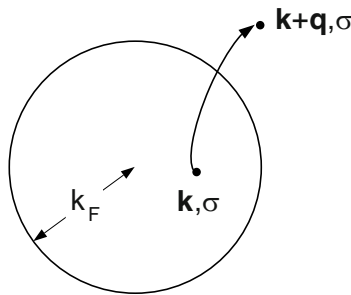


Fig. 4.14. Schematic view of an excited state: Fermi sphere plus electron-hole pair

Finally with $f_{-\mathbf{k}} = f_{\mathbf{k}}$, $\epsilon_{\mathbf{k}} = \epsilon_{-\mathbf{k}}$, and $f_{\mathbf{k}}f_{\mathbf{k}+\mathbf{q}} = 0$ (one of the states is not occupied) one obtains

$$\frac{1}{\varepsilon^{\text{HF}}(\mathbf{q}, \omega)} = 1 + v_{\mathbf{q}}\pi_0(\mathbf{q}, \omega) \quad (4.121)$$

where

$$\pi_0(\mathbf{q}, \omega) = \lim_{\delta \rightarrow 0} \sum_{\mathbf{k}, \sigma} \frac{f_{\mathbf{k}} - f_{\mathbf{k}+\mathbf{q}}}{\hbar\omega - \epsilon_{\mathbf{k}+\mathbf{q}} + \epsilon_{\mathbf{k}} + i\delta}. \quad (4.122)$$

is the *polarization function* of the free noninteracting electron system.

A standard approximation for the inverse longitudinal dielectric function beyond HF is the so-called *random phase approximation* or RPA. Although its derivation in the original literature (where also the name is justified) is quite involved (see [5]) it can be obtained simply by replacing the bare Coulomb interaction $v_{\mathbf{q}}$ by the screened one $v_{\mathbf{q}}/\varepsilon(\mathbf{q}, \omega)$. This gives rise to the following formulation:

$$\begin{aligned} \frac{1}{\varepsilon(\mathbf{q}, \omega)} &= 1 + \frac{v_{\mathbf{q}}}{\varepsilon(\mathbf{q}, \omega)}\pi_0(\mathbf{q}, \omega) \\ &= 1 + v_{\mathbf{q}}\pi_0(\mathbf{q}, \omega)(1 + v_{\mathbf{q}}\pi_0(\mathbf{q}, \omega)(1 + v_{\mathbf{q}}\pi_0(\mathbf{q}, \omega)(\dots))) \\ &= 1 + v_{\mathbf{q}}\pi_0(\mathbf{q}, \omega) + (v_{\mathbf{q}}\pi_0(\mathbf{q}, \omega))^2 + \dots \\ &= \frac{1}{1 - v_{\mathbf{q}}\pi_0(\mathbf{q}, \omega)}. \end{aligned} \quad (4.123)$$

The structure of this expression, reminding of the Born series known from scattering theory, is typical for results obtained for interacting particles and can be cast into a graphic representation in terms of Feynman diagrams [4, 5, 64]. Here we give only the formula for the dielectric function in RPA, also known as the *Lindhard function*,

$$\begin{aligned} \varepsilon^{\text{RPA}}(\mathbf{q}, \omega) &= 1 - v_{\mathbf{q}}\pi_0(\mathbf{q}, \omega) \\ &= 1 - v_{\mathbf{q}} \lim_{\delta \rightarrow 0} \sum_{\mathbf{k}, \sigma} \frac{f_{\mathbf{k}} - f_{\mathbf{k}+\mathbf{q}}}{\hbar\omega - \epsilon_{\mathbf{k}+\mathbf{q}} + \epsilon_{\mathbf{k}} + i\delta}. \end{aligned} \quad (4.124)$$

It should be mentioned, that this result which goes beyond the HF approximation, is not obtained by a more accurate description of the eigenstates rather than by the physical argument of screening applied to the electron–electron interaction in the system. The same result can be obtained in an alternative way known as the *self-consistent field approximation*. The idea here is to consider the induced number density fluctuations together with the external charge as the perturbation of the system but evaluate the response with the HF ground state. This calculation is the subject of Problem 4.9.

4.6 Discussion of the Dielectric Function

Starting from (4.117), the exact expression for the inverse longitudinal dielectric function at $T = 0$ K can be separated with

$$\lim_{\delta \rightarrow 0} \frac{1}{x \pm i\delta} = \mathcal{P} \left(\frac{1}{x} \right) \mp i\pi\delta(x) \quad (4.125)$$

into its real and imaginary part:

$$\operatorname{Re} \frac{1}{\varepsilon(\mathbf{q}, \omega)} = 1 + v_{\mathbf{q}} \sum_m |\langle \Psi_0 | \hat{N}_{\mathbf{q}} | \Psi_m \rangle|^2 \frac{2\hbar\omega_{m0}}{(\hbar\omega)^2 - (\hbar\omega_{m0})^2} \quad (4.126)$$

$$\operatorname{Im} \frac{1}{\varepsilon(\mathbf{q}, \omega)} = -\pi v_{\mathbf{q}} \sum_m |\langle \Psi_0 | \hat{N}_{\mathbf{q}} | \Psi_m \rangle|^2 \{ \delta(\hbar\omega - \hbar\omega_{m0}) - \delta(\hbar\omega + \hbar\omega_{m0}) \}. \quad (4.127)$$

In Sect. 1.3 we have introduced the *dynamic structure factor*

$$S(\mathbf{q}, \omega) = \frac{1}{2\pi} \int_{-\infty}^{\infty} e^{-i\omega t} \langle \hat{N}_{\mathbf{q}}(t) \hat{N}_{-\mathbf{q}}(0) \rangle dt \quad (4.128)$$

which for $T = 0$ K (after resolving the Heisenberg picture for $\hat{N}_{\mathbf{q}}(t)$), introducing a complete set of exact eigenstates, and performing the integration over t) takes the form

$$S(\mathbf{q}, \omega) = \sum_m |\langle \Psi_0 | \hat{N}_{\mathbf{q}} | \Psi_m \rangle|^2 \delta(\omega - \omega_{m0}). \quad (4.129)$$

Thus it is possible to express the imaginary part of the dielectric function as

$$\operatorname{Im} \frac{1}{\varepsilon(\mathbf{q}, \omega)} = -\frac{\pi}{\hbar} v_{\mathbf{q}} (S(\mathbf{q}, \omega) - S(\mathbf{q}, -\omega)). \quad (4.130)$$

Moreover, the differential cross section for inelastic scattering is related with the dynamic structure factor:

$$\frac{d^2\sigma}{d\Omega d\omega} = \frac{k'}{k} \left(\frac{m}{2\pi\hbar} \right)^2 |v_{\mathbf{q}}|^2 S(\mathbf{q}, \omega). \quad (4.131)$$

This relation tells us how to extract information about the excitations in the interacting electron system from inelastic scattering experiments: The cross-section will be enhanced if the experimental settings, \mathbf{q} and ω , correspond to the energy and momentum of an excitation in the electron system. The structure factor or likewise the dielectric function can be expressed in terms of the characteristic excitation energies of the system. Due to this relation $\operatorname{Im}(1/\varepsilon(\mathbf{q}, \omega))$ is known also as the *energy-loss function*.

In order to discuss this in more detail, we look at the dielectric function in RPA $\varepsilon^{\text{RPA}}(\mathbf{q}, \omega) = \varepsilon_1(\mathbf{q}, \omega) + i\varepsilon_2(\mathbf{q}, \omega)$ with

$$\varepsilon_1(\mathbf{q}, \omega) = 1 + v_{\mathbf{q}} \sum_{\mathbf{k}\sigma} \frac{f_{\mathbf{k}+\mathbf{q}} - f_{\mathbf{k}}}{\hbar\omega - \epsilon_{\mathbf{k}+\mathbf{q}} + \epsilon_{\mathbf{k}}} \quad (4.132)$$

$$\varepsilon_2(\mathbf{q}, \omega) = \pi v_{\mathbf{q}} \sum_{\mathbf{k}\sigma} (f_{\mathbf{k}} - f_{\mathbf{k}+\mathbf{q}}) \delta(\hbar\omega - \epsilon_{\mathbf{k}+\mathbf{q}} + \epsilon_{\mathbf{k}}). \quad (4.133)$$

The energy-loss function can be written in terms of $\varepsilon_1(\mathbf{q}, \omega)$ and $\varepsilon_2(\mathbf{q}, \omega)$ as

$$\text{Im} \frac{1}{\varepsilon(\mathbf{q}, \omega)} = - \frac{\varepsilon_2(\mathbf{q}, \omega)}{(\varepsilon_1(\mathbf{q}, \omega))^2 + (\varepsilon_2(\mathbf{q}, \omega))^2}. \quad (4.134)$$

The numerator $\varepsilon_2(\mathbf{q}, \omega)$ gives nonvanishing contributions only for

$$\hbar\omega = \epsilon_{\mathbf{k}+\mathbf{q}} - \epsilon_{\mathbf{k}} = \frac{\hbar^2}{2m} (2\mathbf{k} + \mathbf{q}) \cdot \mathbf{q} \quad (4.135)$$

which in view of the particle-hole excitations out of the Fermi sphere is possible at $\hbar\omega = 0$ for all \mathbf{q} with $0 \leq |\mathbf{q}| \leq 2k_{\text{F}}$ and for $\hbar\omega > 0$ for the same range of $|\mathbf{q}|$ but shifted to higher values. This excitation spectrum is known as the particle-hole continuum (see Fig. 4.15).

Significant contributions to the energy-loss function are also expected if the denominator in (4.134) vanishes, i.e., for $\varepsilon_1(\mathbf{q}, \omega) = \varepsilon_2(\mathbf{q}, \omega) = 0$. Let us consider the case $\hbar\omega \gg \epsilon_{\mathbf{k}+\mathbf{q}} - \epsilon_{\mathbf{k}}$ for which $\varepsilon_2(\mathbf{q}, \omega) = 0$ and (after replacing $\mathbf{k} + \mathbf{q}$ in the first term of $\varepsilon_1(\mathbf{q}, \omega)$ by \mathbf{k})

$$\begin{aligned} \varepsilon_1(\mathbf{q}, \omega) &= 1 + v_{\mathbf{q}} \sum_{\mathbf{k}\sigma} \left\{ \frac{f_{\mathbf{k}}}{\hbar\omega - \epsilon_{\mathbf{k}} + \epsilon_{\mathbf{k}-\mathbf{q}}} - \frac{f_{\mathbf{k}}}{\hbar\omega - \epsilon_{\mathbf{k}+\mathbf{q}} + \epsilon_{\mathbf{k}}} \right\} \\ &= 1 + v_{\mathbf{q}} \sum_{\mathbf{k}\sigma} f_{\mathbf{k}} \frac{2\epsilon_{\mathbf{k}} - \epsilon_{\mathbf{k}+\mathbf{q}} - \epsilon_{\mathbf{k}-\mathbf{q}}}{(\hbar\omega - \epsilon_{\mathbf{k}} + \epsilon_{\mathbf{k}-\mathbf{q}})(\hbar\omega - \epsilon_{\mathbf{k}+\mathbf{q}} + \epsilon_{\mathbf{k}})}. \end{aligned} \quad (4.136)$$

Using $\epsilon_{\mathbf{k}} = \hbar^2 k^2/2m$, the numerator can be rewritten as $-\hbar^2 q^2/m$, and simplifying the denominator for $\hbar\omega \gg \epsilon_{\mathbf{k}+\mathbf{q}} - \epsilon_{\mathbf{k}}$, one obtains for sufficiently small $|\mathbf{q}|$

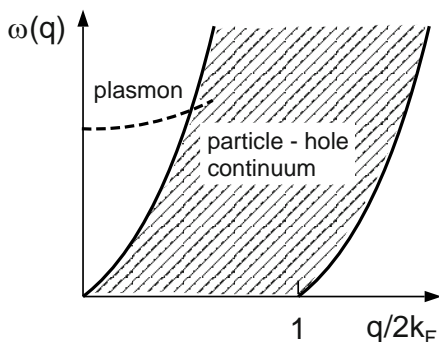


Fig. 4.15. The spectrum of excitations derived from the energy-loss function: RPA spectrum

$$\epsilon_1(\mathbf{q}, \omega) \simeq 1 - v_{\mathbf{q}} \frac{\hbar^2 q^2}{m} \frac{1}{(\hbar\omega)^2} \sum_{\mathbf{k}} f_{\mathbf{k}} = 1 - \frac{Ne^2}{\epsilon_0 V m \omega^2} \quad (4.137)$$

or for $q \rightarrow 0$

$$\epsilon_1(\mathbf{q}, \omega) \simeq 1 - \frac{\omega_{\text{p}}^2}{\omega^2}, \quad \omega_{\text{p}}^2 = \frac{e^2}{\epsilon_0 m} \frac{N}{V}. \quad (4.138)$$

Apparently, the energy-loss function has a singularity at the *plasma frequency* ω_{p} . As the typical result of RPA it represents a collective excitation, the *plasmon*, in which all particles of the electron system participate. Moreover, it obeys a sum rule, which can be expressed in terms of ω_{p} (Problem 4.10).

We note that (4.138) does not contain \hbar . This indicates the possibility of an interpretation in terms of classical physics. In fact, the classical equation of motion of a single electron in an electric field \mathbf{E} , determined by the dielectric polarization $\mathbf{E} = -\mathbf{P}/\epsilon_0 = n e \mathbf{r}/\epsilon_0$ of the electron system with density $n = N/V$, reads

$$m \ddot{\mathbf{r}} = -\frac{e^2}{\epsilon_0} \frac{N}{V} \mathbf{r} \quad \text{or} \quad \ddot{\mathbf{r}} = -\omega_{\text{p}}^2 \mathbf{r}. \quad (4.139)$$

In the long wavelength limit each electron of the system experiences a restoring force characterized by the plasma frequency when (in the collision with a fast charged particle) the system is displaced against the jellium background. For finite \mathbf{q} , one obtains from $\epsilon_1(\mathbf{q}, \omega) = 0$

$$\omega_{\text{p}}^2(q) = \omega_{\text{p}}^2 \left(1 + \frac{3}{10} \frac{q^2 \hbar^2 k_{\text{F}}^2}{m \omega_{\text{p}}^2} + \dots \right), \quad (4.140)$$

where the second and higher order terms indicate quantum mechanical corrections to the classical result.

The typical RPA spectrum, consisting of the particle-hole continuum and the plasmon mode, as depicted schematically in Fig. 4.15, can be translated for small momentum transfer into the real and imaginary part of the dielectric function as shown in Fig. 4.16: $\epsilon_2(\mathbf{q}, \omega)$ is determined by the particle-hole continuum giving contributions only at low frequencies, while $\epsilon_1(\mathbf{q}, \omega)$, showing a more complex frequency dependence, starts at $\omega = 0$ with the value defined by the Thomas-Fermi screening parameter k_{FT} (see Problem 4.11), changes sign around the upper cut-off frequency of the particle-hole excitations, passes through zero at the plasma frequency, and approaches 1 for high frequencies. These characteristic features are also found in the experimental data, e.g., [5, 89].

In metals with electron densities of the order of 10^{23} cm^{-3} (see Table 4.1), the plasmon energy $\hbar\omega_{\text{p}}$ is about 1 Ry and determines the response in an energy-loss experiment in this energy range. In contrast, doped semiconductors represent diluted metallic systems with much lower plasmon energies, which can be tuned by the concentration of the dopands in the range of

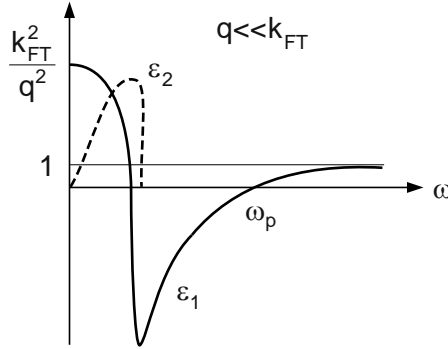


Fig. 4.16. The frequency dependent real and imaginary part of the dielectric function as obtained for the RPA spectrum

optical phonons at $\mathbf{q} = 0$. The response of the system (measured by inelastic light scattering [118]) is then characterized by *coupled plasmon-phonon modes* with frequencies determined by the zeros of the dielectric function in the long-wavelength limit

$$\varepsilon(\omega) = \varepsilon_\infty \left(1 - \frac{\omega_p^2}{\omega^2} + \frac{\omega_L^2 - \omega_T^2}{\omega_T^2 - \omega^2} \right), \quad (4.141)$$

which is the sum of the plasmon and phonon contributions (see Sect. 3.5). Note that the plasmon contribution is modified by the dielectric constant ε_∞ of the semiconductor accommodating the diluted plasma, while the electron mass becomes the effective mass m^* . The biquadratic equation $\varepsilon(\omega) = 0$ has two solutions, which in dependence on the carrier concentration show an anticrossing behavior typical for the coupling between the two modes, which is also experimentally verified.

4.7 Electronic Correlation

The mean energy per electron in the ground state at $T = 0\text{ K}$

$$\epsilon_0 = \frac{1}{N} E_0 = \epsilon_0^{\text{HF}} + \epsilon_c \quad (4.142)$$

can be separated into the HF energy and the correlation energy. The former is determined by the filling of the Fermi sphere and considering the exchange interaction (as a consequence of the Pauli principle). The latter takes into account the electron-electron interaction beyond the HF approximation and will lead to a modified picture of the pair-distribution function of Fig. 4.12, in which the exchange hole is replaced by the correlation hole.

It is helpful to start with the expectation value (per electron) of the electron–electron interaction in (4.107) for the exact ground state $|\Psi_0\rangle$

$$\epsilon_{xc} = \frac{1}{2N} \sum_{\mathbf{q} \neq 0} v_{\mathbf{q}} \langle \Psi_0 | (N_{\mathbf{q}}^\dagger N_{\mathbf{q}} - N) | \Psi_0 \rangle, \quad (4.143)$$

where the index xc refers to exchange and correlation. It can be reformulated by making use of the expression for the *dynamic structure factor*

$$S(\mathbf{q}, \omega) = \frac{1}{2\pi} \int_{-\infty}^{+\infty} e^{-i\omega t} \langle \Psi_0 | (\hat{N}_{\mathbf{q}}(t) \hat{N}_{-\mathbf{q}}(0)) | \Psi_0 \rangle dt \quad (4.144)$$

which can be written also as

$$S(\mathbf{q}, \omega) = \sum_m |\langle \Psi_0 | \hat{N}_{\mathbf{q}} | \Psi_m \rangle|^2 \frac{1}{2\pi} \int_{-\infty}^{+\infty} e^{-i(\omega - \omega_{m0})t} dt. \quad (4.145)$$

The integral is the δ function and thus

$$\begin{aligned} \int_0^\infty S(\mathbf{q}, \omega) d\omega &= \sum_m |\langle \Psi_0 | \hat{N}_{\mathbf{q}} | \Psi_m \rangle|^2 \\ &= \langle \Psi_0 | \hat{N}_{\mathbf{q}} \hat{N}_{-\mathbf{q}} | \Psi_0 \rangle = NS(\mathbf{q}). \end{aligned} \quad (4.146)$$

Here $S(\mathbf{q})$ is the static structure factor which now enters the (still exact) expression for ϵ_{xc} :

$$\epsilon_{xc} = \frac{1}{2} \sum_{\mathbf{q} \neq 0} v_{\mathbf{q}} (S(\mathbf{q}) - 1). \quad (4.147)$$

Due to the isotropy of the free electron system we have $S(\mathbf{q}) = S(q)$ and we may write after integration over the angles

$$\epsilon_{xc} = -\frac{e^2 k_F}{2\pi^2 \epsilon_0} \left(-\frac{1}{2k_F} \int_0^\infty (S(q) - 1) dq \right). \quad (4.148)$$

By introducing the dimensionless function

$$\gamma(k_F) = -\frac{1}{2k_F} \int_0^\infty (S(q) - 1) dq \quad (4.149)$$

and expressing k_F by the density parameter r_s we find (in Ry)

$$\epsilon_{xc}(r_s) = -\frac{4}{\pi r_s} \left(\frac{9\pi}{4} \right)^{1/3} \gamma(r_s). \quad (4.150)$$

The static structure factor $S(q)$ is shown in Fig. 4.17 for different values of r_s .

It should be kept in mind here that the expectation value of the kinetic energy (to be taken for the exact ground state) depends on the interaction.

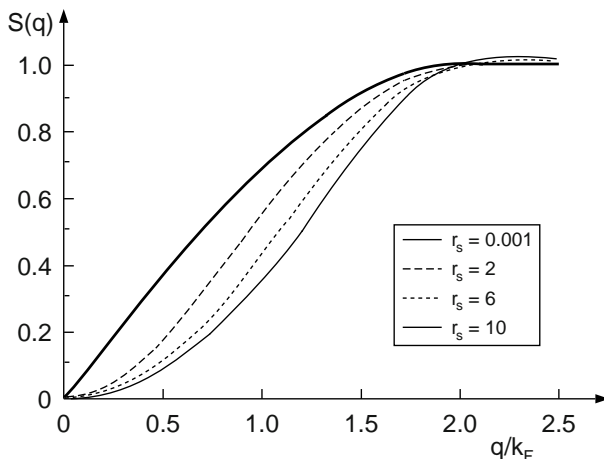


Fig. 4.17. The static structure factor $S(q)$ for different values of the density parameter r_s (after [119])

This is accounted for within the following consideration known as the *ground state theorem*: Let the system Hamiltonian be given by

$$H(g) = H_{\text{kin}} + gH_{\text{int}} \quad (4.151)$$

where $g = e^2$ is the strength of the (electron–electron) interaction. The eigenstates of $H(g)$, including the ground state $|\Psi_0(g)\rangle$, depend on g and

$$E_{\text{int}}(g) = \langle \Psi_0(g) | gH_{\text{int}} | \Psi_0(g) \rangle \quad (4.152)$$

is the exact contribution of the interaction to the ground state energy $E_0(g)$. Then, according to the theorem

$$E_0(g) = E_0(0) + \int_0^g \frac{1}{g'} E_{\text{int}}(g') dg' . \quad (4.153)$$

To prove this theorem one has simply to write

$$\begin{aligned} \frac{dE_0(g)}{dg} &= \langle \Psi_0(g) | \frac{dH(g)}{dg} | \Psi_0(g) \rangle + \left(\frac{d}{dg} \langle \Psi_0(g) | \right) H(g) | \Psi_0(g) \rangle \\ &\quad + \langle \Psi_0(g) | H(g) \left(\frac{d}{dg} | \Psi_0(g) \rangle \right) \\ &= \frac{1}{g} E_{\text{int}}(g) + E_0(g) \frac{d}{dg} \langle \Psi_0(g) | \Psi_0(g) \rangle . \end{aligned} \quad (4.154)$$

The last term vanishes, because $|\Psi_0(g)\rangle$ is normalized, and the resulting differential equation can be integrated directly to yield the statement of the theorem.

For the homogeneous electron gas we can immediately write

$$\epsilon_0 = \frac{3}{5} E_F - \frac{k_F}{2\pi^2 \epsilon_0} \int_0^{e^2} \gamma(g') dg' . \quad (4.155)$$

Thus, in terms of the density parameter r_s , the exact ground state energy per electron reads (in Ry)

$$\epsilon_0(r_s) = \frac{2.2099}{r_s^2} - \frac{4}{\pi r_s} \left(\frac{9\pi}{4} \right)^{1/3} \int_0^1 \gamma(\lambda r_s) d\lambda . \quad (4.156)$$

If γ or $S(q)$ or $\text{Im}1/\epsilon(\mathbf{q}, \omega)$ is given, the ground state energy per electron $\epsilon_0(r_s)$ is also known. The first term is the contribution of the kinetic energy in the Sommerfeld (or noninteracting electron) model, the second term describes the exchange and correlation energy (including also modifications of the kinetic energy due to the electron–electron interaction), and the exact correlation energy per electron can be written as

$$\epsilon_c(r_s) = \frac{0.916}{r_s} - \frac{4}{\pi r_s} \left(\frac{9\pi}{4} \right)^{1/3} \int_0^1 \gamma(\lambda r_s) d\lambda . \quad (4.157)$$

By definition $\epsilon_c(r_s)$ vanishes in the HF approximation.

Calculations of the correlation energy have been carried out in different approximations for $\epsilon(\mathbf{q}, \omega)$ (or $S(q)$ or γ), whose accuracy depends on the density (or r_s) [64, 119]. Typically one uses

$$\epsilon(\mathbf{q}, \omega) = 1 - \frac{v_{\mathbf{q}} \pi_0(\mathbf{q}, \omega)}{1 + v_{\mathbf{q}} G(q) \pi_0(\mathbf{q}, \omega)} \quad (4.158)$$

with different forms of $G(q)$. One particularly simple form is $G(q) = 0$, for which the dielectric function takes the RPA form of (4.125). But also in general, considering correlation means some kind of screening the Coulomb interaction. Results are visualized by plotting the pair–distribution function (see Problem 4.12) which for the homogeneous electron system reads

$$g(r) = 1 + \frac{3}{2rk_F^3} \int_0^\infty q \sin(qr) (S(q) - 1) dq . \quad (4.159)$$

As can be seen in Fig. 4.18, the HF result, with $g(r \rightarrow 0) = 1/2$, is recovered for dense electron systems ($r_s \ll 1$) while in the low-density case (large r_s) $g(r \rightarrow 0) \rightarrow 0$ and the exchange or Fermi hole evolves into a *correlation hole* because the electrons try to avoid each other (irrespective of their spin). We will see in the next chapter how these concepts of exchange and correlation can be considered in describing the electronic states of the inhomogeneous electron systems found in solids.

Let us also briefly discuss the low density limit $r_s \gg 1$, for which the electron–electron interaction is expected to dominate the kinetic energy. The

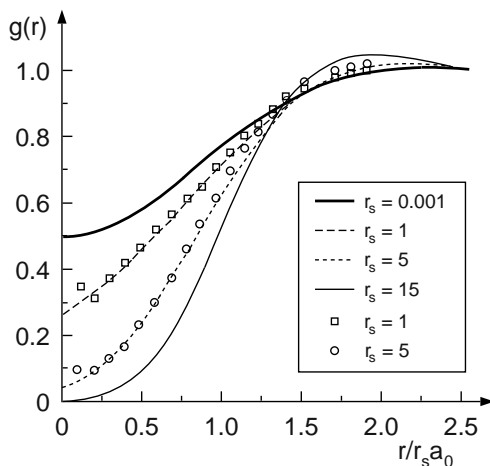


Fig. 4.18. The pair-distribution function $g(r)$ for different values of the density parameter r_s (after [119]). The symbols refer to Monte-Carlo simulations of [120]

ultimate limit, when the kinetic energy can be completely neglected, leads to a problem of classical electrostatics: the ground state is defined by the configuration of point charges with the lowest potential energy. This configuration is a crystalline one: the *Wigner crystal*. Its electrostatic energy shall be evaluated here in the jellium model, in which each electron is assigned the volume of the Seitz sphere with radius $r_0 = r_s a_B$. The potential energy of an electron in the center and the sphere filled with the compensating positive charge of the jellium background is

$$\epsilon_-^{\text{WC}} = - \int_0^{r_0} \frac{e^2}{4\pi\epsilon_0 r} n d^3\mathbf{r} = -\frac{3}{r_s} \text{Ry}. \quad (4.160)$$

The potential energy of the positive jellium background in the Seitz sphere, ϵ_+ , is to be calculated from the electrostatic potential of the homogeneously charged sphere

$$V(r) = \frac{e^2}{r_s^2 a_B^3} \left(-\frac{r^2}{2} \right) + C \quad (4.161)$$

where $C = 3e^2/2r_s a_B$ has to be chosen to establish charge neutrality, thus

$$V(r) = \frac{1}{r_s} \left(3 - \left(\frac{r^2}{r_s a_B} \right)^2 \right) \text{Ry} \quad (4.162)$$

and

$$\epsilon_+ = \frac{1}{2} \int_0^{r_0} V(r) n d^3\mathbf{r} = \frac{6}{5r_s} \text{Ry}. \quad (4.163)$$

The electrostatic energy per electron in the Wigner crystal amounts to

$$\epsilon^{\text{WC}} = \epsilon_-^{\text{WC}} + \epsilon_+ = -\frac{1.8}{r_s} \text{Ry}. \quad (4.164)$$

This expression corresponds to the sum of exchange and correlation energy. With the latter being given by $\epsilon_x = -0.916/r_s \text{Ry}$, the correlation energy per electron in the Wigner crystal turns out to be

$$\epsilon_c(r_s \gg 1) = -\frac{0.88}{r_s}. \quad (4.165)$$

We may finally compare with the electrostatic energy of the smeared (instead of the point-like) electron in the Seitz sphere: it is given by

$$\epsilon_-^{\text{jell}} = -2\epsilon_+ = -\frac{2.4}{r_s} \text{Ry} \quad (4.166)$$

which is larger than ϵ_-^{WC} . Thus, the Wigner crystal is the predicted ground state of the strongly diluted homogeneous electron system. The experimental verification of the Wigner crystal represents a tremendous challenge because the realization of a diluted homogeneous electron system turns out to be very difficult.

Problems

- 4.1 Calculate the interaction energy of a homogeneous electron gas (density $n = N/V$) with a homogeneous jellium background of positive charges with the same density and the electrostatic potential energy of this background. Hint: Make use of the Fourier transform of the Coulomb interaction.
- 4.2 According to (4.25) the chemical potential $\mu(T)$ is determined by the particle density n . For the three-dimensional electron gas, calculate the temperature dependence of μ for low temperatures ($k_B T \ll E_F$) up to the order $(k_B T/E_F)^2$!
- 4.3 Calculate the density of states for a system of electrons, which can move freely in a plane (two-dimensional electron gas) or along a straight line (1-dimensional electron gas). Give an expression for the density of states of bound electrons (zero-dimensional electron gas). Plot and discuss these results.
- 4.4 Typical electron densities are $n \simeq 10^{23} \text{cm}^{-3}$ for metals and $n \simeq 10^{14} \text{cm}^{-3}$ for doped semiconductors (see Table 4.1) Consider the magnetic quantum limit, when all electrons are in the lowest Landau level, and derive for this case a relation between the magnetic field and n . For which of the two systems is it possible to reach the magnetic quantum limit in a laboratory?

- 4.5 The Pauli spin-paramagnetism is determined by the spin-splitting of the electronic energy spectrum due to the Zeeman term (see Fig. 4.7). Express this contribution to the magnetization by the number of non-compensated electron spins and compare the result with (4.53).
- 4.6 Discuss the quality of the HF approximation starting from ϵ_0^{HF} (4.93) for metals and semiconductors (see parameters given in Table 4.1). In terms of the density parameter r_s , which system is of higher density?
- 4.7 In order to go beyond the HF approximation (which is a first order perturbation calculation) one may consider the second order perturbation correction E_2 due to the Coulomb interaction. (a) Make use of the Fermi sphere to find excited states which yield a contribution to E_2 . (b) Distinguish between direct and exchange contributions to E_2 and show that the direct term can be formulated as

$$E_2^{\text{dir}} = -4m \sum_{\mathbf{k}\mathbf{q}\mathbf{p}} v_{\mathbf{k}}^2 \frac{n_{\mathbf{p}}(1-n_{\mathbf{p}+\mathbf{k}})n_{\mathbf{q}}(1-n_{\mathbf{q}+\mathbf{k}})}{\hbar^2 \mathbf{k} \cdot (\mathbf{k} + \mathbf{q} + \mathbf{p})} \quad (4.167)$$

where $n_{\mathbf{p}}$ is the occupation number. (c) Show by expanding $n_{\mathbf{p}+\mathbf{k}}$ for small k that $\sum_{\mathbf{p}} n_{\mathbf{p}}(1-n_{\mathbf{p}+\mathbf{k}}) \sim k$ and use this result to find that (for small k) E_2^{dir} is logarithmically divergent. Interpret this result!

- 4.8 Field operators are defined by

$$\Psi(\mathbf{r}) = \sum_{\alpha} c_{\alpha} \Psi_{\alpha}(\mathbf{r}), \quad \Psi^{\dagger}(\mathbf{r}) = \sum_{\alpha} c_{\alpha}^{\dagger} \psi_{\alpha}^*(\mathbf{r}) \quad (4.168)$$

with fermion operators $c_{\alpha}, c_{\alpha}^{\dagger}$ and a complete orthonormal set of single particle wave functions $\psi_{\alpha}(\mathbf{r})$ (for free electrons $\psi_{\mathbf{k}}(\mathbf{r}) = \exp(i\mathbf{k} \cdot \mathbf{r})/\sqrt{V}$). (a) Discuss the meaning of $\Psi(\mathbf{r})$ and $\Psi^{\dagger}(\mathbf{r})$. (b) Derive the commutation relations for $\Psi(\mathbf{r})$ and $\Psi^{\dagger}(\mathbf{r})$. (c) The density operator is given by $\hat{n}(\mathbf{r}) = \Psi^{\dagger}(\mathbf{r})\Psi(\mathbf{r})$. Give for free electrons the Fourier components $\hat{n}_{\mathbf{q}}$ defined by $\hat{n}(\mathbf{r}) = \sum_{\mathbf{q}} e^{i\mathbf{q} \cdot \mathbf{r}} \hat{n}_{\mathbf{q}}$. What is the meaning of $\hat{n}_{\mathbf{q}}$ for $\mathbf{q} = 0$ and $\mathbf{q} \neq 0$? d) Express the Coulomb interaction in terms of the number fluctuation operators $\hat{N}_{\mathbf{q}} = V \hat{n}_{\mathbf{q}}$.

- 4.9 Calculate the thermal expectation value of the number fluctuation operator $\langle \hat{N}_{\mathbf{q}} \rangle$ by starting from the exact expression

$$\langle \hat{N}_{\mathbf{q}} \rangle = \lim_{\Gamma \rightarrow 0} v_{\mathbf{q}} \frac{1}{i\hbar} \int_0^{\infty} e^{i\omega\tau - \Gamma\tau} \langle [\hat{N}_{\mathbf{q}}(\tau), \hat{N}_{-\mathbf{q}}(0)] \rangle_0 N_{\text{ext}} d\tau \quad (4.169)$$

by replacing the bare external charge eN_{ext} by $e(N_{\text{ext}} + \langle \hat{N}_{\mathbf{q}} \rangle_{\text{RPA}})$ with the induced number fluctuation $\langle \hat{N}_{\mathbf{q}} \rangle_{\text{RPA}}$ in RPA and evaluating the expectation value of the commutator not in the exact ground state of the interacting system but in the ground state of the system without interaction. This is the *self-consistent field approximation*.

4.10 Prove the sum rule

$$\int_0^\infty \text{Im} \left[\frac{1}{\epsilon(\mathbf{q}, \omega)} \right] \omega d\omega = -\frac{\pi}{2} \omega_p^2 \quad (4.170)$$

where ω_p is the plasma frequency. Hint: Calculate the ground state expectation value of $[[H_{\text{jell}}, \hat{n}_{\mathbf{q}}], \hat{n}_{-\mathbf{q}}]$ by making use of the commutation relations of $c_{\mathbf{k}}$ and $c_{\mathbf{k}}^\dagger$ and by introducing a complete set of eigenstates of H_{jell} .

4.11 Evaluate the real part of the dielectric constant (4.132) for the static case ($\omega = 0$) in the long-wavelength limit $|\mathbf{q}| \rightarrow 0$ (Thomas–Fermi approximation). It will depend on the parameter k_{FT} defined by

$$k_{\text{FT}}^2 = \frac{3N e^2}{2\epsilon_0 V E_F}. \quad (4.171)$$

Consider the screened Coulomb potential $v_{\mathbf{q}}/\epsilon_1(\mathbf{q}, 0)$: How does the Fourier transform of this potential look like and what is the obvious meaning of k_{FT}^{-1} ?

4.12 The ground state density–density correlation function is defined as

$$p(\mathbf{r}) = \frac{1}{N} \int \langle \Psi_0 | \hat{n}(\mathbf{r} + \mathbf{r}') \hat{n}(\mathbf{r}') | \Psi_0 \rangle d\mathbf{r}'. \quad (4.172)$$

The Fourier transform of $p(\mathbf{r})$ is $S(\mathbf{k}) = \int e^{i\mathbf{k}\cdot\mathbf{r}} p(\mathbf{r}) d^3\mathbf{r}$. It can be obtained from the dynamic form factor $S(\mathbf{k}, \omega)$ with

$$S(\mathbf{k}) = \frac{1}{N} \int S(\mathbf{k}, \omega) d\omega. \quad (4.173)$$

Use the relation between $S(\mathbf{k}, \omega)$ and $\text{Im}(1/\epsilon(\mathbf{q}, \omega))$ to calculate $p(\mathbf{r})$ in HF approximation.

Electrons in a Periodic Potential

In Chap. 4, the crystal structure of the solid has been suppressed by smearing out the periodic configuration of ions in the jellium model, because the many-body aspects of the electron–electron interaction stood in the focus of interest. Now, our attention will be, in addition, at the effect of the periodic potential formed by the ions in the configuration $\{\mathbf{R}_{\mathbf{n},\tau}^0\}$ of a crystal lattice. Therefore, we reverse the introduction of the jellium term in Sect. 4.3 with the replacement

$$H_+ \Rightarrow \sum_{\mathbf{n},\tau,l} v(\mathbf{r}_l - \mathbf{R}_{\mathbf{n},\tau}^0) + \frac{1}{2} \sum_{\substack{\mathbf{n},\mathbf{n}' \\ \tau,\tau'}} V(\mathbf{R}_{\mathbf{n}\tau}^0 - \mathbf{R}_{\mathbf{n}'\tau'}^0) = \sum_l V(\mathbf{r}_l). \quad (5.1)$$

Note the simplified notation of the single-particle potential $V(\mathbf{r}_l)$, which does not explicitly refer to the ion positions. It is invariant under lattice translations and is the same for all electrons. The Hamiltonian for a system of N electrons in the crystal volume

$$\mathcal{H}_N = \sum_{l=1}^N \left(\frac{p_l^2}{2m} + V(\mathbf{r}_l) \right) + \frac{1}{2} \sum_{\substack{k,l=1 \\ k \neq l}}^N v(\mathbf{r}_l - \mathbf{r}_k), \quad (5.2)$$

with the Coulomb potential

$$v(\mathbf{r}_l - \mathbf{r}_k) = \frac{e^2}{\kappa |\mathbf{r}_l - \mathbf{r}_k|}, \quad \kappa = 4\pi\epsilon_0 \quad (5.3)$$

defines the starting point for this chapter.

The complexity of the eigenvalue problem of \mathcal{H}_N comes from the simultaneous presence of the periodic lattice potential and the electron–electron interaction. As we have already seen in Chap. 4, the latter prevents a rigorous solution of the eigenvalue problem and some approximate treatment has to be applied. In some textbooks, e.g., [6, 7, 13, 121], the potential energy terms of \mathcal{H}_N , namely $\sum_l V(\mathbf{r}_l)$ and the electron–electron interaction, are replaced

by an effective single-particle potential:

$$\mathcal{H}_N \Rightarrow \sum_l \left(\frac{p_l^2}{2m} + V_{\text{eff}}(\mathbf{r}_l) \right) \quad (5.4)$$

which incorporates the many-body aspect in an approximate way. Other textbooks, e.g., [8, 9, 122], provide arguments, on how this replacement can be justified and we shall follow this line in Sect. 5.1. Given such a potential, electrons can be understood as independent particles and in a wave picture, are expected to undergo Bragg reflections due to the periodic potential (as in the case of elastic or electromagnetic waves). The consequence is that the energy spectrum becomes a band structure with energy intervals for which propagation of electrons is possible. They are separated by gaps, where this is not the case.

In this approximation, the Hamiltonian is a sum of identical single-particle terms and can be separated with a product Ansatz into one and the same single-particle Schrodinger equation for all electrons:

$$\left(-\frac{\hbar^2}{2m} \Delta + V_{\text{eff}}(\mathbf{r}) \right) \psi_\alpha(\mathbf{r}) = E_\alpha \psi_\alpha(\mathbf{r}). \quad (5.5)$$

Here, α denotes a complete set of single-particle quantum numbers, which, as will be outlined in Sect. 5.2, are the band index n and the crystal momentum or wave vector \mathbf{k} in the first Brillouin zone. Spin-orbit coupling and a spin index can be added if required. The energy eigenvalues $E_\alpha = E_n(\mathbf{k})$ form the *energy band structure* of electrons. The foremost task is the justification of this approach and the definition of the effective single-particle potential $V_{\text{eff}}(\mathbf{r})$.

5.1 Density Functional Theory

The many-particle problem is defined by the Hamiltonian \mathcal{H}_N in (5.2). The eigenvalue equation $\mathcal{H}_N \Psi_N = E \Psi_N$, is the same as (2.17) or (2.25) with the electron-ion interaction considered for the crystalline equilibrium configuration of the ions. But it corresponds also to that of the jellium model treated in Chap. 4 with the exception, now that the crystal structure of the ions is considered. Thus, we may use the concepts developed for the homogeneous electron gas. The simplest approach would be to apply the Hartree approximation with the product Ansatz

$$\Psi_N(\mathbf{r}_1 \dots \mathbf{r}_N) = \prod_{\alpha=1}^N \psi_\alpha(\mathbf{r}_\alpha). \quad (5.6)$$

The single-particle wave functions ψ_α have to be determined from the condition that the expectation value of \mathcal{H}_N takes a minimum under the constraint of their normalization. This leads to Ritz' variational problem (see Sect. 4.1)

$$\delta \left\{ \langle \Psi_N | \mathcal{H}_N | \Psi_N \rangle - \sum_\alpha E_\alpha (\langle \psi_\alpha | \psi_\alpha \rangle - 1) \right\} = 0 \quad (5.7)$$

where the normalization condition enters with the Lagrangian parameters E_α . The expression in the curly brackets is a functional of the single-particle wave functions ψ_α , thus the variation is to be performed as the functional derivative with respect to ψ_α or ψ_α^* . If this is done with

$$\begin{aligned} \langle \Psi_N | \mathcal{H}_N | \Psi_N \rangle &= \sum_{\alpha=1}^N \int d^3\mathbf{r} \psi_\alpha^*(\mathbf{r}) \left(\frac{p^2}{2m} + V(\mathbf{r}) \right) \psi_\alpha(\mathbf{r}) \\ &\quad + \frac{1}{2} \sum_{\substack{\alpha, \beta=1 \\ \alpha \neq \beta}}^N \int \int d^3\mathbf{r} d^3\mathbf{r}' \psi_\alpha^*(\mathbf{r}) \psi_\beta^*(\mathbf{r}') v(\mathbf{r} - \mathbf{r}') \psi_\alpha(\mathbf{r}) \psi_\beta(\mathbf{r}') \end{aligned} \quad (5.8)$$

one obtains the Euler–Lagrange equations of the variational problem (note that the variational derivative gives two contributions from the double sum of the interaction term)

$$\left(-\frac{\hbar^2}{2m} \Delta + V(\mathbf{r}) + \int d^3\mathbf{r}' \frac{e^2 \sum_{\beta \neq \alpha} |\psi_\beta(\mathbf{r}')|^2}{\kappa |\mathbf{r} - \mathbf{r}'|} \right) \psi_\alpha(\mathbf{r}) = E_\alpha \psi_\alpha(\mathbf{r}). \quad (5.9)$$

They have the form of (5.5) with an effective potential composed of the potential $V(\mathbf{r})$ due to the periodic ion configuration and a contribution from the electron–electron interaction, which can be identified as the Hartree potential: it describes the direct Coulomb interaction of the electron in the state α with the charge distribution of all the other electrons. Remember, that in the jellium model the Hartree contribution exactly compensates the jellium term, to which $V(\mathbf{r})$ simplifies in this case.

Three aspects are to be mentioned here: the Hartree potential for ψ_α

$$V_{H,\alpha}(\mathbf{r}) = \int d^3\mathbf{r}' \frac{e^2}{\kappa |\mathbf{r} - \mathbf{r}'|} \sum_{\substack{\beta \neq \alpha \\ \text{occ}}} |\psi_\beta(\mathbf{r}')|^2 \quad (5.10)$$

depends on all the other occupied single-particle states with $\beta \neq \alpha$ with the consequence that (5.9) can be solved only if the solutions (the eigenfunctions) are known. How such a *self-consistent solution* can be achieved, will be explained at the end of this section. Moreover, the Hartree potential depends also on the state α , and one has to deal with equations containing different potentials. Finally, as we know from Sect. 4.3, the product Ansatz does not prevent double occupation of single-particle states, thus being in contrast with the Pauli principle. Nevertheless, the Hartree approximation indicates in some way, how to arrive at the effective single-particle potential we are looking for, without reaching it.

In the next step, we assume Ψ_N in the form of a Slater determinant as in (4.61) constructed from single-particle wave functions $\psi_\alpha(x)$, where x comprises space and spin variables and α is a complete set of quantum numbers including spin, but proceed as before. By carrying out the variation

(Problem 5.1) we arrive at the Hartree equations (5.9) augmented by an additional term

$$V_{x,\alpha}(\mathbf{r})\psi_\alpha(\mathbf{r}) = - \int d^3\mathbf{r}' v(\mathbf{r} - \mathbf{r}') \sum_{\substack{\beta \neq \alpha, \parallel \\ \text{occ}}} \psi_\beta^*(\mathbf{r}')\psi_\alpha(\mathbf{r}')\psi_\beta(\mathbf{r}). \quad (5.11)$$

This *exchange term* results from the fact that the expansion of the Slater determinant contains products of single-particle wave functions with interchanged particle coordinates, which do not exist in the simple product Ansatz of the Hartree approximation. Here, $V_{x,\alpha}(\mathbf{r})$ is not a simple potential acting as a factor on $\psi_\alpha(\mathbf{r})$ but a nonlocal integral operator, because $\psi_\alpha(\mathbf{r}')$ appears under the integral. The \parallel -sign in the sum under the integral indicates the restriction to contributions from states $\beta \neq \alpha$ with parallel spins and results from the summation over the spin variables. We may include the contributions for $\alpha = \beta$ in the Hartree and the exchange terms, which cancel each other, to obtain the *Hartree-Fock equations*

$$\left(-\frac{\hbar^2}{2m}\Delta + V(\mathbf{r}) + \int d^3\mathbf{r}' n(\mathbf{r}')v(\mathbf{r} - \mathbf{r}') - \int d^3\mathbf{r}' n_\alpha^x(\mathbf{r}, \mathbf{r}')v(\mathbf{r} - \mathbf{r}') \right) \psi_\alpha(\mathbf{r}) = E_\alpha \psi_\alpha(\mathbf{r}). \quad (5.12)$$

Here we have introduced the density

$$n(\mathbf{r}) = \sum_{\beta, \text{occ}} |\psi_\beta(\mathbf{r})|^2 \quad (5.13)$$

and the Hartree-Fock (HF) or *exchange density*

$$n_\alpha^x(\mathbf{r}, \mathbf{r}') = \sum_{\substack{\beta, \parallel \\ \text{occ}}} \frac{\psi_\beta^*(\mathbf{r}')\psi_\alpha(\mathbf{r}')\psi_\alpha^*(\mathbf{r})\psi_\beta(\mathbf{r})}{\psi_\alpha^*(\mathbf{r})\psi_\alpha(\mathbf{r})}. \quad (5.14)$$

For free electrons with $\psi_\alpha(\mathbf{r}) = e^{i\mathbf{k}\cdot\mathbf{r}}/\sqrt{V_c}$ (here we denote the crystal volume by V_c) (5.14) leads back to the results in Sect. 4.4 (Problem 5.2).

As the Hartree potential (5.10), also the exchange potential is state-dependent and the HF equations have to be solved self-consistently. However, by replacing the state-dependent HF density by its average over all occupied states

$$n_\alpha^x(\mathbf{r}, \mathbf{r}') \Rightarrow \bar{n}^{\text{HF}}(\mathbf{r}, \mathbf{r}') = \frac{1}{N} \sum_{\alpha=1}^N n_\alpha^x(\mathbf{r}, \mathbf{r}'), \quad (5.15)$$

we obtain an effective single-particle potential

$$V_{\text{eff}}^{\text{HF}}(\mathbf{r}) = V(\mathbf{r}) + \int d^3\mathbf{r}' \frac{e^2(n(\mathbf{r}') - \bar{n}^{\text{HF}}(\mathbf{r}, \mathbf{r}'))}{\kappa|\mathbf{r} - \mathbf{r}'|}. \quad (5.16)$$

which is the same for all electrons. Besides the electrostatic interaction with the periodic ion configuration, it contains the electron–electron interaction in approximate form. It should be noted, however, that although deriving from the Ansatz with the Slater determinant, it is not exactly the HF approximation because the averaging of the exchange density in (5.15) represents a non-systematic step.

The question arises if one could go systematically beyond HF and consider in $V_{\text{eff}}(\mathbf{r})$ correlation contributions besides exchange also as discussed in Chap. 4. The answer to this question comes from the *density functional theory* (DFT) [9, 122–126], which since its formulation in the sixties has developed into the most frequently used concept in calculating the electronic structure of atoms, molecules, and solids and earned in 1998 the Nobel prize in Chemistry shared by Kohn and Pople. Here we outline the three essential steps of DFT:

1. The *Hohenberg–Kohn*¹ theorem [127]
2. The *Kohn–Sham* equations [128]
3. The *local density approximation* (LDA)

The basic idea of the *Hohenberg–Kohn* theorem is that the ground state energy of the N electron system for a given external potential (here that of the periodic configuration of the ions $V(\mathbf{r})$) is a unique functional of the single-particle density $n(\mathbf{r})$. This idea is conceivable: when adding the electrons to the external potential, they will arrange in a unique way to establish the state with lowest energy. This state will be characterized by a many-particle wave function $\Psi_0(\{\mathbf{r}_i\})$ and a single-particle density (the spin degree of freedom is suppressed here)

$$n(\mathbf{r}) = \int \dots \int d^3\mathbf{r}_2 \dots d^3\mathbf{r}_N |\Psi_0(\mathbf{r}, \mathbf{r}_2 \dots \mathbf{r}_N)|^2, \quad N = \int d^3\mathbf{r} n(\mathbf{r}). \quad (5.17)$$

The *statement of the theorem* is:

Let $n(\mathbf{r})$ be the (inhomogeneous) single particle density for the ground state of a system of interacting electrons in an external potential $V(\mathbf{r})$ and let the density $n'(\mathbf{r})$ have the same relation to the external potential $V'(\mathbf{r})$. Then it follows from $n(\mathbf{r}) = n'(\mathbf{r})$ that $V(\mathbf{r}) = V'(\mathbf{r})$ up to a constant.

The *proof of the theorem* is indirect:

Assume two systems with external potentials $V(\mathbf{r}) \neq V'(\mathbf{r})$, which differ by more than just a constant, but have identical densities $n(\mathbf{r}) = n'(\mathbf{r})$ in the ground state. Then one has the ground state energies

$$E'_0 = \langle \Psi'_0 | T + V' + U | \Psi'_0 \rangle, \quad E_0 = \langle \Psi_0 | T + V + U | \Psi_0 \rangle \quad (5.18)$$

where T and U denote the kinetic energy and the electron–electron interaction, respectively, and $|\Psi_0\rangle$ and $|\Psi'_0\rangle$ the ground states of the system with external potential $V(\mathbf{r})$ and $V'(\mathbf{r})$, respectively. As $|\Psi_0\rangle$ is not the ground state of the system with the external potential V' (and $|\Psi'_0\rangle$ not that of the system

¹ Walther Kohn *1923, shared the Nobel prize in chemistry 1998 with J. Pople.

with V), we may formulate the following relations

$$E'_0 < \langle \Psi_0 | T + V' + U | \Psi_0 \rangle = E_0 + \langle \Psi_0 | V' - V | \Psi_0 \rangle \quad (5.19)$$

and

$$E_0 < \langle \Psi'_0 | T + V + U | \Psi'_0 \rangle = E'_0 + \langle \Psi'_0 | V - V' | \Psi'_0 \rangle. \quad (5.20)$$

Due to the assumption of identical densities, the last terms in both relations are identical (except for the sign) and by taking the sum of these expressions we find the contradictory relation $E_0 + E'_0 < E_0 + E'_0$. Thus, the assumption must be incorrect, while the statement of the theorem is correct. (We note that this proof applies, if the ground state is not degenerate. A more general proof was given by Levy [124].)

The Hohenberg–Kohn theorem can be formulated also by saying that for the given external potential $V(\mathbf{r})$ the exact ground state energy E_0 is a unique functional of the exact ground state density $n(\mathbf{r})$:

$$E_0 = \langle \Psi_0 | T + V + U | \Psi_0 \rangle = E_V[n(\mathbf{r})]. \quad (5.21)$$

It tells us, that in order to find the ground state energy of the N -particle problem with \mathcal{H}_N , it is not required to find the exact many-particle wave function Ψ_0 (which is a function of the coordinates of N electrons), it suffices to find the exact single-particle density $n(\mathbf{r})$ (which depends only on the coordinates of one particle). Note, that the same statement as for the ground state energy E_0 can be made for the expectation value of any observable in this state (and this includes also the response functions). One has to keep in mind, however, that the theorem is restricted to the system ground state.

Now, the problem to be solved is to find E_0 as minimum of the energy functional

$$E_V[n(\mathbf{r})] = T[n(\mathbf{r})] + \int V(\mathbf{r})n(\mathbf{r})d^3\mathbf{r} + \frac{e^2}{2} \iint \frac{n(\mathbf{r})n(\mathbf{r}')}{\kappa|\mathbf{r} - \mathbf{r}'|} d^3\mathbf{r}d^3\mathbf{r}' + E_{xc}[n(\mathbf{r})], \quad (5.22)$$

where the first and last terms describe the exact functionals of the kinetic and exchange–correlation energy, respectively, of the interacting electron system, while the second and third term are the electrostatic energy of the electron density $en(\mathbf{r})$ in the external potential $V(\mathbf{r})$ and the Hartree energy for this charge density. In mathematical language (5.23) represents, for a given external potential, a mapping of the densities onto the energies of which we have to find the minimum. $T[n]$ and $E_{xc}[n]$ are not exactly known and will be considered in an approximate way, as outlined in the following.

The variational problem can be treated by assuming the representation of the density by a complete set of single-particle wave functions

$$n(\mathbf{r}) = \sum_{\alpha=1}^N |\psi_{\alpha}(\mathbf{r})|^2, \quad \langle \psi_{\alpha} | \psi_{\alpha} \rangle = 1, \quad N = \int n(\mathbf{r}) d^3\mathbf{r}. \quad (5.23)$$

Taking the functional derivatives with respect to the ψ_{α}^* (which corresponds to the variation with respect to the density $n(\mathbf{r})$) and assuming $T[n]$ as for non-interacting electrons

$$T[n(\mathbf{r})] \simeq T_0[n(\mathbf{r})] = \sum_{\alpha} \int \psi_{\alpha}^*(\mathbf{r}) \left(-\frac{\hbar^2}{2m} \Delta \right) \psi_{\alpha}(\mathbf{r}) d^3\mathbf{r} \quad (5.24)$$

one arrives at a set of Schroedinger equations for the single-particle functions ψ_{α}

$$\left(-\frac{\hbar^2}{2m} \Delta + V(\mathbf{r}) + \int \frac{e^2 n(\mathbf{r}')}{\kappa |\mathbf{r} - \mathbf{r}'|} d^3\mathbf{r}' + V_{\text{xc}}(\mathbf{r}) \right) \psi_{\alpha}(\mathbf{r}) = E_{\alpha} \psi_{\alpha}(\mathbf{r}), \quad (5.25)$$

the *Kohn–Sham equations*. They have the form of (5.5), but are integro-differential equations due to the fact that, because of

$$V_{\text{xc}}(\mathbf{r}) \psi_{\alpha}(\mathbf{r}) = \frac{\delta}{\delta n} E_{\text{xc}}[n] \frac{\delta n}{\delta \psi_{\alpha}^*}, \quad (5.26)$$

$V_{\text{xc}}(\mathbf{r})$ is a nonlocal integral operator and we may write similar to (5.11)

$$V_{\text{xc}}(\mathbf{r}) \psi_{\alpha}(\mathbf{r}) = \int d^3\mathbf{r}' \Sigma_{\text{xc}}(\mathbf{r}, \mathbf{r}'; E_{\alpha}) \psi_{\alpha}(\mathbf{r}'). \quad (5.27)$$

Here, $\Sigma_{\text{xc}}(\mathbf{r}, \mathbf{r}'; E_{\alpha})$ is the exchange–correlation self-energy or mass operator.

In the last step, the Kohn–Sham equations can be reduced to the form of (5.5) by applying the *local density approximation* (LDA) with the replacement

$$E_{\text{xc}}[n(\mathbf{r})] \Rightarrow E_{\text{xc}}^{\text{LDA}}[n(\mathbf{r})] = \int n(\mathbf{r}) \epsilon_{\text{xc}}(n(\mathbf{r})) d^3\mathbf{r}, \quad (5.28)$$

where $\epsilon_{\text{xc}}(n)$ is the xc energy per electron of a homogeneous system with density n . For each \mathbf{r} of the inhomogeneous system (with external potential $V(\mathbf{r}) \neq \text{const}$) the xc energy of the jellium model (Chap. 4) is taken with the local density $n = n(\mathbf{r})$. This allows one to write the xc term as a local single-particle potential

$$V_{\text{xc}}^{\text{LDA}}(\mathbf{r}) = \frac{d}{dn} (n \epsilon_{\text{xc}}(n))_{n=n(\mathbf{r})} \quad (5.29)$$

with $\epsilon_{\text{xc}}(n) = \epsilon_{\text{xc}}(r_s)$ from (4.150). Thus, we have found the effective single-particle potential to be used in (5.5)

$$V_{\text{eff}}^{\text{LDA}}(\mathbf{r}) = V(\mathbf{r}) + \int n(\mathbf{r}') v(\mathbf{r} - \mathbf{r}') d^3\mathbf{r}' + V_{\text{xc}}^{\text{LDA}}(\mathbf{r}). \quad (5.30)$$

The considerations of this section apply to any interacting fermion system and external potential. The DFT-LDA has been and is currently applied to atoms, molecules, and condensed matter. With the available computer power it has become the dominant tool for solving quantum many-body problems. The input with respect to the exchange–correlation energy comes from the homogeneous electron gas (which accounts also for the replacement made in (5.24)), which we have studied in detail in Chap. 4.

The DFT concepts have been refined to include spatial inhomogeneity of the density in the xc energy (in the generalized gradient approximation), spin polarization (in the spin or SDFT), and time dependent perturbations (in the DFT perturbation theory, mentioned in Chap. 3) [100, 123]. Also, the restriction to the system ground state has been overcome by taking care of the discontinuity of the correlation energy in its dependence on the quasi-particle energy across the Fermi energy (quasi-particle corrections in the GW approximation) for which we refer also to Chap. 7 [123, 129, 130]. But even without the latter, the eigenvalues E_α of the Kohn–Sham equations with the single particle potential (5.30) are usually taken as single particle energies not only for states occupied in the ground state, but also for unoccupied states. This identification is widely supported by the agreement between experimental mapping of the energy bands from photoelectron spectroscopy (PES) and results from DFT calculations [131]. It should be noted, however, that this agreement is not found for optical properties in semiconductors and insulators due to the *band gap problem*: as it turns out, the separation between conduction and valence band states, as obtained from DFT-LDA calculations is too small [130]. This discrepancy can be resolved systematically by considering different xc energies for conduction and valence band states, as is done in the already mentioned GW approximation.

As we have seen in this section, the Hartree, the Hartree–Fock, and the effective LDA potential (5.30) depend on the solutions of the corresponding Schroedinger equations. For this type of problem an iterative procedure applies: for the given external potential one has to choose a single-particle density $n_0(\mathbf{r})$ to start with, calculate the Hartree and LDA contributions and solve the Schroedinger equation. The occupied states of this solution define a density $n_1(\mathbf{r})$, which in general will be different from $n_0(\mathbf{r})$ and is taken to create a modified Hartree and LDA potential. With these modified potentials (or a mixture with the potential of the previous step) the Schroedinger equation is solved again and the procedure is repeated until the calculated densities (or energy eigenvalues) for two successive iteration steps are reproduced within desired limits of accuracy. At this level, the obtained single-particle energies, wave functions and the potential to which they contribute via the occupied states are *self-consistent*.

5.2 Bloch Electrons and Band Structure

In the previous section we have reduced the many-body problem of the electrons in a solid to the single-particle problem

$$H\psi_\alpha = E_\alpha\psi_\alpha, \quad H = -\frac{\hbar^2}{2m}\Delta + V_{\text{eff}}(\mathbf{r}) \quad (5.31)$$

with the periodic effective potential

$$V_{\text{eff}}(\mathbf{r} + \mathbf{R}_n^0) = V_{\text{eff}}(\mathbf{r}). \quad (5.32)$$

The periodicity of the potential means invariance of the Hamiltonian under lattice translations

$$[H, T_{\mathbf{R}_n^0}] = 0, \quad \text{with } T_{\mathbf{R}_n^0} = e^{-\frac{i}{\hbar}\mathbf{p}\cdot\mathbf{R}_n^0} \quad (5.33)$$

and the momentum operator \mathbf{p} . The properties

$$T_{\mathbf{R}_n^0}\psi_\alpha(\mathbf{r}) = \psi_\alpha(\mathbf{r} - \mathbf{R}_n^0) \quad \text{and} \quad |T_{\mathbf{R}_n^0}\psi_\alpha(\mathbf{r})|^2 = |\psi_\alpha(\mathbf{r})|^2 \quad (5.34)$$

of the translation operator allow one to write

$$T_{\mathbf{R}_n^0}\psi_{\mathbf{k}}(\mathbf{r}) = e^{-i\mathbf{k}\cdot\mathbf{R}_n^0}\psi_{\mathbf{k}}(\mathbf{r}) \quad (5.35)$$

where the phase factor, the eigenvalue of the translation operator, is characterized by the wave vector \mathbf{k} (note that $\hbar\mathbf{k}$ is the eigenvalue of the momentum operator \mathbf{p}). Due to the property (5.35) the eigenfunctions of (5.31) can be split into an exponential and a lattice periodic function

$$\psi_{\mathbf{k}}(\mathbf{r}) = e^{i\mathbf{k}\cdot\mathbf{r}}u_{\mathbf{k}}(\mathbf{r}), \quad u_{\mathbf{k}}(\mathbf{r} + \mathbf{R}_n^0) = u_{\mathbf{k}}(\mathbf{r}). \quad (5.36)$$

This form, a modulated plane wave, is characteristic of electrons in a periodic lattice: the *Bloch² function*. It is schematically depicted in Fig. 5.1. The

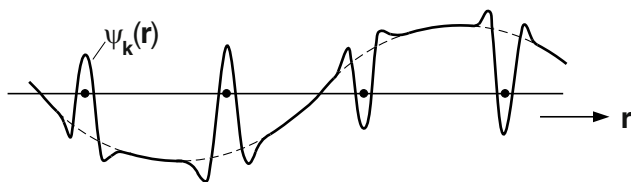


Fig. 5.1. Schematic view of a Bloch function (*solid line*) and its plane wave part (*dashed line*), the dots mark the lattice points

² Felix Bloch 1905–1983, Nobel prize in Physics 1952.

characterization of the Bloch function by the wave vector is unique within the 1st Brillouin zone, because the phase factor in (5.35) is the same for all \mathbf{k} differing by a reciprocal lattice vector.

For a given \mathbf{k} , the eigenvalue equation (5.31) has in general an infinite set of independent solutions, which are distinguished by an energy quantum number, the *band index* n . Thus the solutions of (5.31) are classified by the complete set of quantum numbers $\alpha = (n, \mathbf{k})$ (a spin quantum number can be added where required)

$$\left(-\frac{\hbar^2}{2m}\Delta + V_{\text{eff}}(\mathbf{r})\right)\psi_{n\mathbf{k}}(\mathbf{r}) = E_n(\mathbf{k})\psi_{n\mathbf{k}}(\mathbf{r}) \quad (5.37)$$

and the energy eigenvalues $E_n(\mathbf{k})$ for all n and \mathbf{k} from the 1st Brillouin zone define the energy band structure of electrons in a periodic potential. By applying periodic boundary conditions, one can easily verify, that there are as many different \mathbf{k} in the Brillouin zone as there are unit cells in the crystal volume. Thus, each energy band can accommodate one electron of either spin per Wigner–Seitz cell (Problem 5.3).

Supplement: Symmetry of $E_n(\mathbf{k})$:

Besides the translation symmetry $E_n(\mathbf{k}) = E_n(\mathbf{k} + \mathbf{G})$ considered already by restricting \mathbf{k} to the first Brillouin zone, there are other symmetries of the problem according to which the band structure repeats within the Brillouin zone.

1. Due to *time reversal* invariance the Hamiltonian is hermitian, $H = H^\dagger$, i.e., it is real and we may write the complex conjugate equation to (5.37)

$$H\psi_{n\mathbf{k}}^* = E_n(\mathbf{k})\psi_{n\mathbf{k}}^*. \quad (5.38)$$

The complex conjugate Bloch function $\psi_{n\mathbf{k}}^*$, written in the form of (5.36), is characterized by a phase factor with $-\mathbf{k}$ and belongs to the solutions of (5.37) in the form

$$H\psi_{n-\mathbf{k}} = E_n(-\mathbf{k})\psi_{n-\mathbf{k}}. \quad (5.39)$$

Both these equations are eigenvalue equations for the same operator and yield the same spectrum. If we consider the electron spin (whose direction changes under time inversion) as additional quantum number, we may write

$$\{E_{n\uparrow}(\mathbf{k}), \text{ all } n\} = \{E_{n\downarrow}(-\mathbf{k}), \text{ all } n\}, \quad (5.40)$$

where the curly brackets denote the whole set of eigenvalues. This degeneracy, following from time reversal symmetry, is known as *Kramers degeneracy*.

2. We mentioned already in Chap. 1 the symmetry of the periodic lattice under the operations S of the point group, which now means invariance of the Hamiltonian of (5.37)

$$[H, S] = 0, \quad \text{or} \quad SHS^{-1} = H. \quad (5.41)$$

Application of the point group operation S to the wave function $\psi(\mathbf{r})$ changes \mathbf{r} into $S^{-1}\mathbf{r}$ and we may write

$$S\psi_{n\mathbf{k}}(\mathbf{r}) = \psi_{n\mathbf{k}}(S^{-1}\mathbf{r}) = e^{i\mathbf{k}\cdot(S^{-1}\mathbf{r})}u_{n\mathbf{k}}(S^{-1}\mathbf{r}) \quad (5.42)$$

which because of $\mathbf{k}\cdot(S^{-1}\mathbf{r}) = S\mathbf{k}\cdot\mathbf{r}$ means that the Bloch function (5.42) is one with wave vector $S\mathbf{k}$ and we conclude, as for the time reversal symmetry, that

$$\{E_n(S\mathbf{k}), \text{ all } n\} = \{E_n(\mathbf{k}), \text{ all } n\}. \quad (5.43)$$

Thus, the energy band structure reflects completely the point group symmetry of the crystal structure. This property of the band structure can be exploited in performing sums over \mathbf{k} , which can be restricted to the so-called irreducible wedge of the Brillouin zone.

3. Consider a combination of 1 and 2: if time reversal invariance combines with the point group symmetry, we have for operations S with $S\mathbf{k} = -\mathbf{k}$ that

$$\{E_{n\uparrow}(\mathbf{k}), \text{ all } n\} = \{E_{n\downarrow}(\mathbf{k}), \text{ all } n\}. \quad (5.44)$$

In contrast to (5.40), this situation with the up and down spin states of a given \mathbf{k} having the same energy, is called *spin degeneracy*.

Let us have a look back to the beginning of this chapter with the N electron Hamiltonian (5.2) as starting point. Within the DFT concepts we have reduced this many-particle problem to a single-particle one (of course with the restrictions already mentioned). Nevertheless, we can formulate \mathcal{H}_N in an approximate way (compare with (4.94))

$$\mathcal{H}_N \simeq \sum_{n\mathbf{k}} E_n(\mathbf{k})c_{n\mathbf{k}}^\dagger c_{n\mathbf{k}} \quad (5.45)$$

by making use of the band structure and by introducing fermion creation and annihilation operators $c_{n\mathbf{k}}^\dagger$ and $c_{n\mathbf{k}}$ with

$$\{c_{n\mathbf{k}}^\dagger, c_{n'\mathbf{k}'}\} = c_{n\mathbf{k}}^\dagger c_{n'\mathbf{k}'} + c_{n'\mathbf{k}'} c_{n\mathbf{k}}^\dagger = \delta_{nn'}\delta_{\mathbf{k}\mathbf{k}'}. \quad (5.46)$$

In this approximate formulation, the electron–electron interaction is incorporated in the single-particle properties and we may address these Bloch electrons as the quasi-particles of the density functional theory.

5.3 Almost Free Electrons and Pseudo-Potentials

Starting with this section we present concepts of band structure calculations which are outlined in many textbooks of Solid State Theory [11, 121, 132–134]. The task is to solve the Schroedinger equation (5.37)

$$\left(-\frac{\hbar^2}{2m}\Delta + V_{\text{eff}}(\mathbf{r})\right)\psi_{n\mathbf{k}}(\mathbf{r}) = E_n(\mathbf{k})\psi_{n\mathbf{k}}(\mathbf{r}) \quad (5.47)$$

for Bloch electrons with

$$\psi_{n\mathbf{k}}(\mathbf{r}) = e^{i\mathbf{k}\cdot\mathbf{r}}u_{n\mathbf{k}}(\mathbf{r}). \quad (5.48)$$

The simplest possible concept is to make use of the periodicity of $u_{n\mathbf{k}}(\mathbf{r})$ and expand it in the complete set of normalized plane waves with reciprocal

lattice vectors \mathbf{G}

$$\psi_{n\mathbf{k}}(\mathbf{r}) = \sum_{\mathbf{G}} C_{n\mathbf{k}}(\mathbf{G}) \frac{1}{\sqrt{V_c}} e^{i(\mathbf{k}+\mathbf{G})\cdot\mathbf{r}}. \quad (5.49)$$

The problem of solving (5.47) consists in finding the expansion coefficients $C_{n\mathbf{k}}(\mathbf{G})$. For this purpose we use the expansion (5.49) in (5.47), multiply from left with a normalized plane wave with $\mathbf{k} + \mathbf{G}'$, and integrate over the crystal volume V_c . This leads to a set of coupled homogeneous linear equations

$$\sum_{\mathbf{G}} \left\{ \left(\frac{\hbar^2}{2m} (\mathbf{k} + \mathbf{G})^2 - E \right) \delta_{\mathbf{G}\mathbf{G}'} + V(\mathbf{G} - \mathbf{G}') \right\} C_{n\mathbf{k}}(\mathbf{G}) = 0. \quad (5.50)$$

The first term results from the operator of kinetic energy and the orthogonality of the plane waves, the second is the Fourier component of the effective potential

$$V(\mathbf{G} - \mathbf{G}') = \frac{1}{V_c} \int V_{\text{eff}}(\mathbf{r}) e^{i(\mathbf{G}-\mathbf{G}')\cdot\mathbf{r}} d^3\mathbf{r}. \quad (5.51)$$

The energy eigenvalues are obtained from the secular problem

$$\left\| \left(\frac{\hbar^2}{2m} (\mathbf{k} + \mathbf{G})^2 - E \right) \delta_{\mathbf{G}\mathbf{G}'} + V(\mathbf{G} - \mathbf{G}') \right\| = 0. \quad (5.52)$$

The efficiency of this concept depends essentially on the convergence of the plane wave expansion (5.49) or on the strength of the periodic potential in terms of its Fourier coefficients. When looking at Fig. 5.1 it is conceivable that a strong modulation of the Bloch function (caused by a strong potential) requires more terms in the plane wave expansion than a Bloch function with a weak modulation. In general, one can say that the plane wave expansion is expected to work well if in the secular problem (5.52) the kinetic energy terms (the diagonal terms of the matrix) dominate over the (non-diagonal) potential terms. This is the case for almost free electrons, for which the periodic potential acts as a weak perturbation. In fact (5.52) represents an expression of first order perturbation theory applied to the free electron states and leads to a Brillouin–Wigner perturbation expansion. The anticipation of a weak periodic potential and the occupation of the lowest bands deriving from a free electron parabola with the valence electrons, is consistent with the idea put forward at the beginning of this book that the constituents of the solid are ions and valence electrons. But we have not yet shown how this concept is considered in the effective potential.

Intuitively, the potential of an ion seen by a valence electron is that of a screened uncompensated charge outside of the closed shell radius but approximately zero (due to charge compensation) inside of this shell. This leads to the model of an *empty core potential*

$$V_{\text{ec}}(\mathbf{r}) = \begin{cases} 0 & r < R_c \\ -\frac{Ze^2}{4\pi\epsilon_0 r} e^{-k_{\text{FT}} r} & r > R_c \end{cases} \quad (5.53)$$

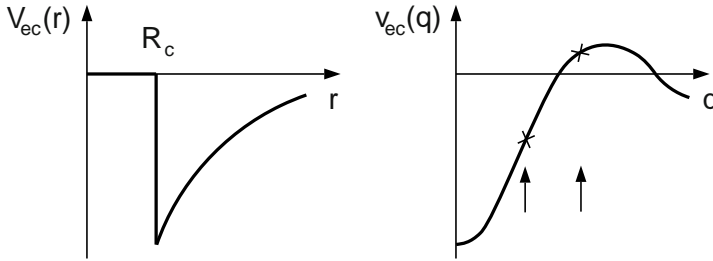


Fig. 5.2. Empty core pseudo-potential and its Fourier transform (the *arrows* indicate the length of reciprocal lattice vectors)

where Z is the ion charge, R_c the core radius, and k_{FT} the inverse Thomas–Fermi screening length (see Problem 4.11). This potential is depicted in Fig. 5.2 together with its Fourier transform

$$v_{\text{ec}}(q) = -\frac{Ze^2}{\varepsilon_0(q^2 + k_{\text{FT}}^2)} \cos qR_c = \frac{v_{\text{ion}}(q)}{\varepsilon(q)}, \quad (5.54)$$

which can be expressed as the ion potential $v_{\text{ion}}(q) = -Ze^2/4\pi\varepsilon_0q^2$ divided by the dielectric constant $\varepsilon(q)$ in the Thomas–Fermi approximation. Characteristic values of the parameters Z, R_c , and k_{FT} , yield values for the Fourier coefficients of the periodic potential of a few tenths of the Rydberg energy, which can in fact be considered as a perturbation on the scale of the free electron energies (which are of the order of 1 Ry).

The empty core potential is a prototype pseudo-potential adapted to the anticipated construction of the solid out of ions and valence electrons [134, 139]. If we had started from nuclei and all electrons, then the effective single-particle potential would have the characteristic form depicted in Fig. 2.1 with strong attractive parts close to the nuclei. Such a potential would have strong Fourier coefficients up to large reciprocal lattice vectors, which are required to obtain a converging representation, especially of the most strongly bound electrons in the inner shell. But as already discussed, these electrons are not relevant for solid state properties and we are interested here only in the valence electrons. In view of the all-electron problem, the valence electrons are in states which are orthogonal to those in closed shells and we can understand the problem of calculating the band structure as that of looking for eigensolutions of the all-electron Hamiltonian in that part of the Hilbert space, which is orthogonal to the core states. This view opens the principle access to pseudo-potentials.

Let us expand for this purpose the Bloch function $\psi_{n\mathbf{k}}(\mathbf{r}) = \langle \mathbf{r} | n\mathbf{k} \rangle$ in terms of plane waves $\langle \mathbf{r} | \mathbf{k} + \mathbf{G} \rangle$ which by construction are made orthogonal to the core states

$$|n\mathbf{k}\rangle = (1 - \mathcal{P})|n\mathbf{k}\rangle_{\text{PW}}, \quad |n\mathbf{k}\rangle_{\text{PW}} = \sum_{\mathbf{G}} C_{n\mathbf{k}}(\mathbf{G})|\mathbf{k} + \mathbf{G}\rangle, \quad (5.55)$$

where

$$\mathcal{P} = \sum_{\nu \in \text{core}} |\nu \mathbf{k}\rangle \langle \nu \mathbf{k}| \quad (5.56)$$

is the projection operated onto the core Bloch states (see (5.67)). Making use of this expansion in the eigenvalue problem with the single-particle Hamiltonian but with all electrons considered in the periodic potential V_{all} , one finds

$$\begin{aligned} H_{\text{all}}|n\mathbf{k}\rangle &= \left(\frac{p^2}{2m} + V_{\text{all}} - \sum_{\nu \in \text{core}} E_{\nu} |\nu \mathbf{k}\rangle \langle \nu \mathbf{k}| \right) |n\mathbf{k}\rangle_{\text{PW}} \\ &= E \left(1 - \sum_{\nu \in \text{core}} |\nu \mathbf{k}\rangle \langle \nu \mathbf{k}| \right) |n\mathbf{k}\rangle_{\text{PW}}. \end{aligned} \quad (5.57)$$

An eigenvalue equation for this expansion is obtained by rearranging (5.57) in the form

$$\left(\frac{p^2}{2m} + V_{\text{all}} + \sum_{\nu \in \text{core}} (E - E_{\nu}) |\nu \mathbf{k}\rangle \langle \nu \mathbf{k}| \right) |n\mathbf{k}\rangle_{\text{PW}} = E |n\mathbf{k}\rangle_{\text{PW}} \quad (5.58)$$

with the nonlocal pseudo-potential operator

$$V_{\text{psp}} = V_{\text{all}} + \sum_{\nu \in \text{core}} (E - E_{\nu}) |\nu \mathbf{k}\rangle \langle \nu \mathbf{k}|. \quad (5.59)$$

By construction, the solutions of (5.58) are orthogonal to the core electron states and yield the electron states of valence and conduction bands. When taking the expectation value of the nonlocal operator with $|n\mathbf{k}\rangle_{\text{PW}}$ one finds (note, that we calculate valence electron states with $E > E_{\nu}$)

$$\sum_{\nu \in \text{core}} (E - E_{\nu}) |\langle \nu \mathbf{k} | n\mathbf{k}\rangle_{\text{PW}}|^2 > 0, \quad (5.60)$$

i.e., the additional potential cancels (partially) the attractive potential of the nuclei and converts the all electron potential into a weak pseudo-potential. In this sense, the effective potential in (5.47) is to be understood as a pseudo-potential and we can safely assume, that the plane wave expansion converges with reasonable effort.

Initially, the Fourier coefficients of the pseudo-potentials have been used as empirical parameters [134, 139] which were determined by fitting a calculated band structure to experimental data, such as Fermi surface parameters or energy gaps. In the course of time, the pseudo-potential concepts have been developed and it is now possible to perform ab initio band calculations which make use of so-called norm conserving and soft pseudo-potentials, which are free of adjustable parameters [140, 141].

Instead of treating the full problem of solving (5.52), we may look for situations where the free electron picture, with the parabolic dispersion of the

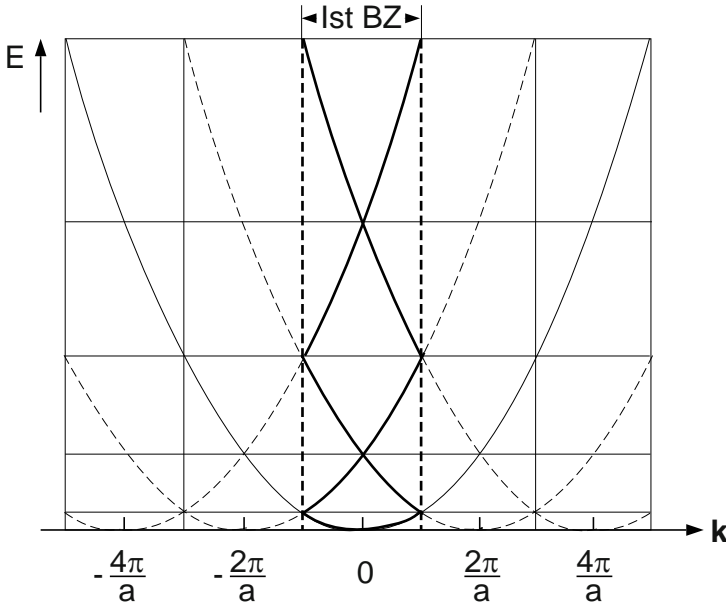


Fig. 5.3. Free electron energy bands in one dimension: extended and repeated zone scheme

energy, is only slightly perturbed by the periodic potential. Figure 5.3 shows the free-electron band structure for a one-dimensional system without periodic potential but with the periodicity taken into account by introducing Brillouin zone boundaries. Due to the translation symmetry, the energy dispersion is periodic in k with periods $2\pi/a$, i.e., the free-electron parabola may start at each value $2n\pi/a$ with integer n . In order to avoid the redundancy in this *repeated zone scheme*, it is sufficient to consider the dispersion only in the first Brillouin zone (*reduced zone scheme*). This picture of the reduced zone scheme can be obtained also from the parabola starting at 0, by shifting those parts, which are outside the first Brillouin zone, by multiples of $2\pi/a$ to bring them back to this zone. This concept is not restricted to the free electron dispersion in 1D but applies as well to any realistic band structure not only of electrons (see e.g., the situation in Problem 3.1 for the linear chain, when the two masses become equal).

Coming back to the secular problem (5.52) we recognize in Fig. 5.3 degeneracies of the free-electron energy dispersion at the Brillouin zone boundaries and in its center, e.g., the parabolas starting at 0 and at $2\pi/a$ cross at $k = \pi/a$. Writing the secular problem for the corresponding states one obtains

$$\left\| \begin{array}{cc} E(k) - E & V(G) \\ V(G) & E(k - G) - E \end{array} \right\| = 0, \quad G = \frac{2\pi}{a}, \quad (5.61)$$

where $E(k)$ is the kinetic energy of free electrons, with the zeros

$$E_{\pm}(k) = \frac{1}{2} \left(E(k) + E(k - G) \right) \pm \left\{ \frac{1}{4} (E(k) - E(k - G))^2 + |V(G)|^2 \right\}^{1/2}. \quad (5.62)$$

For $k = \pi/a$ one has $E(k) = E(k - G) = \hbar^2/2m(\pi/a)^2$ and

$$E_{\pm} \left(\frac{\pi}{a} \right) = \frac{\hbar^2}{2m} \left(\frac{\pi}{a} \right)^2 \pm \left| V \left(\frac{2\pi}{a} \right) \right|. \quad (5.63)$$

The effect of the periodic potential is to remove the degeneracy of the free electron states (here at the boundary of the Brillouin zone) and to create an *energy gap* or *band gap* in the otherwise continuous spectrum. The gap is determined by a Fourier coefficient of the potential for the reciprocal lattice vector connecting the degenerate plane waves. The dispersion of the lowest energy bands $E_{\pm}(k)$ around $k = \pi/a$ is shown in Fig. 5.4 together with the corresponding free electron dispersion (thin dashed lines).

In general, the reciprocal lattice vectors of degenerate plane waves fulfill the *Bragg condition* (Problem 5.4), thus the plane waves being reflected at the crystal planes is characterized by the reciprocal lattice vector forming standing waves. This becomes evident by looking at the eigenfunctions. In our simple example with the energies of (5.63), they take the form

$$\psi_{+\frac{\pi}{a}}(x) \sim i \sin \frac{\pi x}{a} \quad \text{and} \quad \psi_{-\frac{\pi}{a}}(x) \sim \cos \frac{\pi x}{a} \quad (5.64)$$

and their modulus shows minima (maxima) at the lattice points, which leads to the raising (lowering) of the energy due to the periodic potential in comparison with the free electron case. (Note that the potential is attractive for electrons in the vicinity of the ion positions.) The energy gaps and the horizontal slope of energy bands (preferentially) at the boundary of the Brillouin

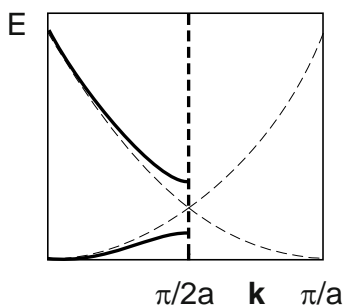


Fig. 5.4. Opening of a gap at the Brillouin zone boundary due to a periodic potential

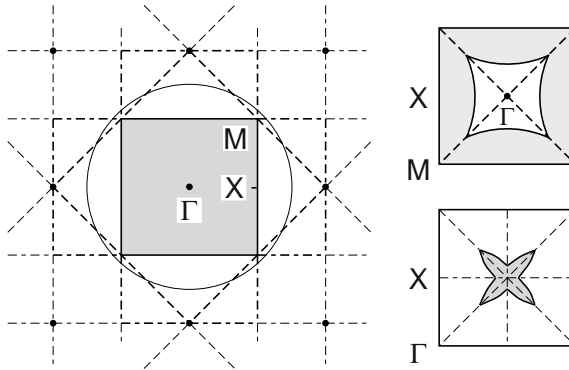


Fig. 5.5. Brillouin zones of the two-dimensional square lattice and Fermi contours

zone, which corresponds to a vanishing group velocity, are the most prominent features of the energy band structure.

Let us now proceed to the situation of a 2D square lattice and look at the Fermi contours as depicted in Fig. 5.5. In the left part, we recognize the reciprocal lattice points and the construction lines for the Brillouin zones: the solid lines mark the central square of the first Brillouin zone (first BZ); the dashed lines, augmenting the first BZ to a square of double size, mark the second Brillouin zone. The four triangles outside of the first BZ can be rearranged by translations with reciprocal lattice vectors to form a square reproducing the 1st BZ as indicated in the right upper part of Fig. 5.5. The third BZ is obtained from the dash-dotted smaller triangles which again can be rearranged to a square of the size of the first BZ around the M point (see lower right part of Fig. 5.5). The free-electron dispersion in the extended zone scheme (Fig. 5.5, left) is a paraboloid with its minimum at the Γ point or $\mathbf{k} = (0,0)$. In the presence of a 2D periodic potential, (causing the square lattice with lattice constant a) this continuous energy dispersion will be deformed in the vicinity of the Brillouin zone boundaries in connection with the opening of gaps (Problem 5.5).

Instead of looking at the band dispersion, we want to discuss here the consequences of the Fermi circle shown in the left part of Fig. 5.5 for an assumed electron density, i.e., the area inside this circle defines the occupied states of the free-electron dispersion at $T = 0$ K. When constructing the Brillouin zones the Fermi circle, breaks into pieces which by rearrangement of the extended to the reduced zone scheme, give the grey areas indicating occupied states in different bands. The first BZ or the lowest energy band is completely occupied, the second and third band (plotted for a BZ around the point M) are only partially filled and the grey areas are only faintly reminiscent of deriving from a circle. In the presence of a weak periodic potential, these contours, which separate the empty from the occupied states, are distorted when the gaps open at the BZ boundaries. These *Fermi contours* (which in 3D become *Fermi*

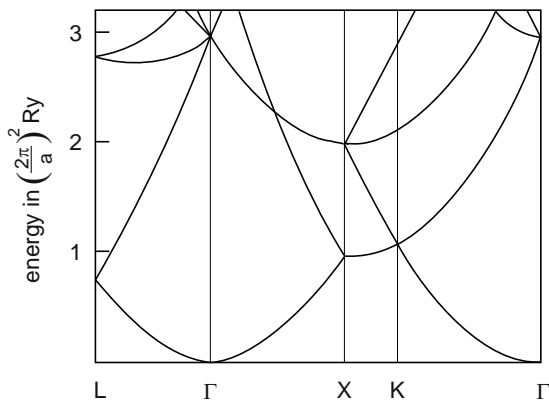


Fig. 5.6. Free electron energy bands in an fcc lattice

surfaces) can experimentally be detected by analyzing the quantum oscillations of the magnetic susceptibility (deHaas–vanAlphen effect) or of the magneto-resistivity (Shubnikov–deHaas effect). These methods are of central importance in band structure investigations of metals.

Modern semiconductor technology has led to man-made two-dimensional electron systems (see Sect. 5.6) with a periodic potential (lateral surface superlattices). The band structure of these systems and their Fermi contours have been analyzed with the band theory of almost free electrons in two dimensions [135].

Let us look at the 3D case. The free electron dispersion in a fcc lattice shown in Fig. 8.6 (Problem 5.6) will serve as the basis to understand in the following some of the electronic properties of a noble metal (Ag), a normal (trivalent) metal (Al), and a semiconductor (Si). The free electron parabola, starting at the Γ point is backfolded to account for Bragg reflection at the BZ boundaries. These backfolded branches can be understood also in the repeated zone scheme as deriving from parabolas starting at reciprocal lattice vectors \mathbf{G} . Some of these branches are degenerate. The characteristic energy scale (and the length of the axes) changes with the lattice constant, but is typically of the order of the Rydberg energy. A weak potential with Fourier coefficients of a few tenths of the Rydberg energy slightly changes this picture by lifting degeneracies (seen here e.g., along the line $\Gamma - K - X$) and opening gaps as depicted in Fig. 5.7 for Al. The density of states for these energy bands, shown in Fig. 5.8, exhibits the similarity with the square root dependence (dashed line) found for free electrons, while the energy gaps are responsible for the deviations seen in the solid curve.

Imagine the filling of these states with electrons: in the free electron picture we have the Fermi sphere in \mathbf{k} space, which is mapped onto the band structure in the reduced zone scheme, where each band can accommodate two electrons per atom in the unit cell (see Problem 5.3). For a monovalent metal

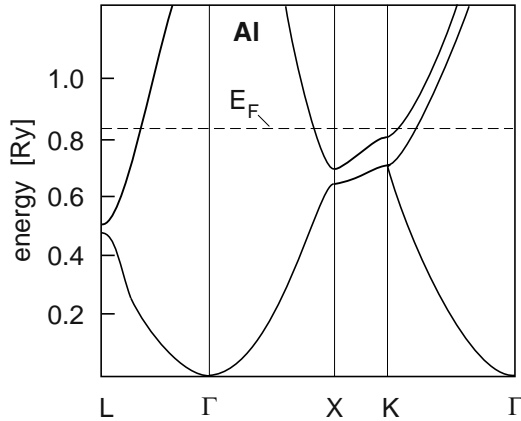


Fig. 5.7. Energy band structure of Al after [134]

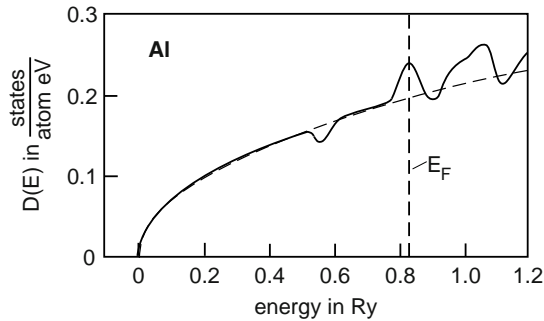


Fig. 5.8. Density of states of electrons in Al

(like Ag), this leads to a half filled lowest band and the Fermi energy cuts the band structure in a region away from zone boundaries where the free electron dispersion is almost unchanged by the periodic potential. In this case, the Fermi surface more or less maintains its spherical shape as for free electrons. Nevertheless, depending on the lattice constant, the Fermi contour can come sufficiently close to the BZ boundaries which (for an fcc lattice around the L points) are closest to the Γ point and one finds the situation shown in Fig. 5.9. It exhibits the Fermi surface of Ag (representative of the noble metals) in the repeated zone scheme. The Fermi sphere is distorted here by the formation of necks close to the L points as a consequence of gap formation. In deHaas–vanAlphen measurements for different orientations of the magnetic field, the extremal cross sections of the Fermi surface perpendicular to the magnetic field (indicated as N for *neck*, B for *belly*, and DB for *dumb-bell* in Fig. 5.9) are detected by the periods of their corresponding oscillations (see discussion at the end of Sect. 4.2).

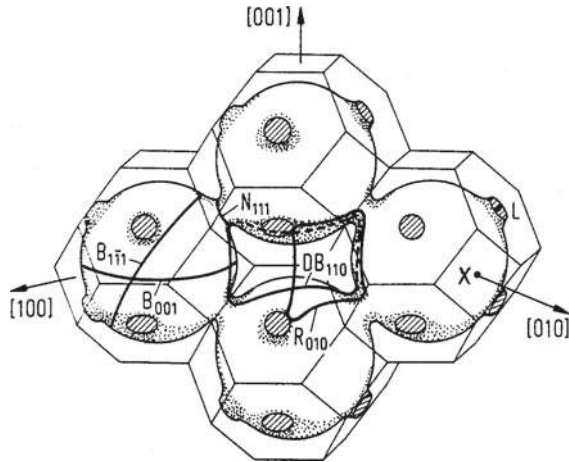


Fig. 5.9. Extended zone scheme with Fermi surfaces and extremal cross sections (see text) of Ag after [136]

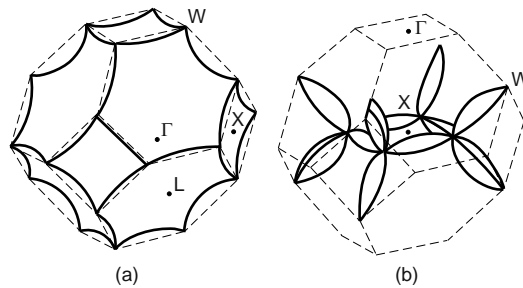


Fig. 5.10. Fermi surfaces of Al in the second and third Brillouin zone after [137]

For the trivalent metal Al the Fermi energy is indicated in Fig. 5.7. All states of the lowest band (or the first BZ) are filled, while the states in the second and third band are only partially filled. The Fermi contours, derived from the Fermi sphere of the free electrons for these bands, are depicted in Fig. 5.10. They will be slightly changed (essentially by rounding off the sharp edges) by gap formation due to the periodic potential. Looking at these strange surfaces, one can imagine that their analysis from deHaas–vanAlphen oscillations, which correspond to extremal cross sections of the Fermi surface perpendicular to the applied magnetic field (see Sect. 4.2), can be quite an involved task.

The last example to be presented in the context of Fig. 8.6 is the band structure of Si. It crystallizes in the diamond structure with two atoms with each four electrons per unit cell. The structure factor of diamond differs from that of the simple fcc lattice and as a consequence, the non-vanishing Fourier components of the periodic potential and the gap structure are different

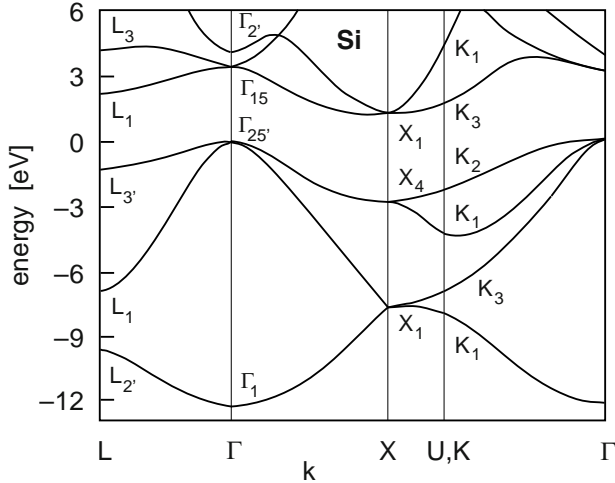


Fig. 5.11. Energy band structure of Si after [138]

(Problem 5.7). This is clearly seen by comparing the band structure of Si (Fig. 5.11) with that of Al (Fig. 5.7) which both derive from the free electron dispersion of the fcc lattice (Fig. 8.6). The eight valence electrons per unit cell in Si, fill the four lowest energy bands in Fig. 5.11 (the *valence bands*), which are separated from the empty *conduction bands* by an *energy gap*, which extends throughout the BZ.

This particular situation of the energy band structure with a gap separating the occupied from the unoccupied states, i.e., the Fermi energy is somewhere in the gap, characterizes the system as a *semiconductor* or *insulator* depending on the size of the gap compared to the thermal energy $k_B T$. At room temperature, and for gap energies around 1 eV (typical for semiconductors like Si) free carriers can be thermally excited and become available for electrical transport, while these solids would be insulating at low temperatures. This band structure is responsible also for a characteristic optical property of semiconductors: at low temperature, light can be absorbed only for $h\nu > E_{\text{gap}}$ by creating electron–hole pairs (see Chap. 10).

5.4 LCAO and Tight-Binding Approximation

An alternative approach to solve (5.47) starts from the isolated atom, for which we may formulate the Schroedinger equation

$$\left(-\frac{\hbar^2}{2m}\Delta + v(\mathbf{r}) \right) \phi_\nu(\mathbf{r}) = E_\nu \phi_\nu(\mathbf{r}) \quad (5.65)$$

with an effective single-particle potential $v(\mathbf{r})$ of the isolated atom. When arranging the atoms to a solid we can imagine the effective single-particle

potential of the solid emerging from a superposition of the atomic potentials

$$V_{\text{eff}}(\mathbf{r}) = \sum_{\mathbf{n}} v(\mathbf{r} - \mathbf{R}_{\mathbf{n}}^0), \quad (5.66)$$

while the overlapping atomic orbitals form Bloch functions

$$\psi_{\nu\mathbf{k}}(\mathbf{r}) = \frac{1}{\sqrt{N}} \sum_{\mathbf{n}} e^{i\mathbf{k}\cdot\mathbf{R}_{\mathbf{n}}^0} \phi_{\nu}(\mathbf{r} - \mathbf{R}_{\mathbf{n}}^0), \quad (5.67)$$

which can be used as a complete set for the expansion

$$\psi_{n\mathbf{k}}(\mathbf{r}) = \sum_{\nu} C_{n\nu} \psi_{\nu\mathbf{k}}(\mathbf{r}). \quad (5.68)$$

It is a *linear combination of atomic orbitals* (LCAO). In contrast to the plane wave expansion used in Sect. 5.3, which exploited the periodicity and weakness of the effective potential, is the LCAO expansion intimately related to the atomic orbitals of valence electrons, which are distorted in the crystalline environment.

We make use of the expansion (5.68) in (5.47) to determine the expansion coefficients $C_{n\nu}$. The *lhs* of (5.47) can be written

$$\begin{aligned} & H \psi_{n\mathbf{k}}(\mathbf{r}) \\ &= \sum_{\nu} C_{n\nu} \frac{1}{\sqrt{N}} \sum_{\mathbf{n}} e^{i\mathbf{k}\cdot\mathbf{R}_{\mathbf{n}}^0} \left(-\frac{\hbar^2}{2m} \Delta + \sum_{\mathbf{n}'} v(\mathbf{r} - \mathbf{R}_{\mathbf{n}'}^0) \right) \phi_{\nu}(\mathbf{r} - \mathbf{R}_{\mathbf{n}}^0) \\ &= \sum_{\nu} C_{n\nu} \frac{1}{\sqrt{N}} \sum_{\mathbf{n}} e^{i\mathbf{k}\cdot\mathbf{R}_{\mathbf{n}}^0} \left(E_{\nu} + \sum_{\mathbf{n}' \neq \mathbf{n}} v(\mathbf{r} - \mathbf{R}_{\mathbf{n}'}^0) \right) \phi_{\nu}(\mathbf{r} - \mathbf{R}_{\mathbf{n}}^0). \end{aligned} \quad (5.69)$$

To arrive at the last line, the solution of (5.65) has been used for the lattice site $\mathbf{R}_{\mathbf{n}}^0$. By multiplying from the left with $\psi_{\nu'\mathbf{k}}^*$ and integrating over the crystal volume, one obtains a set of homogeneous coupled linear equations for the $C_{n\nu}$. In contrast to the plane wave expansion the basis set used here, the atomic orbitals $\phi_{\nu}(\mathbf{r} - \mathbf{R}_{\mathbf{n}}^0)$, are not orthogonal when centered around different lattice sites. Thus, one has to calculate (making use of the lattice periodicity)

$$\begin{aligned} & \frac{1}{N} \sum_{\mathbf{n}'\mathbf{n}} e^{i\mathbf{k}\cdot(\mathbf{R}_{\mathbf{n}}^0 - \mathbf{R}_{\mathbf{n}'}^0)} \int \phi_{\nu'}^*(\mathbf{r} - \mathbf{R}_{\mathbf{n}'}^0) \phi_{\nu}(\mathbf{r} - \mathbf{R}_{\mathbf{n}}^0) d^3\mathbf{r} \\ &= \frac{1}{N} \sum_{\mathbf{m}} \sum_{\mathbf{n}} e^{i\mathbf{k}\cdot\mathbf{R}_{\mathbf{n}}^0} \int \phi_{\nu'}^*(\mathbf{r}) \phi_{\nu}(\mathbf{r} - \mathbf{R}_{\mathbf{n}}^0) d^3\mathbf{r} \\ &= \delta_{\nu'\nu} + \sum_{\mathbf{n} \neq 0} e^{i\mathbf{k}\cdot\mathbf{R}_{\mathbf{n}}^0} S_{\nu'\nu}(\mathbf{R}_{\mathbf{n}}^0) =: S_{\nu'\nu}(\mathbf{k}) \end{aligned} \quad (5.70)$$

with the two-center *overlap integral*

$$S_{\nu'\nu}(\mathbf{R}_n^0) = \int \phi_{\nu'}^*(\mathbf{r})\phi_{\nu}(\mathbf{r} - \mathbf{R}_n^0)d^3\mathbf{r}. \quad (5.71)$$

These integrals depend on the relative position of the centers and on the spatial orientation of the atomic orbitals. Their value decreases with increasing separation of the centers, because the orbitals are localized around the lattice sites.

The terms containing the atomic potentials depend in general on three centers

$$\frac{1}{N} \sum_m \sum_n e^{i\mathbf{k}\cdot(\mathbf{R}_n^0 - \mathbf{R}_m^0)} \sum_{n' \neq n} \int \phi_{\nu'}^*(\mathbf{r} - \mathbf{R}_m^0)v(\mathbf{r} - \mathbf{R}_{n'}^0)\phi_{\nu}(\mathbf{r} - \mathbf{R}_n^0)d^3\mathbf{r}. \quad (5.72)$$

Because the atomic orbitals and the atomic potential decrease rapidly away from their respective centers, these integrals will be small if the three centers are different from each other. A reasonable approximation is to consider only terms where two of the three centers coincide. They can be written

$$K_{\nu'\nu} = \sum_n \int \phi_{\nu'}^*(\mathbf{r})v(\mathbf{r} - \mathbf{R}_n^0)\phi_{\nu}(\mathbf{r})d^3\mathbf{r} \quad (5.73)$$

for $m = n \neq n'$ and

$$J_{\nu'\nu}(\mathbf{k}) = \sum_n e^{i\mathbf{k}\cdot\mathbf{R}_n^0} \int \phi_{\nu'}^*(\mathbf{r} - \mathbf{R}_n^0)v(\mathbf{r} - \mathbf{R}_n^0)\phi_{\nu}(\mathbf{r})d^3\mathbf{r} \quad (5.74)$$

for $m \neq n = n'$. As for the two-center overlap integral these expressions are obtained by making use of the periodicity of the lattice. The term $K_{\nu'\nu}$, which does not depend on the wave vector \mathbf{k} , describes the effect of the off-center atomic potentials on the orbitals at the origin. This *crystal field term* accounts for the lowering of the rotational symmetry of the isolated atom (according to which atomic orbitals can be classified by angular momentum quantum numbers) in the crystalline environment. It can lead to a removal of degeneracy of atomic orbitals which is known as *crystal field splitting* (Problem 5.8).

The term $J_{\nu'\nu}(\mathbf{k})$ is similar to the overlap integral $S_{\nu'\nu}(\mathbf{k})$ except for the additional potential under the integral. It contributes together with $S_{\nu'\nu}(\mathbf{k})$ to the formation of energy bands. The eigenvalue problem can now be written

$$\sum_{\nu} C_{\nu\nu} (H_{\nu'\nu}(\mathbf{k}) - ES_{\nu'\nu}(\mathbf{k})) = 0 \quad (5.75)$$

with the Hamiltonian matrix

$$H_{\nu'\nu}(\mathbf{k}) = E_{\nu}S_{\nu'\nu}(\mathbf{k}) + K_{\nu'\nu} + J_{\nu'\nu}(\mathbf{k}) \quad (5.76)$$

and the eigenvalues are obtained from the secular equation

$$\|H_{\nu'\nu}(\mathbf{k}) - ES_{\nu'\nu}(\mathbf{k})\| = 0. \quad (5.77)$$

This secular problem deviates from the standard form because of the overlapping atomic orbitals. It can be shown, that due to the properties of the overlap matrix, one can find a unitary transformation to reduce (5.77) to the standard form (Problem 5.9). Frequently, the problem is further simplified by considering in the sum over the lattice sites \mathbf{n} only nearest neighbors (which is justified for sufficiently tightly bound atomic orbitals). This *tight-binding approximation* will be used in the following examples.

Supplement: Energy bands in tight-binding approximation:

Let us assume in all these examples the simplified form of the secular problem (5.77) with $S_{\nu'\nu}(\mathbf{k}) \simeq \delta_{\nu'\nu}$ (see Problem 5.9).

1. The simplest example is the energy band in a cubic lattice that derives from an atomic s orbital. For this case $\nu = \nu' = s$ and the energy band is immediately given by $E_s(\mathbf{k}) = H_{ss}(\mathbf{k}) \simeq E_s + J_{ss}(\mathbf{k})$. Note that the s orbital is not degenerate (except for spin) and the crystal field causes only a shift which can be absorbed in the zero of the energy scale. Let us evaluate $J_{ss}(\mathbf{k})$ by summing up the nearest neighbors in a fcc lattice, which under normal conditions is the crystal structure of normal and noble metals. The 12 nearest neighbors are

$$\mathbf{R}_n^0 : \frac{a}{2} (\pm 1, \pm 1, 0), (\pm 1, 0, \pm 1), (0, \pm 1, \pm 1) \\ (\pm 1, \mp 1, 0), (\pm 1, 0, \mp 1), (0, \pm 1, \mp 1). \quad (5.78)$$

Due to the spherical symmetry of the s orbital, the matrix element $J_{ss}(\mathbf{R}_n^0)$ does not depend on the individual lattice vector but only on the nearest neighbor distance $a/\sqrt{2}$ and one finds

$$E_s(\mathbf{k}) = E_s + 12J_{ss} \left(\frac{a}{\sqrt{2}} \right) f(\mathbf{k}) \quad (5.79)$$

with

$$f(\mathbf{k}) = \frac{1}{3} \left(\cos \frac{k_x a}{2} \cos \frac{k_y a}{2} + \cos \frac{k_y a}{2} \cos \frac{k_z a}{2} + \cos \frac{k_z a}{2} \cos \frac{k_x a}{2} \right). \quad (5.80)$$

The function $f(\mathbf{k})$ is characteristic of the crystal structure (Problem 5.10), while the overlap of the atomic orbital together with the strength of the atomic potential, determines the value of the matrix element J_{ss} . The energy band (for obvious reasons called s band) is depicted in Fig. 5.12 for the lines $\Gamma - X$ and $\Gamma - L$. The width of the band is determined by the matrix element $J_{ss}(a/\sqrt{2})$, which for $a \rightarrow \infty$ decreases to zero and the band shrinks to the discrete level at E_s of the isolated atom. This band exhibits a clear similarity with the lowest band of the free electron dispersion in Fig. 8.6, if we take into account that a periodic potential gives rise to gaps around the points X and L , leading to Fig. 5.7. This similarity indicates the strong influence of the crystal structure on the energy bands.

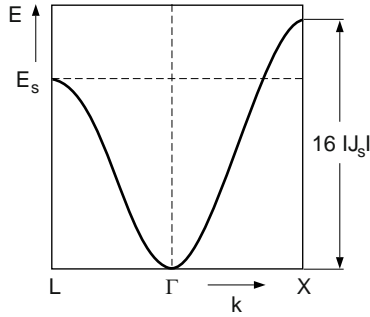


Fig. 5.12. Dispersion of an energy band in an fcc crystal structure deriving from an s orbital

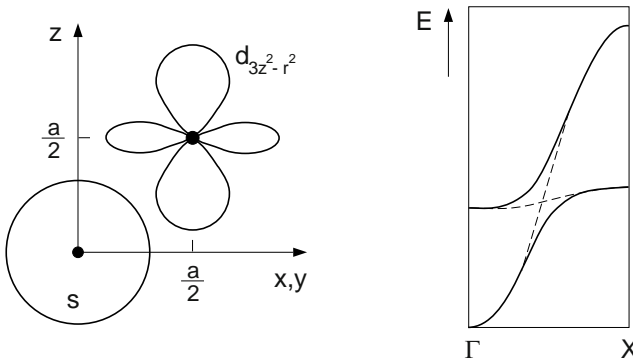


Fig. 5.13. Polar diagrams of atomic orbitals at nearest neighbors for a fcc transition metal (*left*) and schematic of energy bands along $\Gamma - X$ resulting from $s - d$ hybridization (*right*)

- Transition metal atoms differ from those of normal (and noble) metals by the successive filling of d electron states, which are energetically close to the s level of the valence shell. In a solid, when bands are formed due to the wave function overlap, these bands deriving from s and d states fall into the same energy range and intersect each other. This situation can well be described in the tight-binding approximation. We choose $\nu, \nu' = s, d$ to account for the configuration of the $3d$ transition metals (e.g., Fe: $4s^2 3d^6$). For simplicity we assume here, besides the s orbital (shown as polar plot in Fig. 5.13, left part, placed at the origin) only the d orbital with the spatial dependence $3z^2 - r^2$ (in Fig. 5.13 at the nearest neighbor site) and consider the dispersion along $\mathbf{k} = (0, 0, k)$.

With the simplifying assumption $S_{\nu'\nu} = \delta_{\nu'\nu}$ the secular problem (5.77) takes the form

$$\begin{vmatrix} H_{ss}(k) - E & H_{sd}(k) \\ H_{sd}(k) & H_{dd}(k) - E \end{vmatrix} = 0 \quad (5.81)$$

with the solutions

$$E_{\pm}(k) = \frac{1}{2}(H_{ss}(k) + H_{dd}(k)) \pm \left\{ \frac{1}{4}(H_{ss}(k) - H_{dd}(k))^2 + |H_{sd}(k)|^2 \right\}^{1/2}. \quad (5.82)$$

Here $H_{ss}(k)$ (and similarly $H_{dd}(k)$ and $H_{sd}(k)$) takes the form

$$H_{ss}(k) = E_s + 4J_{ss}\left(1 + 2 \cos \frac{ka}{2}\right). \quad (5.83)$$

Without the $s-d$ coupling one gets two similar bands deriving from the s and d orbitals. Their width depends on the corresponding two-center overlap integral $J_{\nu\nu}$, $\nu = s, d$. In Fig. 5.13 we have depicted in the left part the polar diagrams of two orbitals on neighboring lattice sites. If s orbitals are considered on both sites one obtains a significantly larger overlap than from d orbitals (which are stronger localized to the atomic site). Consequently, the s band is much broader than the d band as depicted by the dashed lines in the right part of Fig. 5.13. The overlap between s and d orbitals (described by $H_{sd}(k)$) leads to a coupling and an anti-crossing of these bands as shown by the solid lines in Fig. 5.13. It is known as $s-d$ hybridization and is typical for transition metals. A similar situation can be found for rare earths due to hybridization with f orbitals.

The energy bands for some of the $3d$ transition metals, as obtained from a realistic band structure calculation, are shown for $\mathbf{k} \parallel (001)$ in Fig. 5.14. Note the crystal field splitting of the d bands, which at the Γ point leads to a twofold (Γ_{12}) and a threefold ($\Gamma_{25'}$) state (see Problem 5.8). The group theoretical notation refers to the irreducible representations of the point group. The crystal structure changes with the filling of the d shell, it is body-centered cubic for V and Fe but face-centered cubic for Co and Cu. With the filling of the d shell the corresponding bands get narrower and shift to lower energy until for Cu (Fig. 5.15) they are all below the Fermi energy. In Fig. 5.15 one easily identifies the broad band deriving from the s -orbitals, which is reminiscent of the free electron band of Fig. 8.6. But one also recognizes the small distortions of this band close to the L point at the Fermi energy, which leads to the necks of the almost spherical Fermi surface (see Fig. 5.9).

- Hybridization can take place not only due to overlap of atomic orbitals at different lattice sites but also due to linear combinations of different orbitals

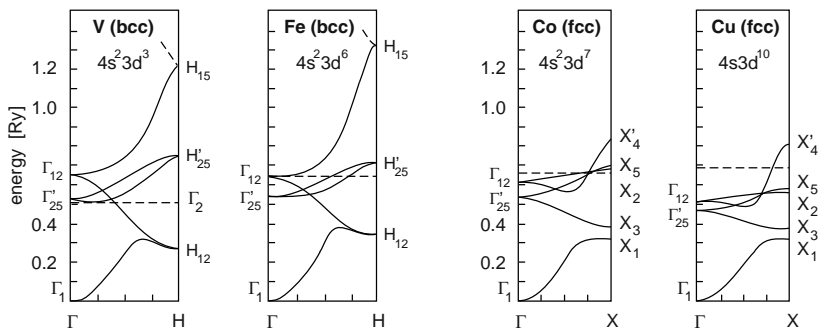


Fig. 5.14. Energy bands of V, Fe, Co, and Cu for $\mathbf{k} \parallel (001)$ after [142]. The dashed line indicates the Fermi energy

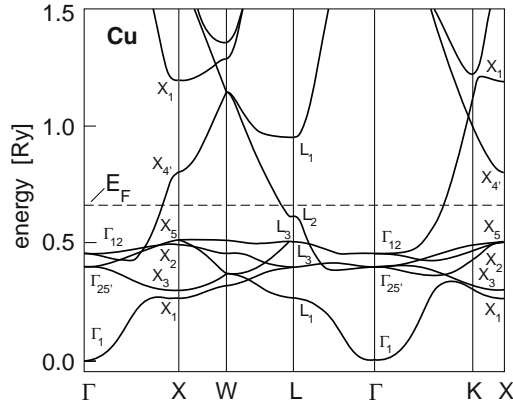


Fig. 5.15. Energy bands of Cu after [143]. The dashed line indicates the Fermi energy

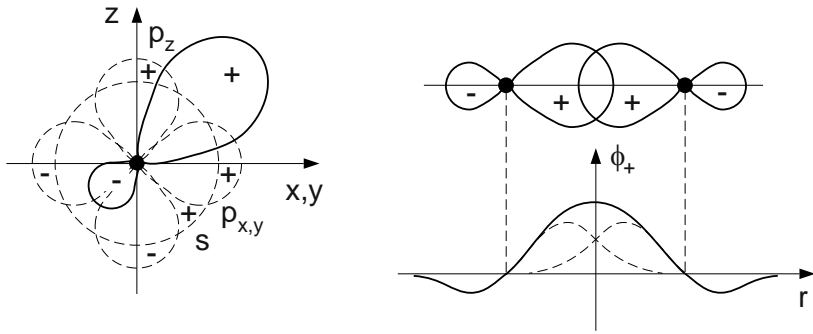


Fig. 5.16. Polar diagram of an sp^3 hybrid orbital and its decomposition into s and p contributions (left) and bonding molecular orbital formed by superposition of sp^3 orbitals from neighboring lattice sites (right)

at the same lattice site. It leads to directed orbitals, which are important in covalent binding. Let us consider the secular problem (5.77) with the orbitals $\nu, \nu' = s, p_x, p_y, p_z$ but use instead their linear combinations

$$\begin{aligned}
 \phi_{111} &= \frac{1}{2}(\phi_s + \phi_{p_x} + \phi_{p_y} + \phi_{p_z}) \\
 \phi_{1-1-1} &= \frac{1}{2}(\phi_s + \phi_{p_x} - \phi_{p_y} - \phi_{p_z}) \\
 \phi_{-11-1} &= \frac{1}{2}(\phi_s - \phi_{p_x} + \phi_{p_y} - \phi_{p_z}) \\
 \phi_{-1-11} &= \frac{1}{2}(\phi_s - \phi_{p_x} - \phi_{p_y} + \phi_{p_z}).
 \end{aligned} \tag{5.84}$$

A polar diagram of the orbital ϕ_{111} and how it is composed of the s and p orbitals is depicted in the left part of Fig. 5.16. Just by accounting for the signs of the latter, it is clear that the resulting orbital has a pronounced positive lobe in the (111) direction, which is the direction towards one of the four nearest neighbors

in the diamond structure. Likewise, the other orbitals point to the direction of the other nearest neighbors. These directed orbitals, called sp^3 hybrid orbitals, are favorable for establishing a network with tetrahedral coordination based on covalent bonds as realized in the diamond structure.

In the same way sp^2 hybrid orbitals can be used to establish planar networks based on covalent bonds as in graphite. In this case the p_z orbitals sticking out of the plane form π bonding and anti-bonding orbitals, which lead to a peculiar band structure with vanishing gap (Problem 5.11). The band structure of this planar network of carbon atoms (graphene) is the basis also for the electronic structure of carbon nanotubes, which result from rolling up the carbon sheets into cylinders.

For the diamond structure, which we pursue here, there are two atoms in the Wigner–Seitz cell with each four directed sp^3 hybrid orbitals, which can be superimposed, as depicted in the right part of Fig. 5.16, such that the positive lobes overlap in the nearest neighbor direction or with the opposite signs to form *bonding* and *anti-bonding* orbitals, respectively,

$$\phi_{\nu}^{\pm}(\mathbf{r}) = \frac{1}{N_{\pm}} \left\{ \phi_{+\nu} \left(\mathbf{r} + \frac{\boldsymbol{\tau}}{2} \right) \pm \phi_{-\nu} \left(\mathbf{r} - \frac{\boldsymbol{\tau}}{2} \right) \right\}. \quad (5.85)$$

Here $\pm\boldsymbol{\tau}/2$ are the positions of the two atoms in the Wigner–Seitz cell and $\pm\nu$ refers to the directions of the positive lobes of the sp^3 hybrid orbitals, which change sign between the nearest neighbor sites. In order to calculate the band structure, Bloch functions have to be composed of these bonding and anti-bonding orbitals and in general, an 8×8 secular problem has to be solved. The bonding orbitals yield the valence bands, the anti-bonding orbitals the conduction bands. Both groups are separated by an energy gap and we obtain the characteristic band structure of a semiconductor.

As an example, the valence bands of Ge calculated by diagonalising the 4×4 matrix for the four bonding orbitals with nearest and next nearest neighbor interaction are shown in Fig. 5.17. These bands exhibit a strong similarity with those of Fig. 5.11 obtained from a pseudo-potential calculation. It is interesting also to look at the spatial electron distribution

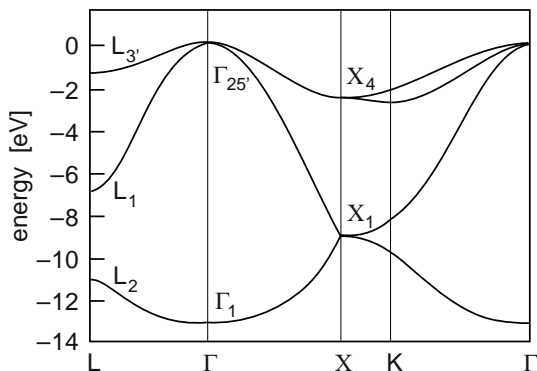


Fig. 5.17. Valence band dispersion (Ge) from an LCAO calculation with nearest and next nearest neighbor coupling after [144]

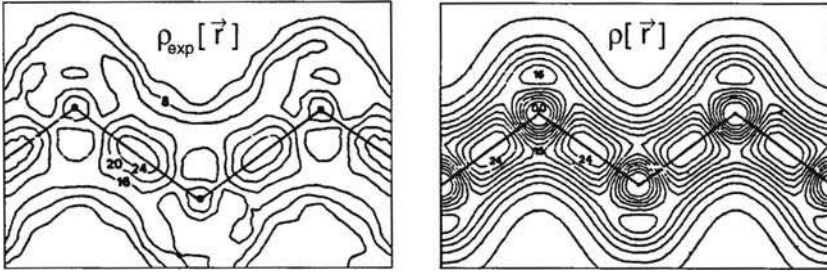


Fig. 5.18. Contour plots of the valence electron charge density of Si showing the bond charge: experiment (*left*), theory (*right*) after [145]

$$\rho(\mathbf{r}) = -e \sum_{n,\mathbf{k},occ.} |\psi_{n\mathbf{k}}(\mathbf{r})|^2 \quad (5.86)$$

determined by all occupied (valence band) states. A calculated contour plot is shown in Fig. 5.18 for Si together with experimental data obtained from X-ray scattering. The dominant feature is the accumulation of charge between the neighboring lattice sites. It is the bond charge characteristic of covalent binding.

The density of states and the energy band dispersion can be determined experimentally using light–matter interaction (see Chap. 10). Photo-electron spectroscopy (PES) is used to analyse the energy distribution of photo-emitted electrons and yields approximately the density of states from which the excitation takes place, while angular resolved photo-electron spectroscopy (ARPES), which analyses the geometry of the photo-emission process, in addition, allows to map out the energy bands.

5.5 Effective-Mass Approximation

Semiconductors differ from metals by the fact that the Fermi energy is in the gap between valence and conduction bands, which is a region with vanishing density of states. At low temperature, there are no free carriers, which could react on a weak perturbation by an applied electric field. At elevated temperatures, the Fermi distribution function is smeared out and thermal population of the lowest conduction band states takes place together with depopulation of the topmost valence band states. The empty valence band states correspond to missing electrons or *holes* which can be understood as particles with positive charge. In doped semiconductors, the Fermi energy is shifted from the middle of the gap to the impurity levels, which can be close to the conduction band minimum (*n* doping) or to the valence band maximum (*p* doping) and the thermal population/depopulation takes place between the impurity states and the nearby band edge. The number of the thermally excited carriers will be small compared with the number of valence electrons and only states close to

the conduction band minimum or valence band maximum become occupied with electrons and holes, respectively. These carriers can follow an applied electric field and carry an electric current. Similarly, optical excitation with photon energies exceeding the gap energy creates *electron-hole pairs* by lifting electrons from the valence band (leaving holes behind) to the conduction band (see Chap. 10). Thus, the near band edge states determine some of the characteristic properties of semiconductors and deserve special attention. In fact, most of the technological applications with semiconductors (transistors, sensors, lasers) are based on these states.

The lowest minimum of the conduction bands is found in Si along the axis from Γ to X (see Fig. 5.11), in Ge at the L point, but it is at the Γ point for most of the compound semiconductors A_3B_5 (A_2B_6) in the zinc blende structure, with one fcc lattice occupied by atoms from the third (second) and the other by atoms from the fifth (sixth) column of the periodic table. For all these tetrahedrally coordinated semiconductors, the valence band maximum is at the Γ point. Si and Ge with valence band maximum and conduction band minimum at different points of the Brillouin zone are called *indirect gap semiconductors*, while those with the band extrema at the same point of the BZ (here the Γ point) are called *direct gap semiconductors*.

The method to describe the dispersion of energy bands around a given point \mathbf{k}_0 in the BZ has been developed in the early days of semiconductor physics [146, 147]. It is an expansion around this point, which in principle can be extended throughout the Brillouin zone but is used mainly under the condition $|\mathbf{k} - \mathbf{k}_0| \ll 2\pi/a$. Let us assume the Schroedinger equation (5.37) to be solved for \mathbf{k}_0

$$H\psi_{n\mathbf{k}_0}(\mathbf{r}) = E_n(\mathbf{k}_0)\psi_{n\mathbf{k}_0}(\mathbf{r}). \quad (5.87)$$

The periodic parts $u_{n\mathbf{k}_0}(\mathbf{r})$ (with fixed \mathbf{k}_0 and all n) of the Bloch functions form a complete set of lattice periodic functions. With the Bloch functions at \mathbf{k} written as

$$\psi_{n\mathbf{k}}(\mathbf{r}) = e^{i(\mathbf{k}-\mathbf{k}_0)\cdot\mathbf{r}} e^{i\mathbf{k}_0\cdot\mathbf{r}} u_{n\mathbf{k}}(\mathbf{r}) \quad (5.88)$$

the Schroedinger equation reads

$$\left(-\frac{\hbar^2}{2m}\Delta + V_{\text{eff}}(\mathbf{r}) + \frac{\hbar^2(\mathbf{k} - \mathbf{k}_0)^2}{2m} + \frac{\hbar}{m}(\mathbf{k} - \mathbf{k}_0) \cdot \mathbf{p} \right) e^{i\mathbf{k}_0\cdot\mathbf{r}} u_{n\mathbf{k}}(\mathbf{r}) = E_n(\mathbf{k}) e^{i\mathbf{k}_0\cdot\mathbf{r}} u_{n\mathbf{k}}(\mathbf{r}). \quad (5.89)$$

Now we make use of the complete set in the expansion

$$u_{n\mathbf{k}}(\mathbf{r}) = \sum_{n'} c_{nn'}(\mathbf{k} - \mathbf{k}_0) u_{n'\mathbf{k}_0}(\mathbf{r}), \quad (5.90)$$

and insert in (5.89) to find

$$\sum_{n'} c_{nn'}(\mathbf{k} - \mathbf{k}_0) \left\{ E_{n'}(\mathbf{k}_0) + \frac{\hbar^2(\mathbf{k} - \mathbf{k}_0)^2}{2m} - E + \frac{\hbar}{m}(\mathbf{k} - \mathbf{k}_0) \cdot \mathbf{p} \right\} e^{i\mathbf{k}_0 \cdot \mathbf{r}} u_{n'\mathbf{k}_0}(\mathbf{r}) = 0. \quad (5.91)$$

Here the eigenvalue equation at \mathbf{k}_0 was applied and the energy $E_n(\mathbf{k})$ we are looking for is now called E . The last term in the curly brackets containing the momentum operator and the difference in \mathbf{k} vectors can be treated as a perturbation and that is why this concept is called $\mathbf{k} \cdot \mathbf{p}$ perturbation theory. The expansion coefficients can be found from the set of coupled linear equations

$$\sum_{n'} c_{nn'}(\mathbf{k} - \mathbf{k}_0) \left\{ \left(E_{n'}(\mathbf{k}_0) + \frac{\hbar^2(\mathbf{k} - \mathbf{k}_0)^2}{2m} - E \right) \delta_{nn'} + \frac{\hbar}{m}(\mathbf{k} - \mathbf{k}_0) \cdot \mathbf{p}_{nn'}(\mathbf{k}_0) \right\} = 0 \quad (5.92)$$

which are obtained from (5.91) by multiplying $\psi_{n\mathbf{k}_0}^*(\mathbf{r})$ from the left and integrating over the crystal volume. Here the matrix elements of the momentum operator

$$\mathbf{p}_{nn'}(\mathbf{k}_0) = \int u_{n\mathbf{k}_0}^*(\mathbf{r}) \mathbf{p} u_{n'\mathbf{k}_0}(\mathbf{r}) d^3\mathbf{r} \quad (5.93)$$

establish a coupling between the different bands. Solving the secular problem

$$\left\| \left(E_n(\mathbf{k}_0) + \frac{\hbar^2(\mathbf{k} - \mathbf{k}_0)^2}{2m} - E \right) \delta_{nn'} + \frac{\hbar}{m}(\mathbf{k} - \mathbf{k}_0) \cdot \mathbf{p}_{nn'}(\mathbf{k}_0) \right\| = 0 \quad (5.94)$$

yields the dispersion relations $E_n(\mathbf{k})$ around \mathbf{k}_0 for given $E_n(\mathbf{k}_0)$ and $\mathbf{p}_{nn'}(\mathbf{k}_0)$. Formally, (5.94) is the matrix of a first order perturbation calculation for degenerate states. The off-diagonal coupling by the momentum matrix elements can be eliminated to any desired order, by matrix perturbation theory as will be outlined below.

From Sect. 5.4 we identify the states at the conduction band minimum at $\mathbf{k}_0 = 0$ as s anti-bonding states, while those of the valence band maximum are p bonding states. As seen in Fig. 5.17, the dispersion around the valence band maximum is more complex than that around the conduction band minimum. Let us start, therefore, with describing the states at the conduction band edge.

Conduction band edge at $\mathbf{k}_0 = 0$:

We choose the band index $n = c$ for the lowest conduction band with the Bloch function $u_{c0}(\mathbf{r}) = \langle \mathbf{r} | S \rangle$ deriving from the s anti-bonding orbital. This state is coupled with the p bonding (or valence band) and with the p anti-bonding (or higher conduction band) states (n'). Denoting these states $|X\rangle, |Y\rangle, |Z\rangle$ and $|X'\rangle, |Y'\rangle, |Z'\rangle$, respectively, we have the momentum matrix elements

$$P = \frac{\hbar}{m} \langle S|p_x|X \rangle = \frac{\hbar}{m} \langle S|p_y|Y \rangle = \frac{\hbar}{m} \langle S|p_z|Z \rangle \quad (5.95)$$

and similar ones for the primed states. These matrix elements are equal due to the symmetry of the diamond or zinc blende structure according to which the cubic axes are equivalent. By eliminating to lowest order the coupling of the s like state at the conduction band minimum to the p like states $n' \neq c$, one arrives at the second order perturbation expression

$$E_c(\mathbf{k}) = E_c(0) + \frac{\hbar^2 k^2}{2m} + \frac{\hbar^2}{m^2} \sum_{n' \neq c} \frac{|\langle S|\mathbf{k} \cdot \mathbf{p}|n' \rangle|^2}{E_c(0) - E_{n'}(0)} \quad (5.96)$$

and by making use of (5.95) one arrives with

$$\sum_{n'=X,Y,Z} |\langle S|\mathbf{k} \cdot \mathbf{p}|n' \rangle|^2 = |\langle S|p_x|X \rangle|^2 (k_x^2 + k_y^2 + k_z^2) \quad (5.97)$$

at the approximate parabolic dispersion around the conduction band minimum

$$E_c(\mathbf{k}) = E_c(0) + \frac{\hbar^2 k^2}{2m} \left(1 + \frac{2}{m} \sum_{n'(p)} \frac{|\langle S|p_x|X_{n'} \rangle|^2}{E_c(0) - E_{n'}(0)} \right). \quad (5.98)$$

The summation here is over all p like states. This dispersion tells us, that the electrons occupying these states behave like free electrons but with an *effective mass* m^* given by

$$\frac{m}{m^*} = 1 + \frac{2}{m} \sum_{n'(p)} \frac{|\langle S|p_x|X_{n'} \rangle|^2}{E_c(0) - E_{n'}(0)}. \quad (5.99)$$

Depending on the energy denominators, only a few terms need to be considered in the sum. For narrow gap semiconductors the contribution of the topmost valence band dominates, while in general the coupling to the p anti-bonding states needs to be considered. Characteristic values are $m^*/m = 0.067$ for GaAs with a band gap $E_{\text{gap}} = E_c(0) - E_v(0) = 1.52 \text{ eV}$ and $m^*/m = 0.0135$ for InSb with $E_{\text{gap}} = 0.25 \text{ eV}$. By applying a magnetic field, a fan chart of Landau levels evolves out of this parabolic dispersion with typical spacings of $\hbar\omega_c^* = eB/m^*$ and the detection of the cyclotron resonance frequency (see Sect. 4.2) provides the information about the effective mass. We note in passing that higher order terms in the dispersion relation account for the flattening and anisotropy of the energy band away from the Γ point [148] as can be seen in e.g., Fig. 5.12. This nonparabolicity and warping would translate into an energy dependence and anisotropy of the effective mass.

Conduction band edge of Si at $\mathbf{k}_0 = (0, 0, k_0)$:

As mentioned already, Si is an indirect gap semiconductor, the minimum of the conduction band is along the Δ axis close to the point X (see Fig. 5.11).

The lowest conduction band derives from the sp^3 anti-bonding states with a \mathbf{k} dependent hybridization. Let us denote them by $|\tilde{S}\rangle$. Along the Δ axis, the threefold valence band maximum splits into a rather flat twofold band connected with the states $|X\rangle$ and $|Y\rangle$ and a band, which evolves from a mixing of $|Z\rangle$ with the s bonding state, is denoted here as $|\tilde{Z}\rangle$. Instead of (5.95) we now have for the momentum matrix elements

$$P_X = \frac{\hbar}{m} \langle \tilde{S} | p_x | X \rangle = \frac{\hbar}{m} \langle \tilde{S} | p_y | Y \rangle \neq \frac{\hbar}{m} \langle \tilde{S} | p_z | \tilde{Z} \rangle = P_Z, \quad (5.100)$$

and the perturbation series reads with $\mathbf{k}' = \mathbf{k} - \mathbf{k}_0$

$$E_c(\mathbf{k}') = E_c(\mathbf{k}_0) + \frac{\hbar^2 k'^2}{2m} + \frac{\hbar^2}{m^2} \sum_{n' \neq c} \frac{|\langle \tilde{S} | \mathbf{k}' \cdot \mathbf{p} | n' \rangle|^2}{E_c(\mathbf{k}_0) - E_{n'}(\mathbf{k}_0)}. \quad (5.101)$$

The inequality in (5.100), caused by the reduced symmetry of the group of the wave vector \mathbf{k}_0 , leads to the anisotropic dispersion relation (with $\mathbf{k}' = (k_x, k_y, k_z - k_0)$)

$$E_c(\mathbf{k}') = E_c(\mathbf{k}_0) + \frac{\hbar^2}{2} \left(\frac{k_x^2 + k_y^2}{m_{\perp}^*} + \frac{k_z^2}{m_{\parallel}^*} \right) \quad (5.102)$$

with m_{\parallel}^* and m_{\perp}^* being the masses parallel and perpendicular to the Δ axis. For Si, the conduction band minimum is at $k_0 = 0.85$ in units of $2\pi/a$. Due to the cubic symmetry there are minima also along the other equivalent directions in the Brillouin zone, thus the conduction band of Si has six minima, which (thermally or by doping) become equally populated. In the presence of a magnetic field, fan charts of Landau levels evolve from these minima, which depend on the orientation of the magnetic field with respect to the inverse mass ellipsoid and so does the cyclotron mass (Problem 5.12).

Valence band maximum at $\mathbf{k}_0 = 0$:

The valence band maximum of semiconductors with diamond or zinc blende structure derives from the p bonding orbitals and is (without spin) threefold degenerate. The energy dispersion is obtained from the 3×3 determinant ($\nu, \nu' = X, Y, Z$)

$$\left\| \left(E_{\nu}(0) + \frac{\hbar^2 k^2}{2m} - E \right) \delta_{\nu\nu'} + \frac{\hbar^2}{m^2} \sum_{n \neq \nu, \nu'} \frac{\langle \nu | \mathbf{k} \cdot \mathbf{p} | n \rangle \langle n | \mathbf{k} \cdot \mathbf{p} | \nu' \rangle}{E_{\nu}(0) - E_n(0)} \right\| = 0. \quad (5.103)$$

Symmetry arguments, for which we refer to the literature [146], allow to write the terms bilinear in the components of the wave vector as a 3×3 matrix (known as the Shockley³ matrix [147])

³ William B. Shockley 1910–1989, received the Noble prize in physics 1956 jointly with J. Bardeen and W.H. Brattain.

$$\mathcal{M} = \begin{pmatrix} Lk_x^2 + M(k_y^2 + k_z^2) & Nk_xk_y & Nk_xk_z \\ Nk_xk_y & Lk_y^2 + M(k_x^2 + k_z^2) & Nk_yk_z \\ Nk_xk_z & Nk_yk_z & Lk_z^2 + M(k_x^2 + k_y^2) \end{pmatrix} \quad (5.104)$$

with

$$L, M, N \sim \sum_{n \neq \nu, \nu'} \frac{\langle \nu | p_\alpha | n \rangle \langle n | p_\beta | \nu' \rangle}{E_\nu(0) - E_n(0)}, \quad (5.105)$$

where different intermediate levels contribute to L , M , and N . The secular problem $\|\mathcal{M} - E\delta_{\nu, \nu'}\| = 0$ is easily solved for special directions of \mathbf{k} . For the Δ axis or $\mathbf{k} = (0, 0, k)$ one finds

$$E_{v1}(k) = Lk^2 \quad \text{and} \quad E_{v2}(k) = Mk^2, \quad (5.106)$$

where the second solution is twofold, which by comparison with Fig. 5.17 can be identified with the upper branch of the valence band. For the Λ axis with $\mathbf{k} = (k, k, k)/\sqrt{3}$ the solutions are

$$E_{v1}(k) = \frac{L + 2M - 2N}{3}k^2 \quad \text{and} \quad E_{v2}(k) = \frac{L + 2M + N}{3}k^2. \quad (5.107)$$

Again, the second solution is twofold and can be identified with the upper branch for this direction. A characteristic feature is the different curvatures of the bands for the two solutions: the twofold band with the small curvature, corresponding to a large mass, is the *heavy hole* band, while the non-degenerate band with the larger curvature is the *light hole* band. The other feature is that these curvatures depend on the direction of \mathbf{k} and the surfaces of constant energy are warped. We note in passing that for all the other directions the secular problem has three different solutions. These degeneracies and the anisotropy of the valence bands are the same as those of the acoustic phonon branches discussed in Sect. 3.4. This is a consequence of the group of the wave vector, which contains at least threefold rotations only for the Δ and Λ axes.

In general, energy bands can be calculated numerically by diagonalizing (5.94) for a finite set of states, provided, the separation of their energy levels at \mathbf{k}_0 and the momentum matrix elements are known. For near band-edge states in direct gap semiconductors around the Γ point, a multi-band $\mathbf{k} \cdot \mathbf{p}$ model is frequently in use, which comprises five bands or (including spin) 14 states [148–150].

5.6 Subbands in Semiconductor Quantum Structures

While in the previous sections of this chapter, we have looked at the electron states in three-dimensional solids, we shall now consider systems with reduced dimensionality, which are in the focus of interest since the development of the planar semiconductor technology of Si based field effect transistors

(MOSFET or metal oxide Si field effect transistor)[151–153]. Here, we would like to describe a semiconductor heterostructure, which can be obtained by epitaxial growth of one semiconductor (say AlAs) onto another one (GaAs). Both systems have the same crystal structure (zinc blende) and almost the same lattice constant, i.e., across the interface it is only the chemical nature of the atoms that changes. Let the growth direction be along z and the interface at $z = 0$ extend in the $x - y$ plane. The electronic structure of this system is determined by the bulk band structure of the two materials with their respective energy gaps and effective masses. In particular, the band edges (the minima of the conduction band and the maxima of the valence band) are shifted against each other and the interface appears as a step-like potential for carriers at these edges. Correspondingly, a double heterostructure AlAs/GaAs/AlAs would represent a confining square well potential which for electrons can be described by the conduction band profile

$$E_c(z) = \begin{cases} 0 & z < 0 \\ -V_0 & 0 < z < L \\ 0 & z > L \end{cases} \quad (5.108)$$

where the minimum of the energy band in AlAs is the zero point of the energy scale and V_0 is the conduction band offset between AlAs and GaAs. As it is only a few 100 meV, the confined states, being close to the conduction band minimum, can be described in the effective-mass approximation with the Hamiltonian

$$H_{\text{EMA}} = -\frac{\hbar^2}{2m^*}\Delta + E_c(z). \quad (5.109)$$

The eigenfunctions of this Hamiltonian

$$\phi_n(\mathbf{k}_{\parallel}\mathbf{r}) = e^{i\mathbf{k}_{\parallel}\cdot\mathbf{r}}\zeta_n(z) \quad (5.110)$$

and the eigenvalues

$$E_n(\mathbf{k}_{\parallel}) = E_n + \frac{\hbar^2 k_{\parallel}^2}{2m^*} \quad (5.111)$$

indicate the quantization with energies E_n due to the confinement potential in growth direction and the free motion parallel to the interface: electrons occupying these states would be free carriers in two dimensions. The quantum number n denotes the subbands evolving from the conduction band of the three-dimensional band structure.

In both, the single heterostructure and in the quantum well, free carriers can be introduced by doping the AlAs barrier with Si. The Si atoms create additional states close to the conduction band minimum (donor states) with a small binding energy. Due to the negative band offset, the donor electrons cross the interface and reside in the GaAs layer, while leaving a positively charged center behind in AlAs. This charge separation gives rise to an electrostatic potential, which is superimposed on the band edge profile. For a single

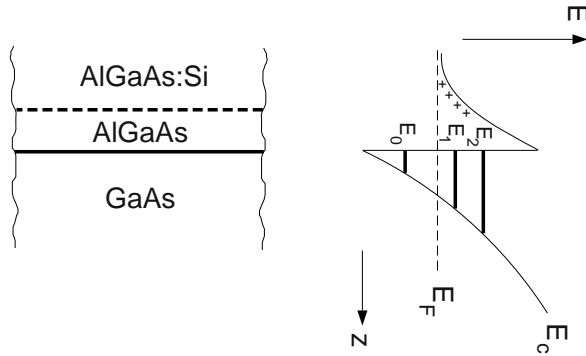


Fig. 5.19. Semiconductor heterostructure (*left*) and conduction band profile across the interface with subband levels and Fermi energy (*right*)

heterostructure this leads to the picture shown in Fig. 5.19 with an almost triangular potential at the interface, which now confines the carriers. The energy spectrum is similar to (5.111) but the subband energies are obtained here from a self-consistent solution of the one-dimensional Schroedinger equation

$$\left(-\frac{\hbar^2}{2m^*}\partial_z^2 + V(z)\right)\zeta_n(z) = E_n\zeta_n(z) \quad (5.112)$$

with the potential $V(z) = V_0\Theta(-z) + V_H(z) + V_{xc}(z)$ and Poisson's equation

$$\partial_z^2 V_H(z) = \frac{e}{\varepsilon\varepsilon_0}\rho(z). \quad (5.113)$$

Here, $V_H(z)$ is the Hartree potential, determined by the charge distribution $\rho(z)$ of ionized donors in the barrier (AlAs) and of the electrons occupying subband states. We recognize (5.112) as the one-dimensional analogue to the Schroedinger equation (5.5) for the three-dimensional case with an effective single-particle potential, which contains also an exchange–correlation part $V_{xc}(z)$. We note in passing that a more accurate description would take into account the change of the effective mass across the interface. The effective mass determines also the density of states, which (without nonparabolicity effects) is a constant (see Problem 4.3 and Fig. 5.20, left part). The number of subbands with occupied states depend on the areal density, which can be controlled by the external gate voltage. The situation, when only states in the lowest subband are occupied, is called the *electric quantum limit*. A more detailed description shows, that the spin-degeneracy of the subbands is removed due to a spin–orbit coupling caused by the asymmetric confinement potential at the interface [153] (Problem 5.13). It can be tuned by an external gate voltage and is important in manipulating the spin dynamics in these structures (Rashba effect).

The effective-mass Hamiltonian (5.109) is obtained from the conduction band dispersion (5.98) by replacing $k^2 \rightarrow -\Delta$, which leads to the operator of

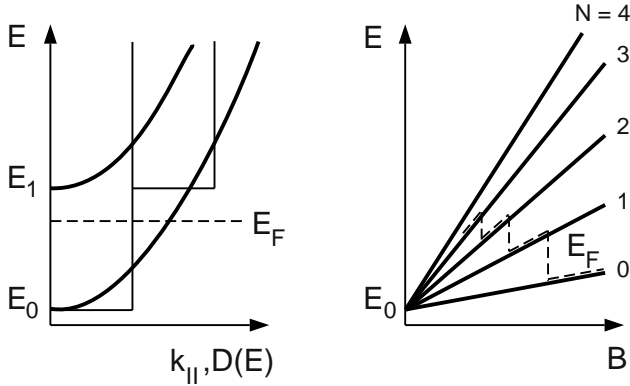


Fig. 5.20. Subband dispersion and density of states for the lowest two subbands (*left*) and fan chart of Landau levels evolving from the lowest subband (*right*), spin splitting is suppressed

kinetic energy for carriers close to the conduction band minimum. The corresponding description of confined holes is more complex because of the valence band degeneracy and would lead (without spin) to three coupled Schrodinger equations, which for $\mathbf{k}_{\parallel} = 0$, decouple and yield subband states for heavy and light holes. Quantitative subband calculations including spin and non-parabolicity effects are performed within the multiband envelope function approximation, which is based on the $\mathbf{k} \cdot \mathbf{p}$ theory [152–154]. Due to the confinement potential, the energy gap, i.e., the energy difference between the lowest electron and the highest hole subband state, is changed as compared with the bulk material. The possible choices of well and barrier material with their respective electron and hole masses and of the width L of the quantum well allow one to design materials with defined gap energies. This *band gap engineering* is exploited in optical devices (see Chap. 10).

In heterostructures, the spatial separation between the free carriers in the confining potential and the ionized donors in the barriers (usually enlarged by growing a spacer layer at the interface) leads to improved mobilities of the carriers at low temperatures (when scattering with ionized impurities is dominating, see Chap. 9). Under these conditions, characteristic transport lengths become comparable or even larger than the lateral system size and phenomena of mesoscopic physics can be investigated [155–160]. Magnetotransport experiments in these systems have led to the discovery of the quantum Hall effects and composite fermions (see Chap. 7).

A magnetic field applied perpendicular to the plane of the two-dimensional electron system leads to a complete discretization of the energy spectrum. The subbands split into highly degenerate Landau levels (see Sect. 4.2) and the filling factor, i.e., the number of occupied Landau levels changes with the magnetic field. The ultimate case, when at sufficiently high magnetic field all electrons can be accommodated in the lowest Landau level of the lowest

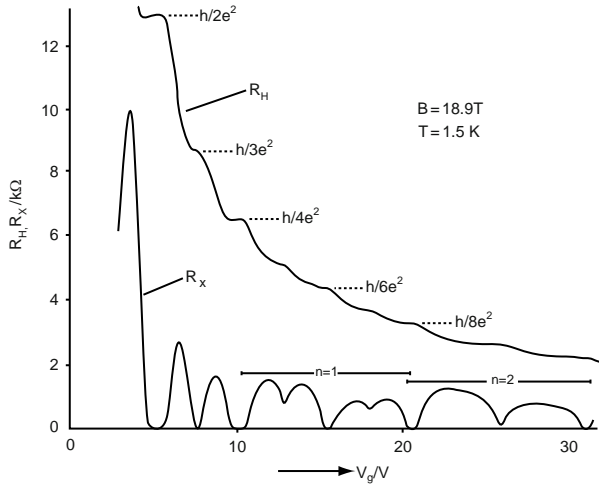


Fig. 5.21. Longitudinal and Hall resistance vs. magnetic field of a Si-MOSFET showing the quantum Hall effect after [161]

subband, is known as the *magnetic quantum limit* (see Problem 4.4). Upon reducing the magnetic field starting from this limit, a point will be reached when all states in the lowest Landau level are occupied, which corresponds to filling factor $\nu = 2$ (due to spin degeneracy). With further reduction of the magnetic field, the Fermi energy moves into the next higher Landau level. Thus, by sweeping the magnetic field, the Fermi energy will jump at field values corresponding to (even) integer filling factors (Fig. 5.20, right). When at sufficiently high magnetic fields (and low temperatures) the Zeeman splitting can be resolved, these jumps take place at all (even and odd) integer filling factors.

In a MOSFET or a gated heterostructure, it is possible to change the carrier density by varying the gate voltage. Thus, for a fixed magnetic field, the Fermi energy can be shifted through the Landau levels by changing the filling factor. At integer filling factors and sufficiently low temperature, magnetotransport data show striking deviations from the classical behavior of the Drude model (Fig. 5.21): the longitudinal resistance (or conductance) vanishes (as typical for an insulator) and the Hall resistance (or conductance) exhibits plateaus, which to extremely high accuracy are inverse integer multiples of e^2/h [161]. This is known as the *integer quantum Hall effect*, discovered by von Klitzing⁴ in 1980. The high accuracy of the plateau values gave rise to a new definition of the resistance, normally defined by precision measurements in a quantum Hall experiment of h/e^2 , which corresponds to the Klitzing constant $R_{K-90} = 25812, 807 \Omega$ introduced by the Meter Convention in 1990. An introduction to the theory of the integer Quantum Hall effect is [162].

⁴ Klaus von Klitzing *1943, Noble prize in physics 1985.

In 1983, Tsui and Störmer⁵ discovered signatures of the quantum Hall effect at very low temperatures and high magnetic fields at the fractional filling $\nu = 1/3$. The confirmation of this signature complemented by the discovery of a whole family of so-called fractional quantum Hall states (see Sect. 7.6) in the following years has stimulated much experimental and theoretical work on electron systems under such extreme conditions. The fractional quantum Hall effect is now understood to be dominated by electron–electron interaction (see Chap. 7) while the integer quantum Hall effect is essentially a single-particle effect caused by disorder (see Chap. 9).

Problems

- 5.1 Derive the Hartree–Fock equations as Euler–Lagrange equations of the variational problem (5.7) with the Slater determinant as ground state wave function. Note that the single-particle wave functions depend on space and spin coordinates.
- 5.2 Show that the exchange potential

$$V_x(\mathbf{r}) = -e^2 \int \frac{\bar{n}^{\text{HF}}(\mathbf{r}, \mathbf{r}')}{|\mathbf{r} - \mathbf{r}'|} d^3\mathbf{r}' \quad (5.114)$$

with the averaged nonlocal HF or exchange density (5.15) reduces for free electrons to the so-called Slater exchange potential

$$V_{x,\text{Slater}}(\mathbf{r}) = -\frac{3e^2}{2\pi} k_{\text{F}}(n(\mathbf{r})). \quad (5.115)$$

Compare it with the exchange potential in the LDA

$$V_x^{\text{LDA}}(\mathbf{r}) = \frac{d}{dn} (n\epsilon_x(n))_{n=n(\mathbf{r})}, \quad (5.116)$$

where $\epsilon_x(n)$ is the exchange energy per electron for the jellium model with density n .

- 5.3 Verify that each energy band can accommodate one electron of either spin per unit cell. Remember the corresponding statement concerning phonon modes.
- 5.4 A point at the Brillouin zone boundary can be characterized by wave vectors \mathbf{k} and \mathbf{k}' drawn from different reciprocal lattice vectors. Give the relation between \mathbf{k} and \mathbf{k}' and verify that the condition of degeneracy of the corresponding free electron states, i.e., of having the same energy, is consistent with the condition for Bragg reflection.

⁵ Daniel C. Tsui *1939, Horst L. Störmer *1949, shared the Noble prize in Physics 1998 with R.B. Laughlin.

- 5.5 Calculate and plot the free electron energy dispersion for the square lattice along the lines $\Gamma \rightarrow M$, $M \rightarrow X$, and $X \rightarrow \Gamma$ for the lowest three bands (the reciprocal lattice vectors can be used as band index). Indicate the position of the Fermi energy, if each atom in the unit cell contributes one, two, or three electrons. Calculate the dispersion for the two lowest bands in the presence of a periodic potential and discuss the modification of the Fermi circle with radius $k_F = \pi/a$ by this potential.
- 5.6 Calculate the free electron energy bands of a fcc lattice as shown in Fig. 8.6. Find out the degeneracies of these bands.
- 5.7 Compare the band structures of Al, Si, and GaAs in the context of the almost free electron or pseudo-potential approximation. What is common (different) in the free electron picture and which of the Fourier coefficients of the periodic potential are responsible for opening of gaps? Which details of the band structure can be understood from this comparison?
- 5.8 The atomic d states are fivefold degenerate (without spin). Calculate the crystal field splitting of these states in a cubic lattice. Is there a difference between the sc, bcc, and fcc crystal structures?
- 5.9 Show that the secular problem (5.77) can be reduced to the standard form

$$\left\| \tilde{H}_{\nu'\nu}(\mathbf{k}) - E_\nu \delta_{\nu'\nu}(\mathbf{k}) \right\| = 0 \quad (5.117)$$

by making use of the properties of the overlap matrix $S_{\nu'\nu}(\mathbf{k})$. Give the explicit expression of $\tilde{H}_{\nu'\nu}(\mathbf{k})$ in terms of $H_{\nu'\nu}(\mathbf{k})$ and $S_{\nu'\nu}(\mathbf{k})$.

- 5.10 Calculate the dispersion of an energy band deriving from an s orbital in a sc and bcc lattice for the lines $\Gamma - X$ and $\Gamma - L$. Compare with each other and with the result for the fcc lattice. How does the width of the energy band depend on the nearest neighbor configuration?
- 5.11 Graphene is a single sheet of carbon atoms arranged in a (two-dimensional) hexagonal lattice with primitive lattice vectors in the (x, y) plane

$$\mathbf{a}_1 = d \left(\frac{\sqrt{3}}{2}, \frac{3}{2} \right), \quad \mathbf{a}_2 = d \left(-\frac{\sqrt{3}}{2}, \frac{3}{2} \right) \quad (5.118)$$

and two carbon atoms in each cell at $\boldsymbol{\tau}_1 = (0, d)$ and $\boldsymbol{\tau}_2 = (0, 2d)$ with the nearest neighbor distance d . The s , p_x , and p_y orbitals can be combined to sp^2 hybrid orbitals directed towards the nearest neighbors, while the p_z orbitals stick out of the lattice plane and form π_z bonding and anti-bonding orbitals. Formulate and solve the eigenvalue problem for graphene using LCAO for the π_z orbitals in the tight-binding approximation and discuss the resulting energy bands.

- 5.12 Find the expression for the cyclotron mass of a spheroidal energy surface

$$E(\mathbf{k}) = \frac{1}{m_t} (k_x^2 + k_y^2) + \frac{1}{m_l} k_z^2 = \text{const.} \quad (5.119)$$

- in dependence on the orientation of the magnetic field in the xz plane. Make use of the Peierls substitution and use a vector potential with $A_x = A_z = 0$. Set up and solve the equations of motion in the xz plane.
- 5.13 Solve the eigenvalue problem of free two-dimensional electrons in the xy plane in the presence of a spin-orbit coupling

$$H_{\text{SO}} = \alpha(\mathbf{k} \times \nabla V) \cdot \boldsymbol{\sigma} \quad (5.120)$$

due to the confinement potential V in z direction, i.e., $\nabla V \parallel (001)$. Calculate and visualize the expectation values of the spin operator $\boldsymbol{\sigma}$ in dependence on the direction of \mathbf{k} . Identify the Kramers pairs.

Spin Waves: Magnons

The electron spin, which does not explicitly appear in the N -particle Hamiltonian of the solid (except for the spin-orbit coupling and Zeeman terms), will be in the focus of this chapter. In Chaps. 4 and 5 we have addressed already the relevance of spin in connection with magnetic properties, which shall be studied now in more detail. The issue here will be to consider the interacting electron system with dominating exchange interaction, which leads to a spin-ordered ground state, and to describe elementary excitations out of this ground state: *spin waves* or (in quantized form) *magnons*. In several aspects, spin dynamics is similar to lattice dynamics (see Chap. 3) with the masses coupled by springs, now being replaced with spins (or their magnetic moments) coupled with exchange interaction. Depending on the complexity of the crystal structures on which these spin systems are realized, their spin or magnetic order can be ferromagnetic, anti-ferromagnetic, ferrimagnetic, or anti-ferrimagnetic [163]. Most standard textbooks on Solid State Theory contain a chapter on spin waves or magnons and magnetic properties, but there are also special review articles [164, 165] and monographs [116, 166–172] on these topics. In solids with disorder, e.g. due to alloying, the magnetic order takes the form of spin glasses [16]. Theoretical concepts developed for spin glasses have turned out to be useful also for neural networks [173]. A variant of magnetic order in disordered solids are diluted magnetic semiconductors of which A_3B_5 with Mn ions randomly replacing the A_3 atoms show ferromagnetic order (see [174–176]). The latter materials have gained much interest in connection with spintronics [177, 178], a concept of electronics using the electron spin rather than its charge. Magnetic order exists as a ground state property only below some critical temperature at which a phase transition takes place. It can be described using the molecular or mean field approximation. For spin excitations at the surface of magnetic solids (*surface magnons*) we refer to [179, 180].

6.1 Preliminaries

In Chap. 4 we have seen how magnetic properties of free electrons can be understood in terms of the single-particle picture and the Pauli principle. The Zeeman term causes a shift of the density of states of up and down spin electrons against each other (see Fig. 4.7). Occupying these states according to the Fermi–Dirac distribution function, leads to a magnetic moment determined by the excess of majority spins: this is the Pauli spin paramagnetism. On the other hand, for the case without external magnetic field, we have found a lowering of the single-particle and ground state energies due to the exchange term in the HF approximation, which becomes effective for electrons with parallel spins. This effect is expected to get stronger with an increase of the number $N_{\uparrow,\downarrow}$ of aligned spins, i.e. with a spin polarization $N_{\uparrow} - N_{\downarrow}$ of the system accompanied by a magnetization $M = g\mu_B(N_{\uparrow} - N_{\downarrow})$. Eventually, one may ask for a condition under which a state with all spins aligned could be the system ground state.

In this consideration, we have completely neglected the influence of the periodic potential. Let us look, therefore, for a moment at the band structure of ferromagnetic Fe in Fig. 6.1 as an example. We note the characteristic features resulting from *s-d* hybridization discussed in Sect. 5.4, but find that for the ferromagnetic state the energy bands of up and down spin electrons differ from each other, $\epsilon_{n\mathbf{k}\uparrow} \neq \epsilon_{n\mathbf{k}\downarrow}$, as is typical for Bloch electrons with incomplete *d* shells. A closer inspection shows that the bands of spin-up and spin-down electrons are very similar but shifted against each other, as can be seen in the density of states (Fig. 6.2) by comparing the position of the pronounced structures, caused by van Hove singularities, for majority and minority spins. This reminds us of the free electron case with external magnetic field, but

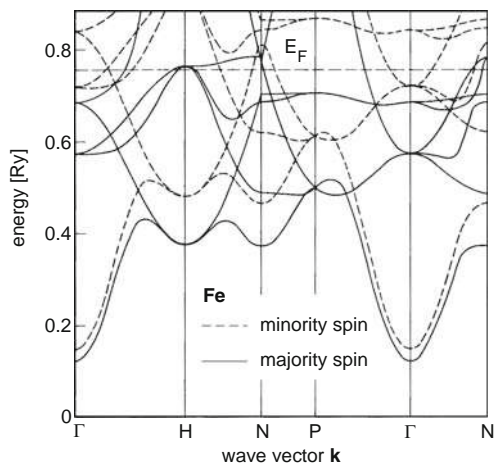


Fig. 6.1. Energy bands of ferromagnetic Fe after [181]

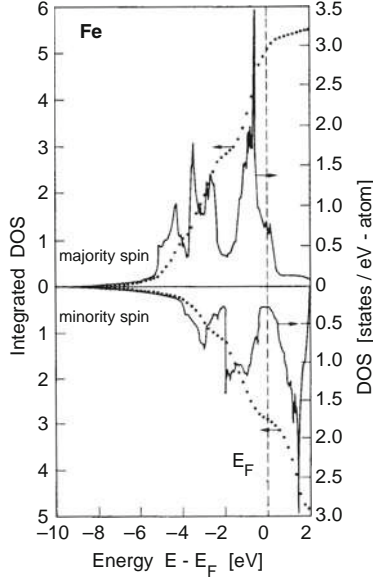


Fig. 6.2. Density of states (*solid lines*) and integrated density of states (*dotted lines*) for the energy bands of ferromagnetic Fe of Fig. 6.1 (after [181])

here, the shift is determined by the spin-polarization that exists even without an external magnetic field, i.e. there is a spontaneous magnetization below a critical temperature. Energy bands as those of Fig. 6.1 result from an extension of the DFT-LDA to the SDF-T-LSDA (spin-density functional theory in the local spin-density approximation) [123, 182].

Turning back to the free electron system of Chap. 4, we recollect the expression for the ground state energy in HF approximation (without magnetic field) with each state with $|\mathbf{k}| \leq k_F$ occupied by a pair of \uparrow, \downarrow spins (see (4.91))

$$E_{0\uparrow\downarrow}^{\text{HF}} = \underbrace{\frac{3}{5} N \frac{\hbar^2}{2m} k_F^2}_a - \underbrace{\frac{3}{16\pi^2\epsilon_0} N e^2 k_F}_b. \quad (6.1)$$

Remember the origin of the second term; it is the exchange part of the Coulomb interaction which results from parallel spins. Instead of occupying each state in the Fermi sphere with a pair of \uparrow, \downarrow electrons one could align all spins to gain exchange energy, but this can be done only at the cost of increasing the kinetic energy because the size of the Fermi sphere has to be doubled, i.e. by now occupying all states with $|\mathbf{k}| \leq 2^{1/3} k_F$ (see Fig. 6.3). The HF ground state energy for this ferromagnetic order (the completely spin-polarized free electron gas) is

$$E_{0\uparrow\uparrow}^{\text{HF}} = 2^{2/3} a k_F^2 - 2^{1/3} b k_F \quad (6.2)$$

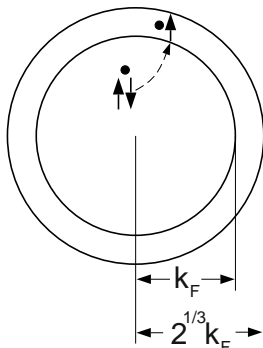


Fig. 6.3. Fermi spheres for a spin-unpolarized and a completely spin-polarized electron system

with a and b from (6.1). In order to have $E_{0\uparrow\uparrow}^{\text{HF}} < E_{0\uparrow\downarrow}^{\text{HF}}$, k_{F} has to fulfill the condition

$$k_{\text{F}} < \frac{2^{1/3} - 1}{2^{2/3} - 1} \frac{b}{a} = 0.44 \frac{b}{a} = \frac{1.1}{\pi} a_{\text{B}}^{-1} \quad (6.3)$$

with the Bohr radius a_{B} or, with $k_{\text{F}} = (9\pi/4)^{1/3} 1/r_{\text{s}} a_{\text{B}}$, this yields for the density parameter

$$r_{\text{s}} > \left(\frac{9\pi}{4}\right)^{1/3} \frac{\pi}{1.1} = 5.45. \quad (6.4)$$

According to this estimate the ferromagnetic ground state should be favored in diluted electron systems with $r_{\text{s}} > 5.45$, which is still in the region of electron densities in metals ($2 < r_{\text{s}} < 6$). However, this estimate should not be taken for a proof of the existence of a ferromagnetic ground state as it does not include the effects of correlation or of the periodic potential.

For a more rigorous treatment, we start from the N -electron Hamiltonian (5.2) that includes the periodic potential. It can be written with the help of (4.76) and (4.77) in terms of fermion operators as

$$\mathcal{H} = \sum_{\alpha} \epsilon_{\alpha} c_{\alpha}^{\dagger} c_{\alpha} + \frac{1}{2} \sum_{\alpha\beta\alpha'\beta'} V_{\alpha\beta\beta'\alpha'} c_{\alpha}^{\dagger} c_{\beta}^{\dagger} c_{\alpha'} c_{\beta'}, \quad (6.5)$$

where α, β, α' , and β' are complete sets of single-particle quantum numbers, which here are those of Bloch states, e.g. $\alpha = n\mathbf{k}\sigma$ and ϵ_{α} are the corresponding single-particle energy values. The potential matrix elements

$$V_{\alpha\beta\beta'\alpha'} = \int dx \int dx' \psi_{\alpha}^{\dagger}(x) \psi_{\beta}^{\dagger}(x') \frac{e^2}{4\pi\epsilon_0 |\mathbf{r} - \mathbf{r}'|} \psi_{\beta'}(x) \psi_{\alpha'}(x') \quad (6.6)$$

can be expressed in terms of the single-electron wave functions $\psi_{\alpha}(x)$ (Problem 6.1), where x stands for space and spin coordinates. Summing up

the spin coordinates results in getting the same spin quantum numbers for the states α, β' and for the states β, α' . In the following, we shall separate the Hamiltonian (6.5) according to $\mathcal{H} = \mathcal{H}_{\text{sp}} + \mathcal{H}_{\text{int}}$ into its single-particle and interaction parts.

Magnetism is known, from the introductory courses on solid state physics [29–31], to arise in materials with incomplete d or f shells. The corresponding electrons form narrow bands (see e.g. Fig.6.1), for which the free electron picture hardly applies. We take this situation into account by switching to the LCAO (or tight-binding) approximation introduced in Sect.5.4. In this picture, contrary to Fig.6.3, the electron spin is not attached to delocalized electrons, and magnetism results from the magnetic moments of the total spin carried by local atomic d or f orbitals.

Let us consider electrons in an energy band deriving from one such orbital. The Bloch function can be expressed (as in Sect. 5.5) by

$$\psi_{\mathbf{k}\sigma}(\mathbf{r}) = \frac{1}{\sqrt{N}} \sum_{\mathbf{R}} e^{i\mathbf{k}\cdot\mathbf{R}} \phi_{\sigma}(\mathbf{r} - \mathbf{R}), \quad (6.7)$$

where we have dropped the band index to simplify notation while the index σ refers to the spin eigenstate. It is advantageous here to adopt the Wannier¹ representation with localized orbitals, which are orthogonal for different lattice sites, although they may still overlap (Problem 6.2). This allows one to switch with

$$c_{\mathbf{k}\sigma} = \frac{1}{\sqrt{N}} \sum_{\mathbf{R}} e^{i\mathbf{k}\cdot\mathbf{R}} c_{\mathbf{R}\sigma} \quad (6.8)$$

to fermion operators and write the single-particle term in the form

$$\begin{aligned} \mathcal{H}_{\text{sp}} &= \sum_{\mathbf{k}\sigma} \epsilon_{\mathbf{k}} c_{\mathbf{k}\sigma}^{\dagger} c_{\mathbf{k}\sigma} \\ &= \sum_{\mathbf{R}\mathbf{R}'\sigma} \underbrace{\frac{1}{N} \sum_{\mathbf{k}} \epsilon_{\mathbf{k}} e^{i\mathbf{k}\cdot(\mathbf{R}-\mathbf{R}')}}_{t_{\mathbf{R}\mathbf{R}'}} c_{\mathbf{R}'\sigma}^{\dagger} c_{\mathbf{R}\sigma} = \sum_{\mathbf{R}\mathbf{R}'\sigma} t_{\mathbf{R}\mathbf{R}'} c_{\mathbf{R}'\sigma}^{\dagger} c_{\mathbf{R}\sigma}. \end{aligned} \quad (6.9)$$

The dispersion of the energy band $\epsilon_{\mathbf{k}}$ (assumed to be independent of σ) is now expressed in terms of the hopping or transfer matrix elements $t_{\mathbf{R}\mathbf{R}'}$, $\mathbf{R} \neq \mathbf{R}'$ which is a two-center integral of the type given in (5.74), while the term with $\mathbf{R} = \mathbf{R}'$ gives the atomic energy level from which the band derives (see Problem 6.2) .

Likewise the electron–electron interaction takes the form (Problem 6.3)

$$\mathcal{H}_{\text{int}} = \frac{1}{2} \sum_{\substack{\mathbf{R}_1 \mathbf{R}_2 \sigma \\ \mathbf{R}'_1 \mathbf{R}'_2 \sigma'}} V_{\mathbf{R}_1 \mathbf{R}_2 \mathbf{R}'_1 \mathbf{R}'_2} c_{\mathbf{R}_1 \sigma}^{\dagger} c_{\mathbf{R}_2 \sigma'}^{\dagger} c_{\mathbf{R}'_2 \sigma'} c_{\mathbf{R}'_1 \sigma} \quad (6.10)$$

¹ Gregory Hugh Wannier 1911–1983.

with the interaction matrix element being now the four-center integral

$$V_{\mathbf{R}_1 \mathbf{R}_2 \mathbf{R}'_1 \mathbf{R}'_2} = \int d^3 r \int d^3 r' \phi^*(\mathbf{r} - \mathbf{R}_1) \phi^*(\mathbf{r}' - \mathbf{R}_2) \times \frac{e^2}{4\pi\epsilon_0 |\mathbf{r} - \mathbf{r}'|} \phi(\mathbf{r} - \mathbf{R}'_1) \phi(\mathbf{r}' - \mathbf{R}'_2). \quad (6.11)$$

Note, that the Wannier (or atomic) orbitals and the single particle energies are assumed to be independent of the spin quantum number σ . This means to neglect all spin-dependent effects deriving from spin-orbit coupling and from the electrons in all other occupied bands of the solid, while here all spin related effects derive from the interaction term.

6.2 The Heisenberg Hamiltonian

The extreme case of strongly localized orbitals would lead to vanishing hopping matrix elements and to a single-particle part of the Hamiltonian, just counting the occupation of the sites multiplied by the atomic level energy. Contrary to the free-electron case (see Fig. 6.3), in a flat band there is no increase in the kinetic energy when all spins are aligned, which is the favorite configuration with respect to the exchange interaction. But this ferromagnetic configuration, with each site being occupied by a single electron with given spin (Fig. 6.4), minimizes the Coulomb repulsion also, because each two electrons are separated in space as much as possible in the given crystal structure. Thus, this configuration can be considered as the ground state.

We have to keep in mind here that the assumption of strongly localized atomic orbitals does not apply to metallic ferromagnets such as the transition metals, which form d bands with a width of the order of one eV, (see Figs. 5.14 and 6.1) due to the overlap between nearest neighbors in a close-packed crystal structure (bcc or fcc). This overlap is, however, essentially reduced in transition metal compounds like MnAs, EuS, EuS with a larger spacing between the metallic ions in a lattice with basis. They appear as ferromagnetic insulators and are the materials, to which the model of Fig. 6.4 applies.

With respect to elementary excitations, this ferromagnetic ground state plays the same role as the filled Fermi sphere for the free electrons. As in Chap. 4, when considering the HF approximation the interaction term in application to this ground state, we can distinguish between a direct and an

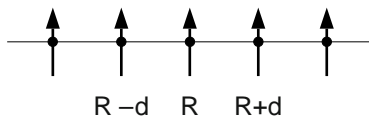


Fig. 6.4. Ferromagnetic configuration of spins on a linear chain

exchange term. The direct process requires $\mathbf{R}_1 = \mathbf{R}'_1 = \mathbf{R}$ and $\mathbf{R}_2 = \mathbf{R}'_2 = \mathbf{R}'$ and can be expressed as

$$\mathcal{H}_d = \frac{1}{2} \sum_{\mathbf{R}\mathbf{R}'} V_{\mathbf{R}\mathbf{R}'\mathbf{R}\mathbf{R}'} \sum_{\sigma\sigma'} c_{\mathbf{R}\sigma}^\dagger c_{\mathbf{R}'\sigma'}^\dagger c_{\mathbf{R}'\sigma'} c_{\mathbf{R}\sigma}. \quad (6.12)$$

When applied to the ferromagnetic ground state, it removes two electrons at sites \mathbf{R} and \mathbf{R}' with spins σ and σ' , respectively, and puts them back where they are taken from. It is clear that this requires $\mathbf{R} \neq \mathbf{R}'$, because at each lattice site, there is only one electron that can be removed, and the operator part can be transformed to yield

$$\sum_{\sigma} c_{\mathbf{R}\sigma}^\dagger c_{\mathbf{R}\sigma} \sum_{\sigma'} c_{\mathbf{R}'\sigma'}^\dagger c_{\mathbf{R}'\sigma'} = 1. \quad (6.13)$$

Thus, we find that \mathcal{H}_d is the energy of the electrostatic interaction between the charge densities located around \mathbf{R} and \mathbf{R}' , i.e. of the electronic configuration associated with the spin configuration of Fig. 6.4.

The exchange term is obtained with $\mathbf{R}_1 = \mathbf{R}'_2 = \mathbf{R}$ and $\mathbf{R}_2 = \mathbf{R}'_1 = \mathbf{R}'$ and reads

$$\mathcal{H}_x = \frac{1}{2} \sum_{\mathbf{R}\mathbf{R}'} V_{\mathbf{R}\mathbf{R}'\mathbf{R}'\mathbf{R}} \sum_{\sigma\sigma'} c_{\mathbf{R}\sigma}^\dagger c_{\mathbf{R}'\sigma'}^\dagger c_{\mathbf{R}\sigma'} c_{\mathbf{R}'\sigma}. \quad (6.14)$$

The operator part can be transformed (again with $\mathbf{R} \neq \mathbf{R}'$):

$$\begin{aligned} \sum_{\sigma\sigma'} c_{\mathbf{R}\sigma}^\dagger c_{\mathbf{R}'\sigma'}^\dagger c_{\mathbf{R}\sigma'} c_{\mathbf{R}'\sigma} &= -c_{\mathbf{R}\uparrow}^\dagger c_{\mathbf{R}\uparrow} c_{\mathbf{R}'\uparrow}^\dagger c_{\mathbf{R}'\uparrow} - c_{\mathbf{R}\downarrow}^\dagger c_{\mathbf{R}\downarrow} c_{\mathbf{R}'\downarrow}^\dagger c_{\mathbf{R}'\downarrow} \\ &\quad - c_{\mathbf{R}\uparrow}^\dagger c_{\mathbf{R}\downarrow} c_{\mathbf{R}'\downarrow}^\dagger c_{\mathbf{R}'\uparrow} - c_{\mathbf{R}\downarrow}^\dagger c_{\mathbf{R}\uparrow} c_{\mathbf{R}'\uparrow}^\dagger c_{\mathbf{R}'\downarrow}. \end{aligned} \quad (6.15)$$

The different combinations of creation and annihilation operators at a given site have the following meaning with respect to the site \mathbf{R} (here we drop the site index):

$$\begin{aligned} c_{\uparrow}^\dagger c_{\uparrow}, c_{\downarrow}^\dagger c_{\downarrow} &: \text{count the } \uparrow, \downarrow \text{ electrons} \\ c_{\uparrow}^\dagger c_{\uparrow} - c_{\downarrow}^\dagger c_{\downarrow} &: \text{counts the difference between } \uparrow \text{ and } \downarrow \text{ electrons} \\ c_{\uparrow}^\dagger c_{\downarrow}, c_{\downarrow}^\dagger c_{\uparrow} &: \text{cause spin flips.} \end{aligned}$$

Taking into account the commutation relation

$$[c_{\uparrow}^\dagger c_{\downarrow}, c_{\downarrow}^\dagger c_{\uparrow}] = c_{\uparrow}^\dagger c_{\uparrow} - c_{\downarrow}^\dagger c_{\downarrow} \quad (6.16)$$

we recognize that the operators $c_{\uparrow}^\dagger c_{\downarrow}$, $c_{\downarrow}^\dagger c_{\uparrow}$, and $c_{\uparrow}^\dagger c_{\uparrow} - c_{\downarrow}^\dagger c_{\downarrow}$ at each site \mathbf{R} fulfill the commutation rules of the $su(2)$ algebra known from the angular momenta (Problem 6.4):

$$[S^i, S^j] = i\varepsilon_{ijk} S^k, \quad i, j, k = x, y, z \quad \text{cycl. perm.} \quad (6.17)$$

with the Levi–Civita symbol ε_{ijk} , and we may identify

$$S^+ = S^x + iS^y = c_{\uparrow}^{\dagger}c_{\downarrow}, \quad S^- = S^x - iS^y = c_{\downarrow}^{\dagger}c_{\uparrow}, \quad S^z = \frac{1}{2}(c_{\uparrow}^{\dagger}c_{\uparrow} - c_{\downarrow}^{\dagger}c_{\downarrow}). \quad (6.18)$$

Thus, it is possible to replace the annihilation and creation operators by spin vector operators $\mathbf{S}_{\mathbf{R}} = (S_{\mathbf{R}}^x, S_{\mathbf{R}}^y, S_{\mathbf{R}}^z)$ at each lattice site. This is achieved by adding and subtracting $(c_{\mathbf{R}\uparrow}^{\dagger}c_{\mathbf{R}'\uparrow}c_{\mathbf{R}'\downarrow}^{\dagger}c_{\mathbf{R}\downarrow} + c_{\mathbf{R}\downarrow}^{\dagger}c_{\mathbf{R}\uparrow}c_{\mathbf{R}'\uparrow}^{\dagger}c_{\mathbf{R}'\downarrow})/2$ on the *rhs* of (6.15) to obtain for the operator part of the exchange term

$$\begin{aligned} \sum_{\sigma\sigma'} c_{\mathbf{R}\sigma}^{\dagger}c_{\mathbf{R}'\sigma'}^{\dagger}c_{\mathbf{R}\sigma'}c_{\mathbf{R}'\sigma} &= - (S_{\mathbf{R}}^+S_{\mathbf{R}'}^- + S_{\mathbf{R}}^-S_{\mathbf{R}'}^+) - 2S_{\mathbf{R}}^zS_{\mathbf{R}'}^z \\ &\quad - \frac{1}{2} \sum_{\sigma\sigma'} c_{\mathbf{R}\sigma}^{\dagger}c_{\mathbf{R}\sigma}c_{\mathbf{R}'\sigma'}^{\dagger}c_{\mathbf{R}'\sigma'}. \end{aligned} \quad (6.19)$$

The first two terms on the *rhs* can be written in the form

$$S_{\mathbf{R}}^+S_{\mathbf{R}'}^- + S_{\mathbf{R}}^-S_{\mathbf{R}'}^+ + 2S_{\mathbf{R}}^zS_{\mathbf{R}'}^z = 2\mathbf{S}_{\mathbf{R}} \cdot \mathbf{S}_{\mathbf{R}'} \quad (6.20)$$

while the last term can be combined with the direct term, and we find for the interaction part, \mathcal{H}_{int} of the Hamiltonian, the form

$$\mathcal{H}_{\text{int}} = - \sum_{\substack{\mathbf{R}\mathbf{R}' \\ \mathbf{R} \neq \mathbf{R}'}} J_{\mathbf{R}\mathbf{R}'} \mathbf{S}_{\mathbf{R}} \cdot \mathbf{S}_{\mathbf{R}'} \quad (6.21)$$

which is the *Heisenberg² Hamiltonian* with the exchange integral

$$J_{\mathbf{R}\mathbf{R}'} = \int d^3\mathbf{r} \int d^3\mathbf{r}' \frac{e^2\phi^*(\mathbf{r} - \mathbf{R})\phi(\mathbf{r} - \mathbf{R}')\phi^*(\mathbf{r}' - \mathbf{R}')\phi(\mathbf{r}' - \mathbf{R})}{4\pi\varepsilon_0|\mathbf{r} - \mathbf{r}'|}. \quad (6.22)$$

It can be shown that $J_{\mathbf{R}\mathbf{R}'} > 0$. We add the Zeeman term and replace the site index \mathbf{R} by a number index i (which can be understood as replacing the 3-dimensional Bravais lattice with a linear chain but is meant also as short notation for \mathbf{R}_i) to write the spin or Heisenberg Hamiltonian in the form

$$\mathcal{H}_{\text{spin}} = - \sum_{\substack{i,j \\ i \neq j}} J_{ij} \mathbf{S}_i \cdot \mathbf{S}_j - g\mu_{\text{B}}H_{\text{ext}} \sum_i S_i^z. \quad (6.23)$$

This Hamiltonian is the canonical starting point in the theory of magnetism [183]. In spite of its simplicity, it bears fundamental properties, one of which is related to symmetry. Without external magnetic field, (6.23) is spherically symmetric, however, its ground state, the ferromagnetic configuration, has only axial symmetry. This situation is known as *spontaneous symmetry breaking*: Due to interaction between the spins and in order to gain energy,

² Werner Heisenberg 1901–1976, Nobel prize in physics 1932.

the system prefers a configuration with lower symmetry than that of the Hamiltonian. The further task of this chapter will be to describe elementary excitations out of this ground state.

There exist several model Hamiltonians related to the Heisenberg Hamiltonian, which have been under investigation in the context of magnetic properties [171]:

1. the anisotropic Heisenberg model

$$\mathcal{H}_{\text{spin}} = - \sum_{\substack{i,j \\ i \neq j}} (J_{ij}(S_i^x S_j^x + S_i^y S_j^y) + \bar{J}_{ij} S_i^z S_j^z), J_{ij} \neq \bar{J}_{ij}, \quad (6.24)$$

2. the Ising model (with $J_{ij} = 0$)

$$\mathcal{H}_{\text{Ising}} = - \sum_{\substack{i,j \\ i \neq j}} \bar{J}_{ij} S_i^z S_j^z, \quad (6.25)$$

3. and the XY model ($\bar{J}_{ij} = 0$)

$$\mathcal{H}_{XY} = - \sum_{\substack{i,j \\ i \neq j}} J_{ij}(S_i^x S_j^x + S_i^y S_j^y). \quad (6.26)$$

The Ising and the XY models are used in statistical mechanics because of their simplicity compared to the Heisenberg model, while still representing reasonable approximations for real spin systems. As it turns out, however, the low-dimensional spin models (except the two-dimensional Ising model) fall short of describing the ferromagnetic phase transition (see Sect. 6.5). Instead the XY model produces a transition between two disordered phases of different topology. This *Kosterlitz–Thouless transition* is caused by the appearance of spin vortices (see [171]).

In all these models, the exchange integrals appear as parameters. The microscopic mechanism, although it is always the exchange interaction, can be quite different depending on the lattice structure of the solid. The easiest case is that of the transition metals, where the exchange takes place directly between the d orbitals on nearest neighbor lattice sites of a close-packed structure like bcc and fcc. Therefore, it is called *direct exchange* to distinguish it from indirect or *super-exchange* in compounds of elements with incomplete d shells, as e.g. the ferromagnetic insulators MnAs, EuO, and EuS. In these solids forming lattices with basis, the orbitals which carry a magnetic moment, are separated by the non-magnetic ions and the exchange coupling has to be mediated by the orbitals of the intervening ions. A similar situation is found in metallic ferromagnetic compounds, where the exchange

coupling between distant magnetic ions is mediated by the free electrons. This is the *Rudermann–Kittel exchange*, which exists together with the direct exchange interaction and is frequently the dominating mechanism. Depending on the mechanism and the lattice configuration, the exchange constant can be positive (as anticipated so far), which leads to the ferromagnetic order, but also negative. In the latter case, neighboring spins align anti-parallel and exhibit the anti-ferromagnetic ordering. More complex crystal structures with sublattices accomodating different spin carrying orbitals, i.e. the spin operator \mathbf{S} depends on the sublattice, lead to the *ferrimagnetic* or *anti-ferrimagnetic order*.

6.3 Spin Waves in Ferromagnets

In this Section, we want to describe low-energy excitations out of the ferromagnetic ground state. Let us assume for the moment the classical picture of spins in Fig. 6.4 as localized magnetic dipoles. They are coupled from site to site by the scalar product of their respective spin vectors, weighted by the exchange integral. If one of the spins is tilted against the preferential direction thus raising the energy, the neighboring spins tend to follow this tilt. If this spin is released from its tilted orientation the whole system will start to perform a collective motion just as the linear chain of masses connected by springs in Chap. 3: The masses now become the magnetic moments of the spins and the role of the springs is taken by the exchange coupling. This collective excitation of the localized interacting spins are the *spin waves* or, in quantized form, the *magnons*.

In order to quantify this consideration, we start from the Heisenberg model in tight-binding approximation, for which the exchange coupling is taken into account only between nearest neighbors ($n.n.i, j$), thus the Hamiltonian (6.23) simplifies to

$$\mathcal{H}_{\text{spin}} = -J \sum_{n.n.i,j} \mathbf{S}_i \cdot \mathbf{S}_j - g\mu_{\text{B}} H_{\text{ext}} \sum_i S_i^z. \quad (6.27)$$

and contains only one exchange integral. The nature of the spin, being an angular momentum, can be exploited by making use of the corresponding representation with

$$S_i^{\pm} |SM\rangle_i = \{S(S+1) - M(M \pm 1)\}^{1/2} |SM \pm 1\rangle_i, \quad (6.28)$$

where $|SM\rangle_i$ is an eigenstate of the spin operators \mathbf{S}_i^2 and S_i^z for the site i . It is convenient here to write the Hamiltonian with raising and lowering operators S_i^{\pm} (see (6.18))

$$\mathcal{H}_{\text{spin}} = -J \sum_{n.n.i,j} \left\{ \frac{1}{2} (S_i^+ S_j^- + S_i^- S_j^+) + S_i^z S_j^z \right\} - g\mu_{\text{B}} H_{\text{ext}} \sum_i S_i^z. \quad (6.29)$$

Let us first calculate the expectation value of $\mathcal{H}_{\text{spin}}$ without external magnetic field ($H_{\text{ext}} = 0$) in the ferromagnetic ground state, formulated as $|\Psi_0\rangle = \prod_i |SS\rangle_i$:

$$\begin{aligned} E_0 &= \langle \Psi_0 | \mathcal{H}_{\text{spin}} | \Psi_0 \rangle \\ &= -J \sum_{n.n.i,j} \langle SS | S_i^z | SS \rangle_i \langle SS | S_j^z | SS \rangle_j = -J\nu S^2 N, \end{aligned} \quad (6.30)$$

where ν is the number of nearest neighbors and N the number of sites in the chain. Note, that the ferromagnetic ground state in angular momentum representation is composed of angular momentum eigenstates with maximum z component. Application of the raising operator to $|SS\rangle$ gives zero, while application of the z components of the spin operators to the ground state yields

$$\sum_j S_j^z |\Psi_0\rangle = \sum_j S_j^z \prod_i |SS\rangle_i = NS |\Psi_0\rangle. \quad (6.31)$$

As we see from (6.30), the ground state energy is negative if the exchange integral J , whose sign depends on the configuration of nearest neighbors and the atomic orbital, is positive. The stability of the ground state increases with J , with the number of nearest neighbors ν , and with the total spin S . The latter changes with the number of electrons in an incomplete shell and takes a maximum value for half-filling of the shell according to *Hund's rule*³.

Before studying the collective excitations of the spin lattice it is quite instructive to have a look at the dynamics of the individual spin operator \mathbf{S}_j . It is straightforward to derive the equation of motion with the Heisenberg Hamiltonian (6.23) (Problem 6.5)

$$\frac{d\mathbf{S}_j}{dt} = \frac{i}{\hbar} [\mathcal{H}_{\text{spin}}, \mathbf{S}_j] = -\frac{1}{\hbar} (\mathbf{H}_j \times \mathbf{S}_j), \quad (6.32)$$

where $\mathbf{H}_j = \sum_i J_{ij} \mathbf{S}_i + g\mu_B \mathbf{H}_{\text{ext}}$ is an effective magnetic field acting on the spin \mathbf{S}_j at the same site. The equation of motion (6.32) is that of an angular momentum, whose dynamics is determined by a torque, or of a magnetic dipole moving in a magnetic field. This ubiquitous equation of motion, originally formulated in the context of magnetic resonance phenomena, is known as *Bloch equation* [184].

In order to solve (6.32) we choose as before $\mathbf{H}_{\text{ext}} = (0, 0, H_{\text{ext}})$, which gives for the transverse spin components the equations of motion

$$\begin{aligned} \hbar \frac{dS_j^x}{dt} &= - \sum_{n.n.i} J_{ij} (S_i^y S_j^z - S_i^z S_j^y) + g\mu_B H_{\text{ext}} S_j^y \\ \hbar \frac{dS_j^y}{dt} &= - \sum_{n.n.i} J_{ij} (S_i^z S_j^x - S_i^x S_j^z) - g\mu_B H_{\text{ext}} S_j^x. \end{aligned} \quad (6.33)$$

³ Friedrich Hund 1896–1997.

Close to the ferromagnetic ground state, i.e. at low temperature, we may use the replacement $S_j^z \rightarrow \langle S_j^z \rangle \simeq S$ (while $\langle S_j^x \rangle, \langle S_j^y \rangle \ll S$) to simplify these equations:

$$\begin{aligned}\hbar \frac{dS_j^x}{dt} &= -S \sum_{n.n.i} J_{ij} (S_i^y - S_j^y) + g\mu_B H_{\text{ext}} S_j^y \\ \hbar \frac{dS_j^y}{dt} &= -S \sum_{n.n.i} J_{ij} (S_j^x - S_i^x) - g\mu_B H_{\text{ext}} S_j^x.\end{aligned}\quad (6.34)$$

They are combined with $S_j^\pm = S_j^x \pm iS_j^y$ in the equation

$$\hbar \frac{dS_j^\pm}{dt} = \mp i \left(S \sum_{n.n.i} J_{ij} (S_j^\pm - S_i^\pm) + g\mu_B H_{\text{ext}} S_j^\pm \right).\quad (6.35)$$

The coupled motion of neighboring spins can be decoupled by exploiting the periodicity of the chain (or solid) with the Bloch representation

$$S_{\mathbf{k}}^\pm = \frac{1}{\sqrt{N}} \sum_j e^{-i\mathbf{k}\cdot\mathbf{R}_j} S_j^\pm.\quad (6.36)$$

With these normal coordinates (see Chap.3, where the same concept was applied in lattice dynamics) we arrive at

$$\frac{\hbar}{i} \frac{dS_{\mathbf{k}}^\pm}{dt} = \left(S \sum_{n.n.i,j} J_{ij} (1 - e^{-i\mathbf{k}\cdot(\mathbf{R}_i - \mathbf{R}_j)}) + g\mu_B H_{\text{ext}} \right) S_{\mathbf{k}}^\pm.\quad (6.37)$$

The exchange integrals J_{ij} to the ν nearest neighbors with $\mathbf{d} = \mathbf{R}_i - \mathbf{R}_j$ are all the same in a cubic lattice and we may write instead the expression in brackets as

$$\hbar\omega_{\mathbf{k}} = 2J\nu S(1 - \gamma_{\mathbf{k}}) + g\mu_B H_{\text{ext}}, \quad \text{with} \quad \gamma_{\mathbf{k}} = \frac{1}{\nu} \sum_{\mathbf{d}} e^{i\mathbf{k}\cdot\mathbf{d}}.\quad (6.38)$$

Thus, we come to the important result, that the whole spin configuration of the lattice (but also the individual localized spin) performs an oscillatory motion with the frequency $\omega_{\mathbf{k}}$, if small deviations from the ferromagnetic ground state are considered. This collective mode, the *spin wave* characterized by the wave vector \mathbf{k} (depicted in Fig.6.5), corresponds to a coherent precession of the

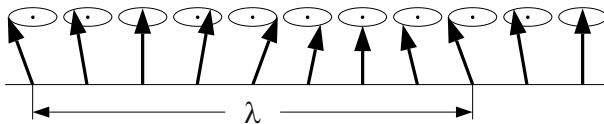


Fig. 6.5. Schematic of a ferromagnetic spin wave on a linear chain

individual spins around the direction of the ferromagnetic orientation. It is completely analogous to the lattice modes in Chap. 3. Its quantized form is called *magnon* as it is related to magnetic properties of the solid.

For methodical reasons, it is worth presenting as an alternative to the Bloch equation, which essentially is a classical concept, a formulation based on the occupation number representation and adapted to the quantized form of elementary excitations. In the previous formulation of excitations out of the ferromagnetic ground state, the emphasis was on the transverse components of the local spins to quantify the precession of the spin vectors around the z direction. The alternative is to quantify the deviation of S_j^z from its maximum value S . This is achieved with a transformation that replaces the ladder operators S_j^\pm by boson operators a_j^\dagger, a_j with $[a_i, a_j^\dagger] = \delta_{ij}$ according to

$$S_j^+ = \sqrt{2S} \left\{ 1 - \frac{1}{2S} a_j^\dagger a_j \right\}^{1/2} a_j, \quad S_j^- = \sqrt{2S} a_j^\dagger \left\{ 1 - \frac{1}{2S} a_j^\dagger a_j \right\}^{1/2} \quad (6.39)$$

without changing the commutation relations among the three angular momentum operators S_j^+, S_j^-, S_j^z . It is the *Holstein⁴-Primakoff⁵ transformation* [185]. The z component of the spin operator follows (with $f(a_j^\dagger a_j) = \{1 - a_j^\dagger a_j / 2S\}^{1/2}$) from

$$\begin{aligned} [S_j^+, S_j^-] &= 2S \left(f(a_j^\dagger a_j) a_j a_j^\dagger f(a_j^\dagger a_j) - a_j^\dagger f^2(a_j^\dagger a_j) a_j \right) \\ &= 2(S - a_j^\dagger a_j) \end{aligned} \quad (6.40)$$

such that

$$S_j^z = S - a_j^\dagger a_j \quad (6.41)$$

describes the deviation from the maximum value S by the number operator $a_j^\dagger a_j$ which will turn out to be that of quantized excitations out of the ferromagnetic ground state.

Let us assume again excitations of low energy which can be quantified by $\langle a_j^\dagger a_j \rangle \ll S$ and allow us to expand the operator function $f(a_j^\dagger a_j)$. Then

$$S_j^+ = \sqrt{2S} \left\{ 1 - \frac{1}{4S} a_j^\dagger a_j + \dots \right\} a_j \simeq \sqrt{2S} a_j, \quad \text{and} \quad S_j^+ \simeq \sqrt{2S} a_j^\dagger, \quad (6.42)$$

and we have a one-to-one correspondence between the ladder operators S_j^\pm and the boson operators a_j and a_j^\dagger . The factor $f(a_j^\dagger a_j)$ is required here only to obtain (6.41). Under the condition of low-energy excitations the Heisenberg Hamiltonian can now be written

$$\begin{aligned} \mathcal{H}_{\text{spin}} &\simeq -J \sum_{n.n.i,j} \left\{ S(a_i a_j^\dagger + a_i^\dagger a_j) + S^2 - S(a_i a_i^\dagger + a_j^\dagger a_j) \right\} \\ &\simeq -E_0 + JS \sum_{n.n.i,j} \left\{ a_i^\dagger a_i + a_j^\dagger a_j - a_i a_j^\dagger - a_i^\dagger a_j \right\} \end{aligned} \quad (6.43)$$

⁴ Theodor D. Holstein, 1915–1985.

⁵ Henry Primakoff, 1914–1983.

where higher order terms in the occupation number operator (corresponding to magnon–magnon coupling analogous to lattice dynamics beyond the harmonic approximation) have been omitted and E_0 is the ground state energy (see (6.30)). The last two terms represent a coupling between nearest neighbor lattice sites which can be removed by transforming to normal coordinates (or switching from the Wannier to the Bloch representation) with

$$a_j = \frac{1}{\sqrt{N}} \sum_{\mathbf{k}} e^{-i\mathbf{k}\cdot\mathbf{R}_j} b_{\mathbf{k}}, \quad a_j^\dagger = \frac{1}{\sqrt{N}} \sum_{\mathbf{k}} e^{i\mathbf{k}\cdot\mathbf{R}_j} b_{\mathbf{k}}^\dagger. \quad (6.44)$$

The individual contributions to (6.43) can be expressed in the new boson operators for the collective excitation as

$$\begin{aligned} \sum_{n.n.ij} a_j^\dagger a_j &= \nu \sum_{\mathbf{k}\mathbf{k}'} \frac{1}{N} \underbrace{\sum_j e^{-i(\mathbf{k}-\mathbf{k}')\cdot\mathbf{R}_j}}_{\delta_{\mathbf{k}\mathbf{k}'}} b_{\mathbf{k}'}^\dagger b_{\mathbf{k}} = \nu \sum_{\mathbf{k}} b_{\mathbf{k}}^\dagger b_{\mathbf{k}} \\ \sum_{n.n.ij} a_i^\dagger a_j &= \sum_{\mathbf{k}\mathbf{k}'} \frac{1}{N} \sum_{n.n.ij} e^{i\mathbf{k}\cdot\mathbf{R}_i} e^{-i\mathbf{k}'\cdot\mathbf{R}_j} b_{\mathbf{k}'}^\dagger b_{\mathbf{k}} \\ &= \sum_{\mathbf{k}\mathbf{k}'} \frac{1}{N} \sum_j e^{i(\mathbf{k}-\mathbf{k}')\cdot\mathbf{R}_j} \sum_{\mathbf{d}} e^{i\mathbf{k}\cdot\mathbf{d}} b_{\mathbf{k}}^\dagger b_{\mathbf{k}'} = \nu \sum_{\mathbf{k}} \gamma_{\mathbf{k}} b_{\mathbf{k}}^\dagger b_{\mathbf{k}} \end{aligned} \quad (6.45)$$

and the Hamiltonian takes the approximate form

$$\mathcal{H}_{\text{spin}} \simeq E_0 + 2J\nu S \sum_{\mathbf{k}} (1 - \gamma_{\mathbf{k}}) b_{\mathbf{k}}^\dagger b_{\mathbf{k}} = E_0 + \sum_{\mathbf{k}} \hbar\omega_{\mathbf{k}} b_{\mathbf{k}}^\dagger b_{\mathbf{k}}. \quad (6.46)$$

It is the Hamiltonian for spin waves in ferromagnets. The meaning of the boson operators $b_{\mathbf{k}}^\dagger$ and $b_{\mathbf{k}}$ can be read from the relation

$$\sum_j S_j^z = NS - \sum_{\mathbf{k}} b_{\mathbf{k}}^\dagger b_{\mathbf{k}}, \quad (6.47)$$

where the first term NS gives the maximum value of the z components of all spin operators in the ferromagnetic ground state and the second term counts the number of quantized collective excitations, the magnons.

Because we have assumed exchange interaction only between nearest neighbors, the magnon dispersion $\omega_{\mathbf{k}}$, depending on the configuration of the magnetic ions, can be expressed in terms of cosine functions as is typical for the tight-binding approximation (see Sect. 5.4). The width of the magnon band, determined by the number of nearest neighbors and the exchange constant, is in the range of a few to some tens meV, which is about the same as for phonons. For $|\mathbf{k}| \ll 2\pi/a$ we may expand

$$1 - \gamma_{\mathbf{k}} \simeq 1 - (1 - \frac{1}{2\nu} \sum_{\mathbf{d}} |\mathbf{k}\cdot\mathbf{d}|^2) \sim k^2 \quad (6.48)$$

and find a quadratic dependence on the wave vector around the minimum at $\mathbf{k} = 0$. This quadratic dispersion has been measured by inelastic neutron scattering, e.g. in the 3d transition metals [186, 187], but will be shown only when we discuss itinerant magnetism in Sect. 6.6. For a more recent introduction into the concepts of neutron scattering in solids with examples of magnetic excitations see [96, 97].

Similar to phonons, magnons also can be thermally excited and contribute to the specific heat. This contribution can be calculated from the thermal expectation value of (6.46)

$$\begin{aligned} E(T) &= E_0 + \sum_{\mathbf{k}} \hbar\omega_{\mathbf{k}} \langle b_{\mathbf{k}}^{\dagger} b_{\mathbf{k}} \rangle \\ &= E_0 + \frac{V}{(2\pi)^3} \int \hbar\omega_{\mathbf{k}} \frac{1}{e^{\beta\hbar\omega_{\mathbf{k}}} - 1} d^3\mathbf{k}. \end{aligned} \quad (6.49)$$

As we are interested in the low-temperature behavior of the specific heat, which is determined by the quantum nature of the excitations, the dispersion can be approximated as $\hbar\omega_{\mathbf{k}} = \alpha k^2$, where for a simple cubic lattice with lattice constant a one has $\alpha = 2JSa^2$. With this isotropic quadratic dispersion the integral can be evaluated in polar coordinates and reads after substituting $x = \beta\alpha k^2$

$$E(T) = E_0 + \frac{\alpha}{2\pi^2} \left(\frac{k_B T}{\alpha} \right)^{5/2} \int_0^{x_{\max}} x^{3/2} \frac{1}{e^x - 1} dx. \quad (6.50)$$

We may compare here with $E(T)$ of (3.64), obtained for the acoustic phonons in the Debye model. For low-temperatures the upper limit of the integral can be shifted to infinity and we obtain one of the Bose integrals (see Appendix), which can be expressed here as $\Gamma(5/2)\zeta(5/2; 1)$. Finally, we find for the magnon contribution to the thermal energy

$$E(T) = E_0 + \frac{0.45}{\pi^2 \alpha^{3/2}} (k_B T)^{5/2} \quad (6.51)$$

and for the specific heat

$$c_V(T) = \left. \frac{dE(T)}{dT} \right|_{V=\text{const.}} = 0.113 k_B \left(\frac{k_B T}{\alpha} \right)^{3/2}. \quad (6.52)$$

This $T^{3/2}$ dependence is characteristic of the magnon contribution to the specific heat and makes it distinct from the contributions of the acoustic phonons ($\sim T^3$) or free electrons ($\sim T$).

6.4 Spin Waves in Anti-Ferromagnets

In the last section, we have assumed a ferromagnetic ground state, which required a positive exchange integral between nearest neighbors. An anti-ferromagnetic order, with the spins on neighboring lattice sites being oriented

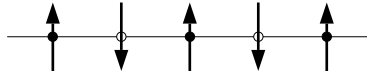


Fig. 6.6. Linear chain with anti-ferromagnetic order, the Wigner–Seitz cell contains two ions with opposite spin

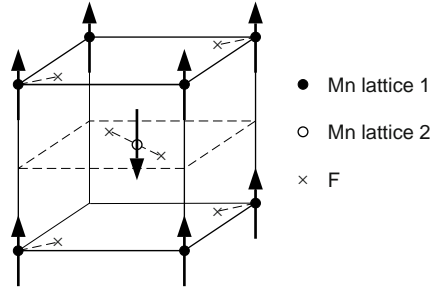


Fig. 6.7. Structure of the anti-ferromagnetic insulator MnF_2

anti-parallel to each other, would mean an enlarged unit cell with a basis consisting of (at least) two atoms with a negative exchange integral between nearest neighbors, as depicted in Fig. 6.6. As a real three-dimensional system we show in Fig. 6.7, the crystal structure of the anti-ferromagnetic insulator MnF_2 . The configuration of the fluorine ions around the Mn ions on the corners of the cube is different from that around the Mn ion in the center, thus the structure is that of two interpenetrating simple cubic lattices each with a basis of one Mn and two F ions.

The Hamiltonian for this system (without external magnetic field) can be written

$$\begin{aligned} \mathcal{H}_{\text{spin}} &= J_a \sum_{n,n,i,j} \mathbf{S}_{1i} \cdot \mathbf{S}_{2j} \\ &= J_a \sum_{n,n,i,j} \left(\frac{1}{2} (S_{1i}^+ S_{2j}^- + S_{1i}^- S_{2j}^+) + S_{1i}^z S_{2j}^z \right). \end{aligned} \quad (6.53)$$

Here $\mathbf{S}_{1i}, \mathbf{S}_{2j}$ are the spin vector operators on the two sublattices and the negative sign of the exchange integral is absorbed in the positive constant J_a . In order to derive a spin wave Hamiltonian similar to (6.46) we employ the Holstein–Primakoff transformation, introduced in the previous section, to replace in a first step, the spin operators on each sublattice by boson operators

$$\begin{aligned} S_{1i}^+ &\simeq \sqrt{2S} a_{1i}, & S_{1i}^- &\simeq \sqrt{2S} a_{1i}^\dagger, & S_{1i}^z &= +S - a_{1i}^\dagger a_{1i} & (\text{sublattice 1}) \\ S_{2i}^+ &\simeq \sqrt{2S} a_{2i}, & S_{2i}^- &\simeq \sqrt{2S} a_{2i}^\dagger, & S_{2i}^z &= -S + a_{2i}^\dagger a_{2i} & (\text{sublattice 2}) \end{aligned} \quad (6.54)$$

and find the approximate Heisenberg Hamiltonian for low-energy excitations out of the anti-ferromagnetic state, i.e. for $\langle a_{1i}^\dagger a_{1i} \rangle, \langle a_{2i}^\dagger a_{2i} \rangle \ll S$,

$$\mathcal{H}_{\text{spin}} \simeq J_a \sum_{n.n.ij} \left\{ -S^2 + S(a_{1i}^\dagger a_{1i} + a_{2i}^\dagger a_{2i} + a_{1i} a_{2j} + a_{1i}^\dagger a_{2j}^\dagger) \right\}. \quad (6.55)$$

The first term $\sim -S^2$ on the right hand side gives the energy of the anti-ferromagnetic configuration $E_a = -2J_a \nu N S^2$. It will be shown later that this configuration does not represent the ground state. The remaining terms can be formulated again in the Bloch representation for each sublattice and we obtain

$$\mathcal{H}_{\text{spin}} \simeq E_a + 2J_a \nu S \sum_{\mathbf{k}} \left\{ b_{1\mathbf{k}}^\dagger b_{1\mathbf{k}} + b_{2\mathbf{k}}^\dagger b_{2\mathbf{k}} + \gamma_{\mathbf{k}} (b_{1\mathbf{k}}^\dagger b_{2\mathbf{k}}^\dagger + b_{1\mathbf{k}} b_{2\mathbf{k}}) \right\}. \quad (6.56)$$

The first terms under the sum, count the elementary excitations on each sublattice, while the last term describes the coupling between the sublattices which still has to be removed. This is achieved by the *Bogoliubov*⁶ *transformation*

$$\begin{aligned} \alpha_{\mathbf{k}} &= u_{\mathbf{k}} b_{1\mathbf{k}} - v_{\mathbf{k}} b_{2\mathbf{k}}^\dagger, & \alpha_{\mathbf{k}}^\dagger &= u_{\mathbf{k}} b_{1\mathbf{k}}^\dagger - v_{\mathbf{k}} b_{2\mathbf{k}}, \\ \beta_{\mathbf{k}} &= u_{\mathbf{k}} b_{2\mathbf{k}} - v_{\mathbf{k}} b_{1\mathbf{k}}^\dagger, & \beta_{\mathbf{k}}^\dagger &= u_{\mathbf{k}} b_{2\mathbf{k}}^\dagger - v_{\mathbf{k}} b_{1\mathbf{k}}, \end{aligned} \quad (6.57)$$

where the coefficients $u_{\mathbf{k}}$ and $v_{\mathbf{k}}$ are real. Also the new operators obey the boson commutation rules (Problem 6.6)

$$[\alpha_{\mathbf{k}}, \alpha_{\mathbf{k}'}^\dagger] = [\beta_{\mathbf{k}}, \beta_{\mathbf{k}'}^\dagger] = \delta_{\mathbf{k}\mathbf{k}'}, \quad [\alpha_{\mathbf{k}}, \beta_{\mathbf{k}'}] = [\alpha_{\mathbf{k}}^\dagger, \beta_{\mathbf{k}'}^\dagger] = [\alpha_{\mathbf{k}}, \beta_{\mathbf{k}'}^\dagger] = 0. \quad (6.58)$$

which leads to the constraint $u_{\mathbf{k}}^2 - v_{\mathbf{k}}^2 = 1$. Note, that the boson operators for different sublattices commute with each other.

The Bogoliubov transformation is an important concept to exactly eliminate a bilinear coupling between two boson systems, of those represented by the spin wave operators on the two sublattices. It can also be applied to phonon–photon or exciton–photon coupling (leading to polaritons, see Chap. 10) or to plasmon–phonon coupling (to yield the coupled plasmon–phonon modes (see Sect. 4.6)). A further example is the magnon–phonon coupling to be treated in Problem 6.7. An analogous transformation for bilinear fermion coupling, the Bogoliubov–Valatin transformation is used in the theory of superconductivity [19].

This transformation is applied here in its inverted form according to which

$$b_{1\mathbf{k}} = u_{\mathbf{k}} \alpha_{\mathbf{k}} + v_{\mathbf{k}} \beta_{\mathbf{k}}^\dagger, \quad b_{2\mathbf{k}} = u_{\mathbf{k}} \beta_{\mathbf{k}} + v_{\mathbf{k}} \alpha_{\mathbf{k}}^\dagger \quad (6.59)$$

and corresponding expressions for Hermitian adjoint operators, to find (Problem 6.8)

$$\begin{aligned} \mathcal{H}_{\text{spin}} &= E_a + 2J_a \nu S \sum_{\mathbf{k}} \left\{ -1 + (u_{\mathbf{k}}^2 + v_{\mathbf{k}}^2 + 2u_{\mathbf{k}} v_{\mathbf{k}}) (\alpha_{\mathbf{k}}^\dagger \alpha_{\mathbf{k}} + \beta_{\mathbf{k}}^\dagger \beta_{\mathbf{k}} + 1) \right. \\ &\quad \left. + (2u_{\mathbf{k}} v_{\mathbf{k}} + \gamma_{\mathbf{k}} (u_{\mathbf{k}}^2 + v_{\mathbf{k}}^2)) (\alpha_{\mathbf{k}}^\dagger \beta_{\mathbf{k}}^\dagger + \alpha_{\mathbf{k}} \beta_{\mathbf{k}}) \right\}. \end{aligned} \quad (6.60)$$

⁶ Nikolai Nikolaevich Bogoliubov 1909–1992.

The last term on the *rhs*, which is bilinear in the α and β operators, vanishes for

$$2u_{\mathbf{k}}v_{\mathbf{k}} + \gamma_{\mathbf{k}}(u_{\mathbf{k}}^2 + v_{\mathbf{k}}^2) = 0, \quad (6.61)$$

which together with $u_{\mathbf{k}}^2 - v_{\mathbf{k}}^2 = 1$ leads to

$$u_{\mathbf{k}}^2 + v_{\mathbf{k}}^2 + 2\gamma_{\mathbf{k}}u_{\mathbf{k}}v_{\mathbf{k}} = \sqrt{1 - \gamma_{\mathbf{k}}^2} \quad (6.62)$$

and

$$u_{\mathbf{k}}^2 = \frac{1}{2} \left(\frac{1}{\sqrt{1 - \gamma_{\mathbf{k}}^2}} + 1 \right), \quad v_{\mathbf{k}}^2 = \frac{1}{2} \left(\frac{1}{\sqrt{1 - \gamma_{\mathbf{k}}^2}} - 1 \right). \quad (6.63)$$

Thus, we arrive at the Hamiltonian for anti-ferromagnetic spin waves

$$\mathcal{H}_{\text{spin}} = -2J_a\nu NS(S+1) + \sum_{\mathbf{k}} \hbar\omega_{\mathbf{k}}(\alpha_{\mathbf{k}}^\dagger\alpha_{\mathbf{k}} + \beta_{\mathbf{k}}^\dagger\beta_{\mathbf{k}} + 1). \quad (6.64)$$

This Hamiltonian differs from that of the ferromagnetic magnons (6.46) by containing number operators of two elementary excitations ($\alpha_{\mathbf{k}}^\dagger\alpha_{\mathbf{k}}$ and $\beta_{\mathbf{k}}^\dagger\beta_{\mathbf{k}}$) with the same energy and in addition, a zero point contribution.

The magnon energy is $\hbar\omega_{\mathbf{k}} = 2J_a\nu S(1 - \gamma_{\mathbf{k}}^2)^{1/2}$ with $\gamma_{\mathbf{k}}$ as defined before. In contrast with the dispersion of the ferromagnetic magnons, we have now for $k \ll \pi/a$ with $1 - \gamma_{\mathbf{k}}^2 \sim k^2$ a linear dependence of the magnon frequency with k . An example for this linear dispersion measured by inelastic neutron scattering in MnF_2 is shown in Fig. 6.8. Note that the dispersion does not exactly follow the linear dependence $\sim k$, but exhibits a small gap at $k = 0$. It is due to an anisotropy field, which removes the degeneracy of the two different magnons and will be the subject of Problem 6.9.

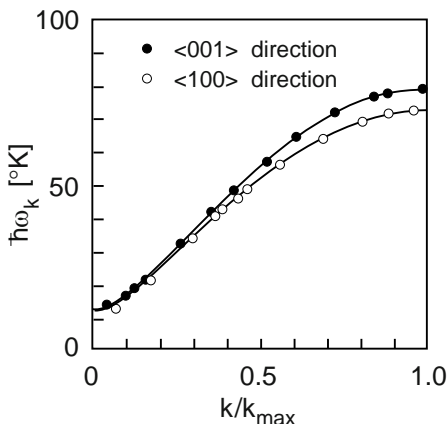


Fig. 6.8. Magnon dispersion in MnF_2 measured by inelastic neutron scattering for two different directions in \mathbf{k} space after [188]. Note the small gap at $\mathbf{k} = 0$ due to a small anisotropy field (see Problem 6.9)

The energy of the ground state (the magnon vacuum, here denoted by $|\Psi_0\rangle$)

$$E_0 = \langle \Psi_0 | \mathcal{H}_{\text{spin}} | \Psi_0 \rangle = -2J_a \nu N S^2 - 2J_a \nu S \sum_{\mathbf{k}} \left(1 - \sqrt{1 - \gamma_{\mathbf{k}}^2} \right) \quad (6.65)$$

is composed of the energy of the perfect anti-ferromagnetic configuration (first term) and the zero-point contribution, which is negative because of $1 - \sqrt{1 - \gamma_{\mathbf{k}}^2} > 0$ (second term). This indicates that the ground state deviates from the exact anti-ferromagnetic order as can be seen more clearly by looking at the departure from the maximum value of the z component of the spin, $NS - \langle \Psi_0 | \sum_j S_j^z | \Psi_0 \rangle$, in the sublattices (which would vanish for the perfect spin alignment). We find for the sublattice 1 (and similar for the sublattice 2) with

$$\begin{aligned} \sum_j S_j^z &= NS - \sum_{\mathbf{k}} b_{1\mathbf{k}}^\dagger b_{1\mathbf{k}} \\ &= NS - \sum_{\mathbf{k}} \left(u_{\mathbf{k}} \alpha_{\mathbf{k}}^\dagger + v_{\mathbf{k}} \beta_{\mathbf{k}} \right) \left(u_{\mathbf{k}} \alpha_{\mathbf{k}} + v_{\mathbf{k}} \beta_{\mathbf{k}}^\dagger \right) \\ &= NS - \sum_{\mathbf{k}} \left(u_{\mathbf{k}}^2 \alpha_{\mathbf{k}}^\dagger \alpha_{\mathbf{k}} + v_{\mathbf{k}}^2 \beta_{\mathbf{k}} \beta_{\mathbf{k}}^\dagger + u_{\mathbf{k}} v_{\mathbf{k}} (\alpha_{\mathbf{k}}^\dagger \beta_{\mathbf{k}}^\dagger + \alpha_{\mathbf{k}} \beta_{\mathbf{k}}) \right) \end{aligned} \quad (6.66)$$

and by making use of the commutation rules for the β operators after taking the expectation value with $|\Psi_0\rangle$

$$NS - \langle \Psi_0 | \sum_j S_j^z | \Psi_0 \rangle = \sum_{\mathbf{k}} v_{\mathbf{k}}^2 = \frac{1}{2} \sum_{\mathbf{k}} \left((1 - \gamma_{\mathbf{k}}^2)^{-1/2} - 1 \right) \neq 0. \quad (6.67)$$

Thus, in the ground state, the magnon vacuum, the spins in the individual sublattices are not perfectly aligned but slightly disordered.

6.5 Molecular Field Approximation

The theory of spin waves outlined in Sects. 6.3 and 6.4 has provided some insight into the low-energy excitations, which means a departure from the state with ferromagnetic or anti-ferromagnetic order. It is known, that magnetic order exists only below a critical temperature at which a phase transition takes place. For ferromagnets, this critical temperature is the *Curie*⁷ *temperature* T_C at which a transition to the paramagnetic phase takes place. The transition temperature for anti-ferromagnets is the *Néel*⁸ *temperature* T_N .

⁷ Pierre Curie 1859–1906, shared the Noble prize in physics 1903 with his wife Marie Curie.

⁸ Louis Néel 1904–2000, Noble prize in physics 1970.

The quantity to be studied here is the magnetization $\mathbf{M}(T)$ and its temperature dependence up to and beyond T_C . Assuming its orientation (which can be defined by a weak external magnetic field) in z direction we may write $\mathbf{M}(T) = (0, 0, M(T))$ with

$$M(T) = g\mu_B \left\langle \sum_j S_j^z \right\rangle, \quad (6.68)$$

i.e., the magnetization is determined by the thermal expectation value of the z components of the localized spin operators. For temperatures below the Curie temperature T_C , it describes the spontaneous magnetization which in terms of ferromagnetic spin waves reads

$$M(T) = g\mu_B \left(NS - \sum_{\mathbf{k}} \langle b_{\mathbf{k}}^\dagger b_{\mathbf{k}} \rangle \right). \quad (6.69)$$

The first term $M(0) = g\mu_B NS$ is the saturation magnetization and the second term accounts for the departure from $M(0)$ by thermal excitation of magnons which follows a temperature dependence given by $T^{3/2}$ (Problem 6.10). When approaching T_C the magnetization vanishes, which in the language of magnons would require $\langle b_{\mathbf{k}}^\dagger b_{\mathbf{k}} \rangle$ to approach NS in contrast with the condition $\langle b_{\mathbf{k}}^\dagger b_{\mathbf{k}} \rangle \ll NS$ for the spin-wave theory, or else, this theory is valid only for $T \ll T_C$.

Let us look, therefore, again at the Heisenberg Hamiltonian with an external magnetic field (to fix the orientation of the spontaneous magnetization) written in the form

$$\mathcal{H}_{\text{spin}} = - \sum_j \left\{ J \sum_{n.n.i \neq j} \mathbf{S}_i + g\mu_B \mathbf{H}_{\text{ext}} \right\} \cdot \mathbf{S}_j. \quad (6.70)$$

It suggests to interpret the content of the curly bracket as an effective magnetic field acting on the spin \mathbf{S}_j . This interpretation requires that the spin operator \mathbf{S}_i is replaced by its thermal expectation value $\langle \mathbf{S}_i \rangle$.

To be more explicit, by splitting the spin operator $\mathbf{S}_i = \langle \mathbf{S}_i \rangle + \delta \mathbf{S}_i$ into its thermal expectation (or mean) value and deviations from it, called spin fluctuations, the spin-spin interaction can be rewritten

$$\mathbf{S}_i \cdot \mathbf{S}_j = \langle \mathbf{S}_i \rangle \cdot \langle \mathbf{S}_j \rangle + \langle \mathbf{S}_i \rangle \cdot \delta \mathbf{S}_j + \delta \mathbf{S}_i \cdot \langle \mathbf{S}_j \rangle + \delta \mathbf{S}_i \cdot \delta \mathbf{S}_j. \quad (6.71)$$

Neglecting the last term quadratic in the fluctuations, which are assumed to be small, the Heisenberg Hamiltonian can be cast into the form

$$\mathcal{H}_{\text{spin}} = - \sum_j \left\{ 2J \sum_{n.n.i \neq j} \langle \mathbf{S}_i \rangle + g\mu_B \mathbf{H}_{\text{ext}} \right\} \cdot \mathbf{S}_j + \sum_{n.n.i \neq j} J \langle \mathbf{S}_i \rangle \cdot \langle \mathbf{S}_j \rangle, \quad (6.72)$$

where the last term is a constant. The first term contains besides the Zeeman term the *molecular field*, defined by

$$2J \sum_{n.n.i \neq j} \langle \mathbf{S}_i \rangle = g\mu_B \mathbf{H}_M \quad (6.73)$$

and the spin Hamiltonian becomes

$$\mathcal{H}_{\text{spin}} \simeq -g\mu_B \sum_j \{ \mathbf{H}_M + \mathbf{H}_{\text{ext}} \} \cdot \mathbf{S}_j + \sum_{n.n.i \neq j} J \langle \mathbf{S}_i \rangle \cdot \langle \mathbf{S}_j \rangle. \quad (6.74)$$

The molecular field \mathbf{H}_M (originally introduced by P. Weiss⁹) accounts for the interaction of the spin \mathbf{S}_j with all the other spins $\mathbf{S}_i, i \neq j$ replaced by $\langle \mathbf{S}_i \rangle$, but can be quantified, only when the thermal expectation values of all these spins are known. Note that this seemingly simple concept is quite general as it can be applied to any system of interacting particles as e.g. in the Hartree–Fock approximation introduced in Sect. 4.4. In this more general context, the molecular field is also called *mean field* and the approximation denoted *mean field approximation*.

According to the translational symmetry of the system, the individual localized spins contribute equally to the magnetization. Therefore, it can be written

$$NM(T) = g\mu_B \sum_j \langle \mathbf{S}_j \rangle = g\mu_B N \langle \mathbf{S}_j \rangle \quad (6.75)$$

and the molecular field can be expressed as

$$\mathbf{H}_M = \frac{2J}{Ng\mu_B} \sum_{n.n.i \neq j} \langle \mathbf{S}_i \rangle = \lambda \mathbf{M}, \quad \lambda = \frac{\nu J}{g^2 \mu_B^2}. \quad (6.76)$$

It is determined by the magnetization $\mathbf{M}(T)$ of the system and a constant $\sim \nu J$, the *Weiss constant*, which is stronger the larger the exchange integral J and the number ν of nearest neighbors in the lattice.

Now, we focus on the temperature dependence of the magnetization. Let the external magnetic field and the magnetization point in the z direction to define an effective field $H_{\text{eff}} = H_{\text{ext}} + \lambda M$. Then the spin Hamiltonian takes the form (up to a constant)

$$\mathcal{H}_{\text{spin}} = -g\mu_B \sum_i S_i^z H_{\text{eff}} \quad (6.77)$$

and the magnetization is to be calculated as thermal expectation value

$$M(T) = g\mu_B \text{Tr} \left(\frac{1}{Z} e^{-\beta \mathcal{H}_{\text{spin}}} S_i^z \right) \quad \text{with} \quad \beta = 1/k_B T. \quad (6.78)$$

⁹ Pierre Ernest Weiss 1865–1940.

The trace can be evaluated with the eigenstates of (6.77) which are

$$\prod_i |SM_S\rangle_i, M_S = -S, -S + 1, \dots, S - 1, S. \quad (6.79)$$

The eigenvalues of S_i^z are independent of the site

$$S_i^z |SM_S\rangle_i = M_S |SM_S\rangle_i \quad (6.80)$$

and we can write

$$M(T) = \sum_i \frac{1}{Z} \sum_{M_S=-S}^{+S} 2\mu_B M_S e^{g\mu_B \beta M_S H_{\text{eff}}} \quad (6.81)$$

which gives

$$M(T) = g\mu_B S \mathcal{B}_S(g\mu_B \beta S H_{\text{eff}}), \quad (6.82)$$

with the Brillouin function (with $y = g\mu_B \beta S H_{\text{eff}}$)

$$\mathcal{B}_S(y) = \frac{2S+1}{2S} \coth\left(\frac{2S+1}{2S}y\right) - \frac{1}{2S} \coth\frac{y}{2S}. \quad (6.83)$$

In the limit of low temperatures, $y \rightarrow \infty$, the Brillouin function $\mathcal{B}_S(y) \rightarrow 1$ and we find

$$T \rightarrow 0: \quad M(T) \rightarrow M(0) = g\mu_B S \quad (6.84)$$

i.e., the magnetization correctly approaches the saturation value.

Actually, according to (6.82) M is a function of the variable $x = H_{\text{eff}}/T$ in which it shows the saturation behavior depicted in Fig. 6.9. Because of its definition, the effective field is itself a function of the magnetization. Thus, (6.82) represents an implicit equation for $M(T)$. It can be solved by considering besides (6.82) the second expression of $M(x)$ obtained from the effective field for the case of vanishing external field

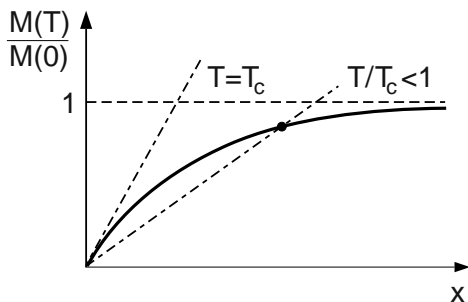


Fig. 6.9. Saturation behavior of the spontaneous magnetization and graphical solution for $M(T)$ with the phase transition for a ferromagnet (after [12])

$$M(x) = \frac{T}{\lambda} x. \quad (6.85)$$

For sufficiently low temperature, the graph of (6.85), which is a straight line (see Fig. 6.9), cuts the saturation curve (6.82) always at a finite value of $M(T)$. With increasing temperature, this crossing point moves to the left until at the critical temperature, the graph of (6.85) becomes the tangent of (6.82) at $M(T) = 0$. This signifies the transition from the ferromagnetic to the paramagnetic phase.

The critical temperature can be obtained from the derivative of the magnetization with respect to x , which is found from the high temperature expansion ($y \ll 1$) of the Brillouin function

$$\mathcal{B}_S(y) = \frac{S+1}{S} \frac{y}{3} - \frac{(2S+1)^4 - 1}{(2S)^4} \frac{y^3}{45} + \dots \quad (6.86)$$

according to which the leading terms of the magnetization in the absence of the external magnetic field ($H_{\text{ext}} \rightarrow 0$) are

$$M(T) = T_C \frac{M(T)}{T} - A \frac{M(T)^3}{T^3}, \quad (6.87)$$

where we have identified the Curie temperature with

$$T_C = \frac{J\nu S(S+1)}{3k_B} \quad (6.88)$$

and A is another constant determined by the system parameters. After dividing by $M(T)$ (6.87) becomes a quadratic equation which gives the qualitative relation

$$M(T \rightarrow T_C) \sim (T_C - T)^{1/2}, \quad T < T_C. \quad (6.89)$$

Thus, the mean field theory allows us to describe the expected vanishing of the magnetization, when approaching the critical temperature from below, and it gives also the temperature dependence with the *critical exponent* 1/2. This behavior is typical for a second order phase transition, which is characterized here by the magnetization $M(T)$ as *order parameter*. The usual plot of $M(T)/M(0)$ versus T/T_C (Fig. 6.10) is universal for a second order phase transition and does not depend on the ferromagnetic material. Thus, the data points for Ni and Fe fall onto the same curve, which is well described by the Brillouin function with $S = 1/2$. The validity of the mean-field approach has been confirmed also by ab-initio calculations with the dynamical mean-field theory.[189]

Above the critical temperature the magnetization in the presence of an external magnetic field is

$$\begin{aligned} M(T > T_C) &= g^2 \mu_B^2 N S(S+1) \frac{1}{3k_B T} (H_{\text{ext}} + \lambda M) \\ &= \frac{C}{T} H_{\text{ext}} + \frac{T_C}{T} M(T) \end{aligned} \quad (6.90)$$

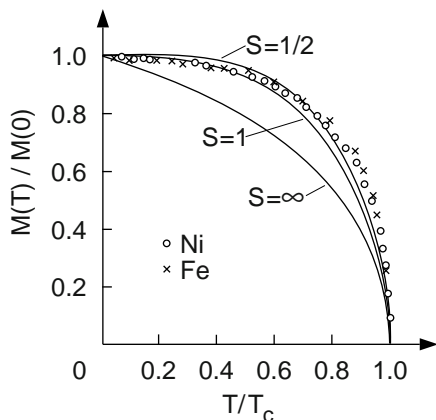


Fig. 6.10. Dependence of the reduced saturation magnetization on the reduced temperature. Symbols are experimental data for Ni and Fe, solid lines are calculated from the Brillouin function with different values for the total spin S (after [30])

Table 6.1. Curie temperatures (T_C in K) and saturation magnetization ($M(0)$ in Gauss) for some ferromagnets and Néel temperatures (T_N in K) for some anti-ferromagnets

Ferromagnets	T_C	$M(0)$	Anti-Ferromagnets	T_N
Fe	1043	1752	MnO	122
Co	1388	1446	FeO	198
Ni	627	510	CoO	291
EuO	77	1910	NiO	600
EuS	16.5	1184	MnF ₂	67.34
MnAs	318	870	CoF ₂	37.7

and it follows the *Curie-Weiss law*

$$M(T > T_C) = \frac{C}{T - T_C} H_{\text{ext}}, \quad T > T_C. \quad (6.91)$$

Similar considerations lead to the phase transition between the anti-ferromagnetic and paramagnetic phases characterized by the Néel temperature as critical temperature. In Table 6.1 some systems with magnetic order are given together with their critical temperatures and (for the ferromagnetic systems) their saturation magnetization at $T = 0$ K. As an example of a ferromagnet we refer to Fe₃O₄ (magnetite) with $T_C = 858$ K and $M(T = 0) = 510$ G. All data are taken from [164]. For further reading about phase transitions and critical exponents we refer to [190–192].

6.6 Itinerant Electron Magnetism

While in the previous sections we have assumed a dominating exchange interaction and strongly localized electrons, we want to study now the opposite situation of Bloch or itinerant electrons with weak exchange interaction. The appropriate Hamiltonian for this case is [166, 171]

$$\mathcal{H} = \sum_{\mathbf{k}\sigma} \epsilon_{\mathbf{k}} c_{\mathbf{k}\sigma}^\dagger c_{\mathbf{k}\sigma} + \frac{1}{2} U \sum_{\substack{\mathbf{k}\mathbf{k}'\mathbf{q} \\ \sigma\sigma'}} c_{\mathbf{k}+\mathbf{q}\sigma}^\dagger c_{\mathbf{k}'-\mathbf{q}\sigma'}^\dagger c_{\mathbf{k}'\sigma'} c_{\mathbf{k}\sigma}. \quad (6.92)$$

It describes electrons in a band $\epsilon_{\mathbf{k}}$ with an interaction independent of \mathbf{k} , which can be understood as a screened Coulomb interaction $e^2/V\epsilon_0(k^2 + k_{\text{FT}}^2)$ with neglect of the dependence on k , i.e. it corresponds to the replacements

$$v_{\mathbf{k}} = \frac{e^2}{\epsilon_0 V k^2} \rightarrow \frac{e^2}{\epsilon_0 V (k^2 + k_{\text{FT}}^2)} \rightarrow \frac{e^2}{\epsilon_0 V k_{\text{FT}}^2} = U. \quad (6.93)$$

We apply the Hartree–Fock approximation by considering only contributions of the interaction with $\mathbf{k}' = \mathbf{k} + \mathbf{q}$ and $\sigma = \sigma'$, which allow us to write the interaction as

$$\mathcal{H}_{\text{int}} = -\frac{1}{2} U \sum_{\mathbf{k}_1 \mathbf{k}_2 \sigma} c_{\mathbf{k}_1 \sigma}^\dagger c_{\mathbf{k}_1 \sigma} c_{\mathbf{k}_2 \sigma}^\dagger c_{\mathbf{k}_2 \sigma} = -\frac{1}{2} U \sum_{\mathbf{k}_1 \mathbf{k}_2 \sigma} n_{\mathbf{k}_1 \sigma} n_{\mathbf{k}_2 \sigma}. \quad (6.94)$$

This can be formulated also with the numbers $N_\sigma = \sum_{\mathbf{k}} n_{\mathbf{k}\sigma}$ of spin-up ($\sigma = +$) and spin-down ($\sigma = -$) electrons as

$$\mathcal{H}_{\text{int}} = -\frac{U}{2} \left(\frac{1}{2} (N_+ - N_-)^2 + \frac{1}{2} N^2 \right), \quad (6.95)$$

where $N = N_+ + N_-$ is the total number of electrons. The HF Hamiltonian, known also as the *Stoner*¹⁰ model then reads

$$\mathcal{H}^{\text{HF}} = \sum_{\mathbf{k}, \sigma} \left(\epsilon_{\mathbf{k}} - \sigma \frac{\Delta}{2} \right) c_{\mathbf{k}\sigma}^\dagger c_{\mathbf{k}\sigma} + \frac{U}{4} ((N_+ - N_-)^2 - N^2). \quad (6.96)$$

The energy spectrum $\epsilon_{\mathbf{k}\sigma} = \epsilon_{\mathbf{k}} - \sigma\Delta/2$ is depicted in Fig. 6.11, where for simplicity, a parabolic dispersion as for free electrons is assumed. The up and down spin electrons differ in their energies by $\Delta = U(N_+ - N_-)$. The number difference between both kinds of electrons determines the magnetization thus indicating the relation with magnetism. We recognize that the exchange interaction leads to a similar result as the Zeeman term in the discussion of the Pauli spin paramagnetism in Sect. 4.2. However, the \mathbf{k} independent shift of the spin-up and spin-down band applies to any dispersion relation $\epsilon_{\mathbf{k}}$ as e.g. in Fig. 6.1.

¹⁰ Edmund Clifton Stoner 1889–1973

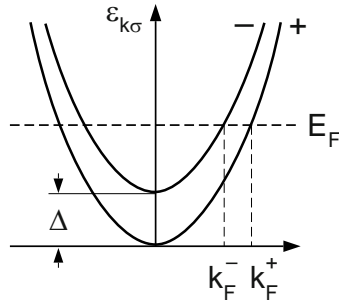


Fig. 6.11. Schematic dispersion for spin-split energy bands

The Stoner model is the starting point for investigating the dependence of the total energy on the degree of spin polarization $\zeta = (N_+ - N_-)/N$. This will lead us to a refinement of the estimate given at the beginning of this Chapter with respect to the existence of ferromagnetic order in a system of itinerant electrons. The ground state energy in HF approximation follows from (6.96) as

$$E_0^{\text{HF}} = \sum_{\mathbf{k}} \left(f_{\mathbf{k}+} \left(\epsilon_{\mathbf{k}} - \frac{U}{2}(N_+ - N_-) \right) + f_{\mathbf{k}-} \left(\epsilon_{\mathbf{k}} + \frac{U}{2}(N_+ - N_-) \right) \right) + \frac{U}{4} ((N_+ - N_-)^2 - n^2) \quad (6.97)$$

with the Fermi distribution function $f_{\mathbf{k}\pm}$. The sums over the band energies are carried out by assuming the free electron dispersion $\epsilon_{\mathbf{k}} = \hbar^2 k^2 / 2m$ and $T = 0$ to give

$$\sum_{\mathbf{k}} f_{\mathbf{k}\pm} \epsilon_{\mathbf{k}} = \frac{3}{5} N_{\pm} E_F(N_{\pm}). \quad (6.98)$$

Using the corresponding results from Sect. 4.4 but with $E_F(N_{\pm}) = 2^{2/3} E_F(N)$, because of single occupancy of the states in \mathbf{k} space with spin aligned electrons, the total energy in HF approximation is

$$E_0^{\text{HF}}(N_+, N_-) = \frac{3}{5} (N_+ E_F(N_+) + N_- E_F(N_-)) - \frac{U}{4} ((N_+ - N_-)^2 + N^2). \quad (6.99)$$

We are interested in the dependence on the degree of spin polarization $\zeta = (N_+ - N_-)/N$, and replace N_{\pm} according to

$$N_{\pm} = \frac{1}{2} N(1 \pm \zeta), \quad (6.100)$$

which gives for the mean energy per particle

$$\begin{aligned}\epsilon^{\text{HF}}(N, \zeta) &= \frac{E_0^{\text{HF}}(N_+) + E_0^{\text{HF}}(N_-)}{N} \\ &= \frac{3}{5} \frac{E_F}{2} ((1 + \zeta)^{5/3} + (1 - \zeta)^{5/3}) - \frac{UN}{4} (\zeta^2 - 1).\end{aligned}\quad (6.101)$$

A minimum of $\epsilon^{\text{HF}}(N, \zeta)$ at finite ζ would indicate the existence of a stable ferromagnetic state. This condition leads to the relation

$$\frac{UN}{E_F} \zeta = (1 + \zeta)^{2/3} - (1 - \zeta)^{2/3}, \quad 0 \leq \zeta \leq 1. \quad (6.102)$$

The *rhs* is a monotonous function, starting for $\zeta = 0$ at zero with a slope of $4/3$ and reaching for $\zeta = 1$ the value $2^{2/3}$ with infinite slope. With respect to (6.102) three situations are possible:

- (a) $UN/E_F < 4/3$, the relation has no solution for finite ζ , which leads to a stable paramagnetic state,
- (b) $4/3 < UN/E_F < 2^{2/3}$, there exists a solution for $0 < \zeta < 1$ representing a stable ferromagnetic state, with partial spin polarization,
- (c) $2^{2/3} < UN/E_F$, there is always a solution with $\zeta = 1$ representing a ferromagnet with perfect alignment of all spins.

The ratio N/E_F is proportional to the density of states at the Fermi energy $D(E_F)$, thus the existence of ferromagnetism in a system of itinerant electrons is ruled by the competition between $D(E_F)$ (which is determined by the dispersion) and the strength of the exchange energy U . If, for the given U , the width of the energy band increases, i.e. $D(E_F)$ decreases, the criterion (c) or even (b) will be missed and ferromagnetism will not be realized. Thus, the Stoner model provides with the criterion (a), the *Stoner condition*, a clear answer with respect to the existence of ferromagnetism for itinerant electrons.

Besides the existence of magnetic order the other basic property of a spin system is the excitation spectrum out of the ground state. In Chap. 4 it was the dielectric function which has led us to the excitation spectrum of the free interacting electrons consisting of single-particle (or electron-hole) and collective excitations (the plasmons). For the latter, it was necessary to employ the random phase approximation. We remember that the inverse dielectric function is a density-density correlation function. Here, we want to put the emphasis on spin-flip excitations. The corresponding response function is the magnetic or spin susceptibility, which is a correlation function between components of the magnetic dipole density. The observable of interest here is the magnetization related to spins \mathbf{S}_l of electrons at \mathbf{r}_l

$$\mathbf{M}(\mathbf{r}) = \frac{\mathbf{m}(\mathbf{r})}{V} = g\mu_B \sum_l \mathbf{S}_l \delta(\mathbf{r} - \mathbf{r}_l) \quad (6.103)$$

as introduced already in Sect. 2.5. This quantity can be addressed by a magnetic field with the interaction term $V_{\text{ext}}(t) = -\mathbf{m} \cdot \mathbf{B}(t)$. Spin flips are caused

by the ladder operators S^\pm , which for a spin-1/2 system are expressed in terms of Pauli spin matrices as

$$S_+ = (\sigma_x + i\sigma_y)/2 = \begin{pmatrix} 0 & 1 \\ 0 & 0 \end{pmatrix}, \quad S_- = (\sigma_x - i\sigma_y)/2 = \begin{pmatrix} 0 & 0 \\ 1 & 0 \end{pmatrix}. \quad (6.104)$$

In the following we assume $B_z = 0$ and choose the appropriate decomposition of the external perturbation

$$V_{\text{ext}}(t) = -(m_+ B_- e^{-i\omega t} + m_- B_+ e^{i\omega t}) \quad (6.105)$$

which describes the interaction with a rotating magnetic field in the xy plane. The observable we are interested in here is $M_+ = m_+/V$. It is related to the susceptibility responsible for spin-flip processes

$$\chi_{+-}^M(\mathbf{q}, \omega) = \frac{i}{\hbar} \int_{-\infty}^{+\infty} e^{i\omega\tau} \Theta(\tau) \langle [M_+(\mathbf{q}, \tau), M_-(-\mathbf{q}, 0)] \rangle_0 d\tau. \quad (6.106)$$

This correlation function, which has the same structure as (2.61), can be evaluated in the occupation number representation. In terms of fermion operators for the Bloch electrons we have

$$M_+(\mathbf{q}) = g\mu_B \sum_{\mathbf{k}} c_{\mathbf{k}+\mathbf{q}\uparrow}^\dagger c_{\mathbf{k}\downarrow}, \quad M_-(-\mathbf{q}) = g\mu_B \sum_{\mathbf{k}} c_{\mathbf{k}-\mathbf{q}\downarrow}^\dagger c_{\mathbf{k}\uparrow}, \quad (6.107)$$

which are spin-density fluctuations (multiplied by $g\mu_B$). We evaluate the expectation value under the integral for $T = 0$ with the eigenstates of the HF Hamiltonian (6.96) analogous to the calculation of the inverse dielectric function in Sect. 4.5 but consider the spin splitting of the HF single-particle energies $\epsilon_{\mathbf{k}\pm} = \epsilon_{\mathbf{k}} \mp \Delta/2$ and obtain as the HF result for the spin susceptibility (Problem 6.11)

$$\chi_{+-}^0(\mathbf{q}, \omega) = \lim_{\delta \rightarrow 0} g^2 \mu_B^2 \sum_{\mathbf{k}} \frac{f_{\mathbf{k}\downarrow} - f_{\mathbf{k}+\mathbf{q}\uparrow}}{\hbar\omega + \epsilon_{\mathbf{k}+\mathbf{q}\uparrow} - \epsilon_{\mathbf{k}\downarrow} + i\delta}. \quad (6.108)$$

It resembles the polarization function $\pi_0(\mathbf{q}, \omega)$ in the HF result for the inverse dielectric function (see (4.122)). Its poles (in the lower half of the complex energy plane) mark the particle-hole excitations with spin flip, the *Stoner continuum* depicted in Fig. 6.12. For $\mathbf{q} = 0$, excitations are possible only for $\hbar\omega = \Delta$, because the two bands are shifted against each other by the exchange energy (see Fig. 6.11). With increasing \mathbf{q} , spin-flip excitations become possible for a continuum with increasing width. In Fig. 6.12, two situations are shown. If Δ is smaller than E_F the continuum reaches down to vanishing excitation energies, for which spin-flip excitations are possible in the interval $k_F^+ - k_F^- < q < k_F^+ + k_F^-$ as can be checked also with Fig. 6.11. This situation is called *weak ferromagnetic case*. In the *strong ferromagnetic case*, $E_F < \Delta$, single-particle excitations with spin flip are possible only for finite excitation energy.

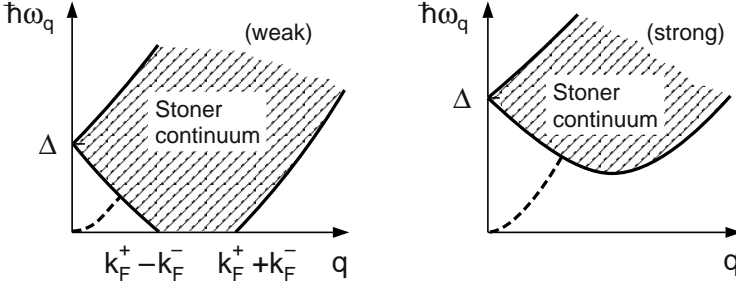


Fig. 6.12. Spectra of single-particle (Stoner continuum) and collective excitations with spin-flip for a weak (*left*) and a strong (*right*) ferromagnet

These results can be compared with those of the dielectric function for the free electron system in Sect. 4.5. There we have obtained the single-particle or electron-hole excitations (without spin flip) in the HF approximation. As we know from the discussion of the dielectric function, this approximation does not yield the collective charge-density excitations (or plasmons) for which we had to go beyond HF to the RPA. It consisted in replacing the free polarization function $\pi_0(\mathbf{q}, \omega)$ by $\pi_0(\mathbf{q}, \omega)/(1 - v_{\mathbf{q}}\pi_0(\mathbf{q}, \omega))$. The corresponding replacement is possible here by identifying $\pi_0(\mathbf{q}, \omega)$ with $\tilde{\chi}_{+-}^0(\mathbf{q}, \omega) = \chi_{+-}^0(\mathbf{q}, \omega)/g^2\mu_B^2$ and $v_{\mathbf{q}}$ with the exchange interaction U . Thus the RPA result for the spin susceptibility is easily obtained as

$$\chi_{+-}^M(\mathbf{q}, \omega) = g^2\mu_B^2 \frac{\tilde{\chi}_{+-}^0(\mathbf{q}, \omega)}{1 - U\tilde{\chi}_{+-}^0(\mathbf{q}, \omega)}. \quad (6.109)$$

Besides the poles of single-particle excitations of $\chi_{+-}^0(\mathbf{q}, \omega)$, the RPA susceptibility has an additional pole due to the vanishing denominator,

$$1 - U\tilde{\chi}_{+-}^0(\mathbf{q}, \omega) = 0, \quad (6.110)$$

giving the collective excitations of the spin system, the magnons.

In order to find the magnon dispersion, we have, in a first step, to evaluate $\tilde{\chi}_{+-}^0(\mathbf{q}, \omega)$ under the conditions of collective excitations outside of the Stoner continuum, which we expect to occur for $\hbar\omega \ll \Delta$ and at small \mathbf{q} . Then we have, using the solution of Problem 6.11

$$\begin{aligned} \tilde{\chi}_{+-}^0(\mathbf{q}, \omega) = & \frac{V}{6\pi^2} \frac{1}{\hbar\omega - \Delta + \epsilon_q} \left(k_F^{+3} + \frac{k_F^{+5}}{5m} \left(\frac{\hbar^2 q}{\hbar\omega - \Delta + \epsilon_q} \right)^2 \right) \\ & - \frac{V}{6\pi^2} \frac{1}{\hbar\omega - \Delta - \epsilon_q} \left(k_F^{+3} + \frac{k_F^{+5}}{5m} \left(\frac{\hbar^2 q}{\hbar\omega - \Delta - \epsilon_q} \right)^2 \right) \end{aligned} \quad (6.111)$$

with $\epsilon_q = \hbar^2 q^2 / 2m$. We substitute this result in (6.110) and find

$$1 - \frac{UV}{6\pi^2} \left\{ \frac{k_F^{-3}}{\hbar\omega - \Delta + \epsilon_q} - \frac{k_F^{+3}}{\hbar\omega - \Delta - \epsilon_q} + \frac{\hbar^4 q^2}{5m^2} \left(\frac{k_F^{+5}}{(\hbar\omega - \Delta + \epsilon_q)^3} - \frac{k_F^{-5}}{(\hbar\omega - \Delta - \epsilon_q)^3} \right) \right\} = 0. \quad (6.112)$$

Being interested in the leading order term in q , we expand the denominators of the first two terms in the bracket with $\Delta \ll \hbar\omega \pm \epsilon_q$ but neglect the small terms in the dominators of the last terms, which are already proportional to q^2 . Making use of the relation

$$\frac{1}{\Delta} \left(k_F^{+3} - k_F^{-3} \right) = \frac{6\pi^2}{UV} \quad (6.113)$$

the condition for the magnon pole simplifies and can be solved for the magnon energy

$$\hbar\omega_q \simeq \frac{\hbar^2 q^2}{2m} \left\{ \frac{k_F^{+3} + k_F^{-3}}{k_F^{+3} - k_F^{-3}} - \frac{2\hbar^2}{5m\Delta} \frac{k_F^{+5} - k_F^{-5}}{k_F^{+3} - k_F^{-3}} \right\}. \quad (6.114)$$

With $k_F^{\pm 3} = k_F^3(1 \pm \zeta)$ and $\Delta = UN\zeta$ this reduces to

$$\hbar\omega_q \simeq \frac{\hbar^2 q^2}{2m\zeta} \left\{ 1 - \frac{2E_F}{5UN} \frac{(1 + \zeta)^{5/3} - (1 - \zeta)^{5/3}}{\zeta} \right\}. \quad (6.115)$$

We find the characteristic q^2 dependence giving a dispersion of the ferromagnetic magnons (see Sect. 6.3) separated from the Stoner continuum as indicated in Fig. 6.12. The magnon dispersion of Fe, measured with inelastic neutron scattering, is shown in Fig. 6.13. It follows more or less that this q^2 law is almost independent of the direction of propagation. With increasing q the magnon dispersion becomes degenerate with the Stoner continuum and decays into single-particle excitations with spin-flip. This situation resembles that of the collective charge density excitations (plasmons, see Sect. 4.6) when they become degenerate with the particle-hole continuum of the free electron gas and decay into particle-hole excitations.

The curvature of the magnon dispersion depends on the relation between density of states (or Fermi energy over N) and interaction strength U . For, complete spin polarization $\zeta = 1$, (6.115) simplifies to

$$\hbar\omega_q(\zeta = 1) = \frac{\hbar^2 q^2}{2m} \left\{ 1 - \frac{2E_F}{5UN} 2^{5/3} \right\} \quad (6.116)$$

while for small spin polarization $\zeta \ll 1$ we have

$$\hbar\omega_q(\zeta \ll 1) = \frac{\hbar^2 q^2}{2m\zeta} \left\{ 1 - \frac{4E_F}{3UN} \right\}. \quad (6.117)$$

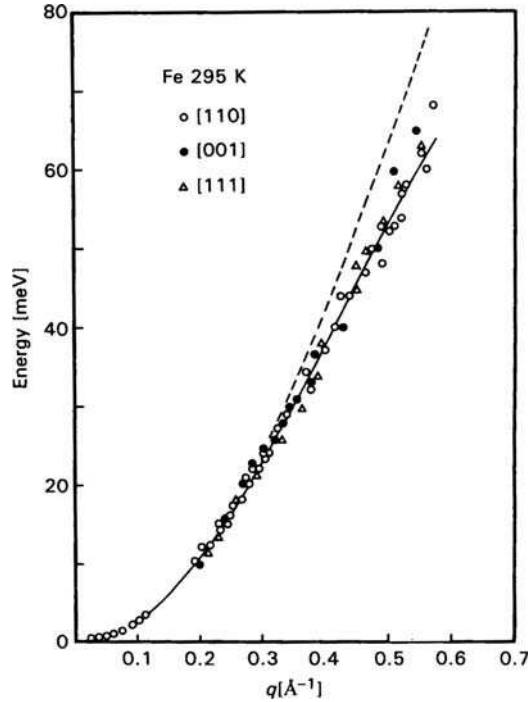


Fig. 6.13. Magnon dispersion of ferromagnetic Fe from inelastic neutron scattering after [186]. The dashed line represents the quadratic dispersion

In this limit ω_q is positive if

$$\frac{UN}{E_F} > \frac{4}{3}. \tag{6.118}$$

Thus, we arrive at the consistent result that collective spin excitations are possible if according to the Stoner condition ferromagnetism and finite spin polarization exist.

Problems

- 6.1 Derive the expression for the matrix element of the electron–electron interaction $V_{\alpha\beta\beta'\alpha'}$ in the general case! Make use of the Fourier expansion of products of the periodic parts of the Bloch functions. Simplify to the single-band case and use only the leading term of this Fourier expansion.
- 6.2 Make use of the orthogonality and normalization of the Bloch functions $\psi_{n\mathbf{k}\sigma}(\mathbf{r})$ to show that

$$\phi_{n\sigma}(\mathbf{r} - \mathbf{R}) = \frac{1}{\sqrt{N}} \sum_{\mathbf{k}} e^{-i\mathbf{k}\cdot\mathbf{R}} \psi_{n\mathbf{k}\sigma}(\mathbf{r}) \tag{6.119}$$

are normalized and that they are orthogonal when centered around different sites \mathbf{R} (Wannier representation)! Derive the commutation relations of $c_{n\mathbf{R}\sigma}, c_{n'\mathbf{R}'\sigma'}^\dagger$ from those of the Bloch states!

- 6.3 Express the interaction matrix element of Problem 6.1 in the Wannier representation with localized atomic orbitals for the single-band case to obtain (6.10)!
- 6.4 Show that the set of operators $c_\uparrow^\dagger c_\downarrow, c_\downarrow^\dagger c_\uparrow$, and $c_\uparrow^\dagger c_\uparrow - c_\downarrow^\dagger c_\downarrow$ fulfills the same commutation relations as the components of the spin-1/2 operators. Make use of the fermion commutation rules for $c_\sigma^\dagger, c_\sigma$!
- 6.5 Derive the equation of motion (6.32) for the spin operator \mathbf{S}_j determined by the Heisenberg Hamiltonian (6.23)!
- 6.6 Given are the commutation rules for the boson operators $b_{i\mathbf{k}}, b_{i\mathbf{k}}, i = 1, 2$ for the magnons in the two sublattices of an anti-ferromagnet. Verify the commutation relations (6.58) for the Boson operators $\alpha_{\mathbf{k}}, \beta_{\mathbf{k}}$ obtained by the Bogoliubov transformation (6.57)!
- 6.7 The Hamiltonian of a solid, in which the simultaneous presence of phonons and magnons shall be studied, can be written as

$$H_{\text{p-m}} = \sum_{\mathbf{k}} \left\{ \hbar\omega_{\mathbf{k}}^{\text{p}} a_{\mathbf{k}}^\dagger a_{\mathbf{k}} + \hbar\omega_{\mathbf{k}}^{\text{m}} b_{\mathbf{k}}^\dagger b_{\mathbf{k}} + c_{\mathbf{k}} (a_{\mathbf{k}} b_{\mathbf{k}}^\dagger + a_{\mathbf{k}}^\dagger b_{\mathbf{k}}) \right\}, \quad (6.120)$$

where $\omega_{\mathbf{k}}^{\text{p}}(\omega_{\mathbf{k}}^{\text{m}})$ is the phonon(magnon) dispersion and $a, a^\dagger(b, b^\dagger)$ are the boson operators for phonons(magnons). The coupling between both elementary excitations is described by the bilinear term with the coupling constant $c_{\mathbf{k}}$. Make use of the following variant of the Bogoliubov transformation to eliminate the coupling (with real $\Theta_{\mathbf{k}}$):

$$a_{\mathbf{k}} = \alpha_{\mathbf{k}} \cos \Theta_{\mathbf{k}} + \beta_{\mathbf{k}} \sin \Theta_{\mathbf{k}}, \quad b_{\mathbf{k}} = \beta_{\mathbf{k}} \cos \Theta_{\mathbf{k}} - \alpha_{\mathbf{k}} \sin \Theta_{\mathbf{k}} \quad (6.121)$$

and express $\Theta_{\mathbf{k}}$ (or a function of $\Theta_{\mathbf{k}}$) by the coupling constant and the frequencies $\omega_{\mathbf{k}}^{\text{p}}(\omega_{\mathbf{k}}^{\text{m}})$! Discuss the solution, especially for $\omega_{\mathbf{k}}^{\text{p}} = \omega_{\mathbf{k}}^{\text{m}}$, and give the eigenfrequencies of the new collective magnon-phonon modes and how their boson operators are composed of the original phonon and magnon operators!

- 6.8 Replace in (6.56) the spin wave operators for the sublattices with the help of the Bogoliubov transformation to get the Hamiltonian (6.60)!
- 6.9 In order to remove the degeneracy of the anti-ferromagnetic magnons, introduce a weak anisotropy field H_{a} in the Hamiltonian (6.53) acting with opposite sign on the two sublattices, and an external magnetic field. How does this change the dispersion relation for the anti-ferromagnetic magnons? Discuss the frequency in the long wavelength limit $\mathbf{k} \rightarrow 0$ and sketch the result to show the effect of the anisotropy field!
- 6.10 Calculate the temperature dependence of $M(T) - M(0)$ for $T \ll T_{\text{C}}$ in the spin-wave approximation and verify Bloch's $T^{3/2}$ law!

- 6.11 Derive the expression (6.108) of the spin susceptibility in HF approximation $\chi_{+-}^0(\mathbf{q}, \omega)$ at $T = 0$! The calculation is strictly analogous to that performed in Sect. 4.5 to obtain the HF result for the inverse dielectric function. Evaluate the formula by assuming a single-particle dispersion of the form $\epsilon_{\mathbf{k}\sigma} = \hbar^2 k^2 / 2m - \sigma \Delta / 2$ with $\Delta = U(N_+ - N_-)$! Make use of the fact that Δ is the dominating quantity, i.e. $\Delta \gg \hbar\omega, \hbar^2 q^2 / 2m$!

Correlated Electrons

In Sect. 4.7, we have studied in some detail the correlation effects for the homogeneous free electron system and figured out their dependence on the electron density. Correlation has been considered in the effective single-particle potential for crystal electrons within the density-functional theory (DFT), which has led to the independent particle description of the electronic band structure in Chap. 5. In Chap. 6, we have stressed the importance of the exchange interaction and of the electron spin for magnetic properties. The aim of this chapter is to introduce concepts of treating correlation effects for electrons in a crystalline surrounding beyond the independent particle picture in a more general sense. One aspect will be to describe model systems, which allow to demonstrate correlation effects [122, 193–196]. The motivation comes from the observation that some group of solids, namely those with the Fermi energy within narrow bands deriving from d or f electrons, exhibit properties which cannot be understood within the single-particle band structure. Among those are besides the magnetic properties (Chap. 6), the insulating behavior of some transition metal oxides, and the heavy fermion effects in compounds of lanthanides and actinides. Another aspect is the quasi-particle concept in the context of the Fermi liquid theory and the deviations from Fermi liquid behavior in systems with reduced dimension [197–201]. Finally, we would like to address also correlation in two-dimensional electron systems in high magnetic fields, known as the fractional quantum Hall regime [202–204].

As in Chap. 6, we start from the N electron Hamiltonian (see (6.5))

$$\mathcal{H} = \sum_{\alpha} \epsilon_{\alpha} c_{\alpha}^{\dagger} c_{\alpha} + \frac{1}{2} \sum_{\alpha\beta\alpha'\beta'} V_{\alpha\beta\beta'\alpha'} c_{\alpha}^{\dagger} c_{\beta}^{\dagger} c_{\alpha'} c_{\beta'}, \quad (7.1)$$

where α, β, α' , and β' are complete sets of single-particle quantum numbers, $\alpha = n\mathbf{k}\sigma$, and ϵ_{α} the corresponding energy values. The matrix elements of the electron–electron interaction

$$V_{\alpha\beta\beta'\alpha'} = \int dx \int dx' \psi_{\alpha}^{\dagger}(x) \psi_{\beta}^{\dagger}(x') \frac{e^2}{4\pi\epsilon_0 |x - x'|} \psi_{\beta'}(x) \psi_{\alpha'}(x') \quad (7.2)$$

can be expressed in terms of the wave functions $\psi_\alpha(x)$, where x stands for space and spin coordinates. We shall separate the Hamiltonian (7.1) according to $\mathcal{H} = \mathcal{H}_{\text{sp}} + \mathcal{H}_{\text{int}}$ into the single-particle and the interaction part. In the context of this chapter, the latter accounts for electrons in partially filled bands only, while the interaction of all other electrons is considered as before in the effective single-particle potential leading to the energy values ϵ_α .

7.1 Retarded Green Function for Electrons

In this section, we introduce the concept of the Green function for electrons, which is advantageous in describing electronic properties of the interacting electrons [64, 205, 206]. In general, a *retarded Green function* is an object defined by (compare with (2.82))

$$G_{AB}^{\text{ret}}(t, t') = -\frac{i}{\hbar}\theta(t-t')\langle[\hat{A}(t), \hat{B}(t')]_{\pm}\rangle, \quad (7.3)$$

where $\langle \dots \rangle$ denotes the thermal expectation value as defined in Sect. 2.32.3 and

$$[\hat{A}(t), \hat{B}(t')]_{\pm} = \hat{A}(t)\hat{B}(t') \pm \hat{B}(t')\hat{A}(t). \quad (7.4)$$

The $+$ ($-$) sign applies if the operators $\hat{A}(t)$ and $\hat{B}(t')$ are fermion(boson) operators. In Sect. 2.6, we have already identified the response function, which is a correlation function for observables, as a special type of retarded Green function. In the context of this chapter, the choice of the operators,

$$\hat{A}(t) = c_\alpha(t) \quad \text{and} \quad \hat{B}(t') = c_\alpha^\dagger(t'), \quad (7.5)$$

will be a creation and an annihilation operator of an electron in a single-particle state with quantum numbers α . Thus, the Green function (we use as before $\{\dots, \dots\}$ for the anti-commutator $[\dots, \dots]_+$)

$$G(\alpha; t, t') = -\frac{i}{\hbar}\theta(t-t')\langle\{c_\alpha(t), c_\alpha^\dagger(t')\}\rangle \quad (7.6)$$

is the probability amplitude to find the particle created at time t' in the state α at a later time $t > t'$ still in the same state. It describes the propagation of an electron in the state α from t' to t and is, therefore, called a *propagator*.

In order to calculate the Green function (7.6), we formulate the equation of motion by taking the derivative with respect to the time argument t . It can be written as

$$\begin{aligned} i\hbar \frac{\partial G(\alpha; t, t')}{\partial t} &= \frac{\partial \theta(t-t')}{\partial t} \langle\{c_\alpha(t), c_\alpha^\dagger(t')\}\rangle \\ &\quad - \frac{i}{\hbar}\theta(t-t') \left\langle \left\{ i\hbar \frac{\partial c_\alpha(t)}{\partial t}, c_\alpha^\dagger(t') \right\} \right\rangle. \end{aligned} \quad (7.7)$$

With

$$\frac{\partial \theta(t-t')}{\partial t} = \delta(t-t'), \quad \{c_\alpha(t), c_\alpha^\dagger(t)\} = 1, \quad (7.8)$$

and the equation of motion for $c_\alpha(t)$

$$i\hbar \frac{\partial c_\alpha(t)}{\partial t} = [c_\alpha(t), \mathcal{H}] \quad (7.9)$$

(here $[\dots, \dots]$ denotes the commutator $[\dots, \dots]_-$) this can be cast into the form

$$i\hbar \frac{\partial G(\alpha; t, t')}{\partial t} = \delta(t-t') - \frac{i}{\hbar} \theta(t-t') \langle \{ [c_\alpha(t), \mathcal{H}], c_\alpha^\dagger(t') \} \rangle. \quad (7.10)$$

The second term on the *rhs* has again the form (7.3) of a retarded Green function, but it has a more complex form. As it will turn out, it contains in general more than two fermion operators due to the electron–electron interaction. One could also formulate, for this higher order Green function, an equation of motion with a similar structure but with an even more complex Green function, and so forth. This is a generic hierarchy problem typical for interacting systems. Concepts of many-particle physics focus on finding for this problem approximate solutions, essentially by truncating the hierarchy at some level.

To become acquainted with the concept of Green functions, let us first look for the simplest solution of (7.10) which can be given for the noninteracting electrons, i.e., by considering the Hamiltonian

$$\mathcal{H}_{\text{sp}} = \sum_{\alpha'} \epsilon_{\alpha'} c_{\alpha'}^\dagger c_{\alpha'}. \quad (7.11)$$

Evaluation of the commutator yields

$$[c_\alpha(t), \mathcal{H}_{\text{sp}}] = e^{\frac{i}{\hbar} \mathcal{H}_{\text{sp}} t} \sum_{\alpha'} \epsilon_{\alpha'} [c_\alpha, c_{\alpha'}^\dagger c_{\alpha'}] e^{-\frac{i}{\hbar} \mathcal{H}_{\text{sp}} t} = \epsilon_\alpha c_\alpha(t). \quad (7.12)$$

Here, we have used the fact that the time argument of all operators is the same and determined by \mathcal{H}_{sp} and that the commutation relation for the fermion operators yields $[c_\alpha, c_{\alpha'}^\dagger c_{\alpha'}] = c_{\alpha'} \delta_{\alpha, \alpha'}$. The equation of motion for the Green function $G^{(0)}(\alpha; t, t')$ of the noninteracting electron

$$\left(i\hbar \frac{\partial}{\partial t} - \epsilon_\alpha \right) G^{(0)}(\alpha; t, t') = \delta(t-t') \quad (7.13)$$

can be easily integrated to obtain

$$G^{(0)}(\alpha; t, t') = -\frac{i}{\hbar} \theta(t-t') e^{-\frac{i}{\hbar} \epsilon_\alpha (t-t')}. \quad (7.14)$$

After carrying out the Fourier transformation (note the time dependence $t-t' = \tau$)

$$G^{(0)}(\alpha, \omega) = \int_{-\infty}^{+\infty} e^{\frac{i}{\hbar}(\hbar\omega + i\delta)\tau} G^{(0)}(\alpha, \tau) d\tau, \quad (7.15)$$

we find the characteristic form of the Green function (with $E = \hbar\omega$)

$$G^{(0)}(\alpha, E) = \lim_{\delta \rightarrow 0} \frac{1}{E - \epsilon_\alpha + i\delta}, \quad (7.16)$$

where the small δ has been introduced to yield, in the back transform again, the retarded Green function. It has a pole in the lower complex energy (or frequency) plane close to the real axis at the single-particle energy ϵ_α . (Compare with the response function for the optical phonons in Sect. 3.5 or with the inverse dielectric function in Sect. 4.5 which exhibit similar structures.) Making use of the relation

$$\lim_{\delta \rightarrow 0} \frac{1}{E - \epsilon_\alpha + i\delta} = \mathcal{P} \left(\frac{1}{E - \epsilon_\alpha} \right) - i\pi\delta(E - \epsilon_\alpha), \quad (7.17)$$

one finds the density of states

$$D(E) = \frac{1}{\pi} \text{Tr} \left(\text{Im} G^{(0)}(\alpha, E) \right) = \sum_{\alpha} \delta(E - \epsilon_\alpha). \quad (7.18)$$

Let us include now the electron–electron interaction for the special case of electrons in a partially filled energy band. For this case, the band index can be dropped, and α is specified by the wave vector \mathbf{k} and the spin σ of the electron (see Problem 6.1). The commutator of $c_{\mathbf{k}\sigma}$ with the interaction term

$$\mathcal{H}_{\text{int}} = \frac{1}{2} \sum_{\substack{\mathbf{k}\mathbf{k}'\mathbf{q} \\ \sigma\sigma'}} V(\mathbf{k}, \mathbf{k}', \mathbf{q}) c_{\mathbf{k}+\mathbf{q}\sigma}^\dagger c_{\mathbf{k}'-\mathbf{q}\sigma'}^\dagger c_{\mathbf{k}'\sigma'} c_{\mathbf{k}\sigma} \quad (7.19)$$

can be calculated as Problem 7.1 and yields

$$[c_{\mathbf{k}\sigma}, \mathcal{H}_{\text{int}}] = \sum_{\mathbf{k}'\mathbf{q}\sigma'} V(\mathbf{k}', \mathbf{k} + \mathbf{q}, \mathbf{q}) c_{\mathbf{k}'+\mathbf{q}\sigma'}^\dagger c_{\mathbf{k}'\sigma'} c_{\mathbf{k}+\mathbf{q}\sigma}. \quad (7.20)$$

The equation of motion for the Green function is now

$$\left(i\hbar \frac{\partial}{\partial t} - \epsilon_{\mathbf{k}\sigma} \right) G(\mathbf{k}\sigma; t, t') = \delta(t - t') + \sum_{\substack{\mathbf{k}'\mathbf{q} \\ \sigma}} V(\mathbf{k}', \mathbf{k} + \mathbf{q}, \mathbf{q}) \Gamma(\mathbf{k}\sigma, \mathbf{k}'\sigma'; t, t') \quad (7.21)$$

where

$$\Gamma(\mathbf{k}\sigma, \mathbf{k}'\sigma'; t, t') = -\frac{i}{\hbar} \theta(t - t') \langle \{ c_{\mathbf{k}'+\mathbf{q}\sigma'}^\dagger(t) c_{\mathbf{k}'\sigma'}(t) c_{\mathbf{k}+\mathbf{q}\sigma}(t), c_{\mathbf{k}\sigma}^\dagger(t') \} \rangle \quad (7.22)$$

is a higher order Green function. It is convenient to introduce, by means of

$$\sum_{\substack{\mathbf{k}' \\ \sigma'}} V(\mathbf{k}', \mathbf{k} + \mathbf{q}, \mathbf{q}) \Gamma(\mathbf{k}\sigma, \mathbf{k}'\sigma'; t, t') = \int \Sigma(\mathbf{k}\sigma; t, t'') G(\mathbf{k}\sigma; t'', t') dt'', \quad (7.23)$$

the single-particle *self-energy* $\Sigma(\mathbf{k}\sigma; t, t')$. If the Hamiltonian does not depend on t , we can exploit the homogeneity of the time, because the Green functions depend only on the time difference and perform the Fourier transformation to obtain

$$G(\alpha, E) = \lim_{\delta \rightarrow 0} \frac{1}{E - \epsilon_\alpha - \Sigma(\alpha, E) + i\delta}. \quad (7.24)$$

This is the same structure as for the Green function without interaction, but now in addition to the single-particle energy there is a self-energy correction, which in general depends on E and changes the pole structure. Thus, (7.24) indicates the structure of the Green function. However, the problem of including the electron–electron interaction is still to be accomplished by calculating the self-energy and to find the poles of the Green function. For the concepts, how this can be done in a systematic way, we refer to the literature [64].

The Green function of the noninteracting particle (7.16) is related to that of the full Green function (7.24) by the *Dyson¹ equation*

$$G = G^{(0)} + G^{(0)} \Sigma G, \quad (7.25)$$

known from scattering theory. It can be obtained also by taking the Fourier transform of (7.21) together with (7.23) (Problem 7.2).

We may look for approximate calculations of the self-energy and do this for $T = 0$, for which the thermal expectation value reduces to the expectation value in the system ground state (see Problem 2.2). The Green function (7.22) can be approximated with the following replacements

$$\begin{aligned} c_{\mathbf{k}'+\mathbf{q}\sigma'}^\dagger(t) c_{\mathbf{k}'\sigma'}(t) c_{\mathbf{k}+\mathbf{q}\sigma}(t) &\rightarrow \langle c_{\mathbf{k}'+\mathbf{q}\sigma'}^\dagger(t) c_{\mathbf{k}'\sigma'}(t) \rangle c_{\mathbf{k}+\mathbf{q}\sigma}(t) \\ &\quad - \langle c_{\mathbf{k}'+\mathbf{q}\sigma'}^\dagger(t) c_{\mathbf{k}+\mathbf{q}\sigma}(t) \rangle c_{\mathbf{k}'\sigma'}(t), \end{aligned} \quad (7.26)$$

which is a factorization of the three-fermion term into an expectation value and a single-fermion term. The former yields the occupation number $n_{\mathbf{k}'\sigma'}$ if $\mathbf{q} = 0$ and $n_{\mathbf{k}+\mathbf{q}\sigma}$ provided $\mathbf{k}' = \mathbf{k}$, and $\sigma' = \sigma$, while the latter combines with the rest of (7.22) to the Green function $G(\alpha; t, t')$. The corresponding expressions for the self-energy, which do not depend on the time arguments, are

$$\Sigma^H(\mathbf{k}\sigma) = \sum_{\mathbf{k}'\sigma'} V(\mathbf{k}, \mathbf{k}', \mathbf{0}) n_{\mathbf{k}'\sigma'}, \quad (7.27)$$

¹ Freeman John Dyson *1923.

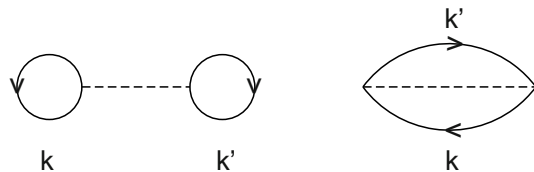


Fig. 7.1. Graphs of the Hartree and Hartree–Fock self-energies

which is the *Hartree self-energy*, and

$$\Sigma^{\text{HF}}(\mathbf{k}\sigma) = - \sum_{\mathbf{k}'\mathbf{q}} V(\mathbf{k}, \mathbf{k}', \mathbf{q}) n_{\mathbf{k}'+\mathbf{q}\sigma}, \quad (7.28)$$

which is the *Hartree–Fock self-energy*. There is a quite intuitive graphical representation of these self-energies (Fig. 7.1): Both graphs are obtained from the interaction graph (see Fig. 4.10) by connecting incoming and outgoing fermion lines, which is possible in just two distinct ways, leading to the Hartree and Hartree–Fock self-energy.

For free electrons, the potential matrix element simplifies according to $V_{\mathbf{k}\mathbf{k}'\mathbf{q}} \rightarrow v_{\mathbf{q}}$, where $v_{\mathbf{q}}$ is the Fourier transform of the bare Coulomb potential and we may compare with the results obtained in the jellium model of Chap. 4. In this case, the Hartree self-energy vanishes, because the contribution for $\mathbf{q} = 0$ is exempt from the summation in the interaction term due to compensation with the jellium term and the Hartree–Fock self-energy becomes the one calculated in Sect. 4.4.

Let us finally reformulate the denominator of the Green function for interacting particles close to the chemical potential with $E \simeq \mu$. Making use of the expansion

$$\Sigma(\alpha, E) \simeq \Sigma(\alpha, \mu) + \left. \frac{\partial \Sigma}{\partial E} \right|_{E=\mu} (E - \mu), \quad (7.29)$$

the denominator of the retarded Green function (7.24) takes the form

$$E - \epsilon_{\alpha} - \Sigma(\alpha, E) \simeq (E - \mu) \left(1 - \left. \frac{\partial \Sigma}{\partial E} \right|_{E=\mu} \right) - (\epsilon_{\alpha} - \mu + \Sigma(\alpha, \mu)) \quad (7.30)$$

and the Green function can be written as

$$G(\alpha, E) = \frac{Z(\alpha)}{E - \mu - \tilde{\epsilon}_{\alpha} - i\gamma_{\alpha}}. \quad (7.31)$$

Here, we introduce

$$Z^{-1}(\alpha) = 1 - \left. \frac{\partial \Sigma}{\partial E} \right|_{E=\mu} \quad (7.32)$$

$$\tilde{\epsilon}_{\alpha} = Z(\alpha) (\epsilon_{\alpha} - \mu + \text{Re}\Sigma(\alpha, \mu)) \quad (7.33)$$

$$\gamma_{\alpha} \simeq Z(\alpha) \text{Im}\Sigma(\alpha, \tilde{\epsilon}_{\alpha}). \quad (7.34)$$

Due to the interaction, the pole of the Green function is now at the energy $\tilde{\epsilon}_\alpha + i\gamma_\alpha$ and has the spectral weight $Z(\alpha)$, which equals 1 if the self-energy does not depend on the energy, as is the case for the Hartree and Hartree–Fock approximation. The pole is in the lower (upper) half plane of complex energies depending on the sign of $E - \mu$ and corresponds to a quasi-particle (quasi-hole). We shall come back to this result in Sect. 7.3. Here, we note only that the Fourier back transformation leads to a time-dependent propagator of the form (see [122], Sect. 10)

$$G(\alpha; t - t') = -\frac{i}{\hbar} Z(\alpha) \theta(t - t') e^{-(i\tilde{\epsilon}_\alpha + \gamma_\alpha)(t - t')/\hbar}. \quad (7.35)$$

The imaginary part of the self-energy indicates a finite lifetime of the quasi-particle or quasi-hole due to particle–particle interaction. A closer inspection shows a decrease of the lifetime with increasing distance from the chemical potential μ (see Sect. 7.3).

7.2 The Hubbard Model

After having gained some insight into the Green function concept and the calculation of self-energies, we turn now to a special model, for which the correlation effects can be evaluated in closed form. This model has been designed to explain the observation that transition metal oxides, which according to their electronic configuration should be metals due to partially filled single-particle energy bands, turn out to be insulators. Take as an example CoO, which crystallizes in the rocksalt structure: the configuration of the valence electrons, Co $4s^2 3d^7$ and O $2s^2 2p^4$, tells us that there is an odd number of electrons for each lattice point (of the fcc lattice), which in the independent particle picture leads to half-filling of the topmost band and means metallic behavior. This topmost band is a narrow d band (see Sect. 5.4), which is even narrower here than for Co (Fig. 5.14), because due to the larger spacing between neighboring Co atoms in CoO the overlap of the d orbitals is smaller. Under this condition the electronic correlation leads to a significant modification of the electronic structure, which – as we shall see – allows one to understand the experimental fact that CoO is not a metal but an insulator [169].

Let us consider electrons in an energy band deriving from one atomic (d or f) orbital. The corresponding Bloch function can be expressed (see (6.7)) by

$$\psi_{\mathbf{k}\sigma}(\mathbf{r}) = \frac{1}{\sqrt{N}} \sum_{\mathbf{R}} e^{i\mathbf{k}\cdot\mathbf{R}} \phi_\sigma(\mathbf{r} - \mathbf{R}), \quad (7.36)$$

where we have dropped the band index and kept only the spin index. We may switch with

$$c_{\mathbf{k}\sigma} = \frac{1}{\sqrt{N}} \sum_{\mathbf{R}} e^{i\mathbf{k}\cdot\mathbf{R}} c_{\mathbf{R}\sigma} \quad (7.37)$$

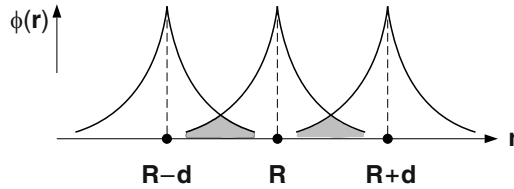


Fig. 7.2. Schematic of atomic orbitals at lattice points of a linear chain and their overlap

to a formulation with fermion operators (see Problem 6.2) and write for the single-particle term as in Sect. 6.1

$$\begin{aligned}
 \mathcal{H}_{\text{sp}} &= \sum_{\mathbf{k}\sigma} \epsilon_{\mathbf{k}} c_{\mathbf{k}\sigma}^{\dagger} c_{\mathbf{k}\sigma} \\
 &= \sum_{\mathbf{R}\mathbf{R}'\sigma} \underbrace{\frac{1}{N} \sum_{\mathbf{k}} \epsilon_{\mathbf{k}} e^{i\mathbf{k}\cdot(\mathbf{R}-\mathbf{R}')} }_{t_{\mathbf{R}\mathbf{R}'}} c_{\mathbf{R}'\sigma}^{\dagger} c_{\mathbf{R}\sigma} = \sum_{\mathbf{R}\mathbf{R}'\sigma} t_{\mathbf{R}\mathbf{R}'} c_{\mathbf{R}'\sigma}^{\dagger} c_{\mathbf{R}\sigma}. \quad (7.38)
 \end{aligned}$$

The dispersion of the energy band $\epsilon_{\mathbf{k}}$ is now expressed in terms of the hopping or transfer matrix elements $t_{\mathbf{R}\mathbf{R}'}$, $\mathbf{R} \neq \mathbf{R}'$, while the term with $\mathbf{R} = \mathbf{R}'$ gives the atomic energy level from which the band derives. For small overlap of the atomic orbitals, as is the case here and illustrated in Fig. 7.2, the tight-binding approximation applies and we may write

$$\sum_{\mathbf{k}\sigma} \epsilon_{\mathbf{k}} c_{\mathbf{k}\sigma}^{\dagger} c_{\mathbf{k}\sigma} \simeq \epsilon_0 \sum_{\mathbf{R}\sigma} c_{\mathbf{R}\sigma}^{\dagger} c_{\mathbf{R}\sigma} + t \sum_{\mathbf{R}\mathbf{d}\sigma} c_{\mathbf{R}+\mathbf{d}\sigma}^{\dagger} c_{\mathbf{R}\sigma} \quad (7.39)$$

with the atomic level energy ϵ_0 and the hopping or transfer matrix element between nearest neighbors $\mathbf{R} - \mathbf{R}' = \mathbf{d}$ (both assumed not to depend on σ)

$$t = \int \phi^*(\mathbf{r}) v(\mathbf{r}) \phi(\mathbf{r} - \mathbf{d}) d^3 r. \quad (7.40)$$

Likewise, the electron–electron interaction takes the form

$$\mathcal{H}_1 = \sum_{\substack{\mathbf{R}_1 \mathbf{R}_2 \sigma \\ \mathbf{R}'_1 \mathbf{R}'_2 \sigma'}} V_{\mathbf{R}_1 \mathbf{R}_2 \mathbf{R}'_1 \mathbf{R}'_2} c_{\mathbf{R}_1 \sigma}^{\dagger} c_{\mathbf{R}'_1 \sigma'}^{\dagger} c_{\mathbf{R}'_2 \sigma'} c_{\mathbf{R}_2 \sigma} \quad (7.41)$$

with the interaction matrix element now being the four-center integral:

$$\begin{aligned}
 V_{\mathbf{R}_1 \mathbf{R}_2 \mathbf{R}'_1 \mathbf{R}'_2} &= \frac{1}{2} \int d^3 r \int d^3 r' \phi^*(\mathbf{r} - \mathbf{R}_1) \phi^*(\mathbf{r}' - \mathbf{R}'_1) \\
 &\quad \times \frac{e^2}{4\pi\epsilon_0 |\mathbf{r} - \mathbf{r}'|} \phi(\mathbf{r}' - \mathbf{R}'_2) \phi(\mathbf{r} - \mathbf{R}_2). \quad (7.42)
 \end{aligned}$$

With the same arguments as used in Sect. 5.4, it is conceivable that the dominating contributions come from two-center terms with $\mathbf{R}_1 = \mathbf{R}_2 = \mathbf{R}$ and $\mathbf{R}'_1 = \mathbf{R}'_2 = \mathbf{R}'$, which give the approximate form

$$\mathcal{H}_{\text{int}} \simeq \sum_{\substack{\mathbf{R}\mathbf{R}' \\ \sigma\sigma'}} V_{\mathbf{R}\mathbf{R}'} c_{\mathbf{R}\sigma}^\dagger c_{\mathbf{R}'\sigma'}^\dagger c_{\mathbf{R}'\sigma'} c_{\mathbf{R}\sigma} = \sum_{\substack{\mathbf{R}\mathbf{R}' \\ \sigma\sigma'}} V_{\mathbf{R}\mathbf{R}'} n_{\mathbf{R}\sigma} n_{\mathbf{R}'\sigma'}. \quad (7.43)$$

The last expression results by identifying the number operator $n_{\mathbf{R}\sigma} = c_{\mathbf{R}\sigma}^\dagger c_{\mathbf{R}\sigma}$ and applying the anticommutation rules for $(\mathbf{R}\sigma) \neq (\mathbf{R}'\sigma')$. If only the term with $\mathbf{R} = \mathbf{R}'$ is considered, which describes double occupancy of the site \mathbf{R} with electrons of opposite spins, we arrive at the single-band *Hubbard² Hamiltonian* [207, 208]

$$\mathcal{H} = \epsilon_0 \sum_{\mathbf{R}\sigma} c_{\mathbf{R}\sigma}^\dagger c_{\mathbf{R}\sigma} + t \sum_{\mathbf{R}d\sigma} c_{\mathbf{R}+d\sigma}^\dagger c_{\mathbf{R}\sigma} + U \sum_{\mathbf{R}} n_{\mathbf{R}\uparrow} n_{\mathbf{R}\downarrow}. \quad (7.44)$$

Here $U = V_{\mathbf{R}\mathbf{R}}$, called the *Hubbard- U* , weighs the strength of the correlation in case of two electrons at the same site. This Hamiltonian contains two competing mechanisms: the hopping term is responsible for band formation and delocalization, while the correlation term, with its energy increase for double occupancy of sites with electrons of opposite spin, favors a ground state with localized magnetic moments of uncompensated spins at each site.

In the following, we replace \mathbf{R} by the site index i and consider the Hubbard Hamiltonian (7.44) in the form

$$\mathcal{H} = \mathcal{H}_0 + \mathcal{H}_1 = \sum_{ij\sigma} t_{ij} c_{i\sigma}^\dagger c_{j\sigma} + \frac{1}{2} U \sum_{i\sigma} n_{i\sigma} n_{i-\sigma}, \quad (7.45)$$

where t_{ij} is the hopping matrix element between two sites (which need not be the nearest neighbors). In order to calculate the spectrum of \mathcal{H} , we calculate the Green function describing the propagation of an electron with spin σ from site j at time t' to site i at time t

$$G(ij\sigma; t, t') = -\frac{i}{\hbar} \theta(t - t') \langle \{ c_{i\sigma}(t), c_{j\sigma}^\dagger(t') \} \rangle. \quad (7.46)$$

This is done by solving the equation of motion

$$i\hbar \frac{\partial}{\partial t} G(ij\sigma; t, t') = \delta(t - t') \delta_{ij} - \frac{i}{\hbar} \theta(t - t') \langle \{ [c_{i\sigma}(t), \mathcal{H}], c_{j\sigma}^\dagger(t') \} \rangle. \quad (7.47)$$

The commutator of $c_{i\sigma}$ with \mathcal{H} can be evaluated with

$$[c_{i\sigma}, c_{j\sigma'}^\dagger c_{m\sigma'}] = c_{m\sigma} \delta_{ij} \delta_{\sigma\sigma'} \quad (7.48)$$

and

² John Hubbard 1931–1980.

$$[c_{i\sigma}, n_{j\sigma'} n_{j-\sigma'}] = \delta_{ij} c_{i\sigma} n_{i-\sigma} (\delta_{\sigma\sigma'} + \delta_{\sigma-\sigma'}) \quad (7.49)$$

giving

$$[c_{i\sigma}, \mathcal{H}] = \sum_m t_{im} c_{m\sigma} + U n_{i-\sigma} n_{i\sigma}. \quad (7.50)$$

Thus, the equation of motion (7.47) reads

$$i\hbar \frac{\partial}{\partial t} G(ij\sigma; t, t') = \delta(t-t') \delta_{ij} + \sum_m t_{im} G(mj\sigma; t, t') + U \Gamma(iij\sigma; t, t') \quad (7.51)$$

with a higher order Green function of the general form

$$\Gamma(iilmj\sigma; t, t') = -\frac{i}{\hbar} \theta(t-t') \langle \{c_{i-\sigma}^\dagger(t) c_{l-\sigma}(t) c_{m\sigma}(t), c_{j\sigma}^\dagger(t')\} \rangle. \quad (7.52)$$

Instead of truncating the hierarchy by factorizing the higher order Green function in (7.51) (which would be the Hartree–Fock approximation to be considered later), we continue by writing its equation of motion as

$$i\hbar \frac{\partial}{\partial t} \Gamma(iij\sigma; t, t') = \langle n_{i-\sigma} \rangle \delta_{ij} \delta(t-t') - \frac{i}{\hbar} \theta(t-t') \langle \{[n_{i-\sigma}(t) c_{i\sigma}(t), \mathcal{H}], c_{j\sigma}^\dagger(t')\} \rangle. \quad (7.53)$$

The commutator with \mathcal{H} gives the two contributions (Problem 7.3)

$$[n_{i-\sigma} c_{i\sigma}, \mathcal{H}_0] = \sum_m t_{im} \left(n_{i-\sigma} c_{m\sigma} + c_{i-\sigma}^\dagger c_{m-\sigma} c_{i\sigma} - c_{m-\sigma}^\dagger c_{i-\sigma} c_{i\sigma} \right) \quad (7.54)$$

and

$$[n_{i-\sigma} c_{i\sigma}, \mathcal{H}_1] = U n_{i-\sigma} c_{i\sigma} \quad (7.55)$$

which leads to

$$\begin{aligned} (i\hbar \frac{\partial}{\partial t} - U) \Gamma(iij\sigma; t, t') &= \langle n_{i-\sigma} \rangle \delta_{ij} \delta(t-t') + \sum_m t_{im} (\Gamma(iimj\sigma; t, t') \\ &\quad + \Gamma(imij\sigma; t, t') - \Gamma(mij\sigma; t, t')). \end{aligned} \quad (7.56)$$

This equation of motion simplifies for the case $t_{im} = \epsilon_0 \delta_{im}$, i.e., for a band without dispersion, known also as the *atomic limit*, to

$$\left(i\hbar \frac{\partial}{\partial t} - \epsilon_0 - U \right) \Gamma(iij\sigma; t, t') = \langle n_{i-\sigma} \rangle \delta_{ij} \delta(t-t'). \quad (7.57)$$

After Fourier transformation, it yields the solution

$$\Gamma(iij\sigma; E) = \frac{\langle n_{-\sigma} \rangle}{E - \epsilon_0 - U} \delta_{ij}, \quad (7.58)$$

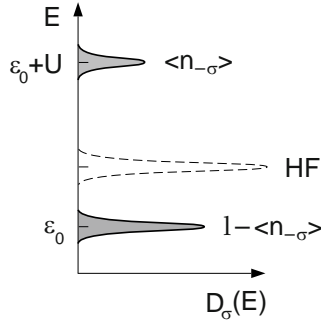


Fig. 7.3. Density of states for the Hubbard model in the atomic limit and comparison with the HF result

with $\langle n_{-\sigma} \rangle = \langle n_{i-\sigma} \rangle$ independent of the site index i due to the translation invariance of the system. For the same situation, (7.51) takes a form, which after Fourier transformation leads to

$$G(ii\sigma; E) = \frac{E - \epsilon_0 - U(1 - \langle n_{-\sigma} \rangle)}{(E - \epsilon_0)(E - \epsilon_0 - U)} \tag{7.59}$$

and can be written in the form

$$G(ii\sigma; E) = \lim_{\delta \rightarrow 0} \left(\frac{1 - \langle n_{-\sigma} \rangle}{E - \epsilon_0 + i\delta} + \frac{\langle n_{-\sigma} \rangle}{E - \epsilon_0 - U + i\delta} \right). \tag{7.60}$$

The surprising result is that $G(ii\sigma; E)$ has two poles, one at $E = \epsilon_0 - i\delta$ with the weight $Z = 1 - \langle n_{-\sigma} \rangle$ and one at $E = \epsilon_0 + U - i\delta$ with the weight $Z = \langle n_{-\sigma} \rangle$ (Fig. 7.3). This pole structure is a consequence of the energy dependence of the self-energy. The second term vanishes for $\langle n_{-\sigma} \rangle \rightarrow 0$ and the remaining first term reduces for $U = 0$ to the Green function of the noninteracting electron

$$G^{(0)}(ii\sigma; E) = \lim_{\delta \rightarrow 0} \frac{1}{E - \epsilon_0 + i\delta}. \tag{7.61}$$

The effect of considering the correlation U is the splitting of the single-particle level into two spin independent quasi-particle levels (separated by U) whose weights depend on the occupation. This is clearly seen also in the density of states

$$\begin{aligned} D_\sigma(E) &= \frac{1}{\pi} \text{Tr}(\text{Im}G(ii\sigma; E)) \\ &= (1 - \langle n_{-\sigma} \rangle)\delta(E - \epsilon_0) + \langle n_{-\sigma} \rangle\delta(E - \epsilon_0 - U) \end{aligned} \tag{7.62}$$

shown in Fig. 7.3. The new quality of the result can be emphasized also by comparing with the Hartree-Fock approximation in (7.51), which means to replace $\Gamma(iij\sigma)$ by $\langle n_{-\sigma} \rangle G(ij\sigma)$. The result for the case $t_{im} = \epsilon_0 \delta_{im}$ is

$$G^{\text{HF}}(ii\sigma; E) = \frac{1}{E - \epsilon_0 - U\langle n_{-\sigma} \rangle + i\delta}, \quad (7.63)$$

which has a single pole only with weight $Z = 1$ at $E = \epsilon_0 + U\langle n_{-\sigma} \rangle$ as indicated in Fig. 7.3.

Let us now consider the band formation by relaxing the approximation $t_{im} \sim \delta_{im}$. Then, (7.56) can be factorized with (for $i \neq m$)

$$\begin{aligned} \Gamma(iimj\sigma) &\rightarrow \langle n_{-\sigma} \rangle G(mj\sigma) \\ \Gamma(imij\sigma) &\rightarrow \langle c_{i-\sigma}^\dagger c_{m-\sigma} \rangle G(ij\sigma) \\ \Gamma(miij\sigma) &\rightarrow \langle c_{m-\sigma}^\dagger c_{i-\sigma} \rangle G(ij\sigma), \end{aligned}$$

where the last two terms compensate each other in (7.56) due to $t_{im} = t_{mi}$ and one obtains with $\tau = t - t'$

$$\left(i\hbar \frac{\partial}{\partial \tau} - \epsilon_0 - U \right) \Gamma(iij\sigma; \tau) = \langle n_{-\sigma} \rangle (\delta_{ij} \delta(\tau) + \sum_{m \neq i} t_{im} G(mj\sigma; \tau)). \quad (7.64)$$

The Fourier transform of this equation

$$\Gamma(iij\sigma; E) = \frac{\langle n_{-\sigma} \rangle}{E - \epsilon_0 - U} \left(\delta_{ij} + \sum_{m \neq i} t_{im} G(mj\sigma; E) \right) \quad (7.65)$$

can be used to write, instead of (7.51), the equation

$$(E - \epsilon_0) G(ij\sigma; E) = \left(\delta_{ij} + \sum_{m \neq i} t_{im} G(mj\sigma; E) \right) \left(1 + \frac{U\langle n_{-\sigma} \rangle}{E - \epsilon_0 - U} \right). \quad (7.66)$$

Finally, we transform into the Bloch representation, which for the one-dimensional model with lattice constant a means

$$G(k\sigma; E) = \frac{1}{N} \sum_{ij} e^{-ik(i-j)a} G(ij\sigma; E), \quad (7.67)$$

to find

$$(E - \epsilon_0) G(k\sigma; E) = (1 - \epsilon_k G(k\sigma; E)) \left(1 + \frac{U\langle n_{-\sigma} \rangle}{E - \epsilon_0 - U} \right) \quad (7.68)$$

with $\epsilon_k = \sum_{n \neq m} t_{im} \exp(-ik(n-m)a)$. This can be solved to yield

$$G(k\sigma; E) = \frac{1}{E - \epsilon_k - \Sigma(\sigma; E)} \quad (7.69)$$

with the self-energy

$$\Sigma(\sigma; E) = U\langle n_{-\sigma} \rangle \frac{E - \epsilon_0}{E - \epsilon_0 - U(1 - \langle n_{-\sigma} \rangle)}. \quad (7.70)$$

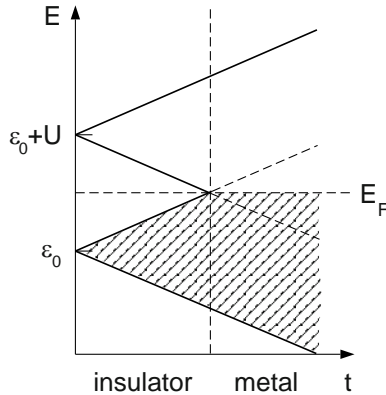


Fig. 7.4. Spectrum of the Hubbard model in dependence on the hopping matrix element t to indicate the insulator–metal transition

Due to the energy dependence of the self-energy, the Green function (7.69) has two separate poles with different spectral weights (as for the atomic limit (Problem 7.4)) for each k . The spectrum, obtained by projecting the eigenvalues onto the energy axes, exhibits two bands whose widths are determined by that of the single-particle energy dispersion ϵ_k (note that the self-energy (7.70) does not depend on k). In tight-binding approximation, the dispersion of the energy band becomes $\epsilon_k = \epsilon_0 + 2t \cos ka$ with t being the hopping matrix element between nearest neighbors.

In Fig. 7.4, the spectrum of the Hubbard model is depicted for fixed U in dependence on t . Two bands evolve with increasing t from the two levels of Fig. 7.3, the upper and lower Hubbard band: they are separated by a gap as long as the band width $4t$ is smaller than U , but they overlap for $4t > U$. For a system with one electron per lattice site, a single band can be completely filled. Thus for $4t > U$ the overlapping Hubbard bands are partially filled (the Fermi energy is in a region with finite density of states) and the model describes a metal, while for $4t < U$ the Hubbard bands are separated by a gap, the lower (upper) band being completely filled (empty), and the model describes an insulator. This *metal–insulator transition* is the important result of the Hubbard model. Systems showing this behavior are called *Mott³–Hubbard insulators*. For the case of half-filling, the Hubbard Hamiltonian can be transformed into a Hamiltonian of the Heisenberg type (Problem 7.5), that allows one to describe the magnetic properties of these systems. However, the Hubbard model is not correct for small values of U , because it always gives the two separate eigenvalues for each \mathbf{k} , while for small correlation we expect the single band solution.

³ Sir Nevill Mott 1905–1996, Nobel prize in Physics 1977, together with Philip W. Anderson and John H. Van Vleck.

For more realistic descriptions, there exist extensions of the Hubbard model which also include transfer to next nearest neighbors, more than one band, and correlation terms including different sites. One of these extensions is the subject of Problem 7.6. These models are used to investigate material systems whose electronic properties are determined by correlation [209–213]. Among those are the high- T_c cuprate superconductors. Their crystal structure contains layers with Cu and O atoms in a quadratic lattice. The overlapping Cu $3d$ and O $2p$ orbitals form a narrow p - d hybrid band. Due to the other constituents of the crystal structure, this band can be partially depopulated (or filled with holes). Thus, by comparing photoemission data for different filling, the spectral weight of the evolving Hubbard bands becomes evident.

The results of this section have uncovered a deficiency of the DFT-LDA concept. Making use of an effective single-particle potential, which is the same for all electrons, irrespective of their orbital, this approach does not account for the correlation effect outlined in presenting the Hubbard model, i.e., it is not capable of describing occupation-dependent energy bands. This deficiency is not problematic for energy bands deriving from s or p orbitals, for which the nearly free electron or pseudo-potential approach applies as well as the LCAO method because the orbital character is diminished due to delocalization. In contrast, for the localized d and f orbitals, this is not the case. In order to overcome this deficiency, the LDA+U concept has been developed [195]. Its essential idea is to replace the LDA Coulomb energy $UN/(N-1)/2$ for d - d interaction, which is assumed to be part of the LDA energy functional $E_{\text{LDA}}[n]$, by the Hubbard correlation by writing

$$E[n] = E_{\text{LDA}}[n] - \frac{1}{2}UN(N-1) + \frac{1}{2}U \sum_{i \neq j} n_i n_j, \quad (7.71)$$

where $N = \sum_i n_i$ is the number of electrons and n_i the orbital occupancy. The orbital energies

$$\epsilon_i = \frac{\partial E[n]}{\partial n_i} = \epsilon_i^{\text{LDA}} + U \left(\frac{1}{2} - n_i \right) \quad (7.72)$$

are changed according to their occupancy with respect to the LDA value. A more recent extension of this concept is the *dynamical mean-field theory* (DMFT) [210, 214].

7.3 Fermi Liquids

Classical liquids are known to exist due to particle–particle interaction, when the average interaction energy cannot be neglected in comparison with the average thermal energy $k_B T$, and condensation, i.e., the phase transition from the gaseous to the liquid phase, takes place. In this condensed phase, the thermal motion is comparable with the mean particle separation. By reducing the

temperature, the thermal motion can get so small that the interaction dominates the kinetic energy. In this situation, the phase transition from the liquid to the solid state, takes place. This systematic, which is based on classical arguments, does not account, however, for quantum effects as has become apparent for He due to its small mass. At sufficiently low temperatures, liquid He does not condense into the solid state. Instead, when the thermal deBroglie wavelength $\lambda_T = (\hbar^2/2Mk_B T)^{1/2}$, a quantum mechanical length scale, becomes comparable to the average particle separation (while at the same time the energy of the zero-point motion is much larger than the interaction energy), it enters a state known as *quantum liquid*. This phase transition is ruled by quantum statistics and leads to a *Fermi liquid* for ${}^3\text{He}$ but to a *Bose liquid* for ${}^4\text{He}$. As the interacting particles are neutral He atoms, these two phases are jointly denoted as neutral quantum liquids.

Especially for ${}^3\text{He}$, Landau developed a theory of Fermi liquids [197], which comprises the interplay between Fermi statistics and particle interaction. As it turned out later on, this theory applies as well to interacting electrons in metals and doped semiconductors, which can be classified as charged Fermi liquids. We note in passing that Landau's Fermi liquid theory is used also for neutron stars. In this section, a brief outline is given of this theory, which is closely connected with the concept of quasi-particles, and we refer for further reading of the literature [64, 194, 197–199].

Fermion systems without interaction, as treated in Chap. 4 in the Sommerfeld model or in Chap. 5 in the independent particle model of electronic band structure, can be characterized by their ground state and low-energy or elementary excitations out of the ground state. The former is defined for $T = 0\text{K}$ by filled states up to the Fermi energy, the latter are particle–hole excitations across the Fermi surface. Here, particle(hole) means an electron(missing electron) above(below) the Fermi energy. We have noticed already that the effect of the interaction is to modify the single-particle energy $\epsilon_{\mathbf{k}\sigma}$ by a self-energy, which incorporates interaction effects (to an extent depending on the applied approximation, see e.g., (7.27) and (7.28)) into the independent particle picture thus leading to the concept of quasi-particles, which we have addressed already in Sects. 4.4, 5.2, and 7.1.

Looking at the quantum numbers, momentum $\mathbf{p} = \hbar\mathbf{k}$ and spin σ (the band index is suppressed here), we have found a one-to-one relation between an independent particle and the corresponding quasi-particle, although via the self-energy, the quasi-particle energy $\epsilon_{\mathbf{k}\sigma}[n_{\mathbf{k}\sigma}]$ becomes a functional of the occupation numbers. Thereby, the spin is not changed and the quasi-particles remain fermions. The self-energy quantifies virtual excitations of electron–hole pairs, which represent charge or spin density waves. Consequently, a quasi-particle is the bare particle of the noninteracting system dressed by a cloud of virtually excited density waves. The lifetime of a quasi-particle, defined by the imaginary part of its self-energy, is determined by the scattering processes which take place under the constraints of energy and momentum conservation. At $T = 0$, this leads to an infinite lifetime for quasi-particles at the Fermi

energy, because the available phase space for scattering shrinks to zero, while the scattering rate increases quadratically with the energy separation from the Fermi energy (or at finite T from the chemical potential) [122, 200]. Thus, quasi-particles are well defined for low-energy excitations. This leads to the concept of Fermi liquids: it is based on the assumption that the excitation spectrum of the interacting Fermi system is similar to that of the noninteracting Fermi system and that the particles (or states) of the latter evolve one-to-one into the quasi-particles (or states) of the former without changing the quantum numbers when the interaction is adiabatically switched on. This concept is supported by the observation that in a certain temperature range some properties (specific heat, spin susceptibility) of many metals (like those of ^3He) correspond, in their temperature dependence, to those of the noninteracting Fermi system, however, with changed kinematic properties such as the particle mass.

Elementary excitations can be described as changing the occupation of states around the chemical potential (or the Fermi energy) with respect to the ground state occupation $n_{\mathbf{k}\sigma}^0$

$$\delta n_{\mathbf{k}\sigma} = n_{\mathbf{k}\sigma} - n_{\mathbf{k}\sigma}^0 = \begin{cases} +1 & |\mathbf{k}| > k_F \\ -1 & |\mathbf{k}| \leq k_F. \end{cases} \quad (7.73)$$

The total energy of the system is a functional of the occupation numbers $n_{\mathbf{k}\sigma}$

$$E = E[n_{\mathbf{k}\sigma}] \text{ but } E \neq \sum_{\mathbf{k}\sigma} \epsilon_{\mathbf{k}\sigma} n_{\mathbf{k}\sigma}, \quad (7.74)$$

because the quasi-particle energy $\epsilon_{\mathbf{k}\sigma} = \delta E / \delta n_{\mathbf{k}\sigma}$ depends on the occupation due to the self-energy and has in general a nonvanishing variational derivative

$$\frac{\delta \epsilon_{\mathbf{k}\sigma}}{\delta n_{\mathbf{k}'\sigma'}} = \frac{\delta^2 E}{\delta n_{\mathbf{k}\sigma} \delta n_{\mathbf{k}'\sigma'}} =: f(\mathbf{k}\sigma; \mathbf{k}'\sigma') \neq 0. \quad (7.75)$$

We may express the total energy as a Taylor series with respect to the elementary excitations (i.e., the changes in the occupation numbers) about the ground state energy E_0

$$\begin{aligned} E[n_{\mathbf{k}\sigma}] &= E_0 + \sum_{\mathbf{k}\sigma} \epsilon_{\mathbf{k}\sigma}[n_{\mathbf{k}\sigma}^0] \delta n_{\mathbf{k}\sigma} \\ &\quad + \frac{1}{2} \sum_{\substack{\mathbf{k}\sigma \\ \mathbf{k}'\sigma'}} f(\mathbf{k}\sigma; \mathbf{k}'\sigma') \delta n_{\mathbf{k}\sigma} \delta n_{\mathbf{k}'\sigma'} + \mathcal{O}(\delta n^3). \end{aligned} \quad (7.76)$$

Denoting the quasi-particle energies for the ground state distribution $\epsilon_{\mathbf{k}\sigma}[n_{\mathbf{k}\sigma}^0]$ by $\epsilon_{\mathbf{k}\sigma}^0$, the quasi-particle energies can be expressed as

$$\epsilon_{\mathbf{k}\sigma} = \frac{\delta E}{\delta n_{\mathbf{k}\sigma}} \simeq \epsilon_{\mathbf{k}\sigma}^0 + \sum_{\mathbf{k}'\sigma'} f(\mathbf{k}\sigma; \mathbf{k}'\sigma') \delta n_{\mathbf{k}'\sigma'}. \quad (7.77)$$

The adequate thermodynamic potential for the grand-canonical ensemble with varying occupation $N = \sum_{\mathbf{k}\sigma} n_{\mathbf{k}\sigma}$ is the free energy $F = E - \mu N$ which under elementary excitations with $N - N_0 = \sum_{\mathbf{k}\sigma} \delta n_{\mathbf{k}\sigma}$, where N_0 is the total occupation in the ground state, changes by

$$\begin{aligned} F - F_0 &= E - E_0 - \mu(N - N_0) \\ &= \sum_{\mathbf{k}\sigma} (\epsilon_{\mathbf{k}\sigma}^0 - \mu) \delta n_{\mathbf{k}\sigma} + \frac{1}{2} \sum_{\mathbf{k}'\sigma'} f(\mathbf{k}\sigma; \mathbf{k}'\sigma') \delta n_{\mathbf{k}'\sigma'} \delta n_{\mathbf{k}\sigma}. \end{aligned} \quad (7.78)$$

Note that we consider a situation where the quasi-particle energies are close to the chemical potential μ and that $\epsilon_{\mathbf{k}\sigma}^0 - \mu \neq 0$ only for $\mathbf{k}\sigma$ with $\delta n_{\mathbf{k}\sigma} \neq 0$; thus, the first term is of the order $(\delta n_{\mathbf{k}\sigma})^2$. As for the noninteracting particles, the free energy is stationary for the equilibrium distribution function

$$n_{\mathbf{k}\sigma} = [1 + \exp(\beta(\epsilon_{\mathbf{k}\sigma} - \mu))]^{-1}, \quad (7.79)$$

with the dispersion of the independent particles replaced by that of the quasi-particles. It has the form of the Fermi–Dirac distribution function but is an implicit equation for $n_{\mathbf{k}\sigma}$ due to the functional dependence of the quasi-particle energies $\epsilon_{\mathbf{k}\sigma}$ on the occupation.

In contrast to a microscopic theory, which aims at a calculation of the quasi-particle energies, the Fermi liquid theory replaces the interaction by parameters and relies on the one-to-one correspondence between independent (or bare) particles and quasi-particles including their statistics. This is outlined in the following by, assuming for better transparency, an isotropic Fermi liquid and a spin degenerate dispersion. The Fermi velocity is defined by

$$v_{k,F} = \frac{1}{\hbar} \left| \nabla_{\mathbf{k}} \epsilon_{\mathbf{k}\sigma} \Big|_{k=k_F} \right| =: \frac{\hbar k_F}{m^*}, \quad (7.80)$$

where m^* denotes the effective mass of the quasi-particle at the Fermi energy. Let us assume the quasi-particle dispersion $\epsilon_{\mathbf{k}\sigma}$ to be a sufficiently smooth function in the vicinity of the Fermi energy E_F (or the chemical potential μ). Then, we can write

$$\epsilon_{\mathbf{k}\sigma} - \mu \simeq \left| \nabla_{\mathbf{k}} \epsilon_{\mathbf{k}\sigma} \Big|_{k=k_F} \right| (k - k_F) = \frac{\hbar^2 k_F}{m^*} (k - k_F) \quad (7.81)$$

as depicted in Fig. 7.5. The same relation holds for the independent particle, however, with a mass m instead of m^* . This difference in the masses is due to the fact that the quasi-particle consists of the bare particle and a cloud of density fluctuations around it, which moves along with the particle and reduces its mobility, i.e., $m^* > m$. One immediate consequence is the enhancement of the density of states at the Fermi energy

$$D(E_F) = \frac{1}{V} \sum_{\mathbf{k}\sigma} \delta(\epsilon_{\mathbf{k}\sigma} - E_F) = \frac{m^* k_F}{\pi^2 \hbar^2}, \quad (7.82)$$

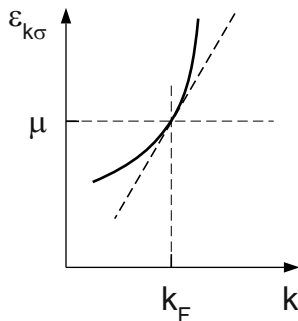


Fig. 7.5. Quasi-particle dispersion (*solid*) and linear approximation around the chemical potential (*dashed*)

which implies an enhancement of all quantities which are proportional to the $D(E_F)$ as e.g., the particle contribution to the specific heat. The effect of the interaction is considered here in the parameter m^* , which is accessible by measuring the Sommerfeld coefficient (see Sect. 4.2).

Let us now take into account the interaction between quasi-particles represented by $f(\mathbf{k}\sigma; \mathbf{k}'\sigma')$. For the isotropic Fermi liquid and dominating exchange interaction (as in Sect. 6.2), this can be written [64] as

$$f(\mathbf{k}\sigma; \mathbf{k}'\sigma') = f^s(\mathbf{k}, \mathbf{k}') + \boldsymbol{\sigma} \cdot \boldsymbol{\sigma}' f^a(\mathbf{k}, \mathbf{k}'). \quad (7.83)$$

Being close to the Fermi energy, we have $|\mathbf{k}|, |\mathbf{k}'| \simeq k_F$ and because of the isotropy, the $f^\lambda(\mathbf{k}, \mathbf{k}')$ depend only on the angle θ between \mathbf{k} and \mathbf{k}' . Therefore, we may expand these functions in terms of Legendre polynomials (normalized for practical reasons by the density of states $D(E_F)$)

$$f^\lambda(\mathbf{k}, \mathbf{k}') = \frac{1}{D(E_F)} \sum_l^\infty F_l^\lambda P_l(\cos \theta). \quad (7.84)$$

The coefficients F_l^λ are the phenomenological Fermi liquid parameters which have to be determined by comparison with experimental data. As it turns out [64, 122], the quasi-particle effective mass is given by

$$m^* = m(1 + F_1^s/3). \quad (7.85)$$

Thus, F_1^s could be determined from the low-temperature behavior of the specific heat (provided the system is isotropic). The Pauli spin susceptibility is enhanced due to interactions and can be expressed as

$$\chi_{\text{spin}} = \frac{m^*}{m(1 + F_0^a)} \chi_{\text{spin}}^0, \quad (7.86)$$

with the spin susceptibility χ_{spin}^0 of free electrons. Its experimental value provides the parameter F_0^a , if the effective mass is already known from specific heat data. Fermi liquid parameters are reported so far only for He [64, 199, 215].

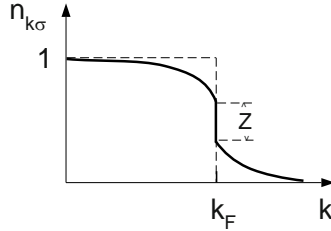


Fig. 7.6. Particle (*dashed*) and quasi-particle (*solid*) distribution at $T = 0$ K. The discontinuity at k_F represents the weight Z

Finally, we look at the momentum distribution $n_{\mathbf{k}\sigma}$, which can be obtained from the Green function with the help of the dissipation–fluctuation theorem

$$n_{\mathbf{k}\sigma} = \langle c_{\mathbf{k}\sigma}^\dagger c_{\mathbf{k}\sigma} \rangle = -\frac{1}{\hbar\pi} \int_{-\infty}^{+\infty} \frac{\text{Im}G(\mathbf{k}\sigma; \epsilon)}{1 + e^{-\beta\epsilon}} d\epsilon, \quad (7.87)$$

with $G(\mathbf{k}\sigma; \epsilon)$ from (7.31). The denominator simplifies for $T = 0$ K and the integration can be extended to a contour in the upper complex plane. This includes only the quasi-particle poles for $k < k_F$ (which are in the upper half plane) but not those for $k > k_F$ (which are in the lower half plane) and results in a jump of $n_{\mathbf{k}}$ at $k = k_F$, which equals the weight $Z(k_F)$ of the quasi-particle pole (Fig. 7.6). The calculation of this jump is the subject of Problem 7.7.

As we have seen by these considerations, the Fermi surface introduced in Chap. 4 for the noninteracting electrons exists also in the presence of the electron–electron interaction, as can be seen from the discontinuity in the momentum distribution (Fig. 7.6). It is the signature of existing quasi-particles. However, when replacing the independent particles by quasi-particles, the kinematic properties and consequently also physical quantities change as compared with the independent particle result. This can be exploited to determine the parameters of the Fermi liquid theory.

The incorporation of particle interaction in the quasi-particle depends essentially on the phase space available for interaction processes close to the Fermi energy. While in three and two dimensions, this phase space is a sphere or a circle, respectively, it shrinks to two points for a one-dimensional system. The dimensionality effect can be demonstrated for the Lindhard function (Problem 7.8). We shall see in the next section how this will dramatically alter the situation when we consider one-dimensional electron systems.

7.4 Luttinger Liquids

The dimensionality and its influence on solid state properties have been mentioned already in several sections. Obviously the two-dimensional systems are the surface of a solid (Sect. 3.6) and the interface between two different

solids (a heterostructure). We have learnt about semiconductor heterostructures that they can accommodate a two-dimensional electron gas (Sect. 5.6). In this section the one-dimensional electron systems will be the focus of interest. There are several realizations, which have stimulated the investigation of such systems. Among those are special molecular crystal structures such as inorganic and organic linear chain compounds that allow band formation by overlapping atomic orbitals in one spatial direction only [201]. Another example is conducting polymers, for which energy bands arise from repeated conjugated bonds along the strand [111, 112]. But one may start also from the 2D electron systems in heterostructures to prepare by etching, cleaved edge overgrowth, or depletion via top gates a 1D channel (a quantum wire) along which electrons can move freely [216–218]. The youngest child in this family is carbon nanotubes, which can be understood as a graphite monolayer rolled up to a cylinder with a diameter of a few nm [21, 113, 114]. All these systems have been and are still under investigation due to their peculiar properties determined by the low dimensionality which do not fit into the framework of Fermi liquid theory. The essential point here is the breakdown of the quasi-particle concept [22, 122, 193, 219–222].

Free electrons in one dimension would be characterized by a quadratic dispersion relation which cuts the Fermi energy at $k = \pm k_F$ as depicted in Fig. 7.7. Being interested in elementary excitations around the Fermi energy, it is advantageous to linearize the dispersion relation as in the previous section by writing (relative to the chemical potential)

$$\epsilon_{\pm,k}^0 \simeq \frac{\hbar^2 k_F}{m} (\pm k - k_F) = \hbar v_F (\pm k - k_F), \quad (7.88)$$

with the Fermi velocity v_F . This spectrum consists of two branches (linear in k) that correspond to electrons traveling left and right along the extension of the 1D system. We can immediately write down the corresponding single-particle part of the Hamiltonian in terms of fermion operators ($\{c_{k\alpha}, c_{k'\alpha'}^\dagger\} = \delta_{\alpha,\alpha'} \delta_{k,k'}$)

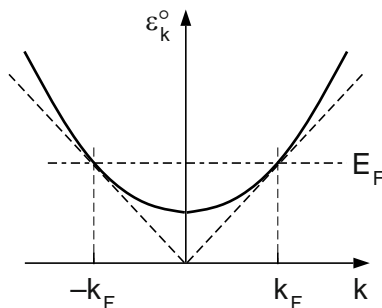


Fig. 7.7. Dispersion relation for a 1D fermion system with linear approximation around the Fermi energy

$$\mathcal{H}_{\text{sp}} = \hbar v_{\text{F}} \sum_{k, \alpha = \pm} (\alpha k - k_{\text{F}}) \left(c_{k\alpha}^{\dagger} c_{k\alpha} - \langle c_{k\alpha}^{\dagger} c_{k\alpha} \rangle_0 \right). \quad (7.89)$$

Here, the ground state expectation value $\langle c_{k\alpha}^{\dagger} c_{k\alpha} \rangle_0$ of the number operator is subtracted to prevent a divergence of the ground state energy due to occupation of states with negative energy.

In the following, we assume a system length L and apply periodic boundary conditions with the consequence of discretizing k in multiples of $2\pi/L$. Number fluctuations would be described here by

$$n_{q\alpha} = \sum_{k\alpha} \left(c_{k+q\alpha}^{\dagger} c_{k\alpha} - \delta_{q,0} \langle c_{k\alpha}^{\dagger} c_{k\alpha} \rangle_0 \right), \quad (7.90)$$

which according to their commutation rule

$$[n_{q\alpha}, n_{-q'\alpha'}] = \alpha \delta_{\alpha, \alpha'} \delta_{q, q'} \frac{qL}{2\pi} \quad (7.91)$$

are boson operators. Moreover, we have

$$[\mathcal{H}_{\text{sp}}, n_{q\alpha}] = \alpha \hbar v_{\text{F}} q n_{q\alpha}, \quad (7.92)$$

indicating that the number fluctuations created by $n_{q\alpha}$ are eigenstates of \mathcal{H}_{sp} with the eigenvalue $\alpha \hbar v_{\text{F}} q$. This leads to an alternative formulation of \mathcal{H}_{sp}

$$\mathcal{H}_{\text{sp}} = \frac{\pi \hbar v_{\text{F}}}{L} \left(\sum_{q \neq 0, \alpha} n_{q\alpha} n_{-q\alpha} + \sum_{\alpha} n_{0\alpha}^2 \right), \quad (7.93)$$

now in terms of boson operators. A closer inspection shows that the existence of these two equivalent formulations of \mathcal{H}_0 , (7.89) and (7.93) is characteristic for the 1D case and the linearized dispersion relation.

Electron–electron interaction can take place within each branch of the spectrum or between the two different branches. For small momentum transfer, corresponding to forward scattering, this can be written in terms of boson operators as

$$\mathcal{H}_{\text{int}} = \frac{1}{2L} \sum_{q, \alpha} v_q (n_{q\alpha} n_{-q\alpha} + n_{q\alpha} n_{-q-\alpha}), \quad (7.94)$$

where v_q quantifies the strength of this scattering. The system Hamiltonian $\mathcal{H} = \mathcal{H}_{\text{sp}} + \mathcal{H}_{\text{int}}$ is a bilinear expression in the boson operators and can be diagonalized by a Bogoliubov transformation

$$\tilde{n}_{q\alpha} = n_{q\alpha} \cosh(\phi(q)) + n_{q-\alpha} \sinh(\phi(q)), \quad (7.95)$$

with the interaction parameter

$$e^{2\phi(q)} = \left(1 + \frac{v_q}{\pi \hbar v_{\text{F}}} \right)^{-1/2} =: K(q). \quad (7.96)$$

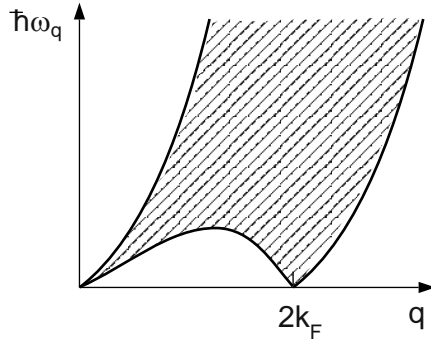


Fig. 7.8. Particle–hole excitations in the 1D fermion system. Note the missing of low-energy excitations for $0 < |k| < 2k_F$

The diagonal form of \mathcal{H} reads

$$\mathcal{H} = \frac{\pi}{L} \sum_{q \neq 0} v_q \tilde{n}_{q\alpha} \tilde{n}_{-q\alpha} + \frac{\pi}{2L} (v_N N^2 + v_J J^2), \quad (7.97)$$

where $v_q = \hbar v_F / K(q)$, $v_N = v_0^2 / \hbar v_F$, and $v_J = \hbar v_F$, while, $N = n_{0+} + n_{0-}$ and $J = n_{0+} - n_{0-}$ describe charge and current excitations respectively. Ultimately, by introducing normalized boson operators

$$b_q^\dagger = \sqrt{\frac{2\pi}{L|q|}} (\theta(q) \tilde{n}_{q+} + \theta(-q) \tilde{n}_{q-}), \quad (7.98)$$

with the step function $\theta(q)$, the Hamiltonian takes the form

$$\mathcal{H} = \sum_{q \neq 0} \hbar\omega_q b_q^\dagger b_q + \frac{\pi}{2L} (v_N N^2 + v_J J^2) \quad (7.99)$$

with the dispersion $\hbar\omega(q) = v_q |q|$. It is the model Hamiltonian for interacting 1D electrons named after Tomonaga⁴ [223] and Luttinger⁵ [224].

The remarkable property of this Hamiltonian is that it is expressed in terms of collective excitations, which are the low-energy excitations of the system similar to the vibrations of a string. This means that low-energy electron–hole pair excitations are absent here, which indicates also the absence of quasi-particles for interacting electrons in 1D. This finding can be confirmed by looking at the excitation spectrum in Fig. 7.8. At low energies, excitations are possible only between states close to the two Fermi points (see Fig. 7.7), but there are no particle–hole excitations and, therefore, no quasi-particles for $0 < |k| < 2k_F$. This nonexistence of quasi-particles can be made explicit by

⁴ Sin-itiro Tomonaga 1906–1979.

⁵ Joaquin Luttinger 1923–1997.

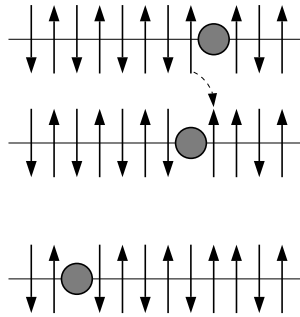


Fig. 7.9. Schematic view of charge and spin separation in a linear spin chain with antiferromagnetic order: a charge excitation (hole) is created (*upper part*) and moves away by hopping leaving a spin excitation behind (*second and third line*)

calculating the momentum distribution, which for the *Tomonaga–Luttinger model* does not exhibit the quasi-particle discontinuity of the Fermi liquids at k_F (see Fig. 7.6) but instead an infinite slope.

Including the spin, the model Hamiltonian \mathcal{H} would contain additional terms corresponding to collective spin excitations. As they are additive, the propagation of collective charge and spin excitations takes place with different velocities. This separation of charge and spin is another characteristic feature of a Luttinger liquid. It can be visualized for a spin chain with antiferromagnetic order (Fig. 6.6), as described by a 1D Hubbard model with half-filling and negative exchange coupling which is a lattice variant of the Luttinger liquid. A charge excitation corresponds to removing an electron with its spin (or to create a hole). This hole is surrounded by two parallel spins (upper part of Fig. 7.9). Its motion (to the left, see lower parts of Fig. 7.9) is ruled by the transfer matrix element and not connected with spin-flips thus, the moving hole is always surrounded by a pair of up/down spins, while the parallel spins remain at the site, where the hole was created.

7.5 Heavy Fermion Systems

Metallic systems with the Fermi energy in a range of the spectrum, where strongly localized states deriving from f electrons hybridize with delocalized states with s, p , or d character, show Fermi liquid behavior, however, with a strong enhancement of the Sommerfeld coefficient γ in the specific heat and also of the Pauli spin susceptibility χ^{Pauli} (see Sect. 7.3). In an independent particle description, both quantities are proportional to the density of states at the Fermi energy, which for isotropic systems is proportional to the effective mass m^* of the quasi-particles. Thus, the observed enhancement can be understood as a dramatic increase of the effective mass and these materials have been named, therefore, *heavy fermion* systems [110, 122, 225].

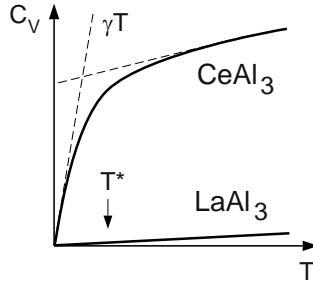


Fig. 7.10. Low-temperature behavior of the specific heat for a heavy fermion system (CeAl_3) compared with a normal metal (LaAl_3). The characteristic temperature T^* indicates the transition from heavy fermion to normal Fermi liquid behavior (after [122])

In general, heavy fermion systems are compounds with ions containing partially filled $4f$ (lanthanides) or $5f$ shells (actinides). For further characterization of their properties, one looks at the ratio $R = \pi^2 k_B^2 \chi^{\text{Pauli}} / 3\mu_{\text{eff}}^2 \gamma$, where μ_{eff} is the effective magnetic moment of the quasi-particles. For non-interacting quasi-particles, $R = 1$, because the effective mass drops out. In contrast, γ and χ^{Pauli} are modified differently by quasi-particle interactions which is reflected in $R \neq 1$. The enhancement of γ and χ^{Pauli} occurs only in a small temperature range below a characteristic temperature T^* of a few Kelvin. Above T^* , it disappears and these systems behave like normal Fermi liquids. This can be seen by comparing the temperature dependence of the specific heat of CeAl_3 and LaAl_3 (Fig. 7.10). The Ce compound differs from the otherwise identical system with La by the partial occupation of the $4f$ shell.

The appropriate Hamiltonian for modeling the electronic properties of heavy fermions is [122]

$$\mathcal{H} = \sum_{\mathbf{k}\sigma} \epsilon_{\mathbf{k}} c_{\mathbf{k}\sigma}^\dagger c_{\mathbf{k}\sigma} + \sum_{im} \epsilon_{fm} f_{im}^\dagger f_{im} + \frac{U}{2} \sum_{i,m \neq m'} n_{im}^f n_{im'}^f + \frac{1}{\sqrt{N}} \sum_{\mathbf{k}, \sigma, i, m} V_{\mathbf{k}\sigma m} \left(c_{\mathbf{k}\sigma}^\dagger f_{im} e^{-i\mathbf{k} \cdot \mathbf{R}_i} + c_{\mathbf{k}\sigma} f_{im}^\dagger e^{i\mathbf{k} \cdot \mathbf{R}_i} \right). \quad (7.100)$$

The first term describes the dispersive energy band $\epsilon_{\mathbf{k}}$ of the delocalized electrons with wave vector \mathbf{k} and spin σ . The second term represents the single-particle energies of the f electrons, localized at lattice sites \mathbf{R}_i , where $m = 1 \dots \nu_f$ counts the orbital degeneracy, while the third term is Hubbard's on-site Coulomb interaction of these electrons (with number operator n_{im}^f). The fourth term accounts for the hybridization of the f electrons with the delocalized Bloch electrons. Equation (7.100) is a variant of the *Anderson⁶ Hamiltonian*, which was originally formulated for only one site

⁶ Philip W. Anderson, *1923, Noble prize in Physics 1977 together with Sir Neville Mott and John H. Van Vleck.

occupied with an ion carrying f electrons (Anderson impurity model). This Hamiltonian combines two aspects of electronic structure: The hybridization (see Sect. 5.4) (which converts the localized f level into a band with finite width) with the correlation of the Hubbard model (which prevents double occupancy of f states at a given site).

Without the correlation term, the problem can be diagonalized as in Sect. 5.4. The correlation can be taken into account by a proper modification of the hybridization or hopping matrix element, which ensures that a conduction band electron does not hop to an already singly occupied f state. In fact, according to Fermi's golden rule, the rate of hopping between the conduction band and an f state is proportional to this matrix element squared. If it is renormalized by a factor $1 - n_f$, where n_f is the occupancy of the f state, the rate will be reduced as desired. For the hopping matrix element, this means the replacement

$$V_{\mathbf{k}\sigma m} \rightarrow rV_{\mathbf{k}\sigma m} = \tilde{V}_{\mathbf{k}\sigma m}, \quad (7.101)$$

where $r^2 = 1 - n_f$. In principle, this modification has to be done site dependent and with the number operator of the localized f electrons. By using r in the following as a parameter, a mean-field approach has been adopted, by which these site-dependent number operators are replaced by their mean value n_f . The relation between r and n_f is to be included as a subsidiary condition with the Lagrange parameter Λ in the Hamiltonian

$$\begin{aligned} \mathcal{H}_{\text{MF}} = & \sum_{\mathbf{k}\sigma} \epsilon_{\mathbf{k}} c_{\mathbf{k}\sigma}^\dagger c_{\mathbf{k}\sigma} + \sum_{im} \tilde{\epsilon}_{fm} f_{\mathbf{k}m}^\dagger f_{\mathbf{k}m} \\ & + \sum_{\mathbf{k},\sigma,m} rV_{\mathbf{k}\sigma m} \left(c_{\mathbf{k}\sigma}^\dagger f_{\mathbf{k}m} + f_{\mathbf{k}m}^\dagger c_{\mathbf{k}\sigma} \right) + \Lambda N(r^2 - 1). \end{aligned} \quad (7.102)$$

Here, the fermion operators of the f electrons are in the Bloch representation and $\tilde{\epsilon}_{fm} = \epsilon_{fm} + \Lambda$. This mean-field version of the Anderson Hamiltonian depends on the two parameters r and Λ which have to be determined at the end. It is advantageous to simplify the model by considering only a nondegenerate conduction band and an f orbital with degeneracy $\nu_f = 2$ by dropping the indices m and σ .

The diagonal form of the simplified mean-field operator

$$\mathcal{H}_{\text{MF}} = \sum_{\mathbf{k}l} E_l(\mathbf{k}) b_{\mathbf{k}l}^\dagger b_{\mathbf{k}l} + \Lambda N(r^2 - 1) \quad (7.103)$$

is obtained by replacing the fermion operators in (7.102) according to

$$f_{\mathbf{k}}^\dagger = \sum_l y_{\mathbf{k}l} b_{\mathbf{k}l}^\dagger, \quad c_{\mathbf{k}}^\dagger = \sum_l x_{\mathbf{k}l} b_{\mathbf{k}l}^\dagger, \quad (7.104)$$

where the index l refers to the two branches of the hybridized bands. The coefficients are determined by the normalization condition

$$|y_{\mathbf{k}l}|^2 + |x_{\mathbf{k}l}|^2 = 1 \quad (7.105)$$

and the coupled linear homogeneous equations

$$\begin{aligned} (\tilde{\epsilon}_f - E_l(\mathbf{k}))y_{\mathbf{k}l} + \tilde{V}_{\mathbf{k}}x_{\mathbf{k}l} &= 0 \\ \tilde{V}_{\mathbf{k}}^*y_{\mathbf{k}l} + (\epsilon_{\mathbf{k}} - E_l(\mathbf{k}))x_{\mathbf{k}l} &= 0. \end{aligned} \quad (7.106)$$

These equations signalize a second order perturbation calculation with respect to the hybridization and by eliminating e.g., $x_{\mathbf{k}ml}$ we have

$$\left(\tilde{\epsilon}_f - E_l(\mathbf{k}) + \frac{\tilde{V}_{\mathbf{k}}\tilde{V}_{\mathbf{k}}^*}{E_l(\mathbf{k}) - \epsilon_{\mathbf{k}}} \right) y_{\mathbf{k}l} = 0. \quad (7.107)$$

The coefficient $y_{\mathbf{k}l}$ is the probability amplitude for the quasi-particle in the band l to be in the f state. From (7.107), one obtains the two quasi-particle bands

$$E_{\pm}(\mathbf{k}) = \frac{1}{2} ((\epsilon_{\mathbf{k}} + \tilde{\epsilon}_f) \pm W(\epsilon_{\mathbf{k}})), \quad \text{with} \quad W(\epsilon_{\mathbf{k}}) = ((\epsilon_{\mathbf{k}} - \tilde{\epsilon}_f)^2 + 4\tilde{V}^2). \quad (7.108)$$

They are depicted in Fig. 7.11, where a linear dispersion is assumed for the conduction band $\epsilon_{\mathbf{k}}$. The requirement that the lower branch crosses the chemical potential for $k = k_F$, $E_-(k_F) = \mu$, allows one to determine from (7.107) the renormalized energy of the f level

$$\tilde{\epsilon}_f = \mu + \frac{\tilde{V}^2}{\epsilon_{k_F} - \mu}, \quad (7.109)$$

which for weak hybridization is slightly above μ .

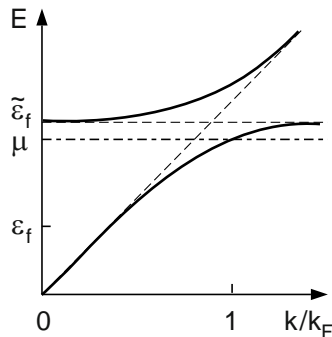


Fig. 7.11. Quasi-particle dispersion for heavy fermion behavior. The linear dispersion of the conduction band hybridizes with the renormalized level at $\tilde{\epsilon}_f$ of the f state (after [122])

The next task is to determine the two parameters r and Λ of the model. One obvious condition is that the ground state expectation value of the mean-field Hamiltonian takes a minimum with respect to the f state occupation n_f or the parameter r . This condition can be formulated as $\partial/\partial r \langle \Psi_0(r) | H_{\text{MF}} | \Psi_0(r) \rangle = 0$, which reduces because of the normalization of the ground state, to $\langle \Psi_0 | \partial H_{\text{MF}} / \partial r | \Psi_0 \rangle = 0$ or with (7.102)

$$\frac{1}{N} \sum_{\mathbf{k}} \tilde{V}_{\mathbf{k}} \langle \Psi_0 | c_{\mathbf{k}}^\dagger f_{\mathbf{k}} + f_{\mathbf{k}}^\dagger c_{\mathbf{k}} | \Psi_0 \rangle + 2\Lambda r^2 = 0. \quad (7.110)$$

The second relation is $n_f = 1 - r^2$, reformulated as

$$\frac{1}{N} \sum_{\mathbf{k}} \langle \Psi_0 | f_{\mathbf{k}}^\dagger f_{\mathbf{k}} | \Psi_0 \rangle + (r^2 - 1) = 0. \quad (7.111)$$

The first terms in these relations with the expectation values can be expressed with the help of the expansions (7.104) and the possibility to create the ground state $|\Psi_0\rangle$ by applying $b_{\mathbf{k}l}^\dagger$ for $|\mathbf{k}| \leq k_F$ to the fermion vacuum

$$\frac{1}{N} \sum_{\mathbf{k}} \langle \Psi_0 | f_{\mathbf{k}}^\dagger f_{\mathbf{k}} | \Psi_0 \rangle = \frac{\nu_f}{2} D(E_F) (\epsilon_{k_F} + W(\epsilon_{k_F}) - W(0)) = n_f \quad (7.112)$$

$$\frac{1}{N} \sum_{\mathbf{k}} \tilde{V} \langle \Psi_0 | c_{\mathbf{k}}^\dagger f_{\mathbf{k}} | \Psi_0 \rangle = -\nu_f D(E_F) \tilde{V}^2 \ln \left(\frac{\epsilon_{k_F} - \tilde{\epsilon}_f + W(\epsilon_{k_F})}{-\tilde{\epsilon}_f + W(0)} \right). \quad (7.113)$$

This leads in the leading logarithmic approximation to

$$r^2 = 1 - \nu_f D(E_F) \left((\epsilon_{k_F} - \mu) - \frac{\tilde{V}^2}{\mu} \right) \quad (7.114)$$

and

$$\Lambda = \nu_f D(E_F) V^2 \ln \left(\frac{(\epsilon_{k_F} - \mu)\mu}{\tilde{V}^2} \right). \quad (7.115)$$

It is useful to define a characteristic temperature T^* by

$$k_B T^* = \mu \exp \left(-\frac{\Lambda}{\nu_f D(E_F) V^2} \right), \quad (7.116)$$

which allows one to express the renormalized energy of the f level as

$$\tilde{\epsilon}_f = \mu + k_B T^* \quad (7.117)$$

and by eliminating ϵ_{k_F} to write

$$n_f = 1 - \frac{k_B T^*}{\nu_f D(E_F) V^2}. \quad (7.118)$$

Inspection of Fig. 7.11 sheds some light on the physics: Without hybridization the f level at ϵ_f would be occupied, $n_f = 1$, and also the conduction band states up to k_F . With hybridization, the f level is shifted above μ , thereby the occupation is reduced, and the conduction band is flattened out close to the chemical potential. The latter is connected with an increase of the density of states and a gain in energy, because the occupied conduction band states are now at lower energy. This gain in total energy can be quantified by comparing the ground state energies without ($E_0^{(0)}$) and with (E_0) hybridization:

$$E_0 - E_0^{(0)} = -k_B T^*. \quad (7.119)$$

Without giving further details of the calculation [122], one obtains for the Sommerfeld coefficient in the specific heat

$$\gamma = \frac{1}{3} \pi^2 k_B^2 \frac{n_f}{\tilde{\epsilon}_f - \mu} (2J + 1) \quad (7.120)$$

and for the spin susceptibility

$$\chi_{\text{spin}} = (gJ\mu_B)^2 \frac{n_f}{\nu_f(\tilde{\epsilon}_f - \mu)} \frac{2J + 1}{3}. \quad (7.121)$$

Both quantities show a strong increase with $\tilde{\epsilon}_f$ being close to the chemical potential μ . This explains the heavy fermion behavior.

7.6 Fractional Quantum Hall States

In this chapter, we have seen so far that the influence of electron correlation increases with the localization of the electrons due to their orbital motion. We found that systems with electrons at the Fermi energy in atomic d and f orbitals are destined to exhibit effects of the electron–electron interaction. There is quite a different system, where the localization is not a genuine property of an atomic orbital, but where it is due the orbital motion enforced by applying a magnetic field. Remember the two-dimensional electron systems of Sect. 5.6 and the discussion of the quantum Hall effects. A magnetic field applied perpendicular to the semiconductor hetero-interface forces the electrons into cyclotron orbits whose radius decreases with increasing magnetic field. This is the localization mechanism which eventually leads to a regime where correlation effects become significant. It is the regime of the fractional quantum Hall effect. This effect has been discovered only a few years after the integer QHE.

In 1982 Tsui, Stoermer, and Gossard [226] reported the observation of a QHE not at integer filling factors ν but at the fractional filling $\nu = 1/3$ of the lowest spin-split Landau level in a high-mobility GaAs/AlGaAs heterostructure. In the following years, with increasing perfections of the heterostructure

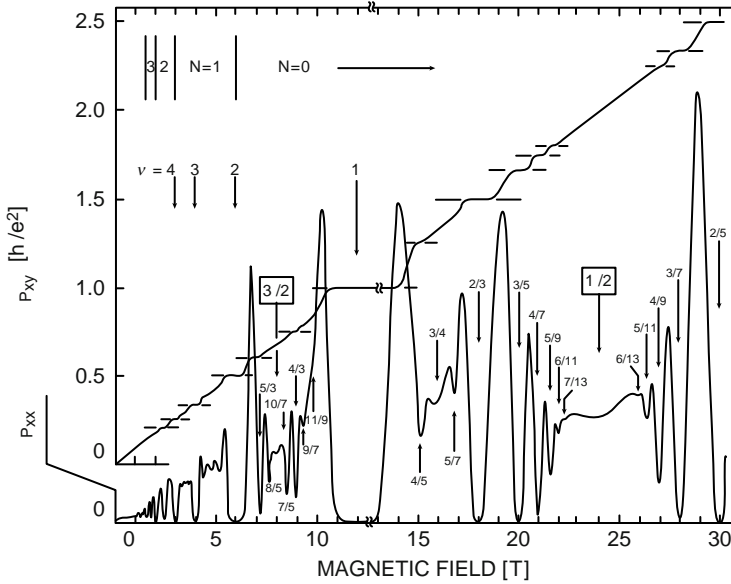


Fig. 7.12. Low-temperature data of the longitudinal (ρ_{xx}) and Hall resistance (ρ_{xy}) of a high-mobility two-dimensional electron system in a GaAs/AlGaAs heterostructure. N indicates the Landau level quantum number and ν the filling factor. After [227]

samples, a whole family of fractional quantum Hall states was discovered preferentially in the same material system (see Fig. 7.12) but also in semiconductor heterostructures with other material combinations. The characteristic features of the QHE, the plateaus of the Hall conductance, and the vanishing of the longitudinal magneto-resistance (in the first observation just a dip at $\nu = 1/3$), appear systematically at filling factors

$$\nu = \frac{p}{2p \pm 1} \quad (7.122)$$

with integer p . Remarkable is here the odd denominator and the convergence of the two series of fractions for the \pm sign from above and below toward the even fractional filling with $\nu = 1/2$, for which no plateau is detected and the longitudinal magneto-resistance does not decrease to zero.

Shortly after the discovery of the effect (and before most of the other fractions were discovered), Laughlin came up with the fundamental idea of an incompressible quantum liquid caused by electron correlation and designed the corresponding N electron wave function [228]. Tsui, Störmer, and Laughlin received jointly in 1998 the Nobel prize in physics for their discovery, which together with other contributions to the subject is well documented in several monographs [202–204].

In order to present Laughlin's idea, we have to briefly go through the single-particle description of two-dimensional electrons in a perpendicular magnetic field.

Supplement: Two-dimensional electrons in a magnetic field

The system Hamiltonian (without Zeeman term)

$$H = \frac{1}{2m^*} (\mathbf{p} + e\mathbf{A})^2 \quad (7.123)$$

can be written with the symmetric gauge of the vector potential $\mathbf{A} = B(y, -x, 0)/2$ in the form

$$H = \frac{1}{2m^*} (p_x^2 + p_y^2) + \frac{m^*}{2} \left(\frac{\omega_c^*}{2} \right)^2 (x^2 + y^2) - \frac{\omega_c^*}{2} L_z. \quad (7.124)$$

The effective mass m^* (and the cyclotron frequency $\omega_c^* = eB/m^*$) accounts for the fact that the electrons are in a subband deriving from the conduction band of a semiconductor. The symmetric gauge restores the cylindrical symmetry of the system according to which the z component of the angular momentum L_z commutes with the system Hamiltonian, which immediately can be recognized as that of two harmonic oscillators in the x, y planes, respectively. Accordingly, two sets of oscillator operators with standard commutation rules are introduced

$$\begin{aligned} a_x^\dagger &= \frac{1}{\sqrt{2}} \left(\frac{x}{l} - \frac{il}{\hbar} p_x \right), & a_x &= \frac{1}{\sqrt{2}} \left(\frac{x}{l} + \frac{il}{\hbar} p_x \right) \\ a_y^\dagger &= \frac{1}{\sqrt{2}} \left(\frac{y}{l} - \frac{il}{\hbar} p_y \right), & a_y &= \frac{1}{\sqrt{2}} \left(\frac{y}{l} + \frac{il}{\hbar} p_y \right), \end{aligned} \quad (7.125)$$

where $l = \sqrt{(\hbar/m^*\omega_c^*)} = \sqrt{(\hbar/eB)}$ is the magnetic length (see Sect. 4.2). The single-particle Hamiltonian

$$H = \frac{\hbar\omega_c^*}{2} \left\{ (a_x^\dagger a_x + a_y^\dagger a_y + 1) - i(a_y a_x^\dagger - a_x a_y^\dagger) \right\} \quad (7.126)$$

can be diagonalized by oscillator operators

$$\begin{aligned} a_+^\dagger &= \frac{1}{\sqrt{2}} (a_x^\dagger + ia_y^\dagger), & a_+ &= \frac{1}{\sqrt{2}} (a_x - ia_y) \\ a_-^\dagger &= \frac{1}{\sqrt{2}} (a_x^\dagger - ia_y^\dagger), & a_- &= \frac{1}{\sqrt{2}} (a_x + ia_y), \end{aligned} \quad (7.127)$$

which obey the commutation relations $[a_\pm, a_\pm^\dagger] = 1$. They can be understood as operators for right/left circular rotations around the direction of the magnetic field. With these operators, one finds

$$H = \frac{\hbar\omega_c^*}{2} (a_+^\dagger a_+ + a_-^\dagger a_- + 1) + \frac{\hbar\omega_c^*}{2} (a_+^\dagger a_+ - a_-^\dagger a_-) \quad (7.128)$$

$$= \hbar\omega_c^* \left(\hat{n}_+ + \frac{1}{2} \right) \quad (7.129)$$

with eigenvalues

$$\epsilon_{n_+n_-} = \hbar\omega_c^* \left(n_+ + \frac{1}{2} \right). \quad (7.130)$$

Note that the eigenvalues depend only on the quantum number n_+ while n_- counts the level degeneracy. The eigenstates of H can be created by multiple application of the raising operators onto the oscillator vacuum

$$|n_+n_-\rangle = \sqrt{\frac{1}{n_+!n_-!}} \left(a_+^\dagger \right)^{n_+} \left(a_-^\dagger \right)^{n_-} |00\rangle. \quad (7.131)$$

Instead of n_\pm , it is advantageous to use the quantum numbers $n = \min(n_+, n_-)$ and the angular momentum quantum number $m = n_+ - n_-$, which are related with the Landau level quantum number $n_L = n + (m + |m|)/2$. (Note: in Fig. 7.12 n_L is denoted N .)

In combining (7.125) and (7.127), it is suggestive to introduce the complex dimensionless variable $z = (x - iy)/l$ and the corresponding derivative $\partial/\partial z = (\partial/\partial x + i\partial/\partial y)l/2$ along with the conjugate definitions. This gives the following convenient properties

$$\frac{\partial}{\partial z} z - z \frac{\partial}{\partial z} = 1, \quad \frac{\partial}{\partial z} z^* - z^* \frac{\partial}{\partial z} = 0 \quad (7.132)$$

and similarly for the complex conjugates. The oscillator operators can now be written as

$$\begin{aligned} a_+^\dagger &= \frac{1}{2} \left(z^* - 2 \frac{\partial}{\partial z} \right), & a_+ &= \frac{1}{2} \left(z + 2 \frac{\partial}{\partial z^*} \right) \\ a_-^\dagger &= \frac{1}{2} \left(z - 2 \frac{\partial}{\partial z^*} \right), & a_- &= \frac{1}{2} \left(z^* + 2 \frac{\partial}{\partial z} \right) \end{aligned} \quad (7.133)$$

which lead to the Hamiltonian in dimensionless coordinate representation

$$H = \frac{1}{2} \hbar\omega_c^* \left(-4 \frac{\partial}{\partial z} \frac{\partial}{\partial z^*} + zz^* \right) - \frac{1}{2} \hbar\omega_c^* \left(z \frac{\partial}{\partial z} - z^* \frac{\partial}{\partial z^*} \right). \quad (7.134)$$

The lowest energy eigenfunction can be obtained from the conditions $a_\pm|00\rangle = 0$, which easily lead to the normalized wave function of the lowest Landau level.

Making use of the complex notation in the (x, y) plane, the normalized wave function for the lowest Landau level ($n_L = 0$) is given by

$$\varphi_{00}(\mathbf{r}) = \frac{1}{\sqrt{2\pi}l} \exp\left(-\frac{r^2}{4l^2}\right) = \frac{1}{\sqrt{2\pi}l} e^{-|z|^2/4}. \quad (7.135)$$

This wave function with angular momentum $m = 0$ is degenerate with finite angular momentum wave functions

$$\varphi_{0m}(z) = \frac{1}{\sqrt{2\pi}2^m m! l} z^m e^{-|z|^2/4}, \quad (7.136)$$

which have a maximum probability $|\varphi_{0m}(\mathbf{r})|^2$ on a circle with radius $\sqrt{2m}l$ and a spread of the order of the magnetic length l . Thus, a sample of circular

shape with radius R can accommodate only states with m values fulfilling the condition $2ml^2 < R^2$. This allows one to count the degeneracy of the Landau level. The maximum value of m is determined by the number of elementary flux quanta threading the sample area. This is the same result as the one obtained in Sect. 4.2 assuming the asymmetric Landau gauge.

Considering fractional quantum Hall states, Laughlin constructed a N -electron wave function from the single-particle wave functions of the lowest Landau level. Their general form, a linear combination of the φ_{0m} , is $\varphi(z) = f(z) \exp(-|z|^2/4)$ with a polynomial $f(z)$. The N -electron wave function, expressed as a linear combination of Slater determinants composed of these single-particle wave functions, has the general form

$$\Psi(z_1, \dots, z_N) = f(z_1, \dots, z_N) \exp\left(-\sum_{i=1}^N |z_i|^2/4\right). \quad (7.137)$$

Here, $f(z_1, \dots, z_N)$ is a polynomial in every variable z_i and its individual terms are products of $z_i^{m_i}$ indicating that the electron i is in an angular momentum eigenstate with m_i . The symmetry of the problem requires that the total angular momentum $\hbar M = \sum_i \hbar m_i$ is conserved and the wave function $\Psi(z_1, \dots, z_N)$ should contain only terms with the same M . Thus, the polynomial f has to be homogeneous. The antisymmetry of the Slater determinants makes this polynomial also antisymmetric in the particle coordinates.

On top of these symmetry requirements, the N -particle wave function, in order to describe a ground state, should by construction take into account that the electrons try to avoid each other due to the repulsive Coulomb interaction. This can be achieved by writing the polynomial as a product of functions $g(z_i - z_j)$ depending on the inter-particle separation. This form, which accounts for two-particle correlations, is known as a Jastrow-type wave function and was used before in atomic physics. Together with the general symmetry considerations $g(z)$ has to be an odd power polynomial. Moreover, Ψ is an eigenfunction of the total angular momentum $\hbar M$ where M counts the powers of the z_i , which are all the same and $M = N(N-1)m/2$. Thus, one arrives at the N electron wave function

$$\Psi_m(z_1, \dots, z_N) = \prod_{i < j} (z_i - z_j)^m \exp\left(-\sum_{i=1}^N |z_i|^2/4\right). \quad (7.138)$$

This is Laughlin's wave function.

As we have seen, the maximum possible angular momentum of a single particle state is determined by the degeneracy of the Landau level which is the sample area divided by $2\pi l^2$ or the number Φ/Φ_0 of flux quanta threading the sample. On the other hand, the maximum power (or angular momentum quantum number) of each z is given by $m(N-1)$ and we can equate (for $N \gg 1$)

$$mN = \frac{\Phi}{\Phi_0} \quad \text{or} \quad m = \frac{\Phi}{N\Phi_0} = \frac{1}{\nu}. \quad (7.139)$$

The last relation connects the angular momentum with the filling factor ν . For fractional filling $\nu = 1/m$ with odd m , the Laughlin wave function is an antisymmetric many-body wave function, where each electron position is an m -fold zero with respect to the dependence on all other electron positions. At the same time, m is the number of flux quanta (or vortices) attached to each electron.

An interpretation of this many-body wave function is possible by looking at

$$|\Psi_m(z_1, \dots, z_N)|^2 = e^{-\Phi_m(z_1, \dots, z_N)} \quad (7.140)$$

where

$$\Phi_m(z_1, \dots, z_N) = -2m \sum_{i < j} \ln |z_i - z_j| + \frac{1}{2l^2} \sum_{i=1}^N |z_i|^2 \quad (7.141)$$

is formally identical with the electrostatic energy of a charge-neutral two-dimensional plasma, where the first term accounts for the electron–electron interaction and the second for the interaction with the neutralizing background. The corresponding expression would be obtained by replacing $2m \rightarrow e^2$ and $1/2m\pi l^2$ by the particle density. Thus, $|\Psi_m(z_1, \dots, z_N)|^2$ is the classical probability distribution of N electrons in a plane with logarithmic interaction.

The quality of Laughlin’s wave function has been tested by projection onto ground state wave functions, which for small N were calculated numerically by exact diagonalization. These projections were found to be very close to 1. Another result, that characterizes Laughlin’s wave function is the radial distribution function

$$g_m(|z_1 - z_2|) = \frac{N(N-1)}{\rho_m^2} \int \dots \int \langle \Psi_m(z_1, \dots, z_N) |^2 d^2 z_3 \dots d^2 z_N. \quad (7.142)$$

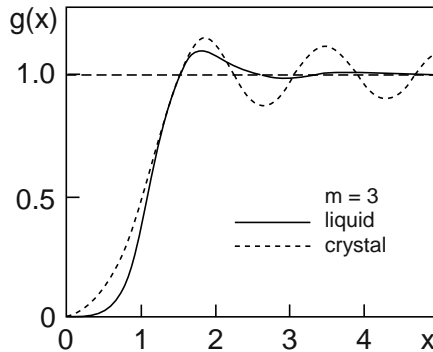


Fig. 7.13. Radial distribution function for the Laughlin state with $m = 3$ (solid line) and the Wigner crystal state in the HF approximation (dashed line) for the same density. Here, x is the inter-particle distance in units of $\sqrt{2ml}$ (after [203])

For $m = 3$ it is shown in Fig. 7.13 (solid line) together with the radial distribution function for the Wigner crystal (dashed line) calculated in the HF approximation. It has been found that the energy of the Laughlin wave function is always lower than that of the Wigner crystal. The radial distribution function indicates that in contrast with the Wigner crystal, the Laughlin state does not exhibit a long-range order and can be identified as a liquid. A more detailed investigation shows also that the excitation spectrum out of the Laughlin state has an energy gap, classifying the fractional quantum Hall states as *incompressible quantum liquids*. The excitation spectra uncover several unexpected properties of these states, such as the hierarchy, the fractional charge, and the composite fermion concept, for which the reader is referred to the literature [202–204, 229, 230].

The geometry of a Hall effect measurement is always connected with the finiteness of the sample with the edge of the sample representing a potential barrier for the electrons. Consequently, the Landau levels, which are constant except for fluctuations due to disorder (see Chap. 9), bend upwards towards the edge of the sample where they cross the Fermi energy. Thus, along the sample boundary, each Landau level represents a one-dimensional electron system, the so-called *edge channel*. In a classical picture, the edge channels correspond to skipping cyclotron orbits along the edge. The quantum Hall effect can be understood as transmission between the different probes of the Hall bar along these edge-channels [231, 232]. In the fractional QH regime, the edge-channels are seen also as a realization of one-dimensional systems of interacting electrons to which the Tomonaga–Luttinger model applies [204].

Problems

- 7.1 Calculate the commutators of $c_{\mathbf{k}\sigma}$ and $c_{\mathbf{k}\sigma}^\dagger$ with the interaction part \mathcal{H}_{int} of the Hamiltonian and verify (7.20).
- 7.2 Derive the Dyson equation (7.25) by making use of the Fourier transform of (7.23) in the equation of motion for the Green function.
- 7.3 Evaluate the commutators of $n_{i-\sigma}c_{i\sigma}$ with the single-particle and with the interaction term of the Hubbard Hamiltonian (7.45) for the one-dimensional case to verify (7.54) and (7.55).
- 7.4 Calculate the spectral weight $Z = (1 - \partial\Sigma/\partial E)^{-1}$ for the lower and upper Hubbard band, especially for the center of the band at $k = \pi/2a$.
- 7.5 Consider the Hubbard Hamiltonian for the case of half-filling and weak hopping or strong correlation. Show by applying perturbation theory in second order and by introducing spin operators

$$S_{iz} = \frac{1}{2} \sum_{\sigma} z_{\sigma} n_{i\sigma}, \quad S_{i\sigma} = c_{i\sigma}^\dagger c_{i-\sigma} \quad (7.143)$$

with $z_{\pm} = \pm 1$, that the Hubbard Hamiltonian can be mapped onto an operator of the Heisenberg type. Identify the sign of the exchange coupling and the magnetic order of the ground state.

- 7.6 Set up the Hamiltonian for a system with localized electrons and on-site correlation (e.g., d or f electrons) overlapping with delocalized electrons deriving e.g., from atomic s states! This Hamiltonian is known in the literature as the *Anderson Hamiltonian*.
- 7.7 Calculate the momentum distribution $n_{\mathbf{k}}$ at $T = 0$ by evaluating (7.87) in order to quantify the quasi-particle jump.
- 7.8 Evaluate the real part of Lindhard function (4.136) at $T = 0$ for the one-dimensional and the three-dimensional electron systems and discuss the behavior for $q \rightarrow k_F$ at $\omega = 0$. While for $d = 1$ the calculation can easily be carried out for finite ω and be discussed for $\omega \rightarrow 0$ it is advantageous to do the calculation for $d = 3$ from the beginning for $\omega = 0$.

Electron–Phonon Interaction

Based on the Born–Oppenheimer (or adiabatic) approximation (Chap. 2), the dynamics of the heavy and light constituents of a solid, the ions and the electrons, respectively, have been presented in the previous chapters as those of independent systems. For the lattice dynamics (Chap. 3), the electrons were considered only by their contribution to the binding forces which determine the dynamical matrix. For the electron systems, their energy spectrum and excitations (Chaps. 4–7), the position of the ions was kept fixed in the periodic configuration of a lattice, while the chemical nature of the ions determined the material specific properties. Releasing the Born–Oppenheimer approximation enables the two subsystems to communicate with each other by exchanging energy. This leads to a variety of effects, which are not restricted to solids but are found in all types of condensed matter including macromolecular systems in chemistry and biology.

The electrons experience the moving lattice as a perturbation of the periodic potential, which can be understood as scattering between electrons and phonons. Four scenarios will be considered here:

1. An excited electron gets rid of its excess energy by emitting phonons and at the same time changes its momentum. This leads to a finite *lifetime* of the carrier in its single-particle state.
2. An electron system in a solid driven by an external field (electric field, temperature gradient) adopts a nonequilibrium state. When the field is switched off, the electrons emit phonons and the system relaxes into an equilibrium state. This process of *electron–lattice relaxation* is characterized by a *transport relaxation time*. (In the same way an excited spin system can transfer its excess energy to the ion system and equilibrate by *spin–lattice relaxation*.) In thermodynamic terminology, the lattice is a heat bath serving as an energy sink or a reservoir. In exchanging energy with this bath, the relaxation processes change the phase of the individual electron wave function which makes these processes incoherent. By discussing these phenomena, electrical transport will become a

topic of this Section. Different physical scattering mechanisms, depending on the phonons involved, determine by their specific contributions the temperature-dependence of the *electric conductivity*.

3. Recalling the effect of electron–electron interaction (Chap. 4), the electron–phonon interaction also can lead to a new ground state of the system. Due to its charge, an electron creates a polarization cloud in a polar lattice, which moves around with the electron and changes its dynamic properties. Thus, electron–phonon interaction leads to a new quasi-particle, the electron and its polarization cloud, called *polaron* because of the polar electron–phonon coupling causing the interaction.
4. Electron–phonon interaction can result also in an attractive electron–electron interaction if the phonon emitted by one electron is absorbed by another one within their lifetimes (virtual phonon exchange). This phonon-mediated electron–electron interaction favors the formation of pairing of electrons, which is one of the basic mechanisms of *superconductivity*.

The different aspects of electron–phonon interaction are subjects of most textbooks in Solid State Theory. For complementary reading, we refer here to [10, 13, 14, 89, 95, 233, 234].

8.1 Preliminaries

Let us recall from Sect. 2.1 the separation of the Hamiltonian (2.1)

$$\mathcal{H}_0 = \mathcal{H}_{\text{el}} + \mathcal{H}_{\text{ion}} + \mathcal{H}_{\text{el-ion}}. \quad (8.1)$$

The electron–ion interaction with the general form

$$\mathcal{H}_{\text{el-ion}} = \sum_{l=1}^{N_e} \sum_{\mathbf{n}, \tau} v(\mathbf{r}_l - \mathbf{R}_{\mathbf{n}\tau}) \quad (8.2)$$

has been considered in the electronic energy $\mathcal{E}_{\text{el}}(\{\mathbf{R}_{\mathbf{n}\tau}\})$ as a contribution to the adiabatic potential $\mathcal{U}(\{\mathbf{R}_{\mathbf{n}\tau}\})$ defined in (2.26), which was the starting point for the lattice dynamics in Chap. 3. This energy, obtained as the eigenvalue of the electron problem (2.25) in a static configuration of the ions, was assumed later to be that of the equilibrium configuration $\{\mathbf{R}_{\mathbf{n}\tau}^0\}$. Here, we have to take into account the moving lattice with time-dependent positions $\mathbf{R}_{\mathbf{n}\tau}(t) = \mathbf{R}_{\mathbf{n}\tau}^0 + \mathbf{u}_{\mathbf{n}\tau}(t)$ and do this by expanding around the equilibrium positions

$$\mathcal{H}_{\text{el-ion}} = \sum_{l, \mathbf{n}, \tau} v(\mathbf{r}_l - \mathbf{R}_{\mathbf{n}\tau}^0) - \sum_{l, \mathbf{n}, \tau} \nabla_l v(\mathbf{r}_l - \mathbf{R}_{\mathbf{n}\tau}) \Big|_{\mathbf{R}_{\mathbf{n}\tau}^0} \cdot \mathbf{u}_{\mathbf{n}\tau} + \dots \quad (8.3)$$

The first term has become part of the effective periodic single-particle potential of the band structure problem (Chap. 5). In the second term, linear in

the displacements $\mathbf{u}_{n\tau}$, ∇_l means the derivative with respect to the position vector of the l th electron. This term will be considered in the following as the linear electron–phonon coupling $\mathcal{H}_{\text{el-ph}}$. The higher order terms, indicated by dots, will be neglected. The linear approximation is sufficient for displacements that are small compared to the lattice spacing, as will be assumed throughout this chapter.

It is advantageous for the illustration and for the evaluation of the interaction to make use of the occupation number representation and write it in terms of creation and annihilation operators. The lattice displacements can be formulated as (see Chap. 3, (3.23, 3.24) together with (3.39))

$$\begin{aligned}\mathbf{u}_{n\tau} &= \frac{1}{\sqrt{NM_\tau}} \sum_{s,\mathbf{q}} Q_{s,\mathbf{q}} \mathbf{e}_\tau^s(\mathbf{q}) e^{i\mathbf{q}\cdot\mathbf{R}_n^0} \\ &= \sum_{s,\mathbf{q}} \sqrt{\frac{\hbar}{2NM_\tau\omega_s(\mathbf{q})}} \mathbf{e}_\tau^s(\mathbf{q}) e^{i\mathbf{q}\cdot\mathbf{R}_n^0} (a_s^\dagger(-\mathbf{q}) + a_s(\mathbf{q}))\end{aligned}\quad (8.4)$$

with the boson operators $a_s^\dagger(\mathbf{q})$ and $a_s(\mathbf{q})$ of phonons with frequency $\omega_s(\mathbf{q})$ and eigenvectors $\mathbf{e}_\tau^s(\mathbf{q})$. The time-dependence is not indicated here to simplify notation.

The gradient of the potential is a single-particle term, which according to (4.76) can be written in terms of fermion operators for Bloch states (Problem 8.1). We want to simplify here the electron–phonon interaction within a single band, for which we adopt the effective mass approximation. For this case, we may write, with the help of the Fourier transform of the potential,

$$\sum_l \nabla_l v(\mathbf{r}_l - \mathbf{R}_{n\tau}) \Big|_{\mathbf{R}_{n\tau}^0} = i \sum_{\mathbf{q}',l} \mathbf{q}' v(\mathbf{q}') e^{i\mathbf{q}'\cdot(\mathbf{r}_l - \mathbf{R}_{n\tau}^0)} \quad (8.5)$$

and use

$$\sum_l e^{i\mathbf{q}'\cdot\mathbf{r}_l} = \sum_{\mathbf{k}} c_{\mathbf{k}+\mathbf{q}'}^\dagger c_{\mathbf{k}} \quad (8.6)$$

with the fermion operators $c_{\mathbf{k}+\mathbf{q}'}^\dagger$ and $c_{\mathbf{k}}$ for free electrons. Making use of (8.4) together with (8.5), we can perform the lattice sum in the second term of (8.3) with

$$\sum_{\mathbf{n}} e^{i(\mathbf{q}-\mathbf{q}')\cdot\mathbf{R}_n^0} = N \sum_{\mathbf{G}} \delta_{\mathbf{q}-\mathbf{q}',\mathbf{G}} \quad (8.7)$$

and write the linear electron–phonon interaction in the convenient operator form

$$\mathcal{H}_{\text{el-ph}} = \sum_{s,\mathbf{k},\mathbf{q},\mathbf{G}} \mathcal{V}_s(\mathbf{q}-\mathbf{G}) (a_s^\dagger(-\mathbf{q}) + a_s(\mathbf{q})) c_{\mathbf{k}+\mathbf{q}-\mathbf{G}}^\dagger c_{\mathbf{k}} \quad (8.8)$$

with the coupling matrix element

$$\mathcal{V}_s(\mathbf{q}-\mathbf{G}) = -i \sum_{\tau} \sqrt{\frac{N\hbar}{2M_\tau\omega_s(\mathbf{q})}} (\mathbf{q}-\mathbf{G}) \cdot \mathbf{e}_\tau^s(\mathbf{q}) e^{-i(\mathbf{q}-\mathbf{G})\cdot\boldsymbol{\tau}} v(\mathbf{q}-\mathbf{G}), \quad (8.9)$$

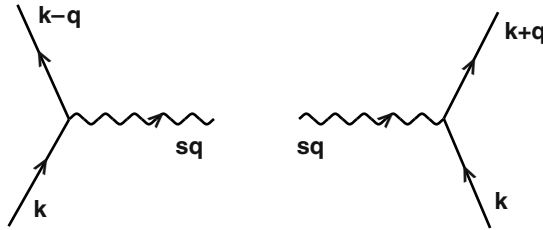


Fig. 8.1. Graphical representation of the electron–phonon interaction: phonon emission (*left*) and phonon absorption (*right*)

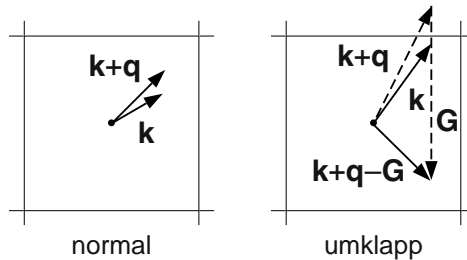


Fig. 8.2. Kinematics of the electron–phonon interaction: normal process (*left*) and Umklapp process (*right*), the thin solid lines mark the boundary of the first Brillouin zone

which depends on the coupling mechanism as will be outlined below.

The operator part of $\mathcal{H}_{\text{el-ph}}$ tells us about the kinematics as determined by the wave vectors. For this, we illustrate the interaction in graphical form (Fig. 8.1) and the kinematics in \mathbf{k} space (Fig. 8.2). The graphs contain the fermion operators as straight lines and the boson operator as a wavy line. $\mathcal{H}_{\text{el-ph}}$ contains only a single phonon operator: a phonon is created or annihilated, and two electron operators: a creation and an annihilation operator. In the interaction process, the electron is scattered between two Bloch states while a phonon is emitted or absorbed (see Fig. 8.1). The total momentum is conserved in the scattering (the sum of the wave vectors of the creation operators equals that of the annihilation operators, up to a reciprocal lattice vector). We note in passing that (8.8), although derived here for the electron–phonon system, is the standard form of a fermion–boson interaction. It applies as well to the coupling of electrons with photons or magnons and also to similar problems in nuclear physics.

Two characteristic scenarios are shown in Fig. 8.2 to demonstrate the kinematics of electron–phonon interaction. If the wave vectors of the electron before and after the scattering are within the 1st Brillouin zone and the momentum transfer is small (\mathbf{k} and $\mathbf{k} + \mathbf{q}$ are almost parallel), the scattering does not strongly change the direction of the moving electron. This is called the *normal process*. If the same small momentum transfer shifts the wave vector across

the Brillouin zone boundary, we have to bring it back by subtracting a reciprocal lattice vector, which almost inverts the direction of the moving electron (\mathbf{k} and $\mathbf{k} + \mathbf{q} - \mathbf{G}$ are almost antiparallel). This is called the *Umklapp process*. It is intuitively clear that the Umklapp processes take a stronger influence on the transport properties of electrons than the normal processes.

Formally, the energy balance of the scattering process will be considered by treating the electron–phonon interaction as a time-dependent perturbation, which leads to self-energy corrections changing the energy of the electrons and giving them a finite lifetime. But, it can be made clear from the graphs: the total energy is conserved and the energy of an emitted (absorbed) phonon has to be provided (is carried away) by the electron. The different coupling mechanisms, which depend on the lattice properties of the solid and exhibit characteristic dependencies on q , will be presented in the following Section.

8.2 Coupling Mechanisms

In Chap. 3, we have demonstrated the physical properties of phonons in different branches. The long-wavelength acoustic phonons were recognized as causing local lattice compression or dilation, while long-wavelength optical phonons have been identified with electrical dipole vibrations. These pictures are helpful in deriving the corresponding mechanisms of electron–phonon coupling.

Deformation Potential Coupling (Acoustic Phonons):

The local homogeneous compression or dilation $\Delta(\mathbf{r})$ caused by acoustic phonons in the long-wavelength limit can be described as a local relative volume change (Fig. 8.3)

$$\Delta(\mathbf{r}) = \left. \frac{\Delta V}{V} \right|_{\mathbf{r}}. \quad (8.10)$$

It is experienced by an electron as a local change of the lattice constant which shifts the single particle energy. If we consider a simple nondegenerate band

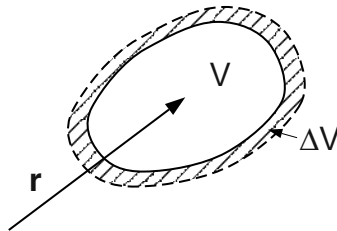


Fig. 8.3. Sketch of the homogeneous dilation caused by a longitudinal acoustic phonon

(deriving from atomic s states as e.g., the conduction band in a normal metal or semiconductor), the electron–phonon interaction can be written as a local potential seen by the electrons

$$\mathcal{H}_{\text{el-ph}} = - \sum_l D \Delta(\mathbf{r}_l), \quad (8.11)$$

where D is the *deformation potential* corresponding to the energy shift for a relative volume change $\Delta V/V = 1$. Deformation potentials are of the order of a few eV (see the data collection of Landolt–Börnstein [1]). The relative volume change caused by phonons, being much smaller than 1, is related with the flux of the continuous lattice displacement field $\mathbf{u}(\mathbf{r})$ through the area enclosing the volume V as depicted in Fig. 8.3. By Gauss’ theorem, we have

$$\Delta V = \oint \mathbf{u} \cdot d\mathbf{A} = \int_V \nabla \cdot \mathbf{u} \, dV \quad (8.12)$$

which for a homogeneous lattice distortion in the volume V (assumed to have a small linear extension compared with the wavelength of the phonon) can be written also as $V \nabla \cdot \mathbf{u}(\mathbf{r})$. Note that $\nabla \cdot \mathbf{u}(\mathbf{r})$ can be expressed as the trace of the strain tensor field, $\text{Tr}\epsilon(\mathbf{r})$ (Problem 8.2). The displacement field $\mathbf{u}(\mathbf{r})$ is obtained in the limit of long wavelengths from the expression for the displacement $\mathbf{u}_{n\tau}$ (3.23) by replacing $\mathbf{R}_n^0 \rightarrow \mathbf{r}$ and using the appropriate expression for the eigenvector $\mathbf{e}_\tau^s(\mathbf{q})$. As the electron–phonon interaction is determined by $\nabla \cdot \mathbf{u}(\mathbf{r})$, only the longitudinal acoustic phonons with $\mathbf{e}_\tau^{\text{LA}}(\mathbf{q}) = \sqrt{M_\tau/M} \mathbf{q}/q$ contribute, where M is the total mass of the ions in the Wigner–Seitz cell. Thus, we can write

$$\mathcal{H}_{\text{el-ph}} = -D \sum_l \nabla_l \cdot \mathbf{u}(\mathbf{r}_l) = -iD \sum_{l,\mathbf{q}} \frac{Q_{\text{LA}\mathbf{q}}}{\sqrt{NM}} \frac{\mathbf{q} \cdot \mathbf{q}}{q} e^{i\mathbf{q} \cdot \mathbf{r}_l} \quad (8.13)$$

and obtain with

$$Q_{\text{LA}\mathbf{q}} = \sqrt{\frac{\hbar}{2\omega_{\text{LA}}(\mathbf{q})}} \left(a_{\text{LA}}^\dagger(-\mathbf{q}) + a_{\text{LA}}(\mathbf{q}) \right) \quad (8.14)$$

and (8.6) the Hamiltonian for the *deformation potential coupling*

$$\mathcal{H}_{\text{el-ph}}^D = \sum_{\mathbf{k},\mathbf{q}} \mathcal{V}_q \left(a_{\text{LA}}^\dagger(-\mathbf{q}) + a_{\text{LA}}(\mathbf{q}) \right) c_{\mathbf{k}+\mathbf{q}}^\dagger c_{\mathbf{k}}. \quad (8.15)$$

The coupling matrix element reads

$$\mathcal{V}_q = -iD \sqrt{\frac{\hbar}{2NM c_{\text{LA}}}} q^{1/2} \quad (8.16)$$

where the use was made of the dispersion relation $\omega_{\text{LA}}(\mathbf{q}) = c_{\text{LA}} q$.

Supplement: Deformation potential coupling of electrons in a p band

In deriving (8.15), we have assumed the electrons to be in a simple s band. For energy bands originating from atomic orbitals with higher angular momentum, we have to consider the orbital degeneracy, according to which the Hamiltonian for the electron–phonon interaction becomes a matrix in the Bloch (or angular momentum) representation. Here, we face the same problem as in the effective-mass approximation for the p type valence band in semiconductors (see Sect. 5.5), which resulted in a 3×3 matrix Hamiltonian with bilinear expressions in the components of the wave vector as matrix elements and three-material specific parameters (L, M, N) , which define the curvature of the bands in different directions in \mathbf{k} space. This matrix can be expressed also in terms of angular momentum matrices for $I = 1$, which in the basis $|x\rangle, |y\rangle, |z\rangle$ read

$$I_x = \begin{pmatrix} 0 & 0 & 0 \\ 0 & 0 & -i \\ 0 & i & 0 \end{pmatrix}, \quad I_y = \begin{pmatrix} 0 & 0 & i \\ 0 & 0 & 0 \\ -i & 0 & 0 \end{pmatrix}, \quad I_z = \begin{pmatrix} 0 & -i & 0 \\ i & 0 & 0 \\ 0 & 0 & 0 \end{pmatrix}. \quad (8.17)$$

As it turns out, the $\mathbf{k} \cdot \mathbf{p}$ matrix \mathcal{M} (5.104) can be decomposed according to

$$\mathcal{M} = Ak^2\mathbf{1} + B \sum_{\alpha} \left(I_{\alpha}^2 - \frac{1}{3}I^2 \right) k_{\alpha}^2 - 2N \sum_{\alpha < \beta} \{I_{\alpha}, I_{\beta}\} k_{\alpha} k_{\beta}, \quad (8.18)$$

where in the first term $k^2 = k_x^2 + k_y^2 + k_z^2$ and $\mathbf{1}$ is a 3×3 unit matrix (which is proportional to $I_x^2 + I_y^2 + I_z^2$) and $\{I_{\alpha}, I_{\beta}\} = (I_{\alpha}I_{\beta} + I_{\beta}I_{\alpha})/2$, while the constants are related by $A = (L + 2M)/3$ and $B = -L + M$.

The individual terms of \mathcal{M} are invariant tensor products under the point group and can be formulated on group theoretical grounds [235, 236]. The symmetry properties of the symmetric second-rank strain tensor with the components $\epsilon_{\alpha\beta}$ are the same as those of the tensor formed by $k_{\alpha}k_{\beta}$. Therefore, in the same degeneracy space (here the 3-fold space of the p states), the Hamiltonian of the deformation potential coupling has the form

$$\mathcal{H}_{\text{el-ph}}^D = D_1 \text{Tr}\epsilon + D_2 \sum_{\alpha} \left(I_{\alpha}^2 - \frac{1}{3}I^2 \right) \epsilon_{\alpha\alpha} + 2D_3 \sum_{\alpha, \beta} \{I_{\alpha}, I_{\beta}\} \epsilon_{\alpha\beta}. \quad (8.19)$$

It consists of three invariant contributions connected with three deformation potentials. D_1 is recognized as the deformation potential of hydrostatic strain (as in (8.11)), while D_2 and D_3 correspond to shear strain in (001) and (111) direction, respectively. This strain Hamiltonian, originally derived for homogeneous static strain, is used here to describe the deformation potential coupling. The components of the strain tensor field $\epsilon_{\alpha\beta}(\mathbf{r})$, which are symmetrized derivatives of the displacement field (see (3.76)), can be expressed in terms of phonon operators as before and one obtains the matrix Hamiltonian for the deformation potential coupling of electrons in a p band. The complexity of this interaction Hamiltonian allows not only for the coupling to be longitudinal but also to transverse phonons (Problem 8.3). The same concept can be applied to energy bands with other orbital degeneracies and to coupling between different bands.

Polar Coupling with Optical Phonons or Fröhlich¹ Coupling

[237, 238]:

In the long-wavelength limit, longitudinal optical phonons cause a macroscopic polarization field

$$\mathbf{P}(\mathbf{r}) = \frac{\mathbf{M}(\mathbf{r})}{V} \quad (8.20)$$

with the electric dipole field $\mathbf{M}(\mathbf{r})$. A charge density $\rho(\mathbf{r})$ placed in this polarization field gives rise to the interaction energy

$$E_{\text{int}} = - \int \mathbf{P}(\mathbf{r}) \cdot \mathbf{E}(\mathbf{r}) d^3\mathbf{r} \quad (8.21)$$

with

$$\mathbf{E}(\mathbf{r}) = -\nabla_{\mathbf{r}} \int \frac{\rho(\mathbf{r}')}{4\pi\epsilon_0\epsilon_{\infty}|\mathbf{r} - \mathbf{r}'|} d^3\mathbf{r}', \quad (8.22)$$

where ϵ_{∞} is the background (or high frequency) dielectric constant. By partial integration, this can also be written as

$$E_{\text{int}} = - \int d^3\mathbf{r} (\nabla_{\mathbf{r}} \cdot \mathbf{P}(\mathbf{r})) \int d^3\mathbf{r}' \frac{\rho(\mathbf{r}')}{4\pi\epsilon_0\epsilon_{\infty}|\mathbf{r} - \mathbf{r}'|} \quad (8.23)$$

with the charge distribution given by

$$\rho(\mathbf{r}') = -\frac{e}{V} \sum_{l, \mathbf{q}'} e^{i\mathbf{q}' \cdot (\mathbf{r}' - \mathbf{r}_l)} = -\frac{e}{V} \sum_{\mathbf{q}'} e^{i\mathbf{q}' \cdot \mathbf{r}'} \sum_{\mathbf{k}} c_{\mathbf{k} - \mathbf{q}'}^{\dagger} c_{\mathbf{k}}. \quad (8.24)$$

The lattice displacement for longitudinal optical phonons in the long-wavelength limit reads in operator form

$$\mathbf{u}_{n\tau}^{\text{LO}} = \sum_{\mathbf{q}} \sqrt{\frac{\hbar}{2NM_{\tau}\omega_{\text{LO}}}} e_{\tau}^{\text{LO}}(\mathbf{q}) e^{i\mathbf{q} \cdot \mathbf{R}_n^0} \left(a_{\text{LO}}^{\dagger}(-\mathbf{q}) + a_{\text{LO}}(\mathbf{q}) \right). \quad (8.25)$$

Here we assume a crystal with two ions in the Wigner–Seitz cell with masses M_1 , M_2 and $M = M_1 + M_2$ for which the phonon eigenvectors are (see Problem 3.1)

$$\mathbf{e}_1^{\text{LO}}(\mathbf{q}) = \sqrt{\frac{M_2}{M}} \frac{\mathbf{q}}{q}, \quad \mathbf{e}_2^{\text{LO}}(\mathbf{q}) = -\sqrt{\frac{M_1}{M}} \frac{\mathbf{q}}{q}. \quad (8.26)$$

The moving ions, carrying the dynamical effective charge $\eta_1 = -\eta_2 = \eta$ (introduced in Sect. 3.5), provide a macroscopic dipole moment

$$\mathbf{M} = \sum_{n, \tau} \eta_{\tau} \mathbf{u}_{n, \tau} = \eta \sum_{n, \mathbf{q}} \sqrt{\frac{\hbar}{2N\mu\omega_{\text{LO}}}} \frac{\mathbf{q}}{q} e^{i\mathbf{q} \cdot \mathbf{R}_n^0} \left(a_{\text{LO}}^{\dagger}(-\mathbf{q}) + a_{\text{LO}}(\mathbf{q}) \right) \quad (8.27)$$

¹ Herbert Fröhlich, 1905 – 1991

where μ is the reduced ion mass. The continuum limit $\mathbf{M}(\mathbf{r})$ is obtained by replacing the discrete lattice vectors \mathbf{R}_n^0 by the local position vector \mathbf{r} . Thus, we can write

$$\nabla \cdot \mathbf{P}(\mathbf{r}) = i\eta \frac{N}{V} \sum_{\mathbf{q}} \sqrt{\frac{\hbar}{2N\mu\omega_{\text{LO}}}} \frac{\mathbf{q} \cdot \mathbf{q}}{q} e^{i\mathbf{q} \cdot \mathbf{r}} \left(a_{\text{LO}}^\dagger(-\mathbf{q}) + a_{\text{LO}}(\mathbf{q}) \right). \quad (8.28)$$

The two volume integrals in (8.23) are performed by taking the Fourier transform of $1/|\mathbf{r} - \mathbf{r}'|$ (see Appendix) to arrive at

$$\frac{1}{V} \int d^3r \int d^3r' e^{i\mathbf{q} \cdot \mathbf{r}} e^{i\mathbf{q}' \cdot \mathbf{r}'} \frac{1}{|\mathbf{r} - \mathbf{r}'|} = \frac{4\pi}{q^2} \delta_{\mathbf{q}, -\mathbf{q}'}. \quad (8.29)$$

Finally, we take the dynamical effective charge from (3.115) and use the Lyddane–Sachs–Teller relation (3.114) to replace the transverse optical phonon frequency by the longitudinal one

$$\eta = \left(\frac{\mu V \varepsilon_0}{N} \left(\frac{1}{\varepsilon_\infty} - \frac{1}{\varepsilon(0)} \right) \right)^{1/2} \varepsilon_\infty \omega_{\text{LO}} \quad (8.30)$$

to write E_{int} as the electron–phonon interaction for the *Fröhlich coupling*

$$\mathcal{H}_{el-ph}^{\text{F}} = \sum_{\mathbf{k}, \mathbf{q}} \mathcal{V}_q \left(a_{\text{LO}}^\dagger(-\mathbf{q}) + a_{\text{LO}}(\mathbf{q}) \right) c_{\mathbf{k}+\mathbf{q}}^\dagger c_{\mathbf{k}} \quad (8.31)$$

with the interaction matrix element

$$\mathcal{V}_q = i \left\{ \frac{e^2 \hbar \omega_{\text{LO}}}{2V \varepsilon_0} \left(\frac{1}{\varepsilon_\infty} - \frac{1}{\varepsilon(0)} \right) \right\}^{1/2} \frac{1}{q}. \quad (8.32)$$

The strength of the interaction is frequently quantified by the Fröhlich coupling constant

$$\alpha^{\text{F}} = \frac{e^2}{8\pi \varepsilon_0 \hbar \omega_{\text{LO}}} \left(\frac{2m^* \omega_{\text{LO}}}{\hbar} \right)^{1/2} \left(\frac{1}{\varepsilon_\infty} - \frac{1}{\varepsilon(0)} \right), \quad (8.33)$$

with the effective electron mass m^* . It is defined in analogy with the fine structure constant, which is the corresponding coupling constant for the electron–photon interaction and shall find an obvious meaning when dealing with the polaron in Sect. 8.4. Depending on the polarity, determined by the difference between ε_∞ and $\varepsilon(0)$ of the solid, on the effective mass and on the energy of the longitudinal optical phonon, α^{F} takes values between 0.07 in GaAs, 0.39 in CdTe, and 6.6 for RbBr (compared with the fine structure constant of $1/137$). For the *weak coupling* regime ($\alpha^{\text{F}} < 1$) the Fröhlich interaction can be treated by perturbation theory (see Sect. 8.4), while special concepts have been developed for the *strong coupling* regime ($\alpha^{\text{F}} > 1$) [239].

Piezoelectric Coupling (Acoustic Phonons):

In crystals without inversion symmetry, a homogeneous strain causes a dielectric polarization \mathbf{P} , known as the *piezoelectric effect*. It is quantified by the relation (double index summation understood)

$$P_i = e_{ijk}\epsilon_{jk}, \quad (8.34)$$

where e_{ijk} is the piezoelectric and ϵ_{jk} the strain tensor. Due to symmetry considerations, a third rank tensor has nonvanishing elements only for crystals lacking inversion symmetry [74, 235]. For the particular case of zinc blende, the piezoelectric tensor takes the form $e_{ijk} = e_{14}|\varepsilon_{ijk}|$ with the Levi–Civita symbol ε_{ijk} and the piezoelectric constant e_{14} (written in Voigt notation, see Sect. 3.4). The piezoelectric effect, originally related to static strain, applies as well to the dynamical case of strain fields connected with acoustic phonons and gives rise to the piezoelectric electron–phonon coupling. For this case, the classical interaction energy is to be formulated with the polarization field $\mathbf{P}(\mathbf{r})$ according to (8.34) with the strain field

$$\epsilon_{jk}(\mathbf{r}) = \frac{i}{2} (q_k u_j + q_j u_k) e^{i\mathbf{q}\cdot\mathbf{r}} \quad (8.35)$$

connected with the displacement field $\mathbf{u}(\mathbf{r}) = \mathbf{u} \exp(i\mathbf{q} \cdot \mathbf{r})$. For acoustic phonons, \mathbf{u} can be written as

$$\mathbf{u} = \sqrt{\frac{N}{M}} \sum_s Q_{s\mathbf{q}} \mathbf{e}^s(\mathbf{q}), \quad \text{with } \mathbf{e}^s(\mathbf{q}) = \sum_\tau \sqrt{\frac{M}{M_\tau}} \mathbf{e}_\tau^s(\mathbf{q}). \quad (8.36)$$

Taking the corresponding displacement field $\mathbf{P}(\mathbf{r})$, the *piezoelectric electron–phonon interaction* can be derived in analogy with the Fröhlich coupling (Problem 8.4). The result is

$$\mathcal{H}_{\text{el-ph}}^{\text{P}} = \sum_{s,\mathbf{k},\mathbf{q}} \mathcal{V}_{s\mathbf{q}} (a_s^\dagger(-\mathbf{q}) + a_s(\mathbf{q})) c_{\mathbf{k}+\mathbf{q}}^\dagger c_{\mathbf{k}} \quad (8.37)$$

with the coupling matrix element

$$\mathcal{V}_{s\mathbf{q}} = -\frac{2e\varepsilon_{14}}{\varepsilon_0\varepsilon_\infty} \sqrt{\frac{\hbar N}{2Mv_s}} \frac{1}{q^{1/2}} \left(\frac{q_x q_y e_z^s(\mathbf{q}) + c.p.}{q^2} \right), \quad (8.38)$$

where v_s is the sound velocity of the phonon branch s .

8.3 Scattering Processes: Lifetime, Relaxation

The electron–phonon interaction represents a link between the electron and phonon systems, which in the previous chapters have been investigated separately. In this Section, we consider it as a perturbation of the electron system by evaluating the scattering processes depicted in Fig. 8.1: phonon emission

and phonon absorption by a single electron. According to the time-dependence of the phonon operators, the electron–phonon interaction is periodic in time and Fermi’s Golden Rule applies. In general, the *scattering rate* between Bloch electron states with energies $\epsilon_{n\mathbf{k}}$ and $\epsilon_{n'\mathbf{k}'}$ under a perturbation H' is

$$r_{n\mathbf{k},n'\mathbf{k}'} = \frac{2\pi}{\hbar} |\langle n'\mathbf{k}' | H' | n\mathbf{k} \rangle|^2 \delta(\epsilon_{n\mathbf{k}} - \epsilon_{n'\mathbf{k}'} - \Delta\epsilon), \quad (8.39)$$

where $\Delta\epsilon$ is the energy change in the case of inelastic scattering. Considering scattering-out from the Bloch state with n, \mathbf{k} to all other possible Bloch states n', \mathbf{k}' , one finds the inverse single-particle or carrier *lifetime*

$$\frac{1}{\tau_{n\mathbf{k}}} = \sum_{n', \mathbf{k}'} r_{n\mathbf{k},n'\mathbf{k}'} (1 - f(n'\mathbf{k}')), \quad (8.40)$$

where $f(n'\mathbf{k}')$ is the distribution function. It vanishes if we consider a single electron in an otherwise empty band. In the language of Green functions, this lifetime is related with the imaginary part of a self-energy contribution $\hbar/\tau_{n\mathbf{k}}$, which represents a level broadening.

Taking now $\mathcal{H}_{\text{el-ph}}$ as the perturbation H' , we have to evaluate the matrix element with the electron and phonon states in the occupation number representation. This can formally be done, but the result is written immediately by inspection of the graphs for phonon absorption and emission processes (see Fig. 8.1). In the one-band approximation adopted in Sect. 8.2, we can drop the band index and know from momentum conservation that $\mathbf{k}' = \mathbf{k} + \mathbf{q}$ for normal processes, to which we can restrict ourselves here. The matrix elements of the phonon operators yield

$$\langle n_s(\mathbf{q}) - 1 | a_s(\mathbf{q}) | n_s(\mathbf{q}) \rangle = \sqrt{n_s(\mathbf{q})} \quad \text{for phonon absorption} \quad (8.41)$$

$$\langle n_s(\mathbf{q}) + 1 | a_s^\dagger(\mathbf{q}) | n_s(\mathbf{q}) \rangle = \sqrt{n_s(\mathbf{q}) + 1} \quad \text{for phonon emission} \quad (8.42)$$

with the phonon occupation numbers $n_s(\mathbf{q})$, and the inverse lifetime is expressed by

$$\begin{aligned} \frac{1}{\tau_{\mathbf{k}}} &= \frac{2\pi}{\hbar} \sum_{s, \mathbf{q}} |V_{s\mathbf{q}}|^2 (1 - f(\mathbf{k} + \mathbf{q})) \\ &\quad \times \left(n_s(\mathbf{q}) + \frac{1}{2} \mp \frac{1}{2} \right) \delta(\epsilon_{\mathbf{k}} - \epsilon_{\mathbf{k}+\mathbf{q}} \mp \hbar\omega_s(\mathbf{q})). \end{aligned} \quad (8.43)$$

Here, the upper(lower) sign refers to phonon absorption(emission). Phonon absorption is possible only if the occupation factor $n_s(\mathbf{q})$ differs from zero. Energy conservation in the scattering process (depicted in Fig. 8.4) is expressed by the δ -function. For conduction electrons in semiconductors with $\epsilon_{\mathbf{k}} \gg \hbar\omega_s(\mathbf{q})$, the scattering with acoustic phonons is almost elastic, while scattering with optical phonons is connected with a substantial change in energy.

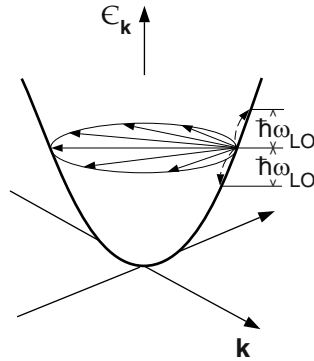


Fig. 8.4. Scattering of conduction electrons in a semiconductor with acoustic and optical phonons

The emission processes describe *energy dissipation* from the electrons to the lattice, which serves as a heat sink. The rate of energy transfer between the electron and phonon systems is given for this process by an expression similar to (8.44) but with an additional factor $\hbar\omega_s(\mathbf{q})/\epsilon_{\mathbf{k}}$ under the sum. For high energy transfer rates, the phonon system will be heated up and one has to consider phenomena related with *hot phonons*.

The general result of (8.44) can be specified for the different mechanisms of the electron–phonon interaction with their particular matrix elements, which differ with respect to their dependence on the wave vector \mathbf{q} of the emitted or absorbed phonon:

$$|\mathcal{V}_{\text{LA}q}|^2 \sim q \quad (\text{deformation potential coupling}) \quad (8.44)$$

$$|\mathcal{V}_{\text{LO}q}|^2 \sim q^{-2} \quad (\text{Fröhlich coupling}) \quad (8.45)$$

$$|\mathcal{V}_{\text{sq}}|^2 \sim q^{-1} \quad (\text{piezoelectric coupling}). \quad (8.46)$$

This has a consequence when evaluating the sum over \mathbf{q} as an integral with the thermal phonon and electron occupations. This is done by substitutions (see Appendix) which lead to different dependencies of these scattering mechanisms, their contribution to electron lifetime and energy dissipation, on the temperature.

The dynamical processes connected with electron–phonon scattering can be studied for two different scenarios. The first applies to semiconductors and insulators, where electrons in the conduction band can be created by optical excitation from the valence band. These electrons thermalize due to carrier–carrier interaction on a very short time scale and form a hot carrier system (with a temperature higher than the lattice temperature), which relaxes due to phonon emission (*energy relaxation*) and finally equilibrates with the lattice before the electrons and holes recombine [240–242]. These processes can be investigated in time-resolved spectroscopy [95, 243].

The second scenario is that of transport, which applies as well to metals as to doped semiconductors. The ensemble of carriers, which in an external electric field are accelerated, is described by a nonequilibrium distribution function $f(\mathbf{k}, T)$. The carriers dissipate their excess energy by emitting phonons. A stationary situation is achieved if the rate of energy gain of the carriers in the electric field equals the rate of energy dissipation by phonon emission. In a homogeneous system, this situation is accounted for by the *Boltzmann equation* (or Boltzmann's stationarity condition) [64, 244–246]

$$-\frac{e}{\hbar} \mathbf{E} \cdot \nabla_{\mathbf{k}} f(\mathbf{k}, T) = \left(\frac{\partial f(\mathbf{k}, T)}{\partial t} \right)_{\text{coll}}, \quad (8.47)$$

where the *lhs* accounts for the rate of energy gain by the carriers in the field \mathbf{E} . The *rhs* of this relation, the scattering or *collision term*, can be formulated in terms of the single-particle scattering rates $r_{\mathbf{k}, \mathbf{k}'}$ and occupation factors

$$\left(\frac{\partial f(\mathbf{k}, T)}{\partial t} \right)_{\text{coll}} = \sum_{\mathbf{k}'} \{ (1 - f(\mathbf{k}, T)) f(\mathbf{k}', T) r_{\mathbf{k}, \mathbf{k}'} - f(\mathbf{k}, T) (1 - f(\mathbf{k}', T)) r_{\mathbf{k}' \mathbf{k}} \}, \quad (8.48)$$

where the first term under the sum on the *rhs* represents the scattering processes into the state with \mathbf{k} while the second term represents scattering-out from this state. For isotropic scattering rates, $r_{\mathbf{k}, \mathbf{k}'} = r_{\mathbf{k}' \mathbf{k}}$, we find

$$\left(\frac{\partial f(\mathbf{k}, T)}{\partial t} \right)_{\text{coll}} = \sum_{\mathbf{k}'} r_{\mathbf{k}, \mathbf{k}'} (f(\mathbf{k}', T) - f(\mathbf{k}, T)). \quad (8.49)$$

Instead of these microscopic expressions, the collision term is frequently treated in the *relaxation time approximation*

$$\left(\frac{\partial f(\mathbf{k}, T)}{\partial t} \right)_{\text{coll}} = -\frac{f(\mathbf{k}, T) - f_0(\mathbf{k}, T)}{\tau_{\text{tr}}(\mathbf{k})}, \quad (8.50)$$

which describes the evolution of the nonequilibrium distribution $f(\mathbf{k}, T)$ into the equilibrium distribution $f_0(\mathbf{k}, T)$ in the characteristic *transport relaxation time* $\tau_{\text{tr}}(\mathbf{k})$. Equations (8.47) and (8.50) can be solved by iteration

$$\begin{aligned} f(\mathbf{k}, T) &= f_0(\mathbf{k}, T) + \frac{e}{\hbar} \tau_{\text{tr}}(\mathbf{k}) \mathbf{E} \cdot \nabla_{\mathbf{k}} f(\mathbf{k}, T) \\ &= f_0(\mathbf{k}, T) + \frac{e}{\hbar} \tau_{\text{tr}}(\mathbf{k}) \mathbf{E} \cdot \nabla_{\mathbf{k}} f_0(\mathbf{k}, T) + \dots \end{aligned} \quad (8.51)$$

For small deviations from the equilibrium distribution, it is sufficient to take into account only the lowest order correction (linear in \mathbf{E}), which defines the regime of *linear transport*, while the higher order terms describe the nonlinear transport [247].

The physical observable to quantify the carrier transport, the electric current density, can be expressed as

$$\mathbf{j} = -\frac{e}{V} \sum_{\mathbf{k}} \mathbf{v}(\mathbf{k}) f(\mathbf{k}, T). \quad (8.52)$$

Here, the carrier velocity $\mathbf{v}(\mathbf{k})$ is the group velocity of electrons in an energy band $\epsilon_{\mathbf{k}}$

$$\mathbf{v}(\mathbf{k}) = \frac{1}{\hbar} \nabla_{\mathbf{k}} \epsilon_{\mathbf{k}}, \quad (8.53)$$

which for a simple parabolic band equals $\hbar \mathbf{k}/m^*$ with the effective mass m^* . Consider now one component of the current density with the nonequilibrium distribution function from (8.51)

$$j_{\alpha} = -\frac{e}{V} \sum_{\mathbf{k}} v_{\alpha}(\mathbf{k}) \left\{ f_0(\mathbf{k}, T) + \frac{e\tau_{\text{tr}}(\mathbf{k})}{\hbar} \sum_{\beta} \frac{\partial f_0(\mathbf{k}, T)}{\partial k_{\beta}} E_{\beta} \right\}. \quad (8.54)$$

The first term on the *rhs* vanishes because the system in equilibrium does not carry a current. By writing the distribution function as $f(\epsilon_{\mathbf{k}}, T)$, the derivative with respect to k_{β} in the second term becomes

$$\frac{\partial f_0(\mathbf{k}, T)}{\partial k_{\beta}} = \frac{\partial f_0(\epsilon, T)}{\partial \epsilon} \frac{\partial \epsilon_{\mathbf{k}}}{\partial k_{\beta}} = \frac{\partial f_0(\epsilon, T)}{\partial \epsilon} \hbar v_{\beta}(\mathbf{k}), \quad (8.55)$$

and we find Ohm's law in the form

$$j_{\alpha} = \sum_{\beta} \sigma_{\alpha\beta} E_{\beta} \quad (8.56)$$

with the *electric conductivity*

$$\sigma_{\alpha\beta} = -\frac{e^2}{V} \sum_{\mathbf{k}} \tau_{\text{tr}}(\mathbf{k}) \frac{\partial f_0(\epsilon, T)}{\partial \epsilon} v_{\alpha}(\mathbf{k}) v_{\beta}(\mathbf{k}). \quad (8.57)$$

This second rank tensor resembles the form derived in Chap. 2 within the concepts of linear response (see Problem 2.4), and we may recognize the correlation between the two components of the velocity. On the other hand, here the appearance of the transport relaxation time is a new aspect. It accounts for the dissipation of energy in collisions, which is essential for obtaining a finite conductivity.

Comparing (8.49) and (8.50) we may identify

$$\frac{f(\mathbf{k}, T) - f_0(\mathbf{k}, T)}{\tau_{\text{tr}}(\mathbf{k})} = \sum_{\mathbf{k}'} r_{\mathbf{k}, \mathbf{k}'} (f(\mathbf{k}, T) - f(\mathbf{k}', T)). \quad (8.58)$$

and see that in general the transport relaxation time depends on the distribution function, which limits the validity of the relaxation time approximation.

However, this is not the case for an isotropic dispersion $\epsilon_{\mathbf{k}} = \epsilon_k$ and elastic scattering for which we may write

$$f(\mathbf{k}) = f_0(\mathbf{k}) + \mathbf{k} \cdot \mathbf{E} \mathcal{C}(k) \quad (8.59)$$

and similar for $f(\mathbf{k}')$ with the electric field \mathbf{E} and a scalar function $\mathcal{C}(k) = \mathcal{C}(k')$. In polar coordinates with respect to the direction of \mathbf{E} , one has

$$\mathbf{k} \cdot \mathbf{E} = kE \cos \vartheta \quad \text{and} \quad \mathbf{k} \cdot \mathbf{k}' = k^2 \cos \vartheta', \quad (8.60)$$

where ϑ' is the angle between \mathbf{k} and \mathbf{k}' , and

$$\mathbf{k}' \cdot \mathbf{E} = kE(\cos \vartheta \cos \vartheta' + \sin \vartheta \sin \vartheta' \cos \varphi'). \quad (8.61)$$

As a consequence, the difference $f(\mathbf{k}) - f(\mathbf{k}')$ can be expressed as

$$f(\mathbf{k}) - f(\mathbf{k}') = kE \mathcal{C}(k) (\cos \vartheta (1 - \cos \vartheta') - \sin \vartheta \sin \vartheta' \cos \varphi') \quad (8.62)$$

where the second term on the *rhs* vanishes by integration over φ' (note that for isotropic scattering $r_{\mathbf{k},\mathbf{k}'}$ depends on $\mathbf{k} - \mathbf{k}'$) which gives with $d\Omega' = d\varphi' \sin \vartheta' d\vartheta'$

$$\int d\Omega' (f(\mathbf{k}) - f(\mathbf{k}')) = kE \mathcal{C}(k) \cos \vartheta \int d\Omega' (1 - \cos \vartheta'). \quad (8.63)$$

With (8.59), we identify the factor in front of the integral on the *rhs* as $f(\mathbf{k}) - f_0(\mathbf{k})$ and obtain, using (8.39), for the relaxation rate

$$\frac{1}{\tau_{\text{tr}}(\mathbf{k})} = \frac{1}{4\pi^2 \hbar} \int |\langle \mathbf{k} | H' | \mathbf{k}' \rangle|^2 \delta(\epsilon_{\mathbf{k}} - \epsilon_{\mathbf{k}'}) (1 - \cos \vartheta') d^3 k' \quad (8.64)$$

which is independent of the distribution function. The factor $1 - \cos \vartheta'$ under the integral tells us that collisions by which the propagation direction of the charge carrier is reversed ($\vartheta' \simeq \pi$, *back scattering*) contribute much to the relaxation rate, while the effect of *forward scattering* with $\vartheta' \ll \pi$ is only small.

For further evaluation of $\sigma_{\alpha\beta}$ (8.57), let us assume the electric field in the z direction. Then, we have σ_{zz} as the only nonvanishing component of the conductivity tensor. The sum over \mathbf{k} can be performed in spherical polar coordinates. By making use of the dispersion relation $\epsilon_{\mathbf{k}} = \hbar^2 k^2 / 2m^*$, we can write with $v_z(\mathbf{k}) = \hbar k_z / m^*$ and $k_z = k \cos \theta$

$$v_z^2(\mathbf{k}) = \frac{2}{m^*} \epsilon \cos^2 \theta \quad (8.65)$$

and formulate the remaining integration over k as an energy integral

$$\sigma_{zz} = -\frac{e^2}{3m^* \pi^2} \left(\frac{2m^*}{\hbar^2} \right)^{3/2} \int \epsilon^{3/2} \tau_{\text{tr}}(\epsilon) \frac{\partial f_0(\epsilon, T)}{\partial \epsilon} d\epsilon. \quad (8.66)$$

The transport relaxation time is a power function of the carrier energy ϵ . Integrals of this type can be evaluated by using the fact that $\partial f_0(\epsilon, T)/\partial\epsilon$ is a symmetric function with a pronounced maximum at $\epsilon = \mu$ (see Appendix).

Depending on the temperature, two limiting cases shall be discussed here. For a degenerate electron system with $E_F \gg k_B T$, the derivative of the Fermi distribution function can be written as $\partial f_0/\partial\epsilon \simeq -\delta(\epsilon - E_F)$ thus giving

$$\sigma_{zz} = \frac{e^2 n \tau(E_F)}{m^*} \quad (8.67)$$

with the degenerate carrier density

$$n = \frac{1}{3\pi^2} \left(\frac{2m^*}{\hbar^2} \right)^{3/2} E_F^{3/2}. \quad (8.68)$$

Formally, this result is identical with that obtained by the classical Drude theory [12, 29, 31]. However, here, the quantum statistical nature of the degenerate electron system becomes relevant in the dependence on the Fermi energy and the transport relaxation time can be traced back to the microscopic scattering processes.

For the nondegenerate carrier system, $k_B T \gg \epsilon$, the derivative of the distribution function takes the form $\partial f_0/\partial\epsilon \simeq -\exp(-\epsilon/k_B T)/k_B T$ and we may write

$$\sigma_{zz} = \frac{e^2 n \langle \tau(\epsilon) \rangle}{m^*} \quad (8.69)$$

with the nondegenerate carrier density

$$n = \frac{1}{2\pi^2} \left(\frac{2m^*}{\hbar^2} \right)^{3/2} \int d\epsilon \epsilon^{1/2} e^{-\epsilon/k_B T} \quad (8.70)$$

and the averaged transport relaxation time

$$\langle \tau(\epsilon) \rangle = \frac{2}{3k_B T} \frac{\int d\epsilon \epsilon^{3/2} \tau(\epsilon) e^{-\epsilon/k_B T}}{\int d\epsilon \epsilon^{1/2} e^{-\epsilon/k_B T}}. \quad (8.71)$$

The effects of the band structure (here the effective mass) and of the scattering processes are comprised in the *mobility*

$$\mu = \frac{e \langle \tau \rangle}{m^*} \quad (8.72)$$

with the temperature-dependent transport relaxation time τ . Thus, the conductivity is written in the form $\sigma = en\mu$. The mobility is frequently measured in magneto-transport experiments making use of the Hall effect and then called *Hall mobility*. An example is shown in Fig. 8.5 for *n*-doped GaAs. The measured values are compared with the calculated mobilities for different scattering mechanisms (Problem 8.5). Besides scattering with phonons, which

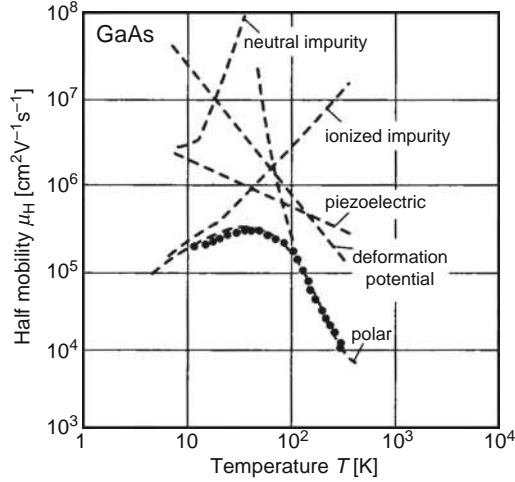


Fig. 8.5. Hall mobility *versus* temperature for *n*-doped GaAs, showing experimental data together with the contributions from different scattering mechanisms, after [89]

limits the mobility at high temperatures, scattering also with impurities (see Chap. 9) is considered. The latter dominates the mobility at low temperature, when the phonons are frozen out. For degenerate electron systems, the relaxation time can be converted into a *mean free path* $l_{\text{mfp}} = v_F \tau$, which is the average distance between collisions covered by a carrier with Fermi velocity v_F .

Note that the momentum selection rule represents a geometrical constraint depending on the system dimension. Thus, compared with the three-dimensional case, electron–phonon interaction is modified in electron systems with reduced dimensionality (e.g., for electrons confined at semiconductor heterostructures or in quantum wells or quantum wires). Moreover, by remote doping, the ionized impurities can be separated from the mobile carriers to suppress the scattering. This leads to an enormous increase of the mobility at low temperatures. Thus, carrier confinement takes influence on the lifetime [242, 243, 248]. At the same time, the mean-free-path, the distance between successive scattering events, can become comparable or larger than the system dimension, as is typical for mesoscopic systems. In this case, the carrier passes through the sample without being scattered and the transport is called ballistic.

8.4 The Fröhlich Polaron

In contrast with the single-particle approximation in Chaps. 4 and 5, where a free electron or a Bloch state was an eigenstate of the electron Hamiltonian, these states are now perturbed by the electron–phonon interaction. We

encounter a similar situation as for interacting electrons: As the electron–electron interaction gives rise to formation of quasi-particles consisting of the bare particle and a cloud of virtual collective excitations, so does the electron–phonon interaction. But now, instead of charge or spin density excitations, the electron (or hole) will be dressed by a cloud of virtual phonons. This composite particle is called *polaron* with particular reference to the lattice deformation in a polar semiconductor or insulator by a charge carrier, which repels the ions with the same charge but attracts those with the opposite charge thus generating a distortion typical for optical phonons. The interaction to be considered in this case is the Fröhlich coupling.

We follow here [4, 14] and adopt the concept of lowest order perturbation theory to calculate the change of the single-electron state $|\mathbf{k}\rangle$ and its energy by the coupling with longitudinal optical phonons. We consider the state $|\mathbf{k}, 0_{\mathbf{q}}\rangle$ as the eigenstate of $\mathcal{H}_{\text{el}} + \mathcal{H}_{\text{ph}}$ characterizing an electron in the undistorted harmonic lattice. Due to electron–phonon interaction, this state gets modified by contributions from states with phonons. The lowest order correction is due to one-phonon contributions

$$|\mathbf{k}, 0_{\mathbf{q}}\rangle^{(1)} = |\mathbf{k}, 0_{\mathbf{q}}\rangle + \sum_{\mathbf{q}} |\mathbf{k} - \mathbf{q}, 1_{\mathbf{q}}\rangle \frac{\langle \mathbf{k} - \mathbf{q}, 1_{\mathbf{q}} | \mathcal{H}_{\text{el-ph}} | \mathbf{k}, 0_{\mathbf{q}} \rangle}{\epsilon_{\mathbf{k}} - \epsilon_{\mathbf{k}-\mathbf{q}} - \hbar\omega_{\text{LO}}}. \quad (8.73)$$

The lattice distortion caused by the carrier can be quantified by the expectation value of the phonon number operator which due to the first order correction is

$$\bar{n} = \sum_{\mathbf{q}} \frac{|\langle \mathbf{k} - \mathbf{q}, 1_{\mathbf{q}} | \mathcal{H}_{\text{el-ph}} | \mathbf{k}, 0_{\mathbf{q}} \rangle|^2}{(\epsilon_{\mathbf{k}} - \epsilon_{\mathbf{k}-\mathbf{q}} - \hbar\omega_{\text{LO}})^2}. \quad (8.74)$$

This expression is still not specified to one of the coupling mechanisms and yields different results for the sum over \mathbf{q} according to the q dependence of the interaction matrix element. For the Fröhlich interaction, we have $\hbar\omega_{\mathbf{q}} \rightarrow \hbar\omega_{\text{LO}}$ and may write with

$$\epsilon_{\mathbf{k}} - \epsilon_{\mathbf{k}-\mathbf{q}} - \hbar\omega_{\text{LO}} = \frac{\hbar^2}{2m^*} (2\mathbf{k} \cdot \mathbf{q} - q^2 - q_{\text{LO}}^2), \quad (8.75)$$

where $q_{\text{LO}}^2 = 2m^*\omega_{\text{LO}}/\hbar$, the sum over \mathbf{q} as an integral over the Brillouin zone

$$\bar{n} = |C|^2 \left(\frac{2m^*}{\hbar^2} \right)^2 \frac{V}{2\pi^3} \int \frac{1}{q^2} \frac{1}{(2\mathbf{k} \cdot \mathbf{q} - q^2 - q_{\text{LO}}^2)^2} d^3\mathbf{q}, \quad (8.76)$$

where $|C|^2 = e^2\hbar\omega_{\text{LO}}/2V\varepsilon_0(1/\varepsilon_{\infty} - 1/\varepsilon(0))$. Let us consider the state with $\mathbf{k} = 0$, representing an electron at rest. Then the integral can be performed in spherical polar coordinates over a sphere with radius q_{BZ} equal to the volume of the Brillouin zone

$$\int \dots d^3\mathbf{q} = 4\pi \left(\frac{2m^*}{\hbar^2} \right)^2 \int_0^{q_{\text{BZ}}} \frac{dq}{(q^2 + q_{\text{LO}}^2)^2}. \quad (8.77)$$

The indefinite integral gives

$$\int \frac{dq}{(q^2 + q_{\text{LO}}^2)^2} = \frac{1}{2q_{\text{LO}}} \left(\frac{q}{q^2 + q_{\text{LO}}^2} + \frac{1}{q_{\text{LO}}} \arctan \frac{q}{q_{\text{LO}}} \right). \quad (8.78)$$

For $q_{\text{LO}} \ll q_{\text{BZ}}$, because the wave vector of an electron at the energy of the LO phonon is much smaller than the Brillouin zone, the upper limit can be extended to infinity and the integral simplifies to $\pi/4q_{\text{LO}}^3$. Taking the interaction constant C from (8.33), we find

$$\bar{n} = \frac{\alpha^{\text{F}}}{2}, \quad (8.79)$$

i.e., in this lowest order perturbation, the composite particle polaron consists, of the electron and a number of phonons which is determined by the coupling constant. A similar calculation can be performed also for the other coupling mechanisms (Problem 8.6). For polar semiconductors, this number is much smaller than one, which *a posteriori* justifies the perturbation treatment. In systems with much larger coupling constants, more elaborate concepts have to be applied [239].

The first order perturbation correction to the free particle energy $\epsilon_{\mathbf{k}} = \hbar^2 k^2 / 2m^*$ is given by

$$\Delta\epsilon_{\mathbf{k}}^{(1)} = \sum_{\mathbf{q}} \frac{|\langle \mathbf{k} - \mathbf{q}, 1_{\mathbf{q}} | \mathcal{H}_{\text{el-ph}} | \mathbf{k}, 0_{\mathbf{q}} \rangle|^2}{(\epsilon_{\mathbf{k}} - \epsilon_{\mathbf{k}-\mathbf{q}} - \hbar\omega_{\text{LO}})}. \quad (8.80)$$

As before, the sum over \mathbf{q} can be written as an integral to have

$$\Delta\epsilon_{\mathbf{k}}^{(1)} = |C|^2 \frac{2m^*}{\hbar^2} \frac{V}{2\pi^3} \int \frac{1}{q^2} \frac{1}{2\mathbf{k} \cdot \mathbf{q} - q^2 - q_{\text{LO}}^2} d^3\mathbf{q}. \quad (8.81)$$

Being interested now in the dispersion relation for the composite particle, we expand the integrand for small \mathbf{k} and find for the leading terms

$$\frac{1}{2\mathbf{k} \cdot \mathbf{q} - q^2 - q_{\text{LO}}^2} = \frac{-1}{q^2 + q_{\text{LO}}^2} \left(1 + \frac{2\mathbf{k} \cdot \mathbf{q}}{q^2 + q_{\text{LO}}^2} + \left(\frac{2\mathbf{k} \cdot \mathbf{q}}{q^2 + q_{\text{LO}}^2} \right)^2 + \dots \right). \quad (8.82)$$

When integrating in spherical polar coordinates, the second term on the *rhs* vanishes while the first and third terms can be evaluated with the integrals

$$\int \frac{d q}{q^2 + q_{\text{LO}}^2} = \frac{1}{q_{\text{LO}}} \arctan \frac{q}{q_{\text{LO}}} \quad \text{and} \quad (8.83)$$

$$\int \frac{q^2 d q}{(q^2 + q_{\text{LO}}^2)^3} = \frac{1}{8q_{\text{LO}}^2} \left(\frac{q(q^2 - q_{\text{LO}}^2)}{(q^2 + q_{\text{LO}}^2)^2} + \frac{1}{q_{\text{LO}}} \arctan \frac{q}{q_{\text{LO}}} \right). \quad (8.84)$$

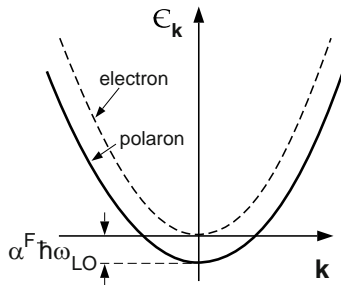


Fig. 8.6. Dispersion of conduction band electron and Fröhlich polaron. In order to show energy and mass renormalization a coupling constant of about 1 has been assumed

By taking the limits from 0 to ∞ as before, these integrals reduce to $\pi/2q_{LO}$ and $\pi/16q_{LO}^3$, respectively, and give for the first order energy correction

$$\Delta\epsilon_{\mathbf{k}}^{(1)} = -\alpha^F \hbar\omega_{LO} - \frac{\alpha^F \hbar^2 k^2}{6 \cdot 2m^*}, \quad (8.85)$$

which again is linear in the coupling constant. It is conceivable that higher order perturbation theory would lead to terms with higher powers in the coupling constant, i.e., the results obtained here are valid only for $\alpha^F < 1$. The polaron energy dispersion can now be written as

$$\epsilon_{\mathbf{k}}^P = -\alpha^F \hbar\omega_{LO} + \frac{\hbar^2 k^2}{2m^*} \left(1 - \frac{\alpha^F}{6}\right). \quad (8.86)$$

The result is shown in Fig. 8.6. There is an energy reduction independent of \mathbf{k} and a change of the particle mass, similar to our finding for the Hartree–Fock quasi-particle in Chap. 4. The mass $m^*/(1 - \alpha^F/6) \simeq m^*(1 + \alpha^F/6)$ is the *polaron mass*. The intuitive physical picture of the polaron is that the carrier has to move around together with the lattice polarization created due to its charge. The coupling constant α^F defines the energy renormalization in units of $\hbar\omega_{LO}$ and the average number of virtual phonons in the polaron.

8.5 Effective Electron–Electron Interaction

In 1911, the Dutch physicist Kamerlingh Onnes² discovered the surprising behavior of Hg that below a critical temperature ($T_c = 4.2\text{K}$) the resistivity dropped suddenly to a value close to zero (see Fig. 8.7), i.e., below this temperature the material can carry an electric current without a voltage drop or dissipation of energy [249]. This behavior, called *superconductivity*, which was found in the following for many other metals, has become and still is one

² Heike Kamerlingh Onnes 1853–1926, Nobel prize in physics 1916

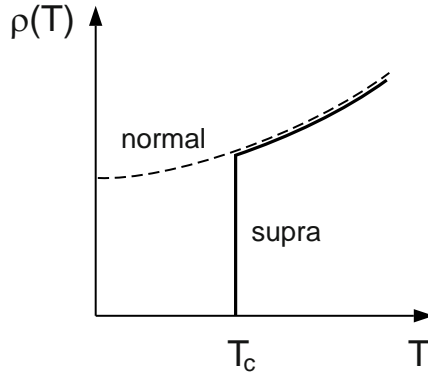


Fig. 8.7. Schematic dependence of the resistivity on the temperature for a normal metal (*dashed*) and a superconductor (*solid*)

of the most challenging problems in solid state physics. Superconductivity has become a standard subject in textbooks on Solid State Physics, but is also well documented in special monographs [250–254].

An indication that the lattices (or precisely the ions) are involved in the mechanism causing superconductivity, was the discovery of the isotope effect, i.e., a dependence of the critical temperature on the ion mass, according to which the critical temperature depends for a given element on the ion mass such that $M^{1/2}T_c = \text{const.}$ But, it took almost half a century before in 1957 a microscopic explanation of the phenomenon was given by Bardeen, Cooper, and Schrieffer³ [255]. According to their theory, known as the BCS theory, electron–phonon coupling can mediate an attractive electron–electron interaction which below T_c gives rise to a new correlated ground state with paired electrons.

In the perspective of promising technical applications, efforts have been made in finding materials with higher critical temperatures which, however, until 1985 remained below 25 K. In 1986, Bednorz and Müller⁴ discovered a new class of superconducting materials, the doped ceramic cuprates, with significantly higher critical temperatures [256]. Within this material class, critical temperatures of up to about 120 K, well above the temperature of liquid nitrogen, were found in the following years. This discovery boosted the research in the field of superconductivity towards both superconducting devices and in theoretical concepts to describe the effect, which is still not completely understood [257]. One of the most recent Nobel prizes in physics

³ John Bardeen, 1908–1991, Leon N. Cooper, *1930, J. Robert Schrieffer, *1931, shared the Nobel prize in physics 1972

⁴ Johannes Georg Bednorz, *1950, Karl Alex Müller, *1927, shared the Nobel prize in physics 1987

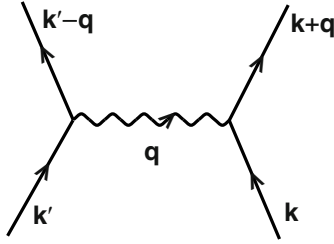


Fig. 8.8. Graphical representation of the effective electron–electron interaction mediated by virtual phonon exchange

has been awarded to Abrikosov, Ginzburg, and Leggett⁵ in recognition of their contributions to this field. In the context of this chapter, the BCS theory - although only the first concept to explain superconductivity - will be presented as an important outcome of electron–phonon interaction.

The system of electrons and phonons, including their interaction, can be described in simplest form by the Hamiltonian introduced in Sect. 8.1

$$\begin{aligned}
 \mathcal{H} &= \mathcal{H}_{\text{el}} + \mathcal{H}_{\text{ph}} + \mathcal{H}_{\text{el-ph}} \\
 &= \sum_{\mathbf{k}} \epsilon_{\mathbf{k}} c_{\mathbf{k}}^{\dagger} c_{\mathbf{k}} + \sum_{\mathbf{q}} \hbar\omega(\mathbf{q}) a^{\dagger}(\mathbf{q}) a(\mathbf{q}) \\
 &\quad + \sum_{\mathbf{k}, \mathbf{q}} \mathcal{V}_{\mathbf{q}} c_{\mathbf{k}+\mathbf{q}}^{\dagger} c_{\mathbf{k}} (a^{\dagger}(-\mathbf{q}) + a(\mathbf{q})). \tag{8.87}
 \end{aligned}$$

Here, we assume the electrons in a simple energy band with dispersion $\epsilon_{\mathbf{k}}$ and the phonons from a branch with dispersion $\omega(\mathbf{q})$. The matrix element of the electron–phonon interaction depends only on the momentum transfer \mathbf{q} and obeys the relation $V_{\mathbf{q}} = V_{-\mathbf{q}}^*$. Considering $\mathcal{H}_{\text{el-ph}}$ as a small perturbation, one can try to eliminate this interaction at least to lowest order in the phonon operators. As will be shown in the following, this leads to an effective electron–electron interaction mediated by virtual exchange of phonons. Its pictorial representation in Fig. 8.8, which can be understood as a composition of the diagrams shown in Fig. 8.1, resembles the corresponding graph for the direct Coulomb interaction (see Fig. 4.10).

The elimination of the terms linear in the phonon operators $a^{\dagger}(-\mathbf{q}), a(\mathbf{q})$ can be achieved by a unitary transformation, the *Schrieffer–Wolff transformation*

$$\begin{aligned}
 H' &= e^{-S} H e^S = \left(1 - S + \frac{1}{2} S^2 \dots\right) H \left(1 + S + \frac{1}{2} S^2 \dots\right) \\
 &= H + [H, S] + \frac{1}{2} [[H, S], S] + \dots, \tag{8.88}
 \end{aligned}$$

⁵ Alexei A. Abrikosov, *1928, Vitaly L. Ginzburg, *1916, Anthony J. Leggett, *1938, shared the Nobel Prize in physics 2003

with a still to be determined operator S . This transformation represents a systematic perturbation expansion. Applied to the Hamiltonian (8.87) the leading terms of the series read

$$\mathcal{H}' = \mathcal{H}_0 + \mathcal{H}_{\text{el-ph}} + [\mathcal{H}_0, S] + [\mathcal{H}_{\text{el-ph}}, S] + \frac{1}{2} [[\mathcal{H}_0, S], S] + \dots, \quad (8.89)$$

where $\mathcal{H}_0 = \mathcal{H}_{\text{el}} + \mathcal{H}_{\text{ph}}$ is the dominating term and all other terms, containing different powers of $\mathcal{H}_{\text{el-ph}}$ or S , represent the perturbation. This expansion can be exploited to eliminate $\mathcal{H}_{\text{el-ph}}$ (in principal to any order) by a proper choice of the operator S . For the lowest order, let us assume the form

$$S = \sum_{\mathbf{k}, \mathbf{q}} \mathcal{V}_{\mathbf{q}} (\alpha a^\dagger(-\mathbf{q}) + \beta a(\mathbf{q})) c_{\mathbf{k}+\mathbf{q}}^\dagger c_{\mathbf{k}} \quad (8.90)$$

which is similar to $\mathcal{H}_{\text{el-ph}}$ but contains α, β as free parameters. The commutator of S with \mathcal{H}_0 yields the two contributions

$$[\mathcal{H}_{\text{el}}, S] = \sum_{\mathbf{k}, \mathbf{q}} (\epsilon_{\mathbf{k}+\mathbf{q}} - \epsilon_{\mathbf{k}}) \mathcal{V}_{\mathbf{q}} (\alpha a^\dagger(-\mathbf{q}) + \beta a(\mathbf{q})) c_{\mathbf{k}+\mathbf{q}}^\dagger c_{\mathbf{k}} \quad (8.91)$$

and

$$[\mathcal{H}_{\text{ph}}, S] = \sum_{\mathbf{k}, \mathbf{q}} \hbar\omega(\mathbf{q}) \mathcal{V}_{\mathbf{q}} (\alpha a^\dagger(-\mathbf{q}) + \beta a(\mathbf{q})) c_{\mathbf{k}+\mathbf{q}}^\dagger c_{\mathbf{k}}, \quad (8.92)$$

where use was made of $\omega(-\mathbf{q}) = \omega(\mathbf{q})$. We recognize that the second and third terms of the perturbation expansion (8.89) are of first order in the electron–phonon interaction, while the fourth and fifth terms are of second order. The condition $\mathcal{H}_{\text{el-ph}} + [\mathcal{H}_0, S] = 0$ for eliminating the first order terms can be fulfilled with the choice

$$\alpha = -(\epsilon_{\mathbf{k}+\mathbf{q}} - \epsilon_{\mathbf{k}} - \hbar\omega(\mathbf{q}))^{-1} \quad (8.93)$$

and

$$\beta = -(\epsilon_{\mathbf{k}+\mathbf{q}} - \epsilon_{\mathbf{k}} + \hbar\omega(\mathbf{q}))^{-1} \quad (8.94)$$

and the transformed Hamiltonian takes the form

$$\mathcal{H}' = \mathcal{H}_0 + [\mathcal{H}_{\text{el-ph}}, S] + \frac{1}{2} [[\mathcal{H}_0, S], S] + \dots \quad (8.95)$$

For this choice of S , the sum of the second and third term is $[\mathcal{H}_{\text{el-ph}}, S]/2$ with

$$[\mathcal{H}_{\text{el-ph}}, S] \simeq \sum_{\mathbf{k}, \mathbf{k}', \mathbf{q}} |\mathcal{V}_{\mathbf{q}}|^2 (-\alpha + \beta) c_{\mathbf{k}+\mathbf{q}}^\dagger c_{\mathbf{k}'-\mathbf{q}}^\dagger c_{\mathbf{k}'} c_{\mathbf{k}}. \quad (8.96)$$

Note that the detailed evaluation (Problem 8.7) of the commutator yields an additional term which is neglected here. Finally, we may write the transformed Hamiltonian by considering all terms up to second order in the electron-phonon coupling as

$$\mathcal{H}' = \mathcal{H}_0 + \sum_{\mathbf{k}, \mathbf{k}', \mathbf{q}} \frac{|\mathcal{V}_{\mathbf{q}}|^2 \hbar\omega(\mathbf{q})}{(\epsilon_{\mathbf{k}} - \epsilon_{\mathbf{k}+\mathbf{q}})^2 - (\hbar\omega(\mathbf{q}))^2} c_{\mathbf{k}+\mathbf{q}}^\dagger c_{\mathbf{k}'-\mathbf{q}}^\dagger c_{\mathbf{k}'} c_{\mathbf{k}}. \quad (8.97)$$

The second term of this Hamiltonian describes an electron-electron interaction caused by a virtual exchange of phonons as depicted by the diagram of Fig. 8.8. It has the same structure as the graph for the Coulomb interaction, but now the interaction line represents the phonon mechanism. It is attractive for $|\epsilon_{\mathbf{k}} - \epsilon_{\mathbf{k}+\mathbf{q}}| < \hbar\omega(\mathbf{q})$ and favors the formation of bound electron pairs.

Starting from the filled Fermi sphere $|\Psi_0\rangle$, which represents the electronic ground state of a normal metal, we may ask if an electron pair formed at the Fermi energy due to the effective electron-electron interaction would be stable. Such a pair can be described by applying two creation operators with $\mathbf{k}_1, \mathbf{k}_2$ from outside the Fermi sphere and superposition to a wave packet

$$|\Psi_{12}\rangle = \sum'_{\mathbf{k}_1, \mathbf{k}_2} F(\mathbf{k}_1, \mathbf{k}_2) c_{\mathbf{k}_1}^\dagger c_{\mathbf{k}_2}^\dagger |\Psi_0\rangle, \quad (8.98)$$

where \sum' indicates that the sum is restricted to $\mathbf{k}_i, i = 1, 2$ in the spherical shell with $E_F \leq \epsilon_{\mathbf{k}_i} \leq E_F + \hbar\omega(\mathbf{q}), i = 1, 2$. The center of mass momentum, $\mathbf{K} = \mathbf{k}_1 + \mathbf{k}_2$, being a good quantum number, limits the states contributing to the wave packet, as depicted in Fig. 8.9. This figure suggests that the condition of forming a stable pair improves by increasing the number of contributing states with attractive interaction. The most favorite situation corresponds to $\mathbf{K} = \mathbf{k}_1 + \mathbf{k}_2 = 0$, for which we can write

$$|\Psi_{12}\rangle = \sum'_{\mathbf{k}} F(\mathbf{k}) c_{\mathbf{k}}^\dagger c_{-\mathbf{k}}^\dagger |\Psi_0\rangle. \quad (8.99)$$

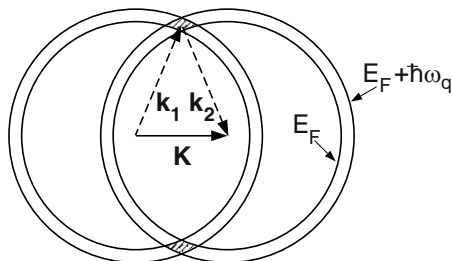


Fig. 8.9. Single particle states at the Fermi energy contributing to a pair state for fixed center-of-mass momentum

If, in addition, the attractive interaction is simplified by writing

$$\frac{|\mathcal{V}_{\mathbf{q}}|^2 \hbar\omega(\mathbf{q})}{(\epsilon_{\mathbf{k}} - \epsilon_{\mathbf{k}'})^2 - (\hbar\omega(\mathbf{q}))^2} \simeq \begin{cases} -\frac{V_{\text{eff}}}{2} \delta_{\mathbf{k}', -\mathbf{k}} & |\epsilon_{\mathbf{k}} - \epsilon_{\mathbf{k}'}| \leq \hbar\omega_{\text{D}} \\ 0 & \text{otherwise} \end{cases}, \quad (8.100)$$

where the Debye frequency ω_{D} introduced in Chap. 3 is taken as a representative cut-off frequency of the phonon spectrum, we obtain the Hamiltonian

$$\mathcal{H}_{\text{eff}} = \sum_{\mathbf{k}} \epsilon_{\mathbf{k}} c_{\mathbf{k}}^{\dagger} c_{\mathbf{k}} - \frac{V_{\text{eff}}}{2} \sum'_{\mathbf{k}, \mathbf{q}} c_{\mathbf{k}+\mathbf{q}}^{\dagger} c_{-\mathbf{k}-\mathbf{q}}^{\dagger} c_{-\mathbf{k}} c_{\mathbf{k}} \quad (8.101)$$

for electrons in the band with $\epsilon_{\mathbf{k}}$ coupled with the phonon-mediated attractive electron–electron interaction.

8.6 Cooper Pairs and the Gap

As mentioned before, this interaction can give rise to the formation of bound electron pairs $|\Psi_{12}\rangle$ at the Fermi surface, the *Cooper pairs*. The condition for this to happen is given by

$$E_{12} = \langle \Psi_{12} | \mathcal{H}_{\text{eff}} | \Psi_{12} \rangle < 2E_{\text{F}}, \quad (8.102)$$

which means an instability of the Fermi sphere against the formation of such pairs. The expectation value of (8.101) for the pair state (8.99) turns out to be (Problem 8.8)

$$E_{12} = 2 \sum'_{\mathbf{k}} \epsilon_{\mathbf{k}} |F(\mathbf{k})|^2 - V_{\text{eff}} \sum'_{\mathbf{k}, \mathbf{q}} F^*(\mathbf{k} + \mathbf{q}) F(\mathbf{k}) \quad (8.103)$$

and is to be minimized with respect to $F(\mathbf{k})$ under the normalization condition $\sum_{\mathbf{k}} |F(\mathbf{k})|^2 = 1$. Thus, we write

$$\frac{\partial}{\partial F^*(\mathbf{k}')} \left\{ E_{12} - \lambda \left(\sum'_{\mathbf{k}} |F(\mathbf{k})|^2 - 1 \right) \right\} = 0 \quad (8.104)$$

or alternatively, after taking the derivatives,

$$\{2\epsilon_{\mathbf{k}'} - \lambda\} F(\mathbf{k}') = V_{\text{eff}} \sum'_{\mathbf{k}} F(\mathbf{k}). \quad (8.105)$$

By setting $\sum'_{\mathbf{k}} F(\mathbf{k}) = C$, we may express

$$F(\mathbf{k}) = \frac{V_{\text{eff}} C}{2\epsilon_{\mathbf{k}} - \lambda} \quad \text{or} \quad C = \sum'_{\mathbf{k}} \frac{V_{\text{eff}} C}{2\epsilon_{\mathbf{k}} - \lambda}, \quad (8.106)$$

where in the last equation C can be dropped.

An expression for λ is obtained by multiplying (8.105) with $F^*(\mathbf{k}')$ and taking the restricted sum over \mathbf{k}'

$$\sum'_{\mathbf{k}'} \{2\epsilon_{\mathbf{k}'} - \lambda\} |F(\mathbf{k}')|^2 = V_{\text{eff}} \sum'_{\mathbf{k}, \mathbf{k}'} F(\mathbf{k}) F^*(\mathbf{k}'). \quad (8.107)$$

By making use on the *lhs* of the normalization condition and replacing the *rhs* \mathbf{k}' by $\mathbf{k} + \mathbf{q}$ with the corresponding change of the summation, this can be written as

$$2 \sum'_{\mathbf{k}'} \epsilon_{\mathbf{k}'} |F(\mathbf{k}')|^2 - V_{\text{eff}} \sum'_{\mathbf{k}, \mathbf{q}} F^*(\mathbf{k} + \mathbf{q}) F(\mathbf{k}) = \lambda. \quad (8.108)$$

Comparing with (8.103), we identify $\lambda = E_{12}$ and find the relation

$$\sum'_{\mathbf{k}} \frac{V_{\text{eff}}}{2\epsilon_{\mathbf{k}} - E_{12}} = 1 \quad (8.109)$$

from which the energy E_{12} of the Cooper pair is to be calculated.

In (8.109), the sum over \mathbf{k} can be formulated as an integral over the energy

$$1 = V_{\text{eff}} \int_{E_{\text{F}}}^{E_{\text{F}} + \hbar\omega_{\text{D}}} \frac{D(E)}{2E - E_{12}} dE, \quad (8.110)$$

with the density of states $D(E)$. Because the integral is to be taken over a narrow interval at the Fermi energy ($\hbar\omega_{\text{D}} \ll E_{\text{F}}$), we may extract the density of states as a factor $D(E_{\text{F}})$ and perform the integration to find

$$1 = \frac{1}{2} V_{\text{eff}} D(E_{\text{F}}) \ln \frac{2(E_{\text{F}} + \hbar\omega_{\text{D}}) - E_{12}}{2E_{\text{F}} - E_{12}}. \quad (8.111)$$

After separating the logarithm to take the exponential, this can be solved for E_{12} and yields

$$E_{12} = 2E_{\text{F}} - 2\hbar\omega_{\text{D}} \frac{\exp(-2/V_{\text{eff}}D(E_{\text{F}}))}{1 - \exp(-2/V_{\text{eff}}D(E_{\text{F}}))}. \quad (8.112)$$

Under the condition of a weak attractive electron–electron interaction, quantified by the relation $2/V_{\text{eff}}D(E_{\text{F}}) \gg 1$, (8.112) is simplified by writing

$$E_{12} \simeq 2E_{\text{F}} - 2\hbar\omega_{\text{D}} \exp(-2/V_{\text{eff}}D(E_{\text{F}})). \quad (8.113)$$

This relation implies that the energy of the Cooper pair is smaller than the energy of the two electrons (without interaction) taken from the Fermi surface. The particular dependence on the interaction in the exponential function, which cannot be represented in a power series, leads to stable bound pairs even for very small V_{eff} . The formation of Cooper pairs means, for the whole electron system, that the Fermi sphere (or in general, the Fermi surface) is

unstable and cannot represent the system ground state. As we shall see, this leads to a new state of the electron system, the superconducting state.

After having confirmed the possibility of pair formation due to the effective electron–electron interaction, we now have to find the ground state of the system. The pairs, consisting of electrons close to E_F with wave vectors \mathbf{k} and $-\mathbf{k}$ and (as we shall assume here) *up* and *down* spin to form spin-singlet pairs, are bosons. Their creation or annihilation changes the number of electrons in the system. This can be accounted for by considering the so-called BCS Hamiltonian

$$\mathcal{H}_{\text{BCS}} = \sum_{\mathbf{k}}' (\epsilon_{\mathbf{k}} - E_F) \left(c_{\mathbf{k}\uparrow}^\dagger c_{\mathbf{k}\uparrow} + c_{-\mathbf{k}\downarrow}^\dagger c_{-\mathbf{k}\downarrow} \right) - V_{\text{eff}} \sum_{\mathbf{k}, \mathbf{k}'}' c_{\mathbf{k}'\uparrow}^\dagger c_{-\mathbf{k}'\downarrow}^\dagger c_{-\mathbf{k}\downarrow} c_{\mathbf{k}\uparrow}, \quad (8.114)$$

which is $\mathcal{H}_{\text{eff}} - \mu N$, with $\mu \simeq E_F$ and $N = \sum_{\mathbf{k}} \left(c_{\mathbf{k}\uparrow}^\dagger c_{\mathbf{k}\uparrow} + c_{-\mathbf{k}\downarrow}^\dagger c_{-\mathbf{k}\downarrow} \right)$. As the energy of the electrons does not differ much from the Fermi energy, it is reasonable to introduce the notation $E(\mathbf{k}) = \epsilon_{\mathbf{k}} - E_F$. Subtracting this energy difference summed over all \mathbf{k} leads to

$$\bar{\mathcal{H}} = - \sum_{\mathbf{k}}' E(\mathbf{k}) \left(1 - c_{\mathbf{k}\uparrow}^\dagger c_{\mathbf{k}\uparrow} - c_{-\mathbf{k}\downarrow}^\dagger c_{-\mathbf{k}\downarrow} \right) - V_{\text{eff}} \sum_{\mathbf{k}, \mathbf{k}'}' c_{\mathbf{k}'\uparrow}^\dagger c_{-\mathbf{k}'\downarrow}^\dagger c_{-\mathbf{k}\downarrow} c_{\mathbf{k}\uparrow}. \quad (8.115)$$

The operators appearing in this Hamiltonian have an obvious meaning when applied to pair states of electrons. Using the occupation number representation, $|0_{\mathbf{k}\uparrow}0_{-\mathbf{k}\downarrow}\rangle$ and $|1_{\mathbf{k}\uparrow}1_{-\mathbf{k}\downarrow}\rangle$ denote the states without and with an electron pair, respectively. The following relations hold:

1. $\left(1 - c_{\mathbf{k}\uparrow}^\dagger c_{\mathbf{k}\uparrow} - c_{-\mathbf{k}\downarrow}^\dagger c_{-\mathbf{k}\downarrow} \right) |0_{\mathbf{k}\uparrow}0_{-\mathbf{k}\downarrow}\rangle = |0_{\mathbf{k}\uparrow}0_{-\mathbf{k}\downarrow}\rangle$
2. $\left(1 - c_{\mathbf{k}\uparrow}^\dagger c_{\mathbf{k}\uparrow} - c_{-\mathbf{k}\downarrow}^\dagger c_{-\mathbf{k}\downarrow} \right) |1_{\mathbf{k}\uparrow}1_{-\mathbf{k}\downarrow}\rangle = -|1_{\mathbf{k}\uparrow}1_{-\mathbf{k}\downarrow}\rangle$
3. $c_{\mathbf{k}\uparrow}^\dagger c_{-\mathbf{k}\downarrow}^\dagger |1_{\mathbf{k}\uparrow}1_{-\mathbf{k}\downarrow}\rangle = 0$
4. $c_{\mathbf{k}\uparrow}^\dagger c_{-\mathbf{k}\downarrow}^\dagger |0_{\mathbf{k}\uparrow}0_{-\mathbf{k}\downarrow}\rangle = |1_{\mathbf{k}\uparrow}1_{-\mathbf{k}\downarrow}\rangle$
5. $c_{\mathbf{k}\uparrow} c_{-\mathbf{k}\downarrow} |1_{\mathbf{k}\uparrow}1_{-\mathbf{k}\downarrow}\rangle = |0_{\mathbf{k}\uparrow}0_{-\mathbf{k}\downarrow}\rangle$
6. $c_{\mathbf{k}\uparrow} c_{-\mathbf{k}\downarrow} |0_{\mathbf{k}\uparrow}0_{-\mathbf{k}\downarrow}\rangle = 0$

For each \mathbf{k} , they can be interpreted as those of spin operators which in the Pauli representation read

$$\begin{aligned} 1./2. : 1 - c_{\mathbf{k}\uparrow}^\dagger c_{\mathbf{k}\uparrow} - c_{-\mathbf{k}\downarrow}^\dagger c_{-\mathbf{k}\downarrow} &= \begin{pmatrix} 1 & 0 \\ 0 & -1 \end{pmatrix}_{\mathbf{k}} = \sigma_{kz} \\ 3./4. : c_{\mathbf{k}\uparrow}^\dagger c_{-\mathbf{k}\downarrow}^\dagger &= \begin{pmatrix} 0 & 0 \\ 1 & 0 \end{pmatrix}_{\mathbf{k}} = \frac{1}{2} (\sigma_{kx} - i\sigma_{ky}) \\ 5./6. : c_{\mathbf{k}\uparrow} c_{-\mathbf{k}\downarrow} &= \begin{pmatrix} 0 & 1 \\ 0 & 0 \end{pmatrix}_{\mathbf{k}} = \frac{1}{2} (\sigma_{kx} + i\sigma_{ky}) \end{aligned} \quad (8.116)$$

and act on corresponding pseudo-spin states

$$|0_{\mathbf{k}\uparrow}0_{-\mathbf{k}\downarrow}\rangle = \begin{pmatrix} 1 \\ 0 \end{pmatrix}_{\mathbf{k}} \quad \text{and} \quad |1_{\mathbf{k}\uparrow}1_{-\mathbf{k}\downarrow}\rangle = \begin{pmatrix} 0 \\ 1 \end{pmatrix}_{\mathbf{k}}. \quad (8.117)$$

In this notation, the Hamiltonian $\bar{\mathcal{H}}$ can be written as

$$\bar{\mathcal{H}} = -\sum_{\mathbf{k}}' E(\mathbf{k})\sigma_{kz} - \frac{V_{\text{eff}}}{4} \sum_{\mathbf{k}, \mathbf{k}'}' (\sigma_{\mathbf{k}'x}\sigma_{\mathbf{k}x} + \sigma_{\mathbf{k}'y}\sigma_{\mathbf{k}y}) \quad (8.118)$$

and turns out to be of the same structure as the Heisenberg spin Hamiltonian in Chap. 6. Therefore, the interaction (second term) can be treated in the same way, i.e., by applying the mean-field approximation. This is done by introducing the fictitious magnetic field (note that it depends on \mathbf{k} and its components represent energies) giving

$$\mathbf{H}_{\mathbf{k}} = E(\mathbf{k})\hat{z} + \frac{V_{\text{eff}}}{2} \sum_{\mathbf{k}'}' (\langle\sigma_{\mathbf{k}'x}\rangle\hat{x} + \langle\sigma_{\mathbf{k}'y}\rangle\hat{y}), \quad (8.119)$$

with Cartesian unit vectors $\hat{x}, \hat{y}, \hat{z}$, and leads to the compact form

$$\bar{\mathcal{H}} = -\sum_{\mathbf{k}}' \mathbf{H}_{\mathbf{k}} \cdot \boldsymbol{\sigma}_{\mathbf{k}}. \quad (8.120)$$

In spite of its simple form, this mean-field Hamiltonian has a remarkable spectrum, determined by the modulus of the fictitious field. The energetically best arrangement requires all pseudo-spins $\langle\boldsymbol{\sigma}_{\mathbf{k}}\rangle$ to be aligned to the corresponding field $\mathbf{H}_{\mathbf{k}}$. Let us discuss first the case without interaction ($V_{\text{eff}} = 0$)

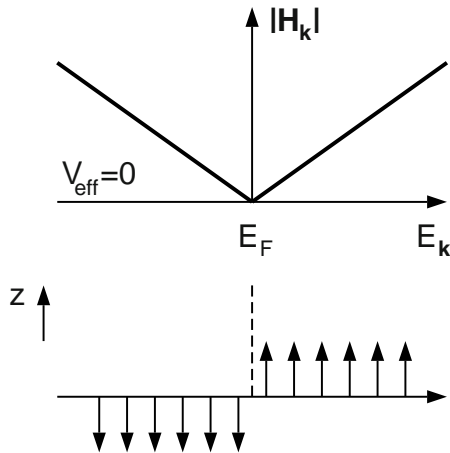


Fig. 8.10. Mean field (*upper part*) and eigenstates (*lower part*) in dependence on the single-particle energy around E_F without effective interaction

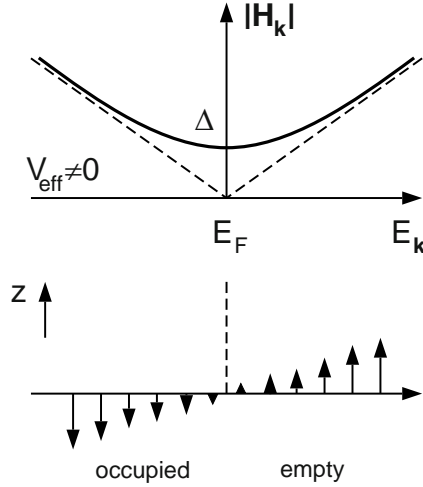


Fig. 8.11. Mean field (*upper part*) and eigenstates (*lower part*) in dependence on the single-particle energy around E_F with effective interaction. Note the opening of a gap at E_F

for which $|\mathbf{H}_{\mathbf{k}}|$ depends linearly on the energy $E(\mathbf{k})$, which is the energy difference of the single particle energy and the Fermi energy. This situation is shown in Fig. 8.10 (upper part). The field points in the positive or negative z direction depending on the sign of $E(\mathbf{k})$. The corresponding eigenstates are pseudo-spin up (down) or occupied (empty) pair states below (above) E_F , i.e., for negative (positive) $E(\mathbf{k})$ (see lower part of Fig. 8.10).

This picture changes for finite V_{eff} (Fig. 8.11). Now, at E_F or $E(\mathbf{k}) = 0$ the fictitious field is finite, pointing somewhere in the xy plane. Its strength depends on the expectation values of the pseudo-spin operators $\sigma_{\mathbf{k}'x}$ and $\sigma_{\mathbf{k}'y}$. But, away from the Fermi energy, this field is turned into the z direction and approaches the linear dependence as for the noninteracting case (upper part of Fig. 8.11). The corresponding eigenstates are pseudo-spin vectors aligned to this field and turn around with $\mathbf{H}_{\mathbf{k}}$. Their projection onto the z direction is shown in the lower part of Fig. 8.11.

In order to quantify the discussion, let us assume $\langle \sigma_{\mathbf{k}'y} \rangle = 0$, i.e., all pseudo-spins together with the fictitious fields are in the xz plane, and introduce the energy parameter $\Delta = V_{\text{eff}} \sum'_{\mathbf{k}'} \langle \sigma_{\mathbf{k}'x} \rangle / 2$. The energy for exciting an electron pair out of the correlated ground state is given by twice the modulus of the field

$$|\mathbf{H}_{\mathbf{k}}| = \{E(\mathbf{k})^2 + \Delta^2\}^{1/2}, \quad (8.121)$$

where Δ is the gap energy at E_F (see Fig. 8.11). Due to the alignment of the pseudo-spin along the field $\mathbf{H}_{\mathbf{k}}$ (Fig. 8.12), the ratios of their x and z components are equal and can be expressed by the angle $\theta_{\mathbf{k}}$. As, in addition, $\langle \sigma_{\mathbf{k}'x} \rangle = \sin \theta_{\mathbf{k}'}$ we may write

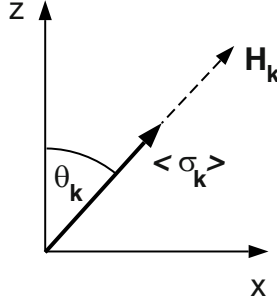


Fig. 8.12. Alignment of pseudo-spin and fictitious field in the xz plane

$$\tan \theta_{\mathbf{k}} = \frac{V_{\text{eff}} \sum_{\mathbf{k}'}' \sin \theta_{\mathbf{k}'}}{2E(\mathbf{k})} = \frac{\Delta}{E(\mathbf{k})}. \quad (8.122)$$

This relation can be solved for Δ by replacing

$$\sin \theta_{\mathbf{k}'} = \frac{\Delta}{(\Delta^2 + E^2(\mathbf{k}'))^{1/2}} \quad (8.123)$$

to obtain

$$\Delta = \frac{1}{2} V_{\text{eff}} \sum_{\mathbf{k}}' \frac{\Delta}{(\Delta^2 + E^2(\mathbf{k}))^{1/2}}. \quad (8.124)$$

The summation, limited to the range of the attractive interaction around the Fermi surface, can again be performed as an integral, giving

$$\begin{aligned} 1 &= \frac{V_{\text{eff}} D(E_F)}{2} \int_{-\hbar\omega_D}^{+\hbar\omega_D} \frac{dE}{(\Delta^2 + E^2(\mathbf{k}))^{1/2}} \\ &= V_{\text{eff}} D(E_F) \sinh^{-1} \left(\frac{\hbar\omega_D}{\Delta} \right). \end{aligned} \quad (8.125)$$

This is easily solved to yield, as the BCS solution, for the gap parameter

$$\Delta = \frac{\hbar\omega_D}{\sinh(1/V_{\text{eff}} D(E_F))} \simeq 2\hbar\omega_D e^{-1/V_{\text{eff}} D(E_F)}, \quad (8.126)$$

where the last expression is obtained for $1 \gg V_{\text{eff}} D(E_F)$. According to this formula, the gap energy (or the stability of the Cooper pairs) increases with the cut-off phonon energy (or the Debye frequency) and the density of single-particle states at the Fermi energy.

In order to find an expression for the critical temperature, we have to ask for the temperature dependence of the gap, which enters through the thermal expectation values of the pseudo-spins

$$\langle \sigma_{\mathbf{k}} \rangle_T = \text{Tr} \left(\frac{1}{Z} e^{-\beta \tilde{\mathcal{H}}} \sigma_{\mathbf{k}} \right) = \tanh \frac{|\mathbf{H}_{\mathbf{k}}|}{k_B T} \quad (8.127)$$

and (using again Fig. 8.12) defines $\Delta(T)$ by the relation

$$\tan \theta_{\mathbf{k}} = \frac{V_{\text{eff}} \sum'_{\mathbf{k}'} \sin \theta_{\mathbf{k}'}}{2E(\mathbf{k})} \tanh \frac{|\mathbf{H}_{\mathbf{k}'}}{k_{\text{B}}T} = \frac{\Delta(T)}{E(\mathbf{k})}. \quad (8.128)$$

Replacing $\sin \theta_{\mathbf{k}'} = \Delta(T)/\{E^2(\mathbf{k}) + \Delta^2(T)\}^{1/2}$ gives

$$\frac{V_{\text{eff}}}{2} \sum'_{\mathbf{k}} \tanh \frac{|\mathbf{H}_{\mathbf{k}}|}{k_{\text{B}}T} \{E^2(\mathbf{k}) + \Delta^2(T)\}^{-1/2} = 1. \quad (8.129)$$

This equation can be solved for $\Delta(T)$. For $T = T_c$ the gap vanishes and $|\mathbf{H}_{\mathbf{k}}| = E(\mathbf{k})$, which simplifies the relation to

$$\frac{V_{\text{eff}}}{2} \sum'_{\mathbf{k}} \frac{1}{E(\mathbf{k})} \tanh \frac{E(\mathbf{k})}{k_{\text{B}}T_c} = 1. \quad (8.130)$$

Extending this result, which is valid for the adopted spin model related to pair states, to include single particle excitations, T_c has to be replaced by $2T_c$. The factor 2 accounts for the doubling of the entropy due to a doubling of the possible excitations (see [4]). The sum over \mathbf{k} is again performed as an energy integral, giving the BCS result for the critical temperature

$$\frac{1}{V_{\text{eff}}D(E_{\text{F}})} = \int_0^{\hbar\omega_{\text{D}}/2k_{\text{B}}T_c} \frac{\tanh(x)}{x} dx. \quad (8.131)$$

For $T_c \ll \Theta_{\text{D}}$, where Θ_{D} is the Debye temperature, this can be evaluated to yield

$$T_c = 1.14 \frac{\Theta_{\text{D}}}{k_{\text{B}}} e^{-1/V_{\text{eff}}D(E_{\text{F}})}. \quad (8.132)$$

This result immediately explains the isotope effect, because the Debye temperature is inversely proportional to the square root of the ion mass. With the help of (8.126), we may also write the direct relation between the gap energy and the critical temperature

$$2\Delta = 3.52k_{\text{B}}T_c. \quad (8.133)$$

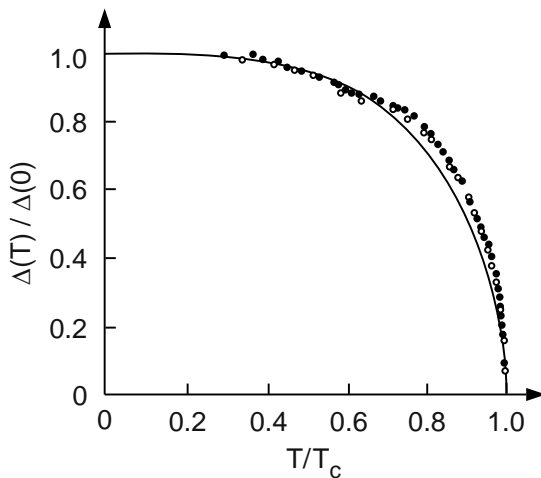
The validity of this relation is demonstrated in Table 8.1 for some representative metals.

The principal correctness of the mean-field approximation is shown in Fig. 8.13 by plotting the reduced value of the gap $\Delta(T)/\Delta(0)$ as the order parameter for different superconductors *versus* the reduced temperature T/T_c . The experimental data for different materials define a universal curve which is well described by the graph from BCS theory. Note the similarity with Fig. 6.10.

Similar to the Fröhlich polaron, a Cooper pair is a composite particle. However, the statistical properties of the polaron are those of the electron

Table 8.1. Debye temperature Θ_D , critical temperature T_c , and ratio $2\Delta(0)/k_B T_c$ for different metals, from [31].

Metal	Θ_D [K]	T_c [K]	$2\Delta(0)/k_B T_c$
An	235	0.9	3.2
Cd	164	0.56	3.2
Hg	70	4.16	4.6
Al	375	1.2	3.4
Sn	195	3.75	3.5
Pb	96	7.22	4.3

**Fig. 8.13.** Dependence of the reduced gap energy on the reduced temperature for different superconductors (*symbols*) and the BCS result (*solid line*) (after [30])

because the phonon cloud does not change the spin, whereas the Cooper pair, which is a particle with integer spin composed of two electrons, is a boson. Due to their bosonic nature, a system of Cooper pairs can undergo *Bose–Einstein condensation* to reach the superconducting state. Depending on the total spin of the two electrons in a Cooper pair, one distinguishes singlet and triplet superconductors.

Bose–Einstein condensation is possible not only for paired electrons in a solid. By cooling atoms confined in electromagnetic traps, degenerate Fermi gases can be realized (see Chap. 4), which consist of atoms. For these Fermi systems, one has, recently, also studied the formation of molecules due to inter-atomic forces. A system of such bosonic molecules can make a phase transformation into the suprafluid state corresponding to the superconducting state of the electrons [258, 259].

Problems

- 8.1 Derive the expression for the electron–phonon interaction in a Bravais lattice without making use of the single-band approximation. In this case the operator form should be

$$(a_s^\dagger(-\mathbf{q}) + a_s(\mathbf{q})) c_{n\mathbf{k}}^\dagger c_{n'\mathbf{k}'}. \quad (8.134)$$

Derive an expression for the interaction matrix element, which leads to a relation between \mathbf{k}, \mathbf{k}' and \mathbf{q} .

- 8.2 Express the divergence of the continuous lattice displacement field $\mathbf{u}(\mathbf{r})$ by the components of the strain tensor field $\epsilon(\mathbf{r})$ and realize that only longitudinal phonons contribute.
- 8.3 Show that charge carriers in an energy band deriving from p states can interact via deformation potential coupling with both longitudinal and transverse phonons.
- 8.4 Derive the expression for the piezoelectric electron–phonon coupling (8.37) by performing the same steps as outlined for the polar optical electron–phonon coupling. Which acoustic branches contribute to the coupling?
- 8.5 Given the scattering rates $1/\tau$ of an electron with energy ϵ due to deformation potential ($\sim T\epsilon^{1/2}$) and piezoelectric coupling ($\sim T\epsilon^{-1/2}$) for large $k_B T$ compared with the phonon energies, calculate the temperature dependence of the contributions of both scattering processes to the mobility of electrons. Compare with Fig. 8.5.
- 8.6 Calculate the number of phonons \bar{n} in a composite particle due to deformation potential coupling with acoustic phonons by using first order perturbation theory. Note that the q dependence of this coupling differs from that of the Fröhlich coupling and that the q integration changes. Discuss the result in dependence on the material parameters. Estimate \bar{n} if the carrier would be an ion (e.g., a proton) moving in the lattice.
- 8.7 Evaluate the commutator between the operators $\mathcal{H}_{\text{el-ph}}$ and S . Discuss the approximation made in writing the expression given in the text.
- 8.8 Calculate the ground state energy of the BCS Hamiltonian (8.120) relative to the normal ground state. Note that only electrons close to E_F are relevant.

Defects, Disorder, and Localization

The crystalline order of a solid, characterized by the configuration $\{\mathbf{R}_n^0\}$ of all atoms with their equilibrium positions at lattice points, has been anticipated throughout this book so far. The essential consequence of the lattice periodicity, deriving from this configuration, is that all states be it of phonons, of electrons, or of magnons follow Bloch's theorem with a modulus that repeats with the lattice period, e.g.,

$$|\psi_{n\mathbf{k}}(\mathbf{r} + \mathbf{R}_n^0)| = |\psi_{n\mathbf{k}}(\mathbf{r})|, \quad \text{for all } \mathbf{R}_n^0. \quad (9.1)$$

Because of this property, Bloch states are *extended states*. In this chapter, deviations from the crystalline order and their consequences shall be considered for the electrons (but they are essentially valid also for the collective excitations of the solid). This is done first for individual *point defects* or *impurities*, which have to be classified, and can lead to discrete bound states localized in the vicinity of the defect. They are described by wave functions that decay (exponentially) away from the defect. A more general deviation from the crystalline structure is *compositional* or *structural disorder*, which will be experienced by the electrons as a random potential. The energy spectrum of the electrons can still exhibit bands with continuous density of states but with a modification of the electronic wave functions depending on their energy: Toward the band edges, the electrons are more strongly influenced by the potential fluctuations and get confined in deep local minima. Such *localized states* have the characteristic form

$$\psi(\mathbf{r}) \sim e^{-|\mathbf{r}|/\lambda}, \quad (9.2)$$

where λ is the *localization length*. Thus, disorder causes localization and becomes responsible for dramatic changes in the transport properties. They show up at low temperatures at which – as one of the prominent features – a *metal–insulator transition* (MIT) can take place due to disorder. The experimental investigations of the MIT and the conceptual theoretical work carried out to understand this phenomenon belong to the outstanding achievements made in solid state physics during the last decades.[275–279]

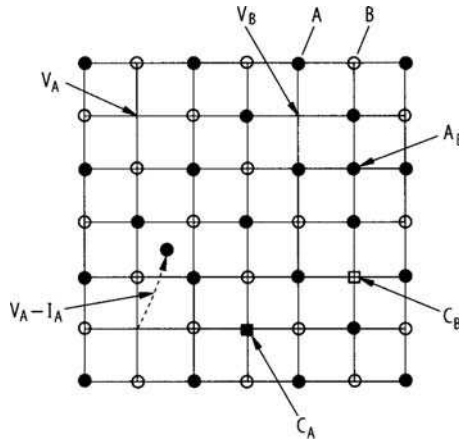


Fig. 9.1. Representation of point defects in a binary solid (*open* and *filled* symbols represent two different atomic species)

9.1 Point Defects

Deviations from the periodic structure can be classified according to their dimension. Point defects represent zero-dimensional perturbations of the periodic lattice structure. Different cases are depicted in Fig. 9.1 for a solid containing two sublattices with atoms A and B , respectively. In a substitutional impurity C_A (or C_B), an atom C differing from those of the host material A (or B) replaces the host atom at a lattice site. An interstitial impurity I means an atom (of the host material, but also different from it) taking a position in some free space between the lattice points. A vacancy V_A (or V_B) refers to an empty lattice point. A Frenkel¹ defect, $V_A - I_A$, is the combination of a vacancy with a nearby interstitial. It can be created by displacing a host atom from its lattice site to the interstitial position. In binary solids AB , especially in compound semiconductors, an anti-site defect A_B is possible with an atom A at the regular site of a B atom. This anti-site defect is more likely, the closer A and B are in the periodic table.

In semiconductors, isolated impurities can change the electronic spectrum by causing states in the fundamental energy gap from which, at elevated temperature carriers are released into the nearby band edges. This is the concept of *doping* which is of great importance in device applications. Therefore, the theory of impurities within the effective-mass approximation originates from the early days of semiconductor physics [260], but was refined and extended following the progress of research [261–268].

For an isolated substitutional impurity in an otherwise crystalline solid, we may write

¹ Yakov Ilyich Frenkel 1894–1954

$$H = -\frac{\hbar^2}{2m}\Delta + V_{\text{eff}}(\mathbf{r}) + U(\mathbf{r}) \quad (9.3)$$

with the periodic effective potential $V_{\text{eff}}(\mathbf{r}) = \sum_{\mathbf{n}} v(\mathbf{r} - \mathbf{R}_{\mathbf{n}}^0)$ introduced in Sect. 5.1 and the impurity potential $U(\mathbf{r}) = v_I(\mathbf{r}) - v(\mathbf{r})$, where the lattice site of the substitution is taken as the origin. Without $U(\mathbf{r})$, the eigenvalue problem of H leads to band structure $E_n(\mathbf{k})$ and Bloch functions $\psi_{n\mathbf{k}}(\mathbf{r})$ which represent the solution of the unperturbed problem. Including the impurity potential, the eigenvalue problem

$$H\phi = E\phi \quad (9.4)$$

can be solved by expanding $\phi(\mathbf{r}) = \sum_{n\mathbf{k}} f_n(\mathbf{k})\psi_{n\mathbf{k}}(\mathbf{r})$ as a wave packet of Bloch waves. The variational principle for the expectation value of the energy leads to the set of coupled linear equations

$$(E_n(\mathbf{k}) - E)f_n(\mathbf{k}) + \sum_{n',\mathbf{k}'} \langle n\mathbf{k}|U|n'\mathbf{k}'\rangle f_{n'}(\mathbf{k}') = 0 \quad (9.5)$$

for the expansion coefficients $f_n(\mathbf{k})$. Using the Fourier transform $U(\mathbf{r}) = \sum_{\mathbf{q}} U_{\mathbf{q}} \exp(i\mathbf{q} \cdot \mathbf{r})$ and expanding the product of the periodic parts of the Bloch functions in a Fourier series, $u_{n\mathbf{k}}^*(\mathbf{r})u_{n'\mathbf{k}'}(\mathbf{r}) = \sum_{\mathbf{G}} C_{nkn'\mathbf{k}'}(\mathbf{G}) \exp(-i\mathbf{G} \cdot \mathbf{r})$, the matrix element of the impurity potential $U(\mathbf{r})$ can be expressed as

$$\langle n\mathbf{k}|U|n'\mathbf{k}'\rangle = \sum_{\mathbf{q}} U_{\mathbf{q}} \sum_{\mathbf{G}} C_{nkn'\mathbf{k}'}(\mathbf{G}) \delta_{\mathbf{q},\mathbf{k}-\mathbf{k}'+\mathbf{G}}. \quad (9.6)$$

For $\mathbf{G} = 0$, one has

$$C_{nkn'\mathbf{k}'}(\mathbf{0}) = \int u_{n\mathbf{k}}^*(\mathbf{r})u_{n'\mathbf{k}'}(\mathbf{r}) \simeq \delta_{nn'} d^3\mathbf{r}, \quad (9.7)$$

(which is exact for $\mathbf{k} = \mathbf{k}'$) and writes

$$(E_n(\mathbf{k}) - E)f_n(\mathbf{k}) + \sum_{\mathbf{k}'} U_{\mathbf{k}-\mathbf{k}'} f_n(\mathbf{k}') + \sum_{n',\mathbf{k}'} \sum_{\mathbf{G} \neq 0} U_{\mathbf{k}-\mathbf{k}'+\mathbf{G}} C_{nkn'\mathbf{k}'}(\mathbf{G}) f_{n'}(\mathbf{k}') = 0. \quad (9.8)$$

The last term in this equation, describing the interband coupling due to the impurity potential, can be neglected if for $\mathbf{G} \neq 0$, the relation

$$\frac{|U_{\mathbf{k}-\mathbf{k}'+\mathbf{G}}|}{|U_{\mathbf{k}-\mathbf{k}'}|} C_{nkn'\mathbf{k}'}(\mathbf{G}) \ll 1 \quad (9.9)$$

holds, which leads to the one-band approximation. Taking the Fourier transform with $f_n(\mathbf{k}) = \int \exp(-i\mathbf{k} \cdot \mathbf{r}) f_n(\mathbf{r}) d^3\mathbf{r}/V$ and by writing

$$E_n(\mathbf{k} \rightarrow \frac{1}{i}\nabla) \simeq E_n(\mathbf{0}) - \frac{\hbar^2}{2m^*}\Delta, \quad (9.10)$$

we find the effective-mass equation for shallow impurities in a simple band [260]

$$\left\{ -\frac{\hbar^2}{2m^*}\Delta + U(\mathbf{r}) \right\} f_n(\mathbf{r}) = (E - E_n(0))f_n(\mathbf{r}). \quad (9.11)$$

The condition (9.9) is fulfilled for $|\mathbf{k} - \mathbf{k}'| \ll |\mathbf{G}|$ and applies if the expansion coefficients $f_n(\mathbf{k})$ differ from zero only for small \mathbf{k} in the vicinity of the band edge. This is the case for charged impurities as, e.g., a substitutional Si (or Ge) at a Ga site in GaAs, for which the impurity potential is essentially a screened Coulomb potential with a short-range correction term U_{cc} (*central-cell correction*) to account for the chemical nature of the impurity

$$U(\mathbf{r}) = U_{cc}(\mathbf{r}) - \frac{e^2}{4\pi\epsilon_0\epsilon r}. \quad (9.12)$$

This leads to a modified hydrogen problem with bound states below the band minimum. The characteristic units of energy and length, the effective Rydberg constant $\text{Ry}^* = (m^*/m\epsilon^2)\text{Ry}$, and the Bohr radius $a_B^* = (\epsilon m/m^*)a_B$, respectively, scale according to the material parameters from the atomic values. For GaAs, one has $\text{Ry}^* \simeq 10^{-3}\text{Ry} \simeq 5 \text{ meV}$ and $a_B^* \simeq 100 a_B \simeq 10 \text{ nm}$. The bound states for hydrogen-like impurities can be classified by the angular momentum quantum numbers. Only the $1s$ state is essentially modified by the central-cell correction. Figure 9.2 draws attention to these bound states at the band edge in \mathbf{k} and in real space. In \mathbf{k} space, the $1s$ wave function is represented by its Fourier transform $f_{1s}(\mathbf{k})$ which extends over a width of the inverse effective Bohr radius around the band minimum. In real space, it is a wave function $f_{1s}(\mathbf{r})$ extending over a distance of about the effective Bohr radius around the impurity site. The real space localization of the state increases with the strength of the impurity potential. Shallow acceptor states have a more complex structure, which derives from the effective-mass Hamiltonian of p -like valence bands [261].

In contrast to (hydrogen-like) shallow impurities, whose spectrum is dominated by the long-range Coulomb interaction with only minor modifications

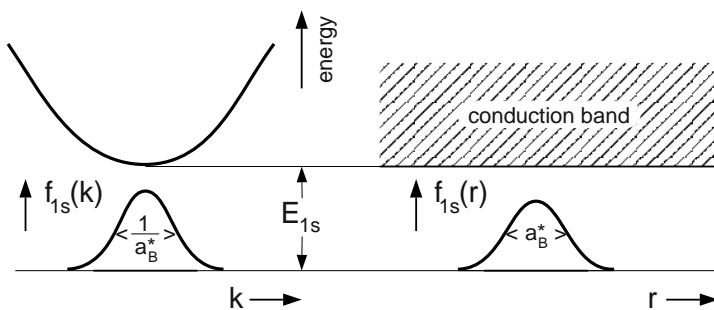


Fig. 9.2. Impurity states at a band edge in \mathbf{k} space (*left*) and in real space (*right*)

due to the central-cell correction (especially for the ground state), the situation is completely reversed for deep impurities. Here, the energy spectrum is determined by the short-range central-cell potential, and the influence of the long-range Coulomb potential (if present at all) is considered as a correction. Consequently, the deep impurity states are strongly localized to the neighborhood of the impurity site accompanied by lattice distortions. This situation cannot be well described by a superposition of extended Bloch states. Here it is more appropriate to use atomic orbitals or concepts of scattering theory with a localized basis.

Starting from the eigenvalue problem of (9.3) with the impurity potential $U(\mathbf{r})$ now dominated by the central-cell correction, we use the Ansatz for the wave function

$$\psi(\mathbf{r}) = \sum_{\alpha, \mathbf{R}} c_{\alpha}(\mathbf{R}) \phi_{\alpha}(\mathbf{r} - \mathbf{R}) \quad (9.13)$$

with atomic orbitals $\phi_{\alpha}(\mathbf{r} - \mathbf{R})$ localized at \mathbf{R} . While in Sect. 5.4, when introducing the LCAO method, we have constructed Bloch functions out of the atomic orbitals, we now remain in the localized representation. The variational principle for the energy leads to the set of coupled linear equations

$$\sum_{\alpha', \mathbf{R}'} (H_{\alpha \mathbf{R}, \alpha' \mathbf{R}'} - E S_{\alpha \mathbf{R}, \alpha' \mathbf{R}'}) c_{\alpha'}(\mathbf{R}') = 0 \quad (9.14)$$

for the expansion coefficients $c_{\alpha}(\mathbf{R})$ and energy eigenvalues following from the secular problem

$$\|H_{\alpha \mathbf{R}, \alpha' \mathbf{R}'} - E S_{\alpha \mathbf{R}, \alpha' \mathbf{R}'}\| = 0. \quad (9.15)$$

Here $H_{\alpha \mathbf{R}, \alpha' \mathbf{R}'}$ and $S_{\alpha \mathbf{R}, \alpha' \mathbf{R}'}$ are the matrix elements of the Hamiltonian and of the overlap between atomic orbitals (see Sect. 5.4), respectively.

Some aspects of deep impurities, in particular the chemical trends, can be understood in this model as exemplified here for an isoelectronic impurity, e.g., GaP:N (meaning that P in GaP is substituted by N) [261, 269]. In the picture of atomic orbitals, the valence and conduction bands of intrinsic semiconductors with tetrahedral coordination are formed by the bonding and anti-bonding states, respectively, of the s and p orbitals. This is sketched for the host atoms in the left hand side of Fig. 9.3, where the shaded regions indicate the continua of the energy bands. Replacing one host atom P by the impurity N leads to different pairs of s and p bonding and anti-bonding states localized at the impurity site (right hand side of Fig. 9.3): in particular, the s -bonding state becomes a resonant impurity level deep in the valence band, while the s -anti-bonding state of the Ga-N pair is lowered with respect to that of the Ga-P pair of the host crystal, thus forming a deep trap in the energy gap. Corresponding impurity states (not shown in the figure) are formed out of the p orbitals.

Chemical trends can be discussed by simulating a continuous change of the impurity (X) with a change of its atomic level energy E_X . For the bonding

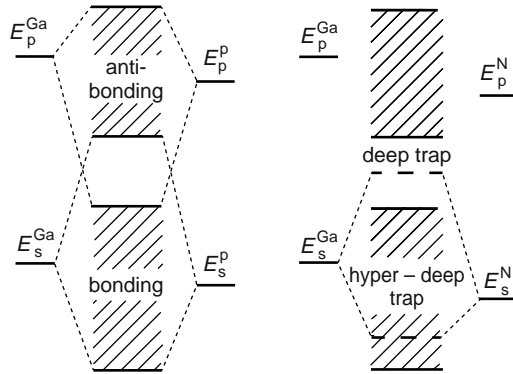


Fig. 9.3. Schematic level diagram with valence and conduction band formed from bonding and anti-bonding states of host atoms Ga and P (*left*) and of deep impurity states formed with s states of a substitutional N impurity (*right*)

and anti-bonding states of the s orbitals of Ga and of the impurity X, one may write the simplified secular problem

$$\begin{vmatrix} E_{\text{Ga}} - E & U \\ U & E_{\text{X}} - E \end{vmatrix} = 0 \quad (9.16)$$

with $E_{\text{Ga(X)}}$ being the energy of the atomic s orbital of the Ga(X) atom, and U the coupling between these orbitals. The eigenvalues of (9.16)

$$E_{\pm} = \frac{E_{\text{Ga}} + E_{\text{X}}}{2} \pm \frac{E_{\text{Ga}} - E_{\text{X}}}{2} \left\{ 1 + \frac{4|U|^2}{(E_{\text{Ga}} - E_{\text{X}})^2} \right\}^{1/2} \quad (9.17)$$

are depicted as a function of $E_{\text{Ga}} - E_{\text{X}}$ in Fig. 9.4. Depending on the sign of $E_{\text{Ga}} - E_{\text{X}}$, the anti-bonding or bonding states are shown: they evolve from the valence or conduction band edge, respectively, and converge with increasing $|E_{\text{Ga}} - E_{\text{X}}|$ toward the energy E_{Ga} of the atomic Ga- s orbital which acts as a pinning level. The symmetry of these impurity states is A_1 due to the s orbital [269]. Similar considerations for the p orbitals lead to deep impurity states with T_2 symmetry.

The other concept to describe deep impurities is based on scattering theory and employs the Green function of the impurity problem [270]

$$G(E) = \lim_{\delta \rightarrow 0} \frac{1}{E - H + i\delta}. \quad (9.18)$$

We make use of the separation of the system Hamiltonian $H = H_0 + U$ into the Hamiltonian H_0 for the unperturbed periodic solid and the impurity potential $U(\mathbf{r})$, now understood as the difference of the self-consistent DFT-LDA single-particle potentials with and without impurity (see Sect. 5.1)

$$U(\mathbf{r}) = V_{\text{eff}}[n(\mathbf{r}), \mathbf{r}] - V_{\text{eff}}^0[n(\mathbf{r}), \mathbf{r}]. \quad (9.19)$$

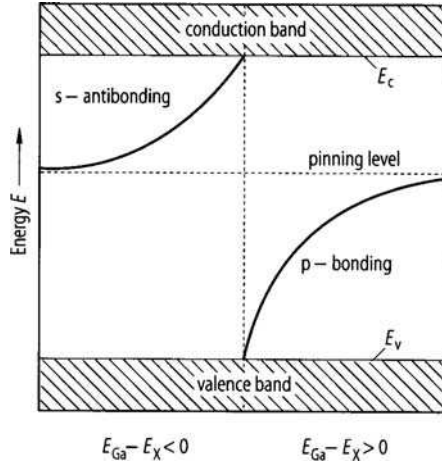


Fig. 9.4. Chemical shift of deep traps evolving from p -bonding and s -anti-bonding states

The Green function $G(E)$ of the full problem can be expanded in the Born series

$$G(E) = G_0(E) + G_0(E)UG_0(E) + \dots = (1 - G_0(E)U)^{-1}G_0(E). \quad (9.20)$$

The first factor in the last expression gives rise to additional poles of $G(E)$ caused by the impurity potential U . They exist besides those of the second factor, the Green function $G_0(E)$ of the unperturbed band structure. For the density of states

$$D(E) = -\frac{2}{\pi} \text{Tr} \text{Im} G(E) \quad (9.21)$$

one finds with $G(E) = G_0(E) + (G(E) - G_0(E))$

$$\begin{aligned} D(E) &= -\frac{2}{\pi} \text{Tr} \text{Im} G_0(E) - \frac{2}{\pi} \text{Tr} \text{Im} (G(E) - G_0(E)) \\ &= D_0(E) + \Delta D(E) \end{aligned} \quad (9.22)$$

where $D_0(E)$ is the density of states of the unperturbed solid and $\Delta D(E)$ its change due to the impurity both in the gap and in the continuum of the valence and conduction bands.

In a representation with localized functions, e.g., Wannier functions

$$\phi_n(\mathbf{r} - \mathbf{R}) = \frac{1}{\sqrt{N}} \sum_{\mathbf{k}} e^{i\mathbf{k} \cdot \mathbf{R}} \psi_{n\mathbf{k}}(\mathbf{r}) \quad (9.23)$$

with

$$\int \phi_n^*(\mathbf{r} - \mathbf{R}) \phi_n(\mathbf{r} - \mathbf{R}') d^3\mathbf{r} = \delta_{nn'} \delta_{\mathbf{R}, \mathbf{R}'} \quad (9.24)$$

the matrix elements (take for simplicity $n = n'$)

$$U_{\mathbf{R}\mathbf{R}'} = \int \phi_n^*(\mathbf{r} - \mathbf{R})U(\mathbf{r})\phi_n(\mathbf{r} - \mathbf{R}')d^3\mathbf{r} \tag{9.25}$$

are different from zero only for a small number of \mathbf{R}, \mathbf{R}' out of a set of lattice points $\{R_I\}$ around the impurity site. This defines a short range defect matrix

$$(U_{\mathbf{R}\mathbf{R}'}) = \begin{pmatrix} U_{\{R_I\}} & 0 \\ 0 & 0 \end{pmatrix} \tag{9.26}$$

for which the additional poles of $G(E)$ in (9.20) can be calculated from (Problem 9.1)

$$\|1 - G_0(E)U\| = \|1 - G_{0,\{R_I\}}(E)U_{\{R_I\}}\| = 0. \tag{9.27}$$

Here $G_{0,\{R_I\}}(E)$ is part of the matrix representation of the Green function connected with the set $\{R_I\}$.

A point defect of particular interest is the anti-site defect, which has been studied intensively in GaAs and found to be responsible for realizing semi-insulating material [271]. Anti-site defects exist also in other compound semiconductors. The schematic level diagram of the As_{Ga} anti-site defect is shown in Fig. 9.5. Besides resonances, deriving from p -anti-bonding and bonding states in the valence and conduction bands, there is a trap in the middle of the gap connected with the s -anti-bonding states of A_1 symmetry. Note the degeneracy of the respective states, it is sixfold (with spin) for T_2 deriving from p -states and twofold for A_1 deriving from s -states.

Transition metal atoms in semiconductors form deep impurity states as a consequence of their tightly bound d electrons.[272] Their orbital multiplets are split by the crystal field into states characterized by the point symmetry (e.g., in zinc blende material A_1, A_2, E, T_1 and T_2 , see Appendix).

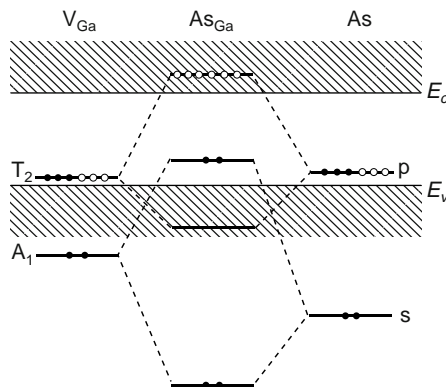


Fig. 9.5. Level diagram of the As_{Ga} anti-site defect (*center*) and its composition out of the Ga vacancy (*left*) and p states of the As atom (*right*). Full (open) dots indicate occupied (empty) states

9.2 Disorder

Following the systematics of dimensionality in the deviations from the crystalline order, we mention briefly the dislocations as one-dimensional defects and may address interfaces (or surfaces) as two-dimensional defects. A particular deviation from crystalline configurations is a disorder by composition or structure, which can exist in all three spatial dimensions. Compositional disorder results, e.g., by placing two or more different kinds of atoms statistically on the otherwise unperturbed lattice points. This is the case in so-called *mixed crystals* or *alloys*, in which the long-range order is destroyed because there is no correlation in the chemical nature of the ions occupying the lattice points. Also statistical occupation of the lattice points with different isotopes of one kind of atoms creates compositional disorder. We mentioned already the broadening of phonon resonances due to isotope disorder in Chap. 3. A more dramatic three-dimensional disorder is the structural disorder, typical for *amorphous solids*, which do not exhibit any crystalline order.

Adopting a single-particle description in the sense of Chap. 5, we write the electron Hamiltonian for a system with disorder as

$$H = -\frac{\hbar^2}{2m}\Delta + \sum_{\mathbf{R}_j} v_j(\mathbf{r} - \mathbf{R}_j) \quad (9.28)$$

with the ion configuration $\{\mathbf{R}_j\}$ and the effective single-particle potentials $v_j(\mathbf{r} - \mathbf{R}_j)$ provided by the specific atom (or ion) at \mathbf{R}_j . Disorder can be accounted for by deviations from the crystalline ion configuration $\{\mathbf{R}_n^0\}$ and/or by varying the atomic species with the potential v_j from site to site.

We may write the Hamiltonian H also in the form

$$H = \sum_j \epsilon_j c_j^\dagger c_j + \sum_{j,l} t_{jl} c_j^\dagger c_l \quad (9.29)$$

by using fermion operators c_j^\dagger, c_j in the site representation. Here the single-particle energies ϵ_j (the site energies) account for disorder in the occupation of the sites \mathbf{R}_j , while the transfer matrix elements t_{jl} do it for the hopping between sites \mathbf{R}_j and \mathbf{R}_l . The actual configuration of a disordered material is not known but is not essential for the physical properties. Instead, disorder is considered by means of probability distributions of the site energies ϵ_j and/or of the transfer matrix elements t_{jl} . For obvious reasons, the former is called *diagonal disorder*, the latter *off-diagonal disorder*. Both are related to probability distributions of the configurations $P(\{\mathbf{R}_j\})$.

A simple case of diagonal disorder is that the single-particle energies scatter around a mean value ϵ_0 , and we may write

$$H = \sum_j \epsilon_0 c_j^\dagger c_j + \sum_{j,l} t_{jl} c_j^\dagger c_l + \sum_j (\epsilon_j - \epsilon_0) c_j^\dagger c_j, \quad (9.30)$$

where the first two terms are the tight-binding Hamiltonian for a single band (see Sect. 5.4), while the last term represents the diagonal disorder. We may switch to the Bloch representation and write

$$H = \sum_{\mathbf{k}} \epsilon_{\mathbf{k}} c_{\mathbf{k}}^{\dagger} c_{\mathbf{k}} + \sum_{\mathbf{k}, \mathbf{q}} u(\mathbf{q}) c_{\mathbf{k}+\mathbf{q}}^{\dagger} c_{\mathbf{k}} = H_0 + H_{\text{disorder}} \quad (9.31)$$

which in a natural way splits into the unperturbed energy band and the perturbation due to disorder. The potential matrix element $u(\mathbf{q})$ is the Fourier transform of the impurity potential $U(\mathbf{r} - \mathbf{R}_j)$ and can be separated according to $u(\mathbf{q}) = \sum_j \exp(i\mathbf{q} \cdot \mathbf{R}_j) U(\mathbf{q}) = \rho(\mathbf{q}) U(\mathbf{q})$ into structure factor $\rho(\mathbf{q})$ and form factor $U(\mathbf{q})$.

For a systematic treatment of the disorder, we study the single-particle Green function (see Sect. 7.1)

$$G(\mathbf{k}, \mathbf{k}', t - t') = -\frac{i}{\hbar} \theta(t - t') \langle \{c_{\mathbf{k}}(t), c_{\mathbf{k}'}^{\dagger}(t')\} \rangle. \quad (9.32)$$

The equation of motion for $G(\mathbf{k}, \mathbf{k}', t - t')$ is easily obtained with H from (9.31) and reads

$$\begin{aligned} (i\hbar \frac{\partial}{\partial t} - \epsilon_{\mathbf{k}}) G(\mathbf{k}, \mathbf{k}', t - t') &= \delta_{\mathbf{k}\mathbf{k}'} \delta(t - t') \\ &+ \sum_{\mathbf{k}''} u(\mathbf{k} - \mathbf{k}'') \underbrace{\frac{-i}{\hbar} \theta(t - t') \langle \{c_{\mathbf{k}''}(t), c_{\mathbf{k}'}^{\dagger}(t')\} \rangle}_{G(\mathbf{k}'', \mathbf{k}', t - t')}. \end{aligned} \quad (9.33)$$

After Fourier transformation with respect to $t - t'$ with $E^+ = \hbar\omega + i\delta$, the retarded Green function of the disorder problem is given by

$$G(\mathbf{k}, \mathbf{k}'; E^+) = \frac{1}{E^+ - \epsilon_{\mathbf{k}}} \left(\delta_{\mathbf{k}\mathbf{k}'} + \sum_{\mathbf{k}''} u(\mathbf{k} - \mathbf{k}'') G(\mathbf{k}'', \mathbf{k}'; E^+) \right). \quad (9.34)$$

By identifying the first factor on the *rhs* as the unperturbed retarded Green function $G_0(\mathbf{k}, E^+)$ for the Bloch band, this can be written in the form of the Dyson equation

$$G(\mathbf{k}, \mathbf{k}'; E^+) = G_0(\mathbf{k}, E^+) \left(\delta_{\mathbf{k}\mathbf{k}'} + \sum_{\mathbf{k}''} u(\mathbf{k} - \mathbf{k}'') G(\mathbf{k}'', \mathbf{k}'; E^+) \right). \quad (9.35)$$

By iteration, it leads to the Born series

$$G = G_0 + G_0 u G_0 + G_0 u G_0 u G_0 + \dots \quad (9.36)$$

and by introducing the t -matrix

$$t = u(1 + G_0u + G_0uG_0u + \dots) = u \sum_{n=0}^{\infty} (G_0u)^n \quad (9.37)$$

it takes the form

$$G(\mathbf{k}, \mathbf{k}'; E^+) = G_0(\mathbf{k}; E^+) (\delta_{\mathbf{k}, \mathbf{k}'} + t(\mathbf{k}, \mathbf{k}'; E^+) G_0(\mathbf{k}'; E^+)). \quad (9.38)$$

We note that the full Green function depends on the configuration $\{\mathbf{R}_j\}$ of the impurities, which in principle is not known. On the other hand, we do not expect, that the physical properties of a sufficiently large sample are determined by its specific impurity configuration. Since on macroscopic length scales (large compared e.g. with the mean free path) different configurations are realized, a statistical average can be taken which depends only on the impurity concentration.

However, this argument does not apply, in the mesoscopic regime with sample sizes comparable to the typical transport lengths. In this regime, the observation of universal conductance fluctuations can be taken as a fingerprint of the distinct impurity configuration realized in the sample [159, 160]. Here we rely on the property of a macroscopic observable A , that it is self-averaging, i.e., for the variance $\text{Var}A = \langle (A - \langle A \rangle)^2 \rangle$ it holds that

$$\lim_{V \rightarrow \infty} \frac{\text{Var}A}{\langle A \rangle^2} = 0, \quad (9.39)$$

where V is the volume of the system. An example can be treated as Problem 9.2.

The averaging over impurity configurations affects only the structure factor and is written as

$$f(\mathbf{q}) = \langle \rho(\mathbf{q}) \rangle_{\text{conf}} = \sum_{\{\mathbf{R}_j\}} P(\{\mathbf{R}_j\}) \sum_{j=1}^N e^{i\mathbf{q} \cdot \mathbf{R}_j}, \quad (9.40)$$

where $P(\{\mathbf{R}_j\})$ is the probability distribution for the configurations of N impurities. The t -matrix consists of terms with different powers of the potential $u(\mathbf{q})$. Thus, the configuration average has to be performed in all orders of $\rho(\mathbf{q})$, and we write for the n th order

$$f(\mathbf{q}_1, \dots, \mathbf{q}_n) = \langle \rho(\mathbf{q}_1) \dots \rho(\mathbf{q}_n) \rangle. \quad (9.41)$$

There is no preference for the impurities to be on particular sites, and we can simplify the double sum over configurations and sites by replacing

$$\sum_{\{\mathbf{R}_j\}} \sum_{j=1}^N \dots \rightarrow c \sum_{\text{all sites}} \dots \quad (9.42)$$

with the impurity concentration c . When taking the sum over all sites and not only over those occupied by an impurity, we have $\sum_{\mathbf{n}} \exp(i\mathbf{q} \cdot \mathbf{R}_{\mathbf{n}}) = N\delta_{\mathbf{q},0}$ and find

$$f(\mathbf{q}_1, \dots, \mathbf{q}_n) = p_n(c) \delta_{\mathbf{q}_1, 0} \dots \delta_{\mathbf{q}_n, 0} \tag{9.43}$$

with a polynomial $p_n(c)$ of degree n in the impurity concentration. The lowest order terms can explicitly be written

$$f(\mathbf{q}_1) = \left\langle \sum_{\mathbf{n}} e^{i\mathbf{q}_1 \cdot \mathbf{R}_{\mathbf{n}}} \right\rangle = N \delta_{\mathbf{q}, 0} \tag{9.44}$$

$$\begin{aligned} f(\mathbf{q}_1, \mathbf{q}_2) &= \left\langle \sum_{\mathbf{n}_1, \mathbf{n}_2} e^{i(\mathbf{q}_1 \mathbf{R}_{\mathbf{n}_1} + \mathbf{q}_2 \mathbf{R}_{\mathbf{n}_2})} \right\rangle \\ &= \left\langle \sum_{i=j} e^{i(\mathbf{q}_1 + \mathbf{q}_2) \cdot \mathbf{R}_i} + \sum_j e^{i\mathbf{q}_1 \cdot \mathbf{R}_j} \sum_{i \neq j} e^{i\mathbf{q}_2 \cdot \mathbf{R}_i} \right\rangle \\ &= N \delta_{\mathbf{q}_1 + \mathbf{q}_2, 0} + N \delta_{\mathbf{q}_1, 0} (N - 1) \delta_{\mathbf{q}_2, 0}. \end{aligned} \tag{9.45}$$

Whenever a sum is to be taken over the wave vectors, it can be converted into an integral with the consequence that the Kronecker symbol becomes a δ function or

$$f(\mathbf{q}_1) = c \delta(\mathbf{q}_1) \quad \text{and} \quad f(\mathbf{q}_1, \mathbf{q}_2) = c \delta(\mathbf{q}_1 + \mathbf{q}_2) + c^2 \delta(\mathbf{q}_1) \delta(\mathbf{q}_2). \tag{9.46}$$

The power of the impurity concentration in these expressions indicates the number of impurities involved in a scattering process. Scattering with single impurities is dominating, while scattering with two or more impurities becomes less likely according to the corresponding power of $c < 1$.

Turning back to the Dyson equation, we now perform the configuration average with the Green function by replacing

$$G(\mathbf{k}, \mathbf{k}'; E^+) \rightarrow \overline{G}(\mathbf{k}, \mathbf{k}'; E^+) = \langle G(\mathbf{k}, \mathbf{k}'; E^+) \rangle_{\text{conf}} \tag{9.47}$$

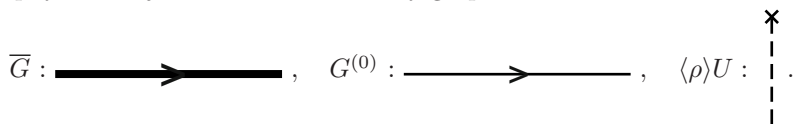
and write (suppressing the energy argument E^+ to simplify notation)

$$\overline{G}(\mathbf{k}, \mathbf{k}') = G^{(0)}(\mathbf{k}) \left(\delta_{\mathbf{k}, \mathbf{k}'} + \frac{V}{(2\pi)^3} \int \Sigma(\mathbf{k}, \mathbf{k}'') \overline{G}(\mathbf{k}'', \mathbf{k}') d^3 k'' \right) \tag{9.48}$$

with the self-energy $\Sigma(\mathbf{k}, \mathbf{k}'')$ due to the disorder, which in general depends on the energy.

9.3 Approximations for Impurity Scattering

The configuration averaged Green function, likewise the self-energy, can be evaluated in different approximations, which can be classified by making use of a diagrammatic representation [9, 206, 273]. This is achieved by replacing the physical objects of our formulas by graphs:



The leading terms of the Dyson equation can be arranged according to their number of interaction lines with the impurities and lead to the following graphical representation of the averaged Green function \bar{G} or the Dyson equation:

$$\begin{aligned}
 \bar{G} = & \begin{array}{c} \text{---} \xrightarrow{k} \text{---} \xrightarrow{k'} \text{---} \\ \text{---} \end{array} = \begin{array}{c} \text{---} \xrightarrow{k} \text{---} \xrightarrow{k} \text{---} \\ \text{---} \end{array} + \begin{array}{c} \text{---} \xrightarrow{k} \text{---} \xrightarrow{k} \text{---} \\ \text{---} \uparrow \text{---} \\ \text{---} \end{array} \\
 & + \begin{array}{c} \text{---} \xrightarrow{k} \text{---} \xrightarrow{k'} \text{---} \xrightarrow{k} \text{---} \\ \text{---} \uparrow \text{---} \uparrow \text{---} \\ \text{---} \end{array} + \begin{array}{c} \text{---} \xrightarrow{k} \text{---} \xrightarrow{k'} \text{---} \xrightarrow{k} \text{---} \\ \text{---} \uparrow \text{---} \uparrow \text{---} \uparrow \text{---} \\ \text{---} \end{array} \\
 & + \begin{array}{c} \text{---} \xrightarrow{k} \text{---} \xrightarrow{k} \text{---} \xrightarrow{k} \text{---} \xrightarrow{k} \text{---} \\ \text{---} \uparrow \text{---} \uparrow \text{---} \uparrow \text{---} \\ \text{---} \end{array} + \begin{array}{c} \text{---} \xrightarrow{k} \text{---} \xrightarrow{k} \text{---} \xrightarrow{k} \text{---} \xrightarrow{k} \text{---} \\ \text{---} \uparrow \text{---} \uparrow \text{---} \uparrow \text{---} \uparrow \text{---} \\ \text{---} \end{array} + \begin{array}{c} \text{---} \xrightarrow{k} \text{---} \xrightarrow{k} \text{---} \xrightarrow{k} \text{---} \xrightarrow{k} \text{---} \\ \text{---} \uparrow \text{---} \uparrow \text{---} \uparrow \text{---} \uparrow \text{---} \\ \text{---} \end{array} \\
 & + \begin{array}{c} \text{---} \xrightarrow{k} \text{---} \xrightarrow{k} \text{---} \xrightarrow{k} \text{---} \xrightarrow{k} \text{---} \xrightarrow{k} \text{---} \\ \text{---} \uparrow \text{---} \uparrow \text{---} \uparrow \text{---} \uparrow \text{---} \\ \text{---} \end{array} + \dots
 \end{aligned} \tag{9.49}$$

We recognize a growing complexity of the individual diagrams. Some of them can be reduced to simpler ones by cutting a free propagator line, while others are irreducible in this sense. This is used in the graphical representation of the self-energy, which contains only the irreducible diagrams

$$\begin{aligned}
 \Sigma(\mathbf{k}, \mathbf{k}''; E^+) = & \begin{array}{c} \text{---} \uparrow \text{---} \\ \text{---} \end{array} + \begin{array}{c} \text{---} \uparrow \text{---} \\ \text{---} \uparrow \text{---} \\ \text{---} \end{array} + \begin{array}{c} \text{---} \uparrow \text{---} \\ \text{---} \uparrow \text{---} \uparrow \text{---} \\ \text{---} \end{array} + \begin{array}{c} \text{---} \uparrow \text{---} \\ \text{---} \uparrow \text{---} \uparrow \text{---} \uparrow \text{---} \\ \text{---} \end{array} \\
 & + \begin{array}{c} \text{---} \uparrow \text{---} \\ \text{---} \uparrow \text{---} \uparrow \text{---} \uparrow \text{---} \uparrow \text{---} \\ \text{---} \end{array} + \begin{array}{c} \text{---} \uparrow \text{---} \\ \text{---} \uparrow \text{---} \uparrow \text{---} \uparrow \text{---} \uparrow \text{---} \\ \text{---} \end{array} + \begin{array}{c} \text{---} \uparrow \text{---} \\ \text{---} \uparrow \text{---} \uparrow \text{---} \uparrow \text{---} \uparrow \text{---} \\ \text{---} \end{array} \\
 & + \begin{array}{c} \text{---} \uparrow \text{---} \\ \text{---} \uparrow \text{---} \uparrow \text{---} \uparrow \text{---} \uparrow \text{---} \\ \text{---} \end{array} + \begin{array}{c} \text{---} \uparrow \text{---} \\ \text{---} \uparrow \text{---} \uparrow \text{---} \uparrow \text{---} \uparrow \text{---} \\ \text{---} \end{array} + \begin{array}{c} \text{---} \uparrow \text{---} \\ \text{---} \uparrow \text{---} \uparrow \text{---} \uparrow \text{---} \uparrow \text{---} \\ \text{---} \end{array} + \dots
 \end{aligned} \tag{9.50}$$

With reference to the graphical form, we may characterize some standard approximations [9, 206, 273].

1. **Virtual Crystal Approximation (VCA):** This simplest approximation consists in taking into account the impurity interaction only in lowest order. The self-energy becomes

$$\Sigma^{\text{VCA}}(\mathbf{k}, \mathbf{k}'') = \begin{array}{c} \text{---} \uparrow \text{---} \\ \text{---} \\ \text{---} \end{array} = \langle \rho \rangle U = cU(0)\delta(\mathbf{k} - \mathbf{k}'') \tag{9.51}$$

and does not depend on the energy. For this case, the Dyson equation

$$\Sigma^{\text{SCBA}}(\mathbf{k}, \mathbf{k}''; E^+) = \text{---} \overset{\times}{\text{---}} + \text{---} \overset{\times}{\triangle} \text{---} \quad (9.59)$$

At the end of this section, we shall apply the SCBA to a system with discrete energy levels in order to demonstrate the mechanism of level broadening due to impurity scattering.

5. **Coherent Potential Approximation (CPA):** It combines the SCBA with the ATA by taking into account all graphs of the latter but with the replacement of the free Green function by the configuration averaged one as in the former. Thus, the self-energy is represented by

$$\Sigma^{\text{CPA}}(\mathbf{k}, \mathbf{k}''; E^+) = \text{---} \overset{\times}{\text{---}} + \text{---} \overset{\times}{\triangle} \text{---} + \text{---} \overset{\times}{\triangle} \text{---} \text{---} \overset{\times}{\triangle} \text{---} + \dots \quad (9.60)$$

In all these approximations, the self-energy turns out to be diagonal in the wave vector, which allows one to solve the Dyson equation to obtain the configuration averaged Green function

$$\overline{G}(\mathbf{k}, \mathbf{k}'; E^+) = \frac{\delta_{\mathbf{k}, \mathbf{k}'}}{E^+ - \epsilon_{\mathbf{k}} - \Sigma(\mathbf{k}; E^+)} \quad (9.61)$$

with the complex self-energy

$$\Sigma(\mathbf{k}; E^+) = cU(0) + c \frac{V}{(2\pi)^2} \int \frac{|t(\mathbf{k} - \mathbf{k}_1)|^2}{E^+ - \epsilon_{\mathbf{k}}} d^3 \mathbf{k}_1. \quad (9.62)$$

Its imaginary part

$$\text{Im}\Sigma(\mathbf{k}; E^+) = c \frac{V}{(2\pi)^2} \int |t(\mathbf{k} - \mathbf{k}_1)|^2 \delta(E^+ - \epsilon_{\mathbf{k}}) d^3 \mathbf{k}_1 = \frac{\hbar}{\tau_{\mathbf{k}}} \quad (9.63)$$

can be expressed by the quasi-particle lifetime $\tau_{\mathbf{k}}$ and quantifies the rate by which the Bloch electron is scattered by disorder out of its state with wave vector \mathbf{k} . Note that the approximations 1–5 consider only scattering from a single impurity, therefore, the self-energy is proportional to the impurity concentration c . In the CPA, all diagrams with up to four interaction lines, except those where these lines cross each other, are included. This point needs further discussion in Sect. 9.5.

The modification of the electron energy by impurity scattering becomes particularly evident for systems with a discrete level spectrum, such as the Hubbard bands in the atomic limit (with energies at t_0 and $t_0 + U$, see Sect. 7.2) and the Landau levels of a two-dimensional electron system (with $\epsilon_n = \hbar\omega_c(n + 1/2)$, see Sect. 5.6). Their density of states has the form

$$D^{(0)}(E) = \sum_n g_n \delta(E - \epsilon_n) \quad (9.64)$$

with the degeneracy factor g_n . Let us assume the impurity potential to be extremely short-ranged as described by

$$U(\mathbf{r} - \mathbf{R}_j) = U_0 \delta(\mathbf{r} - \mathbf{R}_j) \quad (9.65)$$

with the Fourier transform $U(\mathbf{q}) = U_0$. In SCBA, the self-energy can be calculated from

$$\Sigma(E^+) = cU_0 + c \sum_n \frac{U_0^2}{E^+ - \epsilon_n - \Sigma(E^+)}. \quad (9.66)$$

Given that the separation of neighboring energy levels $\epsilon_{n+1} - \epsilon_n$ is much larger than the imaginary part of the self-energy $\text{Im}\Sigma(E^+)$, which determines the level broadening due to the impurity scattering, we may approximate the self-energy for E close to the level energy ϵ_n by

$$\Sigma(E \sim \epsilon_n) = \Sigma_n(E) \simeq \frac{cU_0^2}{E - \epsilon_n - \Sigma_n(E)}, \quad (9.67)$$

which is a quadratic equation in $\Sigma_n(E)$ and can be solved to give

$$\Sigma_n^{\text{SCBA}}(E) = \frac{E - \epsilon_n}{2} - \frac{i}{2} (\Gamma_0^2 - (E - \epsilon_n)^2)^{1/2}, \quad (9.68)$$

where $\Gamma_0^2/4 = cU_0^2$. From the corresponding Green function

$$\overline{G}(E^+) = \sum_n \frac{1}{E^+ - \epsilon_n - \Sigma_n(E)} \quad (9.69)$$

we obtain the density of states $D^{\text{SCBA}}(E) = -\text{Im}\overline{G}(E^+)/\pi$ in the form

$$D^{\text{SCBA}}(E) = \sum_n \begin{cases} \frac{2}{\pi\Gamma_0^2} (\Gamma_0^2 - (E - \epsilon_n)^2)^{1/2} & \text{for } |E - \epsilon_n| < \Gamma_0 \\ 0 & \text{otherwise} \end{cases} \quad (9.70)$$

The result is a broadening due to impurity scattering of the otherwise discrete and highly degenerate levels (Fig. 9.6). The half-elliptic form of the density of states is an artifact of the assumed short-range of the impurity potential. We recognize also the increase of the broadening with the impurity concentration and/or with the strength of the impurity potential. Impurity potentials of some finite range would create states in the gaps between the neighboring peaks thus leading to an overall finite density of states.

9.4 Electric Conductivity

In previous chapters, we have already studied several aspects of the electric conductivity, especially in Chap. 8 we have seen that it is determined by a transport relaxation time $\tau_{\text{tr}}(\mathbf{k})$ which accounts for scattering processes with

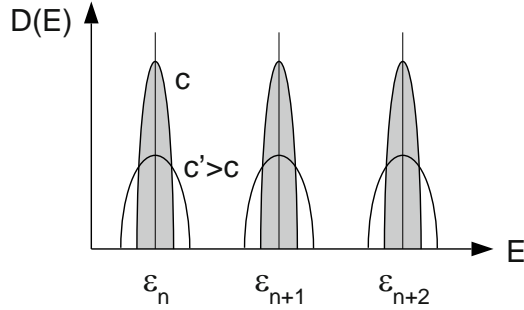


Fig. 9.6. Density of states of Landau levels in a two-dimensional electron system in the SCBA. The broadening increases with the impurity concentration c

phonons. Likewise, scattering with impurities contributes to the relaxation of a non-equilibrium distribution (here written as $f(\mathbf{k})$) which using, Fermi's Golden Rule, can be formulated as [64]

$$\frac{f(\mathbf{k}) - f_0(\mathbf{k})}{\tau_{\text{tr}}(\mathbf{k})} = \frac{2\pi}{\hbar} \frac{c}{(2\pi)^3} \int |t(\mathbf{k} - \mathbf{k}')|^2 \delta(\epsilon_{\mathbf{k}} - \epsilon_{\mathbf{k}'}) (f(\mathbf{k}) - f(\mathbf{k}')) d^3 \mathbf{k}' \quad (9.71)$$

with the t -matrix $t(\mathbf{k} - \mathbf{k}')$ and the impurity concentration c . The δ -function in the integral indicates that the impurity scattering is elastic. For an isotropic dispersion, the same arguments hold here as for the electron-phonon interaction with respect to forward and backward scattering (see Sect. 8.3).

Another and more principal approach to the electric conductivity is the linear response introduced in Sect. 2.5 (see also Problem 2.4). Let us write the Hamiltonian for the electrons in a system with impurities and in the presence of an external field represented by the vector potential $\mathbf{A}(\mathbf{r}, t)$

$$\mathcal{H} = \int d^3 \mathbf{r} \Psi^\dagger(\mathbf{r}) \left\{ \frac{1}{2m} (\mathbf{p} + e\mathbf{A}(\mathbf{r}, t))^2 + \sum_{\mathbf{R}_j} v_j(\mathbf{r} - \mathbf{R}_j) \right\} \Psi(\mathbf{r}). \quad (9.72)$$

Here the notation with field operators $\Psi^\dagger(\mathbf{r}), \Psi(\mathbf{r})$, introduced in Problem 4.8, is used. Without the external field and using the expansion $\Psi(\mathbf{r}) = \sum_{\mathbf{k}} \psi_{\mathbf{k}}(\mathbf{r}) c_{\mathbf{k}}$ in terms of Bloch functions $\psi_{\mathbf{k}}(\mathbf{r})$, the Hamiltonian \mathcal{H} becomes identical with (9.31). Including the vector potential, it takes the form considered in the linear response theory

$$\mathcal{H} = H_0 + H_{\text{disorder}} + V_{\text{ext}}(t), \quad (9.73)$$

and we may identify the external potential by comparing with (9.72) (taking only the terms linear in $\mathbf{A}(\mathbf{r}, t)$) as

$$V_{\text{ext}}(t) = \frac{e}{2m} \int \Psi^\dagger(\mathbf{r}) \{ \mathbf{p} \cdot \mathbf{A}(\mathbf{r}, t) + \mathbf{A}(\mathbf{r}, t) \cdot \mathbf{p} \} \Psi(\mathbf{r}) d^3 \mathbf{r} \quad (9.74)$$

which for the transverse gauge $\nabla \cdot \mathbf{A} = 0$ and with $\mathbf{p} = -i\hbar\nabla$ can be written

$$V_{\text{ext}}(t) = \frac{ie\hbar}{2m} \int \{(\nabla\Psi^\dagger)\Psi - \Psi^\dagger(\nabla\Psi)\} \cdot \mathbf{A}(\mathbf{r}, t) d^3\mathbf{r}. \quad (9.75)$$

The observable connected with the electric conductivity is the current density, which in terms of field operators can be written as

$$\begin{aligned} \hat{\mathbf{j}}(\mathbf{r}) &= -\frac{e}{2m}\Psi^\dagger(\mathbf{r})(\mathbf{p} + e\mathbf{A})\Psi(\mathbf{r}) + h.c. \\ &= \underbrace{\frac{ie\hbar}{2m}(\Psi^\dagger(\nabla\Psi) - (\nabla\Psi^\dagger)\Psi)}_{\hat{\mathbf{j}}^{\text{p}}(\mathbf{r})} - \underbrace{\frac{e^2}{m}\Psi^\dagger\Psi\mathbf{A}}_{\hat{\mathbf{j}}^{\text{d}}(\mathbf{r})}. \end{aligned} \quad (9.76)$$

The two contributions are called *paramagnetic* ($\hat{\mathbf{j}}^{\text{p}}(\mathbf{r})$) and *diamagnetic* ($\hat{\mathbf{j}}^{\text{d}}(\mathbf{r})$) *current density*. The diamagnetic current density is already linear in the external field, while we identify the paramagnetic current density as the one appearing in the external perturbation, which thus takes the form

$$V_{\text{ext}}(t) = - \int \hat{\mathbf{j}}^{\text{p}}(\mathbf{r}) \cdot \mathbf{A}(\mathbf{r}, t) d^3\mathbf{r}. \quad (9.77)$$

The electric conductivity is the response to an external electric field that derives from the electromagnetic potentials according to $\mathbf{E} = -\nabla\phi - \partial\mathbf{A}/\partial t$. Let us assume harmonic external fields, e.g.,

$$\mathbf{A}(\mathbf{r}, t) = \mathbf{A}e^{i(\mathbf{q}\cdot\mathbf{r} - \omega t)}, \quad (9.78)$$

then, with the gauge $\nabla \cdot \mathbf{A} = 0$, we can separate the electric field into a longitudinal ($-\nabla\phi$) and a transverse ($-\partial\mathbf{A}/\partial t$) contribution. The longitudinal field has been the subject of Sects. 4.5 and 4.6 in deriving the energy-loss function and studying screening in the random phase approximation (RPA). Here we are dealing with the transverse response ($\mathbf{q} \perp \mathbf{A}$) with electric field components $E_\alpha = i\omega A_\alpha$. Using the Fourier expansion $\hat{\mathbf{j}}(\mathbf{r}) = \sum_{\mathbf{q}'} \hat{\mathbf{j}}_{\mathbf{q}'} \exp(i\mathbf{q}' \cdot \mathbf{r})$ of the current density operator, we may write the thermal expectation value for one of its Fourier components as

$$\langle \hat{j}_{\alpha, \mathbf{q}} \rangle_t = i\omega \int \sigma_{\alpha\beta}(\mathbf{q}; t, t') A_\beta e^{-i\omega t'} dt' \quad (9.79)$$

with double index summation understood. Assuming homogeneity in the time dependence, this becomes

$$j_{\alpha, \mathbf{q}}(\omega) = i\omega \sigma_{\alpha\beta}(\mathbf{q}; \omega) A_\beta. \quad (9.80)$$

For isotropic systems, the conductivity tensor simplifies to a scalar and the indices α, β can be dropped. We may now identify the operators \hat{A} and \hat{B} used

in Sect. 2.4, when introducing the concept of linear response, as $\hat{j}_{\mathbf{q}} = \hat{j}_{\mathbf{q}}^{\text{p}} + \hat{j}_{\mathbf{q}}^{\text{d}}$ and $\hat{j}_{\mathbf{q}}^{\text{p}}$, respectively, with

$$\langle \hat{j}_{\mathbf{q}}^{\text{d}} \rangle = -\frac{e^2}{m} \langle n_{\mathbf{q}} \rangle A \quad (9.81)$$

giving for the conductivity

$$\sigma(\mathbf{q}; \omega) = -\frac{i}{\omega} \left(\chi(\mathbf{q}, \omega) - \frac{e^2}{m} \langle n_{\mathbf{q}} \rangle \right) \quad (9.82)$$

with the susceptibility of the transverse response

$$\chi(\mathbf{q}, \omega) = \frac{i}{\hbar} \int_{-\infty}^{+\infty} e^{i\omega\tau} \theta(\tau) \langle [\hat{j}_{\mathbf{q}}^{\text{p}}(\tau), \hat{j}_{\mathbf{q}}^{\text{p}}(0)] \rangle_0 d\tau \quad (9.83)$$

The current density operator expressed in terms of fermion operators for free particle states reads

$$\hat{j}_{\mathbf{q}}^{\text{p}} = -e \sum_{\mathbf{k}} \left\langle \mathbf{k} + \mathbf{q} \left| \frac{\hat{p}}{m} \right| \mathbf{k} \right\rangle c_{\mathbf{k}+\mathbf{q}}^{\dagger} c_{\mathbf{k}} \quad (9.84)$$

which for $\mathbf{q} \rightarrow 0$ simplifies to $\hat{j}^{\text{p}} = (e\hbar/m) \sum_{\mathbf{k}} k c_{\mathbf{k}}^{\dagger} c_{\mathbf{k}}$ and yields for the susceptibility

$$\chi(0, \omega) = i \frac{e^2}{\hbar} \frac{\hbar^2}{m^2} \int_0^{\infty} e^{i\omega\tau} \sum_{\mathbf{k}, \mathbf{k}'} k k' \langle [c_{\mathbf{k}}^{\dagger}(\tau) c_{\mathbf{k}}(\tau), c_{\mathbf{k}'}^{\dagger}(0) c_{\mathbf{k}'}(0)] \rangle_0 d\tau. \quad (9.85)$$

In a more general single-particle basis, the current operator is

$$\hat{j}^{\text{p}} = -e \sum_{i,f} \left\langle i \left| \frac{\hat{p}}{m} \right| f \right\rangle c_i^{\dagger} c_f \quad (9.86)$$

and with $c_i^{\dagger}(\tau) = c_i^{\dagger} \exp(i\epsilon_i\tau/\hbar)$ and the Fermi–Dirac distribution function $\langle c_i^{\dagger} c_i \rangle = f(\epsilon_i)$ the current–current response can be cast into the form (Problem 9.3)

$$\chi(0, \omega) = -e^2 \sum_{i,f} |\langle i | \hat{v} | f \rangle|^2 \frac{f(\epsilon_i) - f(\epsilon_f)}{\hbar\omega + \epsilon_i - \epsilon_f + i\delta}. \quad (9.87)$$

When decomposing $\chi(0, \omega)$ for $\delta \rightarrow 0$ into real and imaginary part, one finds that the real part compensates the contribution ne^2/m of the diamagnetic current density in $\sigma(0, \omega)$ (9.82) [64, 274] and obtains the real conductivity

$$\sigma(0, \omega) = \frac{\pi e^2}{\omega} \sum_{i,f} |\langle i | \hat{v} | f \rangle|^2 (f(\epsilon_i) - f(\epsilon_f)) \delta(\hbar\omega + \epsilon_i - \epsilon_f) \quad (9.88)$$

known as the *Kubo–Greenwood formula*. For the metal–insulator transition to be discussed in the next section, we need the dc conductivity σ_{dc} , which is the static limit $\sigma(0, \omega \rightarrow 0)$. As for $\omega \rightarrow 0$, only states close to the Fermi energy contribute to the conductivity, we may finally write

$$\sigma_{\text{dc}} = \pi e^2 \int \left(-\frac{df_0(E)}{dE} \right) \sum_{i,f} |\langle i|\hat{v}|f\rangle|^2 \delta(E - \epsilon_i) \delta(E - \epsilon_f) dE. \quad (9.89)$$

For further discussion, we may cast the double sum under the integral into the form $\text{Tr}(\hat{v}\text{Im}G(E^+)\hat{v}\text{Im}G(E^+))$ (Problem 9.4). This form, with the two Green functions appearing, derives from the fact that the commutator in (9.85) contains four fermion operators, each two of which would be required for a single-particle Green function. In fact, it is possible to formulate the dc conductivity in terms of a configuration averaged product of a retarded (G^+) and an advanced Green function (G^-) [64, 274, 276]. Without going into the details of the derivation, for which we refer to the literature, we quote here in short notation the equation from which it derives. It is the *Bethe²–Salpeter³ equation*

$$\langle G^+ G^- \rangle = \langle G^+ \rangle \langle G^- \rangle + \langle G^+ \rangle \langle G^- \rangle \mathbf{V} \langle G^+ G^- \rangle \quad (9.90)$$

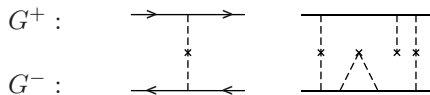
where \mathbf{V} , the *irreducible vertex operator*, plays the same role for the two-particle Green function as the self-energy does for the single-particle Green function. $\langle G^+ G^- \rangle$ describes the propagation of an electron–hole pair (G^- representing the hole) under the influence of impurity scattering, which not only affects the electron or hole propagation separately but can cause also a coupling of electron and hole propagation. The latter is considered in the vertex operator.

Similar to the single-particle Green function, the two-particle propagator can also be represented by diagrams.

A first group of simple diagrams contains the non-connected graphs for electrons and holes and corresponds to the approximation $\mathbf{V} = 0$

$$\langle G^+ G^- \rangle \simeq \langle G^+ \rangle \langle G^- \rangle \quad (9.91)$$

with separate configuration average for the electron and hole propagator. A second group of more complex diagrams (so called ladder diagrams) connects the electron and hole propagator in the simplest way, e.g.,



² Hans Albrecht Bethe 1906–2005, Noble prize in physics 1967

³ Edwin Ernest Salpeter *1924

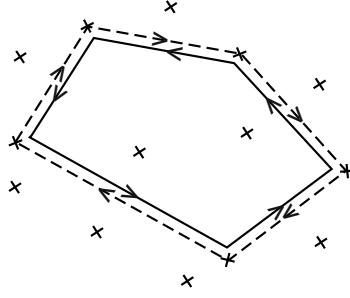


Fig. 9.7. Sketch of an electron path (*solid*) and its time inverted path (*dashed*) in an impurity configuration leading to quantum interference and weak localization

and accounts for coherent scattering of electron and hole at the same impurity. Summing these two groups of diagrams leads to the Drude result of the dc conductivity

$$\sigma = ne^2\tau/m = e^2k_F^2l_{\text{mfp}}/3\pi^2\hbar, \quad (9.92)$$

where τ is the single particle life-time and l_{mfp} the mean free path.

Finally we mention diagrams, which contain crossing interaction lines between the electron and hole propagator, like

$$\begin{array}{l} G^+ : \begin{array}{c} \text{---} \diagdown \text{---} \\ \diagup \text{---} \text{---} \\ \text{---} \diagup \text{---} \\ \text{---} \diagdown \text{---} \end{array} \\ G^- : \begin{array}{c} \text{---} \diagup \text{---} \\ \diagdown \text{---} \text{---} \\ \text{---} \diagdown \text{---} \\ \text{---} \diagup \text{---} \end{array} \end{array}$$

which describe the coherent scattering at an impurity configuration taking place for the hole in the reversed order with respect to that of the electron. Considering these so called *maximally crossing diagrams* is known in the literature as *cooperon approximation*, as they represent an interaction between electrons on their time-inverted paths along an impurity configuration in analogy to the electron–phonon mediated formation of Cooper pairs. The situation is depicted in Fig.9.7. The wave functions corresponding to the two time inverted paths through the impurity configuration interfere positively with each other and lead to a localization due to quantum interference. It is known as *weak localization* and gives a dc conductivity that corresponds to the one found by solving the Boltzmann equation including the effect of the back scattering which is characteristic for the transport relaxation time [274]. Removal of this interference by a magnetic field leads to a decrease of the resistance and can be taken as a signature of weak localization.

9.5 Metal–Insulator Transition

Different sections of this chapter have provided several aspects of disorder, and the influence it takes on the electron states. As we have seen in Sect. 9.1, single impurities can lead to discrete energy levels in the band gap region

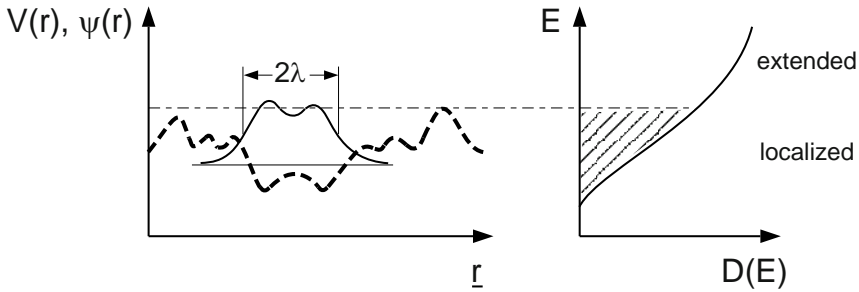


Fig. 9.8. Schematic view of an electron wave function (*thin solid line*) in a random potential (*dashed line, left*) and density of states (*right*) indicating extended and localized states

of semiconductors. These (shallow or deep) bound impurity states are localized, and their wave functions decay exponentially away from the center. But, impurities can modify also the electronic states within a band as resonant states. However, such modifications are expected to be small in regions of high density of extended states. With increasing impurity concentration the bound state wave functions start to overlap and lead to the formation of an impurity band with a continuous density of states, which can eventually merge with that of the nearby energy band. This situation is schematically depicted in Fig. 9.8. Instead of a sharp band edge resulting from the periodic crystal potential as shown in Fig. 9.2, the electrons close to the band edge experience a random potential caused by the impurities. In this potential landscape, states with low energy are localized with a finite localization length λ , while those with sufficiently high energy are not confined and extend over the whole solid as λ increases to infinity. This scenario implies that there must be a certain critical energy ϵ_c which separates the extended from the localized states and that it is likely to be in a region with small density of states or close to the band edges.

Let us consider also a scenario, which does not start from an energy band with a continuous density of states, but from a discrete spectrum as that of Landau levels for two-dimensional electrons (see Sect. 5.6 and Fig. 9.6). Without impurities, we have a homogeneous system which is invariant under translations in the plane perpendicular to the magnetic field. Therefore, the Landau levels are discrete but highly degenerate, and the electron wave functions are delocalized. A random potential breaks the translational invariance and lifts the degeneracy of the Landau levels leading to their broadening into a narrow band. In Sect. 9.3, we have discussed the effect of short-range impurities within SCBA with the result shown in Fig. 9.6. The states in the center of the Landau band with the large density of states are still extended, while those at the edges are localized due to the potential fluctuations, and we have again the scenario sketched in Fig. 9.8.

These conclusions, with respect to a clear separation between extended and localized states, are not restricted to substitutional disorder caused by impurities but are valid also for structural disorder as in amorphous solids. In fact, amorphous solids, especially amorphous semiconductors, have been the systems for which the concepts of a disorder induced metal–insulator transition have been developed [39, 209, 211, 275, 276].

Consider now electron transport in a solid with disorder. As we have seen in the previous section, the dc conductivity is determined by the states around the Fermi energy and would be carried for $T = 0$ K alone by those at the Fermi energy. It follows from the discussion of Fig. 9.8 that we can distinguish between solids or experimental conditions for which the Fermi energy falls into a region of extended states and those with E_F in a region with localized states. For the former, the dc conductivity σ_{dc} at $T = 0$ K is finite, these are the metals, while it vanishes for the latter, which are the insulators. Instead of the dc conductivity, we may also use the relation $\sigma_{dc} = en\mu$ and distinguish these systems by their mobility μ , which at $T = 0$ K is finite for extended states but drops to zero when entering the region of localized states. This defines the *mobility edge* that marks the critical energy ϵ_c for the transition from a metal to an insulator.

In spite of this clear distinction between metals and insulators, the criterion is hard to test in experiments, because of the difficulties to approach the $T = 0$ K limit and also due to the fact that experiments are always performed with finite samples. Let us have a look, therefore, on less restrictive conditions. In an insulator, with the Fermi energy below the mobility edge, already a very low but finite temperature would allow the localized electrons to reach by thermal excitation nearby unoccupied localized states. Thus step by step these electrons carry a current by a hopping process (variable range hopping), which leads to the characteristic dependence of the dc conductivity on the inverse temperature of Mott’s $T^{-1/4}$ law [39, 275].

The existence of a mobility edge in an electron system with disorder is crucial for understanding the vanishing of the longitudinal magneto-resistivity of two-dimensional electron systems for magnetic fields around integer filling factors (see Fig. 5.21). In the original QHE experiments [161], the carrier density and thus the Fermi energy was changed by the external gate voltage while the sample was exposed to a fixed magnetic field. Changing the carrier density shifts the Fermi energy through the spectrum of Landau levels which due to the disorder is broadened. If E_F is close to the center of a Landau band, in a region of extended states, the dc conductivity is finite, while away from the center, and between the Landau levels it hits localized states and the dc conductivity drops to zero. In a Quantum Hall experiment with fixed carrier density (or Fermi energy), an increasing magnetic field increases the degeneracy and separation of the Landau levels, which shift one by one through the Fermi energy. As a function of the magnetic field, $E_F(B)$ coincides with extended or localized states connected with finite or zero dc conductivity, the latter always connected with integer filling factors. Thus, one has a sequence

of metal–insulator transitions within one electron system by sweeping either the magnetic field for fixed carrier density or *vice versa*.

Actually Figs. 5.21 and 7.12 show resistivities, and we have to relate our conclusions to this quantity by inverting the resistivity tensor

$$\boldsymbol{\rho} = \begin{pmatrix} \rho_{xx} & \rho_{xy} \\ \rho_{yx} & \rho_{yy} \end{pmatrix} \quad (9.93)$$

giving

$$\boldsymbol{\sigma} = \frac{1}{\rho_{xx}\rho_{yy} - \rho_{xy}\rho_{yx}} \begin{pmatrix} \rho_{yy} & -\rho_{yx} \\ -\rho_{xy} & \rho_{xx} \end{pmatrix}. \quad (9.94)$$

This simplifies for rotational symmetry around the normal to the plane of the two-dimensional electron system with $\rho_{xx} = \rho_{yy}$ and for finite ρ_{xy} to the relation $\rho_{xx} \sim \sigma_{xx}$. Thus, vanishing longitudinal resistivity means also vanishing longitudinal conductivity.

The question of the quantitative connection between disorder and the quantum mechanical states around the metal–insulator transition found an answer in some fundamental contributions, using scaling arguments to account for the influence of the finite size of the sample [280, 281] and resulted in understanding the MIT as a second order phase transition.

For a finite sample (e.g., a cube of typical length L), the relevant transport quantity is not the conductivity (which is a material property independent of the sample size and shape) but the *conductance* $G(L)$, defined as the ratio of the measured current through the sample and the applied voltage. In terms of the fundamental conductance unit e^2/h , we may define also the dimensionless quantity

$$g(L) = \frac{h}{e^2} G(L). \quad (9.95)$$

If instead of the box of size L a larger box of size $L' > L$ is considered, the scaling argument is applied to find $g(L')$. It is based on the assumption that the ratio between the relative changes of g and of L

$$\frac{dg}{g} \frac{L}{dL} = \frac{d \ln g}{d \ln L} = \beta(g) \quad (9.96)$$

is ruled by a universal function $\beta(g)$ depending on the dimensionless conductance g but not separately on the parameters characterizing the sample such as disorder, energy, or sample size L . Solving the differential equation for the asymptotic limits yields

$$\beta(g) = 1 - \frac{g_c}{g} \quad \text{for large } g \quad (9.97)$$

$$\beta(g) = -e^{g_c/g} \quad \text{for small } g. \quad (9.98)$$

Assuming a monotonous function $\beta(g)$, these results can be connected by an interpolation to obtain the qualitative result shown in Fig. 9.9 (Problem 9.5).

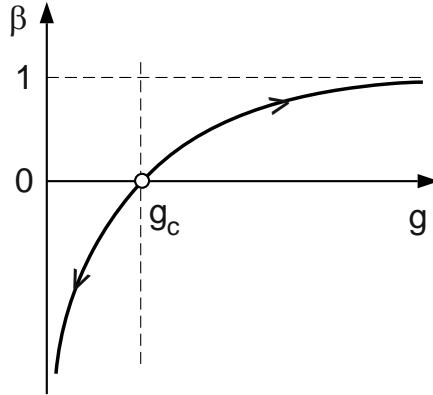


Fig. 9.9. Universal function $\beta(g)$ for the scaling behavior of the conductance $g(L)$ in a three-dimensional system. For $\beta > 0$ the conductance increases while for $\beta < 0$ it decreases with increasing system size L

For $\beta(g) > 0$, the conductance increases with increasing sample size, which corresponds to metallic behavior, while for $\beta(g) < 0$ it goes to zero for $L \rightarrow \infty$, typical for the insulator. The critical value g_c with $\beta(g_c) = 0$ marks the metal–insulator transition. This one-parameter scaling theory has been successful in describing the critical behavior of the conductivity σ_{dc} when approaching the transition from the metallic side ($E > \epsilon_c$) and of the localization length λ , when approaching it from the side of the insulator ($E < \epsilon_c$). In accordance with the properties of a second order phase transition [277], these quantities follow power laws:

$$\begin{aligned}\sigma_{dc} &\sim (E - \epsilon_c)^s, & E > \epsilon_c \\ \lambda &\sim (\epsilon_c - E)^{-\nu}, & E < \epsilon_c.\end{aligned}\tag{9.99}$$

From scaling relations, the critical exponents s and ν are found to be equal.

A particular aspect of this theory, which more recently has attracted renewed interest, is its dependence on the dimension d of the system [280]. As was argued by Thouless [281], it is the ratio of the level broadening due to disorder $\Gamma(L)$ and the level separation $\Delta E(L)$ due to confinement in a system of size L which decides about the character of the quantum states at the Fermi energy as being localized or extended. The former can be expressed as $\Gamma(L) = h/t_D(L)$, where $t_D(L)$ is the time for the electron to pass through the sample by diffusive motion. This time is determined by the diffusion constant D according to $t_D(L) = L^2/D$, thus $\Gamma(L) = hD/L^2$. For a particle in a box of the size L , the level separation at E_F is $\Delta E(L) = (n(E_F)L^d)^{-1}$ with the particle density $n(E_F)$ and the system dimension d . Using the Einstein relation $\sigma = e^2 D n(E_F)$, the ratio $\Gamma(L)/\Delta E(L)$ can be expressed as

$$\frac{\Gamma(L)}{\Delta E(L)} = \frac{h}{e^2} \sigma L^{d-2}\tag{9.100}$$

and we identify the dimensionless conductance $g(L) = \sigma L^{d-2}$, where the conductivity σ characterizes the material property and does not depend on L . Using this relation, the scaling argument (9.96) can be discussed with respect to its dependence on the system dimension d (see Problem 9.5). As it turns out, the universal function $\beta(g)$ passes through zero only for a three-dimensional system. For a two-dimensional system, it approaches zero asymptotically for large g and is always negative for $d = 1$. This means that a disorder-driven metal–insulator transition should be possible only for $d > 2$. Detailed investigations of two-dimensional electron systems seem to disprove this conclusion [278]. The critical discussion in the light of these data leads to the result, that possibly disorder is not the only mechanism but that electron–electron interaction may contribute, which is not included in the scaling theory.

Problems

- 9.1 Verify the eigenvalue equation (9.27) for the additional poles of the full Green function $G(E)$ (9.20) by making use of the block-diagonal form of the short-range defect matrix.
- 9.2 To demonstrate self-averaging, consider the classical resistance $R = \sum_{i=1}^N r_i$ of N resistances r_i , $i = 1 \dots N$ in a row. Make sure that the average $\langle r \rangle$ exists and that $\langle R \rangle = N \langle r \rangle$. Calculate the relative variance of R and show that it tends to zero with increasing N or system size!
- 9.3 Calculate the current–current response $\chi(0, \omega)$ of (9.83) with the current operator \hat{j}^p of (9.86) to obtain the conductivity $\sigma(0, \omega)$ (9.88).
- 9.4 Show that the double sum expression under the integral of σ_{dc} (9.89) can be cast into the form $\text{Tr}(\hat{v}\text{Im}G(E^+)\hat{v}\text{Im}G(E^+))$.
- 9.5 Discuss the asymptotics of $\beta(g)$ for $g \rightarrow \infty$ (using σ independent of L) and for $g \rightarrow 0$ (assuming $g(L) \sim \exp(-L/\lambda)$) in dependence on the system dimension d . Show that $\beta(g) < 0$ for all g and $d \leq 2$ while it changes sign for $d > 2$.

Light–Matter Interaction

The investigation of condensed matter systems using light as a probe is a versatile and powerful concept, which provides various kinds of information not only about the structure but also of the electronic and lattice excitations and their dynamics. Besides linear optical processes, like absorption and emission (including photoemission), light-scattering, two- (or three-)photon absorption, photo-luminescence and high-excitation spectroscopy also belong to the methods to gain information about the single-particle and collective excitations of a solid. In semiconductor samples with a proper design, coherent light emission is possible and used in solid-state lasers. These methods, which allow studies in the frequency or time domain, are all based on the interaction of light with matter. In Sect. 3.5 we have already treated the optical excitation of lattice vibrations as an example. In this chapter, we shall present a systematic theoretical description of light–matter interaction, which can be found in one or the other representation in standard textbooks[7, 14, 89, 95, 282, 283].

10.1 Preliminaries

Let us start with the microscopic *Maxwell equations*¹

$$\begin{aligned}\nabla \cdot \mathbf{E} &= \frac{\rho}{\varepsilon_0}, \quad \nabla \times \mathbf{E} = -\frac{\partial \mathbf{B}}{\partial t} \\ \nabla \cdot \mathbf{B} &= 0, \quad \nabla \times \mathbf{B} = \mu_0 \mathbf{j} + \frac{1}{c^2} \frac{\partial \mathbf{E}}{\partial t}.\end{aligned}\tag{10.1}$$

Here, $\mathbf{E}(\mathbf{r}, t)$ and $\mathbf{B}(\mathbf{r}, t)$ are the space and time dependent electric field and magnetic induction, respectively. The latter can be replaced with $\mathbf{B} = \mu_0 \mathbf{H}$ by the magnetic field $\mathbf{H}(\mathbf{r}, t)$. ε_0 and μ_0 are the vacuum constants and $c = 1/\sqrt{\varepsilon_0 \mu_0}$ is the vacuum velocity of light. In this microscopic formulation, $\rho(\mathbf{r}, t)$ and $\mathbf{j}(\mathbf{r}, t)$ are the charge and current densities, respectively, of

¹ James Clark Maxwell 1831–1879.

all charged particles in the system (nuclei and electrons). We could adopt here the reasonable concept of the previous chapters, according to which we understand the solid as composed of ions and valence electrons. In this case $\rho(\mathbf{r}, t)$ and $\mathbf{j}(\mathbf{r}, t)$ would be connected with the latter, while the electrons in closed shells would belong to the ions, which essentially do not contribute to the material properties of the solid. We come back to this point later in this Chapter.

For what follows, instead of the fields $\mathbf{E}(\mathbf{r}, t)$ and $\mathbf{B}(\mathbf{r}, t)$, it is convenient to introduce the potentials $\mathbf{A}(\mathbf{r}, t)$ and $\phi(\mathbf{r}, t)$, which are related to the fields by

$$\mathbf{B} = \nabla \times \mathbf{A}, \quad \mathbf{E} = -\nabla\phi - \frac{\partial \mathbf{A}}{\partial t}. \quad (10.2)$$

Replacing \mathbf{E} and \mathbf{B} in Maxwell's equations by the potentials \mathbf{A} and ϕ , we may write (using $\nabla \times \nabla \times \mathbf{A} = \nabla(\nabla \cdot \mathbf{A}) - \Delta \mathbf{A}$) the inhomogeneous equations in the form

$$\Delta \mathbf{A} - \frac{1}{c^2} \frac{\partial^2 \mathbf{A}}{\partial t^2} - \nabla \left(\nabla \cdot \mathbf{A} + \frac{1}{c^2} \frac{\partial \phi}{\partial t} \right) = -\mu_0 \mathbf{j} \quad (10.3)$$

and

$$\Delta \phi + \frac{\partial}{\partial t} (\nabla \cdot \mathbf{A}) = -\frac{\rho}{\varepsilon_0}. \quad (10.4)$$

The potentials are free to a gauge transformation with the scalar gauge field $\chi(\mathbf{r}, t)$

$$\mathbf{A} \rightarrow \mathbf{A} + \nabla \chi, \quad \phi \rightarrow \phi - \frac{\partial \chi}{\partial t}, \quad (10.5)$$

which leaves (10.2), i.e., the fields \mathbf{E} and \mathbf{B} , invariant.

Among the commonly used gauges, the *transverse* or *Coulomb gauge*, $\nabla \cdot \mathbf{A} = 0$, is the appropriate one for the interaction of light with matter in the form of solids. With this choice, the third term on the *lhs* of (10.3) vanishes while (10.4) becomes Poisson's equation. Thus, we obtain the potential form of Maxwell's equations in the form of an inhomogeneous wave equation for the vector potential

$$\Delta \mathbf{A} - \frac{1}{c^2} \frac{\partial^2 \mathbf{A}}{\partial t^2} = -\mu_0 \mathbf{j}. \quad (10.6)$$

The inhomogeneity is connected with the nuclei and electrons (or ions and valence electrons) and vanishes outside the solid, where (10.6) describes the free propagation of electro-magnetic waves in vacuum.

Consider now the solid interacting with the electro-magnetic field of the light. In the most general case, it is described by the Schrodinger equation with the Hamiltonian of the solid (2.1), including the electro-magnetic field. After having dealt already with the excitation of optical phonons, which are connected with the moving ions (see Chap. 3.), we would like to consider here only the electrons as movable charged particles in a rigid periodic arrangement

of nuclei or ions. Thus, we restrict in this chapter to the interaction of light with the electrons of the solid and start accordingly with the Hamiltonian (5.2) for the electrons. To include the electro-magnetic field, we have to take into account its energy and to fulfill the requirement, that the time-dependent Schroedinger equation

$$\mathcal{H}_N \Psi_N = i\hbar \frac{\partial \Psi_N}{\partial t} \quad (10.7)$$

has to be invariant under the gauge transformation (10.5), together with a simultaneous gauge transformation of the time-dependent N -electron wave function $\Psi_N(\mathbf{r}_1 \dots \mathbf{r}_N, t)$

$$\Psi(\mathbf{r}_1 \dots \mathbf{r}_N, t) \rightarrow \exp\left(-i\frac{e}{\hbar}\{\chi(\mathbf{r}_1, t) + \dots + \chi(\mathbf{r}_N, t)\}\right) \Psi(\mathbf{r}_1 \dots \mathbf{r}_N, t). \quad (10.8)$$

This is achieved by the replacement

$$\mathbf{p}_l \rightarrow \mathbf{p}_l + e\mathbf{A}(\mathbf{r}_l, t). \quad (10.9)$$

For the rest of this chapter the following Hamiltonian will be the starting point:

$$\begin{aligned} \mathcal{H}_N = & \sum_{l=1}^N \frac{1}{2m} (\mathbf{p}_l + e\mathbf{A}(\mathbf{r}_l))^2 + \frac{1}{2} \sum_{\substack{k,l=1 \\ k \neq l}}^N \frac{e^2}{4\pi\epsilon_0 |\mathbf{r}_k - \mathbf{r}_l|} + \sum_{n,l} v(\mathbf{r}_l - \mathbf{R}_n^0) \\ & + \frac{1}{2} \sum_{mn} V(\mathbf{R}_n^0 - \mathbf{R}_m^0) + \frac{\epsilon_0}{2} \int d^3\mathbf{r} (\mathbf{E}^2 + c^2 \mathbf{B}^2). \end{aligned} \quad (10.10)$$

In the last term, describing the energy of the radiation field, \mathbf{E} and \mathbf{B} can be replaced with (10.2) by the vector potential to yield

$$\mathcal{H}_{\text{rad}} = \frac{\epsilon_0}{2} \int d^3\mathbf{r} \left\{ \left(\frac{\partial}{\partial t} \mathbf{A}(\mathbf{r}, t) \right)^2 + c^2 (\nabla \times \mathbf{A}(\mathbf{r}, t))^2 \right\}. \quad (10.11)$$

Having in mind linear response theory (Sect. 2.4), we may separate \mathcal{H}_N into a Hamiltonian for the uncoupled solid and electro-magnetic field, $\mathcal{H}_0 + \mathcal{H}_{\text{rad}}$, and an interaction term $\mathcal{H}_{\text{el-rad}}$ for the light-matter coupling

$$\mathcal{H}_N = \mathcal{H}_0 + \mathcal{H}_{\text{el-rad}} + \mathcal{H}_{\text{rad}}, \quad (10.12)$$

where \mathcal{H}_0 describes the unperturbed electron system of the solid, (5.2), and (by making use of the transverse gauge)

$$\mathcal{H}_{\text{el-rad}} = \sum_{l=1}^N \left(\frac{e}{m} \mathbf{A}(\mathbf{r}_l, t) \cdot \mathbf{p}_l + \frac{e^2}{2m} (\mathbf{A}(\mathbf{r}_l, t))^2 \right) \quad (10.13)$$

is the time-dependent perturbation by the radiation field, which can be identified as the external potential of (2.37). Using $\mathbf{j} = -e \sum_l \mathbf{p}_l/m$, the first term can also be written as $-\mathbf{j} \cdot \mathbf{A}$ (see Sects. 2.4 and 9.4).

10.2 Single-Particle Approximation

In Chap. 5 we have invoked density-functional theory (DFT) to reduce the many-body problem with \mathcal{H}_0 to a single-particle problem, by accounting for the electron–electron interaction in an effective single-particle potential $V_{\text{eff}}(\mathbf{r})$ (see (5.30)), which is the same for all electrons. This can now be used to write the many-body Hamiltonian \mathcal{H}_N as a sum of single-particle terms. Leaving aside the energy of the radiation field as a constant, the single-particle Hamiltonian of an electron interacting with the radiation field takes the form

$$H = -\frac{\hbar^2}{2m}\Delta + V_{\text{eff}}(\mathbf{r}) + \frac{e}{m}\mathbf{A} \cdot \mathbf{p} + \frac{e^2}{2m}\mathbf{A}^2. \quad (10.14)$$

The eigenstates of the first term are the Bloch states of Chap. 5. The last two terms represent a periodic time-dependent interaction of Bloch electrons with the radiation field. For sufficiently weak amplitudes of the vector potential they can be treated as perturbations of first and second order. Sometimes the $A\mathbf{p}$ -term is also expressed in the form $-e\mathbf{E} \cdot \mathbf{r}$, where $-e\mathbf{r}$ is the dipole operator (Problem 10.1).

Let us first treat the term linear in \mathbf{A} . For monochromatic light, its space and time dependence is given by

$$\mathbf{A}(\mathbf{r}, t) = A_0 \mathbf{e} e^{i(\boldsymbol{\kappa} \cdot \mathbf{r} - \omega t)} + c.c., \quad (10.15)$$

with a scalar amplitude A_0 and the unit vector \mathbf{e} for transverse polarization, $\mathbf{e} \perp \boldsymbol{\kappa}$. The frequency follows the linear dispersion relation $\omega = c|\boldsymbol{\kappa}|$ of light in vacuum.

Because of the periodic time-dependence of the perturbation, Fermi's Golden Rule applies and we can immediately write the rate for the transition probability between Bloch states

$$W_{n\mathbf{k}, n'\mathbf{k}'} = \frac{2\pi}{\hbar} |\langle n\mathbf{k} | H' | n'\mathbf{k}' \rangle|^2 \delta(E_n(\mathbf{k}) - E_{n'}(\mathbf{k}') - \hbar\omega), \quad (10.16)$$

where $H' = eA_0 \exp(i\boldsymbol{\kappa} \cdot \mathbf{r}) \mathbf{e} \cdot \mathbf{p}/m$ is the perturbation without the time-dependent exponential. Together with the time-dependent phase factors of the stationary Bloch functions, it results in the δ -function, which expresses the energy conservation: the energy quantum $\hbar\omega$ of the radiation field equals the energy difference between the Bloch states. Depending on the sign of this difference, the transition between the Bloch states can be an absorption or emission process.

The transition matrix element can be transformed from an integral over the crystal volume V_c

$$\langle n\mathbf{k}|H'|n'\mathbf{k}'\rangle = \int_{V_c} \psi_{n\mathbf{k}}^*(\mathbf{r}) \left(\frac{e}{m} A_0 e^{i\boldsymbol{\kappa}\cdot\mathbf{r}} \mathbf{e} \cdot \mathbf{p} \right) \psi_{n'\mathbf{k}'}(\mathbf{r}) d^3\mathbf{r} \quad (10.17)$$

to an integral over a Wigner-Seitz cell by shifting \mathbf{r} by lattice vectors \mathbf{R}_n and extracting the corresponding phase factors from the Bloch functions

$$\langle n\mathbf{k}|H'|n'\mathbf{k}'\rangle = \int_{WSC} \dots \sum_{\mathbf{n}} e^{i(\boldsymbol{\kappa}+\mathbf{k}'-\mathbf{k})\cdot\mathbf{R}_n} d^3\mathbf{r}. \quad (10.18)$$

Here the dots stand for the integrand of the previous integral. The lattice sum results in a Kronecker $\delta_{\mathbf{k},\mathbf{k}'+\boldsymbol{\kappa}}$, which represents the momentum conservation of the excitation process. The diameter of the Wigner-Seitz cell is about the lattice constant of a few \AA , which is much smaller than the wavelength of the light corresponding to the typical excitation energy $\hbar\omega$ of a few eV . Therefore, the exponential with $\boldsymbol{\kappa}$ in the integral is almost constant over the cell and we may safely replace it by 1. This is the *dipole approximation*. Finally, the transition matrix element can be written (see also Problem 10.2)

$$\begin{aligned} \langle n\mathbf{k}|H'|n'\mathbf{k}'\rangle &= \int_{WSC} u_{n\mathbf{k}}^*(\mathbf{r}) \left(\frac{e}{m} A_0 \mathbf{e} \cdot \mathbf{p} \right) u_{n'\mathbf{k}'}(\mathbf{r}) d^3\mathbf{r} \delta_{\mathbf{k},\mathbf{k}'} \\ &= \frac{e}{m} A_0 \langle n\mathbf{k}|\mathbf{e} \cdot \mathbf{p}|n'\mathbf{k}'\rangle \delta_{\mathbf{k},\mathbf{k}'}. \end{aligned} \quad (10.19)$$

Thus, one obtains a finite transition probability

$$W_{n\mathbf{k},n'\mathbf{k}'}(\omega) = \frac{2\pi}{\hbar} \frac{e^2 A_0^2}{m^2} |\langle n\mathbf{k}|\mathbf{e} \cdot \mathbf{p}|n'\mathbf{k}'\rangle|^2 \delta(E_n(\mathbf{k}) - E_{n'}(\mathbf{k}) - \hbar\omega) \quad (10.20)$$

only for *direct transitions* (or vertical transitions), in which the wave vector of the Bloch state is not changed.

The *absorption* of light passing through a solid of thickness d determines the damping of the light intensity according to

$$I(d) = I_0 e^{-\alpha d}. \quad (10.21)$$

On the other side, the absorption coefficient $\alpha(\omega)$ is connected with the real (n_1) and imaginary (n_2) parts of the complex index of refraction according to

$$\alpha = \frac{2n_1 n_2}{c} \omega, \quad (10.22)$$

where $2n_1 n_2 = \varepsilon_2$ is the imaginary part of the complex dielectric function $\varepsilon(\omega)$. Microscopically, $\alpha(\omega)$ is determined here by the power loss or the rate by which energy of the radiation field is converted into excitations between

Bloch states[14, 89]. Thus,

$$\alpha(\omega) = \frac{2\hbar}{\varepsilon_0 c \omega A_0^2} W(\omega), \quad \text{where } W(\omega) = \sum_{nn'\mathbf{k}} W_{n\mathbf{k},n'\mathbf{k}}(\omega), \quad (10.23)$$

and the imaginary part of the dielectric function is given by

$$\varepsilon_2(\omega) = \frac{4\pi e^2}{\varepsilon_0 m^2 \omega^2} \sum_{nn'\mathbf{k}} |\langle n\mathbf{k} | \mathbf{e} \cdot \mathbf{p} | n'\mathbf{k} \rangle|^2 \delta(E_n(\mathbf{k}) - E_{n'}(\mathbf{k}) - \hbar\omega). \quad (10.24)$$

The real part of $\varepsilon_1(\omega)$ can be obtained using the Kramers–Kronig relation (2.80) formulated for susceptibilities $\chi(\omega)$. Considering the relation $\varepsilon(\omega) = 1 + \chi(\omega)/\varepsilon_0$, we have to use

$$\varepsilon_1(\omega) = 1 + \frac{2}{\pi} \int_0^\infty \frac{\omega' \varepsilon_2(\omega')}{\omega'^2 - \omega^2} d\omega', \quad (10.25)$$

leading to

$$\varepsilon_1(\omega) = 1 + \frac{4e^2}{\varepsilon_0 m} \sum_{nn'\mathbf{k}} \frac{f_{nn'}(\mathbf{k})}{\omega_{nn'}(\mathbf{k})^2 - \omega^2} \quad (10.26)$$

with the *oscillator strength*

$$f_{nn'}(\mathbf{k}) = \frac{2 |\langle n\mathbf{k} | \mathbf{e} \cdot \mathbf{p} | n'\mathbf{k} \rangle|^2}{m \hbar \omega_{nn'}(\mathbf{k})} \quad (10.27)$$

for the transition between Bloch states with the energy difference $\hbar\omega_{nn'}(\mathbf{k}) = E_n(\mathbf{k}) - E_{n'}(\mathbf{k})$.

In cubic solids, the dipole matrix elements do not depend on the polarization direction \mathbf{e} and usually their dependence on the wave vector is not very strong. Thus, we can write

$$\langle n\mathbf{k} | \mathbf{e} \cdot \mathbf{p} | n'\mathbf{k} \rangle \simeq P_{nn'} \quad (10.28)$$

with $P_{nn'}$ independent of \mathbf{k} and $\varepsilon_2(\omega)$ becomes

$$\varepsilon_2(\omega) = \frac{4\pi}{\varepsilon_0} \left(\frac{e}{m\omega} \right)^2 \sum_{nn'} |P_{nn'}|^2 D_{nn'}(\hbar\omega), \quad (10.29)$$

with the *combined density of states*

$$D_{nn'}(\hbar\omega) = \sum_{\mathbf{k}} \delta(E_n(\mathbf{k}) - E_{n'}(\mathbf{k}) - \hbar\omega) \quad (10.30)$$

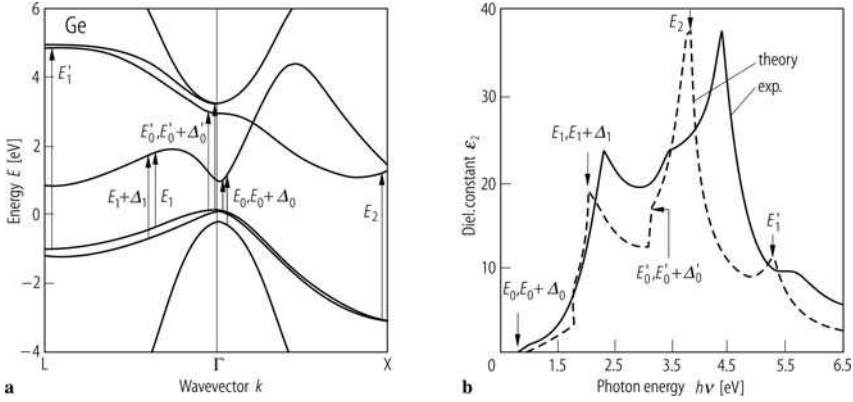


Fig. 10.1. (a) Band structure of Ge with vertical transitions at critical points and (b) comparison of measured and calculated $\varepsilon_2(\omega)$, showing van Hove singularities at these critical points (from Landolt-Börnstein [1])

of the pair of bands n, n' . As in Sect. 3.3, the \mathbf{k} -sum over the Brillouin zone can be converted into an integral

$$D_{nn'}(\hbar\omega) = \frac{V_c}{(2\pi)^3} \int_{BZ} \delta(E_n(\mathbf{k}) - E_{n'}(\mathbf{k}) - \hbar\omega) d^3\mathbf{k}, \quad (10.31)$$

which, due to the δ -function, reduces to an integral over the surface $S_{\mathbf{k}}$, for which the energy difference of the Bloch states equals $\hbar\omega$

$$D_{nn'}(\hbar\omega) = \frac{V_c}{(2\pi)^3} \int_{S_{\mathbf{k}}} \frac{dS_{\mathbf{k}}}{|\nabla_{\mathbf{k}}(E_n(\mathbf{k}) - E_{n'}(\mathbf{k}))|}. \quad (10.32)$$

The points, at which $|\nabla_{\mathbf{k}}(E_n(\mathbf{k}) - E_{n'}(\mathbf{k}))|$ vanishes (*critical points*), give rise to *van Hove singularities* in the combined density of states, by which they can be identified.

As an example, we show in Fig. 10.1 the band structure of Ge in the fundamental band gap region with marked direct transitions at critical points and the measured and calculated imaginary part of the dielectric function, $\varepsilon_2(\omega)$. In spite of discrepancies in the critical point energies, there is a clear correspondence between the experimental and theoretical curves. It turns out, that the optical spectra of semiconductors with tetrahedral coordination resemble each other [89]. Their band structures have the same topology determined by the common crystal structure but differ with respect to their critical point energies E_0, E'_0, \dots . Investigations of the optical spectra have paved the road to the quantitative understanding of semiconductor band structures.

Light-matter interaction stood at the beginning of quantum mechanics with Einstein's explanation of the photo-electric effect, which earned him the Nobel prize in 1922. It is based on the assumption of a quantized radiation field. *Photoemission* can take place if the photon energy suffices to excite an

electron beyond the energy barrier at the surface of the solid so that it can be detected outside the solid as free particle. Einstein found (in accordance with experimental data for metals) the linear dependence of the maximum kinetic energy of the emitted electrons on the photon energy, which is ruled by the ratio \hbar/e . Later, this effect has been exploited by Siegbahn² to develop the concept of *photo-electron spectroscopy* (PES). It is based on analyzing not only the maximum energy but also the energy spectrum of the photo-emitted electrons.

The minimum energy required to free an electron from a metal, is the difference between the vacuum level and the Fermi energy, known as the *work function*. In a semiconductor, with the Fermi energy somewhere in the gap, this energy would not be sufficient for photoemission, because the highest occupied state, in the intrinsic case, is the top of the valence band. Instead it is the *ionization energy* that defines the threshold for photoemission. The photoemissive yield is roughly proportional to the density of the initial states. PES is applied at different photon energies: ultraviolet light (UPS: ultraviolet PES) for the investigation of valence electron structures and X-rays (XPS) for the study of the more tightly bound core electrons[65, 287]. Note, that for the latter case one has to treat the core electrons in the same way as the valence electrons.

The photo-emitted electrons can be also analyzed with respect to their momentum parallel to the surface, which does not change when the electron leaves the solid. This is done in *angular resolved photoemission* (ARPES) experiments, which give information about the energy bands $E_n(\mathbf{k})$, as shown in Fig. 10.2 for Cu as an example. The experimental data points map out all details of the energy bands, which we already know from Chap. 5.

Further variants of photo-electron spectroscopy are spin-polarized UPS (SPUPS) and the inverse photoemission, in which an electron of known energy is injected and the emitted photon is detected. The former method allows to study the bands of minority and majority spins in ferromagnets (see Fig. 6.1), and the latter yields information about the unoccupied states above the Fermi energy.

10.3 Excitons

The basic assumption of the single-particle approximation in Sect. 10.2 is the same effective single-particle potential $V_{\text{eff}}(\mathbf{r})$ for electrons in all bands. This assumption is correct for the ground state of the solid, which, for a semiconductor, is characterized by filled valence and empty conduction bands. But for the excited state an electron in the valence band is missing, because it is in the conduction band. Intuitively, this is the two-particle problem of an

² Kai Manne Börje Siegbahn 1918–2007, Nobel prize in Physics 1981, together with N. Bloembergen and A.L. Schawlow.

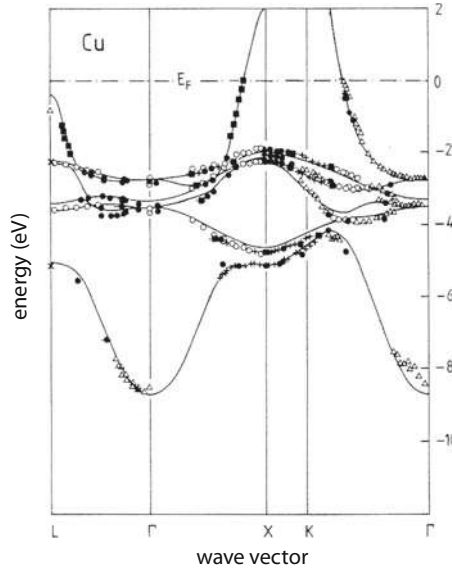


Fig. 10.2. Calculated energy bands of Cu and data from angular resolved photoemission, after [31]

electron-hole pair, if we consider the remaining $N - 1$ electrons in the valence band as the *hole* and the missing contribution to the effective potential as the attractive Coulomb interaction between the electron in the conduction band and the hole in the valence band. In effective-mass approximation, the Hamiltonian for the electron-hole pair can be written

$$H_{e-h} = E_g + \frac{\mathbf{p}_e}{2m_e} + \frac{\mathbf{p}_h}{2m_h} - \frac{e^2}{\kappa|\mathbf{r}_e - \mathbf{r}_h|}. \quad (10.33)$$

Note, that the kinetic energy of the hole increases in the downward bent parabola for the valence band. If we only had the two bands (one valence and one conduction band) in vacuum, then $\kappa = 4\pi\epsilon_0$. However, the correct description has to include all the other valence and conduction bands and the possible excitations between these bands, i.e., the two-band model for electron and hole is embedded in a dielectric with material constant ϵ and, therefore, $\kappa = 4\pi\epsilon_0\epsilon$, i.e., the Coulomb interaction is screened. We would like to mention here, that the electron-hole interaction is just the difference of the Hartree potentials in the excited and ground states, but there should also be exchange and correlation contributions, which we leave aside for the moment.

In relative and center-of-mass coordinates, using for $\mathbf{p}_i = \hbar\mathbf{k}_i$, $i = e, h$,

$$\mathbf{k}_e = \mathbf{k} + \frac{m_e}{M}\mathbf{Q}, \quad \mathbf{k}_h = \mathbf{k} - \frac{m_h}{M}\mathbf{Q}, \quad (10.34)$$

with the total mass $M = m_e + m_h$, we can write the Hamiltonian for the electron–hole pair as

$$H_{e-h} = E_g - \frac{\hbar^2}{2\mu}\Delta + \frac{e^2}{\kappa r} + \frac{\hbar^2 Q^2}{2M}, \quad (10.35)$$

with $r = |\mathbf{r}_e - \mathbf{r}_h|$ and the reduced mass $\mu = (1/m_e + 1/m_h)^{-1}$. Except the last term describing the free center-of-mass motion of the electron–hole pair, this is the hydrogen model characterized by the Rydberg energy $R_{\text{exc}} = R_H \mu / \epsilon^2$ and the Bohr radius $a_{\text{exc}} = a_H \epsilon / \mu$, where R_H and a_H are the corresponding constants of the hydrogen atom. The eigenvalue problem with H_{e-h} for $\mathbf{Q} = 0$

$$H_{e-h}\phi_\nu(\mathbf{r}) = \left(E_g - \frac{\hbar^2}{2\mu}\Delta + \frac{e^2}{\kappa r} \right) \phi_\nu(\mathbf{r}) = E_\nu \phi_\nu(\mathbf{r}) \quad (10.36)$$

gives a series of bound states ($\nu = n = 1, 2, 3, \dots$), the excitons, at $E_n = E_g - R_{\text{exc}}/n^2$. For typical semiconductor data $\epsilon = 10$ and $\mu = 0.1$, the binding energies of the excitons are much smaller than the typical band gap E_g , and a_{exc} extends over many unit cells. Thus the continuum approximation, assuming effective masses and a homogeneous dielectric, is justified. This case of weakly bound excitons is known as the Wannier–Mott exciton, which is similar to the shallow impurities (see Sect. 9.1). Besides these bound states, for energies larger than E_g , there is a continuum of electron–hole pair or band-to-band excitations. For a simple two-band model, the single-particle and exciton pictures are presented in Fig. 10.3. It shows in the left part a valence and a conduction band with a hole at \mathbf{k}_h and an electron at \mathbf{k}_e , respectively, while the exciton picture in the right hand part contains the bound states with their center-of-mass parabolas below the electron–hole continuum and the ground state at $\mathbf{Q} = 0$.

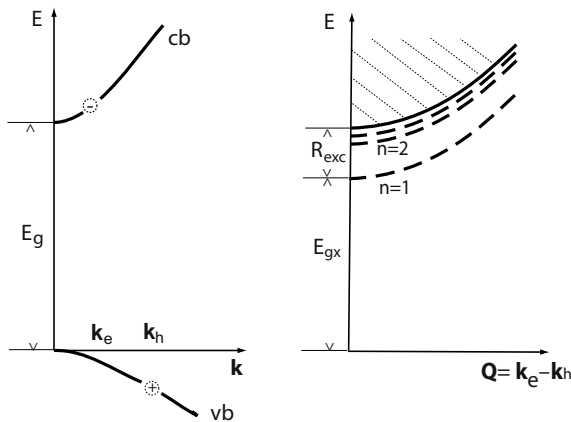


Fig. 10.3. Two-band model with electron–hole pair excitation (*left*) and exciton spectrum with bound states and electron–hole continuum (*right*)

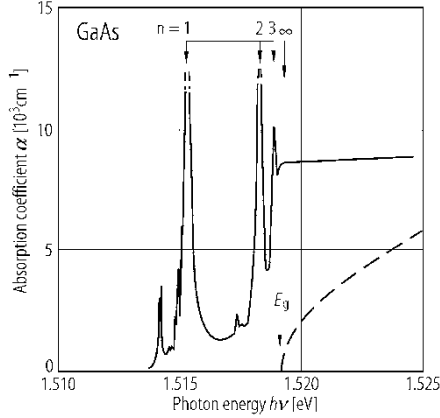


Fig. 10.4. Measured absorption spectrum of GaAs close to the fundamental edge, showing excitonic structure. The dashed curve is the calculated absorption in single-particle approximation (from Landolt-Börnstein [1])

As a representative example, the optical absorption for GaAs close to the fundamental gap is shown in Fig. 10.4. The bound states dominate the spectrum for $\hbar\omega < E_g$, with discrete narrow lines for $n = 1, 2, 3, \dots$ (The small satellites are due to impurities.) The calculated absorption in single-particle approximation drawn for energies $\hbar\omega > E_g$ deviates from the experimental data, thus indicating that the electron–hole interaction also modifies the continuum part of the spectrum.

In order to understand these exciton features in detail, we consider the many-body picture [289]. The ground state of the semiconductor (or insulator) is characterized by filled valence and empty conduction bands. Let us denote it by $|\Psi_0\rangle$ (the same symbol has been used for the filled Fermi sphere in Chap. 4). The simplest excited state is an electron–hole pair

$$|\Psi_{v\mathbf{k}_h, c\mathbf{k}_e}\rangle = c_{c\mathbf{k}_e}^\dagger c_{v\mathbf{k}_h} |\Psi_0\rangle, \quad (10.37)$$

which is obtained by applying appropriate fermion operators to $|\Psi_0\rangle$. We may combine such pairs with same total momentum $\hbar\mathbf{Q}$, $\mathbf{Q} = \mathbf{k}_e - \mathbf{k}_h$, which is a good quantum number for excitations, to form an exciton state

$$|\Psi_{\nu\mathbf{Q}}\rangle = \sum_{\substack{v\mathbf{k}_h, c\mathbf{k}_e \\ \mathbf{k}_e - \mathbf{k}_h = \mathbf{Q}}} \phi_{\nu\mathbf{Q}}(\mathbf{k}) |\Psi_{v\mathbf{k}_h, c\mathbf{k}_e}\rangle, \quad (10.38)$$

where $\phi_{\nu\mathbf{Q}}(\mathbf{k})$ is the Fourier transform of the exciton envelope, which describes the relative motion of the electron–hole pair as a solution for (10.36). In this picture, represented in the *rhs* of Fig. 10.3, optical transitions take place from the ground state (with zero total momentum) to the exciton state with the rate of transition probability

$$W_{0 \rightarrow \nu \mathbf{Q}} = \frac{2\pi}{\hbar} \left(\frac{eA_0}{m} \right)^2 |\langle \Psi_{\nu \mathbf{Q}} | \sum_l e^{i\mathbf{\kappa} \cdot \mathbf{r}_l} \mathbf{e} \cdot \mathbf{p}_l | \Psi_0 \rangle|^2 \delta(E_{\nu \mathbf{Q}} - E_0 - \hbar\omega). \quad (10.39)$$

The Ap -coupling is a sum over single-particle terms and its matrix element

$$\langle \Psi_{\nu \mathbf{Q}} | \sum_l e^{i\mathbf{\kappa} \cdot \mathbf{r}_l} \mathbf{e} \cdot \mathbf{p}_l | \Psi_0 \rangle = \phi_{\nu \mathbf{Q}}(\mathbf{k}) \langle c\mathbf{k}_e | e^{i\mathbf{\kappa} \cdot \mathbf{r}} \mathbf{e} \cdot \mathbf{p} | v\mathbf{k}_h \rangle \quad (10.40)$$

can be expressed as matrix element between the Bloch states of the electron–hole pair. In dipole approximation, replacing the exponential by 1, transitions are possible only to the exciton states with $\mathbf{Q} = 0$ (direct or vertical transitions). Let us assume, as in Sect. 10.2, that the momentum matrix elements are almost independent of $\mathbf{k} = \mathbf{k}_e = \mathbf{k}_h$, to arrive at

$$W_{0 \rightarrow \nu \mathbf{Q}} = \frac{2\pi}{\hbar} \left(\frac{eA_0}{m} \right)^2 |\phi_{\nu}(0) \mathbf{e} \cdot \mathbf{P}_{cv}|^2 \delta(E_{\nu} - E_0 - \hbar\omega), \quad (10.41)$$

where we have dropped the index $\mathbf{Q} = 0$ and replaced $\sum_{\mathbf{k}} \phi_{\nu}(\mathbf{k}) = \phi_{\nu}(\mathbf{r}_e - \mathbf{r}_h = 0)$. By comparing with the corresponding result from Sect. 10.2 for uncorrelated interband excitations, we can immediately express the real part of the dielectric function in terms of exciton quantities:

$$\varepsilon_1(\omega) = 1 + \frac{4e^2}{\varepsilon_0 m} \sum_{\nu} \frac{f_{\nu 0}}{\omega_{0\nu}^2 - \omega^2} \quad (10.42)$$

with the exciton oscillator strength

$$f_{\nu 0} = \frac{2|\phi_{\nu}(0)|^2 |\langle c | \mathbf{e} \cdot \mathbf{p} | v \rangle|^2}{m(E_{\nu} - E_0)}. \quad (10.43)$$

This result already contains, what we need to understand the experimental spectrum of Fig. 10.4, without converting it into the expression for the absorption. The discrete bound states (for $\nu = n = 1, 2, \dots$) are seen as the sharp lines at energies $E_g - E_n$, with intensities scaling according to $|\phi_n(0)|^2 \sim 1/n^3$, if we adopt the wave functions of the hydrogen model (Problem 10.3). But also in the continuum of band-to-band transitions, the transition probability is modified by the factor $|\phi_{\nu}(0)|^2$, which is responsible for the enhancement of the absorption intensity at the fundamental edge. With the solution of Problem 10.3, it is possible to express the absorption coefficient for $\hbar\omega > E_g$ as

$$\alpha(\omega) = \alpha_0(\omega)C(\omega), \quad (10.44)$$

with the absorption coefficient $\alpha_0(\omega)$ of the uncorrelated electron–hole pair of (10.23) and the *Coulomb enhancement factor* or *Sommerfeld correction*

$$C(\omega) = \frac{2\pi\sqrt{x}}{1 - \exp(-2\pi\sqrt{x})}, \quad \text{with } x = \frac{R_{\text{exc}}}{\hbar\omega - E_g}. \quad (10.45)$$

A more rigorous treatment of the electron–hole correlation is possible by using the two-particle Green function G [64, 288], for which we may write

$$G = G_0 + G_0 \Gamma G_0. \quad (10.46)$$

Here, G_0 is the two-particle Green function of the uncorrelated electron–hole pair and the kernel Γ satisfies the Bethe–Salpeter equation (BSE)

$$\Gamma = I + I G_0 \Gamma, \quad (10.47)$$

with the irreducible electron–hole interaction to be specified later. After multiplication from the right by G_0 , the BSE can formally be solved to give

$$\Gamma G_0 = (1 - I G_0)^{-1} I G_0 \quad (10.48)$$

and to express G as

$$G = G_0 \frac{1}{1 - I G_0}. \quad (10.49)$$

Besides the poles of G_0 , the Green function G of the correlated electron–hole pair contains additional poles for $1 - I G_0 = 0$, which we may also write as $G_0^{-1} - I = 0$. For a free electron–hole pair in simple parabolic bands coupled by the Coulomb interaction, this expression can be written in plane wave representation as

$$\sum_{\mathbf{k}'_e, \mathbf{k}'_h} \langle \mathbf{k}_e \mathbf{k}_h | G_0^{-1} - I | \mathbf{k}'_e \mathbf{k}'_h \rangle \langle \mathbf{k}'_e \mathbf{k}'_h | \mathbf{r}_e \mathbf{r}_h \rangle = 0, \quad (10.50)$$

where $\phi_{\mathbf{k}'_e \mathbf{k}'_h}(\mathbf{r}_e, \mathbf{r}_h) = \langle \mathbf{k}'_e \mathbf{k}'_h | \mathbf{r}_e \mathbf{r}_h \rangle$ is the exciton wave function. This leads to

$$\begin{aligned} \langle \mathbf{k}_e \mathbf{k}_h | G_0^{-1} - I | \mathbf{k}'_e \mathbf{k}'_h \rangle &= \left(E_g + \frac{\hbar^2 k_e^2}{2m_e} + \frac{\hbar^2 k_h^2}{2m_h} - E \right) \delta_{\mathbf{k}_e \mathbf{k}'_e} \delta_{\mathbf{k}_h \mathbf{k}'_h} \\ &\quad - \frac{e^2}{\varepsilon_0 V |\mathbf{k}_e - \mathbf{k}'_e|^2} \delta_{\mathbf{k}_e - \mathbf{k}'_e, \mathbf{k}_h - \mathbf{k}'_h}. \end{aligned} \quad (10.51)$$

After introducing relative and center-of-mass coordinates (see (10.34)), taking the Fourier transform, and separating the center-of-mass motion we recover the exciton effective-mass Hamiltonian of (10.36) with the bare Coulomb interaction. We identify the additional poles of the Green function G as the bound states of the electron–hole pair, the excitons. If instead of the plain wave representation the Bloch representation is used, one obtains for the inverse Green function of the uncorrelated electron–hole pair the expression

$$\begin{aligned} \langle c \mathbf{k}_e v \mathbf{k}_h | G_0^{-1} | c' \mathbf{k}'_e v' \mathbf{k}'_h \rangle &= (E_c(\mathbf{k}_e) + E_v(\mathbf{k}_h) \\ &\quad - E) \delta_{cc'} \delta_{vv'} \delta_{\mathbf{k}_e, \mathbf{k}'_e} \delta_{\mathbf{k}_h, \mathbf{k}'_h}. \end{aligned} \quad (10.52)$$

It contains the full expressions of the energy bands but is diagonal in the band indices and in the electron and hole wave vectors.

Let us now turn to the irreducible electron-hole interaction I of the BSE [288]. It is composed of graphs like those represented in Fig. 10.5. The left one is the bare Coulomb interaction as in Fig. 4.10 but now for the electron-hole pair. It propagates in the Bloch states $c\mathbf{k}_e, v\mathbf{k}_h$ and is scattered into the pair $c'\mathbf{k}'_e, v'\mathbf{k}'_h$ by the Fourier component of the Coulomb interaction with wave vector $\mathbf{q} = \mathbf{k}'_e - \mathbf{k}_e = \mathbf{k}'_h - \mathbf{k}_h$. Note, that due to time-inversion the propagation direction of the hole is opposite to that of the electron. The bare Coulomb interaction is modified if intermediate excitation of electron-hole pairs is considered. This is depicted in Fig. 10.6 and means to replace the simple broken Coulomb line of the direct interaction graph by the double broken line which contains the polarization diagrams. It represents the screened Coulomb interaction (see Chap. 4), mentioned already in our intuitive considerations.

The exchange diagram on the right of Fig. 10.5 also contributes to the irreducible electron-hole interaction. It represents a scattering of the electron-hole pair by the Fourier component of the bare Coulomb potential, with wave vector $\mathbf{Q} = \mathbf{k}_e + \mathbf{k}_h = \mathbf{k}'_e + \mathbf{k}'_h$. However, due to the topology of the exchange diagram, a replacement of the bare Coulomb line by the screened one of Fig. 10.6 would lead to diagrams, which could be separated into replicas of the simple one by cutting with a horizontal line (if we forget the band indices for the moment). Such diagrams are called reducible and are excluded. This means that in the simple two-band exciton problem the exchange interaction is not screened [288]. As will be outlined in the following supplement, this argument does not apply if one considers the full band structure instead of the two-band model.

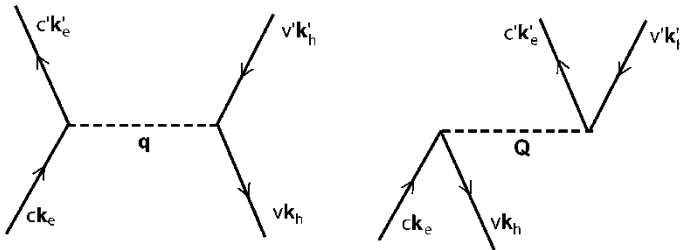


Fig. 10.5. Diagrams for Coulomb and exchange interaction of an electron-hole pair

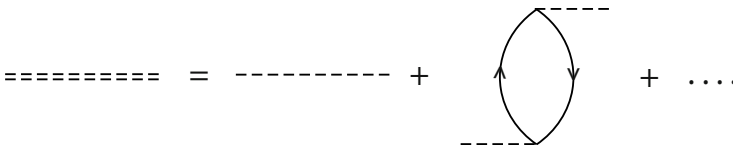


Fig. 10.6. Diagrams showing the screening of the electron-hole interaction

Supplement: Screened Coulomb and exchange interaction

Let us start with the screened Coulomb interaction

$$\begin{aligned} V_{\text{Coul}} &= -\langle c\mathbf{k}_e v\mathbf{k}_h | \frac{e^2}{\kappa|\mathbf{r}-\mathbf{r}'|} | c'\mathbf{k}'_e v'\mathbf{k}'_h \rangle \\ &= -\int d^3\mathbf{r} \int d^3\mathbf{r}' \psi_{c\mathbf{k}_e}^*(\mathbf{r}) \psi_{v\mathbf{k}_h}(\mathbf{r}') \frac{e^2}{\kappa|\mathbf{r}-\mathbf{r}'|} \psi_{c'\mathbf{k}'_e}(\mathbf{r}) \psi_{v'\mathbf{k}'_h}^*(\mathbf{r}'), \end{aligned} \quad (10.53)$$

where $\kappa = 4\pi\varepsilon_0\varepsilon$ and $\varepsilon = \varepsilon_\infty$ is the electronic part of the dielectric constant. Note, that the hole Bloch functions are complex-conjugate because of time-inversion. The products of the lattice periodic parts of the Bloch functions can be expanded in Fourier series with coefficients

$$C_{cc'}(\mathbf{k}_e, \mathbf{k}'_e, \mathbf{G}) = \frac{1}{V_{\text{cell}}} \int u_{c\mathbf{k}_e}^*(\mathbf{r}) u_{c'\mathbf{k}'_e}(\mathbf{r}) e^{i\mathbf{G}\cdot\mathbf{r}} d^3\mathbf{r} \quad (10.54)$$

$$V_{vv'}(\mathbf{k}_h, \mathbf{k}'_h, \mathbf{G}') = \frac{1}{V_{\text{cell}}} \int u_{v\mathbf{k}_h}(\mathbf{r}') u_{v'\mathbf{k}'_h}^*(\mathbf{r}') e^{-i\mathbf{G}'\cdot\mathbf{r}'} d^3\mathbf{r}' \quad (10.55)$$

to write the Coulomb interaction as

$$\begin{aligned} V_{\text{Coul}} &= -\sum_{\mathbf{G}, \mathbf{G}'} C_{cc'}(\mathbf{k}_e, \mathbf{k}'_e, \mathbf{G}) V_{vv'}(\mathbf{k}_h, \mathbf{k}'_h, \mathbf{G}') \\ &\quad \times \int d^3\mathbf{r} \int d^3\mathbf{r}' e^{-i(\mathbf{k}_e - \mathbf{k}'_e - \mathbf{G})\cdot\mathbf{r}} e^{i(\mathbf{k}_h - \mathbf{k}'_h - \mathbf{G}')\cdot\mathbf{r}'} \frac{e^2}{\kappa|\mathbf{r}-\mathbf{r}'|}. \end{aligned} \quad (10.56)$$

The double integration can be performed after replacing the Coulomb potential by its Fourier transform, giving

$$\int d^3\mathbf{r} \int d^3\mathbf{r}' \dots = \frac{e^2}{\varepsilon_0\varepsilon V_c |\mathbf{k}_e - \mathbf{k}'_e - \mathbf{G}|^2} \delta_{\mathbf{k}_e - \mathbf{k}'_e - \mathbf{G}, \mathbf{k}_h - \mathbf{k}'_h + \mathbf{G}'}. \quad (10.57)$$

Let us consider the case with $\mathbf{Q} = 0$, i.e., $\mathbf{k}_e = \mathbf{k}_h = \mathbf{k}$. Then, for weakly bound (or Wannier–Mott) excitons, one has $|\mathbf{k} - \mathbf{k}'| \ll 2\pi/a$ and the Fourier component of the Coulomb potential with $\mathbf{G} = 0$ dominates. The corresponding expansion coefficients $C_{cc'}(\mathbf{k}, \mathbf{k}', 0)$ and $V_{vv'}(\mathbf{k}, \mathbf{k}', 0)$ reduce to $\delta_{cc'}$ and $\delta_{vv'}$, respectively (see Sect. 9.1), and we arrive at the leading term of the screened Coulomb interaction

$$V_{\text{Coul}} = -\frac{e^2}{\varepsilon_0\varepsilon V_c |\mathbf{k} - \mathbf{k}'|^2} \delta_{cc'} \delta_{vv'}, \quad (10.58)$$

which is diagonal in the band indices. For a given band pair with $E_c(\mathbf{k})$ and $E_v(\mathbf{k})$ in isotropic parabolic approximation, this leads back to the exciton problem of (10.49), but now with the screened Coulomb interaction.

In order to treat the exchange interaction in the same way, we have to consider the spin part of the Bloch functions explicitly. According to the diagram rules, spin is conserved at each vertex. This has been tacitly taken into account when evaluating the Coulomb term, for which electron or hole lines meet at each vertex and summation over spin variables gives a factor unity. In the exchange diagram (right hand side of Fig. 10.5), however, at each vertex an electron line meets a hole line. As the hole wave function is a time-inverted electron Bloch function, its spin is opposite to that of the electron and the total spin S of the electron–hole pair has to

be zero. Thus only spin-singlet states, $S = 0$, experience the exchange interaction. This consideration allows one to write the exchange term after summation over the spin variables as

$$V_{\text{exch}} = 2\delta_{S,0} \int d^3\mathbf{r} \int d^3\mathbf{r}' \psi_{c\mathbf{k}_e}^*(\mathbf{r}) \psi_{v'\mathbf{k}'_e}(\mathbf{r}') \frac{e^2}{\kappa|\mathbf{r} - \mathbf{r}'|} \psi_{v\mathbf{k}_h}^*(\mathbf{r}) \psi_{c'\mathbf{k}'_e}(\mathbf{r}'). \quad (10.59)$$

We may again expand the product of the periodic parts of the Bloch functions (here that of a hole and of an electron wave function) in a Fourier series now with coefficients

$$W_{cv}(\mathbf{k}_e, \mathbf{k}_h, \mathbf{G}) = \frac{1}{V_{\text{cell}}} \int u_{c\mathbf{k}_e}^*(\mathbf{r}) u_{v\mathbf{k}_h}(\mathbf{r}) e^{i\mathbf{G}\cdot\mathbf{r}} d^3\mathbf{r} \quad (10.60)$$

and proceed as before. Using $\mathbf{Q} = \mathbf{k}_e + \mathbf{k}_h = \mathbf{k}'_e + \mathbf{k}'_h$, this gives

$$V_{\text{exch}} = 2\delta_{S,0} \sum_{\mathbf{G}} W_{cv}(\mathbf{k}, \mathbf{Q}, \mathbf{G}) W_{c'v'}^*(\mathbf{k}', \mathbf{Q}, \mathbf{G}) \frac{e^2}{\varepsilon_0 V_c |\mathbf{Q} - \mathbf{G}|^2}. \quad (10.61)$$

The center-of-mass wave vector \mathbf{Q} is usually much smaller than a reciprocal lattice vector \mathbf{G} and can be neglected except for $\mathbf{G} = 0$. For the term with $\mathbf{G} = 0$, we use the $\mathbf{k} \cdot \mathbf{p}$ expansion of the Bloch factors around $\mathbf{k} = 0$, while for the terms with $\mathbf{G} \neq 0$ the zone center Bloch functions are taken as a good approximations to write the leading contribution as

$$V_{\text{exch}} = 2\delta_{S,0} \left\{ \lim_{\mathbf{Q} \rightarrow 0} \frac{e^2}{\varepsilon_0 V_c Q^2} \frac{\hbar^2}{m^2} \frac{(\mathbf{P}_{cv} \cdot \mathbf{Q})(\mathbf{P}_{v'c'} \cdot \mathbf{Q})}{(E_c - E_v)(E_{c'} - E_{v'})} + \sum_{\mathbf{G} \neq 0} \frac{e^2}{\varepsilon_0 V_c G^2} W_{cv}(0, 0, \mathbf{G}) W_{c'v'}^*(0, 0, \mathbf{G}) \right\}. \quad (10.62)$$

This result does not depend on \mathbf{k} (or \mathbf{k}'), thus, after Fourier transformation, this exchange interaction is a contact potential $\sim \delta(\mathbf{r})$ in the relative coordinate. Moreover, in contrast to the Coulomb term, it is not diagonal in the band indices. It describes the coupling between the band pair c, v forming the lowest energy gap and the band pairs c', v' with larger energies. Therefore, the argument with the reducibility of exchange diagrams, which was correct for the simple two-band model, is not correct in the more general case, when the dielectric background represented by the band pairs with higher energy is taken into account. It can be considered by a matrix diagonalization procedure (partitioning) of the exchange interaction, which results in a screening of the exchange interaction by the dielectric background. In addition, the first term of (10.62), to be taken in the limit $\mathbf{Q} \rightarrow 0$, has the peculiar property, that it depends on the orientation of the exciton wave vector \mathbf{Q} with respect to the dipole matrix element \mathbf{P}_{cv} and is, therefore, called nonanalytic exchange term. It contributes only to longitudinal excitons with \mathbf{Q} parallel to the transition dipole \mathbf{P}_{cv} . This splitting between longitudinal and transverse excitons is analogous to that of optical phonons (see Chap. 3). We shall come back to this aspect in the following section. The second term in (10.62) is the analytic exchange term [290].

As outlined in this section, excitons are the electronic excitations with the lowest energy (usually in the optical regime) in semiconductors and insulators. For dipole-excitations with this energy, they represent the quanta of the

polarization field as is the case for optical phonons in the far-infrared regime (see Sect. 3.5). Their internal structure, a superposition of electron–hole pair excitations (see (10.37) and (10.38)) suggests to consider them as bosons with operators $B_{\nu\mathbf{Q}}$. Application of $B_{\nu\mathbf{Q}}^\dagger$ to the electronic ground state $|\Psi_0\rangle$ creates an exciton according to $B_{\nu\mathbf{Q}}^\dagger|\Psi_0\rangle = |\Psi_{\nu\mathbf{Q}}\rangle$ and the Hamiltonian for the electron system can be represented in this energy range as

$$H_{\text{el}} = \sum_{\nu,\mathbf{Q}} E_{\nu\mathbf{Q}} B_{\nu\mathbf{Q}}^\dagger B_{\nu\mathbf{Q}}, \quad (10.63)$$

with the exciton energy $E_{\nu\mathbf{Q}}$. Note, however, that the bosonic character of the exciton holds only in the approximation of low excitation densities (Problem 10.4). With increasing excitation densities the internal structure of the exciton, its composition of fermions, becomes relevant and is the origin of high-excitation phenomena like biexcitons (or exciton molecules), polyexcitons, electron–hole droplets, and formation of an electron–hole plasma. Bose–Einstein condensation of excitons is another topic in this field [283].

10.4 Polaritons

Electro-magnetic waves propagate through an insulating solid with reduced velocity of light, $c' = c/n_1$, according to the dispersion relation $\omega = c'|\boldsymbol{\kappa}|$. In the frequency region of a dipole-active oscillator, c' depends on ω due to anomalous dispersion. In a microscopic formulation this is due to the coupling of the propagating light with the oscillator, which, in the context of this section, will be an exciton, but the same considerations also hold for optical phonons. This coupling results in a new kind of excitation, the *polariton* or, to be more specific, the *exciton polariton*. As an introduction to the polariton concept, let us first follow the phenomenological approach.

Light propagation in insulating matter can be described using the macroscopic Maxwell equations

$$\nabla \times \mathbf{E} = -\frac{\partial \mathbf{B}}{\partial t}, \quad \nabla \times \mathbf{H} = \frac{\partial \mathbf{D}}{\partial t}. \quad (10.64)$$

The properties of insulating matter are considered in the dielectric function $\varepsilon(\omega)$, which is determined by the dipole-active oscillators of the solid, here the excitons. It connects the electric field \mathbf{E} with the displacement vector \mathbf{D} , which is connected with the dielectric polarization \mathbf{P} , according to

$$\mathbf{D} = \varepsilon_0 \varepsilon \mathbf{E} = \varepsilon_0 \mathbf{E} + \mathbf{P}. \quad (10.65)$$

The dielectric polarization $\mathbf{P}(\omega) = \chi(\omega)\mathbf{E}(\omega)$ depends on the dielectric susceptibility $\chi(\omega)$, with contributions of the possible dipole excitations in the solid.

The fields \mathbf{B} and \mathbf{H} can be eliminated by combining the two macroscopic Maxwell equations (10.64). One obtains

$$\nabla \times (\nabla \times \mathbf{E}) = -\frac{1}{\varepsilon_0 c^2} \frac{\partial^2 \mathbf{D}}{\partial t^2}. \quad (10.66)$$

Assuming monochromatic light with the electric field given by

$$\mathbf{E}(\mathbf{r}, t) = \mathbf{E}(\omega) e^{i(\boldsymbol{\kappa} \cdot \mathbf{r} - \omega t)} + c.c. \quad (10.67)$$

one finds

$$\boldsymbol{\kappa} \times (\boldsymbol{\kappa} \times \mathbf{E}) = \frac{\omega^2}{c^2} \varepsilon \mathbf{E}. \quad (10.68)$$

For transverse waves, $\mathbf{E} \perp \boldsymbol{\kappa}$, the lhs reduces to κ^2 and we can eliminate the common factor \mathbf{E} . The resulting relation

$$\varepsilon(\omega) = \frac{c^2}{\omega^2} \kappa^2 \quad (10.69)$$

determines, for given $\varepsilon(\omega)$, the dispersion of the coupled light–matter modes, the polaritons as shown in Fig. 10.4 as plots of ω vs. real (κ_1), and imaginary part (κ_2) of the wave vector.

The frequency dependence of $\varepsilon(\omega) = 1 + \chi(\omega)/\varepsilon_0$ results from the oscillators connected with dipole excitations of the solid (here, the excitons). A simple model, assuming a single oscillator with eigenfrequency ω_0 and oscillator strength f_0 , would give $\chi(\omega) = f_0/(\omega_0^2 - \omega^2)$. At frequencies ω much smaller than ω_0 , the propagation follows the linear relation for light in vacuum, but with a reduced velocity $c' = c/n_<$ with $n_< = \sqrt{1 + f_0/\varepsilon_0 \omega_0^2}$. For $\omega \gg \omega_0$, the dielectric susceptibility does not contribute and the propagation takes place with $c' = c/n_>$, where $n_> = 1$. If besides the oscillator at ω_0 , other oscillators contribute to $\chi(\omega)$ but at frequencies $\omega \gg \omega_0$, they can be considered by using $\varepsilon(\omega) = \varepsilon_b + \chi(\omega)/\varepsilon_0$, with a background dielectric constant ε_b , which replaces 1 in the expressions for the refractive indices $n_<$ and $n_>$.

For a longitudinal wave with $\mathbf{E} \parallel \boldsymbol{\kappa}$, the lhs of (10.68) vanishes and the longitudinal frequency ω_L follows from

$$\varepsilon(\omega_L) = \varepsilon_b + \frac{f_0}{\varepsilon_0(\omega_0^2 - \omega_L^2)} = 0 \quad (10.70)$$

to be $\omega_L^2 = \omega_0^2 + f_0/\varepsilon_0 \varepsilon_b$, and we recover the Lyddane–Sachs–Teller relation of Chap. 3

$$\frac{\omega_L^2}{\omega_0^2} = 1 + \frac{f_0}{\varepsilon_0 \varepsilon_b \omega_0^2}. \quad (10.71)$$

It can be used to express the dielectric function in terms of the frequencies ω_0 and ω_L to arrive at the relation

$$\kappa^2 = \varepsilon_b \frac{\omega^2 \omega_L^2 - \omega_0^2}{c^2 \omega_0^2 - \omega^2}, \quad (10.72)$$

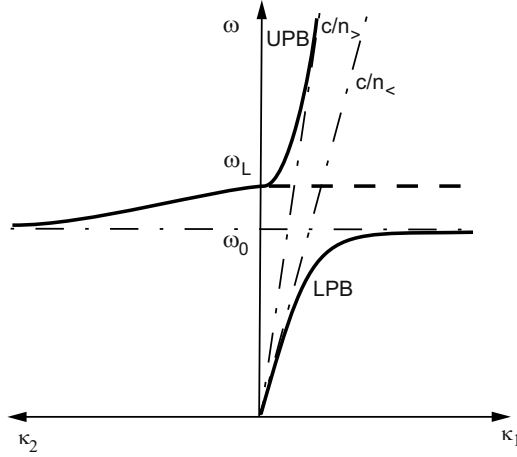


Fig. 10.7. Polariton dispersion: solutions of (10.69) vs. real and imaginary part of κ

which determines the polariton dispersion $\omega(\kappa)$. The difference between the resonance frequency ω_0 of the oscillator (which is a transverse excitation) and the longitudinal frequency ω_L defines the longitudinal-transverse splitting (LT-splitting) of the excitonic resonance, mentioned already in the previous Section. It follows from the Lyddane–Sachs–Teller relation (10.71) by using $\omega_0 + \omega_L \approx 2\omega_0$, and is given by

$$\Delta_{LT} = \omega_L - \omega_0 = \frac{f_0}{2\varepsilon_0\varepsilon_b\omega_0}. \quad (10.73)$$

For $\omega < \omega_0$ and $\omega > \omega_L$ we have $\kappa^2 > 0$ and find two real solutions, the lower and the upper polariton branch, LPB and UPB, respectively in Fig. 10.7. For the frequency interval $\omega_0 < \omega < \omega_L$ κ^2 is negative and leads to a damped solution. The polariton dispersion curves are shown in Fig. 10.7 in a plot of ω vs. the real and imaginary parts of $\kappa = \kappa_1 + i\kappa_2$. It should be noted, that the expression for Δ_{LT} considers the dielectric background by the phenomenological constant ε_b . Its microscopic origin is the coupling of the exciton with the excitations between band pairs with higher energy. With the arguments given in Sect. 10.3 it is possible to relate the LT-splitting with the oscillator strength of the exciton (Problem 10.5).

In Fig. 10.8, we show the polariton dispersion calculated with the exciton parameters of CuCl for a small interval of the wave vector close to the center of the Brillouin zone. (Note, that the Brillouin zone extends out to $k \approx 10^8 \text{ cm}^{-1}$.) The experimental data points are obtained from two-photon absorption (TPA) and hyper-Raman scattering (HRS). In the former case, two photons from different sources are simultaneously absorbed to excite the exciton–polariton, while in the latter a virtually excited biexciton decays into two polaritons, one of which is detected as a scattered photon outside the solid.

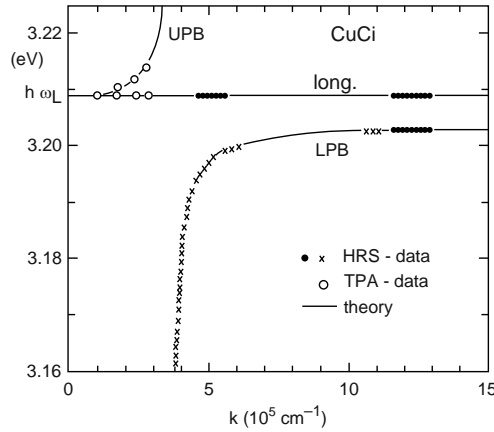


Fig. 10.8. Calculated exciton–polariton dispersion of CuCl with experimental data from two-photon absorption (TPA-data) and hyper-Raman scattering (HRS-data), after [283]

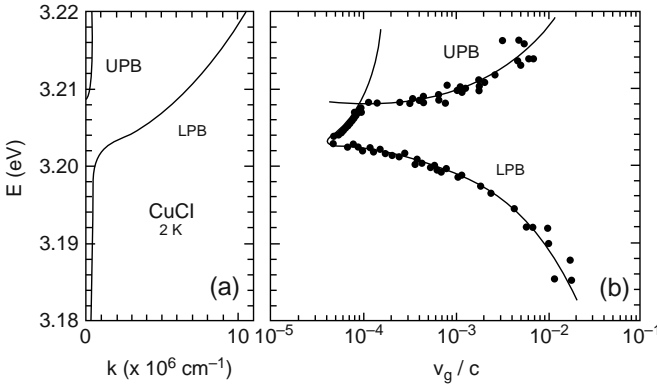


Fig. 10.9. Exciton–polariton dispersion of CuCl (*left*) and measured propagation velocity of polariton modes in CuCl together with values calculated from the dispersion curve (*right*), after [283]

In contrast to simple absorption experiments with one photon, both methods allow to map out the dispersion of the polaritons by exploiting different configurations of the small wave vectors of incident and scattered photons. It is also possible to detect the longitudinal polariton branch.

Fig. 10.9 shows, in the left hand part, the dispersion of the transverse polariton branches on a larger k scale. On this scale, the dispersion of the lower polariton branch (LPB), caused by the free center-of-mass term in the exciton energy, becomes relevant. In the right hand part of the figure the group velocity v_g , calculated from the polariton dispersion, is compared with experimental data obtained from time-of-flight measurements. Away from the exciton resonance, the light pulses propagate through the sample with the velocity of light in matter, the slope of the steep linear parts of the upper

(UPS) and lower polariton branches (LPB). However, close to the resonance the group velocity is reduced by orders of magnitude, because the travelling pulse polarizes the matter by coupling with the exciton.

After this phenomenological survey of exciton–polaritons we turn now to the rigorous formulation that makes use of the quantization of the electromagnetic field and treats light–matter interaction as exciton–photon coupling. The quantization of the electro-magnetic field can be performed analogous to the quantization of the displacement field in Chap. 3 (leading to phonons) with the only difference, that in the Coulomb gauge the vector potential is transverse (Problem 10.6). With the expansion

$$\mathbf{A}(\mathbf{r}, t) = \sum_{\lambda, \boldsymbol{\kappa}} \left(\frac{\hbar}{2\varepsilon_0\omega(\boldsymbol{\kappa})V} \right)^{1/2} \mathbf{e}_{\lambda\boldsymbol{\kappa}} \left(a_{\lambda\boldsymbol{\kappa}}(t) + a_{\lambda\boldsymbol{\kappa}}^\dagger(t) \right) e^{i\boldsymbol{\kappa} \cdot \mathbf{r}} \quad (10.74)$$

in terms of Boson operators $a_{\lambda\boldsymbol{\kappa}}$ for photons, the quanta of the electromagnetic field, and transverse unit vectors $\mathbf{e}_{\lambda\boldsymbol{\kappa}}$ with $\mathbf{e}_{\lambda\boldsymbol{\kappa}} \cdot \boldsymbol{\kappa} = 0$, the Hamiltonian of the radiation field takes the expected form

$$\mathcal{H}_{\text{rad}} = \sum_{\lambda, \boldsymbol{\kappa}} \hbar\omega(\boldsymbol{\kappa}) \left(a_{\lambda\boldsymbol{\kappa}}^\dagger a_{\lambda\boldsymbol{\kappa}} + \frac{1}{2} \right) \quad (10.75)$$

with photon energies $\hbar\omega(\boldsymbol{\kappa})$.

At the end of Sect. 10.3 (in the energy range of excitonic resonances) we have formulated the Hamiltonian for the electron system in terms of exciton operators $B_{\nu\mathbf{Q}}$. We want to extend this concept also to the light–matter interaction. The Ap -coupling of $\mathcal{H}_{\text{el-rad}}$ is linear in the vector potential, which can be replaced by its quantized form (10.74), and it contains the electron momentum operator \mathbf{p}_l . According to (4.76) it can be expressed in terms of Fermion operators giving

$$\begin{aligned} \mathcal{H}_{Ap} = & \sum_{\substack{n n' \mathbf{k} \mathbf{k}' \\ \lambda, \boldsymbol{\kappa}}} \frac{e}{m} \left(\frac{\hbar}{2\varepsilon_0\omega(\boldsymbol{\kappa})V} \right)^{1/2} \langle n' \mathbf{k}' | e^{i\boldsymbol{\kappa} \cdot \mathbf{r}} \mathbf{p} \cdot \mathbf{e}_{\lambda\boldsymbol{\kappa}} | n \mathbf{k} \rangle \\ & \times (a_{\lambda\boldsymbol{\kappa}} + a_{\lambda-\boldsymbol{\kappa}}^\dagger) c_{n' \mathbf{k}'}^\dagger c_{n \mathbf{k}}, \end{aligned} \quad (10.76)$$

which has the same form as the electron–phonon coupling (8.8). However, our concern is not the coupling to an individual electron–hole pair but to an exciton, and we should express the electron part in terms of exciton operators. If we simplify to an exciton formed with Bloch functions from the band pair c, v and with the wave function $\phi(\mathbf{r})$ for the relative motion, then the coupling to one of the photons can be written ($P_{cv} = \langle c | e \cdot \mathbf{p} | v \rangle$)

$$\mathcal{H}_{Ap} = \sum_{\boldsymbol{\kappa}} \frac{e}{m} \left(\frac{\hbar}{2\varepsilon_0\omega(\boldsymbol{\kappa})V} \right)^{1/2} |\phi(0)| |P_{cv}| (a_{\boldsymbol{\kappa}} + a_{-\boldsymbol{\kappa}}^\dagger) (B_{\boldsymbol{\kappa}} + B_{-\boldsymbol{\kappa}}^\dagger), \quad (10.77)$$

which is linear in the Boson operators of both photons and excitons and we may write the polariton Hamiltonian as

$$\begin{aligned} \mathcal{H}_{\text{pol}} = \sum_{\boldsymbol{\kappa}} \left(E_{\boldsymbol{\kappa}} B_{\boldsymbol{\kappa}}^{\dagger} B_{\boldsymbol{\kappa}} + \hbar\omega(\boldsymbol{\kappa}) \left(a_{\boldsymbol{\kappa}}^{\dagger} a_{\boldsymbol{\kappa}} + \frac{1}{2} \right) \right. \\ \left. + C_{\boldsymbol{\kappa}} \left(a_{\boldsymbol{\kappa}} B_{\boldsymbol{\kappa}} + a_{\boldsymbol{\kappa}} B_{-\boldsymbol{\kappa}}^{\dagger} + a_{-\boldsymbol{\kappa}}^{\dagger} B_{\boldsymbol{\kappa}} + a_{-\boldsymbol{\kappa}}^{\dagger} B_{-\boldsymbol{\kappa}}^{\dagger} \right) \right) \end{aligned} \quad (10.78)$$

The coupling reminds of the situation found for anti-ferromagnetic magnons in Sect. 6.4 and can be exactly eliminated by looking for solutions with polariton operators

$$\alpha_{\boldsymbol{\kappa}} = A_1 a_{\boldsymbol{\kappa}} + A_2 B_{\boldsymbol{\kappa}} + A_3 a_{-\boldsymbol{\kappa}}^{\dagger} + A_4 B_{-\boldsymbol{\kappa}}^{\dagger}. \quad (10.79)$$

For the detailed calculation we refer to the literature [10, 14] and to the original paper by Hopfield [291]. The eigenfrequencies of the polaritons are those found with the phenomenological approach and show the anti-crossing behavior (Fig. 10.7), which is typical for hybridization (see Sect. 5.4). The lower polariton branch away from the exciton resonance is photon-like and follows the linear dispersion, but turns over into the exciton dispersion and becomes exciton-like. The upper polariton branch starts at the longitudinal exciton energy but approaches for higher energy the linear dispersion of photons. The existence of polaritons, as coupled exciton–photon modes is clearly demonstrated by the quoted experiments. Thus, photons propagate through the solid as polaritons, which convert to photons when passing back into the vacuum. This means, that absorption is not the conversion of a photon into an electronic excitation like the exciton but due to polariton scattering (e.g., with phonons or impurities), by which energy is dissipated into other excitations of the solid.

10.5 Light-Scattering

Light-scattering, or more precisely *inelastic light scattering*, has, since its discovery 1928 by Raman,³ gained much importance as a spectroscopical method, especially with the availability of lasers as intense light sources. A comprehensive overview of the method, its applications, and the theoretical concepts is given in a series of books with the topic *Light Scattering* [118]. A schematic view, typical for all scattering experiments, is shown in Fig. 10.10.

The incident monochromatic light (vector potential $\mathbf{A}_0(\mathbf{r}, t)$), with photon energy $\hbar\omega_0$ and photon momentum $\hbar\boldsymbol{\kappa}_0$, is scattered at a sample (here the solid), and the cross section for the scattered light (vector potential $\mathbf{A}_1(\mathbf{r}, t)$), with photons of energy $\hbar\omega_1$ and momentum $\hbar\boldsymbol{\kappa}_1$, is measured. It depends on the energy and momentum transfer

³ Chandrasekhara Venkata Raman 1888–1970, Nobel prize in Physics 1930.

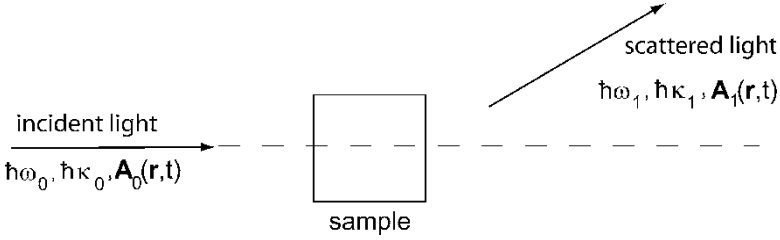


Fig. 10.10. Schematic view of the light-scattering experiment

$$\hbar\omega = \hbar\omega_0 - \hbar\omega_1, \quad \hbar\mathbf{q} = \hbar\boldsymbol{\kappa}_0 - \hbar\boldsymbol{\kappa}_1, \quad (10.80)$$

which, under the assumption of weak light-matter interaction, i.e., validity of the Born approximation, provides information about an elementary excitation with dispersion $\omega(\mathbf{q})$ in the sample. The light-matter interaction can be described by the Hamiltonian $\mathcal{H}_{\text{el-rad}}$ of (10.13), with the vector potential $\mathbf{A}(\mathbf{r}, t) = \mathbf{A}_0(\mathbf{r}, t) + \mathbf{A}_1(\mathbf{r}, t)$. The cross section depends on both the incident and scattered radiation fields, therefore, we expect contributions linear in the product $\mathbf{A}_0\mathbf{A}_1$ not only from the first term of $\mathcal{H}_{\text{el-rad}}$ (Ap -coupling) in second order but also from the second term, which already contains this product, in first order perturbation theory (A^2 -coupling).

Fermi's Golden Rule applied to the A^2 -coupling

$$\mathcal{H}_{\mathbf{A}_0\mathbf{A}_1} = \frac{e^2}{m} A_0 A_1 \mathbf{e}_0 \cdot \mathbf{e}_1 e^{i(\omega_0 - \omega_1)t} \sum_{l=1}^N e^{i(\boldsymbol{\kappa}_0 - \boldsymbol{\kappa}_1) \cdot \mathbf{r}_l} + h.c. \quad (10.81)$$

allows to write down immediately the transition probability

$$W_{i \rightarrow f} = \frac{2\pi}{\hbar} \left(\frac{e^2 A_0 A_1}{m} \right)^2 |\mathbf{e}_0 \cdot \mathbf{e}_1|^2 \left| \langle f | \sum_l e^{i\mathbf{q} \cdot \mathbf{r}_l} | i \rangle \right|^2 \delta(E_f - E_i \pm \hbar\omega) \quad (10.82)$$

and the differential scattering cross section

$$\begin{aligned} \frac{d^2\sigma}{d\Omega d\omega} &= \frac{\hbar}{2\pi} \left(\frac{\omega_1}{\omega_0 A_0 A_1} \right)^2 \sum_{i,f} W_{i \rightarrow f} \\ &= \left(\frac{\omega_1}{\omega_0} \right)^2 \frac{e^4}{m^2} |\mathbf{e}_0 \cdot \mathbf{e}_1|^2 \sum_{i,f} |\langle f | N_{-\mathbf{q}} | i \rangle|^2 \delta(E_f - E_i \pm \hbar\omega). \end{aligned} \quad (10.83)$$

As can be seen from this expression, the scattering due to the A^2 -coupling is caused by number fluctuations $N_{-\mathbf{q}} = \sum_l \exp(i\mathbf{q} \cdot \mathbf{r}_l)$ (see Sect. 4.5) and can be related with the dynamic structure factor

$$\begin{aligned} S(\mathbf{q}, \omega) &= \sum_{i,f} |\langle f | N_{-\mathbf{q}} | i \rangle|^2 \delta(\omega_f - \omega_i \pm \omega) \\ &= \frac{1}{2\pi} \int_{-\infty}^{+\infty} e^{\pm i\omega t} \langle N_{\mathbf{q}}(t) N_{-\mathbf{q}}(0) \rangle dt, \end{aligned} \quad (10.84)$$

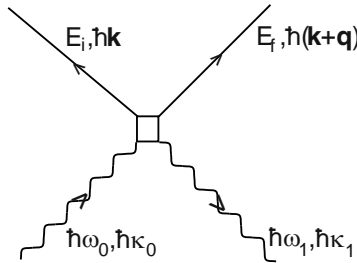


Fig. 10.11. Feynman diagram for the light-scattering process with the A^2 -coupling

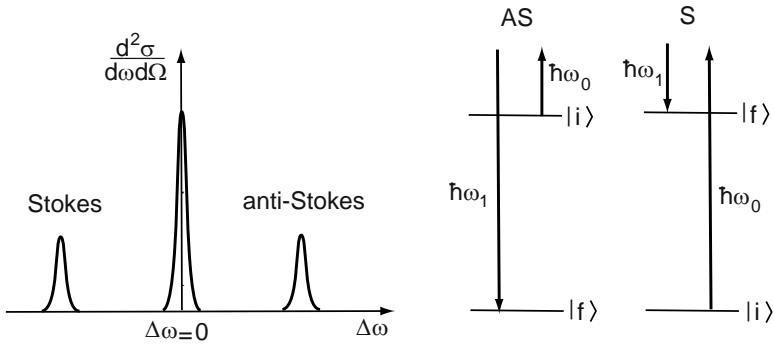


Fig. 10.12. Schematic picture of the scattering cross section and of the diagram of the involved energy levels. The peak of the cross section at $\Delta\omega = 0$ is due to the unscattered light, while the satellites are due to stokes (S) and anti-stokes (AS) scattering

where $E_{i,f} = \hbar\omega_{i,f}$, or expressed by the energy–loss function. Thus, light-scattering, employing the A^2 -coupling is capable to investigate collective modes of the solids like charge or spin density excitations. We note in passing that for inelastic electron scattering the same expression holds if $e^2|\mathbf{e}_0 \cdot \mathbf{e}_1|/m$ is replaced by the Coulomb interaction $v_{\mathbf{q}}$ (see (4.131)). The scattering process can also be visualized in a Feynman diagram (Fig. 10.11). The vertex of the diagram represents the number fluctuation.

A schematic view of the scattering cross section and the energy levels involved in the scattering process is shown in Fig. 10.12. The central peak at $\Delta\omega = \omega - \omega_f + \omega_i = 0$ is caused by the unscattered laser light, the peaks at positive (negative) $\Delta\omega$, called *Stokes* (*anti-Stokes*) *line*, result from creation (annihilation) of an elementary excitation in the solid.

The Ap -coupling

$$\mathcal{H}_{Ap} = \frac{e}{m} \sum_l \left(\mathbf{e}_0 A_0 e^{i(\boldsymbol{\kappa}_0 \cdot \mathbf{r} - \omega_0 t)} + \mathbf{e}_1 A_1 e^{i(\boldsymbol{\kappa}_1 \cdot \mathbf{r} - \omega_1 t)} \right) + h.c. \quad (10.85)$$

contributes in second order perturbation theory by terms linear in both vector potentials of incident and scattered light. The cross section essentially has

the same structure as the one for the A^2 -coupling but $\mathbf{e}_0 \cdot \mathbf{e}_1$ is replaced by $\mathbf{e}_1 \cdot \delta \overleftrightarrow{\chi}_{fi} \cdot \mathbf{e}_0$ under the sum over initial and final states. Here, the components of the Raman tensor $\delta \overleftrightarrow{\chi}_{fi}$ are given by

$$\langle f | \delta \chi^{\mu\nu} | i \rangle \sim \sum_z \frac{M_{1,fz}^\mu M_{0,zi}^\nu}{E_z - E_i - \hbar\omega} + (0 \leftrightarrow 1). \quad (10.86)$$

In dipole approximation, the matrix elements

$$M_{1,fz}^\mu = \langle f | \sum_l e^{-i\boldsymbol{\kappa}_1 \cdot \mathbf{r}_l} p_{l\mu} | z \rangle \text{ and } M_{0,zi}^\nu = \langle z | \sum_l e^{i\boldsymbol{\kappa}_0 \cdot \mathbf{r}_l} p_{l\nu} | i \rangle \quad (10.87)$$

reduce to the momentum matrix elements $\langle f | p_{l\mu} | z \rangle$ and $\langle z | p_{l\nu} | i \rangle$, respectively, if the corresponding transitions are dipole allowed.

In the foregoing, the states $|i\rangle, |z\rangle, |f\rangle$ are to be understood as exact eigenstates of the solid, which are not known, but can be described approximately with the concepts developed in the earlier chapters. Let us assume the Hamiltonian of the solid in the form $\mathcal{H} = \mathcal{H}_{\text{el}} + \mathcal{H}_{\text{ph}} + \mathcal{H}_{\text{el-ph}}$ for electrons, phonons, and electron-phonon interaction as in Chap. 8. The eigenstates $|\gamma\rangle$ of $\mathcal{H}_{\text{el}} + \mathcal{H}_{\text{ph}}$ are products of electron and phonon states in occupation number representation, while the eigenstates of \mathcal{H} can be considered as quasi-particle states with energies $E_\alpha + i\Gamma_\alpha$, with finite lifetime due to the interaction $\mathcal{H}_{\text{el-ph}}$. The exact intermediate state $|z\rangle$ can be expressed by the perturbation expansion

$$|z\rangle = |\gamma\rangle + \sum_{\gamma'} \frac{|\gamma'\rangle \langle \gamma' | \mathcal{H}_{\text{el-ph}} | \gamma \rangle}{E_\gamma - E_{\gamma'}} + \dots \quad (10.88)$$

and one obtains contributions to $\langle f | \delta \chi^{\mu\nu} | i \rangle$ of first order in $\mathcal{H}_{\text{el-ph}}$

$$\langle f | \delta \chi^{\mu\nu} | i \rangle \sim \sum_{\gamma, \gamma'} \frac{M_{f\gamma}^\mu \mathcal{M}_{\gamma\gamma'} M_{\gamma'i}^\nu}{(\hbar\omega_0 - E_{\gamma'} - i\Gamma_{\gamma'}) (\hbar\omega_1 - E_\gamma - i\Gamma_\gamma)} + (0 \leftrightarrow 1), \quad (10.89)$$

where $\mathcal{M}_{\gamma\gamma'} = \langle \gamma | \mathcal{H}_{\text{el-ph}} | \gamma' \rangle$. A graphical picture of such a contribution is shown in Fig. 10.13 together with the energy level scheme. The incoming photon creates *via* Ap -coupling an electron-hole pair or exciton (a), which emits (or absorbs) a phonon (b) and recombines *via* Ap -coupling to the scattered photon (c). Higher order processes with $\mathcal{H}_{\text{el-ph}}$ are possible.

The process described here in detail is used to investigate phonons in bulk material, quantum wells, or at surfaces. If optical phonons are involved, it is called *Raman scattering*, while *Brillouin scattering* is due to emission or absorption of acoustic phonons. Instead of the electron-phonon interaction as the origin of the inelastic light-scattering, one could have also considered the coupling between the electron system and other collective excitations like plasmons, plasmon-phonon modes, or magnons to map out dispersion. The energy denominators in the scattering cross section can be exploited to enhance the scattering efficiency by using the possible resonances of incident or scattered light with the electronic excitation (*resonant light-scattering*).

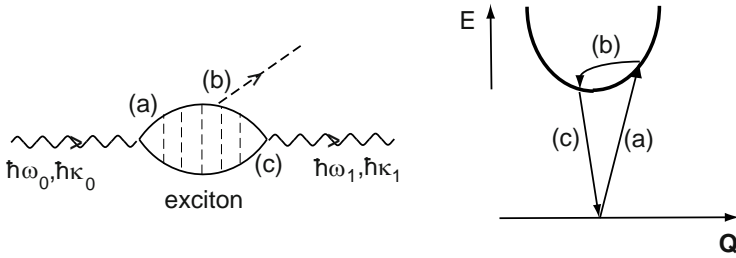


Fig. 10.13. Feynman diagram and level diagram for the light-scattering process with Ap and electron–phonon coupling

10.6 Coherent Interband Dynamics

The light–matter interaction has been treated in the previous sections of this chapter either as a time-dependent perturbation of the electron system on a long time scale by applying Fermi’s Golden Rule or by creating the instantaneous formation of polaritons as coupled modes of electronic excitation and electro-magnetic field. In this section, we focus on the dynamics of the interband transitions by looking at the light–matter system as a system of driven oscillators or two-level systems on the very short time scale after excitation, for which the polarization is in phase with the radiation field. Experimentally, the investigation of this coherent regime is possible with spectroscopy using light pulses in the ps and fs range. The approach of this and the following section, which, besides light–matter interaction also includes many-body aspects, provides a very general view, because previous results of this chapter can be recovered as special cases[95, 284, 285].

Let us start with the Hamiltonian

$$\mathcal{H} = \mathcal{H}_0 + \mathcal{H}_{Ap} + \mathcal{H}_{Coul} . \tag{10.90}$$

We adopt a semiconductor in the form of a two-band model with valence and conduction band ($n = c, v$) separated by a direct gap at $\mathbf{k} = 0$ and formulate the single-particle part of the system Hamiltonian in second quantization:

$$\mathcal{H}_0 = \sum_{\substack{n=c,v \\ \mathbf{k}}} E_n(\mathbf{k}) c_{n\mathbf{k}}^\dagger c_{n\mathbf{k}} . \tag{10.91}$$

The light–matter interaction is reduced to the Ap -coupling written as

$$\mathcal{H}_{Ap} = - \sum_{\mathbf{k}, \boldsymbol{\kappa}} \left(\mathbf{d}_{cv}(\mathbf{k}) \cdot \mathbf{E}(\boldsymbol{\kappa}, t) c_{c\mathbf{k}}^\dagger c_{v\mathbf{k}-\boldsymbol{\kappa}} + h.c. \right) , \tag{10.92}$$

with the dipole matrix element $\mathbf{d}_{cv}(\mathbf{k}) = e \langle c\mathbf{k} | \mathbf{r} | v\mathbf{k} \rangle$ for the transition between the valence and conduction band states at \mathbf{k} and the (real) electric field vector $\mathbf{E}(\boldsymbol{\kappa}, t)$ for a harmonic wave with wave vector $\boldsymbol{\kappa}$ (see Problem 10.1). While the interaction between all electrons in the filled valence band is considered in the energies $E_n(\mathbf{k})$ of the Bloch states (in the vein of DFT discussed in

Chap. 5), we have to explicitly consider the Coulomb interaction between the carriers created by the primary excitation

$$\mathcal{H}_{\text{Coul}} = \frac{1}{2} \sum_{\substack{\mathbf{k}, \mathbf{k}' \\ \mathbf{q} \neq 0}} v_{\mathbf{q}} \left\{ c_{c\mathbf{k}+\mathbf{q}}^\dagger c_{c\mathbf{k}'-\mathbf{q}}^\dagger c_{c\mathbf{k}'} c_{c\mathbf{k}} + c_{v\mathbf{k}+\mathbf{q}}^\dagger c_{v\mathbf{k}'-\mathbf{q}}^\dagger c_{v\mathbf{k}'} c_{v\mathbf{k}} + 2c_{c\mathbf{k}+\mathbf{q}}^\dagger c_{v\mathbf{k}'-\mathbf{q}}^\dagger c_{v\mathbf{k}'} c_{c\mathbf{k}} \right\}. \quad (10.93)$$

Further simplifications can be made with the dipole approximation, according to which the spatial variation of the electric field can be ignored with $\boldsymbol{\kappa} = 0$, and by considering electron–hole pair transitions only close to the fundamental gap at $\mathbf{k} = 0$, which all have the same dipole matrix element \mathbf{d}_{cv} . For an isotropic semiconductor and linearly polarized light we may simplify $\mathbf{d}_{cv} \cdot \mathbf{E}(t)$ to the scalar form $d_{cv}E(t)$ and write the light–matter coupling in the form

$$\mathcal{H}_{Ap} = - \sum_{\mathbf{k}} E(t) \left(d_{cv} c_{c\mathbf{k}}^\dagger c_{v\mathbf{k}} + d_{cv}^* c_{v\mathbf{k}}^\dagger c_{c\mathbf{k}} \right). \quad (10.94)$$

Let us first study the kinetics of optical interband transitions without the Coulomb interaction. This leaves us with a single-particle problem, which can be solved by looking at the equations of motion for the operators $c_{c\mathbf{k}}^\dagger c_{c\mathbf{k}}$, $c_{v\mathbf{k}}^\dagger c_{v\mathbf{k}}$, $c_{c\mathbf{k}}^\dagger c_{v\mathbf{k}}$, and $c_{v\mathbf{k}}^\dagger c_{c\mathbf{k}}$. In the Schrodinger picture these are time-dependent operators, their thermal expectation values $\rho_{nn'}(\mathbf{k}, t) = \langle c_{n\mathbf{k}}^\dagger(t) c_{n'\mathbf{k}}(t) \rangle$ are elements of the time-dependent density matrix

$$\rho_{\mathbf{k}}(t) = \begin{pmatrix} \rho_{cc}(\mathbf{k}, t) & \rho_{cv}(\mathbf{k}, t) \\ \rho_{vc}(\mathbf{k}, t) & \rho_{vv}(\mathbf{k}, t) \end{pmatrix} \quad (10.95)$$

of a two-level system at \mathbf{k} . We switch to the interaction picture with

$$\bar{\mathcal{O}} = e^{\frac{i}{\hbar} \mathcal{H}_0 t} \mathcal{O} e^{-\frac{i}{\hbar} \mathcal{H}_0 t} \quad (10.96)$$

and write down the equation of motion for the density matrix

$$\frac{d}{dt} \bar{\rho}_{\mathbf{k}}(t) = -\frac{i}{\hbar} [\bar{\mathcal{H}}_{Ap}(t), \bar{\rho}_{\mathbf{k}}(t)], \quad (10.97)$$

which for its elements have the following form (here $\epsilon_{n\mathbf{k}} = E_n(\mathbf{k})/\hbar$):

$$\frac{d}{dt} \bar{\rho}_{cv}(\mathbf{k}, t) = \frac{i}{\hbar} d_{cv} E(t) e^{i(\epsilon_{c\mathbf{k}} - \epsilon_{v\mathbf{k}})t} (\bar{\rho}_{vv}(\mathbf{k}, t) - \bar{\rho}_{cc}(\mathbf{k}, t)) \quad (10.98)$$

$$\frac{d}{dt} \bar{\rho}_{cc}(\mathbf{k}, t) = \frac{i}{\hbar} E(t) \left(d_{cv} e^{i(\epsilon_{c\mathbf{k}} - \epsilon_{v\mathbf{k}})t} \bar{\rho}_{vc}(\mathbf{k}, t) - c.c. \right) \quad (10.99)$$

$$\frac{d}{dt} \bar{\rho}_{vv}(\mathbf{k}, t) = \frac{i}{\hbar} E(t) \left(d_{cv}^* e^{-i(\epsilon_{c\mathbf{k}} - \epsilon_{v\mathbf{k}})t} \bar{\rho}_{cv}(\mathbf{k}, t) - c.c. \right). \quad (10.100)$$

The diagonal elements are identical in the Schroedinger and interaction pictures, $\rho_{nn}(\mathbf{k}, t) = \bar{\rho}_{nn}(\mathbf{k}, t)$, and their time derivatives are identical up to a sign change, $d\rho_{vv}(\mathbf{k}, t)/dt = -d\rho_{cc}(\mathbf{k}, t)/dt$, as can be seen from (10.99) and (10.100). These equations describe the interband kinetics of free carriers at \mathbf{k} . It will be shown later, that excitations at different \mathbf{k} are coupled due to $\mathcal{H}_{\text{Coul}}$.

Let us briefly assume quasi-thermal equilibrium, i.e., initially created electrons in the conduction band and holes in the valence band are thermalized within their respective bands. Then, the diagonal elements of the density matrix are Fermi–Dirac distribution functions $f_{c\mathbf{k}}$ and $f_{v\mathbf{k}}$, respectively. For this case, the calculation of the optical polarization $\mathbf{P}(t) = \text{Tr}(\rho(t)\mathbf{d})$, where \mathbf{d} is the electric dipole operator, yields the optical susceptibility $\chi(\omega)$ and the expression for the dielectric function $\varepsilon(\omega)$ derived in Sect. 10.2 (Problem 10.7).

The more interesting case is the time scale, on which the interband excitation follows the same time dependence as the driving electric field, the *coherent regime*. Let us look with

$$E(t) = \frac{E_0}{2} (e^{i\omega t} + e^{-i\omega t}), \quad (10.101)$$

at the equation of motion (10.98) for the off-diagonal element of the density matrix

$$\bar{\rho}_{cv}(\mathbf{k}, t) = e^{i(\epsilon_{c\mathbf{k}} - \epsilon_{v\mathbf{k}})t} \rho_{cv}(\mathbf{k}, t), \quad (10.102)$$

which takes the form

$$\left(\frac{d}{dt} + i(\epsilon_{c\mathbf{k}} - \epsilon_{v\mathbf{k}}) \right) \rho_{cv}(\mathbf{k}, t) = \frac{id_{cv}}{\hbar} E(t) (\rho_{vv}(\mathbf{k}, t) - \rho_{cc}(\mathbf{k}, t)). \quad (10.103)$$

The condition of almost resonant excitation with the *detuning* $\nu_{\mathbf{k}} = \epsilon_{c\mathbf{k}} - \epsilon_{v\mathbf{k}} - \omega$ is considered in the so-called *rotating wave approximation* by dropping the term with $\exp(i\omega t)$ in $E(t)$, which leads to

$$\begin{aligned} \left(\frac{d}{dt} + i\nu_{\mathbf{k}} \right) \rho_{cv}(\mathbf{k}, t)e^{i\omega t} &= -\frac{i\omega_R}{2} (\rho_{cc}(\mathbf{k}, t) - \rho_{vv}(\mathbf{k}, t)) \\ \frac{d}{dt} \rho_{cc}(\mathbf{k}, t) &= -\frac{d}{dt} \rho_{vv}(\mathbf{k}, t) = -\frac{i\omega_R}{2} (\rho_{cv}(\mathbf{k}, t)e^{i\omega t} - c.c.), \end{aligned} \quad (10.104)$$

with the *Rabi*⁴ frequency $\omega_R = d_{cv}E_0/\hbar$. This set of equations is known as *coherent optical Bloch equations* with reference to the Bloch equations used in magnetic resonance spectroscopy. In order to show this relation, the complex elements of the density matrix can be used to define three real components of a vector, the *Bloch vector*

$$\begin{aligned} U_1(\mathbf{k}, t) &= \rho_{cv}(\mathbf{k}, t)e^{i\omega t} + c.c. \\ U_2(\mathbf{k}, t) &= i(\rho_{cv}(\mathbf{k}, t)e^{i\omega t} - c.c.) \\ U_3(\mathbf{k}, t) &= \rho_{cc}(\mathbf{k}, t) - \rho_{vv}(\mathbf{k}, t), \end{aligned} \quad (10.105)$$

⁴ Isaac Isidor Rabi 1898–1988, Nobel prize in Physics 1944.

whose time-dependence is ruled by

$$\begin{aligned}\frac{d}{dt}U_1(\mathbf{k}, t) &= -\nu_{\mathbf{k}}U_2(\mathbf{k}, t) \\ \frac{d}{dt}U_2(\mathbf{k}, t) &= +\nu_{\mathbf{k}}U_1(\mathbf{k}, t) + \omega_{\text{R}}U_3(\mathbf{k}, t) \\ \frac{d}{dt}U_3(\mathbf{k}, t) &= -\omega_{\text{R}}U_2(\mathbf{k}, t),\end{aligned}\tag{10.106}$$

which can also be written also in the compact form as

$$\frac{d}{dt}\mathbf{U}(\mathbf{k}, t) = \mathbf{\Omega} \times \mathbf{U}(\mathbf{k}, t),\tag{10.107}$$

with $\mathbf{\Omega} = -\omega_{\text{R}}\mathbf{e}_1 + \nu_{\mathbf{k}}\mathbf{e}_3$. An equation of this form has been derived already in Sect. 6.3 for the dynamics of spins; its mechanical analogue is the equation of motion for the angular momentum under the action of a torque.

Under resonant excitation, $\nu_{\mathbf{k}} = 0$, the Bloch equation describes the rotation of the Bloch vector around the $-\mathbf{e}_1$ -axis with the Rabi frequency ω_{R} . Let us start at $t = 0$ with a population inversion described by $\mathbf{U}(t = 0) = (0, 0, -U_3)$. After a half period, one has $\mathbf{U}(t = \pi/\omega_{\text{R}}) = (0, 0, U_3)$, i.e., the initial population inversion has changed its sign. This is called *Rabi flopping*. At the intermediate time, $\pi/2\omega_{\text{R}}$ U_3 is completely converted into the component U_2 of the Bloch vector, which is connected with the dielectric polarization $\mathbf{P}(t)$. During the rotation caused by the coupling to the radiation field, the Bloch vector changes periodically between the components U_3 and U_2 , or between population inversion and interband polarization, respectively.

The resonant condition cannot be fulfilled at the same time for interband transitions at different \mathbf{k} , and the detuning $\nu_{\mathbf{k}} \neq 0$ becomes important. Let us consider a group of electron–hole pairs at different \mathbf{k} , but initially with same Bloch vector $\mathbf{U}^{(1)} = (0, 0, U_3)$. A short light pulse of duration $t_1 = \pi/2\Omega_{\text{R}}$ (so-called $\pi/2$ pulse) turns these Bloch vectors into the 2-direction, $\mathbf{U}^{(2)} = (0, U_2, 0)$, and they start to precess around the 3-direction according to their individual detunings, i.e., the Bloch vectors run out of phase and spread in the $U_1 - U_2$ plane. This spreading can be reversed by applying, after some time, T , a π pulse (duration $t_2 = \pi/\Omega_{\text{R}}$), which kicks the Bloch vectors into the directions $\mathbf{U}^{(3)} = (U_1, -U_2, 0)$ such that after $2T$ their further precession around the 3-direction brings them all back to the same phase with $\mathbf{U}^{(4)} = (0, -U_2, 0)$. This Bloch vector, which again is the same for all electron–hole pairs, can be detected as emitted light pulse, the *photon echo*. The photon echo can be observed only, if the phase coherence of each Bloch vector (or electron–hole excitation) with the exciting light is not destroyed.

The coherent optical Bloch equations exhibit some principle features in the dynamics of interband excitations, which, in reality, will be changed due to the finite lifetime of the single-particle states and destroy phase coherence. This can be considered by adding phenomenological damping terms to

the Bloch equations

$$\begin{aligned}
 \frac{d}{dt}U_1(\mathbf{k}, t) &= -\frac{U_1(\mathbf{k}, t)}{T_2} - \nu_{\mathbf{k}}U_2(\mathbf{k}, t) \\
 \frac{d}{dt}U_2(\mathbf{k}, t) &= -\frac{U_2(\mathbf{k}, t)}{T_2} + \nu_{\mathbf{k}}U_1(\mathbf{k}, t) + \omega_{\text{R}}U_3(\mathbf{k}, t) \\
 \frac{d}{dt}U_3(\mathbf{k}, t) &= -\frac{U_3(\mathbf{k}, t) + 1}{T_1} - \omega_{\text{R}}U_2(\mathbf{k}, t).
 \end{aligned} \tag{10.108}$$

The two time constants can be distinguished by their geometrical relation to the components of the Bloch vector: the longitudinal relaxation time T_1 (for U_3) is related with the diagonal elements of the density matrix, while the transverse relaxation time T_2 (for the components U_1 and U_2) refers to its off-diagonal elements. Their physical content discloses by looking at the meaning of the components of the Bloch vector: U_3 describes the population inversion of the two-level system, which decays with T_1 , the *population lifetime*, while $U_{1,2}$, describing the phase-coherent polarization of the two-level system, decay with the *phase relaxation, dephasing or decoherence time* T_2 . Dephasing takes place not only by scattering processes with phonons, lattice defects, and other electronic excitations, but also by electron–hole recombination. If, besides the latter, which is the only process contributing to T_1 , no other processes contribute to T_2 , then $T_2 = 2T_1$, because the number of electron–hole pairs is proportional to $\mathbf{P}^2 \sim \exp(-2t/T_2)$. Including all other processes leads to the relation $T_2 \leq 2T_1$.

10.7 Semiconductor Bloch Equations

In order to include the particle interaction $\mathcal{H}_{\text{Coul}}$ it is convenient to introduce the electron–hole picture by replacing the Fermion operators according to $c_{c\mathbf{k}} \rightarrow \alpha_{\mathbf{k}}$ and $c_{v\mathbf{k}} \rightarrow \beta_{-\mathbf{k}}^\dagger$. With these modifications, making use of $E_n(\mathbf{k}) = E_n(-\mathbf{k})$ and replacing under the sum \mathbf{k} by $-\mathbf{k}$, the terms of the system Hamiltonian can be written as

$$\mathcal{H}_0 = \sum_{\mathbf{k}} \left(E_c(\mathbf{k})\alpha_{\mathbf{k}}^\dagger\alpha_{\mathbf{k}} + E_v(\mathbf{k})\beta_{\mathbf{k}}\beta_{\mathbf{k}}^\dagger \right) \tag{10.109}$$

$$\begin{aligned}
 \mathcal{H}_{\text{Coul}} &= \frac{1}{2} \sum_{\mathbf{k}, \mathbf{k}'; \mathbf{q} \neq 0} v_{\mathbf{q}} \left(\alpha_{\mathbf{k}+\mathbf{q}}^\dagger \alpha_{\mathbf{k}'-\mathbf{q}}^\dagger \alpha_{\mathbf{k}'} \alpha_{\mathbf{k}} + \beta_{\mathbf{k}-\mathbf{q}} \beta_{\mathbf{k}'+\mathbf{q}} \beta_{\mathbf{k}'}^\dagger \beta_{\mathbf{k}}^\dagger \right. \\
 &\quad \left. + 2\alpha_{\mathbf{k}+\mathbf{q}}^\dagger \beta_{\mathbf{k}'+\mathbf{q}} \beta_{\mathbf{k}'}^\dagger \alpha_{\mathbf{k}} \right)
 \end{aligned} \tag{10.110}$$

$$\mathcal{H}_{\text{Ap}} = -E(t) \sum_{\mathbf{k}} \left(d_{cv} \alpha_{\mathbf{k}}^\dagger \beta_{-\mathbf{k}}^\dagger + h.c. \right). \tag{10.111}$$

Bringing the hole operator terms into normal order one finds with

$$\begin{aligned} \sum_{\mathbf{k}, \mathbf{k}'; q \neq 0} v_q \beta_{\mathbf{k}-q} \beta_{\mathbf{k}'+q} \beta_{\mathbf{k}}^\dagger \beta_{\mathbf{k}'}^\dagger &= \sum_{\mathbf{k}, \mathbf{k}', q \neq 0} v_q \beta_{\mathbf{k}+q}^\dagger \beta_{\mathbf{k}'-q}^\dagger \beta_{\mathbf{k}'} \beta_{\mathbf{k}} \\ &+ 2 \sum_{q \neq 0} \sum_{\mathbf{k}} \beta_{\mathbf{k}}^\dagger \beta_{\mathbf{k}} - \sum_{\mathbf{k}; q \neq 0} v_q \end{aligned} \quad (10.112)$$

and single-particle energies $E_e(\mathbf{k}) = E_c(\mathbf{k})$ for electrons and $E_h(\mathbf{k}) = -E_v(\mathbf{k}) + \sum_{q \neq 0} v_q$ for holes

$$\begin{aligned} \mathcal{H}_0 + \mathcal{H}_{\text{Coul}} &= \sum_{\mathbf{k}} \left(E_e(\mathbf{k}) \alpha_{\mathbf{k}}^\dagger \alpha_{\mathbf{k}} + E_h(\mathbf{k}) \beta_{\mathbf{k}}^\dagger \beta_{\mathbf{k}} - \frac{1}{2} \sum_{q \neq 0} v_q \right) \\ &+ \frac{1}{2} \sum_{\mathbf{k}, \mathbf{k}'; q \neq 0} v_q \left(\alpha_{\mathbf{k}+q}^\dagger \alpha_{\mathbf{k}'-q}^\dagger \alpha_{\mathbf{k}'} \alpha_{\mathbf{k}} + \beta_{\mathbf{k}+q}^\dagger \beta_{\mathbf{k}'-q}^\dagger \beta_{\mathbf{k}'} \beta_{\mathbf{k}} \right. \\ &\left. - 2 \alpha_{\mathbf{k}+q}^\dagger \beta_{\mathbf{k}'-q}^\dagger \beta_{\mathbf{k}'} \alpha_{\mathbf{k}} \right). \end{aligned} \quad (10.113)$$

In the first part of this section, we have investigated the dynamics of the two-level system with an electron in the conduction band and a hole in the valence band by taking into account only the single-particle terms in the equation-of-motion of the density matrix. Now, we also consider the contribution of the particle interactions $\mathcal{H}'_{\text{Coul}}$ represented by the four-operator terms in (10.113). This is done in three steps. The first step is the calculation of the commutators between $\mathcal{H}'_{\text{Coul}}$ and the operators $\alpha_{\mathbf{k}}^\dagger \alpha_{\mathbf{k}}$, $\beta_{\mathbf{k}}^\dagger \beta_{\mathbf{k}}$, and $\alpha_{\mathbf{k}}^\dagger \beta_{-\mathbf{k}}^\dagger$ (Problem 10.8). In the second step, we replace the operator terms by their thermal expectation values. The two-operator terms $\langle \alpha_{\mathbf{k}}^\dagger \alpha_{\mathbf{k}} \rangle = f_{e\mathbf{k}}$ and $\langle \beta_{\mathbf{k}}^\dagger \beta_{\mathbf{k}} \rangle = f_{h\mathbf{k}}$ have the obvious meaning of electron and hole populations at wave vector \mathbf{k} , while $\langle \alpha_{\mathbf{k}}^\dagger \beta_{-\mathbf{k}}^\dagger \rangle = P_{\mathbf{k}}^*$ is the macroscopic polarization due to the applied external field. With the results of Problem 10.8, the equations of motion of these quantities take the following form [284]:

$$\begin{aligned} \frac{\partial}{\partial t} P_{\mathbf{k}}^*(t) &= i \frac{(E_e(\mathbf{k}) + E_h(\mathbf{k}))}{\hbar} P_{\mathbf{k}}^*(t) + i d_{cv}^* E^*(t) (f_{e\mathbf{k}}(t) + f_{h\mathbf{k}}(t) - 1) \\ &+ i \sum_{\mathbf{k}'; q \neq 0} v_q (\langle \alpha_{\mathbf{k}-q}^\dagger \alpha_{\mathbf{k}'+q}^\dagger \alpha_{\mathbf{k}'} \beta_{-\mathbf{k}}^\dagger \rangle - \langle \alpha_{\mathbf{k}}^\dagger \alpha_{\mathbf{k}'+q}^\dagger \alpha_{\mathbf{k}'} \beta_{-\mathbf{k}-q}^\dagger \rangle \\ &+ \langle \alpha_{\mathbf{k}}^\dagger \beta_{-\mathbf{k}-q}^\dagger \beta_{\mathbf{k}'+q}^\dagger \beta_{\mathbf{k}'} \rangle - \langle \alpha_{\mathbf{k}+q}^\dagger \beta_{\mathbf{k}'-q}^\dagger \beta_{\mathbf{k}'} \beta_{-\mathbf{k}}^\dagger \rangle), \end{aligned} \quad (10.114)$$

$$\begin{aligned} \frac{\partial}{\partial t} f_{e\mathbf{k}}(t) &= -2 \text{Im}(d_{cv} E(t) P_{\mathbf{k}}^*(t)) \\ &+ i \sum_{\mathbf{k}'; q \neq 0} v_q (\langle \alpha_{\mathbf{k}}^\dagger \alpha_{\mathbf{k}'-q}^\dagger \alpha_{\mathbf{k}-q} \alpha_{\mathbf{k}'} \rangle - \langle \alpha_{\mathbf{k}+q}^\dagger \alpha_{\mathbf{k}'-q}^\dagger \alpha_{\mathbf{k}} \alpha_{\mathbf{k}'} \rangle \\ &+ \langle \alpha_{\mathbf{k}}^\dagger \alpha_{\mathbf{k}-q}^\dagger \beta_{\mathbf{k}'-q}^\dagger \beta_{\mathbf{k}'} \rangle - \langle \alpha_{\mathbf{k}+q}^\dagger \alpha_{\mathbf{k}} \beta_{\mathbf{k}'-q}^\dagger \beta_{\mathbf{k}'} \rangle), \end{aligned} \quad (10.115)$$

$$\begin{aligned}
\frac{\partial}{\partial t} f_{h\mathbf{k}}(t) &= -2\text{Im}(d_{cv}E(t)P_{\mathbf{k}}^*(t)) \\
&+ i \sum_{\mathbf{k}'; \mathbf{q} \neq 0} v_{\mathbf{q}} (\langle \beta_{-\mathbf{k}}^\dagger \beta_{\mathbf{k}'-\mathbf{q}}^\dagger \beta_{-\mathbf{k}-\mathbf{q}} \beta_{\mathbf{k}'} \rangle - \langle \beta_{-\mathbf{k}+\mathbf{q}}^\dagger \beta_{\mathbf{k}'-\mathbf{q}}^\dagger \beta_{-\mathbf{k}} \beta_{\mathbf{k}'} \rangle \\
&+ \langle \alpha_{\mathbf{k}'+\mathbf{q}}^\dagger \alpha_{\mathbf{k}'}^\dagger \beta_{-\mathbf{k}}^\dagger \beta_{-\mathbf{k}+\mathbf{q}} \rangle - \langle \alpha_{\mathbf{k}'+\mathbf{q}}^\dagger \alpha_{\mathbf{k}'}^\dagger \beta_{-\mathbf{k}-\mathbf{q}}^\dagger \beta_{-\mathbf{k}} \rangle). \quad (10.116)
\end{aligned}$$

In the last step we factorize the expectation values of the four-operator terms into expectation values of two-operator terms, following the concept of the Hartree–Fock approximation (see Sect. 4.4). Only those products are considered whose factors are diagonal in the wave vector indices and thus, represent macroscopic expectation values. Let us take as an example:

$$\begin{aligned}
\langle \alpha_{\mathbf{k}-\mathbf{q}}^\dagger \alpha_{\mathbf{k}'-\mathbf{q}}^\dagger \alpha_{\mathbf{k}'} \beta_{-\mathbf{k}}^\dagger \rangle &= -\langle \alpha_{\mathbf{k}-\mathbf{q}}^\dagger \alpha_{\mathbf{k}'} \alpha_{\mathbf{k}'-\mathbf{q}}^\dagger \beta_{-\mathbf{k}}^\dagger \rangle \\
&+ \langle \alpha_{\mathbf{k}'-\mathbf{q}}^\dagger \alpha_{\mathbf{k}'} \alpha_{\mathbf{k}-\mathbf{q}}^\dagger \beta_{-\mathbf{k}}^\dagger \rangle \quad (10.117)
\end{aligned}$$

The two terms can be factorized into products of macroscopic expectation values appearing in the equations of motion to give

$$\begin{aligned}
\langle \alpha_{\mathbf{k}-\mathbf{q}}^\dagger \alpha_{\mathbf{k}'-\mathbf{q}}^\dagger \alpha_{\mathbf{k}'} \beta_{-\mathbf{k}}^\dagger \rangle &\simeq -\delta_{\mathbf{k}-\mathbf{q}, \mathbf{k}'} \underbrace{\langle \alpha_{\mathbf{k}-\mathbf{q}}^\dagger \alpha_{\mathbf{k}-\mathbf{q}} \rangle}_{f_{e\mathbf{k}-\mathbf{q}}} \underbrace{\langle \alpha_{\mathbf{k}'}^\dagger \beta_{-\mathbf{k}}^\dagger \rangle}_{P_{\mathbf{k}}^*} \\
&+ \delta_{\mathbf{q}, 0} \langle \alpha_{\mathbf{k}'}^\dagger \alpha_{\mathbf{k}'} \rangle \langle \alpha_{\mathbf{k}}^\dagger \beta_{-\mathbf{k}}^\dagger \rangle, \quad (10.118)
\end{aligned}$$

where the last term does not contribute under the sum over \mathbf{q} because $\mathbf{q} = 0$ is excluded. In the same way, one finds

$$\langle \alpha_{\mathbf{k}}^\dagger \alpha_{\mathbf{k}'-\mathbf{q}}^\dagger \alpha_{\mathbf{k}-\mathbf{q}} \alpha_{\mathbf{k}'} \rangle \simeq (\delta_{\mathbf{k}, \mathbf{k}'} - \delta_{\mathbf{q}, 0}) f_{e\mathbf{k}}(t) f_{e\mathbf{k}'}(t), \quad (10.119)$$

where the second term does not contribute under the sum over $\mathbf{q} \neq 0$. The neglected terms represent collision terms, while the remaining ones give the following set of equations

$$\begin{aligned}
\frac{\partial}{\partial t} P_{\mathbf{k}}(t) &= -i(\epsilon_{e\mathbf{k}} + \epsilon_{h\mathbf{k}})P_{\mathbf{k}}(t) \\
&- i \frac{f_{e\mathbf{k}}(t) + f_{h\mathbf{k}}(t) - 1}{\hbar} \left[d_{cv}E(t) + \sum_{\mathbf{q} \neq 0} v_{\mathbf{q}} P_{\mathbf{k}-\mathbf{q}}(t) \right] \quad (10.120)
\end{aligned}$$

$$\frac{\partial}{\partial t} f_{e\mathbf{k}}(t) = -\frac{2}{\hbar} \text{Im} \left\{ \left[d_{cv}E(t) + \sum_{\mathbf{q} \neq 0} v_{\mathbf{q}} P_{\mathbf{k}-\mathbf{q}}(t) \right] P_{\mathbf{k}}^*(t) \right\} \quad (10.121)$$

$$= \frac{\partial}{\partial t} f_{h\mathbf{k}}(t). \quad (10.122)$$

Here $\hbar\epsilon_{i\mathbf{k}} = E_n(\mathbf{k}) + \Sigma_i(\mathbf{k})$, $i = e, h$ are the renormalized single-particle energies with the self-energy

$$\Sigma_i(\mathbf{k}) = -\sum_{\mathbf{q}} v_{|\mathbf{k}-\mathbf{q}|} f_{i\mathbf{q}}. \quad (10.123)$$

We introduce the generalized Rabi frequency

$$\omega_{R,\mathbf{k}}(t) = \frac{1}{\hbar} \left[d_{cv} E(t) + \sum_{\mathbf{q} \neq \mathbf{k}} v_{|\mathbf{k}-\mathbf{q}|} P_{\mathbf{q}}(t) \right], \quad (10.124)$$

which combines the applied field with the dipole field of the generated electron–hole pairs, and arrive at the *semiconductor Bloch equations*:

$$\frac{\partial}{\partial t} P_{\mathbf{k}}(t) = -i(\epsilon_{e\mathbf{k}} + \epsilon_{h\mathbf{k}}) P_{\mathbf{k}}(t) - i(f_{e\mathbf{k}}(t) + f_{h\mathbf{k}}(t) - 1) \omega_{R,\mathbf{k}}(t) \quad (10.125)$$

$$\frac{\partial}{\partial t} f_{e\mathbf{k}}(t) = -2\text{Im}(\omega_{R,\mathbf{k}}(t) P_{\mathbf{k}}^*(t)) = \frac{\partial}{\partial t} f_{h\mathbf{k}}(t). \quad (10.126)$$

For $v_{\mathbf{q}} \rightarrow 0$, i.e., when switching off the Coulomb interaction, these equations reduce to the optical Bloch equations.

In spite of their simple form, these equations describe the rather complex dynamics of electron–hole pair excitations in that they include many-body effects within the Hartree–Fock approximaton. This results in the renormalization of the single-particle energies and of the Rabi frequency, but (with the population inversion factor) takes into account also the filling of the phase space by the occupation of the single-particle states due to the light–matter interaction. The occupied states (electrons in the conduction band and holes in the valence band) reduce the available phase space for further excitations because of the Pauli principle. This phase space filling is known as the Pauli blocking. The semiconductor Bloch equations and their extensions, including collision terms, are prerequisite in modelling nonlinear susceptibilities to describe data from time-resolved spectroscopy or in designing semiconductor lasers. Damping terms with longitudinal and transverse relaxation times $T_{1,2}$ can be added as in the optical Bloch equations and part of their microscopic origin can be calculated by considering the collision terms.

Problems

- 10.1 Show with the help of $\mathbf{p}/m = -i/\hbar[\mathbf{r}, H_0]$ that, in matrix representation with eigenstates of H_0 , the Ap -coupling term can be expressed (for resonant excitation) as $\mathbf{d}_{cv} \cdot \mathbf{E}$ with the dipole matrix element $\mathbf{d}_{cv} = -e\langle c0|\mathbf{r}|v0\rangle$ between band edge Bloch functions.
- 10.2 Make use of the Wannier representation (see Problem 6.2) to show that the momentum matrix element between Bloch functions is diagonal in the wave vector.
- 10.3 Make use of the solution of the hydrogen problem to express $|\phi_{\nu}(0)|^2$ in terms of a confluent hypergeometric function for positive and negative energies. Find the dependence of this expression for the bound states

in dependence on the quantum number n and calculate the absorption coefficient for the electron–hole continuum.

- 10.4 Formulate the exciton operators $B_{\nu, \mathbf{Q}}, B_{\nu, \mathbf{Q}}^\dagger$ in terms of products of fermion operators for electrons in the conduction and valence band. Calculate the commutator between the exciton operators and define the condition under which excitons can be considered as bosons.
- 10.5 Start with the phenomenological result of (10.42) close to an excitonic resonance at $E_{\nu 0} = \hbar\omega_{\nu 0}$ and express the LT-splitting of this exciton in terms of its oscillator strength! Consider the first term of the exchange interaction in (10.62) to calculate the LT-splitting as a perturbation correction to the (transverse) exciton energy $E_{\nu 0}$ and verify by comparison with the phenomenological result the expression for the exciton oscillator strength given in (10.43).
- 10.6 Make use of the expansion

$$\mathbf{A}(\mathbf{r}, t) = \sum_{\lambda, \boldsymbol{\kappa}} \left(\frac{\hbar}{2\varepsilon_0\omega(\boldsymbol{\kappa})V} \right)^{1/2} \mathbf{e}_{\lambda\boldsymbol{\kappa}} \left(a_{\lambda\boldsymbol{\kappa}}(t) + a_{\lambda\boldsymbol{\kappa}}^\dagger(t) \right) e^{i\boldsymbol{\kappa}\cdot\mathbf{r}} \quad (10.127)$$

of the vector potential in terms of Boson operators $a_{\lambda\boldsymbol{\kappa}}(t)$, where $\mathbf{e}_{\lambda\boldsymbol{\kappa}}, \lambda = 1, 2$ are transverse unit vectors with $\mathbf{e}_{\lambda\boldsymbol{\kappa}} \cdot \boldsymbol{\kappa} = 0$, to show that the Hamiltonian of the radiation field \mathcal{H}_{rad} takes the form

$$\mathcal{H}_{\text{rad}} = \sum_{\lambda, \boldsymbol{\kappa}} \hbar\omega(\boldsymbol{\kappa}) \left(a_{\lambda\boldsymbol{\kappa}}^\dagger a_{\lambda\boldsymbol{\kappa}} + \frac{1}{2} \right). \quad (10.128)$$

- 10.7 Make use of the equation of motion for the off-diagonal element of the density matrix under quasi-equilibrium condition to calculate the dielectric polarization $\mathbf{P}(t) = \text{Tr}(\rho_{cv}(\mathbf{k}, t)\mathbf{d}_{cv})$ and the dielectric susceptibility $\chi(\omega)$. Recover the result for the imaginary part of the dielectric function $\varepsilon_2(\omega)$ obtained in Sect. 10.2.
- 10.8 Calculate the commutators of $\mathcal{H}'_{\text{Coul}}$ with the operators $\alpha_{\mathbf{k}}^\dagger\alpha_{\mathbf{k}}, \beta_{\mathbf{k}}^\dagger\beta_{\mathbf{k}}$ and $\alpha_{\mathbf{k}}^\dagger\beta_{-\mathbf{k}}^\dagger$ to verify (10.114...116).

A

Appendices

A.1 Elements of Group Theory

Geometrical operations (translation, rotation, inversion), which leave a geometrical object (here, the crystal lattice) invariant, are symmetry operations. Mathematically, they form a group, the symmetry group of the crystal: for the translations it is the *translation group*, for the rotations, inversion, and their combinations it is the *point group*. The number g of elements in the group is its order. The symmetry of a system implies the invariance of the system Hamiltonian H (be it for phonons, electrons, or magnons) under unitary operations corresponding to the geometrical operations of the symmetry group. These unitary operations form a group which is isomorphic to the symmetry group. When applied to a set of eigenfunctions of H , this set is transformed into another set of eigenfunctions, which can be represented as a linear combination of the former ones. The eigenfunctions of a degenerate eigenvalue transform among each other and form an invariant subspace in the Hilbert space of H . In a chosen basis, these unitary operations can be formulated as matrices which define another group isomorphic to the symmetry group. For a proper choice of the basis, all matrices of the matrix representation have block-diagonal form with the dimension of the block matrices indicating the degeneracy of the invariant subspaces. These subspaces, spanned by the set of degenerate eigenfunctions, can be classified by characteristic properties of the corresponding block matrices using the *character tables* of the symmetry group and the concept of *irreducible representations* [47–50].

The symmetry classification of eigenstates is the simplest for the translation group and finds its expression in Bloch's theorem. A translation operator $T_{\mathbf{R}}$ applied to a Bloch function $\psi_{\mathbf{k}}(\mathbf{r})$ yields

$$T_{\mathbf{R}}\psi_{\mathbf{k}}(\mathbf{r}) = \psi_{\mathbf{k}}(\mathbf{r} + \mathbf{R}) = e^{-i\mathbf{k}\cdot\mathbf{R}}\psi_{\mathbf{k}}(\mathbf{r}) \quad (\text{A.1})$$

i.e., it multiplies the Bloch function by a phase factor depending on the wave vector \mathbf{k} and the translation \mathbf{R} . Owing to the fact that translations

commute with each other (the translation group is Abelian), there are only one-dimensional representations, namely the phase factors.

The spherical symmetry of the Coulomb potential leads to the angular momentum classification of the eigenstates of an atom. For the hydrogen problem, we have the $(2l + 1)$ -fold states with angular momentum l . They transform under rotations with the corresponding $(2l + 1) \times (2l + 1)$ matrices $D^l(\alpha, \beta, \gamma)$, which form a $(2l + 1)$ -dimensional irreducible representation of the full rotation group. The group elements depend continuously on the parameters α, β , and γ which define the group element by the three Euler angles.

In contrast with the full rotation group (which is infinite and continuous) the point groups of crystal lattices are finite and discrete. For example, the symmetry group of a cube, O_h , is the same as that of the sc, bcc, and fcc lattices. It consists of 48 elements: the identity (E), three axes with fourfold rotations (C_4, C_4^2), four axes with threefold rotations (C_3), six axes with twofold rotations (C_2), and all these operations combined with the inversion (J). In general, the elements of the point group do not commute (the group is non-Abelian). However, the point group falls into disjunct classes of conjugated elements, where group elements A and B are called conjugated to each other if the relation $A = XBX^{-1}$ holds for all X of the group. For the cubic point group there are 10 classes:

$$E, 3C_4^2, 6C_4, 8C_3, 6C_2, J, 3JC_4^2, 6JC_4, 8JC_3, 6JC_2 \quad (\text{A.2})$$

where the numbers in front of the symbols for the symmetry operations give the number of group elements belonging to the class.

Consider now the block matrices that transform the degenerate invariant subspaces. They are d dimensional irreducible representations of the symmetry group. Different irreducible representations with the same dimension d , $D(X), D'(X)$, are equivalent if there is a d dimensional matrix M with $\|M\| \neq 0$ and $D(X) = MD'(X)M^{-1}$ for all elements X of the group. Note, that with respect to this operation with M , the coefficients of the characteristic polynomial of $D(X)$, especially the trace of $D(X)$ or the *character*, do not change. Thus, inequivalent irreducible representations can be distinguished by looking at their characters. Similarly for the operation of conjugation: all matrices of an irreducible representation belonging to a class have the same character. This leads to the character table listing the characters of the inequivalent irreducible representations for the different classes of conjugated elements. These irreducible representations play the same role in classifying the eigenstates of H with respect to the point group as the crystal momentum \mathbf{k} does for the translation group and the angular momentum l for the rotation group. Their meaning is that of quantum numbers due to the underlying symmetry. Already knowing the classes, it remains now to specify the number of the inequivalent irreducible representations and their dimensions.

According to the theorems of the theory of finite groups, the number of classes equals the number of irreducible representations, i.e., the character table has the same number of rows and columns. Moreover, the sum over the

squared dimensions of the irreducible representations (which is the sum of the characters for the class containing the identity E , because it is represented by d -dimensional unit matrices) must be equal to the order g of the group. As it turns out, the order of the cubic symmetry group can be decomposed only in one way into 10 squared integers:

$$48 = 2(1^2 + 1^2 + 2^2 + 3^2 + 3^2), \tag{A.3}$$

i.e., the group has four one-dimensional, two two-dimensional, and four three-dimensional irreducible representations. As the inversion J is an element of the group, the eigenstates can be classified as having even or odd parity. This is considered in the notation of the irreducible representations by a \pm or g, u (for *gerade* or *ungerade*). Another remarkable property of the character table is that the rows and columns understood as vectors are orthogonal to each other when properly weighted with the number of elements in a class. These are the famous orthogonality relations of the characters.

Different notations are in use for the irreducible representations of the cubic point group O_h (see the character table). The notation with the symbols $A, E,$ and T for one-, two-, and three-dimensional representations, respectively, is applied to characterize localized (e.g., impurity) states of the given point symmetry, while the notation with the symbol Γ refers to the Bloch states at the center of the Brillouin zone with $\mathbf{k} = (0, 0, 0)$. (Note, that this wave vector does not change under the symmetry operations and therefore, the group of this wave vector is the point group of the crystal.) Of the two different notations with the symbol Γ the one with double indices is the older one and indicates the removal of the level degeneracy for finite \mathbf{k} . These symbols are found e.g., in some figures of Chaps. 5 and 9.

Character table of the point group O_h												
			E	$3C_4^2$	$8C_3$	$6C_4$	$6C_2$	J	$3JC_4^2$	$8JC_3$	$6JC_4$	$6JC_2$
A_{1g}	Γ_1^+	Γ_1^+	1	1	1	1	1	1	1	1	1	1
A_{2g}	Γ_2^+	Γ_2^+	1	1	1	-1	-1	1	1	1	-1	-1
E_g	Γ_3^+	Γ_{12}^+	2	2	-1	0	0	2	2	-1	0	0
T_{1g}	Γ_4^+	Γ_{15}^+	3	-1	0	1	-1	3	-1	0	1	-1
T_{2g}	Γ_5^+	Γ_{25}^+	3	-1	0	-1	1	3	-1	0	-1	1
A_{1u}	Γ_1^-	Γ_1^-	1	1	1	1	1	-1	-1	-1	-1	-1
A_{2u}	Γ_2^-	Γ_2^-	1	1	1	-1	-1	-1	-1	-1	1	1
E_u	Γ_3^-	Γ_{12}^-	2	2	-1	0	0	-2	-2	1	0	0
T_{1u}	Γ_4^-	Γ_{15}^-	3	-1	0	1	-1	-3	1	0	-1	1
T_{2u}	Γ_5^-	Γ_{25}^-	3	-1	0	-1	1	-3	1	0	1	-1

It is quite instructive to specify objects (wave functions, operators) that transform according to these irreducible representations. Using the fact, that

the crystal point groups are subgroups of the full rotation group, this can be done by formulating the spherical harmonics in Cartesian coordinates to find the so-called cubic harmonics, which for $l = 0, 1, 2, 3$ are given by

$$\begin{aligned}
 l = 0 &\rightarrow 1 (\Gamma_1^+) \\
 l = 1 &\rightarrow x, y, z (\Gamma_4^-) \\
 l = 2 &\rightarrow z^2 - \frac{1}{2}(x^2 + y^2), x^2 - y^2 (\Gamma_3^+); yz, zx, xy (\Gamma_5^+) \\
 l = 3 &\rightarrow xyz (\Gamma_2^-); z(x^2 - y^2), x(y^2 - z^2), y(z^2 - x^2) (\Gamma_5^-).
 \end{aligned}$$

Thus, the fivefold degeneracy of the $l = 2$ spherical harmonics splits under the reduced symmetry of the cubic point group into a twofold (Γ_3^+) and a threefold level (Γ_5^+), which is the crystal field splitting discussed in Sect. 5.5 and Problem 5.8. Of the seven spherical harmonics with $l = 3$ only four appear in this list, while the remaining three are cubic harmonics which transform as Γ_4^- , i.e., the cubic crystal field causes a mixing of angular momentum states with $l = 1$ and 3.

The point group T_d of the zinc blende lattice is a subgroup of O_h and contains the classes E , $3C_4^2$, $8C_3$, $6JC_4$, and $6JC_2$. Consequently, the number of irreducible representations is reduced to five. Considering only the corresponding columns in the character table of O_h , we find identical rows for pairs of representations which merge into one irreducible representation of T_d . Thus, the character table of T_d is obtained from that of O_h . Note that T_d does not contain the inversion J and eigenstates cannot be classified by parity.

Character table of the point group T_d						
		E	$3C_4^2$	$8C_3$	$6JC_4$	$6JC_2$
A_1	$\Gamma_1 \Gamma_1$	1	1	1	1	1
A_2	$\Gamma_2 \Gamma_2$	1	1	1	-1	-1
E	$\Gamma_3 \Gamma_{12}$	2	2	-1	0	0
T_1	$\Gamma_4 \Gamma_{15}$	3	-1	0	1	-1
T_2	$\Gamma_5 \Gamma_{25}$	3	-1	0	-1	1

The crystal momentum \mathbf{k} is a good quantum number. Thus, for finite \mathbf{k} the eigenstates have to be classified by the irreducible representations of the group of the wave vector, consisting of all elements of the crystal point group which do not change \mathbf{k} . For $\mathbf{k} \parallel (1, 0, 0)$ or along the Δ -axis of the Brillouin zone the cubic point group O_h reduces to C_{4v} with eight elements in five classes, and T_d to C_{2v} with four elements each in one class. Decomposing $8 = 1 + 1 + 1 + 1 + 2^2$ gives the dimensions of the five irreducible representations of C_{4v} , while (obviously) C_{2v} has four one-dimensional representations. The notation of the irreducible representations reminds of the Δ -axis. The group of the wave vector along $(1, 0, 0)$ keeps x unchanged while y and z change. Thus, x transforms as Δ_1 , while for C_{4v} y and z transform into each other like Δ_5 and

the threefold states of symmetry Γ_4^- split into $\Delta_1 + \Delta_5$ (which is considered the notation Γ_{15}^-). This explains the splitting of the phonon dispersion curves (Chap. 3) and of the energy bands (Chap. 5) away from the Γ point. For C_{2v} , y and z transform according to different irreducible representations Δ_3, Δ_4 but due to time invariance these states are degenerate. Similar considerations hold for the other directions in \mathbf{k} space.

C_{4v}	E	C_4^2	$2C_4$	$2JC_4^2$	$2JC_2$
Δ_1	1	1	1	1	1
Δ_2	1	1	1	-1	-1
Δ_3	1	1	-1	1	-1
Δ_4	1	1	-1	-1	1
Δ_5	2	-2	0	0	0

C_{2v}	E	C_4^2	JC_2	JC_2'
Δ_1	1	1	1	1
Δ_2	1	-1	1	-1
Δ_3	1	1	-1	-1
Δ_4	1	-1	-1	1

A.2 Fourier Series and Fourier Transforms

Consider a function $f(x)$ defined in the interval $-L/2 \leq x \leq +L/2$ or a periodic function $f(x+L) = f(x)$. It can be represented by the Fourier series

$$f(x) = \sum_{n=-\infty}^{+\infty} F_{k_n} e^{ik_n x}, \quad \text{with } k_n = \frac{2n\pi}{L}, \quad n \text{ integer.} \tag{A.4}$$

The Fourier coefficients are given by

$$F_{k_n} = \frac{1}{L} \int_{-L/2}^{+L/2} f(x) e^{-ik_n x} dx. \tag{A.5}$$

If the length L is taken as the linear extension of a solid and $f(x)$ as a wave function describing some state of the solid, the periodicity of $f(x)$ reflects the reasonable assumption that the physical properties connected with this state repeat with the period L or, what is equivalent, that they do not depend on L . This is the concept of periodic boundary conditions.

The Fourier series expansion makes use of the fact that complex exponentials are normalized and orthogonal, i.e.,

$$\frac{1}{L} \int_{-L/2}^{+L/2} e^{-ik_m x} e^{ik_n x} dx = \delta_{mn}, \tag{A.6}$$

and that they form a complete set on the interval of length L :

$$\frac{1}{L} \sum_n e^{ik_n(x-x')} = \delta(x-x'). \tag{A.7}$$

In the limit $L \rightarrow \infty$ the discrete k_n become the k space variable and (A.5) the Fourier transform

$$F(k) = \frac{1}{2\pi} \int_{-\infty}^{+\infty} f(x) e^{-ikx} dx. \quad (\text{A.8})$$

In generalizing to the three-dimensional case we may write

$$f(\mathbf{r}) = \sum_{\mathbf{k}} F_{\mathbf{k}} e^{i\mathbf{k} \cdot \mathbf{r}}, \quad (\text{A.9})$$

where the components of the wave vector \mathbf{k} can take the values $k_i = 2\pi n_i/L_i$, $i = 1, 2, 3$ with integer n_i , i.e., the sum over \mathbf{k} is to be understood as the triple sum over all integer values of n_i . The orthogonality and normalization of the complex exponentials is expressed as

$$\frac{1}{V} \int_V e^{i(\mathbf{k}-\mathbf{k}') \cdot \mathbf{r}} d^3\mathbf{r} = \delta_{\mathbf{k}, \mathbf{k}'}, \quad (\text{A.10})$$

and the completeness as

$$\frac{1}{V} \sum_{\mathbf{k}} e^{i\mathbf{k}(\mathbf{r}-\mathbf{r}')} = \delta(\mathbf{r} - \mathbf{r}'), \quad (\text{A.11})$$

where $V = L_1 L_2 L_3$ is the periodicity or crystal volume. The Fourier coefficients take the form

$$F_{\mathbf{k}} = \frac{1}{V} \int_V f(\mathbf{r}) e^{-i\mathbf{k} \cdot \mathbf{r}} d^3\mathbf{r}. \quad (\text{A.12})$$

In this book, discreteness of the \mathbf{k} resulting from the finite volume V is frequently used. Nevertheless, we shall denote $F_{\mathbf{k}}$ as the Fourier transform of $f(\mathbf{r})$. On the other hand, the discrete sum over \mathbf{k} can be evaluated as an integral with the replacement

$$\sum_{\mathbf{k}} \Rightarrow \frac{V}{(2\pi)^3} \int d^3\mathbf{k}, \quad (\text{A.13})$$

where $(2\pi)^3/V$ is the volume for each discrete \mathbf{k} . Let us take $f(\mathbf{r}) = 1/|\mathbf{r}|$ as an example by showing that

$$\frac{1}{r} = \frac{1}{V} \sum_{\mathbf{k}} \frac{4\pi}{k^2} e^{i\mathbf{k} \cdot \mathbf{r}}. \quad (\text{A.14})$$

This is done in the following steps. First, we carry out the summation over \mathbf{k} on the *rhs* as an integral in spherical polar coordinates

$$\frac{1}{V} \sum_{\mathbf{k}} \frac{4\pi}{k^2} e^{i\mathbf{k} \cdot \mathbf{r}} = \frac{V}{(2\pi)^3} \frac{4\pi}{V} \int_0^{2\pi} d\phi \int_0^\pi d\theta \sin \theta \int_0^\infty dk e^{ikr \cos \theta}. \quad (\text{A.15})$$

The integration over ϕ gives a factor 2π and the integration over θ can be performed with the substitution $\cos \theta = z$

$$\dots = \frac{1}{\pi} \int_0^\infty dk \int_{-1}^{+1} dz e^{ikrz} = \frac{1}{\pi} \int_0^\infty dk \frac{1}{ikr} (e^{ikr} - e^{-ikr}). \quad (\text{A.16})$$

With the substitution $x = kr$ and by writing the complex exponentials as the sin-function, we find

$$\dots = \frac{2}{\pi} \frac{1}{r} \int_0^\infty dx \frac{\sin x}{x}. \quad (\text{A.17})$$

The last integral gives $\pi/2$ and we arrive at the *lhs* of (A.14).

A.3 Fermi and Bose Integrals

Frequently, physical quantities of fermion systems are expressed in terms of integrals of the form

$$I_\alpha(\mu, T) = \int_0^\infty E^\alpha f(E, \mu, T) dE, \quad (\text{A.18})$$

with the Fermi–Dirac distribution function

$$f(E, \mu, T) = \frac{1}{e^{(E-\mu)/k_B T} + 1}. \quad (\text{A.19})$$

Examples are the particle density n and the ground state energy $E_0(T)$ of free electrons in Sect. 4.1 with $\alpha = 1/2$ and $\alpha = 3/2$, respectively. By substituting $x = E/k_B T$ and $\eta = \mu/k_B T$ the integral $I_\alpha(\mu, T)$ can be written

$$I_\alpha(\mu, T) = (k_B T)^{\alpha+1} \Gamma(\alpha + 1) F_\alpha(\eta), \quad (\text{A.20})$$

with the Gamma function or Euler integral

$$\Gamma(\alpha) = \int_0^\infty t^{\alpha-1} e^{-t} dt, \quad \text{Re} \alpha > 0 \quad (\text{A.21})$$

and the *Fermi integral* of index α [244, 245, 292]

$$F_\alpha(\eta) = \frac{1}{\Gamma(\alpha + 1)} \int_0^\infty \frac{x^\alpha}{e^{x-\eta} + 1} dx. \quad (\text{A.22})$$

In a three-dimensional system, one has for the particle density (with $\Gamma(3/2) = \sqrt{\pi}/2$)

$$n = \int_0^\infty D(E) f(E, \mu, T) dE = 2 \left(\frac{mk_B T}{2\pi\hbar^2} \right)^{3/2} F_{1/2} \left(\frac{\mu}{k_B T} \right), \quad (\text{A.23})$$

because the density of states $D(E) \sim E^{1/2}$, while the ground state energy can be written (with $\Gamma(5/2) = 3\sqrt{\pi}/4$)

$$\begin{aligned} E_0(T) &= \int_0^\infty ED(E)f(E, \mu, T)dE \\ &= 3 \left(\frac{m}{2\pi\hbar^2} \right)^{3/2} (k_B T)^{5/2} F_{3/2} \left(\frac{\mu}{k_B T} \right). \end{aligned} \quad (\text{A.24})$$

Sometimes also integrals of the form

$$J(\mu, T) = \int_0^\infty \phi(E) \frac{d}{dE} f(E, \mu, T). \quad (\text{A.25})$$

appear [245], e.g., in the transport relaxation times for different scattering processes in Sect. 8.3. For the derivative of the Fermi–Dirac distribution function we may write with $x = (E - \mu)/k_B T$,

$$\frac{df}{dE} = \frac{1}{k_B T} \frac{df}{dx} = -\frac{1}{k_B T} (e^x + 1)^{-1} (e^{-x} + 1)^{-1}, \quad (\text{A.26})$$

which has a pronounced maximum at $x = 0$. Expand the function $\phi(E)$ (which is assumed to be smooth) around $x = 0$ or $E = \mu$

$$\phi(E) = \phi(\mu + xk_B T) = \sum_{n=0}^{\infty} \frac{(k_B T)^n}{n} \phi^{(n)}(\mu) x^n, \quad (\text{A.27})$$

with $\phi^{(n)}(\mu)$ being the n th derivative, to obtain (with $dE = k_B T dx$)

$$J(\mu, T) = \sum_{n=0}^{\infty} \frac{(k_B T)^n}{n} \phi^{(n)}(\mu) \int_{-\mu/k_B T}^{\infty} x^n \frac{df}{dx} dx. \quad (\text{A.28})$$

For $\mu \gg k_B T$, the lower limit of the integral tends to $-\infty$ and one defines

$$J_n = \int_{-\infty}^{\infty} x^{n-1} \frac{df}{dx} dx. \quad (\text{A.29})$$

Because df/dx is an even function, all integrals J_n with even n vanish. For odd n we obtain

$$J_1 = \int_{-\infty}^{\infty} f'(x) dx = -1 \quad (\text{A.30})$$

$$\begin{aligned} J_3 &= \int_{-\infty}^{\infty} x^2 f'(x) dx = -2 \int_0^{\infty} \frac{x^2 e^{-x}}{(1 + e^{-x})^2} dx \\ &= -4 \sum_{k=0}^{\infty} \frac{(-1)^k}{(k+1)^2} = -\frac{\pi^2}{3} \end{aligned} \quad (\text{A.31})$$

(for the last see [293]). Thus, one obtains

$$J(\mu, T) = -\phi(\mu) - \frac{\pi^2}{6}(k_{\text{B}}T)^2\phi''(\mu) + \dots \quad (\text{A.32})$$

For $\mu = 0$ the Fermi integral is given in closed form by [293]

$$\int_0^\infty \frac{x^{\nu-1}}{e^x + 1} dx = (1 - 2^{1-\nu})\Gamma(\nu)\zeta(\nu), \quad \text{Re}\nu > 0 \quad (\text{A.33})$$

and the corresponding Bose integral by

$$\int_0^\infty \frac{x^{\nu-1}}{e^x - 1} dx = \Gamma(\nu)\zeta(\nu), \quad \text{Re}\nu > 1 \quad (\text{A.34})$$

with the Γ -function and Riemann's zeta-function

$$\zeta(z) = \sum_{n=1}^\infty \frac{1}{n^z}, \quad \text{Re}z > 1. \quad (\text{A.35})$$

A.4 Sommerfeld Expansion

In connection with electronic properties, integrals of the form

$$I(T) = \int_{-\infty}^{+\infty} g(E)f(E, \mu, T)dE \quad (\text{A.36})$$

have to be evaluated frequently, where $f(E, \mu, T)$ is the Fermi–Dirac distribution function. Special cases are: the number of electrons in occupied states (with $g(E) = D(E)$, the density of states) and the total energy of these electrons (with $g(E) = ED(E)$). In these cases, the evaluation of the integral is possible if $g(E)$ fulfills the following conditions: (1) it should not be singular for $E \simeq E_{\text{F}}$, (2) it should vanish for $E \rightarrow -\infty$, and (3) it should diverge for $E \rightarrow +\infty$ not stronger than some power in E . These conditions allow to write the integral (A.36) in the form of a series

$$I(T) = \int_{-\infty}^{\mu} g(E)dE + \sum_{n=1}^{\infty} \alpha_n (k_{\text{B}}T)^{2n} g^{(2n-1)}(\mu), \quad (\text{A.37})$$

where $g^{(2n-1)}(\mu)$ is the $(2n - 1)$ th derivative of $g(E)$ taken at the chemical potential μ . The coefficients α_n are determined by Riemann's zeta function

$$\alpha_n = 2 \left(1 - \frac{1}{2^{2n-1}} \right) \zeta(2n), \quad \zeta(n) = \sum_{p=1}^{\infty} \frac{1}{p^n}. \quad (\text{A.38})$$

This expansion, originally derived in [109], is known as the *Sommerfeld expansion*.

The validity of (A.36) can be demonstrated as follows: Define a function $p(E)$ whose derivative is $g(E)$ or

$$p(E) = \int_{-\infty}^E g(x) dx \quad \longleftrightarrow \quad g(E) = \frac{dp(E)}{dE} \quad (\text{A.39})$$

and write the integral (A.36) as

$$\begin{aligned} I(T) &= \int_{-\infty}^{+\infty} \frac{dp(E)}{dE} f(E, \mu, T) dE \\ &= p(E) f(E, \mu, T) \Big|_{-\infty}^{+\infty} - \int_{-\infty}^{+\infty} p(E) \frac{df(E, \mu, T)}{dE} dE. \end{aligned} \quad (\text{A.40})$$

Making use of the Taylor expansion of $p(E)$ about μ

$$p(E) = p(\mu) + \sum_{n=1}^{\infty} \frac{(E - \mu)^n}{n!} p^{(n)}(\mu) \quad (\text{A.41})$$

and of the fact that the derivative of the Fermi–Dirac distribution function (with $\beta = 1/k_B T$)

$$\frac{df(E, \mu, T)}{dE} = -\frac{\beta e^{\beta(E-\mu)}}{(1 + e^{\beta(E-\mu)})^2} = \frac{-\beta}{4 \cosh^2(\beta(E - \mu)/2)} \quad (\text{A.42})$$

is an even function in $E - \mu$, this can be written

$$I(T) = \int_{-\infty}^{\mu} g(E) dE + \beta \sum_{n=1}^{\infty} \frac{1}{2n!} g^{(2n-1)}(\mu) I_{2n}(T), \quad (\text{A.43})$$

where

$$\begin{aligned} I_{2n}(T) &= \int_{-\infty}^{+\infty} (E - \mu)^{2n} \frac{\exp(\beta(E - \mu))}{(\exp(\beta(E - \mu)) + 1)^2} dE, \quad x = \beta(E - \mu) \\ &= \beta^{-(2n-1)} \int_{-\infty}^{+\infty} x^{2n} \frac{e^x}{(e^x + 1)^2} dx \\ &= -2\beta^{-(2n-1)} \left[\frac{d}{d\lambda} \int_0^{\infty} \frac{x^{2n-1}}{\exp(\lambda x) + 1} dx \right]_{\lambda=1}, \quad \lambda x = u \\ &= -2\beta^{-(2n-1)} \left[\frac{d}{d\lambda} \lambda^{-2n} \int_0^{\infty} \frac{u^{2n-1}}{e^u + 1} du \right]_{\lambda=1} \\ &= 4n\beta^{-(2n-1)} \int_0^{\infty} \frac{u^{2n-1}}{e^u + 1} du \\ &= 2 \left(1 - \frac{1}{2^{2n-1}} \right) (2n)! \zeta(2n) \beta^{-(2n-1)}. \end{aligned} \quad (\text{A.44})$$

Thus, we arrive at the expression (A.37).

Usually $g(E)$ is a power function and each derivative means a division by μ . As a consequence, subsequent terms in the series decrease by a factor $(k_B T/\mu)^2$ and for $k_B T \ll \mu$ fast convergence is achieved. The coefficients of the leading terms take the values

$$\alpha_1 = \zeta(2) = \frac{\pi^2}{6} \quad \text{and} \quad \alpha_2 = \frac{7\pi^4}{360}. \quad (\text{A.45})$$

A.5 Calculation of the Exchange Energy

The sums over \mathbf{q} and \mathbf{p} can be performed as integrals over the Fermi sphere after replacing $|\mathbf{p} - \mathbf{q}|$ with the cosine relation

$$\begin{aligned} E_{\text{exch}} &= - \sum_{\substack{\mathbf{q}, \mathbf{p}, \mathbf{q} \neq \mathbf{p} \\ |\mathbf{q}|, |\mathbf{p}| \leq k_F}} \frac{e^2}{\varepsilon_0 V |\mathbf{q} - \mathbf{p}|^2} \\ &= - \frac{e^2}{\varepsilon_0 V} \frac{V_c^2}{(2\pi)^6} \int \int_{|\mathbf{p}|, |\mathbf{q}| \leq k_F} d^3 \mathbf{q} d^3 \mathbf{p} \frac{1}{p^2 + q^2 - 2pq \cos \vartheta}, \end{aligned} \quad (\text{A.46})$$

where ϑ is the angle between \mathbf{q} and \mathbf{p} . The square root of the integrand is known as the generating function of Legendre's polynomials, i.e.,

$$\frac{1}{(1 + x^2 - 2x \cos \vartheta)^{1/2}} = \sum_{L=0}^{\infty} x^L P_L(\cos \vartheta), \quad x < 1. \quad (\text{A.47})$$

In the double integral we have to distinguish $p < q$ ($x = p/q$) and $p > q$ ($x = q/p$), which gives two identical contributions, and we can write

$$\begin{aligned} E_{\text{exch}} &= - \frac{e^2}{\varepsilon_0 (2\pi)^6} 2V \int_{|\mathbf{p}| < k_F} d^3 \mathbf{p} \int_{q < p} 2\pi q^2 dq \frac{1}{p^2} \sum_{LL'} \left(\frac{q}{p}\right)^{L+L'} \\ &\quad \times \int_0^\pi d \cos \vartheta P_L(\cos \vartheta) P_{L'}(\cos \vartheta). \end{aligned} \quad (\text{A.48})$$

The integral over ϑ is performed by making use of the orthogonality of the Legendre polynomials to obtain

$$E_{\text{exch}} = - \frac{e^2 V}{\pi \varepsilon_0 (2\pi)^4} \int_{|\mathbf{p}| < k_F} d^3 \mathbf{p} \sum_L \frac{2}{2L+1} \int_0^p \left(\frac{q}{p}\right)^{2L+2} dq. \quad (\text{A.49})$$

The integral over q yields $p/(2L+3)$ and allows one to perform the integral over \mathbf{p} in spherical polar coordinates:

$$E_{\text{exch}} = - \frac{e^2 V}{\pi \varepsilon_0 (2\pi)^4} \sum_L \frac{2}{(2L+1)(2L+3)} 4\pi \frac{k_F^4}{4}. \quad (\text{A.50})$$

Summing over L with the help of

$$\sum_{L=0}^{\infty} \frac{1}{(2L+1)(2L+3)} = \frac{1}{2} \sum_{L=0}^{\infty} \left(\frac{1}{2L+1} - \frac{1}{2L+3} \right) = \frac{1}{2}, \quad (\text{A.51})$$

we eventually find

$$E_{\text{exch}} = - \sum_{\substack{\mathbf{q}, \mathbf{p}, \mathbf{q} \neq \mathbf{p} \\ |\mathbf{q}|, |\mathbf{p}| \leq k_F}} \frac{e^2}{\varepsilon_0 V |\mathbf{q} - \mathbf{p}|^2} = - \frac{3}{16\pi^2 \varepsilon_0} N e^2 k_F. \quad (\text{A.52})$$

A.6 Operators in Fock Representation

Using field operators (see Problem 4.8) a one-particle operator can be written

$$\hat{A}_1 = \int \Psi^\dagger(\mathbf{r}) \hat{A}_1(\mathbf{r}) \Psi(\mathbf{r}) d^3\mathbf{r}. \quad (\text{A.53})$$

The expansion

$$\Psi(\mathbf{r}) = \sum_i c_{\alpha_i} \psi_{\alpha_i}(\mathbf{r}) \quad (\text{A.54})$$

with fermion operators c_{α_i} and a complete set of single-particle wave functions $\psi_{\alpha_i}(\mathbf{r})$ leads immediately to (4.76)

$$\hat{A}_1 = \sum_{i,j} c_{\alpha_i}^\dagger c_{\alpha_j} \underbrace{\int \psi_{\alpha_i}^*(\mathbf{r}) \hat{A}_1(\mathbf{r}) \psi_{\alpha_j}(\mathbf{r}) d^3\mathbf{r}}_{\langle \psi_{\alpha_i} | \hat{A}_1 | \psi_{\alpha_j} \rangle}. \quad (\text{A.55})$$

If $\psi_{\alpha_j}(\mathbf{r})$ is an eigenfunction of $\hat{A}_1(\mathbf{r})$ with eigenvalue A_{α_j} , this reduces to

$$\hat{A}_1 = \sum_j A_{\alpha_j} c_{\alpha_j}^\dagger c_{\alpha_j}. \quad (\text{A.56})$$

The two-particle operator written in fermion field operators

$$\hat{A}_2 = \int \int \Psi^\dagger(\mathbf{r}_1) \Psi^\dagger(\mathbf{r}_2) \hat{A}_2(\mathbf{r}_1, \mathbf{r}_2) \Psi(\mathbf{r}_2) \Psi(\mathbf{r}_1) d^3\mathbf{r}_1 d^3\mathbf{r}_2 \quad (\text{A.57})$$

takes, with the expansion (A.54), the form

$$\begin{aligned} \hat{A}_2 &= \sum_{i,j,k,l} c_{\alpha_i}^\dagger c_{\alpha_j}^\dagger c_{\alpha_k} c_{\alpha_l} \\ &\times \int \int \psi_{\alpha_i}^*(\mathbf{r}_1) \psi_{\alpha_j}^*(\mathbf{r}_2) \hat{A}_2(\mathbf{r}_1, \mathbf{r}_2) \psi_{\alpha_k}(\mathbf{r}_2) \psi_{\alpha_l}(\mathbf{r}_1) d^3\mathbf{r}_1 d^3\mathbf{r}_2. \end{aligned} \quad (\text{A.58})$$

By convention, the matrix element is written as $\langle \psi_{\alpha_i}^{(1)} \psi_{\alpha_j}^{(2)} | \hat{A}_2 | \psi_{\alpha_l}^{(1)} \psi_{\alpha_k}^{(2)} \rangle$ and one obtains (4.77)

$$\hat{A}_2 = \sum_{i,j,k,l} \langle \psi_{\alpha_i}^{(1)} \psi_{\alpha_j}^{(2)} | \hat{A}_2 | \psi_{\alpha_l}^{(1)} \psi_{\alpha_k}^{(2)} \rangle c_{\alpha_i}^\dagger c_{\alpha_j}^\dagger c_{\alpha_k} c_{\alpha_l}. \quad (\text{A.59})$$

References

1. There are several series publications devoted to solid state physics and collections of data on solids and their properties:
 - *Solid State Physics*, edited by F. Seitz, D. Turnbull, H. Ehrenreich, F. Saepen, since 1955 (Academic Press, New York)
 - *Springer Series in Solid State Sciences*, edited by M. Cardona, P. Fulde, K. von Klitzing, H.-J. Queisser (Springer, Berlin)
 - *Springer Series in Surface Sciences*, edited by G. Ertl, R. Gomer, D.L. Mills (Springer, Berlin)
 - *Springer Series in Materials Sciences*, edited by U. Gonser, A. Mooradian, K.A. Müller, M.B. Panish, H. Sakaki (Springer, Berlin)
 - *Semiconductors and Semimetals* (eds. R.K. Willardson, A.C. Beer) since 1966 (Academic Press, New York)
 - *Springer Tracts in Modern Physics*, G. Höhler (managing editor) (Springer, Berlin)
 - *Topics in Applied Physics*, Series eds. C.E. Ascheron, H.J. Koelsch (Springer, Berlin)
 - *Landolt-Börnstein, Numerical Data and Functional Relationships in Science and Technology*, New Series Group III: Crystal and Solid State Physics, editors K.-H. Hellwege (Vols. 1 to 9), O. Madelung (Vols. 10 to 23), W. Martienssen (since Vol. 24)
 - *Festkörperprobleme/Advances in Solid State Physics*, editors F. Sauter (1962–1966), O. Madelung (1967–1972), H.J. Queisser (1973–1975), J. Treusch (1976–1981), P. Grosse (1982–1987), U. Rössler (1988–1992), R. Helbig (1993–1998), B. Kramer (1999–2000) (Vieweg, Braunschweig) and (2001–2006), R. Haug (2007–present) (Springer, Heidelberg)
2. C.P. Poole (ed.), *Encyclopedic Dictionary of Condensed Matter Physics* (Elsevier, Oxford, 2003)
3. F. Seitz, *The Modern Theory of Solids* (McGraw-Hill, New York, 1940)
4. Ch. Kittel, *Quantum Theory of Solids* (Wiley, New York, 1963)
5. D. Pines, *Elementary Excitations in Solids* (W.A. Benjamin, New York, 1964)
6. R. Kubo, T. Nagamiya, *Solid State Physics* (McGraw-Hill, New York, 1969)
7. J.M. Ziman, *Principles of the Theory of Solids* (Cambridge University Press, Cambridge, 1969)
8. W.A. Harrison, *Solid State Theory* (McGraw-Hill, New York, 1970)

9. W. Jones, N.H. March, *Theoretical Solid State Physics, Vol. 1: Perfect Lattice in Equilibrium, Vol. 2: Non-Equilibrium and Disorder* (Wiley, London, 1973)
10. H. Haken, *Quantenfeldtheorie des Festkörpers* (B.G. Teubner, Stuttgart, 1973), *Quantum Field Theory of Solids* 2nd printing (North-Holland, Amsterdam, 1983)
11. J. Callaway, *Quantum Theory of the Solid State* (Academic, San Diego, 1974)
12. N.W. Ashcroft, N.D. Mermin, *Solid State Physics* (W.B. Saunders Company, Philadelphia, 1976)
13. W. Ludwig, *Festkörperphysik*, 2. Auflage (Akademische Verlagsgesellschaft, Wiesbaden, 1978)
14. O. Madelung, *Introduction to Solid State Theory*. Springer Series in Solid State Sciences, vol. 2, ed. by M. Cardona, P. Fulde, H.-J. Queisser (Springer-Verlag, Berlin, 1978)
15. S.V. Vonsovsky, M.I. Katsnelson, *Quantum Solid State Physics*. Springer Series in Solid State Sciences, vol. 73, ed. by M. Cardona, P. Fulde, K. von Klitzing, H.-J. Queisser (Springer, Berlin, 1989)
16. A. Isihara, *Condensed Matter Physics* (Oxford University Press, New York, 1991)
17. P.W. Anderson, *Concepts in Solids* (World Scientific, Singapore, 1997)
18. P.M. Chaikin, T.C. Lubensky, *Principles of Condensed Matter Physics*, 1st paperback edition with corrections (Cambridge University Press, Cambridge, 2000)
19. P.L. Taylor, O. Heinonen, *A Quantum Approach to Condensed Matter Physics* (Cambridge University Press, Cambridge 2002)
20. E.P. O'Reilly, *Quantum Theory of Solids* (Taylor & Francis, New York, 2002)
21. E. Kaxiras, *Atomic and Electronic Structure of Solids* (Cambridge University Press, Cambridge, 2003)
22. P. Phillips, *Advanced Solid State Physics* (Westview, Boulder Colorado, 2003)
23. H. Bruns, K. Flensberg, *Many-Body Quantum theory in Condensed Matter Physics: An Introduction* (Oxford University Press, New York, 2004)
24. M.P. Marder, *Condensed Matter Physics* (Wiley, New York, 2004)
25. J.V. Chang (ed.), *Frontiers in Condensed matter Physics Research* (Nova Science Hauppauge, New York, 2006)
26. J.V. Chang (ed.), *New Developments in Condensed Matter Physics* (Nova Science Hauppauge, New York, 2006)
27. J.D. Patterson, B.C. Bailey, *Solid State Physics: Introduction to the Theory* (Springer, New York, 2007)
28. G. Czycholl, *Theoretische Festkörperphysik*, 3rd edn. (Springer, Berlin, 2007)
29. Ch. Kittel, *Introduction to Solid State Physics*, 7th edn. (Wiley, New York, 1996)
30. K.H. Hellwege, *Einführung in die Festkörperphysik*, 3. Auflage (Springer, Berlin, 1988)
31. H. Ibach, H. Lüth, *Solid State Physics: An Introduction to Theory and Experiment*, 3rd edn. (Springer, Berlin, 2003)
32. U. Kreibitz, M. Vollmer, *Optical Properties of Metal Clusters*. Springer Series in Material Sciences, vol. 25 (Springer, Berlin, 1995)
33. W. Ekardt, *Metal Clusters* (Wiley, New York 1999)
34. P.-G. Reinhard, E. Suraud, *An Introduction to Cluster Dynamics* (Wiley-VCH, Weinheim, 2003)

35. C. Janot, *Quasicrystals: A Primer* (Clarendon Press, Oxford, 1992)
36. H.-R. Trebin, *Quasicrystals* (Wiley-VCH, Weinheim, 2003)
37. J.B. Suck, M. Schreiber, P. Häussler (eds.), *Quasicrystals*. Springer Series in Solid State Science, vol. 55 (Springer, Berlin 2003)
38. M.H. Brodsky (ed.), *Amorphous Semiconductors*, Topics in Applied Physics, vol. 36, 2nd edn. (Springer, Berlin, 1985)
39. N. Mott, *Conduction in Non-Crystalline Materials* (Clarendon, Oxford, 1987)
40. P.G. deGennes, J. Prost, *The Physics of Liquid Crystals*, 2nd edn. (Clarendon Press, Oxford, 1993)
41. M. Daoud, C.E. Williams (eds.), *Soft Matter Physics* (Springer, Berlin, 1999)
42. I.W. Hamley, *Introduction to Soft Matter* (Wiley, New York, 2000)
43. M. Kleman, O.D. Lavrentovich, *Soft Matter Physics: An Introduction* (Springer, Heidelberg, 2002)
44. R.A.L. Jones, *Soft Condensed Matter* (Oxford University Press, New York, 2002)
45. J.-L. Barrat, J.-P. Hansen, *Basic Concepts for Simple and Complex Liquids* (Cambridge University Press, Cambridge, 2003)
46. G. Strobl, *Condensed Matter Physics: Crystals, Liquids, Liquid Crystals, and Polymers* (Springer, Berlin, 2004)
47. G.F. Koster 'Space Groups and their Representations'. In: *Solid State Physics* Vol. 5, ed. by F. Seitz, D. Turnbull (Academic Press, New York, 1957), pp. 173–256
48. G.F. Koster, J.O. Dimmock, R.G. Wheeler, H. Statz, *Properties of the Thirty-Two Point Groups*, (MIT, Cambridge, 1963)
49. W. Ludwig, L. Falter, *Symmetries in Physics: Group Theory Applied to Physical Problems*. Springer Series in Solid State Sciences vol. 64 (Springer, Berlin, 1988)
50. G. Burns, A.M. Glazer, *Space Groups for Solid State Scientists*, 2nd edn. (Academic Press, Boston, 1990)
51. J.D. Joannopoulos, R.D. Meade, J.N. Winn, *Photonic Crystals* (Princeton University Press, Princeton, 1995)
52. C.M. Soukoulis (ed.), *Photonic Band Gap Materials* (Kluwer Academic Publishers, Dordrecht, 1995)
53. S.G. Johnson, J.D. Joannopoulos, *Photonic Crystals: The Road from Theory to Practice* (Kluwer Academic Publishers, Boston, 2002)
54. K. Inoue, K. Othaka, *Photonic Crystals, Physics, Fabrication and Applications*. Springer Series in Optical Sciences, vol. 94 (Springer, 2004)
55. P. Vukusic, J.R. Sambles, *Nature* **424**, 852 (2003)
56. M. Lannoo, P. Friedel, *Atomic and Electronic Structure of Surfaces*. Springer Series in Surface Sciences, vol. 16 (Springer, Berlin, 1991)
57. H. Lüth, *Surfaces and Interfaces of Solids*. Springer Series in Surface Sciences, vol. 15 (Springer, Berlin, 1993)
58. H. Lüth, *Solid Surfaces, Interfaces, and Thin Films*, 4th edition, Springer Series in Surface Sciences (Springer, Berlin, 2001)
59. F. Bechstedt, *Principles of Surface Physics* (Springer, Berlin, 2003)
60. A. Gross, *Theoretical Surface Science: A Microscopic Perspective* (Springer, Berlin, 2003)
61. G. Binnig, H. Rohrer, *Appl. Phys. Lett.* **40**, 178 (1982); *Phys. Rev. Lett.* **50**, 120 (1983)

62. H.-J. Guentherodt, R. Wiesendanger (eds.), *Scanning Tunneling Microscopy I–III*. Springer Series in Surface Sciences, vols. 20,28,29 (Springer, Berlin, 1994–96)
63. R. Waser (ed.), *Nanoelectronics and Information Technology: Advanced Electronic Materials and Novel Devices* (Wiley-VCH, Weinheim, 2003)
64. G. Mahan, *Many-particle physics*, 3rd edn. (Kluwer Academic/Plenum Publ., New York, 2002)
65. S. Hüfner, *Photoelectron Spectroscopy*, 3rd edn. (Springer, Berlin, 2003)
66. A. Goldmann (ed.), *Landolt–Börnstein, Numerical Data and Functional Relationships in Science and Technology*, New Series Group III: Condensed Matter, Vol. 23 a(1989), b(1994), c(1999)
67. R. Kubo, *J. Phys. Soc. Jpn.* **12**, 570 (1957)
68. D.L. Mills, *Nonlinear Optics* (Springer, Berlin, 1991)
69. G. Rickayzen, *Green Functions and Condensed Matter* (Academic Press, London, 1980)
70. F. Schwabl, *Quantenmechanik für Fortgeschrittene* (Springer, Berlin, 1997)
71. M. Born, K. Huang, *Dynamical Theory of Crystal Lattices* (Clarendon, Oxford, 1954)
72. A.A. Maradudin, E.W. Montroll, G.H. Weiss, *Theory of Lattice Dynamics in the harmonic Approximation*, Solid State Physics Suppl. 3, ed. by F. Seitz and D. Turnbull (Academic, New York, 1966)
73. A.K. Ghatak, L.S. Kothari, *An Introduction to Lattice Dynamics* (Addison-Wesley, Singapore, 1972)
74. B.A. Auld, *Acoustic Fields and Waves in Solids* (Wiley Interscience, New York, 1973)
75. W. Cochran, *The Dynamics of Atoms in Crystals* (William Clowes, London, 1973)
76. H. Bilz, W. Kress, *Phonon Dispersion Relations in Insulators*. Springer Series in Solid State Sciences, vol. 10 (Springer, Berlin, 1979)
77. P. Brüesch, *Phonons: Theory and Experiments I*. Springer Series in Solid State Sciences, vol. 34 (Springer, Berlin, 1982)
78. P. Brüesch, *Phonons: Theory and Experiments II*. Springer Series in Solid State Sciences, vol. 65 (Springer, Berlin, 1986)
79. P. Brüesch, *Phonons: Theory and Experiments III*. Springer Series in Solid State Sciences, vol. 66 (Springer, Berlin, 1987)
80. G.K. Horton, A.A. Maradudin (eds.), *Dynamical Properties of Solids*, vols. 1–7 (Elsevier, Amsterdam, 1974–1995)
81. W. Kress, *Phonon Dispersion Curves, One-Phonon Densities of States and Impurity Vibrations of Metallic Systems*, Physik Daten/Physics Data (FIZ Karlsruhe, 1987)
82. M.T. Dove, *Introduction to Lattice Dynamics*, (Cambridge University Press, Cambridge, 1993)
83. A.M. Kosevich, *The Crystal Lattice: Phonons, Solitons, Dislocations* (Wiley-VCH-Verlag, Berlin, 1999)
84. G. Leibfried, W. Ludwig, *Theory of anharmonic Effects in Crystals*, in: Solid State Physics, vol. 12, ed. by F. Seitz, D. Turnbull (Academic Press, New York, 1961), p. 275
85. W. Kress, F. deWette (eds.), *Surface Phonons*. Springer Series in Surface Sciences, vol. 21 (Springer, Berlin, 1991)

86. J.-P. Leburton, J. Pascual, C. Sotomayor Torres (eds.), *Phonons in Semiconductor Nanostructures*, NATO ASI Series E: Applied Sciences Vol. 236 (Kluwer Academic Publishers, Dordrecht, 1993)
87. G.P. Srivastava: *Theoretical Modelling of Semiconductor Surfaces* (World Scientific, Singapore, 1999)
88. L. van Hove, Phys. Rev. **89**, 1189 (1953)
89. P.Y. Yu, M. Cardona, *Fundamentals of Semiconductors*, 3rd edn. (Springer, Berlin, 2005)
90. J.T. Nye, *Physical Properties of crystals*, (Clarendon, Oxford, 1957)
91. H.B. Huntington 'The Elastic Constants of Crystals'. in *Solid State Physics*, vol. 7, ed. by F. Seitz, D. Turnbull (Academic Press, New York, 1958), p. 213
92. G.A. Northrop, J.P. Wolfe, in *Nonequilibrium Phonon Dynamics*, ed. by W.E. Bron (Plenum Press, New York, 1985), p. 165
93. J.P. Wolfe, *Imaging Phonons: Acoustic Wave Propagation in Solids* (Cambridge University Press, New York, 2005)
94. *Landolt-Börnstein Group III Vol. 41 Semiconductors, Subvolume A1α 'Lattice Properties'*, ed. by U. Rössler (Springer, Berlin, 2001)
95. W. Schäfer, M. Wegener, *Semiconductor Optics and Transport Phenomena*, (Springer, Berlin, 2002)
96. Yu.A. Izyumov, N.A. Chernoplekov, *Neutron Spectroscopy* (Consultants Bureau, New York, 1994)
97. L. Dobrzynski, K. Blinowski, *Neutrons and Solid State Physics* (Ellis Horwood, New York, 1994)
98. D. Strauch, B. Dorner, J. Phys.: Condens. Matter **2**, 1427 (1990)
99. S. Baroni, P. Giannozzi, A. Testa, Phys. Rev. Lett. **58**, 1861 (1987)
100. S. Baroni, S. de Gironcoli, A. Dal Corso, P. Giannozzi, Rev. Mod. Phys. **73**, 515 (2001)
101. P. Giannozzi, S. de Gironcoli, P. Pavone, S. Baroni, Phys. Rev. B **43**, 7231 (1991)
102. M. Wuttig, R. Franchy, H. Ibach, Solid State Commun. **57**, 445 (1986)
103. J. Fritsch, P. Pavone, U. Schröder, Phys. Rev. Lett. **71**, 4194 (1993); J. Fritsch, C. Eckl, P. Pavone, U. Schröder in *Festkörperprobleme/Advances in Solid State Physics*, vol. 36, ed. by R. Helbig (Vieweg, Braunschweig, 1997), p. 135
104. L.L. Chang, K. Ploog (eds.), *Molecular Beam Epitaxy and Heterostructures*, NATO ASI Serie E: Applied Sciences No. 87 (Martinus Nijhoff Publ., Dordrecht, 1985)
105. M.A. Herman, H. Sitter, *Molecular Beam Epitaxy*. Springer Series in Materials Sciences, vol. 7 (Springer, Berlin, 1989)
106. H.D. Fuchs, P. Etchegoin, M. Cardona, K. Itoh, E.E. Haller, Phys. Rev. Lett. **70**, 1715 (1993)
107. J. Spitzer, T. Ruf, M. Cardona, W. Dondl, R. Schorer, G. Abstreiter, E.E. Haller, Phys. Rev. Lett. **72**, 1565 (1994)
108. J.R. Salvador, F. Guo, T. Hogan, M.G. Kanatzidis, Nature **425**, 702 (2003)
109. A. Sommerfeld, H. Bethe, *Elektronentheorie der Metalle* (Springer, Berlin Heidelberg, New York, 1967); reprinted from *Handbuch der Physik* Vol. 24/2
110. N. Grewe, F. Steglich, in *Handbook of Physics and Chemistry of Rare Earths*, Vol. 14, ed. by K.A. Gschneidner jr., L. Eyring (Elsevier, Amsterdam, 1991), p. 343
111. S. Roth, *One-dimensional Metals* (VCH-Verlagsgesellschaft, Weinheim, 1995)

112. H. Kiess (ed.), *Conjugated Conducting Polymers*. Springer Series in Solid-State Sciences, vol. 102 (Springer, Berlin, 1992)
113. P.J.F. Harris, *Carbon Nanotubes and Related Structures*, 1st paperback edition (Cambridge University Press, Cambridge 2001)
114. M.S. Dresselhaus, G. Dresselhaus, Ph. Avouris (eds.), *Carbon Nanotubes: Synthesis, Structure, Properties, and Applications*. Springer Topics in Applied Physics, vol. 80 (Springer, Berlin 2001)
115. A.H. Wilson, *Theory of Metals*, 2nd edn. (Cambridge University Press, Cambridge, 1965)
116. W. Nolting, *Quantentheorie des Magnetismus* (Teubner, Stuttgart, 1986)
117. D. Shoenberg, *J. Low Temp. Phys.* **2**, 483 (1970)
118. M. Cardona (ed.), *Light Scattering in Solids*. Topics in Applied Physics, vol. 8 (Springer, Berlin, 1975)
119. A. Kallio, J. Piilo, *Phys. Rev. Lett.* **77**, 4237 (1996)
120. D.M. Ceperley, *Phys. Rev. B* **18**, 3126 (1978)
121. H. Jones, *The Theory of Brillouin Zones and Electronic Structure in Crystals* (North-Holland, Amsterdam, 1975)
122. P. Fulde, *Electron Correlations in Molecules and Solids*. Springer Series in Solid State Sciences, vol. 100 (Springer, Berlin, Heidelberg, New York, 3rd enlarged edition 1995)
123. R.M. Dreizler, E.K. Gross, *Density Functional Theory: An Approach to the Quantum Many-Body Problem* (Springer, Berlin, 1990)
124. M. Levy, *Proc. Natl. Acad. Sci. USA N.Y.* **76**, 6062 (1979)
125. H. Eschrig, *The Fundamentals of Density Functional Theory* (Teubner Verlagsgesellschaft, Stuttgart, 1996)
126. G.F. Giuliani, G. Vignale, *Quantum Theory of the Electron Liquid* (Cambridge University Press, New York, 2005)
127. P. Hohenberg, W. Kohn, *Phys. Rev.* **136B**, 864 (1964)
128. W. Kohn, L.J. Sham, *Phys. Rev.* **140A**, 1133 (1965)
129. L. Hedin, *Phys. Rev.* **139**, A796 (1965)
130. W.G. Aulbur, L. Jönsson, J.W. Wilkins, in *Solid State Physics*, vol. 54, ed. by H. Ehrenreich (Academic, Orlando, 1999), p. 1
131. J.R. Chelikowski, A. Franciosi (eds.), *Electronic Materials - A New Era in Material Science*. Springer Series in Solid State Sciences, vol. 95 (Springer, Berlin, 1991)
132. W.A. Harrison, *Electronic Structure and the Properties of Solids* (W.H. Freeman and Company, San Francisco 1980; Dover edition, General Publ. Company, Toronto, 1989)
133. J. Kübler, V. Eyert, 'Electronic Structure Calculations'. in *Material Science and Technology: Electronic Properties of Metals and Ceramics*, Part I, ed. by K.H.J. Buschow (VCH-Verlagsgesellschaft, Weinheim, 1991), pp. 1–145
134. W.A. Harrison, *Pseudopotentials in the Theory of Metals* (W.A. Benjamin, New York, 1966)
135. C. Albrecht, J.H. Smet, D. Weiss, K. von Klitzing, R. Hennig, M. Langenbuch, M. Suhrke, U. Rössler, V. Umansky, H. Schweizer, *Phys. Rev. Lett.* **83**, 2234 (1999)
136. *Landolt-Börnstein, Numerical Data and Functional Relationships in Science and Technology*, New Series Group III: Crystal and Solid State Physics, vol. 13b, ed. by O. Madelung, p. 16 (1983)

137. *Landolt-Börnstein, Numerical Data and Functional Relationships in Science and Technology*, New Series Group III: Crystal and Solid State Physics, vol. 13c, ed. by O. Madelung, p. 10 (1984)
138. *Landolt-Börnstein, Numerical Data and Functional Relationships in Science and Technology*, New Series Group III: Crystal and Solid State Physics, vol. 22a, ed. by O. Madelung, p. 263 (1987)
139. M.L. Cohen, V. Heine, 'The Fitting of Pseudopotentials to Experimental Data and Their Subsequent Application'. In: *Solid State Physics* vol. 24, ed. by H. Ehrenreich, F. Seitz, D. Turnbull (Academic, New York, 1970), p. 37
140. D. Vanderbilt, *Phys. Rev. B* **41**, 7892 (1990)
141. N. Troullier, J.L. Martins, *Phys. Rev. B* **43**, 1993 (1991)
142. L.F. Mattheiss, *Phys. Rev.* **134**, A970 (1964)
143. G.A. Burdick, *Phys. Rev. Lett.* **7**, 156 (1961)
144. N.J. Shevchik, J. Tejada, M. Cardona, *Phys. Rev. B* **9**, 2627 (1974)
145. A. Zunger, *Phys. Rev. B* **21**, 4785 (1980)
146. E.O. Kane, in *Semiconductors and Semimetals*, vol. 1, ed. by R.K. Willardson, A.C. Beer (Academic Press, New York, 1966), p. 75
147. W. Shockley, *Phys. Rev.* **78**, 173 (1950)
148. U. Rössler, *Solid State Commun.* **49**, 943 (1984)
149. P. Pfeffer, W. Zawadzki, *Phys. Rev. B* **41**, 1561 (1990)
150. H. Mayer, U. Rössler, *Phys. Rev. B* **44**, 9048 (1991)
151. T. Ando, A.B. Fowler, F. Stern, *Rev. Mod. Phys.* **54**, 437 (1982)
152. G. Bastard, *Wave Mechanics Applied to Semiconductor Heterostructures* (Les Éditions de Physique, Les Ulis, 1988)
153. R. Winkler, *Spin-Orbit Coupling Effects in Two-Dimensional Electron and Hole Systems*. Springer Tracts in Modern Physics, vol. 191 (Springer, Berlin, 2003)
154. R. Winkler, U. Rössler, *Phys. Rev. B* **48**, 8918 (1993)
155. S. Datta, *Electronic Transport in Mesoscopic Systems* (Cambridge University Press, Cambridge, 1995)
156. D.K. Ferry, S.M. Goodnick, *Transport in Nanostructures* (Cambridge University Press, Cambridge, 1997)
157. Y. Murayama, *Mesoscopic Systems: Fundamentals and Applications* (Wiley-VCH, Weinheim, 2001)
158. J.H. Davies, A.R. Long (eds.), *Physics of Nanostructures*, Proc. 38th Scottish Universities Summer School in Physics (IOP, Bristol, 1992)
159. W.P. Kirk, M.A. Reed (eds.), *Nanostructures and Mesoscopic Systems* (Academic, Boston, 1992)
160. Y. Imry, *Introduction to Mesoscopic Physics* (Oxford University Press, Oxford, 1997)
161. K. von Klitzing, G. Dorda, M. Pepper, *Phys. Rev. Lett.* **45**, 494 (1980)
162. J. Hajdu, M. Janssen, *Introduction to the Theory of the Integer Quantum Hall Effect* (VCH-Verlagsgesellschaft, Weinheim 1995)
163. A.P. Cracknell, *Magnetism in Crystalline Materials* (Pergamon, Oxford, 1975)
164. F. Keffer, *Spin Waves* in *Handbuch der Physik* **18/2**, ed. by S. Flügge (Springer, Berlin, 1966)
165. P. Heller, *Rep. Progr. Phys.* **30**/III 731 (1967)
166. R.M. White, *Quantum Theory of Magnetism* (Springer, Berlin, 1983)
167. T. Moriya, *Spin Fluctuations in Itinerant Electron Magnetism*. Springer Series in Solid State Sciences, vol. 56 (Springer, Berlin, 1985)

168. A.S. Borovik-Romanov, S.K. Sinha (eds.), *Spin Waves and Magnetic Excitations*, Modern Problems in Condensed Matter Sciences, vol. 22 (part 1 and 2) (North-Holland, Amsterdam, 1988)
169. A. Auerbach, *Interacting Electrons and Quantum Magnetism*, corrected second printing (Springer, Berlin, 1998)
170. D. Craik, *Magnetism: Principles and Applications* (Wiley, Chichester, 1995)
171. Kei Yosida, *Theory of Magnetism*. Springer Series in Solid State Sciences, vol. 122 (Springer, Berlin, 1996)
172. D.J. Singh, D.A. Papaconstantopoulos, *Electronic Structure and Magnetism of Complex Materials*. Springer Series in Materials Science, vol. 54 (Springer, Berlin, 2003)
173. V. Dotsenko, *The Theory of Spin Glasses and Neural Networks* (World Scientific, Singapore, 1994)
174. T. Dietl, H. Ohno, F. Matsukara, J. Cibert, D. Ferrand, *Science* **287**, 1019 (2000)
175. T. Dietl, *Semicond. Sci. Technol.* **17**, 377 (2002)
176. T. Jungwirth, J. Sinova, J. Mačėk, J. Kučera, A.H. MacDonald, *Rev. Mod. Phys.* **78**, 809 (2006)
177. I. Žutič, J. Fabian, S. Das Sarma, *Rev. Mod. Phys.* **76**, 323 (2004)
178. D.D. Awschalom, D. Loss, N. Samarth (eds.), *Semiconductor Spintronics and Quantum Computation*, Springer Series in NanoScience Technology (Springer, Berlin, 2002)
179. J.C.S. Levy, *Surf. Sci. Rep.* **1**, 39 (1981)
180. D.L. Mills, *Surface Spin Waves in Magnetic Crystals in Surface Excitations* ed. by V.M. Agranovich, A.A. Maradudin (North-Holland, Amsterdam, 1984)
181. V.L. Moruzzi, J.P. Janak, A.R. Williams, *Calculated Electronic Properties of Metals* (Pergamon, New York, 1978)
182. U. von Barth, L. Hedin, *J. Phys. C* **5**, 1269 (1972)
183. W. Heisenberg, *Z. Phys.* **49**, 619 (1928)
184. F. Bloch, *Z. Phys.* **61**, 206 (1930)
185. T. Holstein, H. Primakoff, *Phys. Rev.* **58**, 1098 (1940)
186. G. Shirane, V.J. Minkiewicz, R. Nathans, *J. Appl. Phys.* **39**, 383 (1968)
187. H.A. Mook, D.McK. Paul, *Phys. Rev. Lett.* **54**, 227 (1985)
188. G.G. Low, A. Okazaki, R.W.H. Stevenson, K.C. Turberfield, *J. Appl. Phys.* **35**, 998 (1964)
189. A.I. Lichtenstein, M.I. Katsnelson, G. Kotliar, *Phys. Rev. Lett.* **87**, 067205 (2001)
190. W. Gebhardt, U. Krey, *Pasenübergänge und kritische Phänomene* (Vieweg-Verlag, Braunschweig, 1980)
191. P. Papon, J. Leblond, P.H.E. Meijer, *The Physics of Phase Transitions: Concepts and Applications* (Springer, Heidelberg, 2002)
192. M. Gitterman, V. Halpern, *Phase Transitions: A Brief Account with Modern Applications* (World Scientific, Hackensack, 2004)
193. N.H. March, *Electron Correlation in Molecules and Condensed Phases* (Plenum Press, New York, 1996)
194. A. Isihara, *Electron Liquids*, Springer Series in Solid State Sciences 96, 2nd edn. (Springer, Berlin, 1998)
195. V.I. Anisimov (ed.), *Strong Coulomb Interaction in Electronic Structure Calculations* (Gordon and Breach Science Publishers, New York, 2000)

196. G. Morandi, P. Sodano, A. Tagliacozzo, V. Tognetti (eds.), *Field theories for low-dimensional Condensed Matter Systems - Spin Systems and Strongly Correlated Electrons*. Springer Series in Solid State Sciences, vol. 131 (Springer, Berlin, 2000)
197. L.D. Landau, E.M. Lifshitz, *Lehrbuch der Theoretischen Physik IX, Statistische Physik Teil 2* 4th corrected edition (Akademie-Verlag, Berlin, 1992)
198. D. Pines, P. Nozières, *The Theory of Quantum Liquids* Vol. 1 (Benjamin Press, New York, 1966)
199. G. Baym, Ch. Pethick, *Landau Fermi Liquid Theory* (Wiley, New York, 1991)
200. A.A. Abrikosov, *Fundamentals of the Theory of Metals* (North-Holland, Amsterdam, 1988)
201. G. Grüner, *Density Waves in Solids* (Addison-Wesley, Reading, 1994)
202. R.E. Prange, S.M. Girvin, *The Quantum Hall Effect* (Springer, New York, 1987)
203. T. Chakraborty, P. Pietiläinen, *The Fractional Quantum Hall Effect*. Springer Series in Solid State Sciences, vol. 85 (Springer, Berlin, 1988), 2nd edition 1995
204. D. Yoshioka, *The Quantum Hall Effect*. Springer Series in Solid State Sciences, vol. 133 (Springer, Berlin, 2002)
205. A.A. Abrikosov, *Quantum Field Theoretical Methods in Statistical Physics* (Pergamon, Oxford, 1965)
206. W. Nolting, *Grundkurs Theoretische Physik 7: Vielteilchen-Theorie*, 5. Auflage (Springer, Berlin, 2002)
207. J. Hubbard, Proc. Roy. Soc. A **276**, 238 (1963)
208. M.C. Gutzwiller, Phys. Rev. Lett. **10**, 159 (1963)
209. N. Mott, *Metal-Insulator Transitions* (Taylor & Francis, London, 1974)
210. A. Georges, G. Kotliar, W. Krauth, M.J. Rozenberg, Rev. Mod. Phys. **68**, 13 (1996)
211. F. Gebhard, *The Mott Metal-Insulator Transition*. Springer Tracts in Modern Physics, vol. 137 (Springer, Berlin, 1997)
212. M. Imada, A. Fujimori, Y. Tokura, Rev. Mod. Phys. **70**, 1039 (1998)
213. Y. Tokura (ed.), *Colossal Magnetoresistive Oxides* (Gordon & Breach Science Publ., London, 2000)
214. W. Metzner, D. Vollhardt, Phys. Rev. Lett. **62**, 324 (1989)
215. E.R. Dobbs, *Helium Three* (Oxford University Press, New York, 2000)
216. C. Weisbuch, B. Vinter, *Quantum Semiconductor Structures* (Academic, Boston, 1991)
217. M.J. Kelly, *Low-dimensional Semiconductors* (Clarendon, Oxford, 1995)
218. T. Ando, Y. Arakawa, K. Furuya, S. Komiyama, H. Nakashima (eds.), *Mesoscopic Physics and Electronics* (Springer, Berlin, 1998)
219. V.J. Emery (ed.), *Correlated Electron Systems* (World Scientific, Singapore, 1993)
220. F.D.M. Haldane, J. Phys. C **14**, 2585 (1981)
221. J. Voit, Rep. Progr. Phys. **57**, 977 (1995)
222. M. Sasseti in *Quantum Transport in Semiconductor Submicron Structures*, ed. by B. Kramer (Kluwer Academic Publishers, Dordrecht, 1996)
223. S. Tomonaga, Progr. Theor. Phys. **5**, 544 (1950)
224. J.M. Luttinger, J. Math. Phys. **4**, 1154 (1963)
225. G. Zwicknagl, Adv. in Physics **41**, 203 (1992)
226. D.C. Tsui, H.L. Stoermer, A.C. Gossard, Phys. Rev. Lett. **48**, 1559 (1982)

227. R. Willett, J.P. Eisenstein, H.L. Störmer, D.C. Tsui, A.C. Gossard, J.H. English, *Phys. Rev. Lett.* **59**, 1776 (1987)
228. R.B. Laughlin, *Phys. Rev. Lett.* **50**, 1395 (1983)
229. O. Heinonen (ed.), *Composite Fermions* (World Scientific, Singapore, 1998)
230. J. Jain, *Composite Fermions* (Cambridge University Press, Cambridge, 2007)
231. P. Streda, J. Kucera, A.H. MacDonald, *Phys. Rev. Lett.* **59**, 1973 (1987)
232. M. Büttiker, *Phys. Rev. B* **38**, 9375 (1988)
233. S. Nakajima, Y. Toyozawa, R. Abe, *The Physics of Elementary Excitations*. Springer Series in Solid State Sciences, vol. 12 (Springer, Berlin, 1980)
234. P. Vogl, *The Electron-Phonon Interaction in Semiconductors* in *Physics of Nonlinear Transport in Semiconductors*, ed. by D.K. Ferry, J.R. Barker, C. Jacoboni, NATO ASI Series B: Physics Vol. 52 (Plenum Press, New York, 1980)
235. G.L. Bir, G.E. Pikus, *Symmetry and Strain induced Effects in Semiconductors* (Wiley, New York, 1974)
236. E.L. Ivchenko, G.E. Pikus, *Superlattices and Other Heterostructures*. Springer Series in Solid State Sciences, vol. 110 (Springer, Berlin, 1995)
237. H. Fröhlich, H. Pelzer, S. Zienau, *Phil. Mag.* **41**, 221 (1950)
238. H. Fröhlich, *Proc. Roy. Soc. A* **223**, 296 (1954)
239. J.T. Devreese (ed.), *Polarons in Ionic Crystals and Polar Semiconductors* (North-Holland Publ. Comp., Amsterdam, 1972)
240. L. Reggiani (ed.), *Hot Electron transport in Semiconductors*. Topics in Applied Physics, vol. 58 (Springer, Berlin, 1985)
241. J. Shah (ed.), *Hot Carriers in Semiconductors* (Pergamon, Oxford, 1988)
242. J. Shah (ed.), *Hot Carriers in Semiconductor Nanostructures* (Academic, Boston, 1992)
243. J. Shah, *Ultrafast Spectroscopy of Semiconductors and Semiconductor Nanostructures*. Springer Series in Solid State Sciences, vol. 115 (Springer, Berlin, 1997)
244. K. Seeger, *Semiconductor Physics*. Springer Series in Solid-State Sciences, vol. 40, 8th edn. (Springer, Berlin 2002)
245. V.L. Bonch-Bruевич, S.G. Kalashnikov, *Halbleiterphysik*, translated from Russian (VEB Deutscher Verlag der Wissenschaften, Berlin, 1982)
246. M. Lundstrom, *Fundamentals of Carrier Transport*, 2nd edn. (Cambridge University Press, Cambridge, 2000)
247. D.K. Ferry, J.R. Barker, C. Jacoboni (eds.), *Physics of Nonlinear Transport in Semiconductors*, NATO ASI Series B: Physics, vol. 52 (Plenum, New York, 1980)
248. B.K. Ridley, *Electrons and Phonons in Semiconductor Multilayers* (Cambridge University Press, Cambridge, 1997)
249. H. Kamerlingh Onnes, *Leiden Comm.* **120b**, **122b**, **124c** (1911)
250. P.G. DeGennes, *Superconductivity of Metals and Alloys*, (W.A. Benjamin, New York, 1966)
251. M. Tinkham, *Introduction to Superconductivity*, (McGraw-Hill, New York, 1975)
252. W. Buckel, *Superconductivity: Fundamentals and Applications*, (VCH Verlagsgesellschaft, Weinheim, 1991)
253. V.V. Schmidt, *The Physics of Superconductors*, (Springer, Berlin, 1997)

254. K.-H. Bennemann, J.B. Ketterson (eds.), *The Physics of Superconductors*, Vol. 1: Conventional and High-Tc-Superconductors, Vol. 2: Novel Superconductors (Springer, Berlin, 2003)
255. J. Bardeen, L.N. Cooper, J.R. Schrieffer, *Phys. Rev.* **108**, 1175 (1957)
256. J.G. Bednorz, K.A. Müller, *Z. Physik B* **64**, 189 (1986)
257. H. Kamimura, H. Ushio, S. Matsuno, T. Hamada, *Theory of Copper Oxide Superconductors* (Springer, New York, 2005)
258. A.G. Leggett, *J. Phys.(Paris)* **C7**, 19 (1980)
259. C.A. Regal, C. Ticknor, J.L. Bohn, D.S. Jin, *Nature* **424**, 47 (2003)
260. W. Kohn in *Solid State Physics* vol. 5, 257 (1957)
261. S. Pantelides, *Rev. Mod. Phys.* **50**, 797 (1980)
262. M. Lannoo, J. Bourgoin, *Point Defects in Semiconductors I: Theoretical Aspects*. Springer Series in Solid State Sciences, vol. 22 (Springer, Berlin, 1981)
263. A.K. Ramdas, S. Rodriguez, *Rep. Progr. Phys.* **44**, 1297 (1981)
264. J. Bourgoin, M. Lannoo, *Point Defects in Semiconductors II: Experimental Aspects*. Springer Series in Solid State Sciences, vol. 35 (Springer, Berlin, 1983)
265. W. Schröter (ed.), *Electronic Structure and Properties of Semiconductors*. Materials Science and Technology, vol. 4 (VCH Publishers, New York, 1991)
266. E.F. Schubert, *Doping in III-V Semiconductors* (Cambridge University Press, Cambridge, 1993)
267. J.-M. Spaeth, H. Overhof, *Point Defects in Semiconductors and Insulators. Determination of Atomic and Electronic Structure from Paramagnetic Hyperfine Interactions*, Springer Series in Materials Science, vol. 51 (Springer, Berlin, 2003)
268. D.A. Drabold, S.K. Estreicher (eds.), *Theory of Defects in Semiconductors*. Topics in Appl. Phys., vol. 104 (Springer, New York, 2007)
269. P. Vogl, in *Advances in Solid State Physics*, vol. 21, ed. by J. Treusch (Vieweg, Braunschweig, 1981), p. 191
270. M. Scheffler, in *Advances in Solid State Physics*, vol. 22, ed. by P. Grosse (Vieweg, Braunschweig, 1982), p. 115
271. U. Kaufmann, in *Advances in Solid State Physics*, vol. 29, ed. by U. Rössler (Vieweg, Braunschweig, 1989), p. 183 and B.K. Meyer, K. Krambock, D. Hofmann, J.-M. Spaeth *ibid.* p. 201
272. A. Zunger, *Solid State Physics*, vol. 39, ed. by H. Ehrenreich, D. Turnbull (Academic, New York, 1986), p. 276
273. R.J. Elliott, J.A. Krumhansl, P.L. Leath, *Rev. Mod. Phys.* **46**, 465 (1974)
274. J. Rammer, *Quantum Transport Theory*. Frontiers in Physics, vol. 99, ed. by D. Pines (Perseus Books, Reading Mass, 1998)
275. H. Overhof, P. Thomas, *Electron Transport in Hydrogenated Amorphous Semiconductors*, Springer Tracts in Modern Physics, vol. 114 (Springer, Berlin, 1989)
276. B. Kramer, A. MacKinnon, *Rep. Progr. Physics* **56**, 1469 (1993)
277. D. Belitz, T.R. Kirkpatrick, *Rev. Mod. Phys.* **66**, 261 (1994) (The Anderson-Mott transition)
278. E. Abrahams, S.V. Kravchenko, M.P. Sarachik, *Rev. Mod. Phys.* **73**, 251 (2001)
279. V.F. Gantmakher, *Electrons and Disorder in Solids* (Oxford University Press, Oxford, 2005)
280. E. Abrahams, P.W. Anderson, D.C. Liciardello, T.V. Ramakrishnan, *Phys. Rev. Lett.* **42**, 673 (1979)

281. D.J. Thouless, Phys. Rev. Lett. **39**, 1167 (1977)
282. Y. Toyozawa, *Optical Processes in Solids* (Cambridge University Press, Cambridge, 2003)
283. C. Klingshirn, *Semiconductor Optics* (Springer, Berlin, 2005)
284. M. Lindberg, S.W. Koch, Phys. Rev. B **38**, 3342 (1988)
285. H. Haug, S.W. Koch, *Quantum Theory of the optical and Electronic Properties of Semiconductors*, 2nd edn. (World Scientific, Singapore 1993)
286. T. Meier, P. Thomas, S. Koch, *Coherent Semiconductor Optics* (Springer, Berlin, 2007)
287. W. Schattke, M.A. Van Hove (eds.), *Solid State Photoemission and Related Methods: Theory and experiment* (Wiley-VCH, Weinheim, 2003)
288. L.J. Sham, T.M. Rice, Phys. Rev. **144**, 708 (1966)
289. R.J. Elliott, Phys. Rev. **108**, 1384 (1957)
290. U. Rössler, H.-R. Trebin, Phys. Rev. B **23**, 1961 (1981)
291. J.J. Hopfield, Phys. Rev. **112**, 1555 (1957)
292. J.S. Blakemore, *Semiconductor Statistics* (Pergamon, Oxford, 1962)
293. I.M. Gradsteyn, I.S. Ryshik, *Table of Integrals, Series and Products*, translated from Russian (Academic Press, New York 1965)

Solutions

Solutions for Chap. 1

1.1:

Point lattice: Set of lattice vectors $\mathbf{R}_n = \sum_{i=1}^d n_i \mathbf{a}_i$, n_i integer, \mathbf{a}_i linear independent (d dimension of the system)

Reciprocal lattice: $\mathbf{G}_m = \sum_{j=1}^d m_j \mathbf{b}_j$, m_j integer, \mathbf{b}_j linear independent, and $\mathbf{a}_i \cdot \mathbf{b}_j = 2\pi\delta_{ij}$

Wigner–Seitz cell: Contains all points which are closer to a given \mathbf{R}_n than to any other $\mathbf{R}_{n'} \neq \mathbf{R}_n$

(First) *Brillouin zone:* Wigner–Seitz cell of the reciprocal lattice

$d = 2$, *square lattice:* $\mathbf{a}_1 = a(1, 0)$, $\mathbf{a}_2 = a(0, 1)$
 $\rightarrow \mathbf{b}_1 = 2\pi/a(1, 0)$, $\mathbf{b}_2 = 2\pi/a(0, 1)$

$d = 3$, *simple cubic (sc), body centered cubic (bcc), face centered cubic (fcc)*
sc: $\mathbf{a}_1 = a(1, 0, 0)$, $\mathbf{a}_2 = a(0, 1, 0)$, $\mathbf{a}_3 = a(0, 0, 1)$
 $\rightarrow \mathbf{b}_1 = 2\pi/a(1, 0, 0)$, $\mathbf{b}_2 = 2\pi/a(0, 1, 0)$, $\mathbf{b}_3 = 2\pi/a(0, 0, 1)$

bcc: $\mathbf{a}_1 = a/2(1, 1, -1)$, $\mathbf{a}_2 = a/2(1, -1, 1)$, $\mathbf{a}_3 = a/2(-1, 1, 1)$
 $\rightarrow \mathbf{b}_1 = 2\pi/a(1, 1, 0)$, $\mathbf{b}_2 = 2\pi/a(1, 0, 1)$, $\mathbf{b}_3 = 2\pi/a(0, 1, 1)$

fcc: $\mathbf{a}_1 = a/2(0, 1, 1)$, $\mathbf{a}_2 = a/2(1, 0, 1)$, $\mathbf{a}_3 = a/2(1, 1, 0)$
 $\rightarrow \mathbf{b}_1 = 2\pi/a(-1, 1, 1)$, $\mathbf{b}_2 = 2\pi/a(1, -1, 1)$, $\mathbf{b}_3 = 2\pi/a(1, 1, -1)$

1.2: Create Fibonacci sequence by replacing $LS \rightarrow L$ and $S \rightarrow L$ [21]:

LS

LSL

$LSLLS$

$LSLLSLSL$

$LSLLSLSLLSLLS$

$LSLLSLSLLSLLSLLSLSL$ not periodic

Replacing $LS \rightarrow L'$ and $L \rightarrow S'$ in the last line gives the configuration of the second but last line (self-similarity or fractality). For the Fourier transform see [35].

1.3: Given two vectors $\mathbf{a}_1, \mathbf{a}_2$, with $|\mathbf{a}_1| = a_1$, $|\mathbf{a}_2| = a_2$, and $\mathbf{a}_1 \cdot \mathbf{a}_2 = a_1 a_2 \cos \alpha$, spanning a plane. The following five cases can be distinguished:

$$\begin{aligned} a_1 = a_2, \quad \alpha = \pi/2 & \quad \text{square} \\ \alpha = \pi/3 & \quad \text{triangular or hexagonal} \\ \alpha \neq \pi/2, \pi/3 & \\ a_1 \neq a_2, \quad \alpha = \pi/2 & \quad \text{rectangular} \\ \alpha \neq \pi/2 & \end{aligned}$$

1.4: $T_{\mathbf{R}_n}$ is the translation operator. It acts on a function according to

$$T_{\mathbf{R}_n} \phi(\mathbf{r}) = \phi(\mathbf{r} + \mathbf{R}_n)$$

and commutes with the system Hamiltonian, $[T_{\mathbf{R}_n}, H] = 0$. Therefore, there exist simultaneous eigenfunctions of H and $T_{\mathbf{R}_n}$ with the property

$$T_{\mathbf{R}_n} \phi_{\mathbf{k}}(\mathbf{r}) = e^{i\mathbf{k} \cdot \mathbf{R}_n} \phi_{\mathbf{k}}(\mathbf{r})$$

i.e. the wave eigenfunctions in different Wigner-Seitz cells differ only by a phase factor with wave vector \mathbf{k} from the first Brillouin zone.

1.5: Count nearest neighbors (n.n.) and spheres per cube:

$$\begin{aligned} \text{sc} \quad 6 \text{ n.n., } 1 \text{ sphere} & \rightarrow \frac{4\pi}{3} \left(\frac{a}{2}\right)^3 / a^3 = \frac{\pi}{6} = 0.52, \\ \text{bcc} \quad 8 \text{ n.n., } 2 \text{ spheres} & \rightarrow 2 \frac{4\pi}{3} \left(\frac{\sqrt{3}a}{4}\right)^3 / a^3 = \frac{\sqrt{3}\pi}{8} = 0.68, \\ \text{fcc} \quad 12 \text{ n.n., } 4 \text{ spheres} & \rightarrow 4 \frac{4\pi}{3} \left(\frac{a}{2\sqrt{2}}\right)^3 / a^3 = \frac{\pi}{3\sqrt{2}} = 0.74, \\ \text{diamond} \quad 4 \text{ n.n., } 8 \text{ spheres} & \rightarrow 8 \frac{4\pi}{3} \left(\frac{\sqrt{3}a}{8}\right)^3 / a^3 = \frac{\sqrt{3}\pi}{16} = 0.34. \end{aligned}$$

1.6: A mass density $n(\mathbf{r}) = \delta(\mathbf{r} - \mathbf{r}_i)$ and using $\delta(\mathbf{r} - \mathbf{r}_i) = \sum_{\mathbf{q}} \exp(i\mathbf{q} \cdot (\mathbf{r} - \mathbf{r}_i)) / V$ gives for the scattering amplitude

$$F(\mathbf{k}, \mathbf{k}') = F(\mathbf{k} - \mathbf{k}') = \sum_{i, \mathbf{q}} e^{i\mathbf{q} \cdot \mathbf{r}_i} \frac{1}{V} \int_V e^{i(\mathbf{k} - \mathbf{k}' + \mathbf{q}) \cdot \mathbf{r}} = \sum_{i, \mathbf{q}} e^{i\mathbf{q} \cdot \mathbf{r}_i} \delta_{\mathbf{q}, \mathbf{k} - \mathbf{k}'}$$

and with $\mathbf{r}_i \rightarrow \mathbf{R}_n + \boldsymbol{\tau}$ for a crystalline solid

$$F(\mathbf{q}) = \sum_{\boldsymbol{\tau}} e^{i\mathbf{q} \cdot \boldsymbol{\tau}} \sum_{\mathbf{n}} e^{i\mathbf{q} \cdot \mathbf{R}_n},$$

where the last sum vanishes except for $\mathbf{q} = \mathbf{G}$ and $\sum_{\mathbf{n}} e^{i\mathbf{q} \cdot \mathbf{R}_n} = N \delta_{\mathbf{q}, \mathbf{G}}$. Thus the scattering amplitude, which equals the static structure factor (up to a factor N) has peaks for the reciprocal lattice vectors.

Consider the reciprocal lattice vector $\mathbf{G}_{hkl} = h\mathbf{b}_1 + k\mathbf{b}_2 + l\mathbf{b}_3$ and the lattice plane with Miller indices (hkl) spanned by $\mathbf{a}_1/h' - \mathbf{a}_2/k'$ and $\mathbf{a}_3/l' - \mathbf{a}_2/k'$ with $(hkl) = p(h'k'l')$, $p = \text{integer}$. The normal to the lattice plane is given by

$$\left(\frac{\mathbf{a}_1}{h'} - \frac{\mathbf{a}_2}{k'}\right) \times \left(\frac{\mathbf{a}_3}{l'} - \frac{\mathbf{a}_2}{k'}\right) = -\frac{1}{h'k'}\mathbf{a}_1 \times \mathbf{a}_2 - \frac{1}{k'l'}\mathbf{a}_2 \times \mathbf{a}_3 - \frac{1}{h'l'}\mathbf{a}_3 \times \mathbf{a}_1.$$

Multiplication of this vector with $-2\pi h'k'l'/\mathbf{a}_1 \cdot (\mathbf{a}_2 \times \mathbf{a}_3)$ gives \mathbf{G}_{hkl}/p , thus \mathbf{G}_{hkl} is normal to the lattice planes (hkl) . The distance of the considered plane from the origin of the vectors $\mathbf{a}_1, \mathbf{a}_2, \mathbf{a}_3$ is

$$d'_{hkl} = \frac{a_1}{h'} \frac{\mathbf{a}_1 \cdot \mathbf{G}_{hkl}}{a_1 G_{hkl}} = \frac{2\pi}{G_{hkl}} \frac{h}{h'} = \frac{2\pi}{G_{hkl}} p.$$

Thus, $2\pi/G_{hkl}$ is the distance between neighboring lattice planes.

Solutions for Chap. 2

2.1: The matrix representation of the commutator $[\hat{H}, \hat{\rho}] = 0$ reads

$$\langle m | \hat{H} \hat{\rho} - \hat{\rho} \hat{H} | n \rangle = \sum_{n'} (H_{mn'} \rho_{n'n} - \rho_{mn'} H_{n'n}) = 0.$$

For eigenstates of \hat{H} one has $H_{mn'} = E_m \delta_{m,n'}$ and

$$(E_m - E_n) \rho_{mn} = 0,$$

which means for $E_m \neq E_n$ or $m \neq n$ for nondegenerate states that $\rho_{mn} = 0$. The same result is found by starting from the statistical operator of the canonical (or grand canonical) ensemble.

2.2: Denote the ground state by $|\Psi_0\rangle$ and show that $(\text{Tr} \hat{\rho} \hat{A})_{T=0} = \langle \Psi_0 | \hat{A} | \Psi_0 \rangle$. With $\hat{\rho} = \exp(-\beta \hat{H})/Z$ write

$$\text{Tr}(\hat{\rho} \hat{A}) = \frac{1}{Z} \sum_{m,n} \langle \Psi_m | e^{-\beta \hat{H}} | \Psi_n \rangle \langle \Psi_n | \hat{A} | \Psi_m \rangle = \frac{1}{Z} \sum_m e^{-\beta E_m} \langle \Psi_m | \hat{A} | \Psi_m \rangle.$$

With $Z = e^{-\beta E_0} \sum_m e^{-\beta(E_m - E_0)}$ we can write

$$\text{Tr}(\hat{\rho} \hat{A}) = \frac{\sum_m e^{-\beta(E_m - E_0)} \langle \Psi_m | \hat{A} | \Psi_m \rangle}{\sum_m e^{-\beta(E_m - E_0)}} \xrightarrow{T \rightarrow 0} \langle \Psi_0 | \hat{A} | \Psi_0 \rangle$$

because with $E_m - E_0 > 0$ for all $m \neq 0$ all exponential factors vanish for $T \rightarrow 0$ except the one for the ground state $|\Psi_0\rangle$.

2.3: The thermal expectation value of the number operator is $\hat{N} = \sum_\alpha \hat{n}_\alpha$ where \hat{n}_α is the operator counting the particles in an eigenstate of \hat{H} . The grand canonical partition function can be written

$$Z_G = \sum_{N=0}^{\infty} \sum_{\{n_\alpha\}_N} e^{\beta \sum_\alpha (\mu - E_\alpha) n_\alpha} = \prod_\alpha \sum_{n_\alpha} e^{\beta(\mu - E_\alpha) n_\alpha},$$

where $\{n_\alpha\}_N$ denotes those sets of particle numbers n_α whose sum is N . For fermions: n_α can be 0 or 1 and

$$Z_G = \prod_{\alpha} \left(1 + e^{\beta(\mu - E_{\alpha})} \right),$$

while for bosons n_{α} can be any nonnegative integer and

$$Z_G = \prod_{\alpha} \left(1 + e^{\beta(\mu - E_{\alpha})} + \dots \right) = \prod_{\alpha} \left(1 - e^{\beta(\mu - E_{\alpha})} \right)^{-1}.$$

Now make use of

$$\langle \hat{N} \rangle = \frac{1}{\beta} \frac{\partial \ln Z_G}{\partial \mu} = \frac{1}{\beta} \frac{1}{Z_G} \frac{\partial Z_G}{\partial \mu}$$

$$\text{to obtain for fermions } \langle \hat{N} \rangle = \sum_{\alpha} \langle \hat{n}_{\alpha} \rangle = \sum_{\alpha} \frac{1}{\exp(-\beta(\mu - E_{\alpha})) + 1}$$

$$\text{and for bosons } \langle \hat{N} \rangle = \sum_{\alpha} \langle \hat{n}_{\alpha} \rangle = \sum_{\alpha} \frac{1}{\exp(-\beta(\mu - E_{\alpha})) - 1}.$$

The function

$$f_{\alpha}^{\pm} = \frac{1}{\exp(-\beta(\mu - E_{\alpha})) \pm 1}$$

is the Fermi–Dirac distribution (upper sign) and the Bose–Einstein distribution (lower sign). For large $k_B T \gg \mu$ we have $\exp \beta \mu \simeq 1$ and $f_{\alpha}^{\pm} \rightarrow \exp(-\beta E_{\alpha})$.

2.4: Ohm's law can be written $j_{\lambda} = \sigma_{\lambda\mu} E_{\mu}$, thus the observable to be measured is (a component of) the electrical current density

$$\hat{A} \rightarrow \hat{j}_{\lambda} = e \sum_{l=1}^N \hat{v}_{l,\lambda}$$

with the velocity operator $\hat{v}_{l,\lambda} = \hat{p}_{l,\lambda}/m$. It can be written also as

$$\hat{j}_{\lambda}(\mathbf{r}) = \frac{e}{2m} \sum_l (\hat{p}_{l,\lambda} \delta(\mathbf{r} - \mathbf{r}_l) + \delta(\mathbf{r} - \mathbf{r}_l) \hat{p}_{l,\lambda}).$$

The operator of the kinetic energy in the presence of an electro-magnetic field (here represented by the vector potential $\mathbf{A}(\mathbf{r}, t)$) is for the l th electron

$$\frac{1}{2m} (\hat{\mathbf{p}}_l - e\mathbf{A}(\mathbf{r}_l, t))^2 = \frac{\mathbf{p}_l^2}{2m} - \frac{e}{2m} (\mathbf{p}_l \cdot \mathbf{A}(\mathbf{r}_l, t) + \mathbf{A}(\mathbf{r}_l, t) \cdot \mathbf{p}_l) + \mathcal{O}(A^2).$$

Neglecting the last term on the *rhs*, we identify the perturbation as

$$\begin{aligned} V_{\text{ext}}(t) &= - \sum_l \frac{e}{2m} (\mathbf{p}_l \cdot \mathbf{A}(\mathbf{r}_l, t) + \mathbf{A}(\mathbf{r}_l, t) \cdot \mathbf{p}_l) \quad \text{or} \\ &= - \int d^3r \underbrace{\frac{e}{2m} \sum_l (\mathbf{p}_l \delta(\mathbf{r} - \mathbf{r}_l) + \delta(\mathbf{r} - \mathbf{r}_l) \mathbf{p}_l)}_{j^{(r)}_l} \cdot \mathbf{A}(\mathbf{r}, t) \end{aligned}$$

and the observable \hat{B} as another component of the electric current density. The electric field component is given by

$$E_{\mu} = -\frac{\partial A_{\mu}}{\partial t} = -i\omega A_{\mu} \quad \text{and we can write}$$

$$V_{\text{ext}}(t) = -\frac{i}{\omega} \sum_{\mu} \int d^3r \hat{j}_{\mu}(\mathbf{r}) E_{\mu}(\mathbf{r}) e^{i\omega t}$$

which in the long-wave length limit, when the dependence of the vector potential on \mathbf{r} can be neglected, gives

$$V_{\text{ext}}(t) = -\frac{i}{\omega} \sum_{\mu} \int d^3r j_{\mu}(\mathbf{r}) E_{\mu} e^{i\omega t}$$

and we obtain the electric conductivity

$$\sigma_{\lambda\mu}(\omega) = \frac{i}{\hbar\omega} \int_{-\infty}^{\infty} d\tau e^{i\omega\tau} \theta(\tau) \langle [j_{\lambda}(\tau), j_{\mu}(0)] \rangle_0$$

as a correlation function for the components of the current density.

2.5: With $\Delta\rho(t) = \Delta\rho_1(t) + \Delta\rho_2(t) + \dots$, where the index refers to different orders of V_{ext} , we can write the equations:

1. $[H_0, \Delta\rho_1] + [V_{\text{ext}}, \rho_0] = i\hbar\dot{\rho}_1$ first order in V_{ext} .
2. $[H_0, \Delta\rho_2] + [V_{\text{ext}}, \rho_1] = i\hbar\dot{\rho}_2$ second order V_{ext} .

The solution of (1)

$$\Delta\rho_1(t) = \frac{1}{i\hbar} \int_{-\infty}^t dt' e^{-iH_0(t-t')/\hbar} [V_{\text{ext}}(t'), \rho_0] e^{iH_0(t-t')/\hbar}$$

is to be used in (2), which can be solved in the same way as (1), to yield

$$\Delta\rho_2(t) = \frac{1}{i\hbar} \int_{-\infty}^t dt' \int_{-\infty}^{t'} dt'' e^{-iH_0(t-t')/\hbar} e^{iH_0(t-t'')/\hbar} [\dots, [\dots, \dots]] e^{iH_0(t-t'')/\hbar}$$

where the double commutator

$$[\dots, [\dots, \dots]] = [V_{\text{ext}}(t'), e^{-iH_0(t-t'')/\hbar} [V_{\text{ext}}(t''), \rho_0]]$$

indicates the structure of the second-order response function

$$\langle \Delta A_2 \rangle_t = \dots [\hat{B}(\tau), [\hat{B}(\tau'), \hat{A}(0)]] .$$

It is a two-time correlation function.

2.6: Evaluate the principal value integral

$$\text{Re}\chi(\omega) = \frac{1}{\pi} \mathcal{P} \int_{-\infty}^{+\infty} \frac{\chi_0}{\omega' - \omega} (\delta(\omega_0 - \omega') - \delta(\omega_0 + \omega')) d\omega',$$

which yields

$$\text{Re}\chi(\omega) = \frac{\chi_0}{\pi} \left(\frac{1}{\omega_0 - \omega} + \frac{1}{\omega_0 + \omega} \right) = \frac{2\chi_0\omega_0}{\pi} \frac{1}{\omega_0^2 - \omega^2} .$$

Solutions for Chap. 3

3.1: The potential energy of the linear chain (Fig. 3.16) is

$$\mathcal{U} = \frac{f}{2} \left\{ \sum_{n'} \underbrace{\left[u \binom{n'}{1} - u \binom{n'}{2} \right]^2}_{(1)} + \underbrace{\left[u \binom{n'+1}{1} - u \binom{n'}{2} \right]^2}_{(2)} \right\},$$

here (1) is the contribution due to the relative displacements of M_1 and M_2 in the unit cell n and (2) that due to the relative displacement between M_1 in unit cell $n+1$ and M_2 in unit cell n .

Distinguish the force constants

$$n = m, \tau = \tau' : \phi \binom{n \ n}{1 \ 1} = \phi \binom{n \ n}{2 \ 2} = 2f$$

for the restoring force acting on M_1 (M_2) if the neighbor atoms are kept fixed,

$$n = m, \tau = 1, \tau' = 2 : \phi \binom{n \ n}{1 \ 2} = -f \quad \text{and}$$

$$n = m+1, \tau = 1, \tau' = 2 : \phi \binom{m+1 \ m}{1 \ 2} = -f.$$

Due to *actio = reactio* we have

$$\phi \binom{n \ n}{1 \ 2} = \phi \binom{n \ n}{2 \ 1} \quad \text{and with (3.13)}$$

$$\text{for } \tau = 1 : \phi \binom{n \ n}{1 \ 1} + \phi \binom{n \ n}{1 \ 2} + \phi \binom{n \ n-1}{1 \ 2} = 2f - f - f = 0$$

$$\text{for } \tau = 2 : \phi \binom{n \ n}{2 \ 2} + \phi \binom{n \ n}{2 \ 1} + \phi \binom{n \ n+1}{2 \ 1} = 2f - f - f = 0.$$

Translation invariance allows to shift the cell index.

Considering the equilibrium positions $x_{n1} = na$ for M_1 and $x_{n2} = na + r_0$ for M_2 along the chain, we find the elements of the dynamical matrix

$$D_{11}(q) = \frac{1}{M_1} \phi \binom{n \ n}{1 \ 1} = \frac{2f}{M_1}, \quad D_{22}(q) = \frac{2f}{M_2}$$

and

$$D_{12}(q) = \frac{1}{\sqrt{M_1 M_2}} \sum_n \phi \binom{n \ m}{1 \ 2} e^{iq(x_{n1} - x_{n2})}.$$

For $n = m$, $x_{n1} - x_{n2} = -r_0$ and for $n = m+1$, $x_{m+1,1} - x_{m,2} = a - r_0$, the force constant equals $-f$ and with $a = 2r_0$, we have

$$D_{12}(q) = \frac{-2f}{\sqrt{M_1 M_2}} \cos(qr_0) = D_{21}(q).$$

The eigensolutions of

$$\|D_{\alpha\beta}(q) - \omega^2(q)\delta_{\alpha,\beta}\| = \left\| \begin{array}{cc} \frac{2f}{M_1} - \omega^2 & \frac{-2f}{\sqrt{M_1 M_2}} \cos qr_0 \\ \frac{-2f}{\sqrt{M_1 M_2}} \cos qr_0 & \frac{2f}{M_2} - \omega^2 \end{array} \right\| = 0$$

are (with $M = M_1 + M_2$)

$$\omega_{\pm}^2(q) = \frac{f}{M_1 M_2} \left[M \pm \{M_1^2 + M_2^2 + 2M_1 M_2(1 - 2\sin^2 qr_0)\}^{1/2} \right].$$

There are two solutions for each q . For $q = 0$, the squared frequencies are

$$\omega_+^2(0) = \frac{2fM}{M_1 M_2}, \quad \text{and} \quad \omega_-^2(0) = 0$$

and for $q \simeq 0$ with $1 - 2\sin^2 qr_0 = \cos qa \simeq 1 - q^2 a^2/2$ (for $q \ll \pi/a$)

$$\omega^2(q) \simeq \frac{f}{M_1 M_2} \left[M \pm \{M^2 - M_1 M_2 q^2 a^2\}^{1/2} \right] \simeq \frac{f}{\mu} \left[1 \pm \left\{ 1 - \frac{\mu}{2M} q^2 a^2 \right\} \right]$$

with the reduced mass $\mu = M_1 M_2 / M$ and

$$\omega_+^2(q \ll \frac{\pi}{a}) \simeq \frac{2f}{\mu} \quad \text{independent of } q \quad \text{and}$$

$$\omega_-^2(q \ll \frac{\pi}{a}) \simeq \frac{f}{2M} q^2 a^2 \quad \rightarrow \quad \omega_-(q \ll \frac{\pi}{a}) \simeq \sqrt{\frac{f}{2M}} a q.$$

For $q = \pi/a$ and $\cos qa = -1$ the solutions are

$$\omega_{\pm}^2\left(\frac{\pi}{a}\right) \left(M \pm \{M_1^2 + M_2^2 - 2M_1 M_2\}^{1/2} \right) \quad \text{or}$$

$$\omega_+\left(\frac{\pi}{a}\right) = \sqrt{\frac{2f}{M_2}}, \quad \omega_-\left(\frac{\pi}{a}\right) = \sqrt{\frac{2f}{M_1}}.$$

A plot of the two branches is shown in Fig. 10.1: the lower branch with the linear dependence around $q \simeq 0$ for the acoustic phonons and the flat upper branch for the optical phonons are separated by a gap which results from the different masses $M_1 \neq M_2$. For $M_1 = M_2 = M$ the gap closes and we have a chain with period a and the dispersion

$$\omega(q) = \sqrt{\frac{4f}{M}} \sin qa$$

extends to π/a (thin dashed line in Fig. 10.1), which is the limit of the Brillouin zone for the chain with lattice constant a .

Solving the eigenvector equations, we find

for $q = 0$: $\omega_-(0) = 0$ $e_-(0) \sim (\sqrt{M_1}, \sqrt{M_2})$ move with same phase

$\omega_+(0) = \sqrt{\frac{2f}{\mu}}$ $e_+(0) \sim (\sqrt{M_2}, -\sqrt{M_1})$ move with opposite phase

for $q = \frac{\pi}{a}$: $\omega_-\left(\frac{\pi}{a}\right) = \sqrt{\frac{2f}{M_1}}$ $e_-\left(\frac{\pi}{a}\right) \sim (1, 0)$ M_2 in rest

$\omega_+\left(\frac{\pi}{a}\right) = \sqrt{\frac{2f}{M_2}}$ $e_+\left(\frac{\pi}{a}\right) \sim (0, 1)$ M_1 in rest.

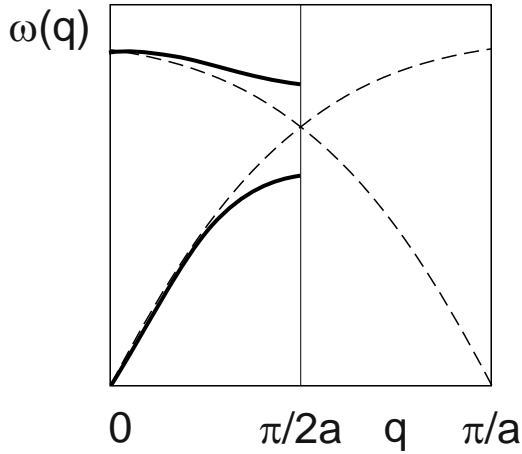


Fig. A.1. Dispersion for the linear chain with two different masses per unit cell (*solid lines*). The *dashed curves* show the result if the two masses are equal

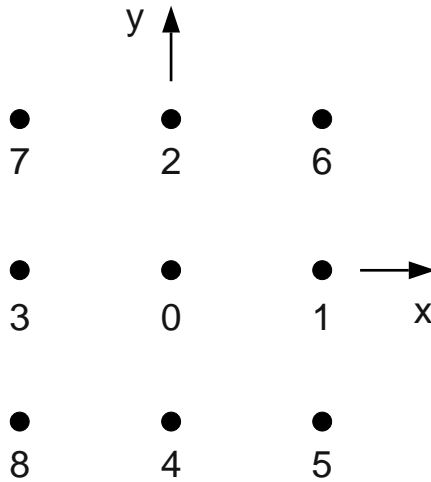


Fig. A.2. Sketch of the two-dimensional quadratic lattice with numbers to address the individual lattice point

3.2: For central forces the adiabatic potential depends on $r_{m,n} = |\mathbf{R}_m^0 + \mathbf{u}_m - \mathbf{R}_n^0 - \mathbf{u}_n|$ and the force constants can be written

$$\phi \begin{pmatrix} m & n \\ i & j \end{pmatrix} = \frac{\partial^2 \mathcal{U}}{\partial r_{m,n}^2} \frac{R_{ki}^0 R_{kj}^0}{|\mathbf{R}_k^0|^2} \quad \text{with} \quad \mathbf{k} = \mathbf{m} - \mathbf{n}.$$

Nearest neighbors to mass in the center (see Fig. 10.2) are

$$\mathbf{R}_1^0 = ae_x, \quad \mathbf{R}_2^0 = ae_y, \quad \mathbf{R}_3^0 = -ae_x, \quad \mathbf{R}_4^0 = -ae_y$$

with force constants

$$\phi \begin{pmatrix} 1 & 0 \\ x & x \end{pmatrix} = \phi \begin{pmatrix} 2 & 0 \\ y & y \end{pmatrix} = \phi \begin{pmatrix} 3 & 0 \\ x & x \end{pmatrix} = \phi \begin{pmatrix} 4 & 0 \\ y & y \end{pmatrix} = \phi_1, \quad \phi \begin{pmatrix} k & 0 \\ x & y \end{pmatrix} = 0$$

next nearest neighbors are

$$\mathbf{R}_5^0 = a\mathbf{e}_x - \mathbf{e}_y, \quad \mathbf{R}_7^0 = -a\mathbf{e}_x + a\mathbf{e}_y$$

with force constants

$$\phi \begin{pmatrix} 5 & 0 \\ x & x \end{pmatrix} = \phi \begin{pmatrix} 5 & 0 \\ y & y \end{pmatrix} = \phi \begin{pmatrix} 7 & 0 \\ x & x \end{pmatrix} = \phi \begin{pmatrix} 7 & 0 \\ y & y \end{pmatrix} = \frac{1}{2}\phi_2,$$

$$\phi \begin{pmatrix} 5 & 0 \\ x & y \end{pmatrix} = \phi \begin{pmatrix} 5 & 0 \\ y & x \end{pmatrix} = \phi \begin{pmatrix} 7 & 0 \\ x & y \end{pmatrix} = \phi \begin{pmatrix} 7 & 0 \\ y & x \end{pmatrix} = -\frac{1}{2}\phi_2$$

and

$$\mathbf{R}_6^0 = a\mathbf{e}_x + a\mathbf{e}_y \quad \text{with} \quad \phi \begin{pmatrix} 6 & 0 \\ x & x \end{pmatrix} = \phi \begin{pmatrix} 6 & 0 \\ y & y \end{pmatrix} = \phi \begin{pmatrix} 6 & 0 \\ x & y \end{pmatrix} = \frac{1}{2}\phi_2$$

and

$$\mathbf{R}_8^0 = -a\mathbf{e}_x - a\mathbf{e}_y \quad \text{with} \quad \phi \begin{pmatrix} 8 & 0 \\ x & x \end{pmatrix} = \phi \begin{pmatrix} 8 & 0 \\ y & y \end{pmatrix} = \phi \begin{pmatrix} 8 & 0 \\ x & y \end{pmatrix} = \frac{1}{2}\phi_2.$$

The force constant

$$\phi \begin{pmatrix} 0 & 0 \\ i & j \end{pmatrix} \quad \text{follows from} \quad \sum_k \phi \begin{pmatrix} k & 0 \\ i & j \end{pmatrix} = 0$$

$$\rightarrow \phi \begin{pmatrix} 0 & 0 \\ i & j \end{pmatrix} = -\sum_{k=1}^8 \phi \begin{pmatrix} k & 0 \\ i & j \end{pmatrix} = -2(\phi_1 + \phi_2)\delta_{i,j}.$$

The elements of the dynamical matrix are

$$\begin{aligned} D_{xx}(\mathbf{q}) &= \frac{1}{M} \sum_k \phi \begin{pmatrix} k & 0 \\ x & x \end{pmatrix} e^{-i\mathbf{q}\cdot\mathbf{R}_k^0} \\ &= -\frac{2}{M} (\phi_1(1 - \cos q_x a) + \phi_2(1 - \cos q_x a \cos q_y a)), \\ D_{yy}(\mathbf{q}) &= -\frac{2}{M} (\phi_1(1 - \cos q_y a) + \phi_2(1 - \cos q_x a \cos q_y a)), \\ D_{xy}(\mathbf{q}) &= -\frac{2}{M} \phi_2 \sin q_x a \sin q_y a. \end{aligned}$$

The secular problem is

$$\left\| \begin{array}{cc} D_{xx}(\mathbf{q}) - \omega^2 & D_{xy}(\mathbf{q}) \\ D_{xy}(\mathbf{q}) & D_{yy}(\mathbf{q}) - M\omega^2 \end{array} \right\| = 0.$$

For $\Gamma - X$: $0 \leq q_x \leq \pi/a$, $q_y = 0$, $\sin q_y a = 0$, $\cos q_y a = 1$ we have two branches

$$\omega_1^2(q_x) = \frac{2}{M}(\phi_1 + \phi_2)(1 - \cos q_x a) \quad \text{and} \quad \omega_2^2(q_x) = \frac{2}{M}\phi_2(1 - \cos q_x a)$$

with $\omega_{q_x} \sim q_x$ for $q_x \ll \pi/a$ but different slopes.

For $\Gamma - M$: $\mathbf{q} = (a, q)/\sqrt{2}$, $0 \leq q \leq \sqrt{2}\pi/a$ the secular problem yields

$$\left(M\omega^2 - \underbrace{2\phi_1 \left(1 - \cos \frac{qa}{\sqrt{2}}\right) - 2\phi_2 \left(1 - \cos^2 \frac{qa}{\sqrt{2}}\right)}_{2a} \right)^2 - \underbrace{4\phi_2^2 \sin^4 \frac{qa}{\sqrt{2}}}_{b^2} = 0$$

with the solutions

$$M\omega^2 = 2a \pm 2b : M\omega_1^2 = 2\phi_1 \left(1 - \cos \frac{qa}{\sqrt{2}}\right),$$

$$M\omega_2^2 = 2\phi_1 \left(1 - \cos \frac{qa}{\sqrt{2}}\right) + 2\phi_2 \left(1 - \cos \frac{2qa}{\sqrt{2}}\right).$$

Again we find two branches with $\omega(q) \sim q$ for $q \ll \pi/a$ and different slopes.

For $X - M$: $\mathbf{q} = (\pi/a, q)$, $0 \leq q \leq \pi/a$ the off-diagonal terms of the dynamical matrix vanish and one has

$$\omega_1^2 = \frac{2}{M}(2\phi_1 + \phi_2(1 + \cos qa)) \quad \text{and} \quad \omega_2^2 = \frac{2}{M}(\phi_1 + \phi_2 - (\phi_1 - \phi_2)\cos qa).$$

The two branches have always finite frequencies and connect those already obtained for the X and M point.

For each of these directions one eigenvector is longitudinal ($\parallel \mathbf{q}$) and one transverse ($\perp \mathbf{q}$).

3.3: Periodic boundaries account for the fact that the physics of a solid repeats over macroscopic distances, i.e., the Bloch phase factor equals one for a translation $\mathbf{R}_N = N_1\mathbf{a}_1 + N_2\mathbf{a}_2 + N_3\mathbf{a}_3$ over a macroscopic length ($N_i \gg 1$, $i = 1, 2, 3$):

$$e^{i\mathbf{k} \cdot \mathbf{R}_N} = 1 \quad \text{or} \quad \mathbf{k} \cdot \mathbf{R}_N = 2\pi \times \text{integer}.$$

This implies (take a simple cubic lattice with $V = L_1L_2L_3$, $L_i = N_i a$ as example) that the components of the wave vector take the discrete values (particle in the box) $k_i = 2\pi n_i/L_i$, $i = 1, 2, 3$ and $0 \leq n_i \leq N_i - 1$. Thus $N = N_1N_2N_3$ is the number of \mathbf{k} in the first Brillouin zone and each \mathbf{k} takes a volume $(2\pi)^3/V$. This can be exploited when replacing a sum over \mathbf{k} by an integral according to

$$\sum_{\mathbf{k}} \dots = \frac{V}{(2\pi)^3} \int \dots d^3k.$$

Similar considerations hold for systems with reduced dimension.

3.4: For the commutator $[a_s(\mathbf{q}), a_{s'}^\dagger(\mathbf{q}')]$ evaluate

$$\begin{aligned} & [\omega_s(\mathbf{q})\hat{Q}_s(\mathbf{q}) + i\hat{P}_s(-\mathbf{q}), \omega_{s'}(\mathbf{q}')\hat{Q}_{s'}(-\mathbf{q}') - i\hat{P}_{s'}(\mathbf{q}')] = \\ & -i\omega_s(\mathbf{q}) \underbrace{[\hat{Q}_s(\mathbf{q}), \hat{P}_{s'}(\mathbf{q}')] }_{i\hbar\delta_{s,s'}\delta_{\mathbf{q},\mathbf{q}'}} + i\omega_{s'}(\mathbf{q}') \underbrace{[\hat{P}_s(-\mathbf{q}), \hat{Q}_{s'}(-\mathbf{q}')] }_{-i\hbar\delta_{s,s'}\delta_{\mathbf{q},\mathbf{q}'}} = 2\hbar\omega_s(\mathbf{q})\delta_{s,s'}\delta_{\mathbf{q},\mathbf{q}'} \end{aligned}$$

to find $[a_s(\mathbf{q}), a_{s'}^\dagger(\mathbf{q}')] = \delta_{s,s'}\delta_{\mathbf{q},\mathbf{q}'}$. The two other commutation relations follow in the same way (note that $\omega_s(\mathbf{q}) = \omega_s(-\mathbf{q})$).

3.5: In the Schrödinger picture, we have

$$[a_s(\mathbf{q}), H_0] = \hbar\omega_{s'}(\mathbf{q}')a_s(\mathbf{q}) \quad \text{or} \quad a_s(\mathbf{q})H_0 = (H_0 + \hbar\omega_{s'}(\mathbf{q}'))a_s(\mathbf{q}).$$

Thus, for any power function $f(H_0)$ we can write

$$a_s(\mathbf{q})f(H_0) = f(H_0 + \hbar\omega_s(\mathbf{q}))a_s(\mathbf{q})$$

and obtain

$$\begin{aligned} a_s(\mathbf{q}, t)a_{s'}^\dagger(\mathbf{q}', 0) &= e^{iH_0t/\hbar}a_s(\mathbf{q}, 0)e^{-iH_0t/\hbar}a_{s'}^\dagger(\mathbf{q}', 0) \\ &= e^{-i\omega_s(\mathbf{q})t}a_s(\mathbf{q}, 0)a_{s'}^\dagger(\mathbf{q}', 0). \end{aligned}$$

Using the commutation relation and taking the thermal expectation value gives

$$\langle a_s(\mathbf{q}, t)a_{s'}^\dagger(\mathbf{q}', 0) \rangle = e^{-i\omega_s(\mathbf{q})t}(n_s(\mathbf{q}, T) + 1)\delta_{s,s'}\delta_{\mathbf{q},\mathbf{q}'}.$$

Similarly we have

$$a_s^\dagger(\mathbf{q})H_0 = (H_0 - \hbar\omega_{s'}(\mathbf{q}'))a_s^\dagger(\mathbf{q})$$

and by following the same steps we find the second relation. For the third relation we have, after extracting the exponential with the time-dependence, the thermal expectation value of a product of two annihilation operators, which vanishes.

3.6: The displacement is a time-dependent operator in the Heisenberg picture. Start by writing (with $[\rho_0, H_0] = 0$)

$$\langle (\mathbf{q} \cdot \mathbf{u}_n(t))^2 \rangle = \text{Tr} \left(\rho_0 e^{iH_0t/\hbar} (\mathbf{q} \cdot \mathbf{u}_n(0))^2 e^{-iH_0t/\hbar} \right)$$

and obtain by cyclic permutation under the trace

$$\langle (\mathbf{q} \cdot \mathbf{u}_n(t))^2 \rangle = \text{Tr} \left((\mathbf{q} \cdot \mathbf{u}_n(0))^2 \right),$$

which is independent of t . Formulate the lattice displacement with (3.23) and (3.39)

$$\mathbf{u}_n = \sum_{s,\mathbf{q}} \left(\frac{\hbar}{2NM\omega_s(\mathbf{q})} \right)^{1/2} (a_s^\dagger(-\mathbf{q}) + a_s(\mathbf{q})) e_s(\mathbf{q}) e^{i\mathbf{q} \cdot \mathbf{R}_n^0}$$

in terms of phonon operators and evaluate

$$\begin{aligned} (\mathbf{q} \cdot \mathbf{u}_n)^2 &= \frac{1}{NM} \sum_{\substack{s',\mathbf{q}' \\ s'',\mathbf{q}''}} (a_{s'}^\dagger(-\mathbf{q}') + a_{s'}(\mathbf{q}')) (a_{s''}^\dagger(-\mathbf{q}'') + a_{s''}(\mathbf{q}'')) \\ &\quad \times \left(\frac{\hbar^2}{4\omega_{s'}(\mathbf{q}')\omega_{s''}(\mathbf{q}'')} \right)^{1/2} e^{i(\mathbf{q}'+\mathbf{q}'') \cdot \mathbf{R}_n^0} (\mathbf{q} \cdot e_{s'}(\mathbf{q}')) (\mathbf{q} \cdot e_{s''}(\mathbf{q}'')). \end{aligned}$$

After multiplying out the operator terms, the thermal expectation value of this expression follows with the formulas of problem 3.4 as

$$\langle (\mathbf{q} \cdot \mathbf{u}_n)^2 \rangle = \frac{1}{NM} \sum_{s',\mathbf{q}'} (2n_{s'}(\mathbf{q}', T) + 1) \frac{\hbar}{2\omega_{s'}(\mathbf{q}')} (\mathbf{q} \cdot e_{s'}(\mathbf{q}'))^2$$

For $T \rightarrow 0$ we have $n_s(\mathbf{q}, T) \rightarrow 0$ which leaves only the contribution of the zero-point motion

$$\langle (\mathbf{q} \cdot \mathbf{u}_n)^2 \rangle = \frac{1}{NM} \sum_{s', \mathbf{q}'} \frac{\hbar}{2\omega_{s'}(\mathbf{q}')} (\mathbf{q} \cdot \mathbf{e}_{s'}(\mathbf{q}'))^2.$$

For $T > 0$, employ the Debye model by writing $\omega_s(\mathbf{q}) = vq$ for all s and independent of the direction of \mathbf{q} . Summation over s' yields a factor 3. Writing $(\mathbf{q} \cdot \mathbf{e}_{s'}(\mathbf{q}'))^2 = q^2 \cos^2 \vartheta^2$ where ϑ is the angle between \mathbf{q} and $\mathbf{e}_{s'}(\mathbf{q}')$, the sum over \mathbf{q}' can be carried out in spherical polar coordinates with the cut-off at $q_D = \omega_D/v$ (with the Debye frequency ω_D) giving

$$\langle (\mathbf{q} \cdot \mathbf{u}_n)^2 \rangle = \frac{6q^2}{M\omega_D^3} \int_0^{\omega_D} \hbar\omega \left(\frac{1}{\exp(\hbar\omega/k_B T) - 1} + \frac{1}{2} \right) d\omega.$$

For high temperatures, $k_B T \gg \hbar\omega$, the distribution function after expanding the exponential yields $k_B T/\hbar\omega$ and by neglecting the term $1/2$ we find for the Debye-Waller factor

$$W = \frac{3q^2}{M\omega_D^3} k_B T \int_0^{\omega_D} d\omega = \frac{3q^2 k_B T}{M\omega_D^2}$$

which is always positive.

For low temperatures, $k_B T \ll \hbar\omega$, the integral over ω reads after substituting $\hbar\omega/k_B T = x$

$$\int_0^{\omega_D} \dots d\omega = \frac{\hbar\omega_D^2}{4} + \frac{(k_B T)^2}{\hbar} \int_0^{x_D} \frac{x dx}{e^x - 1}$$

For $T \rightarrow 0$ the upper limit goes to ∞ and the integral takes the value $\pi^2/6$ (see Appendix A.3). Thus, we may write

$$W = \frac{3q^2}{M\omega_D^3} \left(\frac{\hbar\omega_D^2}{4} + \frac{\pi^2 (k_B T)^2}{6 \hbar} \right) = \frac{3\hbar^2 q^2}{M k_B \Theta_D} \left(\frac{1}{4} + \frac{\pi^2}{6} \left(\frac{T}{\Theta_D} \right)^2 \right)$$

with the Debye temperature Θ_D .

3.7: (a) The point group of a cubic lattice consists of 48 elements (24 rotations, each can be combined with the inversion). Under these operations, which can be represented by orthogonal 3×3 matrices $S_{\alpha i}$, the coordinates x, y, z are interchanged and (under inversion) change their sign. Likewise the components of the elastic tensor transform according to

$$c_{\alpha\beta\gamma\delta} = S_{\alpha i} S_{\beta j} S_{\gamma k} S_{\delta l} c_{ijkl} \quad (\text{double index summation}).$$

The invariance of the elastic tensor under these transformations leaves only those components different from zero, for which pairs of indices are identical and of the nonvanishing components all those are identical which transform into each other by the symmetry operations. Thus, there are only three independent tensor components

$$\begin{aligned} c_{xxxx} &= c_{yyyy} = c_{zzzz} = c_{11} \\ c_{xyxy} &= c_{xzxz} = c_{yxyx} = c_{zxxz} = c_{12} \\ c_{xxyy} &= c_{yyzz} = c_{zzxx} = c_{xxzz} = c_{zzyy} = c_{44} \end{aligned}$$

which are written here in Voigt notation.

(b) Using $u_i(\mathbf{r}, t) = u_i \exp(i(\mathbf{q} \cdot \mathbf{r} - \omega t))$ the wave equation for the elastic displacement field leads to a set of coupled homogeneous linear equations for the components u_i , which has solutions if

$$\|\rho\omega^2\delta_{il} - c_{ijkl}q_jq_k\| = 0.$$

For $\Gamma - X$ or $\mathbf{q} = (q, 0, 0)$ it reads

$$\left\| \begin{array}{ccc} \rho\omega^2 - c_{11}q^2 & 0 & 0 \\ 0 & \rho\omega^2 - c_{12}q^2 & 0 \\ 0 & 0 & \rho\omega^2 - c_{12}q^2 \end{array} \right\| = 0$$

and has solutions

$$\begin{aligned} \omega_L &= \sqrt{\frac{c_{11}}{\rho}} q, \quad \mathbf{e}_L = (1, 0, 0) \quad \text{longitudinal} \\ \omega_T &= \sqrt{\frac{c_{12}}{\rho}} q, \quad \mathbf{e}_T = (0, 1, 0) \quad \text{transverse} \\ &= (0, 0, 1) \quad \text{transverse.} \end{aligned}$$

For $\Gamma - K$ or $\mathbf{q} = (q, q, 0)/\sqrt{2}$, we have $c_{ijkl}q_jq_k = (c_{ixxl} + c_{iyyl} + c_{ixyl} + c_{iyxl})q^2/2$ and the secular problem

$$\left\| \begin{array}{ccc} \rho\omega^2 - \frac{1}{2}(c_{11} + c_{12})q^2 & -\frac{1}{2}(c_{12} + c_{44})q^2 & 0 \\ -\frac{1}{2}(c_{12} + c_{44})q^2 & \rho\omega^2 - \frac{1}{2}(c_{11} + c_{12})q^2 & 0 \\ 0 & 0 & \rho\omega^2 - c_{12}q^2 \end{array} \right\| = 0.$$

One solution is immediately found to be

$$\omega_{T_1} = \sqrt{\frac{c_{12}}{\rho}} q, \quad \mathbf{e}_{T_1} = (0, 0, 1) \quad \text{transverse.}$$

The other two follow from

$$\left\| \begin{array}{cc} \rho\omega^2 - A & -B \\ -B & \rho\omega^2 - A \end{array} \right\| = (\rho\omega^2 - A)2^{-}B^2 = 0$$

with $A = (c_{11} + c_{12})q^3/2$ and $B = (c_{12} + c_{44})q^2/2$ and read

$$\begin{aligned} \omega_{T_2} &= \sqrt{\frac{2c_{12} + c_{11} + c_{44}}{2\rho}} q, \quad \mathbf{e}_{T_2} = (1, -1, 0)/\sqrt{2} \quad \text{transverse} \\ \omega_L &= \sqrt{\frac{c_{11} - c_{44}}{2\rho}} q, \quad \mathbf{e}_L = (1, 1, 0)/\sqrt{2} \quad \text{longitudinal.} \end{aligned}$$

These results can be compared with the phonon dispersion (e.g., those given in Sect. 3.6 which are all for lattices with cubic symmetry). The slope of the acoustic branches for given ρ can be taken to determine the elastic constants.

3.8: The cubic anharmonicity $\Delta(a^\dagger + a)^3$ is first written in normal order

$$(a^\dagger + a)^3 = a^{\dagger 3} + 3a^{\dagger 2}a + 3(a^\dagger + a) + 3a^\dagger a^2 + a^3$$

and then truncated by replacing $a^\dagger a \rightarrow \langle a^\dagger a \rangle = n(T)$ and omitting the terms $a^{\dagger 3}$ and a^3 . Thus the Hamiltonian reduces to

$$H = \hbar\omega_0 a^\dagger a + \Delta(T)(a^\dagger + a) \quad \text{with} \quad \Delta(T) = 3\Delta(n(T) + 1).$$

Calculate now the corrections to the oscillator ground state $|n\rangle$ with $n = 0$ due to the anharmonicity, which by making use of $\langle 0|a|1\rangle\langle 1|a^\dagger|0\rangle = 1$ reads in Brillouin–Wigner perturbation theory

$$\varepsilon = E_0 - \frac{\hbar\omega_0}{2} = \frac{\Delta^2(T)}{\varepsilon - \hbar\omega_0}.$$

The smaller solution of the quadratic equation in ε

$$E_0 = \frac{1}{2}\hbar\omega_0 - \frac{\Delta^2(T)}{\hbar\omega_0}$$

expresses a zero-point energy which decreases as $\Delta(T)$ increases due to thermal phonon excitation with the temperature. This is the behavior of a soft mode.

Solutions for Chap. 4

4.1: The electrostatic potential of a homogeneous positive charge density $+eN(\mathbf{r})$ with $n(\mathbf{r}) = N/V$ is

$$\phi(\mathbf{r}) = \int_V \frac{e n(\mathbf{r}')}{4\pi\varepsilon_0 |\mathbf{r} - \mathbf{r}'|} d^3 r'.$$

Its interaction energy with the homogeneous electron density $-en(\mathbf{r})$ is

$$\mathcal{H}_{\text{el-ion}} = -e \int_V n(\mathbf{r})\phi(\mathbf{r}) d^3 r = -\left(\frac{N}{V}\right)^2 \int d^3 r \int d^3 r' \frac{e^2}{4\pi\varepsilon_0 |\mathbf{r} - \mathbf{r}'|}.$$

With (see Appendix)

$$\frac{e^2}{4\pi\varepsilon_0 |\mathbf{r} - \mathbf{r}'|} = \sum_q v_q e^{i\mathbf{q}\cdot(\mathbf{r}-\mathbf{r}')} , \quad v_q = \frac{e^2}{\varepsilon_0 V q^2} \quad \text{the double integral can be evaluated}$$

$$\int d^3 r \int d^3 r' \frac{e^2}{4\pi\varepsilon_0 |\mathbf{r} - \mathbf{r}'|} = \sum_q v_q \underbrace{\int d^3 r e^{i\mathbf{q}\cdot\mathbf{r}}}_{V\delta_{\mathbf{q},0}} \underbrace{\int d^3 r' e^{i\mathbf{q}\cdot\mathbf{r}'}}_{V\delta_{\mathbf{q},0}} = \sum_q v_q V^2 \delta_{\mathbf{q},0}$$

giving $\mathcal{H}_{\text{el-ion}} = -N^2 v_0$. Similarly the interaction energy of the homogeneous electron and ions systems can be calculated which each give the same result up to a factor $-1/2$. Thus the sum of all these divergent interaction energies vanish for the jellium model.

4.2: The electron density n determines via the density of states $D(E)$ and the Fermi–Dirac distribution function the chemical potential $\mu(T)$. For a 3D electron system we may write $D(E) = 3n\sqrt{E}/2E_F^{3/2}$ define a function $G(E)$ with

$$\int_{-\infty}^E D(E') dE' = G(E) = n \left(\frac{E}{E_F} \right)^{3/2}$$

to express the particle density as

$$n = G(E)f(E, \mu, T)|_0^\infty - \int_{-\infty}^{\infty} dE G(E) \frac{\partial f(E, \mu, T)}{\partial E}.$$

The first term vanishes and the integral can be evaluated by using the fact, that the derivative of $f(E, \mu, T)$ is strongly peaked at $E = \mu$ (for $k_B T \ll \mu$). Expand $G(E)$ in a power series around $E = \mu$

$$G(E) = \int_{-\infty}^{\mu} dE' D(E') + \sum_{n=1}^{\infty} \frac{(E - \mu)^n}{n!} \left. \frac{d^n G(E)}{dE^n} \right|_{E=\mu}.$$

The integral gives $G(\mu)$. Because $\partial f / \partial E$ is an even function only the even powers of the expansion contribute and we find as the two leading terms

$$n = -G(\mu) \int_{-\infty}^{\infty} dE \frac{\partial f}{\partial E} - \frac{3n}{8E_F^{3/2}} \frac{1}{\sqrt{\mu}} \int_{-\infty}^{\infty} dE (E - \mu)^2 \frac{\partial f}{\partial E} \quad (*).$$

The first term gives $n(\mu/E_F)^{3/2}$. With

$$\frac{\partial f}{\partial E} = -\beta \frac{e^{\beta(E-\mu)}}{(e^{\beta(E-\mu)} + 1)^2}, \quad \beta = k_B T \quad \text{and substituting } x = \beta(E - \mu)$$

$$\int_{-\infty}^{\infty} dE (E - \mu)^2 \frac{\partial f}{\partial E} = -\frac{1}{\beta^3} \int_{-\infty}^{\infty} dx x^2 \frac{e^x}{(e^x + 1)^2}.$$

The value of the integral is $\pi^2/6$. Thus (*) reduces to the relation

$$1 \simeq \left(\frac{\mu}{E_F} \right)^{3/2} \left(1 + \left(\frac{k_B T}{\mu} \right)^2 \frac{\pi^2}{8} \right)$$

which can be solved to give

$$\mu(T) \simeq E_F \left(1 - \frac{\pi^2}{12} \left(\frac{k_B T}{\mu} \right)^2 \right).$$

This result corresponds to the Sommerfeld expansion (see Appendix A.4).

4.3: For 2D, the number of states (per unit area) $D(k)dk$ in a circular ring with radius k and thickness dk is

$$D(k)dk = \frac{2}{(2\pi)^2} 2\pi k dk \quad (\text{the factor 2 counts the spins}).$$

Use the dispersion relation for free electrons $E_k = \hbar^2 k^2 / 2m$ to substitute k by E

$$D(E)dE = D(k) \frac{dk}{dE} dE = \frac{1}{\pi} \sqrt{\frac{2m}{\hbar^2}} \sqrt{E} \sqrt{\frac{2m}{\hbar^2}} \frac{1}{2\sqrt{E}} dE$$

$$\text{or } D(E) = \frac{m}{\pi \hbar^2} = \text{const.}$$

For 1D the corresponding number of states per unit length is

$$D(k)dk = \frac{2}{2\pi} dk \quad \text{and} \quad D(k) \frac{dk}{dE} dE = \frac{1}{\pi} \sqrt{\frac{2m}{\hbar^2}} \frac{1}{2\sqrt{E}} dE$$

$$\text{or } D(E) = \sqrt{\frac{m}{2\pi^2\hbar^2}} \frac{1}{\sqrt{E}}.$$

For a zero-dimensional system the spectrum is discrete (with energies E_i) and the density of states is given by

$$D(E) = 2 \sum_i \delta(E - E_i).$$

4.4: The condition to fill n electrons into the lowest (spin-degenerate) Landau level follows from (4.43) or in simplified form from $E_F = \hbar\omega_c$ and reads

$$\frac{\hbar^2}{2m}(3\pi^2 n)^{2/3} = \frac{\hbar e B}{m} \quad \text{which can be solved to give } B = \frac{\hbar}{2e}(3\pi^2 n)^{2/3}.$$

Note, that B is related to the number of elementary flux quanta. Take the value for $\hbar/e = 0.658 \cdot 10^{-15} \text{ Tm}^2$ to obtain for a metal $n = 10^{23} \text{ cm}^{-3}$ a magnetic field of $B \simeq 1.37 \cdot 10^5 \text{ T}$ and for a doped semiconductor with $n = 10^{14} \text{ cm}^{-3}$ $B \simeq 0.137 \text{ T}$. The latter is easily achieved in a laboratory.

4.5: The Zeeman energy for free electrons is $\pm\mu_B B$. It shifts the density of states of up and down spins (Landau quantization is not considered here) against each other

$$D_{\pm}(E, B) = \frac{1}{2}D(E \pm \mu_B B) \simeq \frac{1}{2}D(E) \pm \frac{1}{2}\mu_B B \frac{dD(E)}{dE} \quad \text{which yields}$$

$$D_{\pm}(E, B) \simeq \frac{1}{2} \frac{1}{2\pi^2} \left(\frac{2m}{\hbar^2} \right)^{3/2} \sqrt{E} \left(1 \pm \frac{\mu_B B}{E} \right).$$

The number of spin up and down electrons $N_{\pm}(E, B)$ is obtained by integrating the density of states multiplied with the Fermi-Dirac distribution function and multiplying with the volume V . The first term of $D_{\pm}(E, B)$ gives $N(\mu)/2$ independent of B . The second term is evaluated by employing the Sommerfeld expansion (see Appendix A.4) leading to

$$\dots = \pm \frac{1}{2}\mu_B B \left\{ \int_{-\infty}^{\mu} \frac{dD(E)}{dE} dE + \frac{\pi^2}{6} (k_B T)^2 \frac{d^2 D(E)}{dE^2} \Big|_{E=\mu} \right\}.$$

The integral gives $D(\mu)$ and with $D(E) \sim \sqrt{E}$ the second term can be rewritten using $d^2 D(E)/dE^2 = -D(E)/4E^2$ to obtain

$$N_{\pm}(E, B) \simeq \frac{1}{2}N(\mu) \pm \frac{V}{2}\mu_B B D(\mu) \left\{ 1 - \frac{\pi^2}{24} \left(\frac{k_B T}{\mu} \right)^2 \right\}.$$

The magnetization follows as

$$M = \mu_B (N_+ - N_-)/V = \mu_B^2 B D(\mu) \left\{ 1 - \frac{\pi^2}{24} \left(\frac{k_B T}{\mu} \right)^2 \right\}.$$

For $T = 0$ with $D(\mu \simeq E_F) = 3n/2E_F$ this is identical with (4.53).

4.6: The HF approximation is better for the electron system with the smaller density parameter r_s . According to Table 4.1 the r_s -values of doped semiconductors are smaller than those of metals. On the other hand the electron density (per cm^{-3}) is

higher in metals. Note, that r_s is given in the length scale (effective Bohr radius) of the material.

4.7: Second-order perturbation yields a contribution

$$E_2 = - \sum_m \frac{|\langle \Psi_m | H_{\text{int}} | \Psi_0 \rangle|^2}{E_m - E_0}.$$

(a) Applying the interaction operator to the Fermi sphere $|\Psi_0\rangle$ gives nonvanishing contributions only if the states with \mathbf{p}, \mathbf{q} are inside and those with $\mathbf{p} - \mathbf{k}, \mathbf{q} + \mathbf{k}$ outside of the Fermi sphere. Consider therefore the corresponding excited states $|\Psi_m\rangle$. These states with $E_m - E_0 = \hbar^2 \mathbf{k} \cdot (\mathbf{q} - \mathbf{p} + \mathbf{k})/m$ contribute to E_2 . b) The electron taken from \mathbf{p} to $\mathbf{p} - \mathbf{k}$ is put back to \mathbf{p} in the direct process but to \mathbf{q} in the exchange process. For the former evaluate

$$\langle \Psi_0 | \sum_{\substack{\mathbf{p}' \mathbf{q}' \mathbf{k}' \\ \rho \rho'}} v_{\mathbf{k}'} c_{\mathbf{p}' - \mathbf{k}'}^\dagger c_{\mathbf{q}' + \mathbf{k}'}^\dagger c_{\mathbf{q}' \rho'} c_{\mathbf{p}' \rho} | \Psi_m \rangle \langle \Psi_m | \sum_{\substack{\mathbf{p} \mathbf{q} \mathbf{k} \\ \sigma \sigma'}} v_{\mathbf{k}} c_{\mathbf{p} - \mathbf{k} \sigma}^\dagger c_{\mathbf{q} + \mathbf{k} \sigma'}^\dagger c_{\mathbf{q} \sigma'} c_{\mathbf{p} \sigma} | \Psi_0 \rangle$$

For the direct process the intermediate states have to fulfill the conditions

$$\begin{aligned} \mathbf{p}, \sigma &= \mathbf{p}' - \mathbf{k}', \rho & \mathbf{p} - \mathbf{k}, \sigma &= \mathbf{p}', \rho \\ \mathbf{q}, \sigma' &= \mathbf{q}' + \mathbf{k}', \rho' & \mathbf{q} + \mathbf{k}, \sigma' &= \mathbf{q}', \rho' \end{aligned}$$

or

$$\sigma = \rho, \sigma' = \rho', \mathbf{p}' = \mathbf{p} - \mathbf{k}, \mathbf{q}' = \mathbf{q} + \mathbf{k}, \mathbf{k}' = -\mathbf{k}.$$

It remains to determine

$$\langle \Psi_0 | c_{\mathbf{p} \sigma}^\dagger c_{\mathbf{q} \sigma'}^\dagger c_{\mathbf{q} + \mathbf{k} \sigma'} c_{\mathbf{p} - \mathbf{k} \sigma} c_{\mathbf{p} - \mathbf{k} \sigma}^\dagger c_{\mathbf{q} + \mathbf{k} \sigma'}^\dagger c_{\mathbf{q} \sigma'} c_{\mathbf{p} \sigma} | \Psi_0 \rangle = \dots,$$

which can easily be rearranged as for $\mathbf{k} \neq 0$ all fermion operators anti-commute and one obtains

$$\begin{aligned} \dots &= \langle \Psi_0 | c_{\mathbf{p} \sigma}^\dagger c_{\mathbf{p} \sigma} c_{\mathbf{q} \sigma'}^\dagger c_{\mathbf{q} \sigma'} c_{\mathbf{q} + \mathbf{k} \sigma'}^\dagger c_{\mathbf{q} + \mathbf{k} \sigma'} c_{\mathbf{p} - \mathbf{k} \sigma}^\dagger c_{\mathbf{p} - \mathbf{k} \sigma} | \Psi_0 \rangle \\ &= n_{\mathbf{p} \sigma} n_{\mathbf{q} \sigma'} (1 - n_{\mathbf{q} + \mathbf{k} \sigma'}) (1 - n_{\mathbf{p} - \mathbf{k} \sigma}), \end{aligned}$$

where $n_{\mathbf{q} \sigma} = \theta(k_F - q)$ is the Fermi-Dirac distribution function for $T = 0$ K. Summing over spin indices (factor 4) gives for the direct process

$$E_2^{\text{dir}} = -4 \sum_{\mathbf{p}, \mathbf{q}, \mathbf{k}} v_{\mathbf{k}}^2 \frac{m}{\hbar^2 \mathbf{k} \cdot (\mathbf{q} - \mathbf{p} + \mathbf{k})} n_{\mathbf{p} \sigma} n_{\mathbf{q} \sigma'} (1 - n_{\mathbf{q} + \mathbf{k} \sigma'}) (1 - n_{\mathbf{p} - \mathbf{k} \sigma}).$$

c) For small \mathbf{k} , i.e., excitation close to the Fermi surface

$$n_{\mathbf{p} + \mathbf{k}} \simeq n_{\mathbf{p}} + \mathbf{k} \cdot \nabla_{\mathbf{p}} n_{\mathbf{p}} |_{k_F} = n_{\mathbf{p}} - \mathbf{k} \cdot \mathbf{e}_{\mathbf{p}} \delta(k_F - p) \quad \text{and}$$

$$n_{\mathbf{p}} (1 - n_{\mathbf{p} + \mathbf{k}}) = n_{\mathbf{p}} \{1 - n_{\mathbf{p}} + \mathbf{k} \cdot \mathbf{e}_{\mathbf{p}} \delta(k_F - p)\} = n_{\mathbf{p}} \mathbf{k} \cdot \mathbf{e}_{\mathbf{p}} \delta(k_F - p) \sim k.$$

Replace now the denominator for small \mathbf{k} by $2k k_F$ and perform the sum over \mathbf{p} and \mathbf{q} in polar coordinates. Finally the sum over \mathbf{k} is to be performed over an expression which contains $1/k^4$ from $v_{\mathbf{k}}$, $1/k$ from the denominator, and k^2 from the numerator which together with k^2 from integration in k -space leads to $\int dk/k = \ln k$.

4.8: (a) The meaning of $c_\alpha^\dagger(c_\alpha)$ of creating(annihilating) a fermion in the state α with the probability amplitude $\psi_\alpha(\mathbf{r})$ implies, that $\Psi^\dagger(\mathbf{r})(\Psi(\mathbf{r}))$ creates(annihilates) a fermion at \mathbf{r} . (b) Write

$$\{\Psi^\dagger(\mathbf{r}), \Psi(\mathbf{r}')\} = \sum_{\alpha, \alpha'} \psi_\alpha^*(\mathbf{r})\psi_{\alpha'}(\mathbf{r}') \underbrace{\{c_\alpha^\dagger, c_{\alpha'}\}}_{\delta_{\alpha, \alpha'}} = \sum_{\alpha} \psi_\alpha^*(\mathbf{r})\psi_{\alpha'}(\mathbf{r}') = \delta(\mathbf{r} - \mathbf{r}')$$

and similar for $\{\Psi(\mathbf{r}, \Psi(\mathbf{r}')\} = \{\Psi^\dagger(\mathbf{r}, \Psi^\dagger(\mathbf{r}')\} = 0$. (c) For free electrons the density operator is

$$\begin{aligned} \hat{n}(\mathbf{r}) &= \Psi^\dagger(\mathbf{r})\Psi(\mathbf{r}) = \sum_{\mathbf{k}', \mathbf{k}} e^{-i(\mathbf{k}' - \mathbf{k}) \cdot \mathbf{r}} \frac{1}{V} c_{\mathbf{k}'}^\dagger c_{\mathbf{k}} \quad \text{and with} \quad \mathbf{q} = \mathbf{k}' - \mathbf{k} \\ &= \sum_{\mathbf{q}} e^{-i\mathbf{q} \cdot \mathbf{r}} \frac{1}{V} \sum_{\mathbf{k}} c_{\mathbf{k} + \mathbf{q}}^\dagger c_{\mathbf{k}} \quad \rightarrow \quad \hat{n}_{\mathbf{q}} = \frac{1}{V} \sum_{\mathbf{k}} c_{\mathbf{k} + \mathbf{q}}^\dagger c_{\mathbf{k}}, \end{aligned}$$

$\hat{n}_0 = \sum_{\mathbf{k}} c_{\mathbf{k}}^\dagger c_{\mathbf{k}}/V = \hat{n}$ is the operator of particle density (its eigenvalue being n) while $\sum_{\mathbf{q}} c_{\mathbf{k} + \mathbf{q}}^\dagger c_{\mathbf{k}} = \hat{n}_{\mathbf{q}}$ describes density fluctuations. d) The Coulomb interaction can be rewritten with

$$c_{\mathbf{p} + \mathbf{k}\sigma}^\dagger c_{\mathbf{q} - \mathbf{k}\sigma'}^\dagger c_{\mathbf{q}\sigma'} c_{\mathbf{p}\sigma} = -c_{\mathbf{p} + \mathbf{k}\sigma}^\dagger \left(\delta_{\sigma, \sigma'} \delta_{\mathbf{q} - \mathbf{k}, \mathbf{p}} - c_{\mathbf{p}\sigma} c_{\mathbf{q} - \mathbf{k}\sigma'}^\dagger \right) c_{\mathbf{q}\sigma'}$$

by applying the fermion commutation rules and by using the number operators the Coulomb interaction becomes

$$\frac{1}{2} \sum_{\substack{\mathbf{k} \neq 0, \mathbf{p}, \mathbf{q} \\ \sigma, \sigma'}} v_{\mathbf{k}} c_{\mathbf{p} + \mathbf{k}\sigma}^\dagger c_{\mathbf{q} - \mathbf{k}\sigma'}^\dagger c_{\mathbf{q}\sigma'} c_{\mathbf{p}\sigma} = \frac{1}{2} \sum_{\mathbf{k} \neq 0} v_{\mathbf{k}} \left(\hat{N}_{\mathbf{k}} \hat{N}_{-\mathbf{k}} - N \right).$$

4.9: Replace in the given expression

$$\langle [\hat{N}_{\mathbf{q}}(\tau), \hat{N}_{-\mathbf{q}}(0)] \rangle_{\text{exact}} \rightarrow \langle [\hat{N}_{\mathbf{q}}(\tau), \hat{N}_{-\mathbf{q}}(0)] \rangle_0 \quad \text{and} \quad N_{\text{ext}} \rightarrow N_{\text{ext}} + \langle \hat{N}_{\mathbf{q}} \rangle$$

with the induced number fluctuation $\langle \hat{N}_{\mathbf{q}} \rangle$. From Sect. 4.5, take

$$\lim_{\Gamma \rightarrow 0} \frac{e^2}{\epsilon_0 V q^2} \frac{1}{i\hbar} \int_0^\infty d\tau e^{i\omega\tau - \Gamma\tau} \langle [\hat{N}_{\mathbf{q}}(\tau), \hat{N}_{-\mathbf{q}}(0)] \rangle_0 = v_{\mathbf{q}} \pi_0(\mathbf{q}, \omega)$$

to write

$$\langle \hat{N}_{\mathbf{q}} \rangle = v_{\mathbf{q}} \pi_0(\mathbf{q}, \omega) \left(\langle \hat{N}_{\mathbf{q}} \rangle + N_{\text{ext}} \right) \quad \text{or} \quad \langle \hat{N}_{\mathbf{q}} \rangle = \frac{N_{\text{ext}} v_{\mathbf{q}} \pi_0(\mathbf{q}, \omega)}{1 - v_{\mathbf{q}} \pi_0(\mathbf{q}, \omega)}$$

and identify with

$$\frac{1}{\epsilon(\mathbf{q}, \omega)} = 1 + \frac{\langle \hat{N}_{\mathbf{q}} \rangle}{N_{\text{ext}}} \Rightarrow \epsilon^{\text{RPA}}(\mathbf{q}, \omega) = 1 - v_{\mathbf{q}} \pi_0(\mathbf{q}, \omega).$$

4.10: Using relations given in Sect. 4.6, the lhs of the given equation can be written

$$\int_0^\infty d\omega \omega \text{Im} \frac{1}{\epsilon(\mathbf{q}, \omega)} = -v_{\mathbf{q}} \frac{1}{\hbar} \sum_m |\langle \Psi_0 | \hat{N}_{\mathbf{q}} | \Psi_m \rangle|^2 \int_0^\infty d\omega \omega \delta(\omega - \omega_{m0}).$$

After showing (by inserting a complete set of eigenstates $|\Psi_m\rangle$ of H_{jell}) that

$$-\sum_m 2\hbar\omega_m |\langle\Psi_0|\widehat{N}_q|\Psi_m\rangle|^2 = \langle\Psi_0|[[H_{\text{jell}}, \widehat{N}_q], \widehat{N}_{-q}]|\Psi_0\rangle$$

and one has to evaluate the double commutator. This is done with H_{jell} written in terms of density fluctuations (see (4.107) and Problem 4.8). Realize first with $\widehat{N}_k^\dagger = \widehat{N}_{-k}$ and $[\widehat{N}_k, \widehat{N}_{k'}] = 0$ that the interaction term commutes with \widehat{N}_q . Evaluate

$$[H_{\text{jell}}, \widehat{N}_q] = \left[\sum_{\mathbf{k}} \epsilon_{\mathbf{k}} c_{\mathbf{k}}^\dagger c_{\mathbf{k}}, \widehat{N}_q \right] = \sum_{\mathbf{k}, \mathbf{q}'} \epsilon_{\mathbf{k}} [c_{\mathbf{k}}^\dagger c_{\mathbf{k}}, c_{\mathbf{q}' - \mathbf{q}}^\dagger c_{\mathbf{q}'}]$$

which by applying fermion commutation rules yields

$$[H_{\text{jell}}, \widehat{N}_q] = \sum_{\mathbf{k}} \epsilon_{\mathbf{k}} \left(c_{\mathbf{k}}^\dagger c_{\mathbf{k}+\mathbf{q}} - c_{\mathbf{k}-\mathbf{q}}^\dagger c_{\mathbf{k}} \right) = \sum_{\mathbf{k}} (\epsilon_{\mathbf{k}} - \epsilon_{\mathbf{k}+\mathbf{q}}) c_{\mathbf{k}}^\dagger c_{\mathbf{k}+\mathbf{q}}$$

and with $\epsilon_{\mathbf{k}} = \hbar^2 k^2 / 2m$

$$[H_{\text{jell}}, \widehat{N}_q] = -\frac{\hbar^2 q^2}{2m} n_q - \frac{\hbar^2}{m} \sum_{\mathbf{k}} \mathbf{k} \cdot \mathbf{q} c_{\mathbf{k}}^\dagger c_{\mathbf{k}+\mathbf{q}}$$

The first term $\sim N_q$ does not contribute to the double commutator which, therefore, reads

$$\left[[H_{\text{jell}}, \widehat{N}_q], \widehat{N}_{-q} \right] = -\frac{\hbar^2}{m} \sum_{\mathbf{k}, \mathbf{k}'} \mathbf{k} \cdot \mathbf{q} [c_{\mathbf{k}}^\dagger c_{\mathbf{k}+\mathbf{q}}, c_{\mathbf{k}'+\mathbf{q}}^\dagger c_{\mathbf{k}'}].$$

Evaluating the commutator with the rules for fermion operators leads to

$$\begin{aligned} \left[[H_{\text{jell}}, \widehat{N}_q], \widehat{N}_{-q} \right] &= -\frac{\hbar^2}{m} \sum_{\mathbf{k}} \mathbf{k} \cdot \mathbf{q} \left(c_{\mathbf{k}}^\dagger c_{\mathbf{k}} - c_{\mathbf{k}+\mathbf{q}}^\dagger c_{\mathbf{k}+\mathbf{q}} \right) \quad \text{and with } \mathbf{k} + \mathbf{q} \rightarrow \mathbf{k} \\ &= -\frac{\hbar^2}{m} \sum_{\mathbf{k}} c_{\mathbf{k}}^\dagger c_{\mathbf{k}} = -\frac{\hbar^2}{m} q^2 N. \end{aligned}$$

Consider the factors one has

$$\int_0^\infty d\omega \omega \text{Im} \frac{1}{\varepsilon(\mathbf{q}, \omega)} = -\frac{\pi v_{\mathbf{q}}}{\hbar} \left(-\frac{1}{2\hbar} \right) \left(-\frac{\hbar^2}{m} q^2 N \right) = -\frac{1}{2} \omega_{\text{p}}^2.$$

4.11: Evaluate for $\omega = 0$

$$\varepsilon_1(\mathbf{q}, 0) = 1 - \frac{e^2}{\varepsilon_0 V q^2} \sum_{\mathbf{k}, \sigma} \frac{f_{\mathbf{k}+\mathbf{q}} - f_{\mathbf{k}}}{\epsilon_{\mathbf{k}+\mathbf{q}} - \epsilon_{\mathbf{k}}} \quad \text{by writing for } \mathbf{q} \rightarrow 0:$$

$$f_{\mathbf{k}+\mathbf{q}} - f_{\mathbf{k}} \simeq \mathbf{q} \cdot \nabla_{\mathbf{k}} f_{\mathbf{k}} = \mathbf{q} \cdot \nabla_{\mathbf{k}} \epsilon_{\mathbf{k}} \frac{df}{d\epsilon} \simeq -\mathbf{q} \cdot \nabla_{\mathbf{k}} \epsilon_{\mathbf{k}} \delta(\epsilon_{\mathbf{k}} - E_{\text{F}})$$

$$\text{and } \epsilon_{\mathbf{k}+\mathbf{q}} - \epsilon_{\mathbf{k}} \simeq \mathbf{q} \cdot \nabla_{\mathbf{k}} \epsilon_{\mathbf{k}}$$

Thus one has

$$\begin{aligned}
\varepsilon_1(\mathbf{q}) &\simeq 1 + \frac{e^2}{\varepsilon_0 V q^2} \sum_{\mathbf{k}, \sigma} \delta(\epsilon_{\mathbf{k}} - E_F) \\
&= 1 + \frac{e^2}{\varepsilon_0 V q^2} \frac{2V}{(2\pi)^3} 4\pi \int_0^\infty dk k^2 \delta(\epsilon_{\mathbf{k}} - E_F) \\
&= 1 + \frac{e^2}{\varepsilon_0 q^2} \frac{1}{2\pi^2} \left(\frac{2m}{\hbar^2} \right)^{3/2} E_F^{1/2} \quad \text{and} \\
\varepsilon_1(\mathbf{q}) &\simeq 1 + \frac{e^2}{\varepsilon_0 q^2} \frac{1}{2\pi^2} \frac{2m}{\hbar^2} k_F = 1 + \frac{k_{\text{FT}}^2}{q^2} \quad \text{with} \quad k_{\text{FT}}^2 = \frac{3n e^2}{2\varepsilon_0 E_F}.
\end{aligned}$$

The meaning of k_{FT} becomes evident when looking at the screened Coulomb interaction $v_{\mathbf{q}}/\varepsilon_1(\mathbf{q}, 0)$ whose Fourier transform is of the form $\exp(-k_{\text{FT}}r)/r$: $1/k_{\text{FT}}$ is the Thomas–Fermi screening length.

4.12: Use the pair–distribution function (1.11)

$$\begin{aligned}
g(\mathbf{r}) &= 1 + \frac{1}{N} \sum_{\mathbf{q}} e^{i\mathbf{q}\cdot\mathbf{r}} (S(\mathbf{q}) - 1) \quad \text{and use} \quad \frac{N}{V} = \sum_{\mathbf{p}, \sigma} n_{\mathbf{p}\sigma} \quad \text{and} \\
S(\mathbf{q}) &= \frac{1}{N} \sum_{\mathbf{p}, \sigma} n_{\mathbf{p}\sigma} (1 - n_{\mathbf{p}+\mathbf{q}\sigma}) \quad \text{to write} \\
g(\mathbf{r}) &= 1 + \frac{1}{NV} \sum_{\mathbf{q}} e^{i\mathbf{q}\cdot\mathbf{r}} \left[\frac{V}{N} \sum_{\mathbf{p}, \sigma} n_{\mathbf{p}\sigma} (1 - n_{\mathbf{p}+\mathbf{q}, \sigma}) - 1 \right] \\
&= 1 - \frac{V^2}{N^2} \sum_{\mathbf{q}, \mathbf{p}, \sigma} n_{\mathbf{p}\sigma} n_{\mathbf{p}+\mathbf{q}\sigma} e^{i\mathbf{q}\cdot\mathbf{r}}.
\end{aligned}$$

The summation can be carried out by writing

$$\cdots = \sum_{\mathbf{p}, \sigma} n_{\mathbf{p}} e^{-i\mathbf{p}\cdot\mathbf{r}} \sum_{\mathbf{q}} n_{\mathbf{p}+\mathbf{q}} e^{i(\mathbf{p}+\mathbf{q})\cdot\mathbf{r}} = 2 \sum_{\mathbf{p}} n_{\mathbf{p}} e^{-i\mathbf{p}\cdot\mathbf{r}} \sum_{\mathbf{q}'} n_{\mathbf{q}'} e^{i\mathbf{q}'\cdot\mathbf{r}}.$$

This double sum with the occupation factors was carried out already in Sect. 4.4 for $T = 0$ K by integrating over the Fermi sphere and yields $g(\mathbf{r}) = 1 - \rho^{\text{HF}}/en$ (see Fig. 4.13).

Solutions for Chap. 5

5.1: Taking spin into account, the expectation value of H_N with the Slater determinant Ψ_N is written

$$\begin{aligned}
\langle \Psi_N | H_N | \Psi_N \rangle &= \sum_{\alpha=1}^N \int dx \psi_{\alpha}^*(x) \left(\frac{p^2}{2m} + V(\mathbf{r}) \right) \psi_{\alpha}(x) \\
&\quad + \frac{1}{2} \sum_{\substack{\alpha, \beta=1 \\ \alpha \neq \beta}}^N \int \int dx dx' \psi_{\alpha}^*(x) \psi_{\beta}^*(x') v(\mathbf{r} - \mathbf{r}') \psi_{\alpha}(x) \psi_{\beta}(x') \\
&\quad - \frac{1}{2} \sum_{\substack{\alpha, \beta=1 \\ \alpha \neq \beta}}^N \int \int dx dx' \psi_{\alpha}^*(x) \psi_{\beta}^*(x') v(\mathbf{r} - \mathbf{r}') \psi_{\beta}(x) \psi_{\alpha}(x').
\end{aligned}$$

Carrying out the summation over spin variables, the first two terms become identical with (5.8), while the third term (which appears because the Slater determinant is an antisymmetrized product of N single-particle wave functions) contributes only if ψ_α and ψ_β are states with the same spin. The variational principle leads for the first two terms to the Hartree equations, which become modified by a contribution from the third term, the exchange term (5.11).

5.2: For free electrons with $\psi_{\mathbf{k}}(\mathbf{r}) = \exp(i\mathbf{k} \cdot \mathbf{r})/\sqrt{V}$ the averaged exchange density reads

$$\bar{n}^{\text{HF}}(\mathbf{r}, \mathbf{r}') = -\frac{2}{N} \sum_{\substack{\mathbf{k}, \mathbf{k}' \\ |\mathbf{k}|, |\mathbf{k}'| \leq k_{\text{F}}}} \frac{1}{V} e^{i\mathbf{k}' \cdot (\mathbf{r}-\mathbf{r}')} e^{-i\mathbf{k} \cdot (\mathbf{r}-\mathbf{r}')}$$

and with the Fourier transform of $1/|\mathbf{r} - \mathbf{r}'|$ the exchange potential becomes

$$\begin{aligned} V_{x, \text{Slater}}(\mathbf{r}) &= -\frac{2e^2}{\varepsilon_0 N V} \sum_{\substack{\mathbf{k}, \mathbf{k}' \\ |\mathbf{k}|, |\mathbf{k}'| \leq k_{\text{F}}}} \sum_{\mathbf{q}} \frac{1}{q^2} \frac{1}{V} \underbrace{\int_V e^{i(\mathbf{k}' - \mathbf{k} + \mathbf{q}) \cdot (\mathbf{r}-\mathbf{r}')} d^3 r'}_{\delta_{\mathbf{k}-\mathbf{k}', \mathbf{q}}} \\ &= -\frac{2e^2}{\varepsilon_0 N V} \sum_{\substack{\mathbf{k}, \mathbf{k}' \\ |\mathbf{k}|, |\mathbf{k}'| \leq k_{\text{F}}}} \frac{1}{|\mathbf{k} - \mathbf{k}'|^2} = -\frac{3}{8\pi^2 \varepsilon_0} e^2 k_{\text{F}}. \end{aligned}$$

With the exchange energy $\epsilon_x(n) = -3e^2 k_{\text{F}}^2 / 16\pi^2 \varepsilon_0$ from Sect. 4.4 one finds

$$V_x^{\text{LDA}}(\mathbf{r}) = \frac{4}{3} \epsilon_x^{\text{LDA}}(n(\mathbf{r})) = \frac{2}{3} V_{x, \text{Slater}}(\mathbf{r}).$$

5.3: The number of discrete $\mathbf{k} = (k_1, k_2, k_3)$ with $k_i = 2\pi n_i / L_i$, $i = 1, 2, 3$ with $0 \leq n_i < N_i$ in a Brillouin zone is $N = N_1 N_2 N_3$, which is the number of unit cells in the crystal or periodicity volume. Thus, for each electron in the unit cell with given spin there is one state in the energy band, i.e. each band can accommodate $2N$ electrons.

5.4: A point at the Brillouin zone boundary is characterized by the relation $\mathbf{k}' = \mathbf{k} - \mathbf{G}$. The condition of degeneracy is $k^2 = k'^2$, thus $(\mathbf{k} - \mathbf{G})^2 = (\mathbf{k}')^2$ becomes $2\mathbf{k} \cdot \mathbf{G} = \mathbf{G}^2$, which is the condition for Bragg reflection.

5.5: The primitive reciprocal lattice vectors of the square lattice are $\mathbf{b}_1 = (1, 0)2\pi/a$, and $\mathbf{b}_2 = (0, 1)2\pi/a$. Write the free electron energies

$$E(\mathbf{k}) = \frac{\hbar^2}{2m} (\mathbf{k} + \mathbf{G})^2 = \frac{\hbar^2}{2m} \left(\frac{2\pi}{a} \right)^2 \kappa^2$$

for the smallest \mathbf{G} at the points Γ , M , and X and connect corresponding points by parabolas defined by \mathbf{G} .

If $\nu = 1, 2, 3$ is the number of electrons per atom then, for one atom per unit cell, $n_s = \nu/a^2$ is the areal electron density. The radius of the Fermi circle is given by $k_{\text{F}} = \sqrt{2\pi n_s}$ and the Fermi energy by

$$E_{\text{F}} = \frac{\hbar^2}{2m} k_{\text{F}}^2 = \frac{\hbar^2}{2m} \left(\frac{2\pi}{a} \right)^2 \frac{\nu}{2\pi}$$

or $\kappa_{\text{F}}^2 = \nu/2\pi$ which is 0.159 for $\nu = 1$.

5.6: Proceed as in Problem 5.5 and see [121] for the free-electron bands along $\Gamma - L$.

5.7: In the almost free-electron picture, the energy bands of Al, Si, and GaAs derive from the free-electron bands of the *fcc* lattice (see Problem 5.6). Due to the different crystal structures (Bravais lattice for Al, diamond structure for Si, zinc blende structure for GaAs) the energy gaps are determined by different Fourier components of the pseudo-potential:

$$V_{\text{psp}}(\mathbf{r}) = \sum_{\mathbf{n}, \boldsymbol{\tau}} v_{\text{psp}}^{(\boldsymbol{\tau})}(\mathbf{r} - \mathbf{R}_{\mathbf{n}}^0 - \boldsymbol{\tau}) \quad \rightarrow \quad V_{\text{psp}}(\mathbf{G}) = e^{-i\mathbf{g} \cdot \boldsymbol{\tau}} v_{\text{psp}}^{(\boldsymbol{\tau})}(\mathbf{G}).$$

For Al with $\boldsymbol{\tau} = 0$, the structure factor $S(\mathbf{G}) = \sum_{\boldsymbol{\tau}} \exp(-i\mathbf{G} \cdot \boldsymbol{\tau})$ equals 1 for all \mathbf{G} . For diamond and zinc blende with $\boldsymbol{\tau} = \pm\boldsymbol{\tau}'$ with $\boldsymbol{\tau}' = (1, 1, 1)a/8$ one has

$$\begin{aligned} V_{\text{psp}}(\mathbf{G}) &= e^{-i\mathbf{G} \cdot \boldsymbol{\tau}'} v^{(+)}(\mathbf{G}) + e^{i\mathbf{G} \cdot \boldsymbol{\tau}'} v^{(-)}(\mathbf{G}) \\ &= \cos(\mathbf{G} \cdot \boldsymbol{\tau}') v_{\text{S}}(\mathbf{G}) - i \sin(\mathbf{G} \cdot \boldsymbol{\tau}') v_{\text{A}}(\mathbf{G}), \end{aligned}$$

where

$$v_{\text{S}}(\mathbf{G}) = v^{(+)}(\mathbf{G}) + v^{(-)}(\mathbf{G}) \quad \text{and} \quad v_{\text{A}}(\mathbf{G}) = v^{(+)}(\mathbf{G}) - v^{(-)}(\mathbf{G}).$$

In Si the anti-symmetric potential $v_{\text{A}}(\mathbf{G})$ vanishes. Thus, Fourier components at different reciprocal lattice vectors determine the energy bands as Al, Si, GaAs. Especially, for $\mathbf{G} = (2, 0, 0)2\pi/a$ we have $\cos(\mathbf{G} \cdot \boldsymbol{\tau}) = 0$ but $\sin(\mathbf{G} \cdot \boldsymbol{\tau}) = 1$ and the anti-symmetric potential present in GaAs removes the degeneracy of the level X_1 in Si (see Fig. 5.11).

5.8: The crystal field splitting is determined by the matrix formed by

$$K_{\nu'\nu} = \sum_{\mathbf{n}} \int d^3r \phi_{\nu'}^*(\mathbf{r}) v(\mathbf{r} - \mathbf{R}_{\mathbf{n}}^0) \phi_{\nu}(\mathbf{r})$$

with $\nu = xy, yz, zx, 3z^2 - r^2, x^2 - y^2$. The point group operations of the cubic lattice turn the coordinate triple x, y, z into any other permutation including sign changes of x, y , and z , while leaving $\sum_{\mathbf{n}} v(\mathbf{r} - \mathbf{R}_{\mathbf{n}}^0)$ invariant. Thus, the groups of orbitals d_{xy}, d_{yz}, d_{zx} and $d_{3z^2 - r^2}, d_{x^2 - y^2}$ form invariant sets under the cubic point group, which are classified by the irreducible representations $\Gamma_{25'}$ and Γ_{12} , respectively, and the matrix with the elements $K_{\nu'\nu}$ has block-diagonal form. Further inspection shows, that each of the diagonal blocks is itself diagonal for the given basis with identical diagonal matrix elements, thus, the crystal field splitting gives a threefold ($\Gamma_{25'}$) and a twofold (Γ_{12}) state as can be seen at the Γ point of the band structures depicted in Figs. 5.14 and 5.15. There is no difference between sc, bcc, and fcc crystal structure because they have the same point group.

5.9: The overlap matrix $S_{\nu'\nu}(\mathbf{k})$ is hermitian and can be diagonalized by a unitary transformation $U: USU^{-1} = S'$ with $S'_{\mu'\mu} = S'_{\mu}\delta_{\mu',\mu}$. The diagonal elements S'_{μ} of the transformed overlap matrix represent the norms of the new basis states which are always positive. Thus the eigenvalue equation can be rewritten

$$\underbrace{UHU^{-1}}_{H'} \underbrace{UC}_{C'} = E \underbrace{USU^{-1}}_{S'} \underbrace{UC}_{C'}.$$

One can multiply this equation with the inverse square root of the diagonal matrix S' to arrive at the eigenvalue equation

$$S'^{-1/2}H'S'^{-1/2}S'^{1/2}C' = ES'^{1/2}C'$$

and with $\tilde{H} = S'^{-1/2}H'S'^{-1/2}$, $\tilde{C} = S'^{1/2}C'$ one has the standard eigenvalue problem with the secular equation

$$\left\| \tilde{H}_{\mu'\mu} - E\delta_{\mu',\mu} \right\| = 0$$

with $\tilde{H} = S'^{-1/2}UH'U^{-1}S'^{-1/2}$.

5.10: The nearest neighbors in the sc crystal structure are

$$\mathbf{R}_n^0 : a(\pm 1, 0, 0), (0, \pm 1, 0), (0, 0, \pm 1)$$

leading to the dispersion

$$E_s(\mathbf{k}) = E_s + 2J_{ss}(a)(\cos(k_x a) + \cos(k_y a) + \cos(k_z a))$$

which for $\mathbf{k} = (k, 0, 0)$ becomes $E_s(\mathbf{k}) = E_s + 2J_{ss}(a)\cos(ka)$ and for $\mathbf{k} = (k, k, k)$, $E_s(\mathbf{k}) = E_s + 6J_{ss}(a)\cos(ka)$ with band widths $E(0) - E((\pi/a, 0, 0)) = 4J_{ss}(a)$ and $E(0) - E((\pi/a, \pi/a, \pi/a)) = 12J_{ss}(a)$, respectively.

For the bcc crystal structure one has

$$\mathbf{R}_n^0 : \frac{a}{2}(\pm 1, \pm 1, \pm 1), (\mp 1, \pm 1, \pm 1), (\pm 1, \mp 1, \pm 1), (\pm 1, \pm 1, \mp 1)$$

leading to the dispersion

$$E_s(\mathbf{k}) = E_s + 2J_{ss} \left(\frac{a}{\sqrt{3}} \right) \left\{ \cos \left(\frac{a}{2}(k_x + k_y + k_z) \right) + \cos \left(\frac{a}{2}(-k_x + k_y + k_z) \right) \right. \\ \left. + \cos \left(\frac{a}{2}(k_x - k_y + k_z) \right) + \cos \left(\frac{a}{2}(k_x + k_y - k_z) \right) \right\}$$

which for $\mathbf{k} = (k, 0, 0)$ becomes $E_s(\mathbf{k}) = E_s + 8J_{ss}(a/\sqrt{3})\cos(ka/2)$ and for $\mathbf{k} = (k, k, k)$, $E_s(\mathbf{k}) = E_s + 2J_{ss}(a/\sqrt{3})(\cos(3ka/2) + 3\cos(ka/2))$ with band widths $E(0) - E((2\pi/a, 0, 0)) = 16J_{ss}(a/\sqrt{3})$ and $E(0) - E((\pi/a, \pi/a, \pi/a)) = 8J_{ss}(a/\sqrt{3})$.

5.11: For a solution see P.R. Wallace, Phys. Rev. **71**, 622 (1947) and the article by S.E. Louis in [114].

5.12: Use the Peierls substitution $\epsilon(\mathbf{k}) \rightarrow H(\mathbf{p} - e\mathbf{A})^2$ with the vector potential $\mathbf{A} = (0, B(x \cos \theta + z \sin \theta), 0)$ corresponding to $\mathbf{B} = B(\sin \theta, 0, \cos \theta)$ to write

$$H = \frac{p_x^2}{2m_t} + \frac{1}{2m_t} (p_y - eB(x \cos \theta + z \sin \theta))^2 + \frac{p_z^2}{2m_t}.$$

The equations of motion for the components of the momentum are (up to terms $\sim p_y$ which vanish later due to $\dot{p}_y = 0$)

$$\dot{p}_x = -\frac{i}{\hbar}[p_x, H] = -\frac{e^2 B^2}{m_t}(x \cos \theta + z \sin \theta) \cos \theta \\ \dot{p}_z = -\frac{i}{\hbar}[p_z, H] = -\frac{e^2 B^2}{m_t}(x \cos \theta + z \sin \theta) \sin \theta.$$

Take the derivatives of these equation with respect to t and replace $\dot{x} = p_x/m_t$, $\dot{z} = p_z/m_t$ to obtain

$$\begin{aligned} -\ddot{p}_x &= \omega_t^2 \cos^2 \theta p_x + \omega_t \omega_l \sin \theta \cos \theta p_z \\ -\ddot{p}_z &= \omega_t^2 \sin \theta \cos \theta p_x + \omega_t \omega_l \sin^2 \theta p_z \end{aligned}$$

with $\omega_{l,t} = eB/m_{l,t}$. With $p_{x,z} \sim \exp(-i\omega t)$ this becomes a set of homogeneous linear equations and the eigenfrequencies follow from

$$\left\| \begin{array}{cc} \omega_t^2 \cos^2 \theta - \omega^2 & \omega_t \omega_l \sin \theta \cos \theta \\ \omega_t^2 \sin \theta \cos \theta & \omega_t \omega_l \sin^2 \theta - \omega^2 \end{array} \right\| = 0$$

with the nontrivial solution

$$\omega^2 = \omega_t^2 \cos^2 \theta + \omega_t \omega_l \sin^2 \theta = e^2 B^2 \left(\frac{\cos^2 \theta}{m_t^2} + \frac{\sin^2 \theta}{m_l m_t} \right).$$

The expression in the bracket is the squared inverse cyclotron mass for the anisotropic energy surface if the magnetic field includes the angle θ with the z -axis. See [4].

5.13: For $\mathbf{k} = (k_x, k_y, 0)$ and $\nabla V \parallel (001)$ the interface spin-orbit (or Rashba)-term reads

$$H_{\text{SO}}(\mathbf{k}) = \alpha |\nabla V| (k_y \sigma_x - k_x \sigma_y)$$

and with $k_{\pm} = k_x \pm ik_y = k \exp(\pm i\varphi)$ and $\sigma_{\pm} = (\sigma_x \pm i\sigma_y)/2$

$$H_{\text{SO}}(k, \varphi) = i\alpha |\nabla V| (k_+ \sigma_- - k_- \sigma_+) = i\alpha' (e^{i\varphi} \sigma_- - e^{-i\varphi} \sigma_+).$$

The subband Hamiltonian with spin-orbit interaction becomes

$$H(k, \varphi) = \begin{pmatrix} \epsilon_k & i\alpha' e^{-i\varphi} \\ -i\alpha' e^{-i\varphi} & \epsilon_k \end{pmatrix}.$$

Its eigenvalues $\epsilon_{\pm}(k) = \epsilon_k \pm \alpha |\nabla V| k$ do not depend on φ and are two parabolas shifted against each other. Use the eigenvectors

$$|\mathbf{k}, \pm\rangle = \frac{1}{\sqrt{2}} \left| \begin{array}{c} 1 \\ \mp i e^{i\varphi} \end{array} \right\rangle$$

to calculate the expectation value of the vector of Pauli spin matrices:

$$\langle \mathbf{k}, \pm | \boldsymbol{\sigma} | \mathbf{k}, \pm \rangle = \pm (e_x \sin \varphi - e_y \cos \varphi).$$

Thus, the spin is always oriented perpendicular to the wave vector $\mathbf{k} = (k_x, k_y, 0)$ and rotates with φ . Note, that the states on each parabola form a Kramers pair. See [153].

Solutions for Chap. 6

6.1: Choose the quantum numbers for the Bloch states

$$\alpha = n\mathbf{k}\sigma, \beta = \bar{n}\bar{\mathbf{k}}\bar{\sigma}, \alpha' = n'\mathbf{k}'\sigma', \beta' = \bar{n}'\bar{\mathbf{k}}'\bar{\sigma}'.$$

After carrying out the summation over spin variables the matrix element reduces to

$$V_{\alpha\beta\beta'\alpha'} = \int d^3r \int d^3r' \psi_{n\mathbf{k}\sigma}^*(\mathbf{r}) \psi_{\bar{n}\bar{\mathbf{k}}\bar{\sigma}}^*(\mathbf{r}') \frac{e^2}{\kappa|\mathbf{r}-\mathbf{r}'|} \psi_{\bar{n}'\bar{\mathbf{k}}'\bar{\sigma}'}(\mathbf{r}) \psi_{n'\mathbf{k}'\sigma'}(\mathbf{r}').$$

Decompose the Bloch function into plane wave and lattice periodic parts, expand the products of periodic parts with the same argument in a Fourier series

$$u_{n\mathbf{k}\sigma}^*(\mathbf{r})u_{\bar{n}'\bar{\mathbf{k}}'\sigma}(\mathbf{r}) = \sum_{\mathbf{G}} B_{n\bar{n}\bar{\mathbf{k}}\sigma}(\mathbf{G})e^{i\mathbf{G}\cdot\mathbf{r}},$$

and use the Fourier transform of the Coulomb interaction to perform the integration over the space variables to find

$$\begin{aligned} V_{\alpha\beta\beta'\alpha'} &= \sum_{\mathbf{G},\mathbf{G}',\mathbf{q}} B_{n\bar{n}'\bar{\mathbf{k}}\bar{\sigma}}(\mathbf{G})B_{\bar{n}n'\bar{\mathbf{k}}\bar{\sigma}'}(\mathbf{G}') \\ &\times \frac{e^2}{\varepsilon_0 V q^2} \int d^3r e^{-i(\mathbf{k}-\bar{\mathbf{k}}'-\mathbf{q}-\mathbf{G})\cdot\mathbf{r}} \int d^3r' e^{-i(\bar{\mathbf{k}}-\mathbf{k}'+\mathbf{q}-\mathbf{G}')\cdot\mathbf{r}'}. \end{aligned}$$

For the single-band approximation set $n = \bar{n} = \bar{n}' = n'$ and with only leading terms in the Fourier series, $\mathbf{G} = \mathbf{G}' = 0$, write

$$B_{n\bar{n}'\bar{\mathbf{k}}\bar{\sigma}}(\mathbf{G}) \rightarrow B_{\mathbf{k}\mathbf{q}}, \quad B_{\bar{n}n'\bar{\mathbf{k}}\bar{\sigma}'}(\mathbf{G}') \rightarrow B_{\bar{\mathbf{k}}\mathbf{q}}$$

and obtain

$$V_{\alpha\beta\beta'\alpha'} = \sum_{\mathbf{q}} v(\mathbf{q})V^2 B_{\mathbf{k}\mathbf{q}}B_{\bar{\mathbf{k}}\mathbf{q}}\delta_{\bar{\mathbf{k}}',\mathbf{k}-\mathbf{q}}\delta_{\bar{\mathbf{k}},\mathbf{k}'-\mathbf{q}}.$$

6.2: To check normalization and orthogonality write

$$\begin{aligned} &\sum_{\mathbf{s}} \int d^3r \phi_{n\sigma}^*(\mathbf{r}-\mathbf{R})\phi_{n'\sigma'}(\mathbf{r}-\mathbf{R}') \\ &= \frac{1}{N}\delta_{\sigma,\sigma'} \sum_{\mathbf{k},\mathbf{k}'} e^{-i\mathbf{k}\cdot\mathbf{R}-i\mathbf{k}'\cdot\mathbf{R}'} \underbrace{\int d^3r \psi_{n\mathbf{k}\sigma}^*(\mathbf{r})\psi_{n'\mathbf{k}'\sigma'}(\mathbf{r})}_{\delta_{n,n'}\delta_{\mathbf{k},\mathbf{k}'}} \\ &= \frac{1}{N} \underbrace{\sum_{\mathbf{k}} e^{-i\mathbf{k}\cdot(\mathbf{R}-\mathbf{R}')} \delta_{n,n'}}_{\delta_{\mathbf{R},\mathbf{R}'}} = \delta_{n,n'}\delta_{\mathbf{R},\mathbf{R}'} \end{aligned}$$

Thus localized functions, represented by Bloch functions, are orthogonal when centered on different sites. Insofar the Wannier representation differs from the LCAO. Introduce fermion operators for these localized Wannier states by

$$c_{n\mathbf{R}\sigma} = \frac{1}{\sqrt{N}} \sum_{\mathbf{k}} e^{i\mathbf{k}\cdot\mathbf{R}} c_{n\mathbf{k}\sigma}$$

and calculate the anti-commutator

$$\begin{aligned} \{c_{n\mathbf{R}\sigma}, c_{n'\mathbf{R}'\sigma'}^\dagger\} &= \frac{1}{N} \sum_{\mathbf{k},\mathbf{k}'} e^{i\mathbf{k}\cdot\mathbf{R}-i\mathbf{k}'\cdot\mathbf{R}'} \underbrace{\{c_{n\mathbf{k}\sigma}, c_{n'\mathbf{k}'\sigma'}^\dagger\}}_{\delta_{n,n'}\delta_{\mathbf{k},\mathbf{k}'}\delta_{\sigma,\sigma'}} \\ &= \delta_{n,n'}\delta_{\sigma,\sigma'} \frac{1}{N} \sum_{\mathbf{k}} e^{i\mathbf{k}\cdot(\mathbf{R}-\mathbf{R}')} = \delta_{n,n'}\delta_{\sigma,\sigma'}\delta_{\mathbf{R},\mathbf{R}'}. \end{aligned}$$

The other anti-commutators yield

$$\left\{ c_{n\mathbf{R}\sigma}^\dagger, c_{n'\mathbf{R}'\sigma'}^\dagger \right\} = \{ c_{n\mathbf{R}\sigma}, c_{n'\mathbf{R}'\sigma'} \}.$$

6.3: Use the representation (6.7) of the Bloch functions to write

$$V_{\alpha\beta\beta'\alpha'} = \frac{1}{N^2} \sum_{\mathbf{R}_1, \mathbf{R}_2, \mathbf{R}'_1, \mathbf{R}'_2} e^{-i\mathbf{k}\cdot\mathbf{R}_1} e^{-i\mathbf{k}\cdot\mathbf{R}_2} e^{i\mathbf{k}'\cdot\mathbf{R}'_1} e^{i\mathbf{k}'\cdot\mathbf{R}'_2} \\ \times \int d^3r \int d^3r' \phi^*(\mathbf{r} - \mathbf{R}_1) \phi^*(\mathbf{r}' - \mathbf{R}_2) \frac{e^2}{\kappa|\mathbf{r} - \mathbf{r}'|} \phi(\mathbf{r} - \mathbf{R}'_1) \phi(\mathbf{r}' - \mathbf{R}'_2).$$

Use (6.8) with the exponentials and sums over the wave vectors to replace the fermion operators of Bloch states in the interaction term by those of Wannier states to find (6.10).

6.4: The commutator between $c_\downarrow^\dagger c_\downarrow$ and $c_\uparrow^\dagger c_\uparrow$

$$[c_\downarrow^\dagger c_\downarrow, c_\uparrow^\dagger c_\uparrow] = c_\uparrow^\dagger c_\downarrow c_\downarrow^\dagger c_\uparrow - c_\downarrow^\dagger c_\uparrow c_\uparrow^\dagger c_\downarrow$$

is evaluated by using the anti-commutator for fermion operators and writing

$$c_\downarrow^\dagger c_\downarrow c_\uparrow^\dagger c_\uparrow = c_\uparrow^\dagger (1 - c_\downarrow^\dagger c_\downarrow) c_\uparrow = c_\uparrow^\dagger c_\uparrow - c_\uparrow^\dagger c_\downarrow^\dagger c_\downarrow c_\uparrow \\ = c_\uparrow^\dagger c_\uparrow - c_\downarrow^\dagger (1 - c_\uparrow c_\uparrow^\dagger) c_\downarrow = c_\uparrow^\dagger c_\uparrow - c_\downarrow^\dagger c_\downarrow + c_\downarrow^\dagger c_\downarrow c_\uparrow c_\uparrow^\dagger,$$

where the last term cancels in the commutator. Thus we have

$$[c_\downarrow^\dagger c_\downarrow, c_\uparrow^\dagger c_\uparrow] = c_\uparrow^\dagger c_\uparrow - c_\downarrow^\dagger c_\downarrow.$$

The other commutation relations

$$[c_\uparrow^\dagger c_\downarrow, c_\uparrow^\dagger c_\uparrow - c_\downarrow^\dagger c_\downarrow] = -2c_\uparrow^\dagger c_\downarrow, \quad \text{and} \quad [c_\uparrow^\dagger c_\uparrow, c_\uparrow^\dagger c_\uparrow - c_\downarrow^\dagger c_\downarrow] = 2c_\downarrow^\dagger c_\downarrow$$

follow in a similar way. These three commutators are the same as those between S^\pm and S^z and correspond to the operator algebra of the Cartesian components of the angular momentum S^x , S^y , and S^z .

6.5: Evaluate the commutator

$$[S_i^\beta S_k^\beta, S_j^x] = S_k^\beta S_j^x S_i^\beta - S_j^x S_i^\beta S_k^\beta \\ = -i\varepsilon_{x\beta\gamma} S_j^\gamma S_k^\beta \delta_{i,j} - S_i^\beta i\varepsilon_{x\beta\gamma} S_j^\gamma \delta_{j,k},$$

to write the commutator of S_j^x with the first term of the Heisenberg hamiltonian

$$\sum_{\substack{i,k \\ i \neq k}} J_{ik} \sum_{\beta} [S_i^\beta S_k^\beta, S_j^x] = \begin{cases} -\sum_{k \neq j} \sum_{\beta, \gamma} J_{jk} i\varepsilon_{x\beta\gamma} S_j^\gamma S_k^\beta & \text{for } i = j, k \neq j \\ -\sum_{i \neq j} \sum_{\beta, \gamma} J_{ij} i\varepsilon_{x\beta\gamma} S_i^\beta S_j^\gamma & \text{for } k = j, k \neq i \end{cases} \\ = -i \sum_{i \neq j} J_{ij} (\mathbf{S}_i \times \mathbf{S}_j)_x$$

where for obtaining the last line use was made of $i \neq k$ and of the meaning of the Levi-Civita symbol. For the commutator with the second term of the Heisenberg hamiltonian evaluate

$$\sum_i [S_i^z, S_j^x] = \sum_{i, \beta} i\varepsilon_{z\alpha\beta} S_j^\beta \delta_{i,j} = iS_j^y.$$

Putting together both contributions find

$$\frac{dS_j^x}{dt} = \frac{i}{\hbar} [\mathcal{H}_{\text{spin}}, S_j^x] = -\frac{1}{\hbar} \left(\sum_i J_{ij} (\mathbf{S}_i \times \mathbf{S}_j)_x + g\mu_B (\mathbf{H}_{\text{ext}} \times \mathbf{S}_j)_x \right).$$

6.6: Evaluate the commutator

$$\begin{aligned} [\alpha_k, \alpha_{k'}^\dagger] &= [u_k b_{1k} - v_k b_{2k}^\dagger, u_{k'} b_{1k'}^\dagger - v_{k'} b_{2k'}] \\ &= u_k u_{k'} \underbrace{[b_{1k}, b_{1k'}^\dagger]}_{\delta_{k,k'}} + v_k v_{k'} \underbrace{[b_{2k}^\dagger, b_{2k'}]}_{-\delta_{k,k'}}, \end{aligned}$$

which for $(u_k^2 - v_k^2) = 1$ is a boson commutation relation. In the same way, calculate

$$\begin{aligned} [\alpha_k, \beta_{k'}] &= [u_k b_{1k} - v_k b_{2k}^\dagger, u_{k'} b_{2k'} - v_{k'} b_{1k'}^\dagger] \\ &= -u_k v_{k'} [b_{1k}, b_{1k'}^\dagger] - v_k u_{k'} [b_{2k}^\dagger, b_{2k'}] = 0. \end{aligned}$$

The remaining commutation relations are obtained in a similar way.

6.7: Using the new boson operators for coupled magnon–phonon modes, the hamiltonian becomes

$$\begin{aligned} H_{\text{p-m}} &= \sum_k \{ \alpha_k^\dagger \alpha_k (\hbar\omega_k^{\text{p}} \cos^2 \Theta_k + \hbar\omega_k^{\text{m}} \sin^2 \Theta_k - 2c_k \sin \Theta_k \cos \Theta_k) \\ &\quad + \beta_k^\dagger \beta_k (\hbar\omega_k^{\text{p}} \sin^2 \Theta_k + \hbar\omega_k^{\text{m}} \cos^2 \Theta_k + 2c_k \sin \Theta_k \cos \Theta_k) \\ &\quad + \alpha_k^\dagger \beta_k [(\hbar\omega_k^{\text{p}} - \hbar\omega_k^{\text{m}}) \sin \Theta_k \cos \Theta_k + c_k (\cos^2 \Theta_k - \sin^2 \Theta_k)] \\ &\quad + \alpha_k \beta_k^\dagger [(\hbar\omega_k^{\text{p}} - \hbar\omega_k^{\text{m}}) \sin \Theta_k \cos \Theta_k + c_k (\cos^2 \Theta_k - \sin^2 \Theta_k)] \}. \end{aligned}$$

It can be diagonalized with

$$(\hbar\omega_k^{\text{p}} - \hbar\omega_k^{\text{m}}) \sin \Theta_k \cos \Theta_k + c_k (\cos^2 \Theta_k - \sin^2 \Theta_k) = 0$$

or

$$\tan 2\Theta_k = \frac{-2c_k}{\hbar\omega_k^{\text{p}} - \hbar\omega_k^{\text{m}}}.$$

For $\omega_k^{\text{p}} = \omega_k^{\text{m}} = \omega_k$ we have $\cos^2 \Theta_k = \sin^2 \Theta_k = 1/2$ and find for the eigenenergies of the coupled modes

$$\hbar\omega_k^\alpha = \hbar\omega_k - c_k \quad \text{and} \quad \hbar\omega_k^\beta = \hbar\omega_k + c_k$$

and for the corresponding boson operators

$$\alpha_k = \frac{1}{\sqrt{2}}(a_k - b_k) \quad \text{and} \quad \beta_k = \frac{1}{\sqrt{2}}(a_k + b_k).$$

6.8: With the inverted transformation relations (6.59) write the terms of (6.56):

$$\begin{aligned} b_{1\mathbf{k}}^\dagger b_{1\mathbf{k}} &= \alpha_{\mathbf{k}}^\dagger \alpha_{\mathbf{k}} u_{\mathbf{k}}^2 + \beta_{\mathbf{k}}^\dagger \beta_{\mathbf{k}} v_{\mathbf{k}}^2 + (\alpha_{\mathbf{k}}^\dagger \beta_{\mathbf{k}}^\dagger + \alpha_{\mathbf{k}} \beta_{\mathbf{k}}) u_{\mathbf{k}} v_{\mathbf{k}} \\ b_{2\mathbf{k}}^\dagger b_{2\mathbf{k}} &= \beta_{\mathbf{k}}^\dagger \beta_{\mathbf{k}} u_{\mathbf{k}}^2 + \alpha_{\mathbf{k}} \alpha_{\mathbf{k}}^\dagger v_{\mathbf{k}}^2 + (\beta_{\mathbf{k}}^\dagger \alpha_{\mathbf{k}}^\dagger + \beta_{\mathbf{k}} \alpha_{\mathbf{k}}) u_{\mathbf{k}} v_{\mathbf{k}} \\ b_{1\mathbf{k}}^\dagger b_{2\mathbf{k}}^\dagger &= (\alpha_{\mathbf{k}}^\dagger \alpha_{\mathbf{k}} + \beta_{\mathbf{k}} \beta_{\mathbf{k}}^\dagger) u_{\mathbf{k}} v_{\mathbf{k}} + \alpha_{\mathbf{k}}^\dagger \beta_{\mathbf{k}}^\dagger u_{\mathbf{k}}^2 + \beta_{\mathbf{k}} \alpha_{\mathbf{k}} v_{\mathbf{k}}^2 \\ b_{1\mathbf{k}} b_{2\mathbf{k}} &= (\alpha_{\mathbf{k}} \alpha_{\mathbf{k}}^\dagger + \beta_{\mathbf{k}}^\dagger \beta_{\mathbf{k}}) u_{\mathbf{k}} v_{\mathbf{k}} + \alpha_{\mathbf{k}} \beta_{\mathbf{k}} u_{\mathbf{k}}^2 + \beta_{\mathbf{k}}^\dagger \alpha_{\mathbf{k}}^\dagger v_{\mathbf{k}}^2 \end{aligned}$$

to obtain

$$\begin{aligned} \mathcal{H}_{\text{spin}} &\simeq E_a + 2J_a \nu S \sum_{\mathbf{k}} \left\{ (\alpha_{\mathbf{k}}^\dagger \alpha_{\mathbf{k}} + \beta_{\mathbf{k}}^\dagger \beta_{\mathbf{k}}) (u_{\mathbf{k}}^2 + v_{\mathbf{k}}^2 + 2\gamma_{\mathbf{k}} u_{\mathbf{k}} v_{\mathbf{k}}) \right. \\ &\quad \left. + (\alpha_{\mathbf{k}}^\dagger \beta_{\mathbf{k}}^\dagger + \alpha_{\mathbf{k}} \beta_{\mathbf{k}}) (2u_{\mathbf{k}} v_{\mathbf{k}} + \gamma_{\mathbf{k}} (u_{\mathbf{k}}^2 + v_{\mathbf{k}}^2)) + 2(\gamma_{\mathbf{k}} u_{\mathbf{k}} v_{\mathbf{k}} + v_{\mathbf{k}}^2) \right\}. \end{aligned}$$

Add and subtract $u_{\mathbf{k}}^2$ under the sum to find with $u_{\mathbf{k}}^2 - v_{\mathbf{k}}^2 = 1$ the expression (6.60).

6.9: Extend (6.53) by the terms due to the anisotropy field H_A and the external field H_{ext}

$$\mathcal{H}_{\text{spin}} = J_a \sum_{n,n',ij} \mathbf{S}_{1i} \cdot \mathbf{S}_{2j} - g\mu_B \sum_i ((H_A + H_{\text{ext}}) S_{1i}^z - (H_A - H_{\text{ext}}) S_{2i}^z)$$

and replace the spin operators by boson operators on each sublattice using the Holstein–Primakoff transformation to obtain

$$\begin{aligned} \mathcal{H}_{\text{spin}} &= -2J_a \nu N S^2 - 4g\mu_B H_A N S \\ &\quad + 2J_a \nu S \sum_{\mathbf{k}} \left\{ b_{1\mathbf{k}}^\dagger b_{1\mathbf{k}} + b_{2\mathbf{k}}^\dagger b_{2\mathbf{k}} + \gamma_{\mathbf{k}} (b_{1\mathbf{k}}^\dagger b_{2\mathbf{k}}^\dagger + b_{1\mathbf{k}} b_{2\mathbf{k}}) \right\} \\ &\quad + 2g\mu_B H_A \sum_{\mathbf{k}} (b_{1\mathbf{k}}^\dagger b_{1\mathbf{k}} + b_{2\mathbf{k}}^\dagger b_{2\mathbf{k}}) + g\mu_B H_{\text{ext}} \sum_{\mathbf{k}} (b_{1\mathbf{k}}^\dagger b_{1\mathbf{k}} - b_{2\mathbf{k}}^\dagger b_{2\mathbf{k}}). \end{aligned}$$

Eliminate the coupling between the sublattices using the Bogoliubov transformation (6.57) and write with the abbreviations

$$\begin{aligned} C &= -2J_a \nu N S^2 - 4g\mu_B H_A N S, \quad A = 2J_a \nu S, \quad B = 2g\mu_B H_A, \quad C = g\mu_B H_{\text{ext}} \\ \mathcal{H}_{\text{spin}} &\simeq C + \sum_{\mathbf{k}} \left\{ A\gamma_{\mathbf{k}} \left(2u_{\mathbf{k}} v_{\mathbf{k}} (\alpha_{\mathbf{k}}^\dagger \alpha_{\mathbf{k}} + \beta_{\mathbf{k}}^\dagger \beta_{\mathbf{k}} + 1) + (u_{\mathbf{k}}^2 + v_{\mathbf{k}}^2) (\alpha_{\mathbf{k}}^\dagger \beta_{\mathbf{k}}^\dagger + \alpha_{\mathbf{k}} \beta_{\mathbf{k}}) \right) \right. \\ &\quad + (A + B) \left((u_{\mathbf{k}}^2 + v_{\mathbf{k}}^2) (\alpha_{\mathbf{k}}^\dagger \alpha_{\mathbf{k}} + \beta_{\mathbf{k}}^\dagger \beta_{\mathbf{k}}) + 2u_{\mathbf{k}} v_{\mathbf{k}} (\alpha_{\mathbf{k}}^\dagger \beta_{\mathbf{k}}^\dagger + \alpha_{\mathbf{k}} \beta_{\mathbf{k}}) + 2v_{\mathbf{k}}^2 \right) \\ &\quad \left. + C (\alpha_{\mathbf{k}}^\dagger \alpha_{\mathbf{k}} - \beta_{\mathbf{k}}^\dagger \beta_{\mathbf{k}}) \right\}. \end{aligned}$$

Diagonalize with $A\gamma_{\mathbf{k}} (u_{\mathbf{k}}^2 + v_{\mathbf{k}}^2) = -2(A + B)u_{\mathbf{k}} v_{\mathbf{k}}$. Square this relation and use $u_{\mathbf{k}}^2 - v_{\mathbf{k}}^2 = 1$ to get a biquadratic equation for $u_{\mathbf{k}}$. Take its solution to find

$$u_{\mathbf{k}}^2 + v_{\mathbf{k}}^2 = \pm \left\{ \frac{(A + B)^2}{(A + B)^2 - A^2 \gamma_{\mathbf{k}}^2} \right\}^{1/2}, \quad u_{\mathbf{k}} v_{\mathbf{k}} = \mp \frac{1}{2} \left\{ \frac{A^2 \gamma_{\mathbf{k}}^2}{(A + B)^2 - A^2 \gamma_{\mathbf{k}}^2} \right\}^{1/2}.$$

Identify the prefactor of the magnon number operators as the magnon energy

$$\hbar\omega_{\mathbf{k}} = \{(A+B)^2 - A^2\gamma_{\mathbf{k}}^2\}^{1/2}$$

which without anisotropy field ($B=0$) reduces to the dispersion relation for the antiferromagnetic magnons which for small k is linear. With anisotropy field one finds a finite magnon energy for $\mathbf{k}=0$ and a quadratic dispersion for small k as can be seen in Fig. 6.8.

6.10: Evaluate for low temperature ($T \ll T_C$) the magnetization (per unit volume)

$$M(T) = g\mu_B \left(NS - \sum_{\mathbf{k}} \langle b_{\mathbf{k}}^\dagger b_{\mathbf{k}} \rangle \right) \quad \text{or}$$

$$\begin{aligned} M(0) - M(T) &= g\mu_B \sum_{\mathbf{k}} \frac{1}{\exp(\hbar\omega_{\mathbf{k}}/k_B T) - 1} \\ &= g\mu_B \frac{4\pi}{(2\pi)^3} \int_0^\infty \frac{k^2 dk}{\exp(Dk^2/k_B T) - 1} \end{aligned}$$

where the quadratic dispersion for small k is used. The integral (it is a Bose integral) can be solved as described in the Appendix (A.3) to yield Bloch's $T^{3/2}$ law:

$$M(0) - M(T) = \zeta\left(\frac{3}{2}\right) \frac{g\mu_B}{M(0)} \left(\frac{k_B}{4\pi D}\right)^{3/2} T^{3/2}.$$

See [166].

6.11: Calculate the expectation value in (6.106) for $T=0$:

$$\begin{aligned} \langle \dots \rangle_0 &= \sum_m \{ \langle \Psi_0 | M_+(\mathbf{q}, \tau) | \Psi_m \rangle \langle \Psi_m | M_-(-\mathbf{q}, 0) | \Psi_0 \rangle \\ &\quad - \langle \Psi_0 | M_-(-\mathbf{q}, 0) | \Psi_m \rangle \langle \Psi_m | M_+(\mathbf{q}, \tau) | \Psi_0 \rangle \}. \end{aligned}$$

Replace the operators M_\pm by the fermion operators and extract the exponentials with the time dependence. The energy difference $E_m - E_0$ of exact eigenstates becomes in HF approximation the energy difference of single-particle energies for particle-hole excitations with spin-flip across the Fermi energy. By manipulations as in Sect. 4.5 one arrives at the spin susceptibility (6.108).

To evaluate (6.108), use

$$\epsilon_{\mathbf{k}+\mathbf{q}\uparrow} - \epsilon_{\mathbf{k}\downarrow} = -\Delta + \frac{\hbar^2}{m} \mathbf{k} \cdot \mathbf{q} + \epsilon_{\mathbf{q}}, \quad \epsilon_{\mathbf{k}\uparrow} - \epsilon_{\mathbf{k}-\mathbf{q}\downarrow} = -\Delta + \frac{\hbar^2}{m} \mathbf{k} \cdot \mathbf{q} - \epsilon_{\mathbf{q}}$$

with $\epsilon_{\mathbf{q}} = \hbar^2 q^2 / 2m$ and perform the sum over \mathbf{k} with the substitution $\mathbf{k} \cdot \mathbf{q} = kq \cos \theta$, $\cos \theta = x$. The first term can be written

$$\begin{aligned} A_{\downarrow} &= \sum_{|\mathbf{k}| \leq k_{F\downarrow}} \frac{1}{\hbar\omega + \epsilon_{\mathbf{k}+\mathbf{q}\uparrow} - \epsilon_{\mathbf{k}\downarrow}} \\ &= \frac{V}{(2\pi)^2} \int_0^{k_{F\downarrow}} dk k^2 \int_{-1}^{+1} \frac{1}{\hbar\omega - \Delta + \epsilon_{\mathbf{q}} + \hbar^2 kq x / m} dx. \end{aligned}$$

The integral over x can be solved according to

$$\int_{-1}^{+1} \frac{dx}{a+bx} = \frac{1}{b} \int_{a-b}^{a+b} \frac{dz}{z} = \frac{1}{b} \ln \left| \frac{1+b/a}{1-b/a} \right|.$$

Looking for collective excitations at small q one has $b/a \ll 1$ and can use the expansion

$$\frac{1}{b} \ln \left| \frac{1+b/a}{1-b/a} \right| \simeq \frac{2}{b} \left\{ \frac{b}{a} + \frac{1}{3} \left(\frac{b}{a} \right)^3 \right\} = \frac{2}{a} \left\{ 1 + \frac{1}{3} \left(\frac{b}{a} \right)^2 \right\}$$

to obtain

$$A_{\downarrow} = \frac{2V}{(2\pi)^2} \frac{1}{\hbar\omega - \Delta + \epsilon_q} \int_0^{k_F^-} dk k^2 \left\{ 1 + \frac{k^2}{3} \left(\frac{\hbar^2 q}{m} \right)^2 \left(\frac{1}{\hbar\omega - \Delta + \epsilon_q} \right)^2 \right\}.$$

After integration and corresponding evaluation of the second term A_{\uparrow} one arrives at (6.108).

Solutions for Chap. 7

7.1: Evaluate the commutator $[c_{\bar{k},\bar{\sigma}}, c_{\mathbf{k}+\mathbf{q}\sigma}^{\dagger} c_{\mathbf{k}'-\mathbf{q}\sigma'}^{\dagger} c_{\mathbf{k}'\sigma'} c_{\mathbf{k}\sigma}]$ by successively interchanging $c_{\bar{k},\bar{\sigma}}$ with the four operators appearing in the interaction term. Each step leads to a change in sign and in addition gives a Kronecker δ for exchange with the creation operators, thus

$$c_{\bar{k},\bar{\sigma}}^{\dagger} c_{\mathbf{k}+\mathbf{q}\sigma}^{\dagger} c_{\mathbf{k}'-\mathbf{q}\sigma'}^{\dagger} c_{\mathbf{k}'\sigma'} c_{\mathbf{k}\sigma} = \delta_{\bar{k},\mathbf{k}+\mathbf{q}} \delta_{\bar{\sigma},\sigma} c_{\mathbf{k}'-\mathbf{q}\sigma'}^{\dagger} c_{\mathbf{k}'\sigma'} c_{\mathbf{k}\sigma} - \delta_{\bar{k},\mathbf{k}'-\mathbf{q}} c_{\mathbf{k}+\mathbf{q}\sigma}^{\dagger} c_{\mathbf{k}'\sigma'} c_{\mathbf{k}\sigma}.$$

Interchange the last two operators in the second term and replace σ by σ' and \mathbf{k} by \mathbf{k}' . Replace in the first term \mathbf{q} by $-\mathbf{q}$ and consider the properties of the interaction matrix element to find the expression for $[c_{\bar{k}}, \mathcal{H}_{\text{int}}]$ (7.20). The commutator $[c_{\bar{k}}^{\dagger}, \mathcal{H}_{\text{int}}]$ is evaluated by analogous steps.

7.2: The equation of motion of the full Green function $G(\mathbf{k}\sigma; t-t')$ (7.21) can be written with (7.23) as

$$\left(i\hbar \frac{\partial}{\partial t} - \epsilon_{\mathbf{k}\sigma} \right) G(\mathbf{k}\sigma; t-t') = \delta(t-t') + \int dt'' \Sigma(\mathbf{k}\sigma; t-t'') G(\mathbf{k}\sigma; t''-t').$$

Replace the Green function and the self-energy by their Fourier transform with respect to the time arguments and identify the integrands to obtain

$$(\hbar\omega - \epsilon_{\mathbf{k}\sigma}) G(\mathbf{k}\sigma; \omega) = 1 + \Sigma(\mathbf{k}\sigma; \omega) G(\mathbf{k}\sigma; \omega).$$

After multiplication with the Green function of the noninteracting system

$$G^0(\mathbf{k}\sigma; \omega) = (\hbar\omega - \epsilon_{\mathbf{k}\sigma})^{-1}$$

one arrives at the Dyson equation

$$G(\mathbf{k}\sigma; \omega) = G^0(\mathbf{k}\sigma; \omega) + G^0(\mathbf{k}\sigma; \omega) \Sigma(\mathbf{k}\sigma; \omega) G(\mathbf{k}\sigma; \omega).$$

7.3: The commutator of $n_{i-\sigma} c_{i\sigma}$ with the single-particle part H_0 yields three terms due to interchange of creation and annihilation operators:

$$\begin{aligned}
[n_{i-\sigma}c_{i\sigma}, H_0] &= \sum_{mj\sigma'} t_{mj} \left(c_{i-\sigma}^\dagger c_{i-\sigma} c_{i\sigma} c_{m\sigma'}^\dagger c_{j\sigma'} - c_{m\sigma'}^\dagger c_{j\sigma'} c_{i-\sigma}^\dagger c_{i-\sigma} c_{i\sigma} \right) \\
&= \sum_{mj\sigma'} t_{mj} \left(\delta_{im} \delta_{\sigma\sigma'} n_{i-\sigma} c_{j\sigma} - \delta_{im} \delta_{\sigma-\sigma'} c_{i-\sigma}^\dagger c_{i\sigma} c_{j-\sigma} \right. \\
&\quad \left. - \delta_{ij} \delta_{\sigma-\sigma'} c_{m-\sigma}^\dagger c_{i-\sigma} c_{i\sigma} \right) \\
&= \sum_m t_{im} \left(n_{i-\sigma} c_{m\sigma} + c_{i-\sigma}^\dagger c_{m-\sigma} c_{i\sigma} - c_{m-\sigma}^\dagger c_{i-\sigma} c_{i\sigma} \right),
\end{aligned}$$

where the last line is obtained by proper choice of the summation indices and rearranging the operators. Similarly the commutator with the interaction term is evaluated

$$\begin{aligned}
[n_{i-\sigma}c_{i\sigma}, H_1] &= \frac{1}{2}U \sum_{m\sigma'} (n_{i-\sigma}c_{i\sigma}n_{m\sigma'}n_{m-\sigma'} - n_{m\sigma'}n_{m-\sigma'}n_{i-\sigma}c_{i\sigma}) \\
&= \frac{1}{2}U \sum_{m\sigma'} n_{i-\sigma} \left(c_{i\sigma}c_{m\sigma'}^\dagger c_{m\sigma'}n_{m-\sigma'} - n_{m\sigma'}n_{m-\sigma'}c_{i\sigma} \right) \\
&= \frac{1}{2}U \sum_{m\sigma'} n_{i-\sigma} (\delta_{im}\delta_{\sigma\sigma'}c_{i\sigma}n_{i-\sigma} + \delta_{im}\delta_{\sigma-\sigma'}n_{i-\sigma}c_{i\sigma}),
\end{aligned}$$

which using $n_{i-\sigma}^2 = n_{i-\sigma}$ becomes (7.55).

7.4: Calculate the derivative of the self-energy (7.70) and obtain the spectral weight

$$Z(E) = \left(1 - \frac{\partial \Sigma}{\partial E}\right)^{-1} = \frac{(E - \epsilon_0 - U(1 - \langle n_{-\sigma} \rangle))^2}{(E - \epsilon_0 - U(1 - \langle n_{-\sigma} \rangle))^2 + U^2 \langle n_{-\sigma} \rangle (1 - \langle n_{-\sigma} \rangle)}.$$

For the lower Hubbard band with $E = \epsilon_0 + 2t \cos ka$ this becomes

$$Z_{\text{lower}} = \frac{(2t \cos ka - U(1 - \langle n_{-\sigma} \rangle))^2}{(2t \cos ka - U(1 - \langle n_{-\sigma} \rangle))^2 + U^2 \langle n_{-\sigma} \rangle (1 - \langle n_{-\sigma} \rangle)}$$

and reduces for $k = \pi/2a$ to $Z_{\text{lower}} = 1 - \langle n_{-\sigma} \rangle$. For the upper Hubbard band with $E = \epsilon_0 + U + 2t \cos ka$ the result is

$$Z_{\text{upper}} = \frac{(2t \cos ka + U \langle n_{-\sigma} \rangle)^2}{(2t \cos ka + U \langle n_{-\sigma} \rangle)^2 + U^2 \langle n_{-\sigma} \rangle (1 - \langle n_{-\sigma} \rangle)}$$

and $Z_{\text{upper}} = \langle n_{-\sigma} \rangle$ for $k = \pi/2a$. Note that the spectral weights for $k = \pi/2a$ are those of the atomic limit (see Fig. 7.3).

7.5: This problem is solved in some detail in [169, 206]. It leads to the so-called $t-J$ model, where t is the hopping integral and $J \sim t^2/U$ is the effective exchange matrix element.

7.6: Describing the delocalized electrons by fermion operators $c_{\mathbf{k}\sigma}^\dagger, c_{\mathbf{k}\sigma}$ in a band with dispersion $\epsilon_{\mathbf{k}}$ and the localized electrons with energy ϵ_d by fermion operators $d_\sigma^\dagger, d_\sigma$, the Hamiltonian is formulated as

$$\begin{aligned}
H &= \sum_{\mathbf{k}, \sigma} \epsilon_{\mathbf{k}} c_{\mathbf{k}\sigma}^\dagger c_{\mathbf{k}\sigma} + \sum_{\sigma} \epsilon_d d_\sigma^\dagger d_\sigma \\
&\quad + \sum_{\mathbf{k}, \sigma} V_{\mathbf{k}\sigma} \left(d_\sigma^\dagger c_{\mathbf{k}\sigma} + c_{\mathbf{k}\sigma}^\dagger d_\sigma \right) + U n_\uparrow^d n_\downarrow^d.
\end{aligned}$$

Here the third term describes the hybridization between the localized and delocalized electrons. This is the Anderson impurity model. It can be extended by considering instead of a single impurity a periodic configuration of sites i with d electrons. For this case the fermion operators for d electrons become $d_{i\sigma}^\dagger, d_{i\sigma}$ and summation over the sites i is to be considered. See P.W. Anderson: Phys. Rev. **124** 41 (1961) and [64] Sect. 6.2, [122, 195].

7.7: For the solution see [122, 195]. It uses a contour integration in the complex frequency plane taking into account the position of the poles for quasi-particles and holes.

7.8: Start from (4.136) for the real part of the dielectric function, which for $T = 0$ reads

$$\epsilon_1(\mathbf{q}, \omega) = 1 + v_q \sum_{|\mathbf{k}| \leq k_F} \frac{2\epsilon_{\mathbf{k}} - \epsilon_{\mathbf{k}+\mathbf{q}} - \epsilon_{\mathbf{k}-\mathbf{q}}}{(\hbar\omega - \epsilon_{\mathbf{k}} + \epsilon_{\mathbf{k}-\mathbf{q}})(\hbar\omega - \epsilon_{\mathbf{k}+\mathbf{q}} + \epsilon_{\mathbf{k}})}.$$

Making use of the free electron dispersion $\epsilon_{\mathbf{k}} = \hbar^2 k^2 / 2m$ the numerator simplifies to $-\hbar^2 q^2 / m$ while the denominator takes the form

$$(\hbar\omega - \epsilon_{\mathbf{k}} + \epsilon_{\mathbf{k}-\mathbf{q}})(\hbar\omega - \epsilon_{\mathbf{k}+\mathbf{q}} + \epsilon_{\mathbf{k}}) = \left(\hbar\omega - \frac{\hbar^2}{m} \mathbf{k} \cdot \mathbf{q} \right)^2 - \left(\frac{\hbar^2}{2m} q^2 \right)^2$$

and the expression to be evaluated by integration is

$$\sum_{|\mathbf{k}| \leq k_F} \frac{1}{\left(\hbar\omega - \frac{\hbar^2}{m} \mathbf{k} \cdot \mathbf{q} \right)^2 - \left(\frac{\hbar^2}{2m} q^2 \right)^2} = \left(\frac{2m}{\hbar^2} \right)^2 \sum_{|\mathbf{k}| \leq k_F} \frac{1}{(q_s^2 - 2\mathbf{k} \cdot \mathbf{q})^2 - q^4},$$

with $q_s^2 = 2m\hbar\omega/\hbar^2$.

For $d = 1$ the vectors become scalars and the sum can be written as the integral (using the substitution $x = 2kq$)

$$I(q, \omega) = \frac{L}{2\pi} \int_{-k_F}^{k_F} \frac{dk}{q_s^4 - q^4 - 4q_s^2 kq + 4k^2 q^2} = \frac{L}{2\pi} \int_{-x_F}^{x_F} \frac{dx}{x^2 - 2q_s^2 x + q_s^4 - q^4}.$$

The integral can be found in integral tables giving

$$I(q, \omega) = \frac{L}{2\pi} \frac{1}{4q^3} \ln \left| \frac{(2k_F q - 2q^2)^2 - 4q_s^4}{(2k_F q + 2q^2)^2 - 4q_s^4} \right|.$$

For $\omega = 0$ (or $q_s = 0$) this integral diverges for $q \rightarrow k_F$.

For $d = 3$, considering from the beginning the simpler case $\omega = 0$, the corresponding integral is

$$I(q) = \frac{L^3}{(2\pi)^3} 2\pi \int_0^{k_F} dk k \int_{-1}^{+1} \frac{d \cos \vartheta}{4k^2 q^2 \cos^2 \vartheta - q^4} = \frac{L^3}{8\pi^2 q^3} \int_0^{k_F} dk \ln \left| \frac{k-q}{k+q} \right|,$$

and yields by integration

$$I(q) = \frac{L^3}{8\pi^2 q^2} \left\{ \left(\frac{k_F}{q} - 1 \right) \ln \left(\frac{k_F}{q} - 1 \right) - \left(\frac{k_F}{q} + 1 \right) \ln \left(\frac{k_F}{q} + 1 \right) \right\}.$$

For $q \rightarrow k_F$ this integral remains finite.

Solutions for Chap. 8

8.1: The operator for linear electron–phonon interaction

$$\mathcal{H}_{\text{el-ph}} = - \sum_{l, \mathbf{n}, \tau} \nabla_l v(\mathbf{r}_l - \mathbf{R}_{\mathbf{n}\tau}) \Big|_{\mathbf{R}_{\mathbf{n}\tau}^0} \cdot \mathbf{u}_{\mathbf{n}\tau}$$

can be written in terms of phonon and electron operators using (3.22) together with (3.39) and by replacing with (4.76)

$$\sum_l \nabla_l v(\mathbf{r}_l - \mathbf{R}_{\mathbf{n}\tau}) \Big|_{\mathbf{R}_{\mathbf{n}\tau}^0} \rightarrow \sum_{n, \mathbf{k}, n', \mathbf{k}'} \langle n\mathbf{k} | \nabla v | n'\mathbf{k}' \rangle c_{n\mathbf{k}}^\dagger c_{n'\mathbf{k}'}$$

The sum over the lattice sites \mathbf{n} effects only the gradient of the potential and has the form of a Bloch function

$$\sum_n e^{i\mathbf{q} \cdot \mathbf{R}_n^0} \nabla v(\mathbf{r} - \mathbf{R}_{\mathbf{n}\tau}) \Big|_{\mathbf{R}_{\mathbf{n}\tau}^0} = e^{i\mathbf{q} \cdot \mathbf{r}} \mathcal{U}_{\mathbf{q}\tau}(\mathbf{r})$$

where $\mathcal{U}_{\mathbf{q}\tau}(\mathbf{r})$ is a lattice periodic function. After decomposition of the electron Bloch functions in the matrix element into plane wave and lattice periodic part the product $u_{n\mathbf{k}}^*(\mathbf{r}) u_{n'\mathbf{k}'}(\mathbf{r}) \mathcal{U}_{\mathbf{q}\tau}(\mathbf{r})$ can be expanded in a Fourier series. Thus the integration over the crystal volume can be carried out with

$$\int d^3r e^{-i(\mathbf{k}-\mathbf{k}'-\mathbf{q}-\mathbf{G}) \cdot \mathbf{r}} \sim \delta_{\mathbf{k}, \mathbf{k}'+\mathbf{q}+\mathbf{G}}$$

and yields the relation between the involved wave vectors.

8.2: Using (3.76) one has $\partial u_i / \partial x_i = \epsilon_{ii}$ and can write

$$\nabla \cdot \mathbf{u}(\mathbf{r}) = \sum_i \frac{\partial}{\partial x_i} u_i(\mathbf{r}) = \sum_i \epsilon_{ii} = \text{Tr} \epsilon.$$

For $\mathbf{u}(\mathbf{r}) \sim e^{i\mathbf{q} \cdot \mathbf{r}}$ follows $\nabla \cdot \mathbf{u} = i\mathbf{q} \cdot \mathbf{u}$ which differs from zero only for longitudinal phonons.

8.3: For transverse phonons with $\mathbf{q} = \sum_\alpha q_\alpha \mathbf{e}_\alpha$, $\mathbf{u} = \sum_\beta u_\beta \mathbf{e}_\beta$ we have in general $\mathbf{q} \cdot \mathbf{u} = \sum_\alpha q_\alpha u_\alpha = -i \text{Tr} \epsilon = 0$ but e.g. for the special case $\mathbf{q} = (q, 0, 0)$, $\mathbf{u} = (0, u_2, u_3)$ the strain tensor components are

$$\epsilon_{11} = \epsilon_{22} = \epsilon_{33} = \epsilon_{23} = 0, \text{ but } \epsilon_{12} = \frac{i}{2} q u_2, \quad \epsilon_{13} = \frac{i}{2} q u_3,$$

giving a nonvanishing contribution to the electron–phonon interaction.

8.4: Start with the classical expression for the interaction energy (8.23) with

$$\begin{aligned} \nabla \cdot \mathbf{P}(\mathbf{r}) &= -\frac{1}{4} e_{14} |\varepsilon_{ijk}| (q_i q_k u_j + q_i q_j u_k) e^{i\mathbf{q} \cdot \mathbf{r}} \quad \text{double index summation} \\ &= -2e_{14} (q_y q_z u_x + q_z q_x u_y + q_x q_y u_z) e^{i\mathbf{q} \cdot \mathbf{r}}. \end{aligned}$$

Using (8.24) for the charge density, expressing the displacement field by phonon operators, and integrating over the crystal volume converts E_{int} into the operator

$$\mathcal{H}_{\text{el-ph}}^{\text{P}} = -\frac{2e\epsilon_{14}}{\epsilon_0\epsilon_\infty} \sum_{s,\mathbf{q}} \sqrt{\frac{\hbar N}{2M\omega_s(\mathbf{q})}} \frac{q_x q_y e_z^s(\mathbf{q}) + c.p.}{q^2} \times \left(a_s^\dagger(-\mathbf{q}) + a_s(\mathbf{q}) \right) \sum_{\mathbf{k}} c_{\mathbf{k}+\mathbf{q}}^\dagger c_{\mathbf{k}}.$$

8.5: To be calculated is the expression $\langle \tau \rangle$ (8.71) with the given dependencies of τ . The integrals are solved with the substitution $\epsilon/k_{\text{B}}T = x$ and we may write

$$\int_0^\infty \epsilon^{3/2} e^{-\epsilon/k_{\text{B}}T} d\epsilon = (k_{\text{B}}T)^{5/2} \int_0^\infty x^{3/2} e^{-x} dx \sim T^{5/2}.$$

Similar for $\tau \sim T^{-1}\epsilon^{-1/2}$

$$\int_0^\infty \tau \epsilon^{3/2} e^{-\epsilon/k_{\text{B}}T} d\epsilon = T^{-1} (k_{\text{B}}T)^2 \int_0^\infty x e^{-x} dx \sim T$$

and for $\tau \sim T^{-1}\epsilon^{1/2}$

$$\int_0^\infty \tau \epsilon^{3/2} e^{-\epsilon/k_{\text{B}}T} d\epsilon = T^{-1} (k_{\text{B}}T)^3 \int_0^\infty x e^{-x} dx \sim T^2.$$

Thus for deformation potential coupling $\mu(T) \sim T^{-3/2}$ and for piezoelectric coupling $\mu(T) \sim T^{-1/2}$. This explains the different slopes of the corresponding graphs in Fig. 8.5. For more details see [4, 246].

8.6: For the solution see [4], Chap. 7. The calculation is essentially the same as for the Fröhlich coupling but with the $1/q$ dependence of the interaction potential replaced by a \sqrt{q} dependence. The number of virtually excited phonons being proportional to the square of the effective mass of the electron turns out to be much smaller than 1. Replacing the electron by the much heavier ion would increase this number to a value much larger than 1 indicating that the perturbation calculation is not appropriate.

8.7: We have to evaluate the commutator

$$[\mathcal{H}_{\text{el-ph}}, S] = \sum_{\substack{\mathbf{k}, \mathbf{q} \\ \mathbf{k}', \mathbf{q}'}} \mathcal{V}_{\mathbf{q}} \mathcal{V}_{\mathbf{q}'} \left[c_{\mathbf{k}+\mathbf{q}}^\dagger c_{\mathbf{k}} \left(a_{-\mathbf{q}}^\dagger + a_{\mathbf{q}} \right), c_{\mathbf{k}'+\mathbf{q}'}^\dagger c_{\mathbf{k}'} \left(\alpha a_{-\mathbf{q}'}^\dagger + \beta a_{\mathbf{q}'} \right) \right]$$

and write

$$\begin{aligned} [\dots, \dots] &= \left[a_{-\mathbf{q}}^\dagger + a_{\mathbf{q}}, \alpha a_{-\mathbf{q}'}^\dagger + \beta a_{\mathbf{q}'} \right] c_{\mathbf{k}+\mathbf{q}}^\dagger c_{\mathbf{k}} c_{\mathbf{k}'+\mathbf{q}'}^\dagger c_{\mathbf{k}'} \\ &\quad + \left[c_{\mathbf{k}+\mathbf{q}}^\dagger c_{\mathbf{k}}, c_{\mathbf{k}'+\mathbf{q}'}^\dagger c_{\mathbf{k}'} \right] \left(\alpha a_{-\mathbf{q}'}^\dagger + \beta a_{\mathbf{q}'} \right) \left(a_{-\mathbf{q}}^\dagger + a_{\mathbf{q}} \right). \end{aligned}$$

The electron part of the first term can be rearranged giving

$$c_{\mathbf{k}+\mathbf{q}}^\dagger c_{\mathbf{k}} c_{\mathbf{k}'+\mathbf{q}'}^\dagger c_{\mathbf{k}'} = c_{\mathbf{k}+\mathbf{q}}^\dagger c_{\mathbf{k}'+\mathbf{q}'}^\dagger c_{\mathbf{k}'} c_{\mathbf{k}} + \delta_{\mathbf{k}, \mathbf{k}'-\mathbf{q}} \hat{n}_{\mathbf{k}'}$$

where the first term has the structure of an electron–electron interaction (this is the one we are looking for). The phonon part of the first term gives

$$\left[a_{-q}^\dagger + a_q, \alpha a_{-q'}^\dagger + \beta a_{q'} \right] = (-\alpha + \beta) \delta_{q, q'}.$$

The second term, being bilinear in the phonon operators, is neglected as well as the term with the electron number operator to obtain the approximate form of the commutator $[\mathcal{H}_{\text{el-ph}}, S]$.

8.8: Using (8.120) the ground state expectation value of $\bar{\mathcal{H}}$ relative to the ground state of the normal system is

$$E_0 = \langle \bar{\mathcal{H}} \rangle + \sum_{\mathbf{k}} |E(\mathbf{k})|$$

and can be written with

$$\langle \sigma_{kz} \rangle = \cos \theta_{\mathbf{k}}, \quad \langle \sigma_{kx} \rangle = \sin \theta_{\mathbf{k}} \quad \text{and} \quad \frac{V_{\text{eff}}}{4} \sum_{\mathbf{k}'} \sin \theta_{\mathbf{k}'} = E(\mathbf{k}) \tan \theta_{\mathbf{k}}$$

as

$$E_0 = - \sum_{\mathbf{k}} E(\mathbf{k}) \left(\cos \theta_{\mathbf{k}} + \frac{1}{2} \tan \theta_{\mathbf{k}} \sin \theta_{\mathbf{k}} \right) + \sum_{\mathbf{k}} |E(\mathbf{k})|.$$

With

$$E(\mathbf{k}) \tan \theta_{\mathbf{k}} \sin \theta_{\mathbf{k}} = \frac{2\Delta^2}{V_{\text{eff}}} \quad \text{and} \quad \cos \theta_{\mathbf{k}} = \frac{E(\mathbf{k})}{(E^2(\mathbf{k}) + \Delta^2)^{1/2}}$$

and by replacing the sum over \mathbf{k} by an energy integral over the shell with thickness $\hbar\omega_{\text{D}}$ at the Fermi energy, one finds

$$E_0 = 2D(E_{\text{F}}) \int_0^{\hbar\omega_{\text{D}}} d\epsilon \left\{ \epsilon - \frac{\epsilon^2}{(\epsilon^2 + \Delta^2)^{1/2}} \right\} - \frac{\Delta^2}{V_{\text{eff}}},$$

where $D(E_{\text{F}})$ is the density of states at the Fermi energy. The integration can easily be performed and yields

$$E_0 = D(E_{\text{F}})(\hbar\omega_{\text{D}})^2 \left\{ 1 - \left[1 + \left(\frac{\Delta}{\hbar\omega_{\text{D}}} \right)^2 \right]^{1/2} \right\} \simeq - (D(E_{\text{F}})\hbar\omega_{\text{D}})^2 V_{\text{eff}}.$$

The last expression, obtained for $1 \gg D(E_{\text{F}})V_{\text{eff}}$, tells us that the superconducting state is stable as long as the effective interaction is positive.

Solutions for Chap. 9

9.1: Besides the poles of $G_0(E)$ the full Green function $G(E)$ has additional poles for $1 - G_0(E)U = 0$. In site representation U has block-diagonal form with a non-zero block $U^1 = U_{\{R_I\}}$ only in the diagonal for lattice sites around the impurity. With $G_0(E)$ written in the corresponding block form (with $G_{0, \{R_I\}}(E) = G_0^1(E)$ and corresponding matrices for the other blocks), the matrix multiplication can be performed to give

$$G_0(E)U = \begin{pmatrix} G_0^1(E) & G_0^2(E) \\ G_0^3(E) & G_0^4(E) \end{pmatrix} \begin{pmatrix} U & 0 \\ 0 & 0 \end{pmatrix} = \begin{pmatrix} G_0^1(E)U^1 & 0 \\ G_0^3(E)U^1 & 0 \end{pmatrix}.$$

The determinant of $1 - G_0(E)U$ is the product of the determinants of its diagonal blocks or $\|1 - G_{0, \{R_I\}}(E)U_{\{R_I\}}\| = 0$.

9.2: The average of the individual resistances is

$$\langle r \rangle = \frac{1}{N} \sum_{i=1}^N r_i \quad \text{and therefore} \quad \langle R \rangle = \left\langle \sum_{i=1}^N r_i \right\rangle = \sum_{i=1}^N \langle r_i \rangle = N \langle r \rangle.$$

The variance of R is given by

$$\text{Var}R = \left\langle \sum_{ij} r_i r_j \right\rangle - N^2 \langle r \rangle^2 = \left\langle \sum_i r_i^2 \right\rangle + \left\langle \sum_{i \neq j} r_i r_j \right\rangle - N^2 \langle r \rangle^2$$

and with uncorrelated fluctuations of the r_i

$$\text{Var}R = N \langle r^2 \rangle + N(N-1) \langle r \rangle^2 - N^2 \langle r \rangle^2 = N (\langle r^2 \rangle - \langle r \rangle^2).$$

The relative variance given by

$$\frac{\text{Var}R}{\langle R \rangle^2} = \frac{1}{N} \frac{\text{Var}r}{\langle r \rangle^2} \quad \text{vanishes for } N \rightarrow \infty.$$

9.3: The transverse response reads

$$\chi(0, \omega) = e^2 \sum_{i, f, i', f'} \langle i | \hat{v} | f \rangle \langle f' | \hat{v} | i' \rangle \frac{i}{\hbar} \int_0^\infty d\tau \langle [c_i^\dagger(\tau) c_f(\tau), c_{f'}^\dagger c_{i'}] \rangle_0.$$

The time dependence of the operators gives a factor $\exp(i(\epsilon_i - \epsilon_f)\tau/\hbar)$ and the integral over τ yields

$$\frac{i}{\hbar} \int_0^\infty d\tau e^{\frac{i}{\hbar}(\hbar\omega + \epsilon_i - \epsilon_f + i\delta)\tau} = -\frac{1}{\hbar\omega + \epsilon_i - \epsilon_f + i\delta},$$

where the small parameter δ is introduced to regularize the integral. To evaluate the remaining thermal expectation value first calculate the commutator

$$[c_i^\dagger c_f, c_{f'}^\dagger c_{i'}] = c_i^\dagger c_{i'} \delta_{f, f'} - c_{f'}^\dagger c_f \delta_{i, i'}.$$

With the thermal expectation value of $\langle c_i^\dagger c_{i'} \rangle_0 = f(\epsilon_i) \delta_{i, i'}$ the response function takes the form of (9.87)

$$\chi(0, \omega) = -e^2 \sum_{i, f} |\langle i | \hat{v} | f \rangle|^2 \frac{f(\epsilon_i) - f(\epsilon_f)}{\hbar\omega + \epsilon_i - \epsilon_f + i\delta}.$$

9.4: Write (for finite ω) the δ function in the form

$$\delta(\hbar\omega + \epsilon_i - \epsilon_f) = \int dE \delta(E - \epsilon_i) \delta(E + \hbar\omega - \epsilon_f)$$

so that with $\epsilon_i = E$ and $\epsilon_f = E + \hbar\omega$ the conductivity is expressed by

$$\sigma(0, \omega) = \pi e^2 \int dE \frac{f(E) - f(E + \hbar\omega)}{\omega} \sum_{i, f} |\langle i | \hat{v} | f \rangle|^2 \delta(E - \epsilon_i) \delta(E + \hbar\omega - \epsilon_f).$$

The δ functions can be replaced with (2.77) and $E^+ = E + i\delta$ by the imaginary part of the corresponding single-particle Green functions and give for the double sum

expression under the integral

$$\begin{aligned} \sum_{i,f} \dots &= \sum_{i,f} \langle i|\hat{v}|f\rangle \langle f|\hat{v}|i\rangle \text{Im}G_{ii}(E^+) \text{Im}G_{ff}(E^+ + \hbar\omega) \\ &= \frac{1}{\pi^2} \sum_{i,f} \langle i|\hat{v}G(E^+ + \hbar\omega)|f\rangle \langle f|\hat{v}G(E^+)|i\rangle, \end{aligned}$$

which for $\omega \rightarrow 0$ leads to $\text{Tr}(\hat{v}\text{Im}G(E^+)\hat{v}\text{Im}G(E^+))$.

9.5: Write $\beta(g)$ in the form

$$\beta(g) = \frac{dg}{dL} \frac{L}{g}.$$

For $g \rightarrow \infty$ use $g(L) = \sigma L^{d-2}$ and σ independent of L to find

$$\frac{dg}{dL} = \sigma(d-2)L^{d-3} = (d-2)\frac{g}{L}$$

which means

$$\lim_{g \rightarrow \infty} \beta(g) = d-2.$$

For $g \rightarrow 0$ use $g(L) \sim \exp(-L/\lambda)$ with $dg/dL = -g/\lambda$ and

$$\lim_{g \rightarrow 0} \beta(g) = -\frac{L}{\lambda}.$$

The sign of $\beta(g)$ is determined by dg/dL . For $d \leq 2$ and assuming a monotonous function it is always negative while for $d > 2$ there is a sign change.

Solutions for Chap. 10

10.1: For Bloch states ck, vk' write

$$\frac{1}{m} \langle ck|p|vk'\rangle = -\frac{i}{\hbar} \langle ck|rH_0 - H_0r|vk'\rangle = \frac{i}{\hbar} (E_c(\mathbf{k}) - E_v(\mathbf{k}')) \langle ck|r|vk'\rangle$$

which for direct transitions at $\mathbf{k} = 0$ gives $e\mathbf{p}_{cv} = -iE_g\mathbf{d}_{cv}/\hbar$. Use $\mathbf{E}(t) = -\partial\mathbf{A}/\partial t$ and $\mathbf{A}(t) \exp(i\omega t)$ with $\hbar\omega = E_c(\mathbf{k}) - E_v(\mathbf{k})$ to obtain

$$\frac{e}{m} \mathbf{p}_{cv} \cdot \mathbf{A} = \frac{i}{\omega} \frac{e}{m} \mathbf{p}_{cv} \cdot \mathbf{E} = \frac{E_g}{\hbar\omega} \mathbf{d}_{cv} \cdot \mathbf{E} \simeq \mathbf{d}_{cv} \cdot \mathbf{E}$$

with $\hbar\omega \simeq E_g$ for near band gap excitations.

10.2: Express Bloch functions by Wannier functions (see Problem 6.2) to write

$$\langle n\mathbf{k}|p|n'\mathbf{k}'\rangle = \frac{1}{N} \sum_{\mathbf{R}, \mathbf{R}'} e^{-i\mathbf{k}\cdot\mathbf{R}} e^{i\mathbf{k}'\cdot\mathbf{R}'} \int \phi_n^*(\mathbf{r} - \mathbf{R}) \mathbf{p} \phi_{n'}(\mathbf{r} - \mathbf{R}') d^3r.$$

Replace $\mathbf{R}' = \mathbf{R} - \mathbf{R}''$ and change integration variable to $\mathbf{r}' = \mathbf{r} - \mathbf{R}$ to find

$$\langle n\mathbf{k}|p|n'\mathbf{k}'\rangle = \frac{1}{N} \sum_{\mathbf{R}} e^{-i(\mathbf{k}-\mathbf{k}')\cdot\mathbf{R}} \sum_{\mathbf{R}''} e^{i\mathbf{k}'\cdot\mathbf{R}''} \int \phi_n^*(\mathbf{r}') \mathbf{p} \phi_{n'}(\mathbf{r}' - \mathbf{R}'') d^3r'.$$

The first sum gives $N\delta_{\mathbf{k}, \mathbf{k}'}$.

10.3: The solution of the Schroedinger equation with a spherically symmetric potential is

$$\phi_{nlm}(\mathbf{r}) = R_{nl}(r)Y_{lm}(\theta, \varphi).$$

The radial solution for the Coulomb problem is given by

$$R_{nl}(r) = N_n \rho^l e^{(-\rho/2)} F(l + 1 - \eta; 2l + 2; \rho)$$

with the hypergeometric function depending on the variables η (for the energy) and ρ (for the radial coordinate). For bound states one has $E_n = -R_{exc}/n^2$ and $\rho = 2r/na_B$. Only s-states with $l = 0$ have a nonvanishing amplitude at $r = 0$, thus $\phi_n(0) = N_n F(1 - n; 2; 0)$ with $N_n = 1/na_B$ and $|\phi_n(0)|^2 = (\pi a_B^3 n^3)^{-1}$. For the continuum ($E = \hbar\omega - E_g > 0$), $\eta = i\gamma$, $\gamma = (R_{exc}/(\hbar\omega - E_g))^{1/2}$ and $N = \Gamma(1 - i\gamma) \exp(\pi\gamma/2)$ one obtains

$$|\phi(0)|^2 = \pi\gamma \frac{\exp(\pi\gamma)}{\sinh(\pi\gamma)}.$$

The absorption coefficient is the one of (10.23) for the uncorrelated electron-hole pairs multiplied by the enhancement factor $C(\omega)$.

10.4: Using (10.37) and (10.38) one can write

$$B_{\nu Q}^\dagger |\Psi_0\rangle = |\Psi_{\nu Q}\rangle = \sum_{\substack{c\mathbf{k}_h, c\mathbf{k}_e \\ \mathbf{k}_e - \mathbf{k}_h = \mathbf{Q}}} \Phi_{\nu Q}(\mathbf{k}) c_{c\mathbf{k}_e}^\dagger c_{v\mathbf{k}_h} |\Psi_0\rangle.$$

Thus, in application to the ground state $|\Psi_0\rangle$, the exciton operator is a linear combination of products $c_{c\mathbf{k}_e}^\dagger c_{v\mathbf{k}_h}$. Let us assume a two-band model, i.e. the excitons are formed from states with fixed c, v , and consider for simplicity the exciton with $\mathbf{Q} = 0$ which implies $\mathbf{k}_e = \mathbf{k}_h = \mathbf{k}$. Then, the commutator $[B_{\nu,0}^\dagger, B_{\nu',0}]$ is determined by the commutators

$$\begin{aligned} [c_{v\mathbf{k}}^\dagger c_{c\mathbf{k}}, c_{c\mathbf{k}'}^\dagger c_{v\mathbf{k}'}] &= c_{v\mathbf{k}}^\dagger c_{c\mathbf{k}} c_{c\mathbf{k}'}^\dagger c_{v\mathbf{k}'} - c_{c\mathbf{k}'}^\dagger c_{v\mathbf{k}'} c_{v\mathbf{k}}^\dagger c_{c\mathbf{k}} \\ &= c_{v\mathbf{k}}^\dagger c_{v\mathbf{k}'} \delta_{\mathbf{k}, \mathbf{k}'} - c_{c\mathbf{k}'}^\dagger c_{c\mathbf{k}} \delta_{\mathbf{k}, \mathbf{k}'} \\ &= \delta_{\mathbf{k}, \mathbf{k}'} \left(c_{v\mathbf{k}}^\dagger c_{v\mathbf{k}} - c_{c\mathbf{k}}^\dagger c_{c\mathbf{k}} \right) = (1 - n_e(\mathbf{k}) - n_h(\mathbf{k})) \delta_{\mathbf{k}, \mathbf{k}'} . \end{aligned}$$

Without the electron and hole occupation this relation would lead to $[B_{\nu,0}, B_{\nu',0}^\dagger] = \delta_{\nu, \nu'}$, classifying excitons as bosons. This relation is valid, however, only if we consider a single exciton. The electron and hole occupations remind of the fact, that excitons are composed of fermions.

10.5: The zero of (10.42) close to the exciton resonance at $\omega_{\nu 0}$ determines the frequency of the corresponding longitudinal exciton:

$$\varepsilon_1(\omega_L) \simeq 1 + \frac{4e^2}{\varepsilon_0 m} \frac{f_{\nu 0}}{\omega_{\nu 0}^2} - \omega_L^2 = 0,$$

which for $\omega_L \simeq \omega_{\nu 0}$ and $\Delta_{LT} = \hbar(\omega_L - \omega_{\nu 0})$ allows to express the LT-splitting in terms of the exciton oscillator strength:

$$\Delta_{LT} = \frac{2e^2 \hbar^2}{\varepsilon_0 m} \frac{f_{\nu 0}}{E_{\nu 0}} \quad \text{with} \quad E_{\nu 0} = \hbar\omega_{\nu 0}.$$

On the other hand the first term of the exchange interaction V_{exch} in (10.62) gives a contribution only for longitudinal excitons (with $\mathbf{Q} \parallel \mathbf{P}_{cv}$) which can be calculated as a perturbation correction to the transverse exciton energy $E_{\nu 0}$ with the exciton envelope function $\phi_{\nu 0}(\mathbf{r})$ after taking the Fourier transform of V_{exch} (note: $1/V_c \int \exp(i\mathbf{k} \cdot \mathbf{r}) d^3\mathbf{k} = \delta(\mathbf{r})$) and yields (for singlet excitons with $S = 0$)

$$\Delta_{\text{LT}} = \frac{2e^2}{\varepsilon_0} \frac{\hbar^2}{m^2} \frac{|P_{cv}|^2 |\phi_{\nu 0}(0)|^2}{E_{\nu 0}^2}.$$

With $E_{\nu 0} \simeq E_g$ one finds by comparison between the two obtained expressions for Δ_{LT}

$$f_{\nu 0} = \frac{1}{m} \frac{|P_{cv}|^2 |\phi_{\nu 0}(0)|^2}{E_{\nu 0}}$$

in accordance with (10.43).

10.6: Use the expansion of $\mathbf{A}(\mathbf{r}, t)$ with $a_{\lambda\kappa}(t) = a_{\lambda\kappa} e^{i\omega(\kappa)t}$ to write the two contributions of \mathcal{H}_{rad} as

$$\begin{aligned} \left(\frac{\partial}{\partial t} \mathbf{A}(\mathbf{r}, t) \right)^2 &= \frac{\hbar}{2\varepsilon_0 V} \sum_{\lambda, \kappa} \sum_{\lambda', \kappa'} \mathbf{e}_{\lambda\kappa} \cdot \mathbf{e}_{\lambda'\kappa'} (\omega(\kappa)\omega(\kappa'))^{1/2} \\ &\quad \times (a_{\lambda\kappa}(t) - a_{\lambda-\kappa}^\dagger(t)) (a_{\lambda'\kappa'}(t) - a_{\lambda'-\kappa'}^\dagger(t)) e^{i(\kappa+\kappa') \cdot \mathbf{r}} \end{aligned}$$

and

$$\begin{aligned} c^2 (\nabla \times \mathbf{A}(\mathbf{r}, t))^2 &= -\frac{\hbar}{2\varepsilon_0 V} \sum_{\lambda, \kappa} \sum_{\lambda', \kappa'} (\boldsymbol{\kappa} \times \mathbf{e}_{\lambda\kappa}) \cdot (\boldsymbol{\kappa}' \times \mathbf{e}_{\lambda'\kappa'}) \\ &\quad \times (a_{\lambda\kappa}(t) + a_{\lambda-\kappa}^\dagger(t)) (a_{\lambda'\kappa'}(t) + a_{\lambda'-\kappa'}^\dagger(t)) e^{i(\kappa+\kappa') \cdot \mathbf{r}} \end{aligned}$$

and perform the volume integral with

$$\frac{1}{V} \int e^{i(\kappa+\kappa') \cdot \mathbf{r}} d^3\mathbf{r} = \delta_{\boldsymbol{\kappa}, -\boldsymbol{\kappa}'}$$

With $\mathbf{e}_{\lambda\kappa} \cdot \mathbf{e}_{\lambda'\kappa'} = \delta_{\lambda, \lambda'}$ and $(\boldsymbol{\kappa} \times \mathbf{e}_{\lambda\kappa}) \cdot (-\boldsymbol{\kappa}' \times \mathbf{e}_{\lambda'\kappa'}) = -\kappa^2 \delta_{\lambda, \lambda'}$ for transverse unit vectors this reduces with $\omega(\boldsymbol{\kappa}) = \omega(-\boldsymbol{\kappa}) = c\kappa$ to

$$\mathcal{H}_{\text{rad}} = \sum_{\lambda, \kappa} \frac{1}{2} \hbar \omega(\boldsymbol{\kappa}) (a_{\lambda\kappa} a_{\lambda\kappa}^\dagger + a_{\lambda\kappa}^\dagger a_{\lambda\kappa}) = \sum_{\lambda, \kappa} \hbar \omega(\boldsymbol{\kappa}) \left(a_{\lambda\kappa}^\dagger a_{\lambda\kappa} + \frac{1}{2} \right).$$

10.7: In quasi-equilibrium one has to find only the solution for the off-diagonal elements of the density matrix, because the diagonal elements are the equilibrium distribution functions (Fermi–Dirac distribution). Therefore, one finds from

$$\frac{d}{dt} \bar{\rho}_{cv}(\mathbf{k}, t) = \frac{i}{\hbar} d_{cv} E(t) e^{i(\epsilon_{c\mathbf{k}} - \epsilon_{v\mathbf{k}})t} (f_{v\mathbf{k}} - f_{c\mathbf{k}})$$

with

$$E(t) = \frac{1}{2\pi} \int E(\omega) e^{-i\omega t} d\omega$$

and integration over t

$$\bar{\rho}_{cv}(\mathbf{k}, t) = \frac{1}{2\pi\hbar} \int d\omega \frac{d_{cv} E(\omega) e^{i(\epsilon_{c\mathbf{k}} - \epsilon_{v\mathbf{k}} - \omega)t}}{\epsilon_{c\mathbf{k}} - \epsilon_{v\mathbf{k}} - \omega - i\gamma} (f_{v\mathbf{k}} - f_{c\mathbf{k}}).$$

The dielectric polarization is obtained by

$$\begin{aligned}
 \mathbf{P}(t) &= \text{Tr}(\bar{\rho}(t)\bar{d}(t)) \\
 &= \frac{1}{V} \sum_{\mathbf{k}} (\bar{\rho}_{cv}(t)\bar{d}_{vc}(t) + \bar{\rho}_{vc}(t)\bar{d}_{cv}(t)) \\
 &= \frac{1}{2\pi\hbar V} \sum_{\mathbf{k}} \int d\omega \frac{|d_{cv}|^2(f_{v\mathbf{k}} - f_{c\mathbf{k}})}{\epsilon_{c\mathbf{k}} - \epsilon_{v\mathbf{k}} - \omega - i\gamma} E(\omega) e^{-i\omega t} + c.c.
 \end{aligned}$$

and the dielectric susceptibility with $\chi(\omega) = P(\omega)/E(\omega)$ is

$$\begin{aligned}
 \chi(\omega) &= -\frac{1}{V} \sum_{\mathbf{k}} |d_{cv}|^2 (f_{v\mathbf{k}} - f_{c\mathbf{k}}) \left(\frac{1}{\hbar(\epsilon_{v\mathbf{k}} - \epsilon_{c\mathbf{k}} + \omega + i\gamma)} \right. \\
 &\quad \left. - \frac{1}{\hbar(\epsilon_{c\mathbf{k}} - \epsilon_{v\mathbf{k}} + \omega + i\gamma)} \right).
 \end{aligned}$$

Finally one recovers the result from Sect. 10.2 with $\varepsilon_2(\omega) = \text{Im}\chi(\omega)/\varepsilon_0$.

10.8: We demonstrate here the calculation only for one term, the others follow in similar way. The example is $[\alpha_{\mathbf{k}}^\dagger \alpha_{\mathbf{k}}, \sum_{\bar{\mathbf{k}}, \mathbf{k}'; q \neq 0} v_q \alpha_{\bar{\mathbf{k}}+q}^\dagger \alpha_{\mathbf{k}'-q}^\dagger \alpha_{\mathbf{k}'} \alpha_{\bar{\mathbf{k}}}]$. The commutator is evaluated by using the fermion commutation rules when changing the order of the operators:

$$\begin{aligned}
 &[\alpha_{\mathbf{k}}^\dagger \alpha_{\mathbf{k}}, \alpha_{\bar{\mathbf{k}}+q}^\dagger \alpha_{\mathbf{k}'-q}^\dagger \alpha_{\mathbf{k}'} \alpha_{\bar{\mathbf{k}}}] = \alpha_{\mathbf{k}}^\dagger \alpha_{\mathbf{k}} \alpha_{\bar{\mathbf{k}}+q}^\dagger \alpha_{\mathbf{k}'-q}^\dagger \alpha_{\mathbf{k}'} \alpha_{\bar{\mathbf{k}}} - \leftrightarrow \\
 &= \underbrace{\delta_{\mathbf{k}, \bar{\mathbf{k}}+q} \alpha_{\mathbf{k}}^\dagger \alpha_{\mathbf{k}'-q}^\dagger \alpha_{\mathbf{k}'} \alpha_{\bar{\mathbf{k}}}}_{(1)} - \alpha_{\mathbf{k}}^\dagger \alpha_{\bar{\mathbf{k}}+q}^\dagger \alpha_{\mathbf{k}} \alpha_{\mathbf{k}'-q}^\dagger \alpha_{\mathbf{k}'} \alpha_{\bar{\mathbf{k}}} - \leftrightarrow \\
 &= (1) + \underbrace{\delta_{\mathbf{k}, \bar{\mathbf{k}}+q} \alpha_{\bar{\mathbf{k}}+q}^\dagger \alpha_{\mathbf{k}}^\dagger \alpha_{\mathbf{k}'} \alpha_{\bar{\mathbf{k}}}}_{(2)} - \alpha_{\bar{\mathbf{k}}+q}^\dagger \alpha_{\mathbf{k}}^\dagger \alpha_{\mathbf{k}'-q}^\dagger \alpha_{\mathbf{k}} \alpha_{\mathbf{k}'} \alpha_{\bar{\mathbf{k}}} - \leftrightarrow \\
 &= (1) + (2) + \underbrace{\delta_{\mathbf{k}, \mathbf{k}'} \alpha_{\bar{\mathbf{k}}+q}^\dagger \alpha_{\mathbf{k}'-q}^\dagger \alpha_{\bar{\mathbf{k}}} \alpha_{\mathbf{k}}}_{(3)} - \alpha_{\bar{\mathbf{k}}+q}^\dagger \alpha_{\mathbf{k}'-q}^\dagger \alpha_{\mathbf{k}} \alpha_{\bar{\mathbf{k}}} \alpha_{\mathbf{k}'} \alpha_{\mathbf{k}} - \leftrightarrow \\
 &= (1) + (2) + (3) - \underbrace{\delta_{\mathbf{k}, \bar{\mathbf{k}}} \alpha_{\bar{\mathbf{k}}+q}^\dagger \alpha_{\mathbf{k}'-q}^\dagger \alpha_{\mathbf{k}'} \alpha_{\mathbf{k}}}_{(4)} + \alpha_{\bar{\mathbf{k}}+q}^\dagger \alpha_{\mathbf{k}'-q}^\dagger \alpha_{\mathbf{k}'} \alpha_{\bar{\mathbf{k}}} \alpha_{\mathbf{k}}^\dagger \alpha_{\mathbf{k}} - \leftrightarrow .
 \end{aligned}$$

In the last line, the last two terms cancel each other and one obtains the four contributions (1)–(4) which under the sum combine to the final result

$$\begin{aligned}
 &[\alpha_{\mathbf{k}}^\dagger \alpha_{\mathbf{k}}, \sum_{\bar{\mathbf{k}}, \mathbf{k}'; q \neq 0} v_q \alpha_{\bar{\mathbf{k}}+q}^\dagger \alpha_{\mathbf{k}'-q}^\dagger \alpha_{\mathbf{k}'} \alpha_{\bar{\mathbf{k}}}] = \\
 &= \sum_{\mathbf{k}'; q \neq 0} v_q \left(\alpha_{\mathbf{k}}^\dagger \alpha_{\mathbf{k}'-q}^\dagger \alpha_{\mathbf{k}-q} \alpha_{\mathbf{k}'} - \alpha_{\bar{\mathbf{k}}+q}^\dagger \alpha_{\mathbf{k}'-q}^\dagger \alpha_{\mathbf{k}} \alpha_{\mathbf{k}'} \right) .
 \end{aligned}$$

The thermal expectation values of these terms are found in (10.115).

Index

- absorption, 295
- absorption coefficient, 58
- acoustic phonon, 48
- adiabatic
 - approximation, 21, 37, 231
 - potential, 37, 44, 232
- alkali halide, 7
- alloy, 273
- Anderson model, 219
- anti-ferromagnet, 176, 179
- approximation
 - adiabatic, 21, 231
 - Born, 278
 - Born, self-consistent, 278
 - Born–Oppenheimer, 21, 39, 231
 - coherent potential, 279
 - continuum, 52
 - Cooperon, 285
 - dipole, 295
 - effective-mass, 147, 153, 266, 268, 299
 - harmonic, 39
 - Hartree, 98, 120
 - Hartree–Fock, 97, 98, 167, 181, 185, 322
 - local density, 123, 125
 - local spin density, 163
 - mean field, 100, 181, 258
 - molecular field, 179
 - one-band, 267
 - random phase, 106, 189, 282
 - relaxation time, 243
 - self-consistent field, 106
 - t-matrix, 278
 - Thomas–Fermi, 131
 - tight-binding, 142, 165, 202
 - virtual crystal, 277
- atomic limit, 204
- back scattering, 285
- band
 - conduction, 139
 - heavy hole, 152
 - index, 120, 128
 - light hole, 152
 - structure, 120, 127, 128, 136
 - valence, 139, 146
- band gap, 134, 146
 - engineering, 155
 - problem, 126
- band offset, 153
- band structure
 - free electron, 136
 - of Al, 137
 - of Cu, 145
 - of Fe, 162
 - of Si, 139
 - of transition metals, 144
 - photonic, 8
- BCS theory, 251
- Bethe–Salpeter equation, 284, 303
- binding
 - chemical, 4, 61, 75
 - covalent, 16, 62, 65, 145, 147
 - heteropolar, 16, 61
 - homopolar, 16
 - ionic, 16

- metallic, 16
- van der Waals, 16
- Bloch
 - electron, 127, 129, 185
 - equation, 171
 - function, 127, 129, 140, 267, 281, 326
 - representation, 172, 174, 177
 - state, 265
 - theorem, 6, 41, 326
 - vector, 318
- Bloch equations
 - optical, 318, 323
 - semiconductor, 320, 323
- Bogoliubov transformation, 177, 215
- Boltzmann equation, 243
- bond charge, 62, 147
 - model, 62
- Born
 - approximation, 278
 - series, 271, 274
- Born–Oppenheimer
 - approximation, 21, 39, 231
- Bose–Einstein
 - condensation, 262
 - distribution, 47
- Bragg condition, 134
- Brillouin
 - function, 182
 - zone, 6, 41, 43, 49, 120
- bulk modulus, 71
- carbon nanotubes, 146, 214
- center coordinate, 86
- central-cell
 - correction, 268, 269
 - potential, 269
- character table, 325
- chemical potential, 81, 82, 89, 200
- cluster, 4, 17
- collective
 - excitation, 42
 - mode, 42, 44
- collision term, 243
- compliance constant, 53
- composite fermion, 228
- compressibility, 54
- conditions
 - periodic boundary, 41, 77
- conductance, 288
- conductivity
 - dc, 283, 287
 - electric, 25, 32, 232, 244, 280
 - heat, 32
- configuration
 - average, 275
 - equilibrium, 18, 64
 - of ions, 38
- constant
 - compliance, 53
 - elastic, 52
 - Madelung, 19
 - stiffness, 52
- Cooper pairs, 255
- cooperon approximation, 285
- correlation, 12
 - density–density, 9, 32, 69
 - effects, 195
 - electron, 195
 - electronic, 83
 - energy, 110
 - hole, 113
 - spin–spin, 30
- Coulomb enhancement, 302
- coupling
 - deformation potential, 235
 - exciton–photon, 177
 - Fröhlich, 238
 - phonon–photon, 177
 - piezoelectric, 240
 - plasmon–phonon, 177
 - spin–orbit, 18
- critical
 - exponent, 183
 - point, 48, 297
 - temperature, 161, 179, 250, 261
- crystal
 - liquid, 4
 - mixed, 7, 273
 - molecular, 7
 - momentum, 5
 - photonic, 8
 - quasi, 4
 - structure, 6
- crystal field splitting, 141
- crystalline structure, 4
- Curie temperature, 184
- Curie–Weiss law, 184

- current density, 282
 - diamagnetic, 282
 - electric, 25
 - heat, 25
 - paramagnetic, 282
- cyclotron frequency, 84
- de Haas–van Alphen
 - oscillations, 136, 137
- Debye
 - frequency, 49, 255, 260
 - law, 50
 - model, 49, 175
 - temperature, 49, 261
- Debye–Waller factor, 50, 69, 74
- defect
 - anti-site, 266, 272
 - Frenkel, 266
 - point, 266
- deformation potential, 236
- degeneracy
 - Kramers, 128
 - spin, 129
- density
 - average, 11
 - fluctuation, 11, 211, 215
 - matrix, 317
 - parameter, 79, 99, 111
- density functional theory, 64, 120, 123
- density of states, 154, 187, 260, 271, 286
 - combined, 297
 - electron, 81
 - phonon, 47
- DFT-LDA, 126, 163
- diagram
 - exchange, 304
 - ladder, 284
 - maximally crossing, 285
- diamagnetism
 - Landau–Peierls, 91
- diamond, 50
- dielectric
 - function, 25, 32, 296
 - polarization, 25
 - screening, 31
- dielectric constant
 - high frequency, 58
 - static, 58
- dielectric function, 57
 - electronic part, 102
 - longitudinal, 103
 - transverse, 103
- dimensionality, 8, 153, 213, 214, 289
- dipole
 - approximation, 56, 295
 - moment, 55
 - operator, 56, 294
- direct
 - exchange, 169
 - term, 98
- dislocation, 273
- disorder
 - compositional, 8, 67, 265, 273
 - diagonal, 273
 - isotope, 273
 - off-diagonal, 273
 - structural, 5, 8, 265, 273, 287
 - substitutional, 287
- distribution
 - Bose–Einstein, 47
 - Fermi–Dirac, 82, 283
- doping, 266
- Dulong–Petit law, 49
- dynamical matrix, 41
- Dyson equation, 199, 274, 277
- edge channel, 228
- effect
 - de Haas–van Alphen, 91, 136
 - quantum Hall, 155
- effective
 - g factor, 86
 - mass, 86, 91, 150
 - single-particle potential, 120, 154
- Einstein relation, 289
- elastic
 - constant, 52, 54
 - modulus, 53
- electric conductivity, 25, 232
- electron
 - closed shell, 15
 - core, 75, 131
 - gas, 76
 - valence, 15, 75, 131
- electron system
 - low-dimensional, 84
 - two-dimensional, 153, 195, 222

electron–electron interaction, 75, 96,
 110, 120, 157, 165, 195, 198, 290
 electron–hole
 excitation, 189
 electron–hole excitation, 299
 electron–hole pair, 299
 electron–phonon interaction, 231
 elementary flux quantum, 86
 energy
 band structure, 120
 dissipation, 58, 242
 functional, 124
 gap, 134, 269
 loss spectroscopy, 105
 relaxation, 242
 energy bands
 of Al, 137
 of Cu, 145, 298
 of ferromagnetic Fe, 162
 of Ge, 146
 of Si, 139
 of transition metals, 144
 energy gap, 139, 146
 energy–loss
 function, 32, 107, 109, 282, 314
 ensemble
 canonical, 24
 grand-canonical, 24
 mean value, 22
 equilibrium
 configuration, 18
 position, 18, 38
 thermodynamic, 20
 exchange
 density, 122
 diagram, 304
 direct, 169
 energy, 163
 hole, 102
 Rudermann–Kittel, 170
 term, 98
 excitation
 collective, 42, 109, 170, 189
 electron–hole, 105, 299
 elementary, 44
 particle–hole, 108
 spin-flip, 187

exciton
 longitudinal, 306
 polariton, 307
 transverse, 306
 Wannier–Mott, 300
 Fermi
 circle, 135
 contour, 136
 energy, 79, 144, 147, 210
 gas, ideal, 78
 hole, 102, 113
 integral, 82, 331
 liquid, 195
 sphere, 77, 78, 92, 97, 98, 105, 108,
 110, 163
 surface, 91, 136, 257
 temperature, 79
 velocity, 79
 wavelength, 79
 Fermi surface
 of Ag, 138
 of Al, 138
 Fermi–Dirac
 distribution, 82, 211
 fermion
 annihilation operator, 94
 composite, 155, 228
 creation operator, 94
 heavy, 83, 91, 217
 vacuum, 94
 ferromagnet, 179
 ferromagnetic
 ground state, 167, 171
 insulator, 167, 169
 ferromagnetism, 187
 strong, 188
 weak, 188
 field quantization, 45
 filling factor, 87, 155, 156
 fine structure constant, 239
 fluctuation
 density, 103
 number, 103
 spin, 180
 Fock representation, 95
 force constant, 40, 52, 61
 four-center integral, 202

- Fröhlich
 - coupling constant, 239
 - polaron, 247
- fractional
 - charge, 228
 - filling, 223
 - quantum Hall states, 222
- free energy, 71, 89, 211
- function
 - density–density correlation, 9
 - dielectric, 30, 296
 - pair–distribution, 9, 10, 102
 - Wannier, 165, 271
- gap
 - direct, 148
 - indirect, 148
 - parameter, 260
- Grüneisen
 - parameter, 72
 - relation, 72
- gradient approximation, 126
- grand-canonical
 - ensemble, 24
 - potential, 89
- Green function, 28
 - exciton, 303
 - retarded, 33, 196
 - spectral representation, 34
 - two-particle, 284, 303
- ground state, 4, 78, 97
 - energy, 79, 99
 - of the lattice, 38, 45
 - theorem, 112
- group
 - of the wave vector, 7, 328
 - point, 6, 40, 237, 325
 - space, 7
 - translation, 5, 325
- harmonic
 - approximation, 39, 44
 - oscillator, 39
- Hartree
 - approximation, 98
 - equation, 121
 - self-energy, 200
- Hartree–Fock
 - approximation, 97, 105, 162, 185, 322
 - equation, 122
 - self-energy, 200
- heavy fermion, 83, 91, 217
- Heisenberg
 - Hamiltonian, 166, 168, 180
 - model, 169
- heterostructure, 153, 214
- hierarchy problem, 197
- Hohenberg–Kohn theorem, 123
- hole, 147
- Holstein–Primakoff transformation, 173
- Hooke’s law, 52
- hopping matrix element, 165, 219
- Hubbard
 - band, 207, 279
 - Hamiltonian, 203
 - model, 201
- Hund’s rule, 171
- hybridization, 144, 162, 219
- impurity, 265, 286
 - concentration, 275
 - deep, 269
 - interstitial, 266
 - shallow, 268, 269
 - substitutional, 266
- insulator, 139, 201, 287
 - anti-ferromagnetic, 176
 - ferromagnetic, 169
 - Mott–Hubbard, 207
- interaction
 - effective electron–electron, 252
 - electron–electron, 75, 96, 110, 120, 157, 195, 198
 - electron–phonon, 231, 233
 - electron–phonon, deformation potential, 236
 - electron–phonon, Fröhlich, 239
 - electron–phonon, piezoelectric, 240
 - exchange, 161
 - fermion–boson, 234
 - light–matter, 291, 293, 317
 - van der Waals, 62
- interface, 273
- ionization energy, 298

- irreducible
 - diagram, 277
 - representation, 144, 325
- Ising model, 169
- isotope, 67
 - disorder, 273
 - effect, 251, 261
- Jastrow-type wave function, 226
- jellium model, 19, 76, 96, 119
- k.p theory, 149
- Kohn–Sham equation, 123, 125
- Kramers degeneracy, 128
- Kramers–Kronig relation, 58, 296
- Kubo formula, 28
- Kubo–Greenwood formula, 284
- Lamé constants, 54
- Landau
 - level, 85, 279, 286
 - quantization, 92
- lattice
 - body-centered cubic, 7
 - Bravais, 6
 - displacement, 18, 38
 - distortion, 269
 - dynamics, 37, 42
 - dynamics, nonlinear, 44
 - face-centered cubic, 7
 - point, 5
 - reciprocal, 6, 11
 - thermal expansion, 44
 - translation, 40
 - vector, 5
 - with basis, 6
- Laughlin wave function, 226
- LCAO method, 269
- LDA + U, 208
- lifetime, 231, 241
 - population, 320
 - quasi-particle, 279
 - single-particle, 285
- light–matter interaction, 291, 293, 317
- light-scattering, 312
- Lindhard function, 106, 213
- linear response, 24
- liquid, 9
 - Bose, 209
 - classical, 208
 - Fermi, 209
 - Luttinger, 213
 - quantum, 208
- localization, 222
 - length, 265
 - weak, 285
- longitudinal
 - phonon, 56
- Lyddane–Sachs–Teller relation, 60, 308
- Madelung constant, 19
- magnetic
 - length, 85, 224
 - order, 161
- magnetism, 165
 - itinerant electron, 185
 - theory of, 168
- magnetization, 181, 185
- magnon, 161, 170, 173, 189, 234
- magnon dispersion, 190
- mass
 - effective, 150, 154
 - operator, 125
- matrix element
 - hopping, 165
 - transfer, 165, 273
- matter
 - condensed, 4
 - soft, 4
- mean field, 181
- mean free path, 285
- mesoscopic
 - physics, 155
 - regime, 275
 - system, 17, 247
- metal, 16, 50, 61, 110, 201, 287
 - alkali, 83
 - noble, 6, 80, 83, 136, 142
 - normal, 6, 80, 136, 142
 - transition, 6, 83, 143, 169
- metal–insulator transition, 207, 265, 286, 287, 289
- mobility, 246
 - edge, 287

- model
 - Anderson, 219
 - bond charge, 62
 - Hubbard, 219
 - jellium, 76
 - rigid ion, 61
 - shell, 61
 - Stoner, 185
 - Tomonaga–Luttinger, 217, 228
- modulus
 - bulk, 54
 - rigidity, 54
 - Young, 54
- molecular field, 181

- nanophysics, 8
- nonlinear lattice dynamics, 44
- nonparabolicity, 150
- normal coordinate, 42, 44, 56

- occupation
 - number, 46, 95
 - number operator, 46, 95
- operator
 - annihilation, 44
 - creation, 44
 - dipole, 294
 - field, 281
 - statistical, 23
- orbital
 - sp^2 , 146
 - sp^3 , 146
 - anti-bonding, 146
 - bonding, 146
 - directed, 146
 - hybrid, 146
 - localized, 166
- order
 - ferrimagnetic, 170
 - ferromagnetic, 170
 - parameter, 183, 261
- oscillations
 - de Haas–van Alphen, 91, 138
 - quantum, 136
 - Shubnikov–de Haas, 92, 136
- oscillator strength, 296, 302
- overlap integral, 141

- pair
 - Cooper, 255
 - electron–hole, 139, 148
- pair–distribution
 - function, 10, 12, 102, 113
- paramagnetism
 - Pauli spin, 90, 162
- particle
 - independent, 195
- particle–hole
 - continuum, 108, 190
 - excitation, 108
- partition function
 - canonical, 24
 - grand-canonical, 24, 46
- Pauli
 - blocking, 323
 - principle, 93, 98
- periodic
 - boundary condition, 128, 329
 - potential, 119, 130, 138
- phase
 - ferromagnetic, 183
 - liquid, 4
 - paramagnetic, 183
 - solid, 4
 - transition, 179, 183, 184, 209
- phonon, 19, 37, 45
 - acoustic, 48
 - confined modes, 67
 - dispersion curves, 60
 - energy, 45
 - focusing, 54
 - hot, 242
 - lifetime, 58
 - longitudinal, 56
 - operator, 56
 - optical, 55
 - surface, 66
 - transverse, 56
 - vacuum, 45
 - virtual, 248
- phonon dispersion
 - of α -Fe, 62
 - of Al, 61
 - of Cu(100), 67
 - of GaAs, 64
 - of GaAs(110), 68
 - of KI, 62

- of Si, 63
- of solid ^4He , 63, 64
- phonons
 - acoustic, 235
 - optical, 238
- photo-electron spectroscopy, 298
- photoemission, 298
- photon echo, 319
- photonic
 - band structure, 8
 - crystal, 8
- piezoelectric
 - coupling, 240
 - effect, 240
 - tensor, 240
- plasma frequency, 109
- plasmon, 109
- plasmon dispersion, 190
- plasmon–phonon modes, 110
- point defect, 265
- point group, 325
- polariton, 307
- polarization
 - dielectric, 307
 - function, 106
- polaron, 232, 248
 - energy, 250
 - Fröhlich, 248
 - mass, 250
- polymer, 214
- potential
 - effective, 120
 - adiabatic, 22, 52, 63, 232
 - chemical, 24, 46, 81, 82, 89, 210
 - effective, 122
 - effective single-particle, 18, 120
 - empty core, 130
 - exchange–correlation, 154
 - grand-canonical, 89
 - Hartree, 121, 154
 - self-consistent, 270
- process
 - normal, 235
 - Umklapp, 235
- propagator, 196
- pseudo-potential, 132

- quantum
 - liquid, 209
 - oscillations, 89
 - well, 153
 - wire, 214
- quantum Hall
 - effect, 92, 155
 - effect, integer, 156
 - plateau, 156
- quantum limit
 - electric, 154
 - magnetic, 89, 156
- quasi-crystal, 4
- quasi-hole, 201
- quasi-particle, 101, 129, 201, 205, 209–211, 213, 217, 218, 232
 - correction, 126
 - dispersion, 220
 - distribution, 213
 - effective mass, 212
 - energy, 126, 210
 - lifetime, 279
 - weight, 213
- Rabi frequency, 318, 323
- random phase approximation, 106
- Rashba effect, 154
- reflection coefficient, 59
- relation
 - dispersion, 33
 - Kramers–Kronig, 33, 58
- relaxation
 - electron–lattice, 231
- relaxation time
 - transport, 231, 281
- representation
 - Bloch, 174
 - occupation number, 44, 46, 93, 241, 257
 - Wannier, 165, 174
- resonance
 - cyclotron, 85
 - electron spin, 86
 - paramagnetic, 86
 - spin–flip, 86
- response
 - function, 28, 35, 52, 55
 - linear, 24, 281

- nonlinear, 32
 - transverse, 282
- Reststrahlen band, 59, 66
- RPA, 106, 189
- Rudermann–Kittel exchange, 170
- scaling theory, 289
- scanning tunneling microscopy, 8
- scattering
 - back, 245
 - backward, 281
 - cross section, 313
 - forward, 245, 281
 - inelastic, 60
 - neutron, 60
 - rate, 241, 243
- screening, 103
 - Thomas–Fermi, 109, 131
- SDFT-LDA, 163
- self-averaging, 275
- self-consistent
 - harmonic approximation, 74
 - solution, 121, 126
- self-energy, 199, 205, 206, 209, 235, 241, 276, 284
 - exchange–correlation, 125
 - Hartree, 200
 - Hartree–Fock, 200
 - single-particle, 199
- semiconductor, 7, 16, 80, 110, 136, 139, 146–148, 266
- shell model, 61
- Shubnikov–de Haas oscillations, 136
- Slater determinant, 93, 121
- soft mode, 74
- solid
 - amorphous, 4, 9, 273
 - crystalline, 4, 9
- Sommerfeld
 - coefficient, 82, 212, 217, 222
 - correction, 302
 - expansion, 82, 333
 - model, 78, 97
- sound
 - propagation, 48, 54
 - velocity, 49
- sound propagation
 - longitudinal, 54
 - transverse, 54
- specific heat, 48, 72, 175, 210, 212
 - of electrons, 82
 - of phonons, 48
- spectral function, 34
- spin, 17
 - degeneracy, 18, 129
 - density, 163
 - dynamics, 154
 - paramagnetism, 162
 - polarization, 126, 162, 186, 191
 - susceptibility, 188, 189, 210, 222
- spin polarized electrons, 163
- spin waves, 161, 170, 173
 - in anti-ferromagnets, 175
 - in ferromagnets, 170
- spin–orbit coupling, 18
- spintronics, 161
- splitting
 - longitudinal–transverse, 66
- state
 - anti-bonding, 146
 - bonding, 146
 - extended, 6, 265, 286
 - localized, 8, 265, 286
- states
 - anti-bonding, 269
 - bonding, 269
 - extended, 287
 - localized, 287
- stiffness constant, 52
- Stoner
 - condition, 187, 191
 - continuum, 188
 - model, 185, 187
- strain tensor, 52, 53, 240
- structure
 - diamond, 7
 - rocksalt, 7
 - zinc blende, 7
- structure factor, 9, 71
 - dynamic, 11, 69, 107, 111, 313
 - static, 9, 10, 111
- subband, 152
- super-exchange, 169
- superconductivity, 232, 250
- superconductor
 - high- T_c , 7
- superlattice, 67, 136
- isotope, 68

- surface, 8, 273
 - magnon, 161
 - phonon, 66
- susceptibility, 28
 - dielectric, 28, 55
 - magnetic, 29, 90
- system
 - mesoscopic, 17

- t-J model, 379
- t-matrix, 274, 281
- temperature
 - critical, 179
 - Curie, 184
 - Néel, 179
- term
 - direct, 167
 - exchange, 167
- theorem
 - dissipation–fluctuation, 35, 213
 - ground state, 112
 - Hohenberg–Kohn, 123
- thermal
 - average, 9
 - energy, 48
 - expansion, 44, 71
 - expectation value, 22, 46, 196, 282
 - lattice expansion, 44
- time
 - decoherence, 320
 - dephasing, 320
 - phase relaxation, 320
- time reversal, 128
- transfer matrix element, 165, 202, 273
- transformation
 - Bogoliubov, 177, 215
 - Holstein–Primakoff, 173
 - Schrieffer–Wolff, 252
- transition
 - direct, 295, 302
 - metal–insulator, 207, 265, 287, 289
 - vertical, 295, 302
- translation
 - group, 325
 - operator, 127
- transport
 - ballistic, 247
 - linear, 243
 - nonlinear, 243
 - relaxation time, 231, 243, 285
- transverse
 - effective charge, 60
 - phonon, 56
- truncation, 197

- vacuum
 - fermion, 94
 - phonon, 45
- van Hove singularity, 48, 297
- velocity
 - Fermi, 79
 - of sound, 49
 - sound, 49, 54
- vertex operator, 284
- Voigt notation, 53, 240

- Wannier
 - function, 165
 - representation, 165, 174
- Wannier function, 271
- Wannier–Mott exciton, 300
- warping, 54, 150, 152
- Weiss constant, 181
- Wigner crystal, 114, 228
- Wigner–Seitz cell, 5, 128
- work function, 298

- XY model, 169

- Zeeman term, 84
- zero point
 - contribution, 178
 - motion, 45
- zone scheme
 - extended, 133
 - reduced, 133
 - repeated, 133